CHINESE CRITICAL CARE CONGRESS 2026

中国危重病医学大会

第17届中国医师协会重症医学医师分会年会暨危重病医学大会-2026

Chinese Critical Care Congress 2026, Chinese Medical Doctor Association

济南 中国

2026年9月3日-6日

September 3 – 6, 2026

壁报交流论文汇编

塑造重症未来

Shape the Future of Critical Care



目录

Neuroprotective Effects of Testosterone on Sevoflurane-Induced Neurotoxicity in Testosterone-Deprived Male Mice	05
Serum exosomal proteomics reveals molecular characteristics of sepsis patients at high risk of death	06
The gut-to-lung pathogen translocation occurs in critically ill patients with pneumonia	33
Time-dependent effects of prone position on ventilation-perfusion matching assessed by electrical impedance tomography in patients with COVID-19 ARDS: sub-analysis of a prospective physiological study	46
急性 A 型主动脉夹层患者应用一氧化氮治疗对急性肾损伤和 90 天肾脏不良事件发生率的影响：一项随机对照试验	63
间充质干细胞来源的外泌体改善老年脓毒症患者免疫功能和预后结局的临床研究	75
脓毒症诱导凝血病患者的凝血表型分析	79
普通肝素通过 Ang/Tie2 通路对组蛋白造成的凝血活化发挥保护作用	93
首次发病和复发性高甘油三酯血症性急性胰腺炎患者临床特征比较的全国多中心临床研究	101
治疗性低温调控 PINK1/Parkin-VDAC3 信号通路改善神经细胞缺血 / 再灌注损伤的研究	107
A questionnaire on the current situation of resignation intention of nurses in intensive care units in China – A descriptive quantitative study	116
Frontier and hot topics in family-centered care research: A Bibliometrics Study and Visualization Analysis via CiteSpace	136
ICU 外周静脉血液标本质量管理的最佳证据总结	147
IKAP 理论教育联合主动循环呼吸训练对 ICU 拔管后经鼻高流量氧疗患者肺康复的影响	156
Risk Prediction Models for intra-abdominal hypertension in adult ICU patients	164
非计划重返重症监护病房预测模型的系统评价	180

The influence of dynamic trajectories of red blood cell distribution width on prognosis in sepsis patients：a longitudinal study with external validation

姓名：LiangWen Cui[1], MingLiang Lu[2], YuTao Zha[1], Juan Li[1], Cheng Zhang[1], Nian Liu[1],Yun Sun[2], Min Shao[1], XiaoChun Peng[1]
单位：1 The First Affiliated Hospital of Anhui Medical University，2 The Second Affiliated Hospital of Anhui Medical University

Background: Sepsis is a highly heterogeneous syndrome, and static clinical data do not provide a comprehensive characterization of the full spectrum of patient conditions. This study investigated sepsis subtypes based on the dynamic trajectory of red cell 32

distribution width (RDW) aiming at better risk stratification of patients.

Methods: This retrospective study included a derived cohort of sepsis patients from the Medical Informatics Marketplace Intensive Care Database (MIMIC IV) and an external validation cohort of sepsis patients from the First Affiliated Hospital of AnHui Medical University department of Critical Care medicine Data Mart (AHCCDM) between January 2019 and June 2025. Latent Class Trajectory Modeling (LCTM) was employed to identify distinct RDW trajectories over the first 5 days following ICU admission. We 39

compared the clinical characteristics and outcomes of patients in these subphenotypes to evaluate the prognostic significance of RDW trajectory patterns in sepsis.

Results: A total of 20,485 sepsis patients from the MIMIC-IV database were included in the study as the derived cohort, and 627 sepsis patients from the AHCCDM dataset served as the external validation cohort. Based on the RDW trajectory analysis, three 44

different subtypes were identified, Class 1: stable, normal RDW; Class 2: rapidly increasing and severely abnormal RDW; Class 3: stable, elevated RDW. Among them, the clinical characteristics of patients in category 2 included higher severity, more 47

severe inflammatory response, and more severe organ damage. Using Kaplan-Meier survival curve analysis to compare the incidence of the primary outcome between groups, patients with class 2 sepsis had a significantly higher risk of death at 30, 60, 50

and 90 days than class 3 and 1. External validation revealed that the RDW trajectories were also classified into three distinct groups, with patients in all three groups exhibiting similar mortality trends.

Conclusion: Dynamic RDW trajectories identify distinct sepsis subphenotypes associated with disease severity and mortality. Serial RDW monitoring may serve as a simple tool for early risk stratification and individualized sepsis management.

Keywords: RDW, Sepsis, Mortality, Trajectories analysis

Background

Sepsis is a dysregulation of the inflammatory response to infection, leading to multiple organ dysfunction[1]. Mortality and morbidity from sepsis affect millions of people worldwide, in both developing and developed countries[2]. In recent years, some progress has been made in intensive treatment of sepsis and intensive care models, but the mortality rate of septic patients, especially those with septic shock, is remain high[3]. However, sepsis is complex and dynamically changing, static indicators do not represent the overall course of disease progression, and there is a lack of dynamic clinical biomarkers that can be widely used in the early assessment of sepsis. Red cell distribution width (RDW) is a simple and easy-to-obtain counting value in routine blood tests, which reflects the size and dispersion of red blood cells and is often used in the differential diagnosis of anemia, and is calculated by dividing the standard deviation (SD) of red blood cell volume by the average red blood cell volume and expressing the result as a percentage, The normal range is 11%~15%[4]. Recent studies have shown that RDW is also associated with the prognosis of patients with heart failure, acute myocardial infarction, pulmonary embolism, critical illness, and cardiac arrest. The pathophysiological mechanisms associated with RDW and the above mentioned diseases have not been very well explained, and most of the studies have hypothesized that the above mentioned pathological processes are associated with inflammatory responses and oxidative stress[5-7]. Sadaka et al [8]found in their study, there is a correlation between the incidence of sepsis and RDW. Wang [9]et al found that RDW was an independent predictor of hospitalized mortality in elderly patients with sepsis. Elevated RDW is associated with inflammatory biomarkers[10], and its levels increase in response to oxidative stress [11].

Inflammation can impair iron metabolism, promote erythrocyte apoptosis, suppress erythropoietin production, and inhibit bone marrow hematopoiesis[12, 13], all of which contribute to elevated RDW levels. A study reported that RDW has moderate discriminatory power for mortality in critically ill patients[14], suggesting that RDW may be a potential biomarker for assessing the severity of sepsis. However, the progression of sepsis is dynamic, while most existing clinical studies have focused on the prognostic significance of static RDW measurements[8, 9, 14]. Therefore, the aim of this study was to investigate the association between dynamic changes in the readily available biomarker RDW and long-term prognosis in patients with sepsis, and to provide valuable insights for guiding clinical decision-making by evaluating the potential mediating role of RDW dynamics in survival outcomes.

Materials and Methods

Data source

This study was a retrospective observational study based on two independent cohorts. The primary (derivation) cohort was obtained from the Medical Information Mart for Intensive Care IV (MIMIC-IV, version 3.1) database, a large, freely accessible critical care database developed by the Massachusetts Institute of Technology and the Beth Israel Deaconess Medical Center. The database contains comprehensive electronic health records of 546,028 hospital admissions and 94,458 ICU stays between 2008 and 2019. Access to the MIMIC-IV database requires completion of the "Protecting Human Subjects Research" training and signing of a data use agreement. The use of the MIMIC-IV database was approved by the Institutional Review Boards of the Beth Israel Deaconess Medical Center (2001-P-001699/14) and the Massachusetts Institute of Technology (No. 0403000206), with a waiver of informed consent because all patient data are fully de-identified. Therefore, no additional ethical approval was required for this study. The external validation cohort was derived from the Data Mart of the Department of Critical Care Medicine at the First Affiliated Hospital of Anhui Medical University (AHCCDM, Hefei, China), which includes clinical data from patients admitted to the ICU between January 2019 and June 2025. The study protocol was reviewed and approved by the Ethics Committee of the First Affiliated Hospital of Anhui Medical University (Approval No.Ethics Review: Fast Track PJ2024-02-24). Since this study was retrospective and utilized de-identified patient data, the requirement for informed consent was waived. All methods were conducted in accordance with relevant guidelines and regulations. The clinical trial number for this study is not applicable.

Study design and eligible criteria

All patients with a diagnosis of sepsis in the MIMIC database and AHCCDM dataset were eligible for inclusion in this study. Patients with sepsis who met any of the following criteria were excluded: (1) absence of multiple RDW measurements within the first 5 days of ICU admission; (2) age under 18 years; (3) ICU length of stay less than 24 hours; or (4) not the first ICU admission. To ensure the accuracy of the analysis, patients with an ICU stay of less than 24 hours were excluded, as such a short stay may not adequately capture the true trajectory of RDW changes over the 5-day period.

Variables Measurement and Outcomes

Longitudinal RDW trajectories for 5 days after ICU were included and summarized daily. If there were multiple measurements in a single day, the worst value was used for analysis. Variables included age, gender, vital sign measurements [(heart rate, respiration, temperature, MAP, oxygen saturation (SpO2)], comorbidities (hypertension, diabetes mellitus, cardiac, pulmonary, and renal diseases, etc.), laboratory investigations (white blood cell count, lymphocyte count, erythrocyte count, erythrocyte distribution width, platelet count, aspartate aminotransferase, alanine aminotransferase, total bilirubin, creatinine , urea nitrogen, lactate, PT and APTT, etc.), SAPSII score, SOFA score, and length of hospitalization. The outcomes of this study were 30-day mortality, 60-day mortality and 90-day mortality. With or without mechanical ventilation and with or without CRRT.

Statistical analysis

Latent Class Trajectory Model Development

In the cohort, a latent category trajectory model (LCTM) was used to identify subcategories of septic patients based on the trajectory of RDW measurements 5 days after ICU admission. The selection of the optimal model was guided by several key reference criteria[15, 16]: (1) Bayesian information criterion (BIC), which measures model complexity and goodness-of-fit, where

lower values indicate better fit; (2) to confirm clinical significance and robust results of statistical analyses, it was ensured that each trajectory group included at least 2% of the participants to maintain statistical significance; and (3) Akaike's information criterion (AIC), which, similarly to BIC, assesses model fit, but emphasizes fit over complexity, making it more appropriate for smaller sample sizes; (4) Entropy measures the degree of separation between trajectory groups within the model. Higher entropy values indicate more pronounced group distinctions, usually ranging from 0 to 1. Values greater than 0.8 are considered optimal. The final model will provide a posteriori categorized individual category membership probabilities for each patient trajectory, which will result in division into subcategories and the next step in the analysis. The 5-day RDW levels in ICU septic patients have a very complex fluctuation patterns, making it insufficient to differentiate these patients based solely on baseline RDW levels. To address this limitation, the area under the receiver operating characteristic curve (AUROC) was calculated to evaluate the performance of the model. Model interpretation was performed using the SHapley Additive exPlanations (SHAP) algorithm.

Clinical Characteristics and Outcomes Compared Between Trajectory Model

Subclasses

Continuous variables following a normal distribution are presented as mean ± standard deviation (SD), and differences between groups are assessed using the t-test. Non- normally distributed variables are expressed as interquartile range (IQR), with group comparisons performed using the Wilcoxon rank-sum test. Categorical variables are reported as counts and percentages, and compared using the chi-square test. Patients are classified according to dynamic trajectory models, and survival differences are analyzed using Kaplan-Meier curves and the log-rank test. Multiple Cox proportional hazards models are applied to evaluate the association between dynamic RDW trajectories and clinical outcomes. Mediation analysis is conducted to assess the potential mediating role of dynamic RDW trajectories in survival outcomes among sepsis patients. Subgroup analyses are performed to explore potential effect modifiers, including gender, age, and comorbidities. Multivariate imputation for missing data is conducted using the "mice" package, and latent class trajectory modeling (LCTM) is performed using the "lcmm" package. The SHAP algorithm is applied using the "SHAPforxgBoost" package. All statistical analyses are conducted using R (version 4.5.0), with visualizations generated using the "ggplot2" package. A two-tailed p-value of <0.05 is considered statistically significant.

Results

Construction of a dynamic trajectory model for RDW

The study included 31,911 adult sepsis patients who were first admitted to the ICU in MIMIC-IV, excluded 202 who stayed in the ICU for less than 24 hours, 11,224 who did not have five consecutive days of RDW tests, and finally 20,485 sepsis patients who were included in the study **(Supplementary Figure1A).** In this study, trajectory analysis of RDW was performed using the lcmm package for patients who met the inclusion criteria during the first 5 days of ICU admission. The package conducted trajectory modeling using parametric criteria, including the Bayesian Information Criterion (BIC), Akaike Information Criterion (AIC), entropy, and the proportion of patients assigned to each subgroup **(Supplementary Table 1).** The optimal number of trajectories was determined by selecting the model with the lowest BIC, while ensuring adequate posterior class probabilities (>0.80) and sufficient class size (⩾ 2% of the study population). Based on these criteria, the 3-class model (LCTM-3) was identified as the final model. A total of 20,485 patients with sepsis who met the criteria were ultimately enrolled in this study, and the trajectories were categorized into 3 categories based on changes in Red blood cell distribution width (RDW) trajectories **(Figure 1).** The first trajectory, **Class 1: Low Stabilization,** represented patients whose RDW remained stable around 15%. The second trajectory, labeled **Class 2: Rapid Increase**, included patients whose RDW fluctuated at abnormally elevated levels, ranging from 17% to 20%. The third trajectory, labeled **Class 3: Stable at High Levels,** represented patients whose RDW remained persistently elevated between 17% and 18%. The proportions of patients in Class 1, Class 2, and Class 3 were 76.13%, 20.92%, and 2.95%, respectively.

Baseline characteristics of patients

The baseline characteristics of the three RDW trajectory groups are presented in **Table 1**.The mean age of the sepsis patients in this study was 66.36 years and 11,826 (57.73%) were male. Category 1 included the largest number of patients, while patients in Categories 2 and 3 had more severe underlying diseases, with higher prevalence rates of mild liver disease and renal disease at baseline compared to Category 1. Patients in Category 2 exhibited more pronounced abnormalities in vital signs and laboratory

parameters, including poorer oxygenation, higher lactate levels, lower hemoglobin and platelet counts, and worse liver function, renal function, and coagulation indices. In terms of disease severity, Charlson Comorbidity Index, SOFA score, and SAPS II score were higher in Categories 2 and 3 compared to Category 1, with Category 2 representing the most severe condition. Detailed baseline characteristics for all patients are presented in

Table 1.

Outcomes between subgroups of the RDW trajectory model

In terms of in-hospital 30-day, 60-day, and 90-day mortality, Category 2 patients had the highest mortality rates, followed by Category 3 and then Category 1. The rate of mechanical ventilation use was highest in Category 3, followed by Category 2, and lowest in Category 1. Regarding acute kidney injury (AKI), the incidence was highest in Category 3, followed by Category 2, and lowest in Category 1. However, the utilization rate of continuous renal replacement therapy (CRRT) was highest among Category 2 patients, followed by Category 3, and was significantly lower in Category 1 compared to Categories 2 and 3**(Table 1) Relationship between RDW trajectory and prognosis** Based on the trajectory model subgroups, Kaplan-Meier survival curve analysis was performed to compare the incidence of the primary outcome among the different groups **(Figure 2)**.The risk of 30-day mortality faced among patients with sepsis in category 2 was significantly higher than in categories 3 and 1, with category 1 having the lowest risk of mortality (log-rank $p < 0.001$), as shown in **Figure 2A.** The cumulative risk curves, illustrated in **Figure 2B,** demonstrated a continuously increasing cumulative risk of death over time for patients in Category 2, which was substantially higher than that observed in Category 3, while patients in Category 1 showed the slowest increase in cumulative mortality risk. In addition, similar findings were observed when plotting the 60-day Kaplan-Meier survival curves and cumulative risk curves, as shown in **Supplementary Figures 2A** and **2B,** respectively. Consistent results were also obtained for the 90-day Kaplan-Meier survival curves and cumulative risk curves, as shown in **Supplementary Figures 3A** and **3B**, respectively.

Sensitivity analysis

The research team constructed four Cox regression models to validate the association between RDW trajectories and patient outcomes (Table 3). In Model 1, which was unadjusted, patients in Category 2 had a significantly higher risk of 30-day mortality compared to those in Category 1 (all $p < 0.05$), with RDW being the most significant predictor [hazard ratio (HR) = 2.103, 95% confidence interval (CI): 1.954–2.263, $p < 0.001$]. Patients in Category 3 also showed a significantly elevated mortality risk [HR = 1.683, 95% CI: 1.406–2.013, $p < 0.001$]. In Model 2, after adjusting for age and gender, patients in Category 2 remained at significantly increased risk of 30-day mortality relative to Category 1 [HR = 2.154, 95% CI: 2.001–2.318, $p < 0.001$], while patients in Category 3 continued to show elevated risk [HR = 1.762, 95% CI: 1.473– 2.108, $p < 0.001$]. Model 3 further adjusted for comorbidities, including chronic pulmonary disease, congestive heart failure, mild liver disease, diabetes, and renal disease. After adjustment, the association remained significant for both Category 2 [HR = 1.913, 95% CI: 1.772–2.064, $p < 0.001$] and Category 3 [HR = 1.567, 95% CI: 1.308– 2.064, $p < 0.001$]. Finally, Model 4 included additional adjustments for disease severity using SOFA and SAPS II scores. Even after full adjustment, RDW trajectories remained significantly associated with 30-day mortality for both Category 2 [HR = 1.756, 95% CI: 1.626–1.896, $p < 0.001$] and Category 3 [HR = 1.370, 95% CI: 1.143–1.643, $p = 0.001$] compared to Category 1. These findings are consistent with the trends observed in the Kaplan-Meier survival analysis. Similarly, four multivariable Cox regression models were constructed to assess the association between RDW trajectories and 60- day and 90-day survival, and the results remained consistent, as presented in **Table 2.**

Model Performance and Explanation for Classifier to Identify Class 2 Patients

Based on the XGBoost algorithm, the classifier was trained by developing and validating a cohort combination dataset to recognize data labeled as “Class 2: Fast Growth”.The final model showed strong discriminative performance with an AUROC of 0.7821 for the training set and 0.7963 for the training set **(Figure 3A)**. Feature importance evaluation using the SHAP algorithm indicated that hemoglobin, total bilirubin, red blood cell count, prothrombin time (PT), and mild liver disease were the most influential predictors for identifying Class 2 sepsis patients in the XGBoost classifier **(Figure 3B).**

External validation

To validate our grouping method, we applied the same procedure to 627 patients with sepsis from the First Affiliated Hospital of

AnHui Medical University department of Critical Care medicine Data Mart (AHCCDM) . The patient selection flowchart is shown in **Supplementary Figure 1B.** The optimal number of trajectories was determined through trajectory modeling based on parametric criteria including the Bayesian Information Criterion (BIC), Akaike Information Criterion (AIC), entropy values, and patient proportions across subgroups **(Supplementary Table 2).** The three- category model (LCTM-3) was ultimately selected as the final model. In the validation cohort, **Supplementary Table 3** summarizes baseline characteristics and outlines outcomes for subgroups of the RDW trajectory. RDW trajectories consistent with the derived cohort were obtained in the validation cohort, also categorized into three groups. Patients across the three groups exhibited similar trends in mortality rates. Category 1 (“Low Stability,” 55.98%), Category 2 (“Rapid Increase,” 29.82%), and Category 3 (“ High Stable,” 14.19%), as depicted in Supplementary Figure 4. Category 2 demonstrated the poorest 30-day survival rate, followed by Category 3, while Category 1 exhibited the highest survival rate (log-rank P<0.001), as shown in **Supplementary Figure 5.** To further evaluate the prognostic significance of RDW trajectories in patients with sepsis from the validation cohort, a Cox proportional hazards model was constructed using a stepwise approach to adjust for potential confounders **(Supplementary Table 4).** In the unadjusted model (Model 1), patients in Category 2 exhibited a significantly higher 30-day mortality risk compared to those in Category 1 (HR = 7.284, 95% CI: 5.086–10.431, p<0.001). This association remained significant after sequential adjustment for age and sex (Model 2), comorbidities (hypertension, diabetes, coronary heart disease, kidney disease, malignancy, and cerebrovascular disease) (Model 3), and further adjustment for disease severity indicators (SOFA score and APACHE II score) (Model 4) (HR=5.998, 95% CI: 4.081–8.816, p < 0.001).Conversely, patients in Category 3 showed no statistically significant difference in 30-day survival compared to Category 1 across all models (p > 0.05).

RCS curve

Lastly, RCS was employed to further explore the average RDW values over the first five days associated with lower mortality **risk (Figure 4)**. RDW values exhibited a nonlinear relationship with mortality (P<0.001). In the MIMIC-IV database, the association between RDW and mortality in patients with sepsis exhibited a J-shaped curve: 30-day, 60-day, and 90-day mortality trends are shown in **Figures 4A, 4B, and 4C,** respectively, with higher mortality risk observed when RDW exceeded 13%. In the AHCCDM database, the relationship between RDW values and 30-day mortality in sepsis patients showed a nonlinear pattern: mortality risk increased when RDW exceeded 12%, but did not increase further when RDW exceeded 20%**(Figure 4D). Discussion** In this cohort study, In this cohort study, latent class trajectory modeling (LCTM) was utilized to analyze the 5-day RDW trajectories among patients with sepsis, resulting in the identification of three distinct trajectory classes. We identified and externally validated three distinct RDW trends. Compared with patients exhibiting a stable, low- level RDW trajectory (Class 1: Low Stable), those with rapidly increasing RDW (Class 2: Rapidly Increasing) and persistently elevated RDW (Class 3: Stable Elevated) trajectories demonstrated significantly poorer prognoses. Notably, the Class 2 trajectory, characterized by rapidly rising RDW levels, was most strongly associated with adverse clinical outcomes, including higher ICU and hospital mortality rates and prolonged ICU stays. Furthermore, while the incidence of acute kidney injury (AKI) was highest in Class 3, patients in Class 2 had the highest utilization rate of continuous renal replacement therapy (CRRT). These trajectories were also reproducible within the First Affiliated Hospital of AnHui Medical University department of Critical Care medicine Data Mart (AHCCDM) used in this study. The identification of these distinct RDW trajectories underscores the dynamic nature of this biomarker and suggests its potential utility in guiding clinical decision-making and patient management in ICU settings. RDW, as a routine laboratory parameter, is widely available and easily accessible in ICU settings, and existing evidence suggests that RDW serves as a reliable predictor of in-hospital mortality[14,17-20]. The relationship between RDW and clinical outcomes can be attributed to the underlying pathophysiological mechanisms of sepsis and critical illness. RDW measures the variability in red blood cell size [21], which may reflect inflammation, oxidative stress, and microvascular dysfunction. Sepsis is characterized by systemic inflammation, which affects red blood cell production and morphology, leading to changes in RDW[22, 23]. Consequently, RDW trajectories may reflect both the severity of illness upon ICU admission and subsequent disease progression dynamics. Time-dependent ROC analyses have also demonstrated good predictive accuracy of RDW levels for sepsis-related mortality[24, 25]. Although previous studies have reported using serial RDW measurements [26, 27], longitudinal analyses examining RDW trajectories have not been adequately explored. Since RDW is dynamic and fluctuates over time, measuring RDW at multiple time points can more accurately reflect its prognostic significance compared to a single baseline measurement. In a previous study evaluating the prognosis of 203 patients with sepsis, RDW values were measured at admission and again at 24-hour, 48-hour, 72- hour, and 7-day intervals, demonstrating a positive correlation between elevated RDW and ICU mortality[26]. However, simply using RDW values at several

discrete time points to assess RDW levels overlooks the longitudinal trends of RDW during the follow-up period. This approach does not account for temporal variations, lacks stratification of RDW trajectories, and fails to compare dynamic changes across different patient subgroups. In a study conducted in China investigating the association between dynamic RDW changes and the development of disseminated intravascular coagulation (DIC) in sepsis patients[28], all RDW measurements obtained during hospitalization were used to calculate both the standard deviation of RDW (RDW-SD) and the rate of RDW increase. The results demonstrated that when the RDW increase rate reached or exceeded 6%, there was a continuous rise in both DIC incidence and mortality. However, this study only summarized RDW using descriptive statistics such as mean, maximum, and minimum values, without modeling or visualizing the longitudinal trajectories of RDW. As a result, it could not fully capture the complex and dynamic nature of RDW fluctuations in sepsis patients. Previous studies [28-31]have focused on static measurements of the RDW, which may not accurately reflect the dynamic pathophysiologic changes that occur during the development of sepsis. Our present study highlights the prognostic significance of RDW trajectory patterns in the management of sepsis, highlighting the need for 366

continuous monitoring and individualized therapeutic strategies based on dynamic changes in RDW rather than relying solely on static baseline values. In this study, stratification of RDW by exploring the erythrocyte distribution width (RDW) trajectories of sepsis patients with different clinical characteristics and prognosis under different RDW trajectories has provided new insights into the heterogeneity of sepsis. The identification of different RDW trajectories represents a significant advance in the characterization of sepsis subtypes and fills an important gap in our current understanding. Limitations: This retrospective study has inherent limitations that make it difficult to establish a causal relationship between RDW trajectories and clinical outcomes in patients with sepsis. Although the MIMIC-IV and AHCCDM databases provide comprehensive clinical information sources, reliance on electronic health records may introduce potential biases related to data accuracy, completeness, and missing information. Notably, the AHCCDM database cannot directly determine 30-day mortality, requiring estimation based on discharge summaries. In this study, successful discharge was defined as survival, while discharge for other reasons and automatic discharge due to treatment abandonment were classified as death. This approach may influence outcomes. Furthermore, unmeasured or residual confounding variables not fully accounted for in the analysis may have affected the observed association between RDW trajectories and mortality. Prospective studies are needed to validate these findings and further investigate the underlying biological mechanisms driving the observed correlations in this study.

Conclusion

In critically ill patients with sepsis, longitudinal monitoring of RDW may serve as a simple and readily available biomarker to facilitate early risk stratification and individualized management. Dynamic RDW trajectories offer more informative prognostic value compared to baseline measurements. Prospective studies are warranted to validate these findings and further elucidate the underlying mechanisms driving RDW alterations in sepsis.

Declarations

Ethics approval and consent to participate

The MIMIC-IV database is publicly available, and researchers who agree to the data use agreement and have completed "protecting human subjects training" can request access. The MIMIC database was approved by the institutional review boards of the Beth Israel Deaconess Medical Center (2001-P-001699/14) and the Massachusetts Institute of Technology (No.0403000206), which waived the requirement for individual patient consent because the datasets contained deidentified information. The external validation cohort was derived from the Data Mart of the Department of Critical Care Medicine at the First Affiliated Hospital of Anhui Medical University (AHCCDM, Hefei, China), which includes clinical data from patients admitted to the ICU between January 2019 and June 2025. The study protocol was reviewed and approved by the Ethics Committee of the First Affiliated Hospital of Anhui Medical University (Approval No.Ethics Review: Fast Track PJ2024-02-24).

Consent for publication

Not applicable.

Data availability

The datasets generated and/or analyzed during the current study are available in the MIMIC-IV 3.1 database (https://physionet.

org/ content/ mimic iv/3.1/). This database can be used after obtaining the official permission of the database. Author (Cheng Zhang) obtained database access credentials (ID 47400446) and was responsible for data extraction. The data from this study can be obtained by contacting the author(Cheng Zhang, e-mail: ahmuzc@sina.cn). Sepsis patients were obtained from the First Affiliated Hospital of AnHui Medical University department of Critical Care medicine Data Mart (AHCCDM).For further information, please contact the author LiangWen Cui (e-mail: cuiliangwen1991@fy.ahmu.edu.cn).

Competing interests

The authors have declared no conflict of interest exists.

Funding

This work supported by National Natural Science Foundation of China (Grant NO. 82370605), Special Funding for the Institute of Healthy People Data and Population Medicine, Greater Health Research Institute (Grant NO. JKS2023002), University Natural Science Research Project of Anhui Province (Grant NO. 2023AH053300), Anhui Province Clinical Medical Research Translational Special Project (Grant NO. 202304295107020046).Anhui Province Clinical Medical Research and Transformation Special Project (Grant NO. 202527C10020045).

Author contributions

CLW, LML,ZYT and ZC analyzed the data. CLW, LML, ZYT, LN, LJ and SM interpreted the data. SY,SM and PXC drafted the work. All authors conceived, designed and revised the work. All authors read and approved the final manuscript.

Acknowledgements

Not applicable.

Competing interests

The authors declare that they have no competing interests.

References

1. Fleischmann C SA, Adhikari NK, et al: Assessment of Global Incidence and Mortality of Hospital-treated Sepsis. Current Estimates and Limitations. Am J Respir Crit Care Med 2016, 193(3):259-272.

2. Hotchkiss RS KI: The pathophysiology and treatment of sepsis. N Engl J Med 2003, 348(2):138-150.

3. Cecconi M, Evans L, Levy M, Rhodes A: Sepsis and septic shock. The Lancet 2018, 392(10141):75-87.

4. Salvagno GL S-GF, Picanza A, Lippi G: Red blood cell distribution width: A simple parameter with multiple clinical applications. Crit Rev Clin Lab Sci 2015, 52(2):86-105.

5. Braun E, Domany E, Kenig Y, Mazor Y, Makhoul BF, Azzam ZS: Elevated red cell distribution width predicts poor outcome in young patients with community acquired pneumonia. Critical Care 2011, 15(4):R194.

6. Zorlu A, Bektasoglu G, Kukul Guven FM, Dogan OT, Gucuk E, Refiker Ege M, Altay H, Cınar Z, Tandogan I, Yilmaz MB: Usefulness of Admission Red Cell Distribution Width as a Predictor of Early Mortality in Patients With Acute Pulmonary Embolism. The American Journal of Cardiology 2012, 109(1):128- 134.

7. Dabbah S HH, Markiewicz W,et al: Relation between red cell distribution width and clinical outcomes after acute myocardial infarction. Am Cardiol 2010, 105(3).

8. Sadaka F, O’ Brien J, Prakash S: Red Cell Distribution Width and Outcome in Patients With Septic Shock. Journal of Intensive Care Medicine 2012, 28(5):307-313.

9. Wang A-Y, Ma H-P, Kao W-F, Tsai S-H, Chang C-K: Red blood cell distribution width is associated with mortality in elderly patients

with sepsis. The American Journal of Emergency Medicine 2018, 36(6):949-953.

10. Lippi G TG, Montagnana M, Salvagno GL, Zoppini G, Guidi GC: Relation between red blood cell distribution width and inflammatory biomarkers in a large cohort of unselected outpatients. Arch Pathol Lab Med 2009, 133(4):628-632.

11. Friedman JS, Lopez MF, Fleming MD, Rivera A, Martin FM, Welsh ML, Boyd A, Doctrow SR, Burakoff SJ: SOD2-deficiency anemia: protein oxidation and altered protein expression reveal targets of damage, stress response, and antioxidant responsiveness. Blood 2004, 104(8):2565-2573.

12. Ghali JK: Anemia and heart failure. Current Opinion in Cardiology 2009, 24(2):172-178.

13. Weiss G GL: Anemia of chronic disease. N Engl J Med 2005, 352(10):1011- 1023.

14. Bazick HS, Chang D, Mahadevappa K, Gibbons FK, Christopher KB: Red cell distribution width and all-cause mortality in critically ill patients*. Critical Care Medicine 2011, 39(8):1913-1921.

15. Nguena Nguefack HL, Pagé MG, Katz J, Choinière M, Vanasse A, Dorais M, Samb OM, Lacasse A: Trajectory Modelling Techniques Useful to Epidemiological Research: A Comparative Narrative Review of Approaches. Clinical Epidemiology 2020, 12:1205-1222.

16. Mirza SS, Wolters FJ, Swanson SA, Koudstaal PJ, Hofman A, Tiemeier H, Ikram MA: 10-year trajectories of depressive symptoms and risk of dementia: a population-based study. The Lancet Psychiatry 2016, 3(7):628-635.

17. van Kimmenade RRJ, Mohammed AA, Uthamalingam S, van der Meer P, Felker GM, Januzzi JL: Red blood cell distribution width and 1-year mortality in acute heart failure. European Journal of Heart Failure 2010, 12(2):129-136.

18. Al-Najjar Y, Goode KM, Zhang J, Cleland JGF, Clark AL: Red cell distribution width: an inexpensive and powerful prognostic marker in heart failure. European Journal of Heart Failure 2009, 11(12):1155-1162.

19. Hao M, Jiang S, Tang J, Li X, Wang S, Li Y, Wu J, Hu Z, Zhang H: Ratio of Red Blood Cell Distribution Width to Albumin Level and Risk of Mortality. JAMA Network Open 2024, 7(5):e2413213.

20. Lam AP, Gundabolu K, Sridharan A, Jain R, Msaouel P, Chrysofakis G, Yu Y, Friedman E, Price E, Schrier S et al: Multiplicative interaction between mean corpuscular volume and red cell distribution width in predicting mortality of elderly patients with and without anemia. American Journal of Hematology 2013, 88(11):E245-E249.

21. Wang J, He L, Jin Z, Lu G, Yu S, Hu L, Fang M, Jin X: Immune Dysfunction- Associated Elevated RDW, APACHE-II, and SOFA Scores Were a Possible Cause of 28-Day Mortality in Sepsis Patients. Infection and Drug Resistance 2024, Volume 17:1199-1213.

22. Lan W, Liu E, Sun D, Li W, Zhu J, Zhou J, Jin M, Jiang W: Red cell distribution in critically ill patients with chronic obstructive pulmonary disease. Pulmonology 2025, 30(1):34-42.

23. Kim CH PJ, Kim EJ, et al: An increase in red blood cell distribution width from baseline predicts mortality in patients with severe sepsis or septic shock. Crit Care 2013, 17(6):R282.

24. Zhang H-B, Chen J, Lan Q-F, Ma X-J, Zhang S-Y: Diagnostic values of red cell distribution width, platelet distribution width and neutrophil-lymphocyte count ratio for sepsis. Experimental and Therapeutic Medicine 2016, 12(4):2215-2219.

25. Song K, Guo C, Zeng Z, Li C, Ding N: Factors associated with in-hospital mortality in adult sepsis with Escherichia coli infection. BMC Infectious Diseases 2022, 22(1):197.

26. Moreno-Torres V, Royuela A, Múñez-Rubio E, Gutierrez-Rojas Á, Mills-Sánchez P, Ortega A, Tejado-Bravo S, García-Sanz J, Muñoz-Serrano A, Calderón-Parra J et al: Red blood cell distribution width as prognostic factor in sepsis: A new use for a classical parameter. Journal of Critical Care 2022, 71:154069.

27. Fan YW LD, Chen JM, Li WJ, Gao CJ: Fluctuation in red cell distribution width predicts disseminated intravascular coagulation morbidity and mortality in sepsis: a retrospective single-center study. Minerva Anestesiol 2021, 87(1):52- 64.

28. Zhang L, Huang T, Xu F, Li S, Zheng S, Lyu J, Yin H: Prediction of prognosis in elderly patients with sepsis based on machine learning (random survival forest). BMC Emergency Medicine 2022, 22(1):26.

29. Niu T, Wang Y, Lu L, Li J, Cheng T, Dai Y: The value of preoperative RDW for post-pancreatectomy haemorrhage and surgical prognosis in patients with pancreatic cancer: a retrospective study. BMC Cancer 2025, 25(1):437.

30. Kc S, Kc R, Yadav BK, Basnet B, Basnet A: The role of TLC, RDW, and ESR in predicting short-term prognosis among admitted patients with acute ischemic stroke: Insights from a cross-sectional study. Health Science Reports 2024, 7(6):e2168.

31. Feng J HY, Huang L, et al: Association between RDW-SD and prognosis across glycemic status in patients with dilated cardiomyopathy. BMJ Open Diabetes Res Care 2024, 12(6):e004478.

Table 1. Baseline characteristics and outcomes between subgroups of the RDW trajectory model

Variables	Total (n = 20485)	1 (n = 15595)	2 (n = 4285)	3 (n = 605)	*P*
Age(years)	66.36 ± 16.01	66.57 ± 16.13	65.84 ± 15.55	64.50 ± 15.95	<0.001
Gender, n(%)					<0.001
Female	8659 (42.27)	6389 (40.97)	1980 (46.21)	290 (47.93)	
Male	11826 (57.73)	9206 (59.03)	2305 (53.79)	315 (52.07)	
Complications					
Chronic Pulmonary Disease, n(%)	5460 (26.65)	4116 (26.39)	1203 (28.07)	141 (23.31)	0.015

Variables	Total (n = 20485)	1 (n = 15595)	2 (n = 4285)	3 (n = 605)	*P*
Myocardial Infarct, n(%)	3698 (18.05)	2857 (18.32)	739 (17.25)	102 (16.86)	0.200
Congestive Heart Failure, n(%)	3698 (18.05)	2857 (18.32)	739 (17.25)	102 (16.86)	<0.001
Mild Liver Disease, n(%)	3218 (15.71)	1705 (10.93)	1307 (30.50)	206 (34.05)	<0.001
Diabetes, n(%)	6522 (31.84)	4921 (31.55)	1453 (33.91)	148 (24.46)	<0.001
Renal Disease, n(%)	4893 (23.89)	3365 (21.58)	1382 (32.25)	146 (24.13)	<0.001
Vital signs					
Temperature(°C)	36.72 (36.39, 37.11)	36.78 (36.39,37.17)	36.72 (36.39,37.06)	36.67 (36.33,37.00)	<0.001
Respiratory rate (per minute)	19.00 (16.00, 23.00)	19.00 (15.00,23.00)	20.00 (16.00,24.00)	19.00 (16.00,23.00)	<0.001
Heart Rate(per minute)	88.00 (77.00, 104.00)	88.00 (76.00,103.00)	99.00 (79.00,108.00)	90.00 (79.00,104.00)	<0.001
Mean Arterial Pressure (mmHg)	83.67 (73.00, 96.33)	84.33 (73.33,97.33)	64.00 (71.67,94.00)	79.00 (70.17,91.00)	<0.001
Laboratory testing					
PH	7.37 (7.31, 7.42)	7.37 (7.31,7.42)	7.36 (7.30,7.42)	7.37 (7.30,7.43)	0.002
PO2/FIO2(mmHg)	218.00 (118.00, 336.00)	223.33 (122.00,339.00)	195.00 (104.29,323.00)	220.50 (112.50,362.00)	<0.001
PCO2(mmHg)	41.00 (35.00, 47.00)	41.00 (36.00,48.00)	40.00 (34.00,47.00)	39.00 (34.00,46.00)	<0.001
Lactate(mmol/L)	1.80 (1.20, 2.80)	1.80 (1.20,2.70)	2.90 (1.30,3.10)	2.30 (1.50,3.40)	<0.001
White blood	11.80 (8.20, 16.40)	11.80	16.40 (7.30,17.00)	11.40	<0.001

Variables	Total (n = 20485)	1 (n = 15595)	2 (n = 4285)	3 (n = 605)	*P*
cell (K/uL)		(8.45,16.20)		(7.50,17.40)	
Lymphocytes(K/uL)	1.01 (0.59, 1.61)	1.04 (0.62,1.65)	0.87 (0.49,1.43)	1.04 (0.56,1.72)	<0.001
Red blood cell (K/uL)	3.45 (2.93, 4.02)	3.56 (3.08,4.11)	3.11 (2.63,3.67)	2.65 (2.25,3.15)	<0.001
Hemoglobin (g/L)	10.30 (8.80, 12.00)	10.80 (9.30,12.30)	8.90 (7.80,10.30)	8.50 (7.50,9.80)	<0.001
Platelet(K/uL)	182.00 (126.00, 253.00)	187.00 (134.00,254.00)	102.00 (99.00,257.00)	138.00 (84.00,205.00)	<0.001
ALT(U/L)	29.00 (17.00, 65.00)	29.00 (17.00,64.00)	96.00 (17.00,70.00)	32.00 (18.00,66.00)	0.051
AST(U/L)	43.00 (25.00, 98.00)	41.00 (24.00,90.00)	82.00 (27.00,125.00)	56.00 (30.00,139.00)	<0.001
Total bilirubin(mg/dL)	0.70 (0.40, 1.40)	0.60 (0.40,1.20)	1.60 (0.50,2.90)	1.10 (0.60,3.70)	<0.001
Bun (mg/dL)	21.00 (14.00, 36.00)	20.00 (14.00,32.00)	31.00 (17.00,48.00)	25.00 (15.00,43.00)	<0.001
Creatinine (mg/dL)	1.10 (0.80, 1.70)	1.00 (0.70,1.50)	1.60 (0.90,2.60)	1.20 (0.80,1.90)	<0.001
Calcium (mg/dL)	8.20 (7.70, 8.70)	8.20 (7.70,8.70)	8.00 (7.60,8.70)	8.10 (7.50,8.70)	<0.001
Chloride (mmol/L)	104.00 (100.00, 109.00)	105.00 (101.00,109.00)	103.00 (98.00,108.00)	105.00 (100.00,109.0 0)	<0.001
Potassium (mmol/L)	4.10 (3.70, 4.60)	4.10 (3.70,4.60)	4.20 (3.70,4.70)	4.20 (3.70,4.70)	<0.001
Sodium (mmol/L)	139.00 (135.00, 141.00)	139.00 (136.00,141.00)	138.00 (134.00,141.00)	138.00 (135.00,141.0 0)	<0.001

Variables	Total (n = 20485)	1 (n = 15595)	2 (n = 4285)	3 (n = 605)	*P*
Glucose(mg/dL)	135.00 (110.00, 176.00)	137.00 (111.00,177.00)	130.00 (104.00,171.00)	137.00 (110.00,177.00)	<0.001
PT(s)	14.60 (12.80, 17.40)	14.20 (12.60,16.60)	16.30 (13.90,21.00)	16.20 (13.40,20.80)	<0.001
APTT(s)	31.10 (27.30, 38.20)	30.60 (27.00,36.70)	33.50 (28.70,42.50)	33.40 (28.40,43.90)	<0.001
Scoring system					
SOFA	5.00 (3.00, 8.00)	5.00 (3.00,7.00)	7.00 (5.00,10.00)	6.00 (4.00,9.00)	<0.001
SAPSII	39.00 (31.00, 49.00)	38.00 (31.00,47.00)	46.00 (34.00,52.00)	43.00 (35.00,52.00)	<0.001
Main outcomes					
Hospital Outcome 30d, n(%)	3258 (15.90)	2032 (13.03)	1099 (25.65)	127 (20.99)	<0.001
Hospital Outcome 60d, n(%)	4288 (20.93)	2649 (16.99)	1471 (34.33)	168 (27.77)	<0.001
Hospital Outcome 90d, n(%)	4850 (23.68)	3026 (19.40)	1645 (38.39)	179 (29.59)	<0.001
Secondary outcomes					
Is Ventilator, n(%)	18404 (89.84)	14113 (90.50)	3742 (87.33)	549 (90.74)	<0.001
AKI n(%)	17396 (84.92)	13105 (84.03)	3744 (87.37)	547 (90.41)	<0.001
CRRT, n(%)	1594 (7.78)	885 (5.67)	627 (14.63)	82 (13.55)	<0.001

Table 2. Relationship between RDW and survival in patients with sepsis

Variables	Model 1 [HR (95% CI), p-value]	Model 2 [HR (95% CI), p-value]	Model 3 [HR (95% CI), p-value]	Model 4[HR (95% CI), p-value]
30-day survival				
Class 1	Reference	Reference	Reference	Reference
Class 2	2.103(1.954,2.263),<0.001	2.154(2.001,2.318), <0.001	1.913(1.772,2.064),<0.001	1.756(1.626,1.896),<0.001
Class 3	1.683(1.406,2.013),<0.001	1.762(1.473,2.108),<0.001	1.567(1.308,2.064),<0.001	1.370(1.143,1.643),0.001
60-day survival				
Class 1	Reference	Reference	Reference	Reference
Class 2	2.227(2.089,2.374),<0.001	2.286(2.145,2.437),<0.001	2.038(1.907,2.177),<0.001	1.883(1.762,2.013),<0.001
Class 3	1.739(1.488,2.032),<0.001	1.819(1.557,2.126),<0.001	1.634(1.397,1.912),<0.001	1.441(1.231,1.687),<0.001
90-day survival				
Class 1	Reference	Reference	Reference	Reference
Class 2	2.219(2.089,2.356),<0.001	2.279(2.146,2.421),<0.001	2.044(1.920,2.175),<0.001	1.896(1.781,2.019),<0.001
Class 3	1.637(1.408,1.903),<0.001	1.709(1.470,1.998),<0.001	1.551(1.333,1.805),<0.001	1.376(1.182,1.602),<0.001

Model 1 was a non-adjusted model

Model 2 was adjusted for age, gender

Model 3 was adjusted for the same parameters as Model 2 with additional adjustments for comorbidities of chronic pulmonary disease、congestive heart failure、mild liver disease、diabetes and renal disease Model 4 was adjusted for the same parameters as Model 3 with additional adjustments for SOFA score and SAPSII

score

HR, hazard ratio; 95% CI, 95% confidence interval. The bold values indicate statistically significant values ($p < 0.05$)

Figure Legends

Figure 1. Latent class trajectory analysis of red blood cell distribution width (RDW) in patients with sepsis.

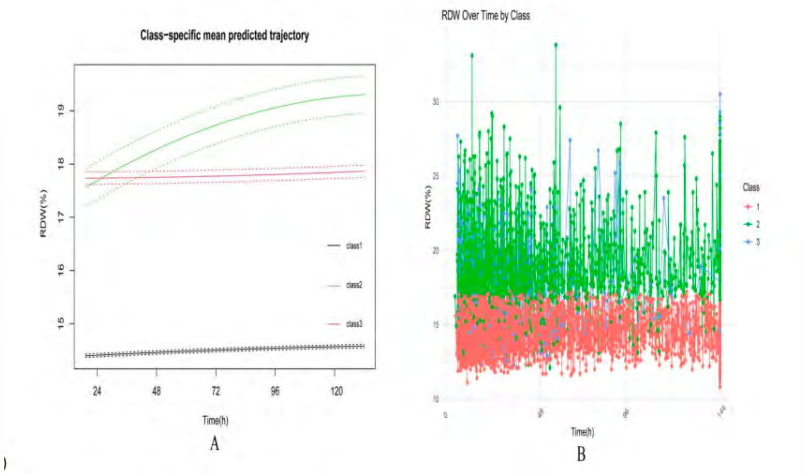


Figure 2. 30-day Kaplan-Meier survival curves(A) and cumulative risk curves (B)by RDW trajectory class in patients with sepsis.

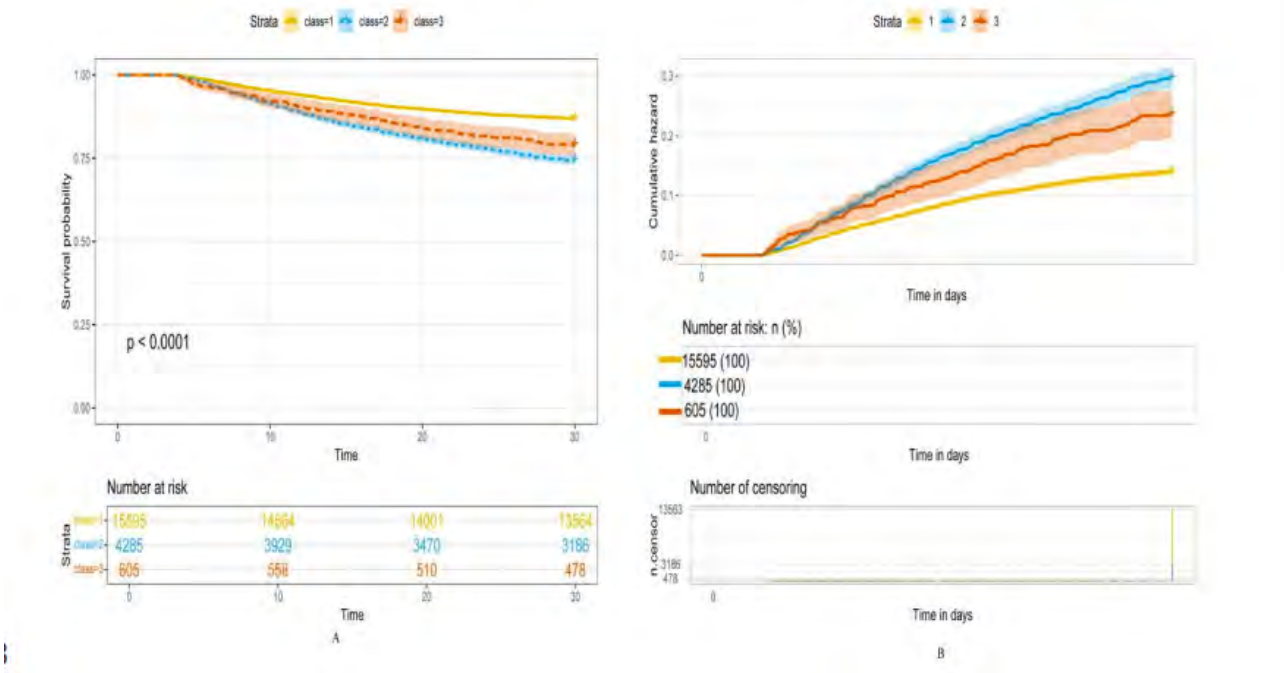


Figure 3. Performance and key features of the XGBoost model for recognizing Type 2 RDW trajectories(A: AUROC performance of the model in the training and validation sets; B: SHAP plot).

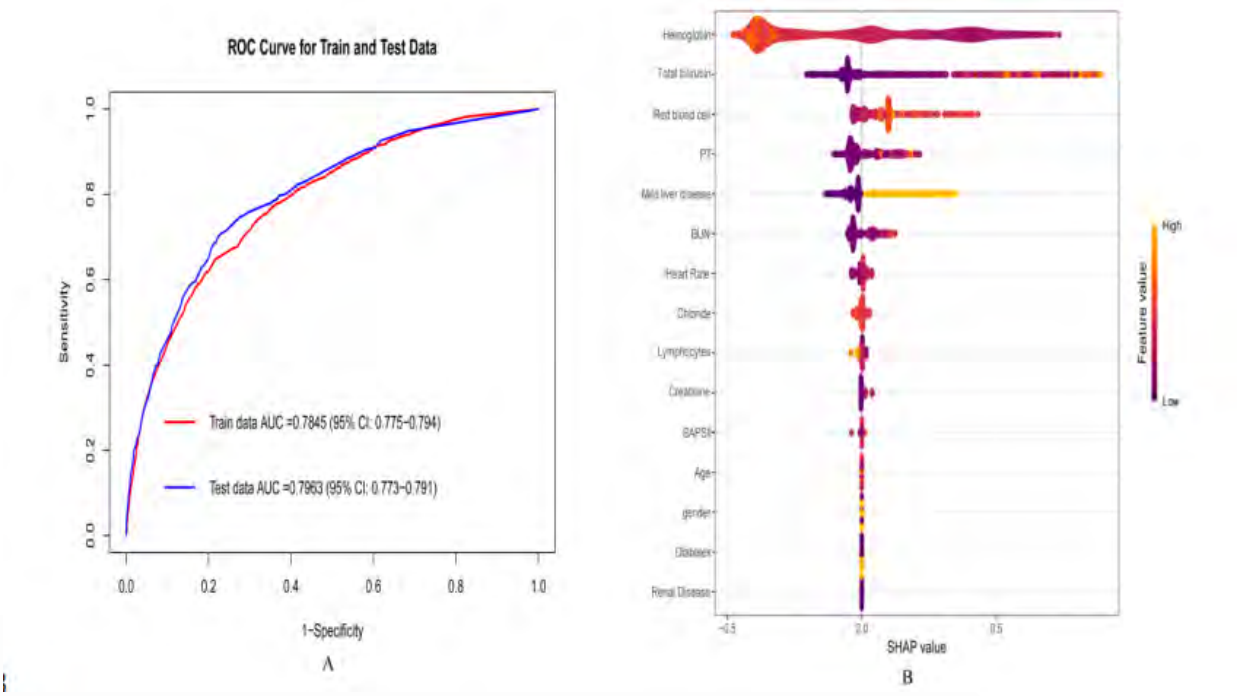
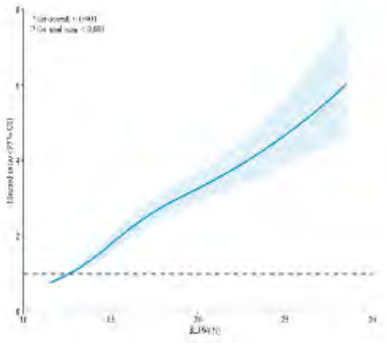
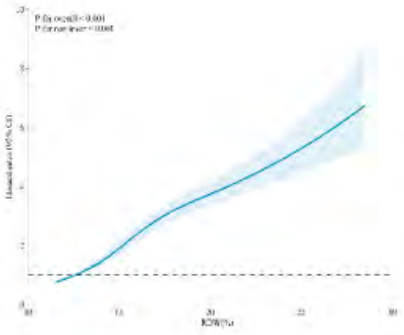


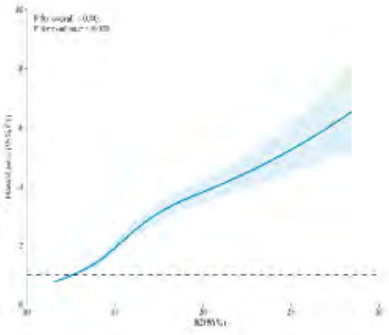
Figure 4. RCS curves showing the association between the mean RDW value in the first 5 days and the risk of 30-day (Figure 4A), 60-day (Figure 4B), and 90-day (Figure 4C) mortality in sepsis patients from the MIMIC IV database. RCS curve showing the association between the mean RDW value in the first 5 days and the risk of 30-day mortality (Figure 4D) in sepsis patients from the AHCCDM database.



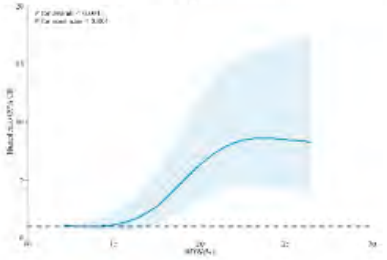
A



B



C



D

类别 :// 基础研究：涉及重症相关问题的基础研究

肺部共生狄氏副拟杆菌来源的 γ- 亚麻酸改善铜绿假单胞菌肺炎预后的机制研究

姓名：张莉，陶哲影，张博顺，徐静，柒晓玲，刘嘉琳

单位：上海交通大学医学院附属瑞金医院

探究肺部共生菌及其代谢产物在铜绿假单胞菌肺炎中的局部免疫调控作用，系统阐明“共生菌 - 代谢物 - 宿主免疫”的完整分子通路，并基于此机制探索具有临床转化价值的靶向治疗方案。

本研究遵循“临床发现问题—功能验证—机制解析—转化探索”的递进逻辑：①收集铜绿假单胞菌 VAP 患者下呼吸道分泌物，通过 16S rRNA 测序、PICRUSt2 功能预测及 GC-MS 代谢物定量，筛选并验证与患者预后相关的关键菌群和代谢物；②利用小鼠菌群清除、宿主 GLA 合成抑制及肺部菌群移植回补等实验，明确肺内 γ- 亚麻酸（GLA）的组织来源；③结合同源建模、分子对接及大肠杆菌异源过表达技术，鉴定狄氏副拟杆菌（P. distasonis）合成 GLA 的关键酶；④运用流式细胞术、氯膦酸盐脂质体清除、转录组测序和表面等离子体共振等技术，明确 GLA 作用的靶细胞及其分子靶点；⑤制备 DPPC-GLA 脂质体雾化系统，比较雾化吸入与口服给药的时效差异；⑥在金黄色葡萄球菌和肺炎克雷伯菌肺炎模型中验证 GLA 的广谱抗感染效能。

①临床发现，存活组患者下呼吸道 P. distasonis 检出率、菌群 GLA 合成潜能及局部 GLA 浓度均显著高于死亡组，GLA 水平与 SOFA/APACHE II 评分呈负相关。②肺内 GLA 主要来源于肺部共生菌的原位合成，而非肝脏供给。③鉴定出 P. distasonis 中 fabF 基因编码的 FabF 蛋白具有 Δ6- 去饱和酶活性，是催化 GLA 合成的关键酶。④ GLA 作为天然配体直接结合并激活肺泡巨噬细胞内的 PPARγ，一方面促进巨噬细胞增殖以增加细胞数量，另一方面增强单个细胞的吞噬和胞内杀菌功能。⑤ DPPC-GLA-Liposome 雾化系统单次给药可在 24 小时内实现肺部 GLA 快速蓄积，起效速度和便捷性均显著优于需连续 7 天预处理的口服给药。⑥ GLA 对金黄色葡萄球菌和肺炎克雷伯菌肺炎同样具有显著的保护效果，表明该免疫调节策略具有广谱抗感染潜力。

肺部共生 P. distasonis 通过其 FabF 蛋白在感染局部原位合成 GLA，GLA 通过激活肺泡巨噬细胞 PPARγ 信号轴，协同增强巨噬细胞的数量和功能，从而改善铜绿假单胞菌肺炎预后。该机制驱动的免疫防御策略对多种呼吸道病原体均有效，基于此开发的雾化吸入 DPPC-GLA-Liposome，因其快速起效和靶向递送优势，为耐药菌肺炎的临床治疗提供了一种具有良好转化前景的新方案。

类别 :// 基础研究：涉及重症相关问题的基础研究

AARS1/HDAC2 失衡介导 IDH2 乳酸化驱动铁死亡在脓毒症相关肌肉萎缩中的作用机制

姓名：彭渝皓

单位：南华大学附属第二医院

（1） 明确脓毒症高乳酸微环境是驱动肌萎缩发生的始动因素；确证铁死亡是导致肌肉质量丢失的主导性死亡方式。

（2）明确 IDH2 K413 乳酸化修饰是介导高乳酸致肌萎缩的关键靶点；阐明该修饰通过抑制 IDH2 酶活并破坏氧化还原稳态（NADPH/GSH），驱动铁死亡发生的分子机制。

（3）阐明脓毒症高乳酸环境下，AARS1 线粒体异常积累（Writer 增强）与 HDAC2 表达缺失（Eraser 减弱）协同驱动 IDH2 异常修饰的“双重酶系失衡”机制。

（4）验证靶向“AARS1-IDH2”轴的 AAV 基因干预对脓毒症肌萎缩的治疗潜力；评估 IDH2 乳酸化水平作为 SAMA 早期诊断及预后判断生物标志物的临床价值。

方法：

(1) 选取 8-10 周龄 C57BL/6J 雄性小鼠，随机分为 Sham 组和 CLP 组，采用盲肠结扎穿孔术（CLP）构建脓毒症肌萎缩模型。术后每日监测小鼠体重变化，利用前肢抓力测定仪检测肌肉功能，并记录术后 0-96 小时生存率，旨在评估脓毒症导致的机体分解代谢状态。采集胫骨前肌（TA），采用 H&E 染色及 WGA 荧光染色观察肌纤维形态，利用 MyHC-F/S 免疫荧光分型技术统计不同类型肌纤维比例，旨在明确肌萎缩是否具有糖酵解纤维（Type II）特异性。利用 Western blot 检测肌肉组织中 E3 泛素连接酶（Atrogin-1, MuRF1）的表达，同时在术后 24 小时及 96 小时分别检测血清及肌肉内的乳酸浓度，分析高乳酸微环境与肌萎缩发生的相关性。

(2) 提取小鼠全肌肉蛋白，利用泛乳酸化抗体（Pan-Kla）进行 Western blot 检测，旨在分析脓毒症状态下肌肉蛋白质组的整体乳酸化修饰水平变化。制作肌肉组织超薄切片，利用透射电镜（TEM）观察线粒体膜密度增加、嵴断裂及外膜破裂等特征，旨在从超微结构层面捕捉铁死亡迹象。采用生化试剂盒检测肌肉组织中的 MDA、亚铁离子（Fe^{2+}）、GSH 及 GSH/GSSG 比值，利用 Western blot 检测 GPX4、SLC7A11、FTH1、ACSL4、TFRC 等核心标志物及 Caspase-3/p-MLKL，旨在综合确立脓毒症肌纤维的主导死亡方式。

(3) 在 C2C12 肌管模型中，利用 LPS 联合 LDH 抑制剂（草氨酸钠）或外源乳酸钠（Na-Lac）处理，旨在构建具有不同乳酸梯度的细胞模型。利用 Western blot 检测不同处理组细胞内乳酸水平与 Pan-Kla 丰度及 GPX4 表达的关系，旨在分析乳酸积累与乳酸化水平及抗氧化蛋白丢失的相关性。利用倒置荧光显微镜进行 C11-BODIPY（脂质 ROS）和 FerroOrange（亚铁离子）活细胞成像及 ATP 测定，评估干预乳酸代谢（阻断或加重）对肌细胞铁死亡敏感性及供能状态的直接影响。结合 MyHC 免疫荧光染色及萎缩基因（Atrogin-1, MuRF1）检测，验证阻断乳酸生成对 LPS 诱导肌管萎缩的挽救作用。

结果：

(1) 脓毒症肌萎缩伴随持续的高乳酸微环境与糖酵解纤维特异性损伤

为了明确脓毒症肌萎缩的代谢特征，我们构建了小鼠盲肠结扎穿孔（CLP）脓毒症模型。生存分析显示 CLP 组小鼠术后 96 小时死亡率约为 50%（图 1A）。存活小鼠表现出严重的分解代谢表型，前肢抓力显著下降，胫骨前肌（TA）湿重 / 体重比降低（图 1B-C）。H&E 染色及 WGA 荧光染色定量分析显示，CLP 组肌纤维横截面积（CSA）显著减小，且呈现向小直径偏移的趋势（图 1D-F）。此外，Western blot 结果证实，CLP 组小鼠肌肉中经典萎缩蛋白（Atrogin-1 和 MuRF1）的表达水平显著上调（图 1G）。进一步利用 MyHC-I/II 免疫荧光染色分析发现，CLP 组糖酵解型（Type II）肌纤维的比例显著减少（图 1H）。代谢检测结果显示，CLP 组小鼠血清及肌肉组织内的乳酸浓度在术后 24 小时显著升高（图 1I-J）。

(2) 铁死亡是脓毒症肌纤维的主导性死亡方式

为了探究细胞死亡的具体形式，我们利用透射电镜（TEM）观察发现，CLP 组线粒体呈现典型的铁死亡特征：体积皱缩、膜密度增加、嵴断裂消失（图 2A）。生化检测显示，肌肉组织中脂质过氧化产物 MDA 及亚铁离子（Fe2+）水平显著升高，而抗氧化剂 GSH 与 GSH/GSSH 比值降低（图 2B）。Western blot 结果证实，铁死亡核心护盾 GPX4 、FTH1 及 SLC7A11 蛋白水平显著下调，而促铁死亡蛋白 ACSL4 及 TFRC 上调（图 2C）。

(3) 细胞内乳酸累积直接驱动泛乳酸化修饰升高与线粒体铁死亡

为了确证高乳酸微环境对肌细胞的直接毒性作用，我们通过药理学手段正反向调控 C2C12 肌管内的乳酸水平。在 LPS 模拟脓毒症炎症背景下，我们分别给予 LDH 抑制剂草氨酸钠（Sodium Oxamate）以阻断内源性乳酸生成，或额外添加外源性乳酸钠（Na-Lac）以加剧乳酸负荷。Western blot 结果证实，泛乳酸化修饰（Pan-Kla）丰度与细胞内乳酸负荷水平呈正向协同关系，而抗氧化蛋白 GPX4 的表达则随之显著受抑（图 3A-B），提示乳酸累积导致了广泛的蛋白修饰改变及抗氧化能力的丧失。活细胞荧光成像结果进一步显示，外源添加乳酸钠显著加剧了 LPS 诱导的细胞内总 ROS（CM-H2DCFDA 指示）及亚铁离子（FeRhNOX-1 指示）的异常累积；相反，给予草氨酸钠阻断内源性乳酸生成后，上述铁死亡信号得到有效逆转（图 3C）。此外，WB 检测证实，高乳酸负荷会直接导致萎缩蛋白（MuRF1）表达上调（图 3D）。以上结果确证，细胞内乳酸累积是驱动铁死亡与肌管萎缩的始动因素。

(4) 蛋白质修饰组学锁定 IDH2 为高乳酸环境下的关键乳酸化靶点

为了揭示高乳酸致病的分子机理，我们提取了小鼠胫骨前肌进行定量乳酸化修饰组学分析。将差异蛋白与 FerrDb 铁死亡数据库交叉比对后，我们筛选出 7 个候选蛋白及其 12 个修饰位点，最终聚焦于变化最显著的线粒体关键代谢酶 IDH2（图 4A-B）。高分辨质谱（LC-MS/MS）确证了 IDH2 的乳酸化修饰肽段，且空间结构与序列分析显示，该修饰精确发生于跨物种高度保守的 K413 位点（图 4C-E）。体内 IP-WB 实验首先证实，脓毒症（CLP 组）显著上调了小鼠肌肉中 IDH2 的泛乳酸化（Pan-Kla）水平（图 4F）。更重要的是，单纯注射外源性乳酸（Na-lac 组）即可独立诱导该修饰的发生；而在脓毒症叠加乳酸负荷（CLP+Na-lac 组）时 IDH2 的乳酸化水平被进一步激化（图 4G）。

结论：脓毒症肌萎缩导致的高乳酸微环境通过诱导广泛的蛋白修饰重编程，特异性地触发线粒体铁死亡；IDH2 K413 位点的乳酸化修饰从分子结构层面抑制酶活性，导致 NADPH/GSH 代谢中断，进而引发线粒体抗氧化防御系统的崩溃；在脓毒症病理条件下，AARS1 的异常累积（Writer 增强）与 HDAC2 的表达缺失（Eraser 减弱），形成协同效应，共同打破 IDH2 的修饰稳态并驱动不可逆的氧化损伤。

ACSL1 靶向 PDK1-cGAS-STING 通路激活小胶质细胞介导脓毒症相关性脑病远期认知功能障碍的机制研究

姓名：黄佩贤

单位：广东省人民医院

1、论文摘要

论文题目：ACSL1 靶向 PDK1-cGAS-STING 通路激活小胶质细胞介导脓毒症相关性脑病

远期认知功能障碍的机制研究

背景：脓毒症相关性脑病（SAE）是脓毒症患者常见的严重并发症，发生率高达 70%，其导致的远期认知功能障碍严重影响患者生存质量，且缺乏有效治疗手段。小胶质细胞介导的神经炎症与突触异常修剪被认为是 SAE 认知功能障碍的核心病理基础，但急性炎症消退后小胶质细胞驱动远期认知障碍的分子机制尚不明确。

目的：本项目旨在阐明小胶质细胞 ACSL1 通过靶向结合 PDK1 激活 cGAS-STING 信号通路，诱导突触过度吞噬及 p-Tau 蛋白异常聚积，从而介导 SAE 远期认知功能障碍的分子机制，为 SAE 的临床防治提供新靶点。

方法：采用盲肠结扎穿孔术构建小鼠 SAE 模型，结合小胶质细胞特异性 Acsl1 条件性敲除小鼠、PLX5622 靶向消融、AAV 介导的体内功能拯救、免疫共沉淀、单细胞转录组测序、透射电镜、高尔基染色及全细胞膜片钳等多种技术手段，系统评估小胶质细胞 ACSL1-PDK1-cGAS-STING 信号轴在 SAE 远期突触损伤及认知功能障碍中的作用。

结果与结论：前期研究发现，SAE 小鼠在急性炎症消退后仍出现明显认知功能障碍，伴随小胶质细胞持续激活、突触过度吞噬、突触超微结构损伤及海马 CA3 区 p-Tau 异常聚积。动态转录组测序显示 ACSL1 在小胶质细胞中特异性持续高表达，其敲除可显著减轻突触损伤及 p-Tau 聚积并改善认知功能。机制上，ACSL1 与 PDK1 存在直接相互作用，并通过激活下游 cGAS-STING 通路介导小胶质细胞致病效应。本项目将系统阐明 ACSL1-PDK1-cGAS-STING 信号轴驱动 SAE 远期认知功能障碍的分子机制，为靶向小胶质细胞治疗 SAE 提供理论依据和潜在干预靶点。

2、研究内容

研究背景和现状

脓毒症相关性脑病是脓毒症患者最常见的严重并发症之一，临床发生率高达 70%，不仅显著增加急性期病死率，更导致幸存者出现长期认知与运动功能障碍，严重影响患者生存质量并带来沉重的社会经济负担。目前 SAE 远期认知障碍缺乏特效治疗手段，根本原因在于其发病机制尚未被完全阐明。现有研究表明，SAE 导致远期认知功能障碍的病理生理机制具有高度复杂性，涉及神经炎症、血脑屏障破坏、线粒体功能障碍、神经递质失衡及突触损伤等多因素交织作用。其中，小胶质细胞介导的神经炎症与突触过度修剪被认为是 SAE 认知功能障碍的核心病理基础。全身性炎症反应通过破坏血脑屏障驱动外周促炎介质进入中枢，激活小胶质细胞并形成神经炎症风暴介导神经损伤，这是脓毒症早期神经损伤的经典机制。然而，急性炎症消退后小胶质细胞是否持续激活、以及其如何驱动远期认知功能障碍的分子机制，目前尚不清楚。近年来，小胶质细胞功能研究为 SAE 机制解析提供了新见解，如海马小胶质细胞线粒体 TRPV1 通道通过诱导线粒体应激与糖代谢重编程介导神经毒性表型，cGAS-STING 通路被证实为小胶质细胞介导 SAE 神经炎症的关键调控节点。然而，上述研究主要聚焦于脓毒症急性期的小胶质细胞炎症反应，对小胶质细胞在慢性期持续激活的分子开关及其驱动远期认知障碍的机制尚缺乏系统研究。

研究目的

本项目旨在系统阐明小胶质细胞 ACSL1-PDK1-cGAS-STING 信号轴在 SAE 远期认知功能障碍中的作用与分子机制，具体目标包括：（1）明确小胶质细胞过度吞噬突触及诱导 p-Tau 聚积在 SAE 远期认知功能障碍中的核心作用；（2）揭示 ACSL1 作为小胶质细胞介导 SAE 突触损伤及 p-Tau 病理的关键分子；（3）阐明 ACSL1 与 PDK1 相互作用及其对下游信号通路的调控关系；（4）验证 PDK1-cGAS-STING 通路在小胶质细胞介导 SAE 突触损伤中的功能地位。

实验设计

本项目以盲肠结扎穿孔术构建小鼠 SAE 模型为核心动物模型，结合小胶质细胞特异性条件性基因敲除、药理学靶向消融、AAV 介导的体内功能拯救及通路干预等多元手段。研究设置 Sham 组、CLP 组、CLP+ 基因敲除 / 抑制剂组、CLP+ 过表达 / 激动剂组等多层次对照，分

别在 CLP 术后 60 天进行行为学、组织病理、突触超微结构、电生理及分子水平的多维度评估。

实验方法

（1）动物模型与认知行为评估： 采用 CLP 法构建 SAE 小鼠模型，术后 60 天通过 Morris 水迷宫和旷场实验评估空间学习记忆能力及自主活动能力。

（2）小胶质细胞靶向消融：利用 CSF1R 抑制剂 PLX5622 在 CLP 术后 14–28 天（急性炎症消退期）喂养小鼠，实现小胶质细胞可逆性消融，停药后观察其再生及对远期认知功能的影响。

（3）条件性基因敲除与过表达： 采用 CRISPR/Cas9 技术构建小胶质细胞特异性 Acsl1 条件性敲除小鼠，术后 14 天腹腔注射他莫昔芬诱导敲除。通过脑立体定位注射 AAV-CD68-Pdk1 过表达病毒实现小胶质细胞靶向功能拯救。

（4）单细胞转录组测序与动态转录组分析： 流式分选海马小胶质细胞进行 RNA-seq 及单细胞测序，筛选差异表达基因，结合拟时序分析追踪小胶质细胞从稳态向激活态转化的动态轨迹。

（5）分子互作验证： 在 HEK293T 细胞中共表达 ACSL1 与 PDK1，通过免疫共沉淀验证蛋白相互作用，构建截短突变体明确关键结合域。

（6）突触结构与功能评估： 免疫荧光染色检测 Iba1 与突触前膜蛋白 Synaptophysin 共定位以评估小胶质细胞突触吞噬；透射电镜观察突触超微结构；高尔基染色分析树突棘形态与密度；全细胞膜片钳记录海马 CA1 区锥体神经元长时程增强及兴奋性突触后电流。

（7）通路干预实验： 采用 cGAS-STING 抑制剂或激动剂脑定位注射，验证 PDK1-cGAS-STING 信号轴的上下游关系及功能效应。

结果及结论

前期研究结果

（1）小胶质细胞在急性炎症消退后持续激活并介导远期认知障碍。 CLP 术后海马炎症因子于术后 7 天达峰、14 天基本恢复基线，但 $Iba1^{+}$ 小胶质细胞数量在术后 60 天仍显著高于对照组，小鼠出现明显空间学习记忆障碍。术后 60 天检测显示，小胶质细胞对突触前膜蛋白的吞噬显著增加，突触前后膜共定位位点减少，透射电镜见突触间隙模糊、突触后致密物变薄，高尔基染色示树突棘密度及成熟型蘑菇状树突棘比例降低，伴随海马 CA3 区 p-Tau 显著异常聚积。PLX5622 靶向消融实验显示，急性炎症消退期短暂清除小胶质细胞可显著改善术后 60 天认知功能，证实小胶质细胞在炎症消退后仍持续驱动病理进程。

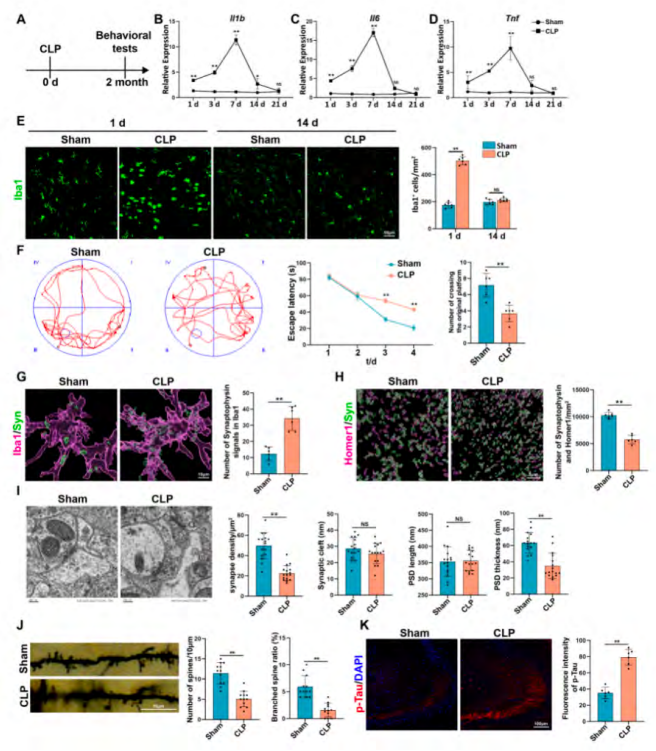
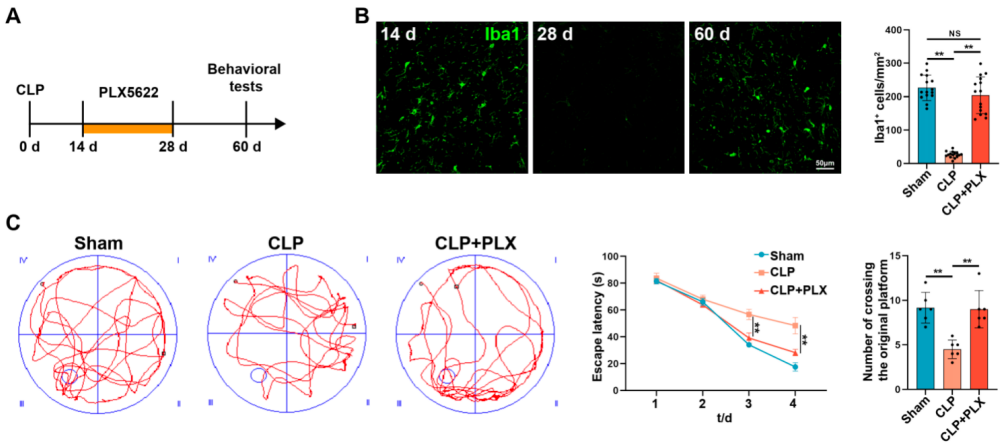


Fig. 1 脓毒症模型中小鼠出现远期神经行为学障碍。（A）CLP 模型的模式图。（B-D）RT-qPCR 检测海马中 Il1b、Il6 和 Tnf 的 mRNA 表达水平（n=6）。（E）荧光染色检测海马 CA1 区中小胶质细胞（Iba1+）的数量变化及其统计图（scale bar = 50 μm，n=6）。（F）水迷宫第六天训练轨迹代表图，水迷宫训练期 1-4 d 的逃避潜伏期以及穿越平台统计图（n=6）。（G）小胶质细胞（Iba1，粉色）及突触前膜蛋白（Syn，绿色）共定位染色，使用 Imaris 三维重建（scale bar = 10 μm，n=6）。（H）突触前膜蛋白（Syn）和突触后面蛋白（Homer1）的共定位染色，使用 Imaris 三维重建（scale bar = 5 μm，n=6）。（I）通过电镜检测海马组织中的突触代表图，突触的数量、突触间隙、突触后膜的长度以及突触后膜的厚度统计图（scale bar = 200nm，n=12）。（J）通过高尔基染色，树突棘的代表图，统计图数据为树突棘的数量以及分枝状树突棘的比例（scale bar = 10nm，n=12）。（K）海马 CA3 区的 p-Tau 蛋白的荧光染色及 p-Tau 蛋白荧光强度统计图（scale bar = 100 μm，n=6）。

(NS 代表 p>0.05，*p<0.05，**p<0.01)



（Fig. 2 小胶质细胞靶向消融减轻脓毒症脑病的认知功能障碍。（A）在脓毒症脑病中靶向消融小胶质细胞的模式图。（B-C）荧光染色检测海马 CA1 区中小胶质细胞（Iba1+）在 14 d、28 d 和 60 d 的数量变化（scale bar = 50 μm，n=6）。（C）第六天测试水迷宫的轨迹图代表图、训练期 1-4d 的逃避潜伏期及其穿越平台次数的统计（n=6）。(NS 代表 p>0.05，*p<0.05，**p<0.01)

（2）ACSL1 是小胶质细胞持续激活的关键分子。 动态转录组测序（术后 7、14、30、60 天）鉴定出 69 个持续高表达基因，富集于脂肪酸氧化及免疫激活通路，其中 Acsl1 变化最为显著。RT-qPCR 及免疫荧光双标验证其在小胶质细胞中特异性持续高表达。小胶质细胞特异性 Acsl1 敲除可显著减轻突触吞噬、改善突触超微结构、减少 p-Tau 聚积并改善认知功能，而不影响炎症因子基线水平。

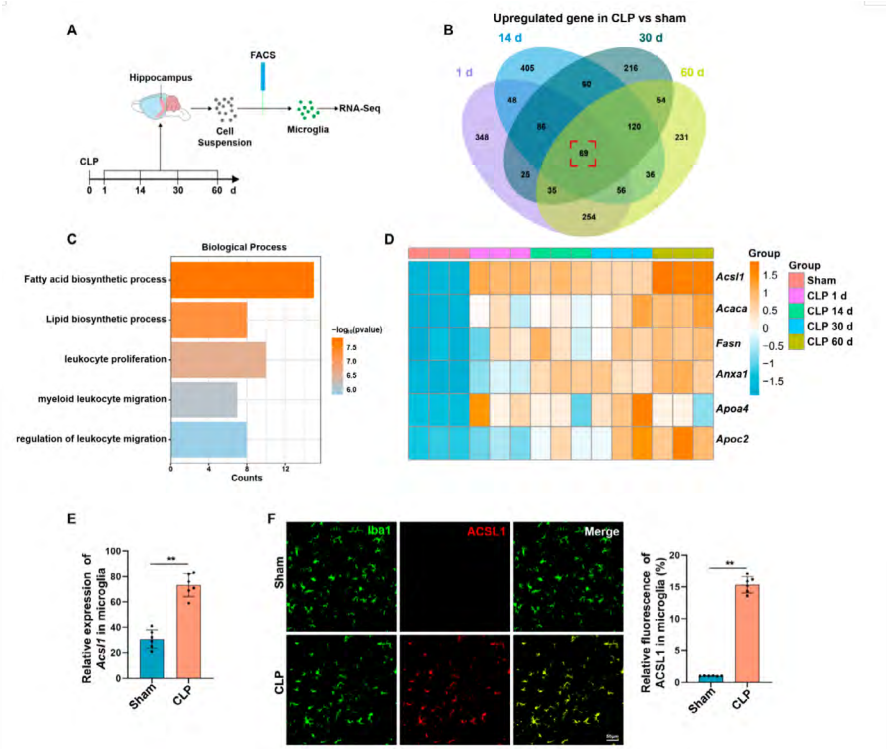


Fig. 3 小胶质细胞在脓毒症中 ACSL1 表达上升。（A）小胶质细胞流式分选的模式图。（B）韦恩图展示 CLP 术后 1、14、30 和 60 d 后小胶质细胞转录水平升高的基因。（C）GO 分析展示（B）中 69 个基因的信号通路富集。（D）基因热图展示（C）中 Fatty acid biosynthetic process 信号通路表达水平前 6 的基因水平。（E）RT-qPCR 检测小胶质细胞 Acsl1 的表达（n=6）。（F）海马中小胶质细胞（Iba1+）和 ACSL1 的抗体染色代表图及其相对荧光统计图（scale bar = 50 μm，n=6）。(NS 代表 p>0.05，*p<0.05，**p<0.01)

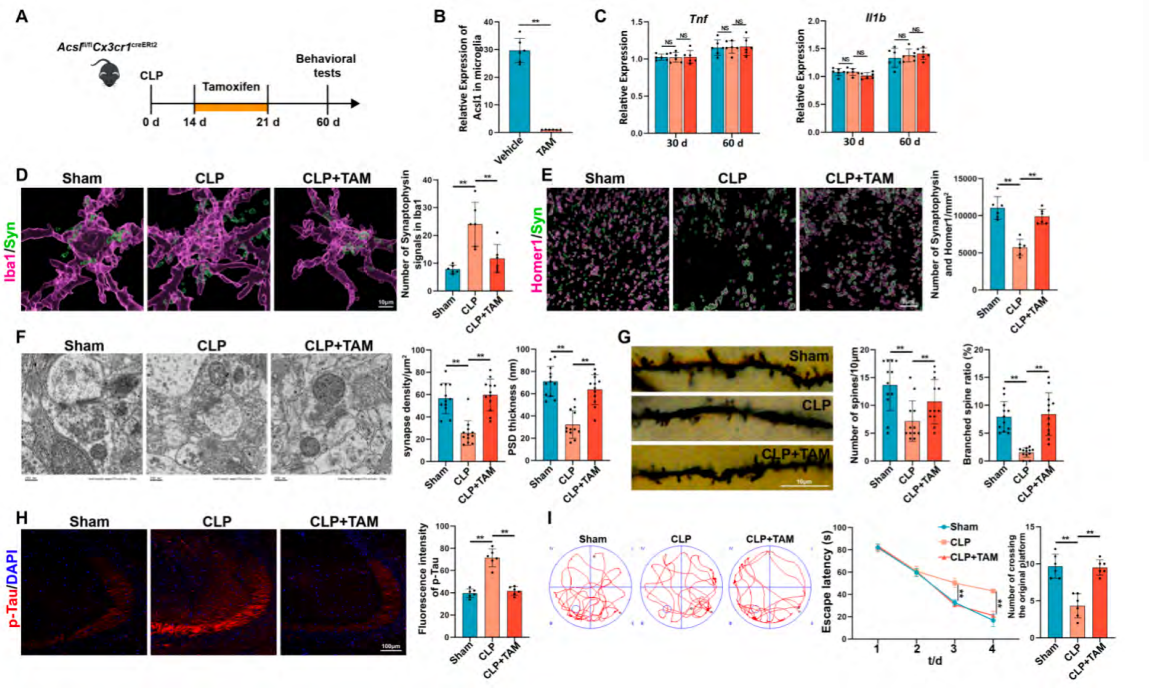
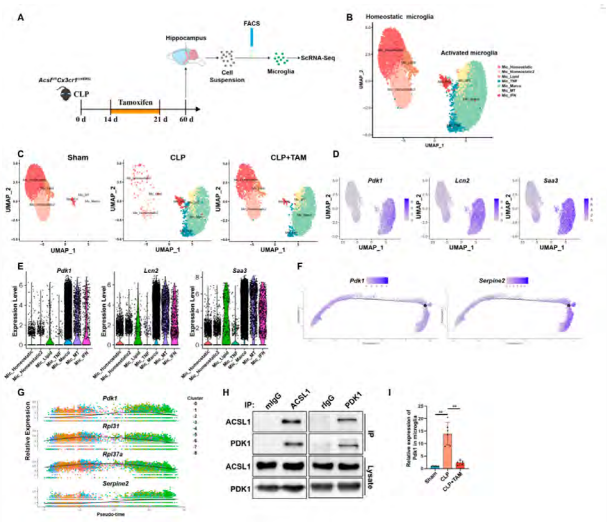


Fig. 4 小胶质细胞 Acsl1 基因条件性敲除可减轻 SAE 突触的损伤及认知功能障碍。（A）小胶质细胞在脓毒症中条件性敲除 Acsl1 的模式图。（B）q-PCR 检测小胶质细胞 Acsl1 的表达水平（n=6）。（C）q-PCR 检测 CLP 术后 60 d 海马中 Tnf 和 Il1b 的表达水平（n=6）。（D）免疫荧光染色检测小胶质细胞（Iba1+）吞噬突触前膜蛋白（Syn+）的代表图及其统计柱状图（scale bar = 10 μm，n=6）。（E）免疫荧光染色检测突触前膜 Synaptophysin 和突触后膜 Homer1 的代表图及其统计柱状图（scale bar = 5 μm，n=6）。（F）电镜检测突触的超微结构的代表图（scale bar = 200 μm, n=12）。（G）通过高尔基染色，树突棘的代表图，统计图数据为树突棘的数量以及分枝状树突棘的比例（scale bar = 10 nm，n=12）。（K）海马 CA3 区的 p-Tau 蛋白的荧光染色及 p-Tau 蛋白荧光强度统计图（scale bar = 100 μm，n=6）。（I）第六天测试水迷宫的轨迹图代表图、训练期 1-4d 的逃避潜伏期及其穿越平台次数的统计（n=6）。(NS 代表 p>0.05，*p<0.05，**p<0.01)

（3）ACSL1 通过 PDK1-cGAS-STING 通路介导下游效应。 单细胞测序揭示 Acsl1 敲除后激活态小胶质细胞比例显著降低，Pdk1 为关键差异基因。免疫共沉淀证实 ACSL1 与 PDK1 存在直接相互作用。Acsl1 敲除抑制 cGAS-STING 通路活化，而 PDK1 过表达可逆转该抑制效应并加重突触损伤。KEGG 富集分析显示 cGAS-STING 为 PDK1 过表达后差异最显著通路。



（Fig. 5 ACSL1 可能通过靶向结合 PDK1 持续激活小胶质细胞。（A）分选海马小胶质细胞进行单细胞测序的模式图。（B）总的小胶质细胞散点图，并分为两大类小胶质细胞，即稳态小胶质细胞（Homeostatic microglia）以及激活态小胶质细胞（Activated microglia）。（C）Sham 组、CLP 组和 CLP+TAM 组中小胶质细胞的分群情况。（D）激活态小胶质细胞特异性最强的三个基因在散点图的表达。（E）Pdk1、Lcn2 和 Saa3 基因在各群小胶质细胞的数量分布统计图。（F-G）拟时序分析筛选激活态小胶质细胞的关键基因。（H）在 BV2 细胞中，通过免疫共沉淀检测 ACSL1 蛋白和 PDK1 蛋白的相互作用关系。（I）q-PCR 检测小胶质细胞中 Pdk1 的 mRNA 表达水平（n=6）。(NS 代表 p>0.05，*p<0.05，**p<0.01)

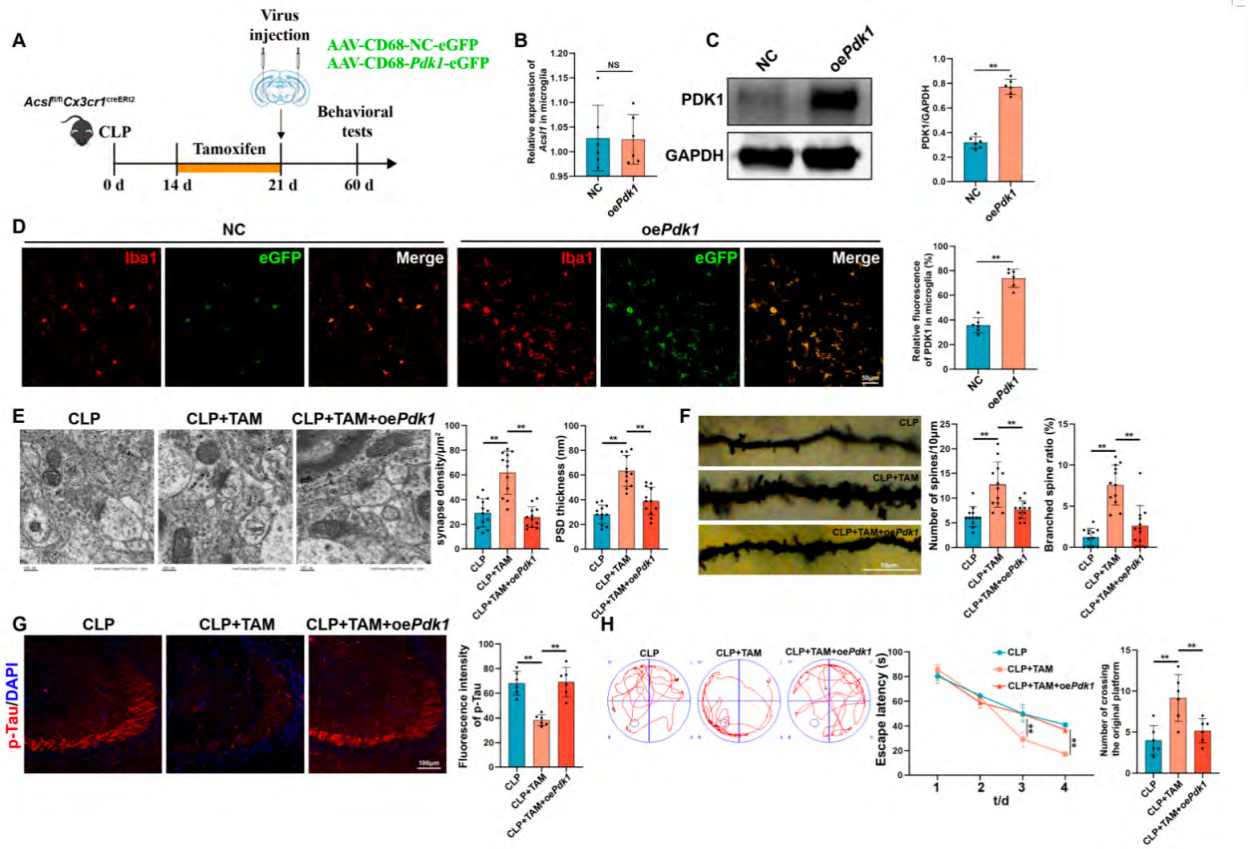


Fig. 6 小胶质细胞过表达 Pdk1 加重 SAE 突触的损伤及认知功能障碍。（A）小胶质细胞在脓毒症中靶向过表达 Pdk1 的模式图。（B）q-PCR 检测 CLP 术后 60 d 海马中小胶质细胞 Acsl1 的表达水平（n=6）。（C）WB 检测 CLP 术后 60 d 海马中 PDK1 蛋白的表达水平（n=6）。（D）荧光染色检测小胶质细胞 PDK1 的表达水平（n=6）。（E）电镜检测突触的超微结构的代表图（scale bar = 200 μm, n=12）。（F）通过高尔基染色，树突棘的代表图，统计图数据为树突棘的数量以及分枝状树突棘的比例（scale bar = 10 nm，n=12）。（G）海马 CA3 区的 p-Tau 蛋白的荧光染色及 p-Tau 蛋白荧光强度统计图（scale bar = 100 μm，n=6）。（H）第六天测试水迷宫的轨迹图代表图、训练期 1-4d 的逃避潜伏期及其穿越平台次数的统计（n=6）。(NS 代表 p>0.05，*p<0.05，**p<0.01)

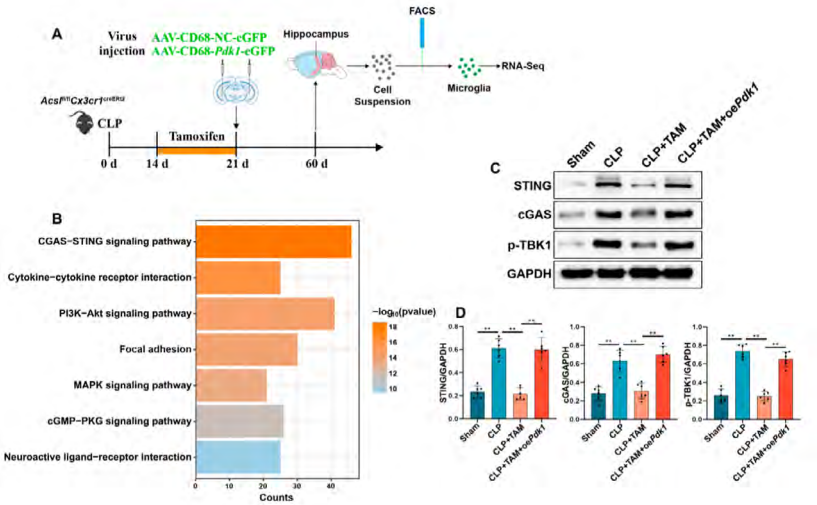


Fig. 7 小胶质细胞可能通过 PDK1 激活 cGAS-STING 信号通路。（A）小胶质细胞在过表达 Pdk1 后流式分选的模式图。（B）KEGG 分析过表达 Pdk1 后信号通路的激活。（C）WB 检测海马中 cGAS-STING 信号通路关键蛋白 STING、cGAS 和 p-TBK1 的表达水平（n=6）。(NS 代表 p>0.05，*p<0.05，**p<0.01)

（二）预期结论

本项目预期证实以下科学假设：在 SAE 病理进程中，海马小胶质细胞持续高表达的 ACSL1 通过直接结合 PDK1，激活下游 cGAS-STING 信号通路，进而诱导小胶质细胞对突触的过度吞噬及 p-Tau 蛋白异常聚积，最终驱动 SAE 远期认知功能障碍。该研究将从“ACSL1-PDK1-cGAS-STING”信号轴的全新视角揭示 SAE 远期认知障碍的分子机制，为靶向小胶质细胞治疗 SAE 提供理论依据和潜在干预靶点。本项目预计发表 SCI 论文 2–3 篇（其中 IF>10 一篇），并申请相关专利 1 项。

类别 :// 基础研究：涉及重症相关问题的基础研究

Agreement between the confusion assessment method for the intensive care unit and the intensive care delirium screening checklist in neurosurgical intensive care unit patients: A prospective observational study

姓名：莫逊，何达，武丹洋，黄华玮，余姗姗，吴蕾

单位：贵阳市第二人民医院，北京天坛医院

Background: The Confusion Assessment Method for the Intensive Care Unit (CAM-ICU) and the Intensive Care Delirium Screening Checklist (ICDSC) are the two most widely used bedside instruments for delirium screening in critically ill patients. However, the extent to which these tools agree under different intensive care unit (ICU) conditions remains unclear, particularly in the presence of sedation, invasive mechanical ventilation, and altered arousal.

Method: This prospective single-center observational study included 202 adult patients admitted to a neurosurgical intensive care unit who underwent paired delirium assessments using CAM-ICU and ICDSC within 24 h of admission. Agreement between the two instruments was evaluated using observed agreement, positive agreement, negative agreement, Cohen’s kappa, and the McNemar test. Prespecified subgroup analyses were performed according to sedation status, invasive mechanical ventilation, and Richmond Agitation-Sedation Scale (RASS) category. A restricted sensitivity analysis was additionally conducted in non-sedated, non-ventilated patients with RASS = 0. Factors associated with disagreement between CAM-ICU and ICDSC were examined using multivariable logistic regression.

Result: Overall agreement between CAM-ICU and ICDSC was 77.2%, corresponding to moderate agreement beyond chance (kappa = 0.55, 95% CI: 0.44-0.66). Agreement was substantially higher in non-sedated than in sedated patients (kappa = 0.632, 95% CI: 0.475-0.789 vs. 0.053, 95% CI: -0.191to 0.297) and in non-ventilated than in invasively ventilated patients (kappa = 0.696, 95% CI: 0.549-0.844 vs. -0.225, 95% CI: -0.467to 0.018). According to arousal level, agreement was highest in patients with RASS = 0 (kappa = 0.715, 95% CI: 0.540-0.889), intermediate in those with RASS +1 to +2 (kappa = 0.403, 95% CI: 0.145-0.662), and absent in those with RASS -2 to -1 (kappa = -0.002, 95% CI: -0.280to 0.276). In the restricted sensitivity analysis of non-sedated, non-ventilated patients with RASS = 0, concordance was 84/95 (88.4%), with substantial agreement (kappa = 0.691, 95% CI: 0.494-0.888). Among 46 discordant paired assessments, disagreement was more often characterized by CAM-ICU positivity with concurrent ICDSC negativity than by the reverse pattern (36/46 [78.3%] vs. 10/46 [21.7%]; exact McNemar p = 0.0002). In multivariable analyses, invasive mechanical ventilation was the most consistent independent predictor of disagreement.

Conclusion: CAM-ICU and ICDSC should not be assumed to be interchangeable across all ICU conditions. Their agreement is strongly state-dependent and is substantially reduced in patients receiving sedation, undergoing invasive mechanical ventilation, or exhibiting depressed arousal. These findings suggest that delirium screening results should be interpreted in light of the patient’s clinical state and that the same instrument should be used consistently when delirium is analyzed as an outcome.

Assessing the Immediate Benefit of Lung Recruitment in ARDS Patients Using CT Imaging Features: A Single-Center Prospective Observational Study

姓名：Liu Youwei，Wang Yan，Hu Dan

单位：Qingdao Municipal Hospital, University of Health, and Rehabilitation Sciences

Abstract

Objective

To investigate the relationship between quantitative analysis findings of different CT patterns and the immediate benefits of lung recruitment in patients with ARDS.

Design

Prospective observational clinical study.

Setting

Intensive Care Unit from a tertiary-level hospital.

Patients

ARDS patients requiring invasive mechanical ventilation.

Main variables of interest

Demographic characteristics, respiratory mechanics parameters, and chest CT features. Based on the rate of improvement in PaO_2/FiO_2 following lung recruitment, patients were divided into an improvement group and a non-improvement group.

Results

Compared with the non-improvement group, patients in the improvement group demonstrated significantly lower proportions of poorly-aerated ($Z = -2.658$, $P = 0.008$) and non-aerated ($Z = -2.360$, $P = 0.018$). Multivariate logistic regression analysis revealed that the proportion of poorly-aerated served as an independent inhibitory factor for immediate benefit following lung recruitment ($\beta = -0.374$, $P = 0.035$), whereas the proportion of non-aerated was not an independent predictor ($P > 0.05$), with no significant interaction detected between these two factors. ROC curve analysis further showed that the proportion of poorly-aerated, the proportion of non-aerated, and their combined indicator each yielded an AUC exceeding 0.7 in predicting immediate post-recruitment benefit.

Conclusion

The proportion of poorly-aerated serves as a valuable imaging biomarker for predicting immediate oxygenation improvement following lung recruitment.

Introduction

Acute Respiratory Distress Syndrome (ARDS) is a severe critical illness, characterized definitively by refractory hypoxemia and diffuse pulmonary inflammation.1 It constitutes a major complication within the Intensive Care Unit (ICU), presenting with an estimated incidence of 10.4% and a notably high in-hospital mortality ranging from 40% to 46%.2, 3

The management of ARDS is grounded in lung-protective ventilation.4 Lung recruitment, a critical element, is defined as the application of controlled pressures to reopen collapsed alveoli. The primary objective is to improve oxygenation and minimize ventilator-induced lung injury by optimizing transpulmonary pressure.5 Although a majority of ARDS patients derive benefit, an estimated 10 — 13% are at risk for complications like pneumothorax following unsuitable recruitment maneuvers.6 Nevertheless, findings from a pivotal multicenter randomized controlled trial in the Journal of the American Medical Association

associated these maneuvers with higher mortality, sparking renewed debate and reflection on their therapeutic profile.7 This is likely attributed to the variable responsiveness of individual patients to lung recruitment. This variability in patient response necessitates a meticulous assessment of recruitability, which has become a vital step in guiding individualized clinical decisions.

Currently, a range of modalities, including imaging, respiratory mechanics, and bedside monitoring, are employed to assess lung recruitment.8-10 Computed Tomography (CT) is the gold standard for assessing lung recruitment.8 The quantitative analysis of CT images capitalizes on strengths such as robust objectivity, excellent reproducibility, and high result comparability.11 Although it has demonstrated established value in the diagnosis and prognosis of diverse pathologies including COVID-19 and pulmonary fibrosis,12-14 the body of literature specifically exploring its utility for lung recruitment assessment in ARDS is still developing, indicating a need for more targeted investigation.

Guided by this imperative, our study is designed to investigate which CT-derived features predict favorable recruitment outcomes and to explore how distinct radiographic phenotypes correlate with lung recruitability. By conducting an in-depth investigation into the characteristics of quantitative CT during the progression of ARDS, this research may offer new perspectives and approaches for ARDS treatment, thereby improving patient prognosis and quality of life.

Methods

Patients

The study population comprised adult ARDS patients who required invasive mechanical ventilation and were admitted to the ICU of Qingdao Municipal Hospital between December 2024 and December 2025. According to the New Global Definition for ventilator-managed ARDS: PEEP $\geqslant$ 5 cmH_2O, $PaO_2/FiO_2 \leqslant 300$ mmHg, or $SpO_2/FiO_2 \leqslant 315$ (when $SpO_2 \leqslant 97\%$).15 The following exclusion criteria applied: intracranial hypertension, hemodynamic instability, decompensated heart failure, severe or very severe chronic obstructive pulmonary disease, lung cancer, bronchopleural fistula, pneumothorax, pulmonary bullae, chronic respiratory diseases requiring long-term oxygen therapy or assisted ventilation, and pregnancy. This study was reviewed and approved by the Hospital Ethics Committee (Approval No. KTLL2024-081). Prior to any study procedures, detailed information was provided to the families of potential participants, from whom written informed consent was subsequently obtained.

CT Imaging Analysis

Prior to recruitment maneuvers, each patient underwent a chest CT scan within a 24-hour window. Chest CT image analysis was carried out utilizing the 3D Slicer platform (version 5.6.1).16 Upon import of the DICOM data, the lung parenchyma was isolated through application of a semi-automatic segmentation algorithm. Consensus-based Regions of Interest (ROIs) were subsequently delineated. Within these ROIs, Hounsfield Unit (HU) value measurement and classification was performed based on standard thresholds: over-aerated (− 1000 to − 900 HU), normally-aerated (− 900 to − 500 HU), poorly-aerated (− 500 to − 100 HU), and non-aerated (− 100 to +100 HU).17 To obtain volumetric data, three-dimensional reconstruction techniques were applied to compute total lung volume and the volume of pathological areas.

PEEP Titration

Following the administration of adequate sedation, analgesia, and neuromuscular blockade to eliminate spontaneous breathing, patients are positioned semi-recumbent (prone positioning permitted if required). Suctioning is permitted prior to, but strictly prohibited during, the trial unless clinically indicated. A standardized ventilation period of at least 30 minutes is then instituted under volume control mode with a tidal volume of 6–8 mL/kg. The respiratory rate and I:E ratio are adjusted based on PaCO2, while PEEP is titrated to maintain SpO_2 at 93–100%. A singlebreath measurement method is then applied.18 The protocol comprises three consecutive 30-minute phases: Baseline, High PEEP, and Low PEEP, with constant FiO2. Arterial blood gas analysis is conducted at the end of each phase, after which ventilator settings are reverted to baseline. Continuous hemodynamic and respiratory monitoring is maintained. If the patient exhibits refractory hypoxemia ($SpO_2 < 88\%$) or persistent hypotension (MAP < 55 mmHg) despite vasopressor therapy, the patient must be withdrawn from the study.

During the implementation of lung recruitment maneuvers, hemodynamic stability is always prioritized. Considering that increased intrathoracic pressure induced by recruitment may reduce venous return, decrease cardiac output, and cause blood

pressure fluctuations, invasive arterial blood pressure, central venous pressure (if available), and heart rate are continuously monitored before, during, and after the procedure, with close attention to their dynamic trends. Peripheral perfusion indicators such as urine output, skin temperature of the extremities, and capillary refill time are also observed. Throughout the maneuver, rapid fluid resuscitation access and vasoactive medications are readily available to ensure that the mean arterial pressure is consistently maintained above 55 mmHg, thereby preserving adequate perfusion of vital organs. Every step of the procedure is carried out without compromising circulatory stability, ensuring that the potential benefits of lung recruitment and changes in oxygenation indices are not significantly offset by hemodynamic disturbances. This approach achieves a balance between improving oxygenation and maintaining overall circulatory stability.

Record the following parameters at baseline, high PEEP, and low PEEP levels, respiratory rate (RR), peak pressure (Ppeak), plateau pressure (Pplat), tidal volume (VT), PEEP, endexpiratory lung volume (EELV), and PaO_2/FiO_2. Subsequently calculate static lung compliance (Cst), mechanical power (MP), the change in mechanical power before and after recruitment (ΔMP), the recruitmenttoinflation ratio (R/I ratio), and the improvement rate in PaO_2/FiO_2.

Statistics

CT data were analyzed using 3D Slicer software to estimate the volume of each region and calculate the ratio of the corresponding pattern to the total lung volume. Statistical analysis and graphing were performed with SPSS 25 and GraphPad Prism 10.1.2 software. The Shapiro-Wilk test was used to assess the normality of data distribution. Continuous variables not conforming to a normal distribution were analyzed using the Mann-Whitney U test and expressed as median (interquartile range). Categorical variables were expressed as frequency and percentage, with intergroup comparisons performed using the chi-square test or Fisher's exact test. For variables that do not conform to a normal distribution or are ordinal, the Spearman rank correlation coefficient is used for correlation analysis. Multivariate logistic regression analysis was employed to explore imaging factors influencing the immediate improvement in oxygenation following lung recruitment. A multiplicative interaction model was also used to evaluate the interaction effects of CT imaging features on the immediate improvement in oxygenation after recruitment. Receiver operating characteristic (ROC) curves were constructed to evaluate the predictive value of CT imaging features for immediate post-recruitment benefit in ARDS patients. The predictive performance was quantified using the area under the curve (AUC). A P-value < 0.05 was considered statistically significant.

Results

Population

38 patients were ultimately included (Fig 1). Patients with a PaO_2/FiO_2 improvement rate ⩾ 20% were defined as the improvement group, with the remainder classified as the non-improvement group.19 A total of 15 patients were included in the improvement group, and 23 in the non-improvement group. In contrast to the non-improvement group, patients in the improvement group exhibited a significantly lower proportion of pre-existing underlying diseases (Z = –2.143, P = 0.032). However, no statistically significant differences were observed between the two groups in terms of other demographic characteristics or respiratory mechanics parameters (all P > 0.05; Table 1).

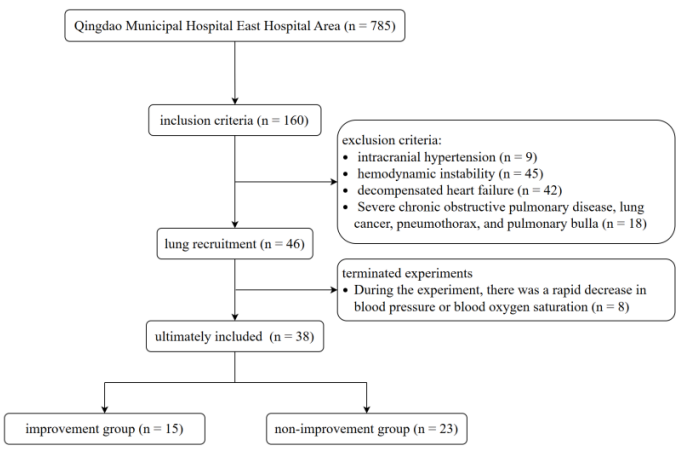


Figure 1 Inclusion and exclusion flowchart

Table 1 Comparison of clinical data between the improved group and the non-improved group

Indicator	Improvement group (n = 15)	Non-improvement group (n = 23)	P
Demography			
Age (years)	71[62-80]	75[60-83]	0.952
Man (cases)	9(60.0)	16(69.6)	0.728
BMI (kg/m^2)	22.09[20.81-30.86]	26.12[20.81-29.14]	0.560
Pulmonary (cases)	9(60.0)	15(65.2)	1.000
Underlying conditions (cases)	9(60.0)	21(91.3)	0.039
SOFA (points)	8[7-12]	10[8-11]	0.216
APACHE Ⅱ (points)	21[18-24]	23[19-28]	0.274
PaO_2/FiO_2 (mmHg)	191.17[175.11-232.67]	194.00[141.6-221.00]	0.601
Respiratory mechanics			
VT (mL)	360[350-450]	420[370-450]	0.435
RR (times/min)	15[15-18]	16[15-20]	0.501
PEEP (cmH_20)	5[5-7]	5[5-8]	0.760
Ppeak (cmH_20)	22[19-27]	24[19-26]	0.834
Pplat (cmH_20)	15[13-18]	17[13-21]	0.409
ΔP (cmH_20)	9[7-11]	12[8-13]	0.212
Cst (ml/cmH_20)	43.75[32.73-60.00]	40.00[32.14-56.25]	0.676
MP (J/min)	10.67[7.94-13.97]	11.85[8.11-15.99]	0.633
ΔMP (J/min)	0.24[-0.51-0.46]	0.00[-0.66-0.86]	0.962
R/I ratio	0.33[0.17-0.53]	0.23[-0.10-0.49]	0.420

Underlying conditions include hypertension, diabetes mellitus, coronary heart disease, and cerebrovascular disease; BMI, body mass index; SOFA, the Sequential Organ Failure Assessment score; APACHE II, the Acute Physiology and Chronic Health Evaluation II score; PaO_2/FiO_2, the oxygenation index; VT, tidal volume; RR, respiratory rate; PEEP, positive end-expiratory pressure; Ppeak, peak inspiratory pressure; Pplat, plateau pressure; Cst, static compliance; ΔP, driving pressure; MP, mechanical power; R/I ratio, recruitment-to-inflation ratio.

Correlation analysis

Correlation analysis revealed that the rate of improvement in PaO_2/FiO_2 demonstrated a significant positive correlation with the proportion of over-aerated ($r = -0.333$, $P = 0.041$; Fig 2A), and significant negative correlations with the proportions of poorly-aerated ($r = -0.540$, $P < 0.001$; Fig 2C) and non-aerated ($r = -0.412$, $P = 0.010$; Fig 2D). No significant correlation was found with the proportion of normally-aerated ($P > 0.05$; Fig 2B).

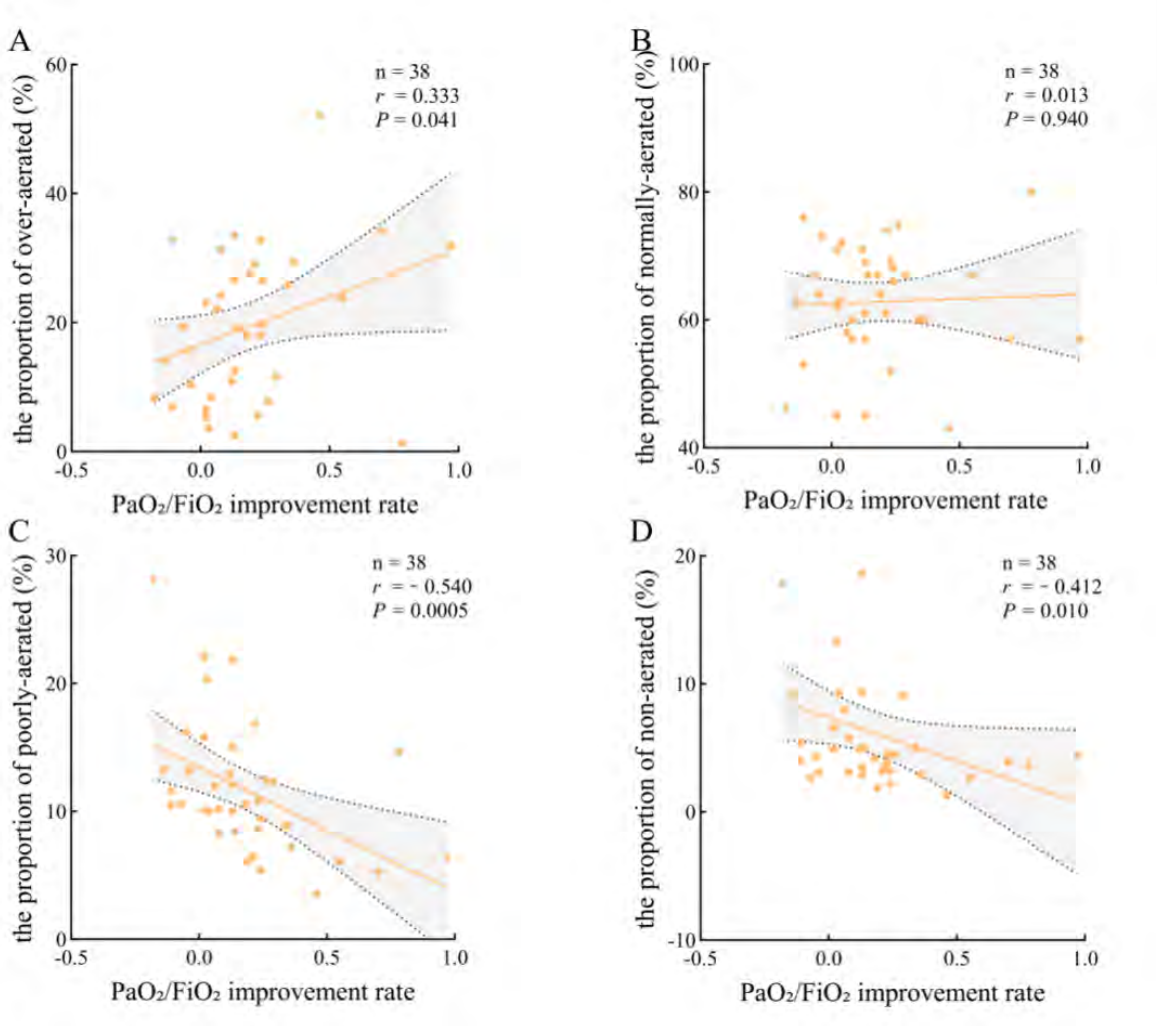


Figure 2 Correlation analysis between CT imaging characteristics and PaO2/FiO2 improvement rate

A: Correlation between the proportion of over-aerated and PaO_2/FiO_2 improvement rate; B: Correlation between the proportion of normally-aerated and PaO2/FiO2 improvement rate; C: Correlation between the proportion of poorly-aerated and PaO2/FiO2 improvement rate; D: Correlation between the proportion of non-aerated and PaO2/FiO2 improvement rate.

Differential analysis

Compared with the non-improvement group, patients in the improvement group exhibited significantly lower proportions of poorly-aerated (Z = –2.658, P = 0.008; Fig 3C) and non-aerated (Z = –2.360, P = 0.018; Fig 3D). In contrast, no statistically significant differences were observed between the two groups in the proportions of over-aerated or normally-aerated (both P > 0.05; Fig 3B, D).

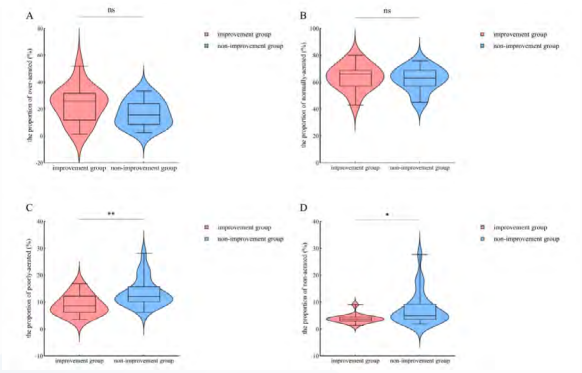


Figure 3 Analysis of the differences in CT imaging characteristics between the improvement group and the non-improvement group

A: Comparison of the proportion of over-aerated between the improvement group and the non-improvement group; B: Comparison of the proportion of normally-aerated between the improvement group and the non-improvement group; C: Comparison of the proportion of poorly-aerated between the improvement group and the non-improvement group; D: Comparison of the proportion of non-aerated between the improvement group and the non-improvement group. Red represents the improvement group, and blue represents the non-improvement group. ns indicates P > 0.05, * indicates P < 0.05, and ** indicates P < 0.01.

Regression analysis

Multivariate logistic regression analysis revealed that, after adjusting for the proportion of over-aerated, the proportion of poorly-aerated emerged as an independent inhibitory factor for immediate benefit following lung recruitment (β = –0.374, P = 0.035). In contrast, the proportion of non-aerated was not identified as an independent predictor of immediate post-recruitment benefit (β = –0.319, P = 0.101). Moreover, no interaction was found between these two factors (P > 0.05).

Table 2 Multivariate logistic regression analysis of the proportion of poorly-aerated and non-aerated

Predictive variables	Model 1			Model 2		
	β	P	OR(95%CI)	β	P	OR(95%CI)
the proportion of poorly-aerated	-0.271	0.018	0.762(0.609, 0.954)	-0.374	0.035	0.688(0.485, 0.974)
the proportion of non-aerated	-0.355	0.060	0.701(0.484, 1.015)	-0.319	0.101	0.727(0.497, 1.064)
the proportion of poorly-aerated * non-aerated	-0.029	0.046	0.971(0.944, 0.999)	-0.030	0.090	0.970(0.937, 1.005)

Model 1 did not adjust for other variables, while Model 2 adjusted for the proportion of over-aerated

ROC

ROC curves were constructed to evaluate the predictive value of the proportion of poorly-aerated, the proportion of non-aerated, and their combination for immediate benefit following lung recruitment in mechanically ventilated patients with ARDS (Fig 4). The analysis demonstrated that the proportion of poorly-aerated predicted immediate recruitment benefit with an AUC of 0.758 (P = 0.008), an optimal cutoff value of 9.7%, a sensitivity of 66.7%, and a specificity of 87.0%. The proportion of non-aerated yielded an AUC of 0.729 (P = 0.018) for predicting immediate benefit, with an optimal cutoff of 4.7%, a sensitivity of 86.7%, and a specificity of 60.9%. When combined, the two parameters achieved an AUC of 0.780 (P = 0.004), with a sensitivity of 60.0% and a specificity of 91.3%. All three indicators exhibited comparable AUC values exceeding 0.7, indicating favorable predictive performance.

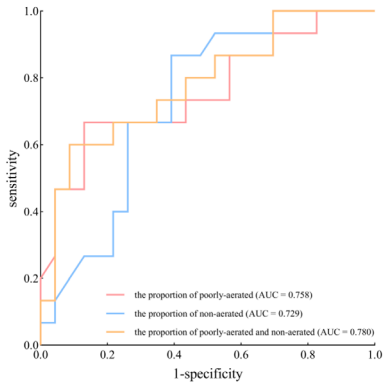


Figure 4 ROC curve for predicting immediate benefit after lung recruitment based on the proportion of poorly-aerated and non-aerated

ROC, the Receiver Operating Characteristic curve; AUC, the area under the ROC curve. Red represents the proportion of poorly-aerated, blue represents the proportion of non-aerated, and yellow represents the combined proportion of poorly-aerated and non-aerated.

Conclusion

The proportion of poorly-aerated serves as a valuable imaging biomarker for predicting immediate oxygenation improvement following lung recruitment. Monitoring this parameter facilitates a pre-recruitment assessment of the risk-benefit balance, enabling clinicians to identify patients most likely to benefit from the maneuver while avoiding ineffective or potentially harmful procedures in those unlikely to respond.

类别 :// 重症护理

Association between early urea-to-creatinine ratio trajectories and accelerated skeletal muscle loss in critically ill patients: a retrospective cohort study

姓名：罗振，陈管洁，李晓青

单位：东南大学附属中大医院

Background Critically ill patients often experience rapid muscle loss. The urea-to-creatinine ratio (UCR) reflects the muscle breakdown and catabolism. While UCR has been proposed as a surrogate marker for muscle mass, the predictive value of its dynamic early trajectory for acute muscle depletion remains unexplored. This study aimed to investigate whether dynamic trajectories of early UCR can predict the development of rapid muscle loss in critically ill patients.

Methods

This retrospective observational study involved adult patients admitted to the ICU. The primary outcome was the incidence of rapid muscle loss during ICU hospitalization. Group-based trajectory modeling (GBTM) was used to identify distinct UCR trajectories over the first 5 days of ICU admission. Changes in the cross-sectional muscle area at the third lumbar vertebra were measured using CT images to evaluate muscle loss. Rapid muscle loss was defined as a muscle loss rate greater than 2% per day. Multivariable logistic regression was used to examine the association between early UCR trajectories and rapid muscle loss. Kaplan-Meier analysis was performed to evaluate ICU survival.

Results

Of the 642 patients, 184 (28.7%) experienced rapid muscle loss during the early phase of their ICU stay. Three distinct early UCR trajectories were identified: a Stable-Low trajectory (80.5%), a High-Declining trajectory (8.3%), and a Steadily-Increasing trajectory (11.2%). Multivariable logistic regression analysis revealed that the High-Declining trajectory was significantly associated with an increased risk of rapid muscle loss compared to the Stable-Low trajectory, with an odds ratio (OR) of 2.76 [95% CI: 1.45~5.24]. Furthermore, the High-Declining trajectory was significantly associated with a higher risk of early ICU mortality (P = 0.011), despite no significant difference in overall ICU length of stay (P = 0.18).

Conclusion

The results demonstrate that an early high-declining UCR trajectory is independently associated with rapid muscle loss and poor survival in critically ill patients. Though additional prospective data are needed, our results suggest that monitoring early UCR trajectories may be useful in the early identification of critically ill patients at risk of rapid muscle loss and adverse outcomes.

Association between Respiratory Phenotypes and Successful Ventilator Liberation in Early-Onset and Late-Onset ARDS: A Multicenter Cohort Study

姓名：Hongyan Wang[2#],Lina Zhao[1#], Zhe Chen[2*], Keliang Xie[1*]

单位：1 Department of Critical Care Medicine, 2 Department of Geriatrics, Tianjin Geriatrics Institute, Tianjin Medical University General Hospital

Abstract

Background: Early-onset and late-onset acute respiratory distress syndrome (ARDS) differ in clinical course and outcomes, but their longitudinal respiratory trajectories remain unclear. We aimed to characterize respiratory trajectories in early- and late-onset ARDS and identify trajectory-based phenotypes associated with ventilator liberation and mortality.

Methods: In this multicenter retrospective cohort study, 907 patients with ARDS (519 early-onset, 388 late-onset) were analyzed. Partitioning around medoids clustering was applied to longitudinal trajectories of the PaO2/FiO2 ratio, tidal volume, and driving pressure in the overall cohort and onset-specific subgroups. Associations with outcomes were evaluated using multivariable regression, propensity score matching, and inverse probability weighting.

Results: Early-onset and late-onset ARDS showed distinct respiratory trajectories and clinical outcomes. Three reproducible respiratory trajectory phenotypes were identified across the overall cohort and onset-specific subgroups. The high-risk phenotype was characterized by persistent oxygenation impairment, elevated driving pressure, and higher tidal volume. Compared with the reference phenotype, the high-risk phenotype was associated with lower odds of successful ventilator liberation within 7 days (OR 0.15, 95% CI 0.06–0.34) and higher 28-day mortality (OR 7.50, 95% CI 4.74–12.05). Mediation analysis suggested that APACHE II score, SOFA score, and work of breathing partly mediated the association with ventilator liberation failure, whereas APACHE II score was the main mediator of 28-day mortality.

Conclusion: Early-onset and late-onset ARDS exhibit distinct longitudinal respiratory trajectories. Trajectory-based respiratory phenotyping identifies a high-risk subgroup associated with ventilator liberation failure and mortality, supporting the use of dynamic respiratory phenotyping for risk stratification in ARDS.

类别 :// 临床研究：设计规范的各类临床研究及研究方案报告

Association of Adjunctive Nonsteroidal Anti-inflammatory Drug Therapy with Reduced Sepsis Risk in Patients with Severe Post-traumatic Pulmonary Infection: A Multicenter Retrospective Cohort Study

姓名：谢开晶，敬慧丹

单位：重庆市九龙坡区人民医院

To evaluate the clinical efficacy of nonsteroidal anti-inflammatory drugs (NSAIDs) combined with antibiotics in patients with severe post-traumatic pulmonary infection, and to assess their impact on the risk of developing downstream sepsis.

This multicenter retrospective cohort study enrolled 181 patients with severe post-traumatic pulmonary infection admitted to the Intensive Care Unit (ICU) of the Jiulongpo District People's Hospital of Chongqing, Qianjiang Hospital affiliated to Chongqing University, and Army Medical Center of PLA (Daping Hospital) between June 2017 and June 2024. Patients were stratified into an antibiotic monotherapy group (control group, n=45) and an NSAIDs-supplemented antibiotic group (observation group, n=136) according to NSAIDs administration. Baseline demographics, laboratory parameters, and microbiological data were collected. Temporal trajectories of vital signs, hematologic indices, inflammatory markers, coagulation profiles, metabolic parameters, arterial blood gases, electrolytes, and organ function markers were compared between groups. The incidence of sepsis and in-hospital mortality were also evaluated.

The mean age of the cohort was 47.07±15.29 years, and 79.6% were male. The cohort presented a high injury burden, with a mean Injury Severity Score (ISS) of 30.2±10.25, Traffic accident trauma (57.5%) were the predominant mechanisms. Microbiological analysis identified Acinetobacter baumannii as the most frequent pathogen (18.0%). Post-treatment, the observation group exhibited a robust reinvigoration of lymphocyte percentage (LYM%) ($Z = -2.337$, $P = 0.019$), coordinated by synchronized systemic declines in white blood cell count (WBC) ($Z = -2.582$, $P = 0.010$), neutrophil-to-lymphocyte ratio (NLR) ($Z = -2.334$, $P = 0.020$), D-dimer ($Z = -2.970$, $P = 0.003$), blood glucose (Glu) ($Z = -2.231$, $P = 0.026$), total bilirubin (TBIL) ($Z = -2.384$, $P = 0.017$), indirect bilirubin (IBIL) ($Z = -2.557$, $P = 0.011$), blood urea nitrogen (BUN) ($Z = -2.245$, $P = 0.025$), and serum creatinine (SCr) ($Z = -2.245$, $P = 0.025$) compared to the control group. These findings indicate that the combinatorial paradigm effectively blunts systemic phlogistic cascades, ameliorates hypercoagulable disturbances, dampens metabolic stress, and promotes parenchymal organ recovery. Crucially, the incidence of sepsis was profoundly attenuated in the observation group compared to controls (8.1% vs. 22.2%, $\chi^2 = 6.586$, $P = 0.012$). Although in-hospital mortality demonstrated a favorable downward trend in the trial group, the discrepancy did not reach statistical significance.

In patients wrestling with severe post-traumatic pulmonary infections, the synergy of NSAIDs and antibiotics holds promise to mitigate secondary sepsis accrual and optimize clinical trajectories by concurrently uncoupling hyperinflammation, restoring immunological homeostasis, and reversing multiorgan vulnerability. This framework supports the clinical rationale of adjunctive anti-inflammatory modulation, although its definitive long-term benefits warrant further validation in prospective randomized controlled trials.

Association of HDL-C and ApoA-I with persistent organ failure in hypertriglyceridemia-associated acute pancreatitis: insights from a multicenter registry

姓名：王兰庭

单位：中国人民解放军东部战区总医院

Background: Circulating triglycerides have been believed to play a key role in aggravating hypertriglyceridemia-associated acute pancreatitis (HTG-AP), and therefore, existing therapies primarily focus on managing serum triglyceride levels. However, current early triglyceride-lowering therapies have failed to demonstrate significant clinical benefits, prompting efforts to identify novel treatment targets. Mechanistic studies have shown that lipoproteins, such as high-density lipoprotein cholesterol (HDL-C) and apolipoprotein A-I (ApoA-I), may also be involved in the pathophysiology of HTG-AP. This study aimed to investigate whether admission levels of HDL-C and ApoA-I were associated with adverse outcomes in HTG-AP.

Methods: Participants enrolled in the national PERFORM registry between November 2020 and November 2023, with available HDL-C and ApoA-I levels at enrollment, were retrospectively analyzed. The PERFORM is a large-scale, long-running, multicenter, prospective cohort study recruiting HTG-AP patients across China. The primary outcome was persistent organ failure (POF) within 14 days. A Cochran-Armitage test for trend was used to evaluate trends in proportions across tertiles of baseline HDL-C and ApoA-I levels. We employed the multivariable logistic regression models to investigate the association between serum levels of HDL-C and ApoA-I on admission and POF. Additionally, subgroup analyses were performed according to triglyceride level at enrollment ($\geqslant$ 22.6 mmol/L or not). Restricted cubic splines with knots set at the 10th, 50th, and 90th percentiles of the baseline HDL-C and ApoA-I levels examined the dose-response association with the primary outcome.

Results: Among the 325 HTG-AP patients eventually included, 52 (16.0%) developed POF. Within each low-to-high tertile of ApoA-I, the rate of POF decreased proportionally ($p<0.001$ by Cochran-Armitage trend test). After controlling for selected confounders (age, Sequential Organ Failure Assessment score, organ failure at enrollment, total cholesterol, and triglyceride), compared to the lowest tertile of ApoA-I, the highest tertile was significantly associated with reduced risk of POF (adjusted OR=0.16, 95% CI 0.05 to 0.56, $p=0.004$). In subgroup analysis, a similar finding was observed regardless of whether patients had a triglyceride level above 22.6 mmol/L. Spline analyses demonstrated a decrease in the risk of POF with increasing ApoA-I levels (p for overall=0.021). However, no significant association between HDL-C levels and POF was identified, regardless of regression and trend analyses.

Conclusions: Using large-sample real-world data, we found that low ApoA-I levels, continuous or tertile grouped, were associated with increased risk of developing POF in HTG-AP patients, independently of the serum triglyceride level. However, we did not detect a significant relationship between the levels of HDL-C and POF. These observations may inform the development of novel treatment strategies for HTG-AP.

Beyond Norepinephrine Dose: A Two-Stage Analytical Framework for Adjunctive Vasopressin Decision-Making in Septic Shock

姓名：王涛
单位：解放军总医院第四医学中心

Title

Beyond Norepinephrine Dose: A Two-Stage Analytical Framework for Adjunctive Vasopressin Decision-Making in Septic Shock

Abstract

Background

Vasopressin is widely used as an adjunctive vasopressor in septic shock, but the optimal strategy for patient selection and initiation timing remains uncertain. Norepinephrine dose alone may not capture the heterogeneous hemodynamic states underlying septic shock.

Objective

To develop and evaluate a two-stage analytical framework separating vasopressin treatment selection from initiation timing after treatment selection.

Methods

This multicenter observational study used target trial emulation principles. MIMIC-IV was used as the primary cohort and eICU-CRD for external validation. Vasoactive exposure was reconstructed from actual infusion events. Norepinephrine landmark cohorts were analyzed using overlap weighting.

Results

In the MIMIC-IV NE ⩾ 0.25 μg/kg/min landmark cohort (n=1,987), early vasopressin initiation was associated with higher 28-day mortality odds (OR 1.434, 95% CI 1.160–1.773). Threshold analyses across NE ⩾ 0.10, ⩾ 0.25, and ⩾ 0.50 μg/kg/min did not identify a clear beneficial initiation window. Among eventual vasopressin users, earlier initiation was associated with lower mortality (OR 0.747, 95% CI 0.574–0.972), although this analysis was exploratory due to eventual-user conditioning.

Conclusion

Vasopressin decision-making requires separating treatment selection from treatment timing. Norepinephrine dose alone may be insufficient for individualized vasopressin strategies.

Research Content

Background and Current Status

Septic shock management frequently requires escalating vasopressor support. Although vasopressin is recommended as adjunctive therapy, uncertainty remains regarding which patients should receive therapy and when therapy should be initiated.

Study Design

The study applied a two-stage target trial emulation framework. Stage 1 evaluated early vasopressin strategy among norepinephrine-escalated septic shock patients. Stage 2 explored initiation timing among patients who eventually received vasopressin.

Methods

Actual ICU infusion events were used to reconstruct vasopressor exposure. Landmark cohorts were constructed at norepinephrine

thresholds. Pre-treatment covariates were adjusted using propensity score overlap weighting. Outcomes included mortality, vasopressor-free days, shock reversal, renal outcomes, and external validation.

Results

Early vasopressin initiation among all eligible norepinephrine escalation patients was associated with higher mortality odds. Among eventual users, earlier initiation showed an exploratory association with improved outcomes. Hemodynamic phenotype analysis identified persistent hypotension as an exploratory effect-modification signal.

Conclusion

These findings suggest that vasopressin decisions involve distinct treatment selection and timing processes and support future phenotype-guided prospective evaluation.

Important Figures

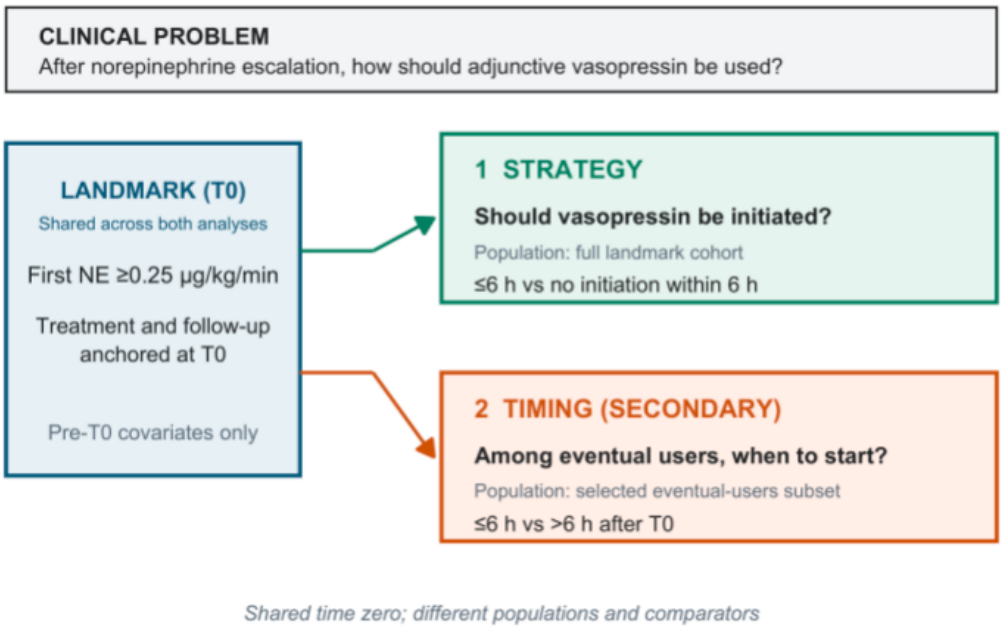


Figure 1. Two-stage analytical framework for vasopressin decision-making.

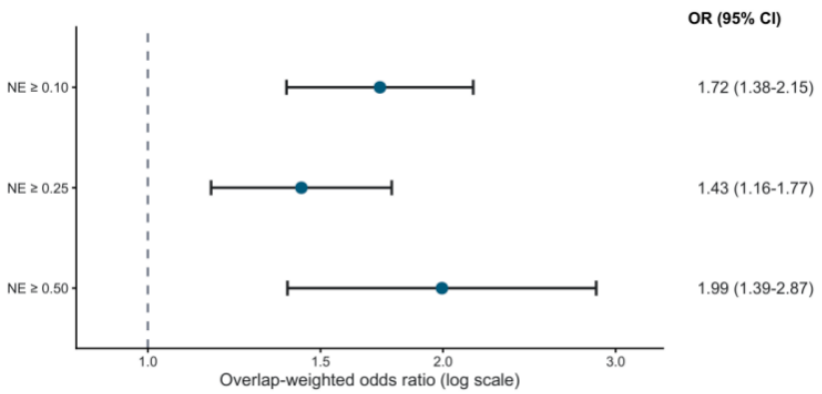


Figure 2. Association of early vasopressin initiation across norepinephrine thresholds.

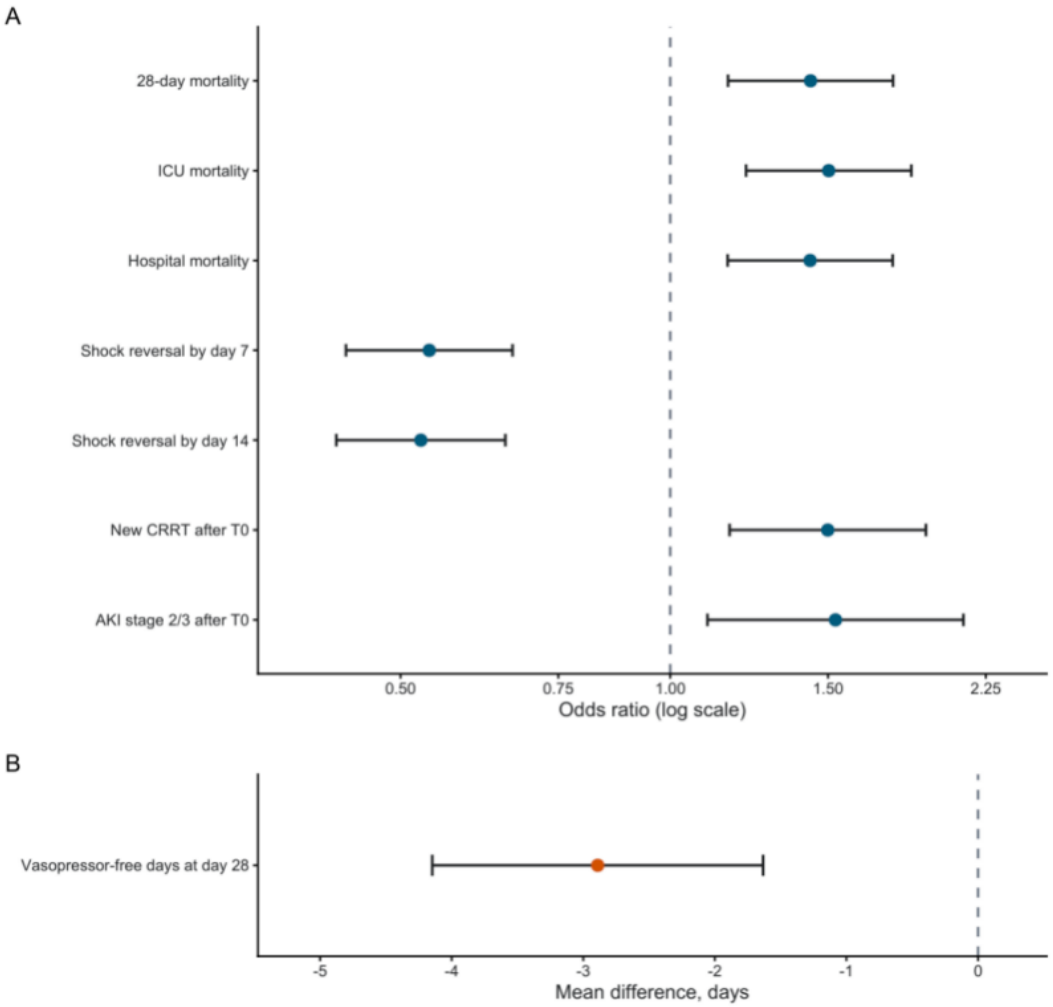


Figure 3. Primary strategy outcomes including mortality, shock reversal, renal outcomes, and vasopressor-free days.

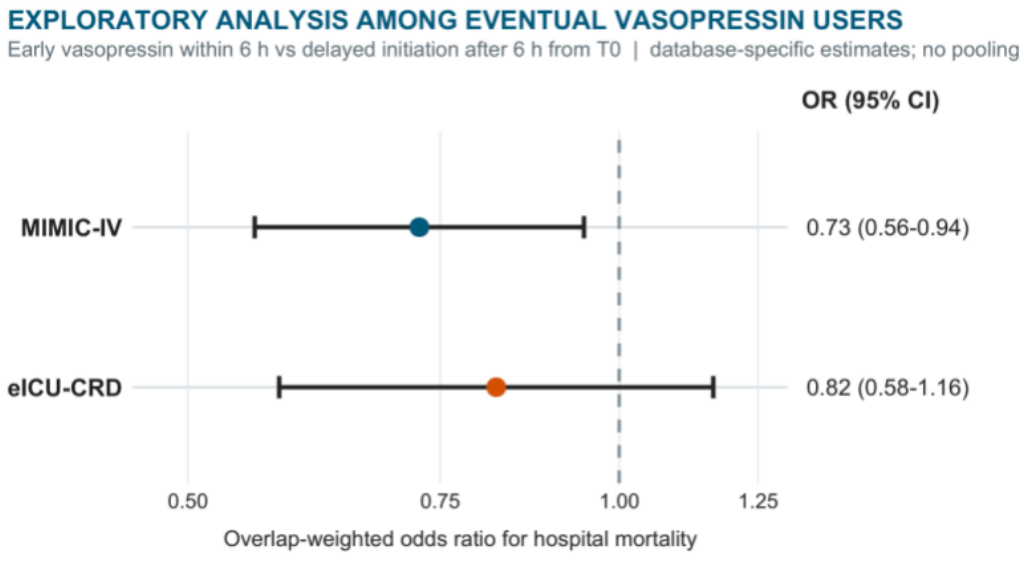


Figure 4. Exploratory timing analysis among eventual vasopressin users.

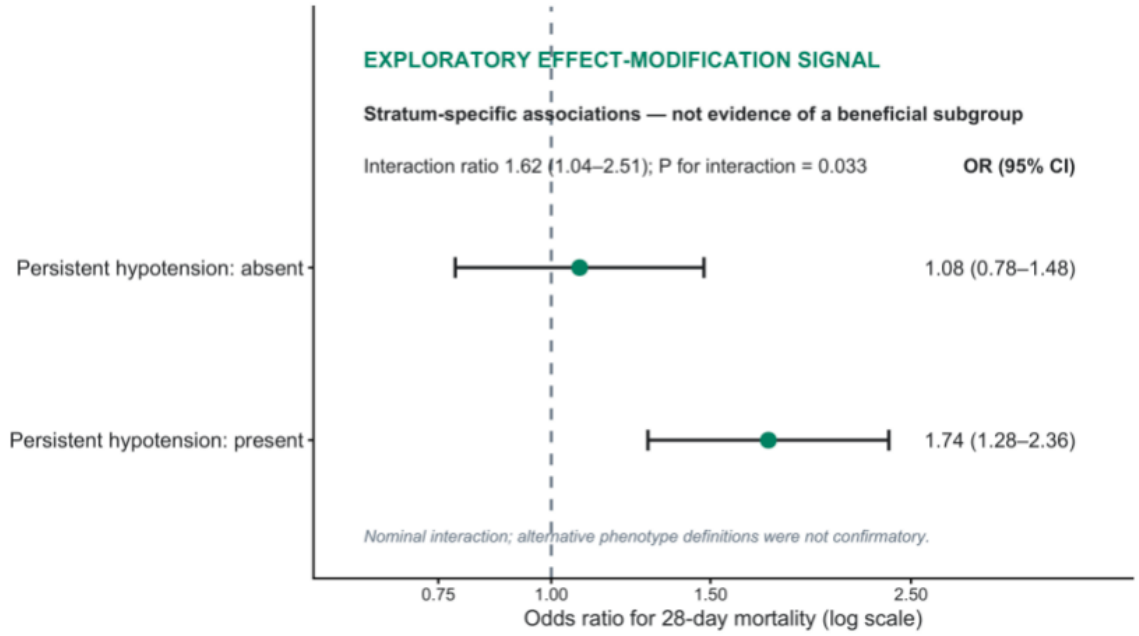


Figure 5. Exploratory effect-modification signal by persistent hypotension phenotype.

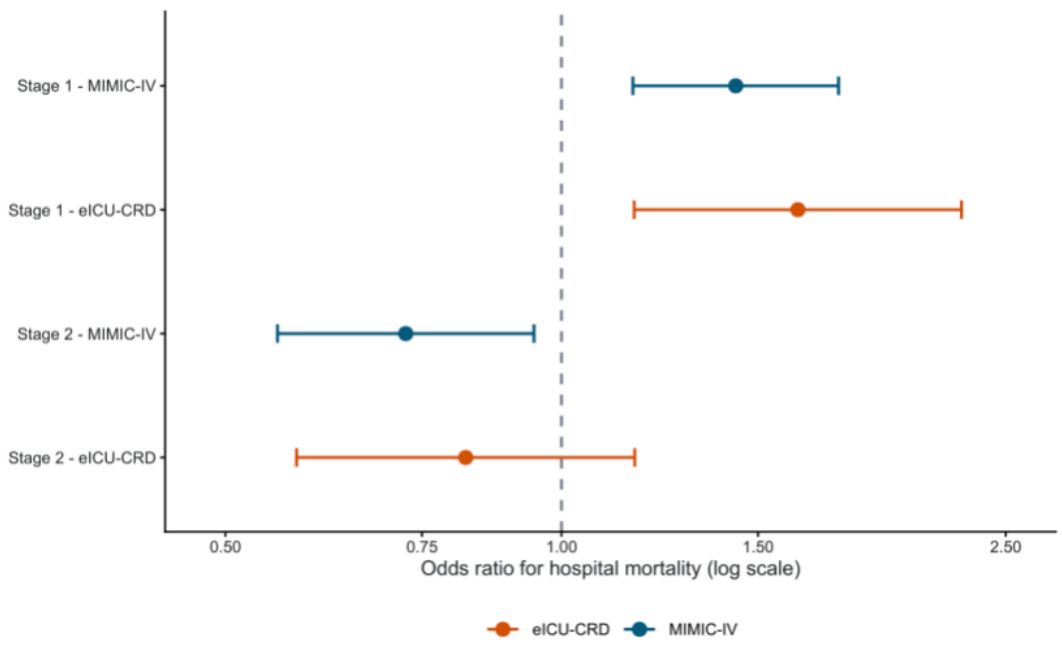


Figure 6. External validation comparing MIMIC-IV and eICU-CRD estimates.

Beyond Pressure: Development and External Validation of a Hemodynamic-Metabolic Framework for Interpreting Norepinephrine Response in Critically Ill Patients

姓名：Zhu xiaowei[1#]，Zhong Ming[2*]

单位：1 Zhongshan Hospital, Fudan University，2 Zhongshan Hospital, Fudan University

Background

Despite substantial heterogeneity in metabolic status, norepinephrine (NE) treatment duration, and vasopressor burden among critically ill patients, the clinical interpretation of NE escalation is frequently limited to arterial pressure alone. This over-reliance on a single hemodynamic parameter may obscure the complex physiological response to NE. Thus, we aimed to develop and externally validate a comprehensive hemodynamic–metabolic framework to contextualize NE response beyond isolated arterial pressure monitoring.

Methods

A retrospective observational cohort study was conducted in a primary ICU cohort, with external validation in MIMIC-IV. We included patients admitted to ICU, who had hypotension (MAP ⩽ 65 mmHg) and initiated NE infusion after ICU admission. The framework included three domains: heterogeneous early NE responses, state-dependent NE intensification interpretation (by concurrent MAP and lactate), and modification by treatment duration/vasopressor burden. Favorable downstream response was defined as simultaneous MAP improvement of at least 10% and lactate reduction of at least 20% within 6 hours after NE initiation. Hourly state-space analyses were performed in NE-exposed patients with paired MAP/lactate. External validation in MIMIC-IV included two levels: derived-cohort exposure–outcome analysis and hourly raw-table replication. Sensitivity analyses involved missing-data imputation and multivariable modeling for 28-day mortality.

Results

Among the patients who were started on NE alone at a dose between 0.01 (first percentile) and 0.5 (99th percentile) mg/kg/min were analyzed. Early response after NE initiation was heterogeneous, with distinct good responder, pressure-only responder, and poor responder phenotypes. In the primary state-space analysis, the apparent value of higher contemporaneous NE intensity varied across current MAP–lactate states rather than following pressure alone. The final decision map was derived through sequential refinement from a raw 4×4 grid to an intermediate 3×3 representation and then to a clinically optimized publication-ready map. Treatment duration modified the meaning of a given norepinephrine dose, and reaching MAP targets under high vasopressor burden was associated with less favorable downstream profiles than achieving those goals with lower vasopressor requirements. In MIMIC-IV, higher NE exposure remained associated with worse 28-day mortality, and the hourly MAP–lactate state-space pattern was directionally replicated. In sensitivity analyses addressing missing data, the low-MAP, high-lactate region continued to exhibit the most unfavorable prognosis, although the strength of the adverse signal was attenuated relative to the complete-case analysis. In additional supplementary analyses using clustered bootstrap inference for external hourly validation, the most robust and consistent adverse signal remained localized to the low-MAP, high-lactate phenotype.

Conclusions

Arterial pressure alone incompletely captures NE response in critical illness. A framework integrating MAP–lactate state, NE treatment duration, and vasopressor burden enables more clinically meaningful NE interpretation. These findings support the framework and generate hypotheses but not definitive causal treatment effects.

Keywords: Norepinephrine, Lactate, Hemodynamic metabolic framework, Septic shock

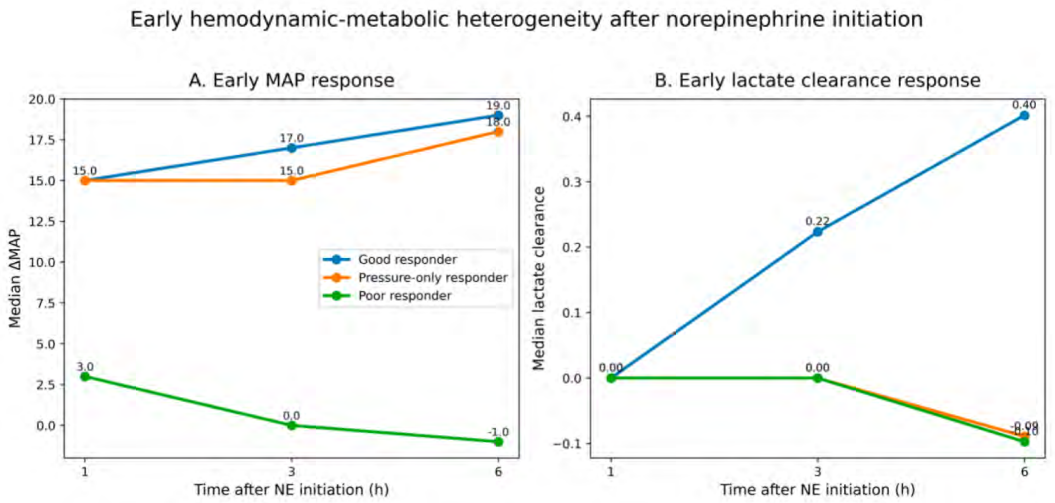


Figure 1. Early hemodynamic–metabolic heterogeneity after norepinephrine initiation.

Panel A shows the MAP response trajectory over the first 6 hours after NE initiation across early responder phenotypes. Panel B shows the corresponding lactate-response pattern. Good responders were defined as patients achieving both a ⩾ 10% increase in MAP and a ⩾ 20% decrease in lactate within 6 hours after NE initiation; pressure-only responders met the MAP criterion only, and poor responders met neither criterion. This figure illustrates that early NE-associated response is heterogeneous even during the initial treatment window.

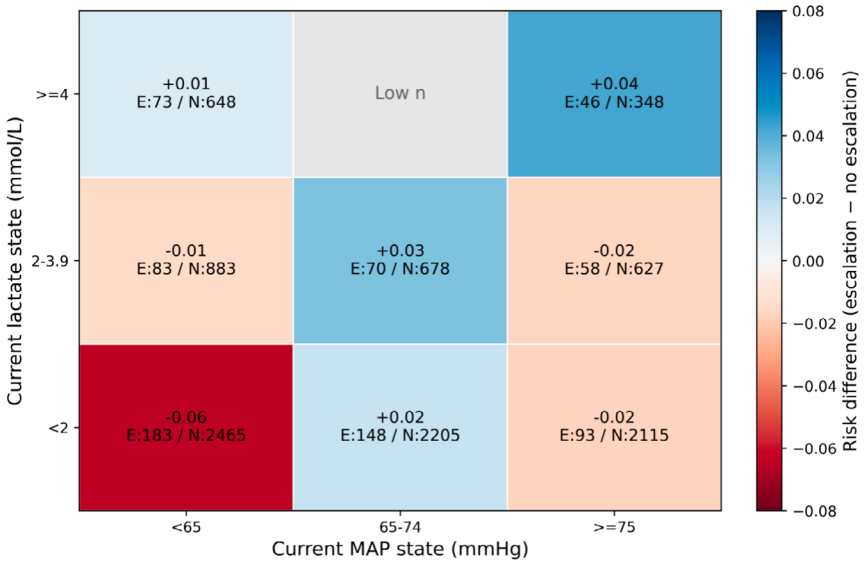


Figure 2. State-dependent interpretation of norepinephrine intensification across current MAP and lactate conditions.

Heatmap showing the observed difference in favorable downstream response across current MAP–lactate states. Cell values represent descriptive risk differences between higher-intensity and lower-intensity NE strata within each state cell. Blue indicates relatively greater favorable response with higher-intensity support, whereas red indicates lower favorable response. Cells were classified as low-information when either comparison stratum contained fewer than 50 observations; these cells were retained descriptively but not formally interpreted.

Bioelectrical Impedance Analysis for Early Sepsis Identification, Severity Assessment, and Post-Stabilization Risk Stratification in Critically Ill Patients With Cancer

姓名：Lyu Yang，王东浩
单位：天津市肿瘤医院（天津医科大学肿瘤医院）

Objective： Early sepsis identification and risk stratification remain particularly challenging in critically ill patients with cancer. Conventional inflammatory biomarkers do not fully capture host physiological vulnerability. We evaluated whether bioelectrical impedance analysis (BIA), particularly phase angle (PhA), provides incremental value for early sepsis identification, severity assessment, exploratory post-stabilization risk stratification, and longitudinal recovery monitoring in cancer patients with sepsis.

Methods： This single-center prospective observational study comprised two prespecified analytic components: a cross-sectional diagnostic component at sepsis onset (T0) and a longitudinal cohort component within the sepsis group. A total of 417 participants were included, including 296 patients with sepsis and 121 non-septic cancer controls. BIA and clinical data were collected at T0, after initial clinical stabilization (T1), and after 3-5 days of nutritional support (T2). For diagnostic analysis, elastic net logistic regression was used to develop traditional, BIA-only, and combined models. Internal validation was performed using 500 bootstrap resamples and repeated 10-fold cross-validation. Severity associations were examined using Spearman correlation and adjusted linear regression. Exploratory prognostic analyses were performed as T1 landmark analyses. Longitudinal changes were evaluated using mixed-effects models, with inverse probability weighting as a sensitivity analysis for incomplete T2 follow-up.

Results： The combined diagnostic model showed the best discrimination (AUC 0.970, 95% CI 0.949-0.991), followed by the traditional model (AUC 0.951) and the BIA-only model (AUC 0.915). Bootstrap optimism-corrected AUCs were 0.955, 0.944, and 0.897, respectively. PhA remained independently associated with sepsis in the combined model (OR 0.460, 95% CI 0.275-0.801; P = 0.003). In adjusted severity analyses, higher PhA was associated with lower SOFA and APACHE II scores, whereas higher ECW/TBW was associated with higher SOFA. In the T1 landmark analysis, each 1-degree increase in PhA was associated with lower odds of adverse outcome (OR 0.207, 95% CI 0.121-0.332; AUC 0.825, 95% CI 0.766-0.885). PhA increased significantly during recovery, including in inverse probability-weighted sensitivity analysis.

Conclusion： BIA-derived parameters, especially PhA, provide clinically relevant host-centered information beyond conventional biomarkers for early sepsis identification in critically ill cancer patients. PhA was also associated with disease severity and recovery-phase improvement, while its post-stabilization prognostic value should be interpreted as exploratory and hypothesis-generating.

Cg12712415 位点甲基化抑制 TAK1 表达介导重症肺炎免疫麻痹的分子机制

姓名：张佳敏，谢剑锋，张实

单位：山东大学附属第三医院，东南大学附属中大医院，山东大学附属第三医院

摘要：

背景：重症肺炎患者在感染过程中常由早期炎症反应过度逐渐转入免疫抑制状态，即免疫麻痹，该状态与继发感染及高死亡率密切相关，但其分子调控机制及精准干预靶点尚不明确。目的：系统解析重症肺炎免疫麻痹的关键表观遗传调控机制，并筛选潜在干预靶点。方法：基于临床队列、体外免疫麻痹细胞模型及动物模型，结合 DNA 甲基化芯片与转录组测序开展多组学整合分析，并通过染色质可及性分析、蛋白 -DNA 互作检测及基因功能实验对关键调控轴进行验证。结果：鉴定 Cg12712415 为关键 DNA 甲基化位点，其在免疫麻痹状态中显著高甲基化，并与 TAK1 表达呈负相关。进一步研究表明，该位点由 DNMT3A 催化甲基化，通过降低染色质开放性并抑制 RNA 聚合酶 II 结合，从而下调 TAK1 转录并抑制 NF-κB/MAPK 信号通路，导致免疫细胞功能受损。临床分析显示，该位点甲基化与继发感染风险及不良预后显著相关。动物实验表明，外源性补充 TAK1 可部分恢复免疫功能并改善生存结局。结论：DNMT3A-Cg12712415-TAK1 轴在重症肺炎免疫麻痹中发挥关键作用，具有潜在诊断标志物及干预靶点价值。

研究内容

1. 研究背景与现状

重症肺炎是临床常见的危重感染性疾病，其病情进展迅速且病死率较高，仍是住院患者死亡的重要原因之一。当前临床治疗以抗感染及多器官功能支持为核心，虽可在一定程度上控制感染，但部分患者在治疗过程中逐渐出现免疫功能低下，表现为继发感染、病原清除能力下降以及持续炎症失衡。这种由炎症过度反应向免疫抑制转变的过程被称为免疫麻痹，是影响患者预后的关键病理阶段。

已有研究表明，免疫麻痹并非单一因素所致，而是多层次调控失衡的结果。其中，单核 - 巨噬细胞在该过程中发挥核心作用，其功能受损不仅直接削弱机体清除病原体的能力，还可通过细胞因子网络抑制 T 细胞及其他免疫效应细胞功能，形成全身性免疫抑制状态。然而，目前针对其功能抑制的分子机制仍缺乏系统阐述。

近年来，表观遗传调控逐渐成为解释免疫功能重塑的重要理论基础。DNA 甲基化作为重要的表观遗传修饰方式，能够通过改变染色质结构及转录活性，实现对基因表达的稳定调控。研究发现，在严重感染及炎症耐受过程中，免疫细胞可发生广泛的 DNA 甲基化重编程，但针对具体功能性甲基化位点、其调控靶基因以及信号通路的研究仍较为有限，成为制约精准干预策略发展的关键科学问题。

2. 研究目的

本研究以重症肺炎免疫麻痹为研究对象，旨在通过多组学整合分析筛选关键 DNA 甲基化位点，解析其对靶基因表达及免疫功能的调控机制，并进一步评估其在疾病风险预测及靶向干预中的潜在应用价值。

3. 研究设计与方法

本研究采用“临床样本 - 细胞模型 - 动物实验”相结合的研究策略，以提高研究结果的系统性与可靠性。

在体外实验中，通过持续 LPS 刺激构建单核 - 巨噬细胞免疫麻痹模型，以模拟感染后期免疫抑制状态。利用转录组测序及 450K DNA 甲基化芯片对模型细胞进行分析，筛选差异表达基因及差异甲基化位点，并通过相关性分析构建潜在调控网络。

在临床研究部分，纳入肺炎患者及健康对照，分离 PBMCs 并进行转录组与甲基化检测，同时结合临床随访数据，采用多因素回归模型评估关键分子与继发感染风险之间的关系，从而验证其临床相关性。

在机制研究中，采用 ChIP-seq 分析 DNA 结合蛋白与目标区域的结合情况，利用 ATAC-seq 评估染色质开放程度，并通过 EMSA 检测蛋白 -DNA 相互作用，以解析关键甲基化位点对基因转录调控的分子机制。同时，通过基因敲低及回补实验验证目标基因在免疫功能调控中的作用。

在动物实验中，构建免疫麻痹模型，并通过巨噬细胞来源外泌体递送目标分子进行干预，系统评估其对免疫功能及生存结局的影响。

4. 研究结果

（1）免疫麻痹模型的建立及表型特征

经 LPS 持续刺激后，单核 - 巨噬细胞表现出典型免疫麻痹特征，包括吞噬能力显著下降、HLA-DR 表达降低以及 IL-1β、IL-6、TNF 等炎症

因子分泌减少。GSEA 分析显示炎症反应及免疫激活相关通路显著受抑，提示模型成功模拟免疫抑制状态。（图 1 a-d）

（2）多组学整合筛选关键调控轴

通过整合转录组与 DNA 甲基化数据，筛选出多个差异表达基因及差异甲基化位点。进一步相关性分析发现，部分基因表达与特定位点甲基化呈显著负相关。结合临床数据进行交叉筛选，最终确定 TAK1 为关键靶基因，其对应的 Cg12712415 位点被鉴定为核心调控位点。（图 1 e-j）

（3）临床相关性分析及风险评估

在肺炎患者队列中，Cg12712415 位点甲基化水平在发生继发感染的患者中显著升高。进一步分析显示，该位点甲基化与炎症通路活性下降及免疫抑制表型密切相关。风险模型提示，该位点甲基化可作为继发感染的独立预测因素之一，具有潜在临床应用价值。（图 2）

（4）DNMT3A 介导的甲基化修饰机制

差异表达分析表明，DNMT3A 在免疫麻痹状态中显著上调，而其他 DNA 甲基转移酶变化不明显。ChIP 实验显示，DNMT3A 可直接结合 Cg12712415 位点附近区域并催化其甲基化。干扰 DNMT3A 表达后，该位点甲基化水平下降，同时 TAK1 表达上调，提示其在该调控过程中的关键作用。

ATAC-seq 结果表明，该位点甲基化可降低 TAK1 启动子区域的染色质开放程度。进一步研究发现，甲基化状态可阻碍 RNA 聚合酶 II 与启动子区域结合，从而抑制转录起始。报告基因实验进一步证实，甲基化启动子活性显著下降，表明该位点甲基化直接参与 TAK1 转录调控。（图 3）

（5）TAK1 在免疫功能中的作用及机制

功能实验表明，TAK1 表达降低可显著抑制单核 - 巨噬细胞吞噬能力、炎症因子分泌及抗原呈递功能，同时抑制 NF-κB 及 MAPK 信号通路活化。恢复 TAK1 表达后，上述功能可部分恢复，提示其在维持免疫反应中的关键作用。此外，TAK1 缺失还可通过细胞间调控抑制 $CD8^+$T 细胞功能并促进调节性 T 细胞扩增，进一步加重免疫抑制状态。（图 4、5）

（6）靶向干预的治疗效果验证

在免疫麻痹小鼠模型中，通过外泌体递送 TAK1 后，可显著改善免疫抑制表型，包括炎症因子表达恢复、吞噬功能增强及免疫细胞比例改善。生存分析显示，干预组小鼠生存时间显著延长，提示该调控轴具有潜在治疗价值。（图 6、7）

5. 结论

本研究从表观遗传调控角度系统阐明了重症肺炎免疫麻痹的分子机制，明确 DNMT3A 介导的 Cg12712415 位点甲基化通过抑制 TAK1 表达，进而调控 NF-κB/MAPK 信号通路并导致免疫功能抑制。该调控轴不仅参与疾病发生发展，还与临床预后密切相关，具有潜在的诊断及靶向干预价值，为重症肺炎的精准治疗提供了新的理论依据。

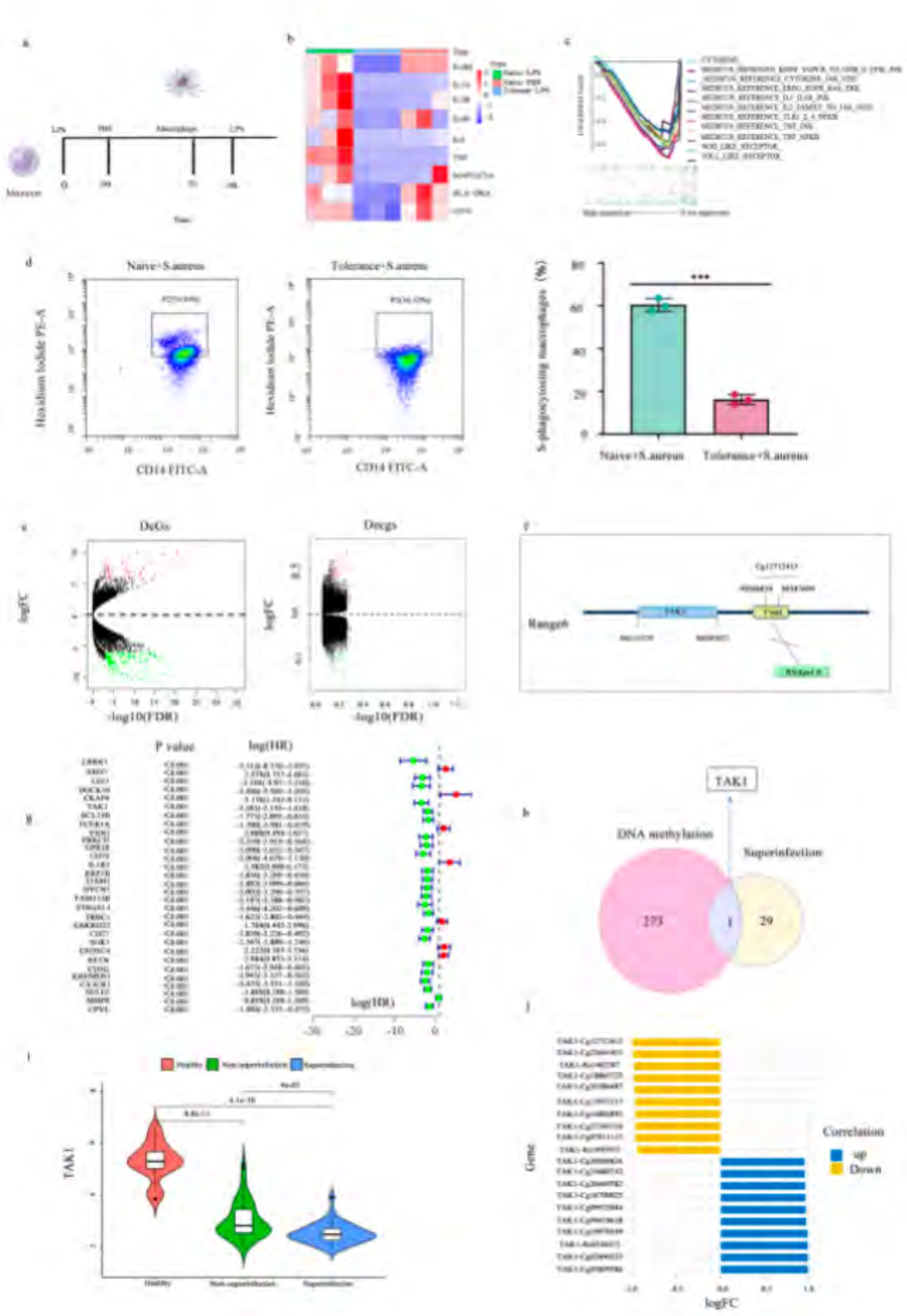

Naive+S.aureus
Tolerance+S.aureus
Hoechst Iodide PE-A
CD14 FITC-A
Sphagocytosing macrophages (%)
***
DeGs
logFC
-log10(FDR)
Rangeh
TAK1
DNA methylation
Superinfection
273
1
29
P value
log(HR)
Correlation
up
Down
Gene
logFC

图 1

图 2

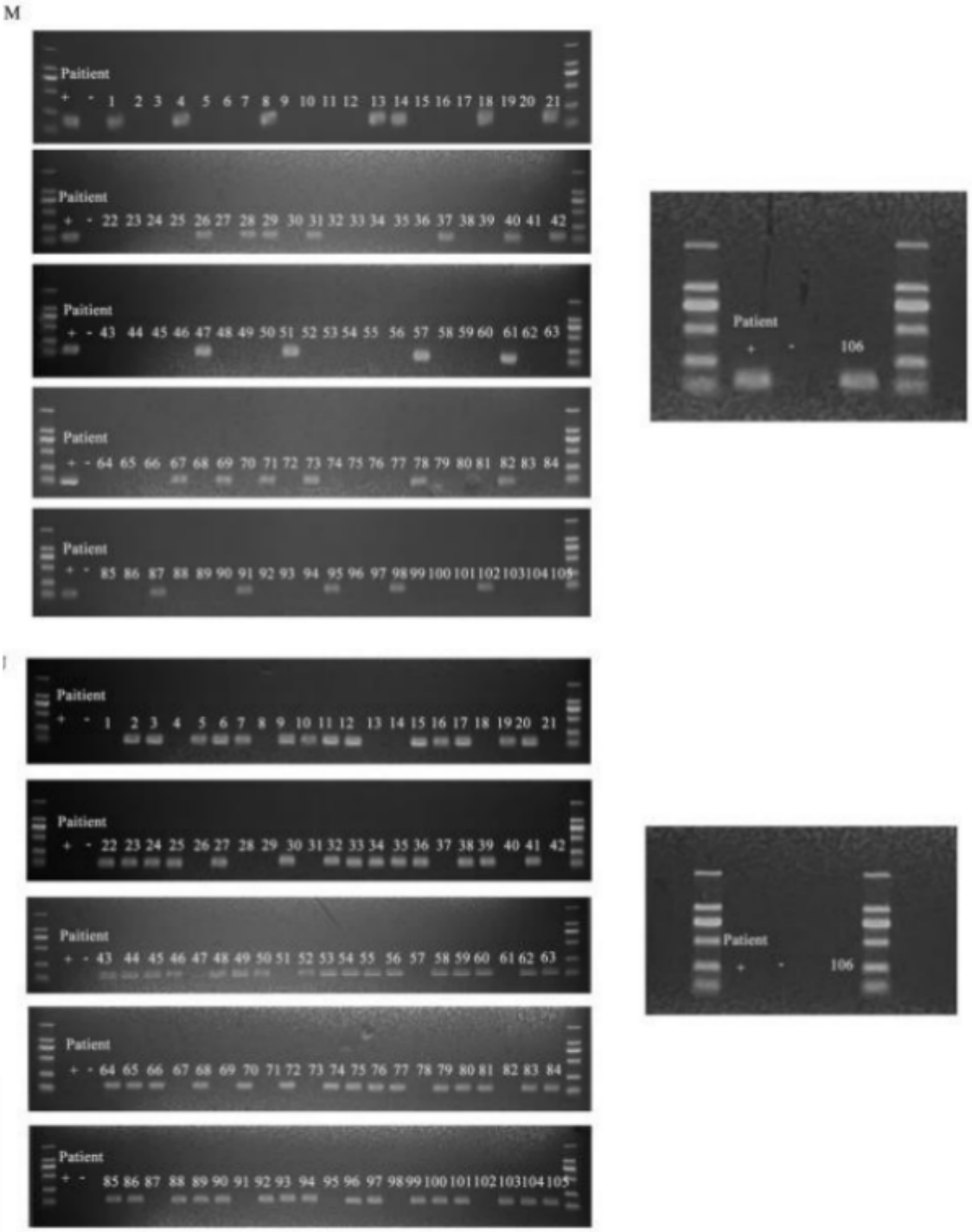

M
Paitient
+ - 1 2 3 4 5 6 7 8 9 10 11 12 13 14 15 16 17 18 19 20 21
Paitient
+ - 22 23 24 25 26 27 28 29 30 31 32 33 34 35 36 37 38 39 40 41 42
Paitient
+ - 43 44 45 46 47 48 49 50 51 52 53 54 55 56 57 58 59 60 61 62 63
Patient
+ - 64 65 66 67 68 69 70 71 72 73 74 75 76 77 78 79 80 81 82 83 84
Patient
+ - 85 86 87 88 89 90 91 92 93 94 95 96 97 98 99 100 101 102 103 104 105
Patient
+ - 106
Paitient
+ - 1 2 3 4 5 6 7 8 9 10 11 12 13 14 15 16 17 18 19 20 21
Paitient
+ - 22 23 24 25 26 27 28 29 30 31 32 33 34 35 36 37 38 39 40 41 42
Paitient
+ - 43 44 45 46 47 48 49 50 51 52 53 54 55 56 57 58 59 60 61 62 63
Patient
+ - 64 65 66 67 68 69 70 71 72 73 74 75 76 77 78 79 80 81 82 83 84
Patient
+ - 85 86 87 88 89 90 91 92 93 94 95 96 97 98 99 100 101 102 103 104 105
Patient
+ - 106

图 3

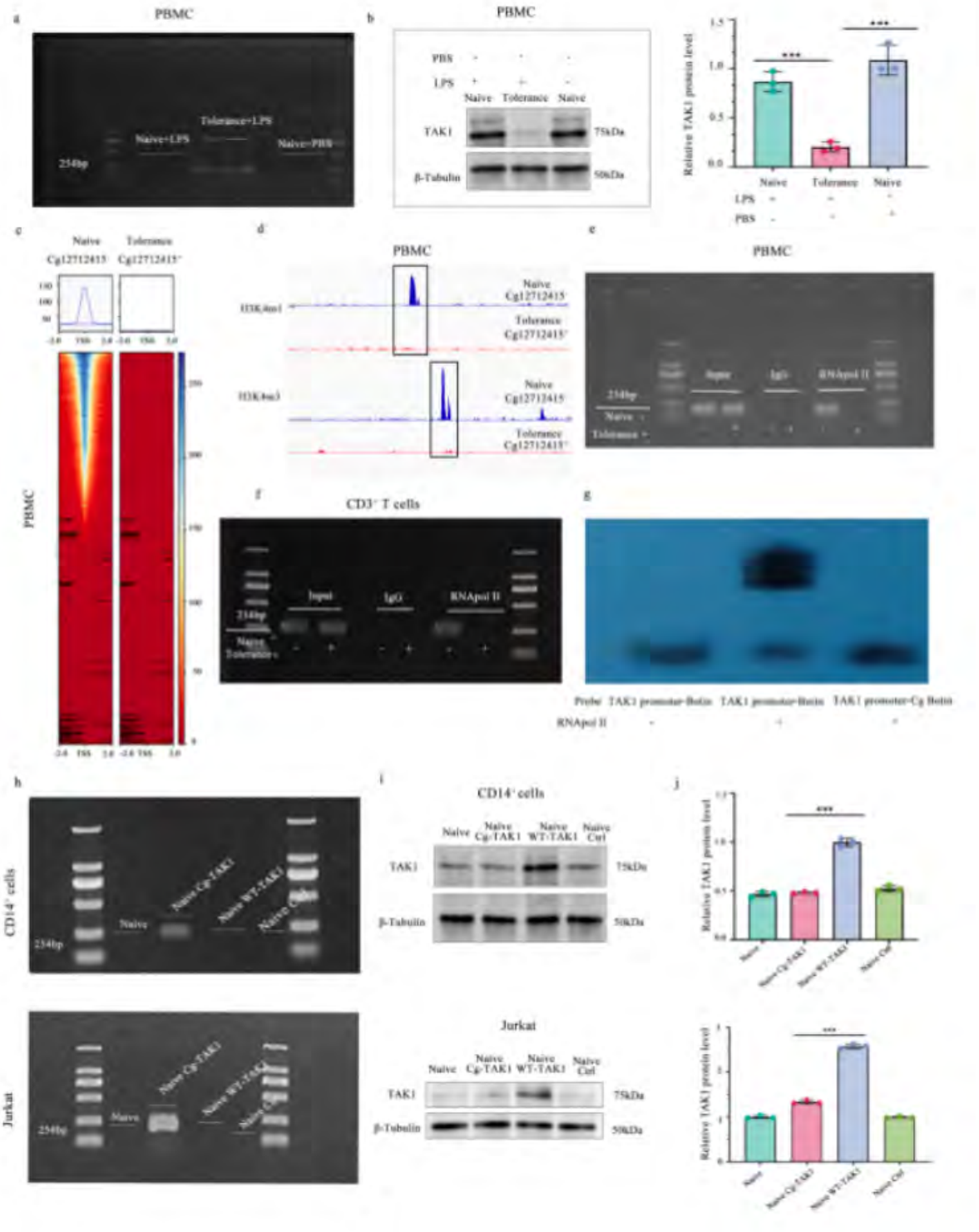

a
PBMC
Tolerance+LPS
Naive+LPS
Naive+PBS
254bp
b
PBMC
PBS
LPS
Naive
Tolerance
Naive
TAK1
75kDa
β-Tubulin
50kDa
Relative TAK1 protein level
***
***
Naive
Tolerance
Naive
LPS
PBS
c
Naive
Tolerance
Cg12712415
Cg12712415'
PBMC
d
PBMC
H3K4me1
H3K4me3
Naive
Cg12712415
Tolerance
Cg12712415'
e
PBMC
Input
IgG
RNApol II
254bp
Naive
Tolerance
f
CD3⁺ T cells
Input
IgG
RNApol II
254bp
Naive
Tolerance
g
Probe: TAK1 promoter-Biotin
TAK1 promoter-Biotin
TAK1 promoter-Cg Biotin
RNApol II
h
CD14⁺ cells
Naive
Naive Cg-TAK1
Naive WT-TAK1
Naive Ctrl
254bp
Jurkat
Naive
Naive Cg-TAK1
Naive WT-TAK1
Naive Ctrl
254bp
i
CD14⁺ cells
Naive
Naive Cg-TAK1
Naive WT-TAK1
Naive Ctrl
TAK1
75kDa
β-Tubulin
50kDa
Jurkat
Naive
Naive Cg-TAK1
Naive WT-TAK1
Naive Ctrl
TAK1
75kDa
β-Tubulin
50kDa
j
Relative TAK1 protein level
***
Naive
Naive Cg-TAK1
Naive WT-TAK1
Naive Ctrl
Relative TAK1 protein level
***
Naive
Naive Cg-TAK1
Naive WT-TAK1
Naive Ctrl

图 4

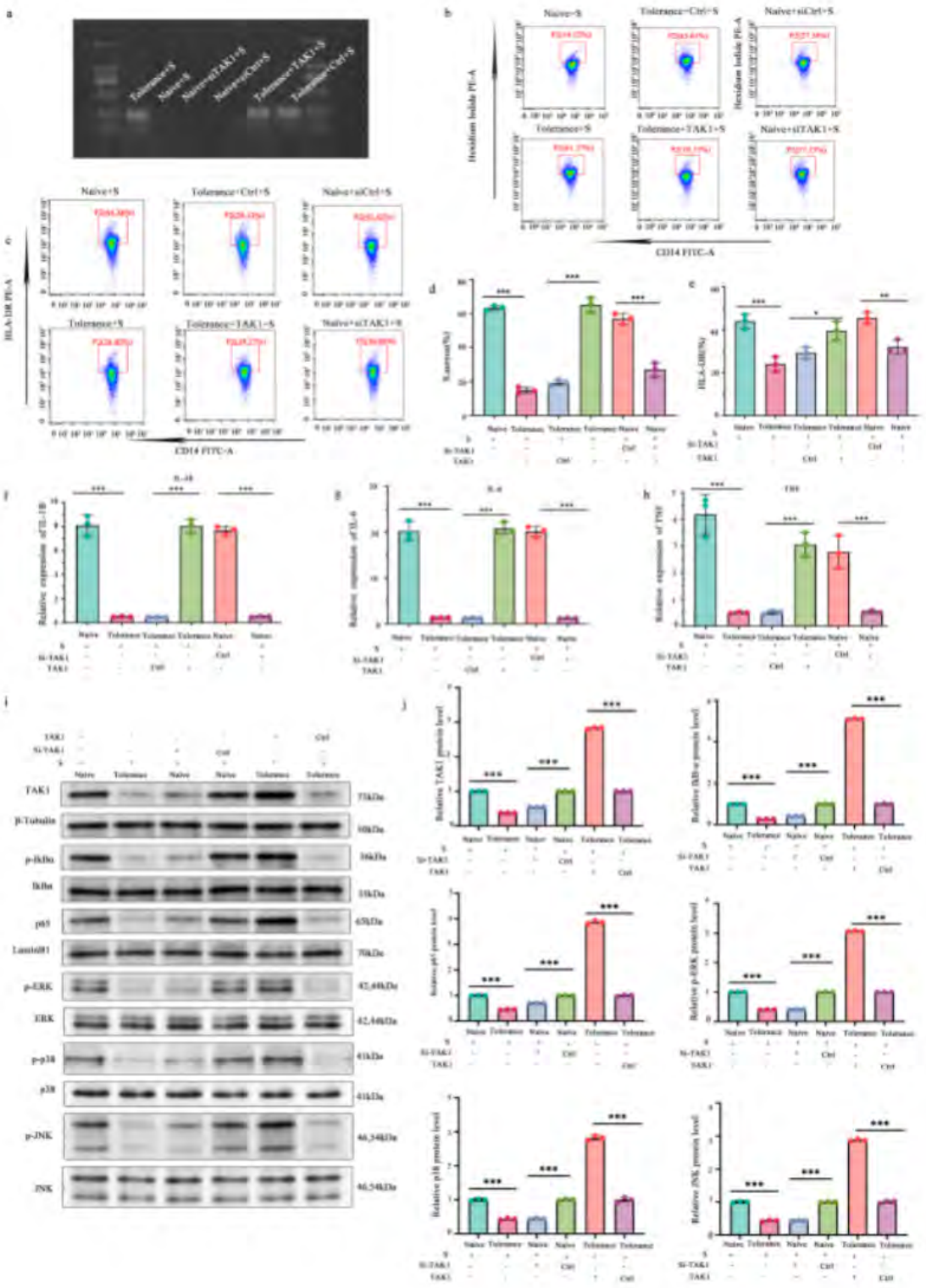


图 5

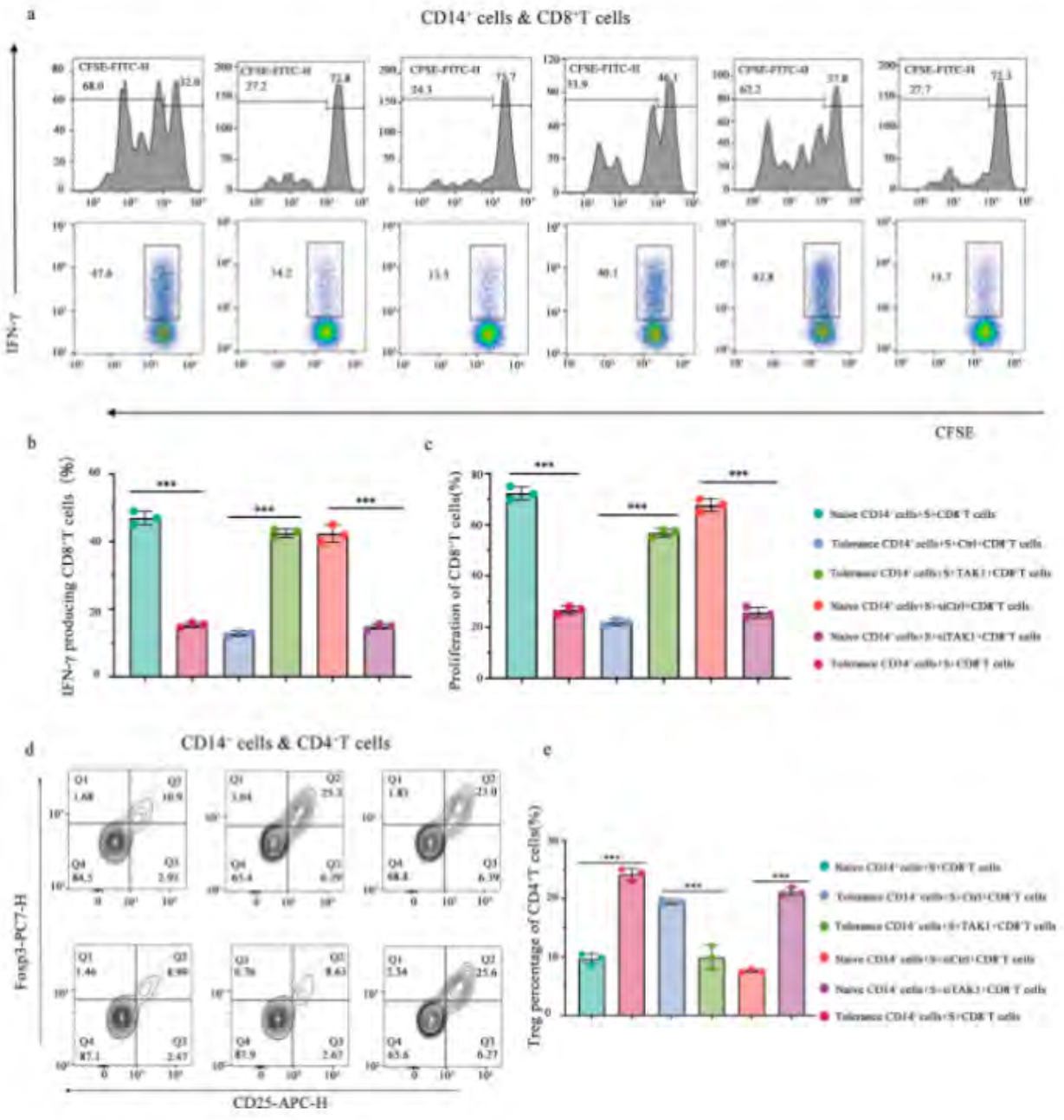

a
CD14+ cells & CD8+T cells
IFN-γ
CFSE
b
IFN-γ producing CD8+T cells (%)
c
Proliferation of CD8+T cells(%)
d
CD14+ cells & CD4+T cells
Foxp3-PC7-H
CD25-APC-H
e
Treg percentage of CD4+T cells(%)

图 6

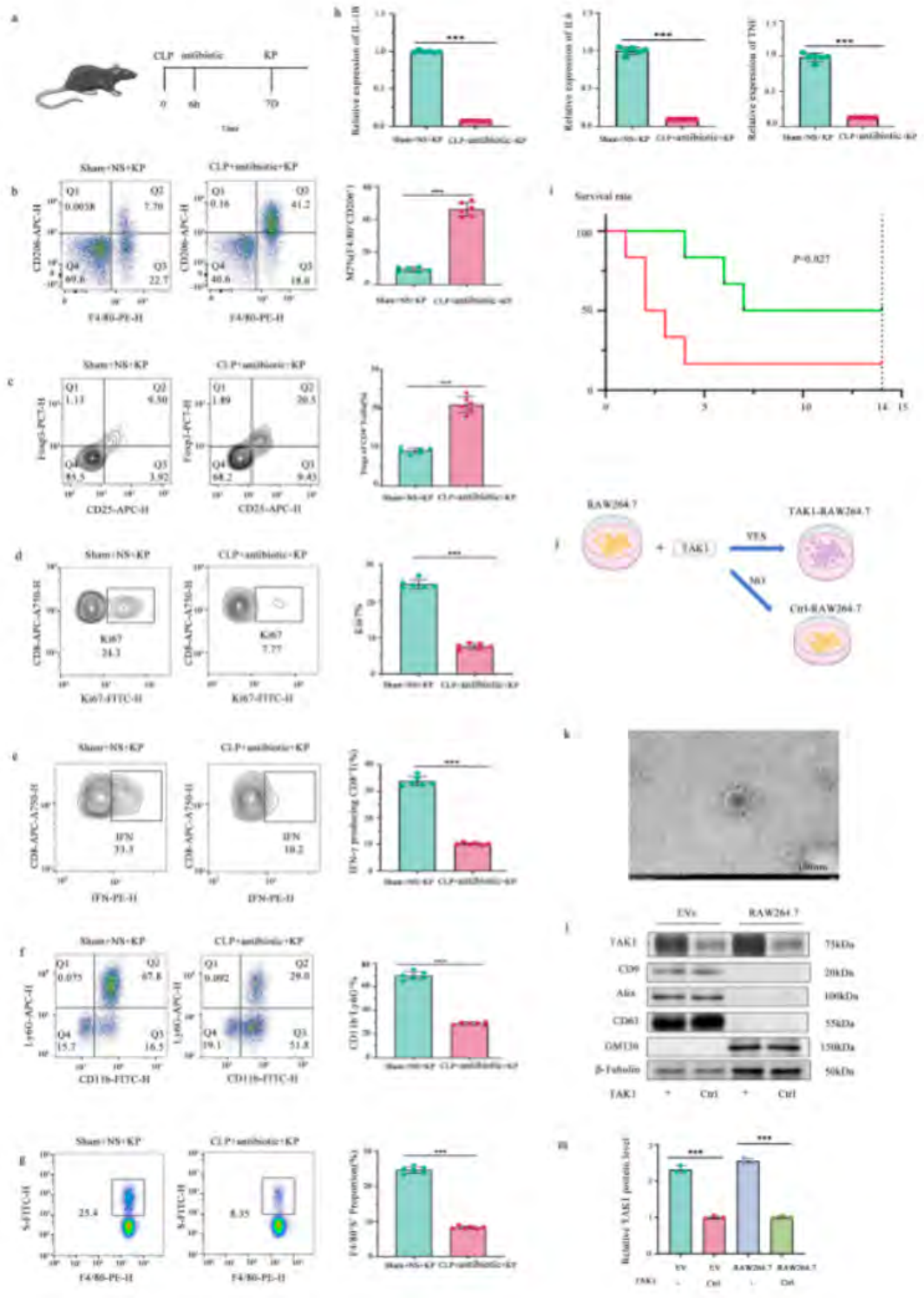
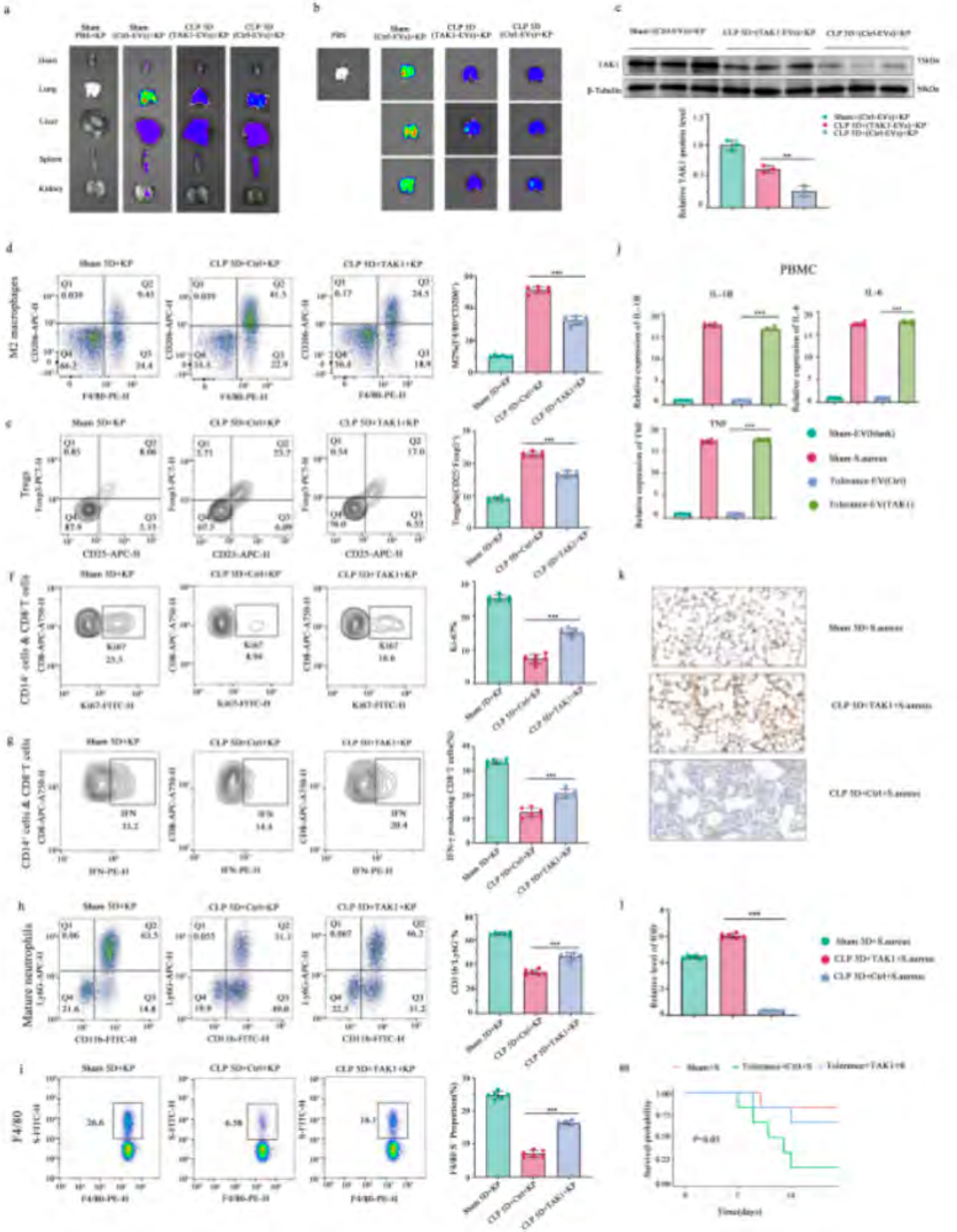
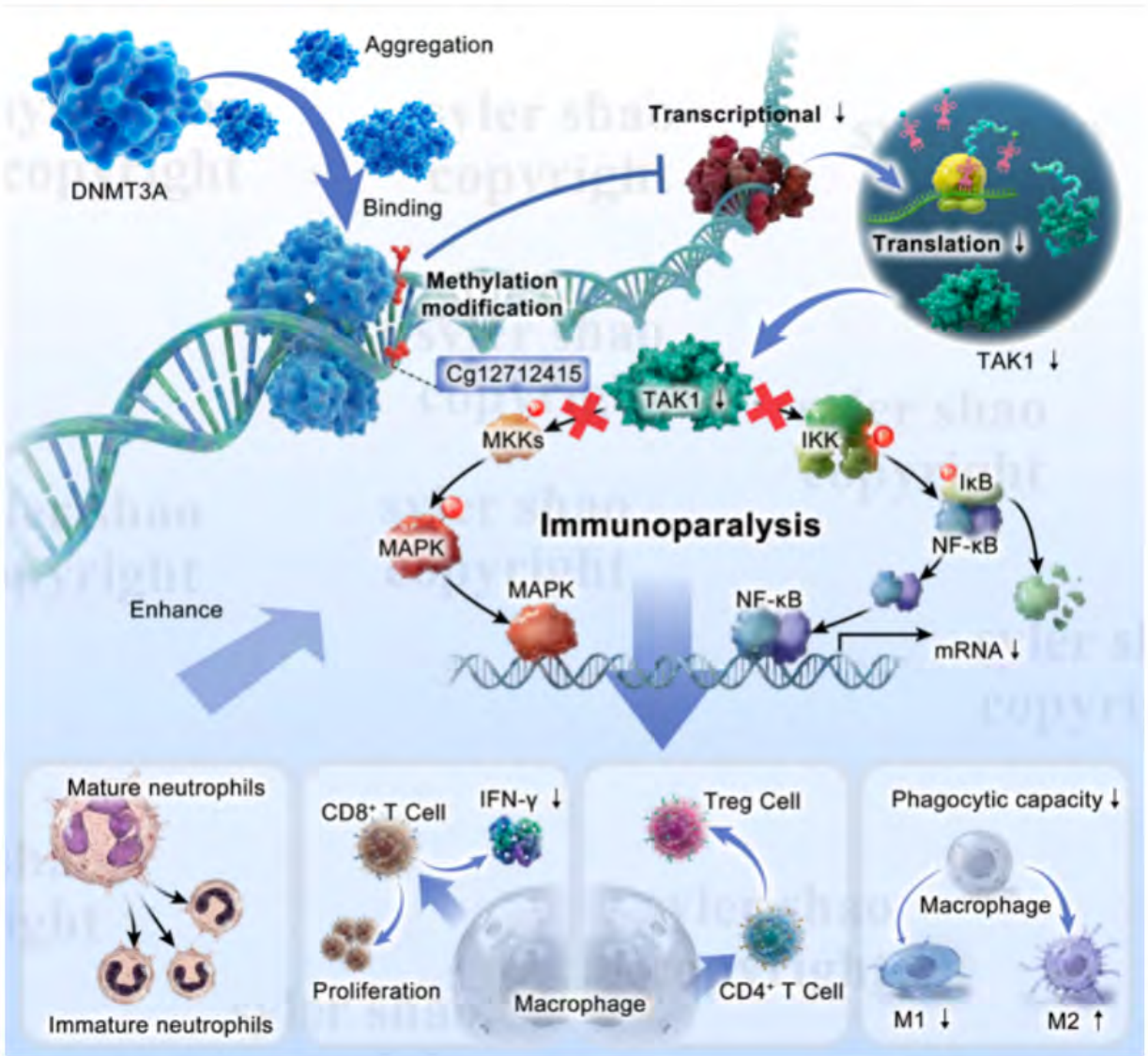


图 7




Aggregation
DNMT3A
Binding
Transcriptional ↓
Translation ↓
TAK1 ↓
Methylation modification
Cg12712415
TAK1 ↓
MKKs
IKK
IκB
NF-κB
MAPK
Immunoparalysis
MAPK
NF-κB
Enhance
mRNA ↓
Mature neutrophils
Immature neutrophils
CD8⁺ T Cell
IFN-γ ↓
Proliferation
Macrophage
Treg Cell
CD4⁺ T Cell
Phagocytic capacity ↓
Macrophage
M1 ↓
M2 ↑

类别 :// 临床研究：设计规范的各类临床研究及研究方案报告

Chronic Critical Illness and Persistent Inflammation Immunosuppression Catabolism Syndrome: A Comparative Clinical Outcomes Study

姓名：周青青，刘军

单位：南京医科大学附属苏州医院

Chronic critical illness (CCI) and persistent inflammation immunosuppression and catabolism syndrome (PICS) represent significant challenges in intensive care medicine, contributing to prolonged hospitalizations, poor functional outcomes, and increased mortality. However, the relationship between these conditions remains incompletely understood. This study aimed to investigate the clinical features, laboratory parameters, and prognostic outcomes in patients with CCI, PICS, or both conditions, while exploring whether PICS serves as an independent factor or a consequence of prolonged CCI.

This prospective observational study enrolled patients from the intensive care units (ICUs) of Suzhou Municipal Hospital and Suzhou Ninth People's Hospital between July 2021 and March 2022. Inclusion criteria comprised ICU stay ⩾ 14 days and age ⩾ 18 years. Exclusion criteria included immunosuppressant/corticosteroid use, congenital/acquired immunodeficiency, pregnancy, and refusal of informed consent. Patients were classified into four distinct groups based on established diagnostic criteria: PICS only, CCI only, combined CCI+PICS, and neither CCI nor PICS (NCCI+NPICS). CCI was defined by ICU stay ⩾ 14 days plus at least one of the following: continuous mechanical ventilation, tracheotomy, serious infection, severe trauma, or multiple organ failure. PICS was defined by persistent ICU stay ⩾ 14 days, CRP >150 μg/dL, lymphocyte count $<0.8\times10^9$/L, and albumin <30 g/L or other catabolic markers. We collected comprehensive clinical data including demographics, hospital diagnoses, severity scores (APACHE II, SOFA), inflammatory markers (CRP), immunological parameters (lymphocyte counts), nutritional indices (serum albumin), and outcomes (length of stay, secondary infections, 28-day mortality). Statistical analyses included ANOVA, Kruskal-Wallis tests, chi-square tests, and univariate and multivariate logistic regression.

Among 687 ICU admissions during the study period, 168 patients met the inclusion criteria after applying exclusion parameters: 17 with PICS only (10.1%), 71 with CCI only (42.3%), 50 with CCI+PICS (29.8%), and 30 with NCCI+NPICS (17.8%). Baseline characteristics revealed significant differences in SOFA scores (median: PICS=9, CCI=8, CCI+PICS=8.5, NCCI+NPICS=4.5; p=0.008), hospital length of stay (median days: PICS=27, CCI=24, CCI+PICS=36.5, NCCI+NPICS=20; p=0.001), and 28-day mortality rates (PICS=35.3%, CCI=21.1%, CCI+PICS=48.0%, NCCI+NPICS=26.7%; p=0.016). Multiple comparisons demonstrated that the CCI+PICS group had significantly longer hospitalizations compared to both CCI and NCCI+NPICS groups (p<0.05), as well as higher mortality than the CCI group (p<0.05). Laboratory parameters showed distinctive patterns across groups, with absolute lymphocyte counts significantly lower in PICS and CCI+PICS groups compared to CCI and NCCI+NPICS groups on days 14 and 21 (p<0.001). Similarly, albumin levels were lower in the CCI+PICS group versus CCI group on day 14 (30.15 vs. 33.90 g/L; p<0.05) and versus NCCI+NPICS on day 21 (31.00 vs. 34.60 g/L; p<0.05). CRP values were higher in the CCI+PICS group compared to both PICS and NCCI+NPICS groups on day 21 (67.70 vs. 33.58 and 21.36 mg/L, respectively; p<0.05). Respiratory and cardiovascular causes were the predominant reasons for ICU admission across all groups. In multivariate analysis, age (OR=0.94, 95%CI 0.91-0.98; p=0.001), CRP on days 14 (OR=0.99, 95%CI 0.98-1.00; p=0.001) and 21 (OR=6.15, 95%CI 1.03-36.60; p=0.046), and albumin on days 1 (OR=1.09, 95%CI 1.01-1.17; p=0.035) and 21 (OR=0.98, 95%CI 0.97-0.99; p<0.001) emerged as independent prognostic factors, while lymphocyte counts did not maintain significance in the multivariate model.

This study demonstrates a progressive worsening of clinical outcomes across the four patient groups, with the combined CCI+PICS group exhibiting the poorest prognosis. The identification of clinically isolated PICS suggests it may function as an inducement or independent factor that exacerbates CCI, rather than merely representing a consequence of prolonged critical illness. The synergistic negative impact when both conditions coexist supports a potential vicious cycle model where persistent organ dysfunction in CCI leads to PICS, which in turn further worsens organ function. Age emerged as a non-modifiable prognostic factor, potentially reflecting age-related immunosenescence and diminished compensatory mechanisms. The persistent elevation of inflammatory markers (CRP) and decline in nutritional indices (albumin) throughout the ICU stay highlight the central role of ongoing inflammation and catabolism in determining outcomes.

Our findings suggest two potential pathophysiological pathways. In the first, external threats trigger inflammation, immunosuppression, and/or catabolism leading to organ dysfunction (SOFA ⩾ 2), which if persistent, results in CCI and eventually

PICS through a vicious inflammatory-immunosuppressive-catabolic cycle. Alternatively, particularly strong external threats or poor baseline patient condition may directly trigger the complete PICS phenotype from the outset. The lymphocyte findings raise questions about current PICS diagnostic criteria, as lymphopenia did not emerge as an independent prognostic factor despite being central to the immunosuppression component of PICS.

These results have important clinical implications. Early identification of high-risk patients—particularly elderly individuals with persistent inflammatory and catabolic markers—could facilitate targeted interventions to prevent progression to the combined CCI+PICS state. Such interventions might include enhanced nutritional support, early mobilization, personalized immune modulation, and aggressive infection prevention strategies. Furthermore, the study underscores the need for multidisciplinary approaches addressing the complex interplay between persistent inflammation, immunosuppression, and catabolism in critically ill patients with prolonged ICU stays. Future research should focus on validating more precise diagnostic markers, developing predictive models for early identification, and exploring targeted therapeutic interventions that could interrupt the CCI-PICS vicious cycle and improve long-term outcomes in this challenging patient population.

类别 :// 临床研究：设计规范的各类临床研究及研究方案报告

Clinical and Prognostic Insights into Pneumocystis Pneumonia in Non-HIV-Infected Patients: A single-center Retrospective Analysis

姓名：承韶晖，周敏

单位：中国科学技术大学附属第一医院（安徽省立医院）

This study aims to characterize the clinical features, prognostic factors, and treatment outcomes of Pneumocystis pneumonia (PCP) in non-HIV-infected patients, as its incidence continues to rise in this population.

Clinical data from 375 non-HIV-infected PCP patients treated at a tertiary medical center in Anhui, China, between January 2018 and December 2022 were retrospectively analyzed.

Among the 375 patients with PCP included in the study, 271 (72.3%) were male and 104 (27.7%) were female, showing a significant gender difference ($P < 0.001$). There were 243 patients in the survival group and 132 in the non-survival group, resulting in an overall mortality rate of 32.5%. Of the 159 patients admitted to the ICU, 31 survived while 128 did not, leading to an ICU mortality rate of 80.5%.

A total of 274 (73.1%) patients (124 in the survival group and 132 in the non-survival group) had co-infections, which were identified as a significant risk factor for poor prognosis ($P < 0.001$).

A total of 146 (38.9%) patients (14 in the survival group and 132 in the non-survival group) required mechanical ventilation (both invasive and non-invasive). Patients requiring ICU admission and/or mechanical ventilation demonstrated significantly worse outcomes ($P < 0.001$), while the length of ICU stay did not significantly affect prognosis.

Regarding laboratory indicators, decreased albumin levels and increased blood urea nitrogen and/or blood glucose were identified as risk factors associated with non-survival ($P = 0.001$, $P = 0.001$, and $P = 0.03$, respectively). Other laboratory indicators were not significantly associated with prognosis.

Logistic multivariate regression analysis identified the following as independent risk factors for poor prognosis in the non-survival group: male gender (OR = 1.238, 95% CI: 1.094–1.402, $P = 0.001$), elevated serum urea nitrogen (OR = 1.167, 95% CI: 1.056–1.290, $P = 0.002$), co-infection with multiple viruses (OR = 4.605, 95% CI: 1.418–14.953, $P = 0.011$), and co-infection with cytomegalovirus (OR = 4.423, 95% CI: 1.172–16.695, $P = 0.028$).

Pneumocystis pneumonia in non-HIV-infected patients is marked by acute onset, rapid progression, severe symptoms, and a poor prognosis. Key risk factors associated with poor outcomes in this population include male gender, elevated urea nitrogen levels, co-infection with multiple viruses, and co-infection with cytomegalovirus (CMV). A thorough understanding of the disease's characteristics and prognostic factors is crucial for identifying high-risk patients, implementing preventive strategies, and making timely and informed medical decisions after disease onset.

类别 :// 临床研究：设计规范的各类临床研究及研究方案报告

Demographic and socioeconomic disparities in invasive mechanical ventilation use across China: a national cross-sectional study

姓名：Cao，Weng Li，Du Bin

单位：中国医学科学院北京协和医院

To describe the utilization, incidence, and in-hospital mortality rates of IMV and examine the association between provincial human development level (HDI) and IMV epidemiological profiles.

In this national cross-sectional study, we used data from the National Data Center for Medical Service and public databases covering 4111 hospitals in 30 provinces of mainland China, including all patients receiving IMV between Jan 1 and Dec 31, 2022. We estimated age-standardized utilization, incidence, and in-hospital mortality, stratified by age, sex, and provincial HDI stratum. Regional inequality was quantified with the Gini coefficient and HDI associations with Spearman's rank correlation.

A total of 1,334,939 IMV patients were included (mean age 60.2 years [SD 22.4]; 64.1% male). Pneumonia and influenza were the leading primary diagnoses in non-surgical patients (19.3%), while cerebrovascular diseases predominated among surgical patients (20.3%). The national age-standardized IMV incidence was 146 (95% CI: 145–147) per 100,000 population, higher in upper-middle HDI regions (155, 95% CI: 154-155) than lower-middle region (134, 95% CI: 133-135). Males had a 1.9-fold higher incidence than females (195 vs 104 per 100,000 population). IMV incidence increased progressively with age. A significant positive correlation was observed between HDI and IMV utilization (Spearman R = 0.464, P = 0.010). Gini coefficients were 0.34 and 0.33 in upper-middle and lower-middle regions, respectively. Age-standardized in-hospital mortality varied widely across provinces (range: 7%–33%) and was higher in lower-middle regions.

IMV utilization in China is shaped by pronounced demographic and socioeconomic disparities. The divergence between HDI-driven capacity and clinical need underscores the urgency of need-based critical care resource allocation, equitable infrastructure investment, and long-term capacity planning amid China's rapidly ageing population.

类别 :// 临床研究：设计规范的各类临床研究及研究方案报告

Development and evaluation of a machine learning-based risk prediction model for enteral feeding intolerance in sepsis patients

姓名：魏振港，刘聪聪，张继承

单位：山东省立医院

Early detection and prediction of enteral nutrition intolerance (EFI) are essential for effective management of septic patients. This study seeks to develop an interpretable machine learning (ML) model for predicting EFI in septic patients.

Data were collected from septic patients admitted to the ICU and receiving enteral nutrition at a tertiary hospital in Shandong Province between January 2023 and July 2025. A retrospective cohort was randomly divided into training and validation sets in a 7:3 ratio. Feature selection was performed using univariate analysis and binary logistic regression. Five independent machine learning models—Random Forest (RF), Support Vector Machine (SVM), Neural Networks, and XGBoost—were developed and evaluated based on the area under the receiver operating characteristic curve (AUROC), accuracy, sensitivity, specificity, and F1 score. The Shapley Additive Explanation (SHAP) method was applied to interpret the predictive model.

The study included 549 septic patients, with an EFI incidence of 34.6%. Six key features were selected for model development: age, APACHE II score, albumin levels, receipt of continuous renal replacement therapy, enteral nutrition start time, and intra-abdominal pressure. Among the models, the RF model demonstrated the best performance, with an AUC of 0.891, accuracy of 0.830, F1 score of 0.771, specificity of 0.869, and sensitivity of 0.763. SHAP analysis identified albumin levels as a protective factor for EFI in septic patients.

The RF model showed strong predictive performance for EFI in septic patients; however, further validation in large multicenter cohorts is needed before clinical application. Future research should focus on early identification of high-risk patients through clinical data analysis, enabling timely intervention and more efficient use of limited healthcare resources.

Development and Internal Validation of an Interpretable Machine Learning Model for Predicting 28-Day Mortality in Critically Ill Patients Undergoing Invasive Prone Position Ventilation

姓名：Yilin Wei[1#], Yongsheng Guo[2#], Xin Zheng[3#], Yuxian Wang[3*], Ming Zhong[1,3*]

单位：1 Shanghai Institute of Infectious Disease and Biosecurity, Fudan University, Shanghai, China

2 Shanghai Geriatric Medical Center, Shanghai, China

3 Department of Critical Care Medicine, Zhongshan Hospital, Fudan University, Shanghai, China.

Abstract

Background: Acute respiratory distress syndrome (ARDS) is a life-threatening form of acute hypoxemic respiratory failure with substantial mortality. Prone position ventilation (PPV) is a key supportive therapy for moderate-to-severe ARDS, yet patient outcomes remain highly heterogeneous. An interpretable prognostic model may help identify high-risk patients before PPV and support clinical decision-making.

Methods: We retrospectively enrolled ARDS patients who received PPV in the ICU of Zhongshan Hospital, Fudan University, between October 2019 and August 2025. The primary outcome was 28-day mortality. Candidate predictors measured within 24 hours before the first PPV session were collected. The dataset was split into a stratified training set (70%) and test set (30%) (seed = 123). Feature selection and model training were performed in the training set, and four models—logistic regression (LR), random forest (RF), support vector machine (SVM), and XGBoost—were developed with 5-fold cross-validation. Model discrimination and classification performance were assessed using ROC-AUC, PR-AUC, accuracy, sensitivity, specificity, precision, F1-score, and Brier score. The best-performing model was further compared with the APACHE II score to assess relative predictive performance. SHapley Additive exPlanations (SHAP) were applied to interpret the contribution of individual predictors in the optimal model.

Results: A total of 358 patients were included, with a 28-day mortality of 69.3%. XGBoost showed the best discrimination on the test set (ROC-AUC = 0.790, PR-AUC = 0.927). SHAP analysis demonstrated that age, pH, potassium, ionized calcium, platelet count (PLT), monocyte percentage (MO%), systolic blood pressure (SBP), dynamic compliance (Cdyn), and continuous renal replacement therapy (CRRT) contributed substantially to mortality prediction in the XGBoost model.

Conclusions: An XGBoost model incorporating variables collected within 24 hours before first PPV initiation showed favorable discrimination for predicting 28-day mortality in ARDS patients undergoing prone position ventilation. The model may facilitate early risk stratification and support individualized clinical decision-making by identifying patients at high risk of poor outcomes despite PPV. Further multicenter validation is required to confirm generalizability.

Keywords:

Acute respiratory distress syndrome; Prone position ventilation; Mortality; Machine learning; Prediction model; XGBoost; Intensive care unit.

Introduction

ARDS is an acute hypoxemic respiratory failure caused by pulmonary inflammation, characterized by rapid onset, severe clinical manifestations, and high mortality[1]. Global data show that ARDS accounts for approximately 10.4% of all ICU admissions, with about 40% of patients dying duringhospitalization[2]. Currently, etiological treatment, respiratory support, and anti-infective therapy constitute the main treatment strategies for ARDS[3]. As a form of respiratory support, PPV hasbeen shown to improve oxygenation and confer substantial survival benefits since it was first applied in patients with ARDS in 1976[4]. Compared with the supine position, PPV improves ventilation–perfusion (V/Q) matching, reduces intrapulmonary shunt, enhances oxygenation, and decreases overdistension in nondependent lung regions as well as cyclic collapse of alveoli independent regions[5]. Some studies have suggested that PPV may also exert beneficial effects on cardiac function. For example, in conditions of increased right ventricular load or cardiac output–dependent states, PPV may help improve venous return and pulmonary circulation perfusion

[6]. Since large randomized controlled trials such as PROSEVA demonstrated a survival benefit[7], PPV has been incorporated into multiple international guidelines and is recommended as a key therapeutic strategy for patients with moderate to severe ARDS[8]. The COVID-19 pandemic and the updated definitions of ARDS[9] have further expanded the application of PPV to non-intubated, awake patients with hypoxemic respiratory failure, making it a routine clinical intervention. However, in clinical practice, not all ARDS patients receiving PPV exhibit consistent treatment responses; some show only limited or no improvement in oxygenation after pronepositioning[10,11]. In recent years, with the rapid development of artificial intelligence and machine learningtechnologies, an increasing number of studies have utilized large-scale, multivariable data todevelop predictive models for clinical decision-making and risk stratification in critically ill patients. Some studies have attempted to predict the effects of PPV on oxygenation using demographic, physiological, and laboratory variables; however, an interpretable model for predicting 28-day mortality in ARDS patients before PPV remains lacking. Therefore, this study aims to develop and internally validate a prognostic model that estimates the individual probability of 28-day mortality at the time of first prone positioning initiation (t0) in mechanically ventilated ARDS patients, using predictors routinely available within the 24 hours preceding t0. The model is intended to support early risk stratification and shared decision-making regarding escalation strategies, rather than to infer causal treatment effects.

Methods

Study Design and Population

This was a single-center, retrospective observational cohort study including patients with ARDS admitted to the ICU of Zhongshan Hospital, Fudan University, between October 2019 and August 2025. This study was approved by the Institutional Ethics Committee (NO. B2026-019) and registered at ClinicalTrials.gov (NCT07445061). The inclusion criteria were:

(1) Diagnosis of ARDS according to the Berlin definition[12];

(2) Receipt of at least one session of PPV during hospitalization;

(3) Requirement for mechanical ventilation. The exclusion criteria were:

(1) Age <18 years;

(2) Duration of PPV <6 hours[13];

(3) Receipt of awake prone positioning;

(4) Pregnancy;

(5) ICU length of stay <2 days. To ensure sample representativeness, no selective inclusion was performed among patients receiving PPV. All patients received standardized critical care treatment and nursing. Clinical data were extracted from the hospital information system, including demographic characteristics, vital signs, laboratory results, therapeutic interventions, and ICU outcomes. This study was approved by the Ethics Committee of Zhongshan Hospital, Fudan University (B2026-019) and conducted in accordance with the Declaration of Helsinki. All data were de-identified prior to analysis to ensure patient confidentiality **(Figure 1).**

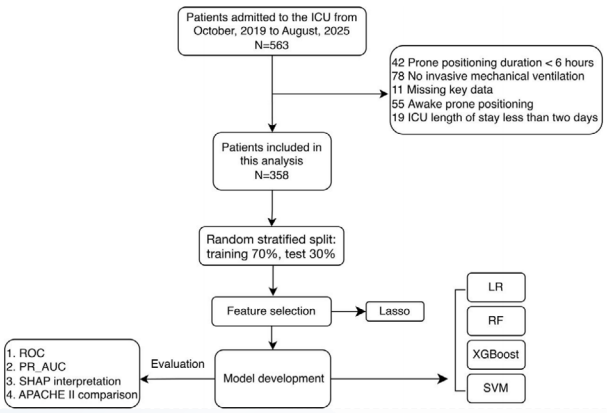


Figure 1. Study flowchart and machine learning model development.

ICU, intensive care unit; LASSO, least absolute shrinkage and selection operator; LR, logistic regression; RF, random forest; SVM, support vector machine; XGBoost, extreme gradient boosting; ROC, receiver operating characteristic; PR, precision–recall; SHAP, SHapley Additive exPlanations; APACHE II, Acute Physiology and Chronic Health Evaluation II.

Outcome Variable Index time (t0) was defined as the start time of the first prone positioning session. The primary outcome was all-cause mortality within 28 days after t0, ascertained from the hospital death registry and electronic medical records. All patients were followed up for 28 days, and no censoring occurred.

Predictor Variables Baseline clinical characteristics and key variables were collected within 24 hours before first PPV. If multiple measurements were available for the same variable, the value closest to t0 was used. These included:

(1) Demographic factors: age, sex, body mass index (BMI), major comorbidities (diabetes, hypertension, chronic lung disease, immunosuppression, etc.), and ARDS etiologies (pneumonia, aspiration, sepsis, malignancy, etc.);

(2) Disease severity: APACHE II score at ICU admission, ARDS severity classification, and COVID-19 infection status;

(3) Laboratory variables: arterial blood gas results, complete blood count, inflammatory markers, biochemical parameters, and coagulation indices prior to the first PPV session;

(4) Organ support measures: use of CRRT or extracorporeal membrane oxygenation (ECMO) before the first PPV session;

(5) Microbiological findings: presence of bacterial, fungal, or viral infections before the first PPV session;

(6) Other variables: lung compliance and CT classification (1 = focal, 2 = diffuse). All variables were measured using standard clinical procedures. Arterial blood gas analysis was performed on arterial samples, laboratory parameters were tested in the hospital’ s central laboratory, and respiratory mechanics were obtained from ventilator monitoring data.

Data Preprocessing The proportion of missing data was calculated for each variable. Variables with more than 20% missing values or with evidence of non-random missingness were excluded to reduce potential bias. For variables with a lower proportion of missing data that were assumed to be missing at random, multiple imputation (MI) was performed. Multiple imputation was conducted using five imputations (m = 5). The proportion of missing data for variables included in the LASSO analysis (missingness <20%) is presented in **Figure S1.**

To reduce the impact of multicollinearity, Pearson or Spearman correlation matrices were calculated for all continuous candidate predictors. Variance inflation factors (VIFs) were also computed. When the correlation coefficient between two variables exceeded 0.7, only the clinically more meaningful variable was retained. Variables with VIF >5 were considered to have significant multicollinearity and were either excluded or transformed (e.g., logarithmic transformation or ratio calculation). After these preprocessing steps, the final feature set was used for model development.

Feature Selection

The dataset was randomly divided into a training set and a test set at a ratio of 7:3 using stratified sampling to preserve the distribution of the outcome variable. Feature selection was performed using LASSO in the training set, and selected non-zero-coefficient variables were used for downstream modeling. By introducing an L1-norm penalty into the LR model, LASSO shrinks regression coefficients toward zero and eliminates less informative variables, thereby enabling variable selection.

Cross-validation methods include k-fold cross-validation and leave-one-out cross-validation. Since leave-one-out cross-validation may lead to overfitting in small samples, k-fold cross-validation is generally preferred [14]. Therefore, five-fold cross-validation was used to determine the optimal regularization parameter (λ) in the LASSO model. Model Development and Evaluation Four commonly used supervised machine learning algorithms were employed to build prediction models: LR, RF, SVM, and XGBoost. LR is a traditional generalized linear model with good interpretability. RF and XGBoost are tree-based ensemble methods: RF aggregates multiple decision trees using bagging, whereasXGBoost trains trees sequentially using gradient boosting; these methods are advantageous forcapturing nonlinear relationships and complex feature interactions. SVM is a margin-based

supervised learning algorithm that constructs an optimal hyperplane to maximize class separation and can effectively model nonlinear boundaries through kernel-based transformations. Within the training set, random search combined with five-fold cross-validation was used to optimize model hyperparameters, and the parameter set yielding the highest cross-validated AUC was selected. The final models were then trained using the optimal parameters and evaluated on the independent test set using receiver operating characteristic (ROC) analysis and multiple performance metrics. The AUC, accuracy, sensitivity, specificity, precision, F1-score and Brier score obtained from the test set were used to evaluate the overall performance of the models. Model performance was evaluated using both ROC-AUC and PR-AUC to provide a more informative assessment under class imbalance. Threshold-dependent metrics (accuracy, sensitivity, specificity, precision, and F1-score) were computed using a cutoff selected by the Youden index on the training set ROC curve, and then fixed for evaluation on the independent test set.

SHAP-Based Model Interpretability

To enhance interpretability, we applied SHapley Additive exPlanations (SHAP) to the best-performing model. SHAP values were computed to quantify the marginal contribution of each feature to the predicted mortality risk at both the individual and global levels, and were visualized using summary plots.

Statistical Analysis

All statistical analyses were performed using R version 4.4.2. Baseline characteristics of the study population were described using descriptive statistics. Continuous variables were presented as median (interquartile range). Categorical variables were presented as counts (percentages). Comparisons between survivors and non-survivors were conducted using the independent-samples t-test or Mann–Whitney U test for continuous variables, and the chi-square test or Fisher’ s exact test for categorical variables. All statistical tests were two-sided, and a p value <0.05 was considered statistically significant.

Results

Clinical Characteristics

A total of 358 ARDS patients who received PPV were included in this study (Table S1). Among them, 110 patients (31%) survived and 248 patients (69%) died. The cohort comprised 275 males (77%) and 83 females (23%). The median age was 71 years (IQR: 64–79), and the median body mass index (BMI) was 23.26 kg/m^2 (IQR: 20.76–25.40). The median APACHE II score was 21 (IQR: 14–27). The burden of comorbidities was relatively high, with hypertension being the most common (59%, n=213), followed by tumor (32%, n=116) and diabetes (25%, n=91). Most patients received invasive mechanical ventilation on the day of ICU admission. Some patients were initially treated with noninvasive ventilation or high-flow oxygen therapy and were subsequently intubated due to worsening oxygenation. During the course of ARDS, 29 patients required extracorporeal membrane oxygenation (ECMO) because adequate oxygenation could not be maintained with conventional therapy, and 109 patients received CRRT. Compared with survivors, non-survivors were older (72.5 vs. 68 years, $p < 0.05$), had higher APACHE II scores (21 vs. 20, $p = 0.037$), more frequent diffuse CT patterns (61% vs. 39%, $p < 0.05$), a higher rate of CRRT use (35% vs. 19%, $p < 0.05$), and a shorter ICU stay (13.9 vs.22.86, $p < 0.05$). At enrollment, significant differences were observed between survivors and non-survivors in arterial blood gas, biochemical, and hemodynamic parameters (Table S2). Compared with survivors, non-survivors had lower ionized calcium levels (1 mmol/L vs. 1.02 mmol/L, $p < 0.05$), platelet (132 $\times 10^9$/L vs. 176 $\times 10^9$/L, $p < 0.05$), and monocyte percentages (3.3% vs. 4%, $p < 0.05$). In contrast, non-survivors showed higher lactate levels (1.83 vs. 1.47 mmol/L, $p < 0.05$), international normalized ratio (1.26 vs. 1.22, $p < 0.05$), cardiac troponin T (0.05 vs. 0.02 ng/L, $p < 0.05$), interleukin-8 (87 vs. 61 pg/mL, $p < 0.05$), and systolic blood pressure (118.5 vs. 130 mmHg, $p < 0.05$). CRP levels appeared numerically higher in survivors than in non-survivors (103.35 vs. 90.00, $P < 0.05$), although the distributions overlapped considerably. This counterintuitive pattern in the univariate comparison may reflect underlying confounding factors and heterogeneity in inflammatory responses at the time of measurement.

Feature Selection Results

A total of 63 candidate variables were entered into the LASSO regression. For LASSO, five-fold cross-validation was used to determine the optimal regularization parameter (λ); the minimum cross-validation error was achieved at λ = 0.03026484 (λmin), and a more parsimonious model was obtained using the one–standard error rule at λ = 0.04819018 (λ1se). As λ increased, less informative predictors were progressively shrunk toward zero coefficients. Using λ1se, the LASSO procedure selected 9 variables

with nonzero coefficients: Age, pH, potassium, ionized calcium, PLT, MO%, SBP, Cdyn, and use of CRRT **(Figure 2)**. All subsequent machine learning models were trained and compared using these 9 selected features as inputs.

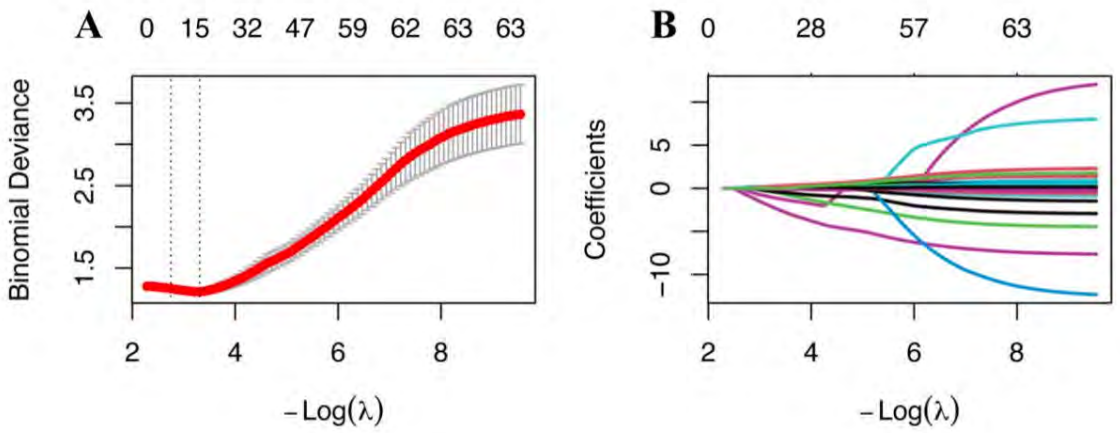


Figure 2. Feature selection.

(A) LASSO cross-validation error plot: This panel illustrates the process of selecting the optimal regularization parameter in the LASSO model using cross-validation. The left dashed line indicates the λ value corresponding to the minimum cross-validation error and the number of variables included at that point, whereas the right dashed line represents the λ value that yields the most parsimonious model within one standard error of the minimum error; (B) LASSO coefficient path plot: This panel shows the coefficient trajectories of the predictors during LASSO regression. Each colored curve represents the coefficient of a variable. As λ decreases (i.e., − log(λ) increases), the coefficients gradually emerge from zero. By combining the − log(λ) scale on the bottom axis with the number of nonzero coefficients on the top axis, the plot visually demonstrates the dynamic process of variable selection and the trade-off between regularization strength and model complexity.

Model Evaluation and Comparison

Based on the selected features, four prediction models—LR, RF, SVM, and XGBoost—were developed to predict 28-day mortality in ARDS patients receiving PPV. Five-fold cross-validation was applied within the training set for model tuning , and the corresponding ROC curves are presented in **Figure S2.** The final performance was evaluated on the test set **(Figure 3).**

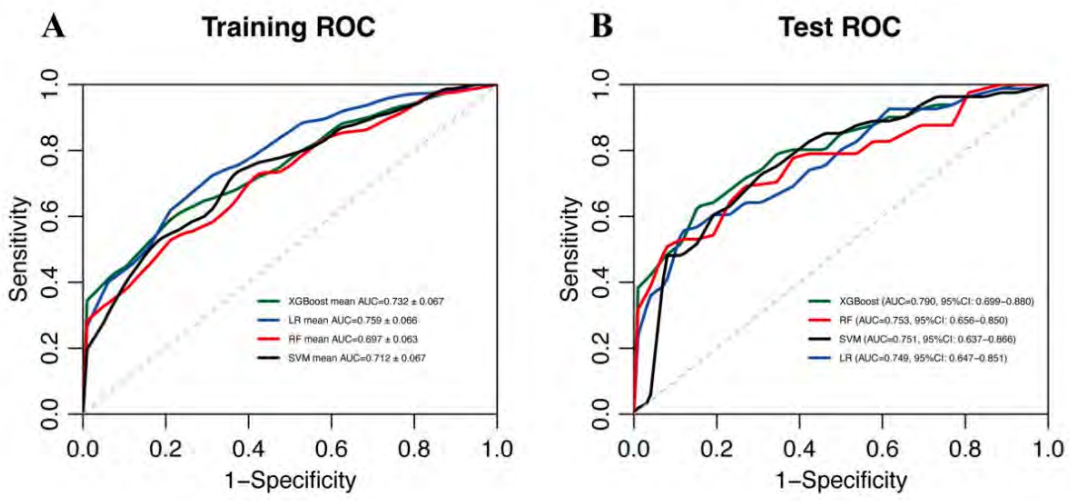


Figure 3. Model performance evaluated by receiver operating characteristic (ROC) curves.

(A) ROC curves of four machine learning models in the training set based on 5-fold cross-validation. The x-axis represents 1 − specificity and the y-axis represents sensitivity. The area under the curve (AUC) values are presented as mean ± standard deviation across the cross-validation folds. (B) ROC curves of four machine learning models in the independent test set. The

AUC value with 95% confidence intervals (CIs) are reported for each model. The diagonal dashed line indicates no discriminative ability (AUC = 0.5). Among the four models evaluated, XGBoost achieved the best performance, with an accuracy of 0.692, ROC-AUC of 0.790, precision of 0.887, and a PR-AUC of 0.927, indicating robust performance in identifying high-risk patients under class imbalance. RF demonstrated the most balanced overall performance, with an AUC of 0.753 and the highest F1-score (0.815). LR and SVM yielded comparable results (AUC: 0.749 and 0.751; F1-score: 0.743 and 0.651). Overall, all models showed acceptable discrimination, while XGBoost demonstrated relatively better predictive performance **(Table 1).**

	AUC	PR-AUC	Accuracy	Sensitivity	Specificity	Precision	F1-score	Brier
LR	0.749	0.906	0.664	0.642	0.731	0.881	0.743	0.216
RF	0.753	0.913	0.720	0.815	0.423	0.815	0.815	0.170
SVM	0.751	0.866	0.589	0.506	0.846	0.911	0.651	0.165
XGBoost	0.790	0.927	0.692	0.679	0.731	0.887	0.769	0.181

Table 1 Performance of machine learning models for predicting 28-day mortality

LR, logistic regression; RF, random forest; SVM, support vector machine; AUC, area under the receiver operating characteristic curve; PR-AUC, area under the precision–recall curve. To further evaluate the clinical utility of the model, XGBoost was compared with the APACHE II score. Compared with APACHE II, XGBoost showed higher discrimination (AUC 0.790 vs 0.610). The difference between the two AUCs was statistically significant (P < 0.05, DeLong test). These results suggest that the machine learning model provides superior predictive accuracy compared with the traditional scoring system for 28-day mortality in ARDS patients receiving PPV **(Figure4).**

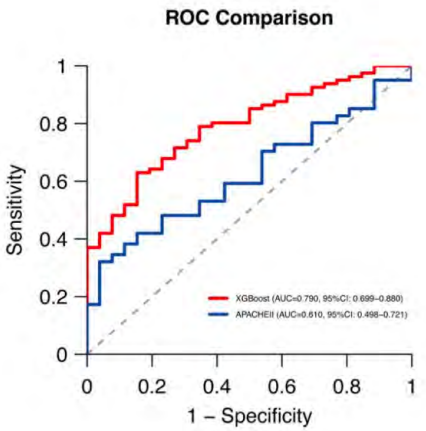


Figure 4. ROC curve comparison between the XGBoost model and the APACHE II score.

The ROC curves illustrate the discriminative performance of the two models in predicting 28-day mortality. The x-axis represents 1 − specificity, and the y-axis represents sensitivity. The diagonal dashed line indicates no discrimination (AUC = 0.5). The XGBoost model demonstrated superior predictive performance compared with the APACHE II score. AUC values are shown in the figure, and the difference between the two ROC curves was statistically significant according to the DeLong test (P < 0.05).

Variable importance and variable interpretation

SHAP analysis demonstrated that PLT was the most influential predictor in the XGBoost model, followed by Age and MO%. Potassium, Ionized Calcium, SBP, Cdyn, CRRT, and pH also showed relevant contributions, although with lower relative importance. The beeswarm plot indicated that lower PLT, lower MO%, lower Ionized Calcium, lower SBP, lower Cdyn, and lower pH were associated with positive SHAP values and increased predicted mortality risk. Conversely, advanced age and elevated Potassium levels contributed positively to mortality prediction. The use of CRRT was likewise associated with higher SHAP values, suggesting an increased predicted risk of 28-day mortality **(Figure 5).**

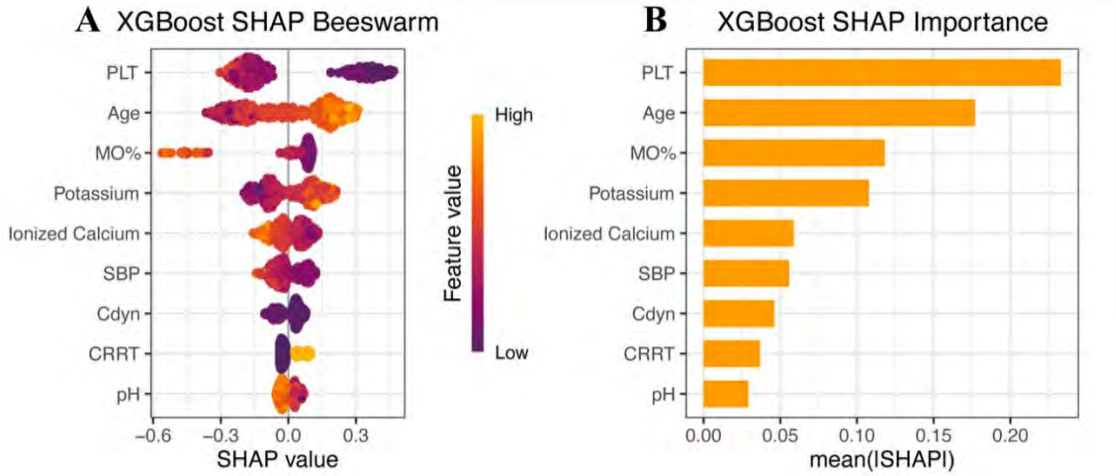


Figure 5. SHAP analysis of the XGBoost model.

(A) SHAP beeswarm plot showing the distribution of SHAP values for each feature across all patients. Each dot represents an individual observation, with color indicating the feature value; (B) SHAP importance plot showing the mean absolute SHAP values of each feature, reflecting their overall contribution to the model; PLT, platelet count; MO%, monocyte percentage; SBP, systolic blood pressure; Cdyn, dynamic lung compliance; CRRT, continuous renal replacement therapy.

Discussion

In this study, we developed a machine learning–based model to predict 28-day mortality in ARDS patients receiving PPV. Using variables obtained within 24 hours prior to PPV initiation, the XGBoost model demonstrated good discriminative performance (AUC = 0.791) with balanced accuracy, suggesting potential clinical utility for early risk stratification. Although prone positioning is widely recommended for moderate to severe ARDS [15], its survival benefit remains heterogeneous across patients. While improvements in oxygenation are frequently observed, they do not consistently translate into reduced mortality, highlighting a "physiological–clinical dissociation [16]". A meta-analysis of five randomized controlled trials involving 1,372 patients similarly concluded that although PaO_2/FiO_2 significantly improved, prone positioning was not associated with a significant reduction in mortality in ALI/ARDS patients [17]. In contrast, the PROSEVA trial demonstrated a substantial survival benefit, with a 28-day mortality of 16.0% in the prone group compared with 32.8% in the supine group, representing a 50% relative reduction in mortality [7]. More recent studies have confirmed that PPV not only improves oxygenation but also optimizes ventilation–perfusion matching and reduces overdistension in nondependent lung regions, thereby facilitating lung-protective ventilation strategies and decreasing the risk of ventilator-induced lung injury [18,19]. Based on these physiological and survival benefits, multiple guidelines now recommend PPV as a standard therapy for patients with moderate to severe ARDS [20]. However, clinical responses to PPV remain highly heterogeneous. Therefore, identifying patients at high risk of poor outcomes despite PPV in terms of survival should become a key focus of clinical assessment and management. These patients essentially represent a higher-risk subgroup, and early identification may allow clinicians to initiate more aggressive rescue therapies, such as extracorporeal membrane oxygenation (ECMO). Previous studies have explored prediction of nonresponse to prone positioning [13] or identification of ARDS subphenotypes among patients receiving PPV[21] , but these studies primarily focused on oxygenation outcomes rather than survival. The 28-day mortality rate in our cohort was substantially higher than that reported in landmark trials such as PROSEVA. This likely reflects differences in patient populations, as our study was conducted in a large tertiary referral center, where patients tend to have more advanced disease severity and a higher burden of multiorgan dysfunction. In addition, the inclusion of patients during the COVID-19 pandemic may have further contributed to the increased mortality. These factors may limit the external generalizability of the model and should be considered when interpreting the results.The model leverages variables obtained within 24 hours prior to PPV initiation. When coagulopathy or renal failure is already present, the benefit of PPV may be limited. Early identification may facilitate timely escalation of care, such as ECMO. Among the evaluated models, XGBoost achieved the best overall performance, likely due to its ability to capture nonlinear relationships and complex feature interactions while incorporating regularization to reduce overfitting. In contrast, RF showed higher sensitivity but lower specificity, possibly reflecting bias toward the majority class in this imbalanced cohort. The slightly lower

AUC observed in cross-validation compared with the test set is expected, as cross-validation provides a more conservative estimate based on out-of-fold predictions. SHAP analysis further revealed that the model primarily reflects integrated pathophysiological domains. Variables related to coagulation and inflammation (e.g., platelet count and monocyte percentage), electrolyte and metabolic disturbances (e.g., potassium, ionized calcium, and pH), and hemodynamic and organ dysfunction (e.g., SBP, dynamic compliance, and CRRT) jointly contributed to mortality prediction. Specifically, thrombocytopenia, advanced age, hyperkalemia, hypocalcemia, and hemodynamic instability were consistently associated with increased predicted risk. These findings are consistent with prior evidence indicating that multiorgan dysfunction, rather than isolated respiratory failure, is a key determinant of prognosis in ARDS. This study has several limitations. First, it was a single-center retrospective study with a relatively limited sample size, which may restrict generalizability. Second, only variables at the time of PPV initiation were included, and dynamic changes over time were not analyzed. Third, some potentially important variables, such as detailed hemodynamic indices and ventilatory parameters (e.g., driving pressure and tidal volume), were not incorporated. Finally, although COVID-19 status was recorded, it was not retained in the final model, and further validation in different subgroups is warranted.

Conclusions

In this study, we developed and internally evaluated a machine learning–based model using variables collected within 24 hours prior to PPV initiation to predict 28-day mortality in ARDS patients after PPV, demonstrating acceptable discriminative performance. The final predictor set included Age, pH, potassium, ionized calcium, PLT, MO%, SBP, Cdyn, and CRRT. Among the evaluated algorithms, XGBoost achieved the best overall performance. SHAP analysis further enhanced model interpretability by illustrating the relative importance and direction of each predictor. This model enables early risk stratification and may help identify patients at high risk of poor outcomes despite PPV, thereby supporting early risk stratification at the time of PPV initiation. Further multicenter studies are warranted to validate its generalizability and clinical applicability

Abbreviations

Abbreviation	Full term
AG	Anion gap
APTT	Activated partial thromboplastin time
ARDS	Acute respiratory distress syndrome
AUC	Area under the receiver operating characteristic curve
BA	Basophil count
BE	Base excess
BMI	Body mass index
Cdyn	Dynamic compliance
Cl^-	Chloride
CRP	C-reactive protein
CRRT	Continuous renal replacement therapy
cTnT	Cardiac troponin T
DBP	Diastolic blood pressure
EO	Eosinophil count
ECMO	Extracorporeal membrane oxygenation
F1 score	Harmonic mean of precision and recall
Hb	Hemoglobin
HCO_3^-	Bicarbonate
Hct	Hematocrit
ICU	Intensive care unit
IL	Interleukin
IL-2R	Interleukin-2 receptor
INR	International normalized ratio
K^+	Potassium
Lac	Lactate
LR	Logistic regression
LY	Lymphocyte count
Mb	Myoglobin
MO	Monocyte count
Na^+	Sodium
NE	Neutrophil count

NT-proBNP	N-terminal pro–brain natriuretic peptide
$PaCO_2$	Partial pressure of arterial carbon dioxide
PaO_2/FiO_2	Ratio of arterial oxygen partial pressure to fractional inspired oxygen
PCT	Procalcitonin
PEEP	Positive end-expiratory pressure
PLT	Platelet count
PPV	Prone position ventilation
PR	Precision–recall
PR-AUC	Area under the precision–recall curve
RF	Random forest
ROC	Receiver operating characteristic
SBP	Systolic blood pressure
SHAP	SHapley Additive exPlanations
SpO_2	Peripheral oxygen saturation
SVM	Support vector machine
t0	Index time (start time of first prone positioning)
TNF-α	Tumor necrosis factor alpha
TT	Thrombin time
V/Q	Ventilation–perfusion
WBC	White blood cell count
XGBoost	Extreme gradient boosting

Declarations

Ethics approval and consent to participate

Ethics approval was obtained from Medical Ethics Committee of Fudan University Zhongshan Hospital (NO. B2026-019). Informed consent was obtained from all individual participants. The study was conducted in accordance with the International Council for Harmonization and good clinical practice principles.

Consent for publication

Not applicable.

Availability of data and material

The datasets used and/or analyzed in the present study are available from the corresponding author on reasonable request.

Code availability

The code used to develop the models and perform the analysis is available from the corresponding author on reasonable request due to institutional and data privacy restrictions.

Competing interests

The authors declare no competing interests.

Funding

This work was supported by the Shanghai Municipal Health Commission Fund(GWVI-11.1-14), the Open Project of State Key Laboratory of Respiratory Disease (SKLRD-OP-202321), the Shanghai Key Laboratory of Lung Inflammation and Injury, the Shanghai Health Commission Clinical Research Project (202240334), and the Youth Fund of Zhongshan Hospital, Fudan University (No.2024ZSQN48).

Authors' contributions

Yilin Wei, Yuxian Wang and Ming Zhong conceived and designed the study. Yilin Wei, Yuxian Wang, Yongsheng Guo and Xin Zheng collected data. Yilin Wei analyzed and interpreted the data, and wrote the manuscript. Yuxian Wang and Ming Zhong provided

critical revisions and approved the final version of the manuscript. Yilin Wei, Yongsheng Guo, Xin Zheng, Yuxian Wang and Ming Zhong are responsible for the entire manuscript. All authors reviewed the manuscript.

Acknowledgments

The authors thank all the subjects for their participation in this study.

References

[1] Ashbaugh D G, Bigelow D B, Petty T L, et al. Acute respiratory distress in Adults[J]. Lancet, 1967, 2(7511): 319 ～ 323.

[2] Bellani G, Laffey J G, Pham T, et al. Epidemiology, Patterns of Care, and Mortality for Patients With Acute Respiratory Distress Syndrome in Intensive Care Units in 50 Countries[J]. JAMA, 2016, 315(8): 788.

[3] Meyer N J, Gattinoni L, Calfee C S. Acute respiratory distress Syndrome[J]. The Lancet, 2021, 398(10300): 622 ～ 637.

[4] PIEHL M A, BROWN R S. Use of extreme position changes in acute respiratory Failure[J]. Critical Care Medicine, 1976, 4(1): 13 ～ 14.

[5] Guérin C, Albert R K, Beitler J, et al. Prone position in ARDS patients: Why, when, how and for Whom[J]. Intensive Care Medicine, 2020, 46(12): 2385 ～ 2396.

[6] Vieillard-Baron A, Charron C, Caille V, et al. Prone Positioning Unloads the Right Ventricle in Severe ARDS[J]. Chest, 2007, 132(5): 1440 ～ 1446.

[7] Guérin C, Reignier J, Richard J-C, et al. Prone Positioning in Severe Acute Respiratory Distress Syndrome[J]. New England Journal of Medicine, 2013, 368(23): 2159 ～ 2168.

[8] Angus D C, Seymour C W, Bibbins-Domingo K. Caring for Patients With Acute Respiratory Distress Syndrome[J]. JAMA, 2023, 330(4): 368.

[9] Wick K D, Ware L B, Matthay M A. Acute respiratory distress Syndrome[J]. BMJ, 2024, 387: e076612.

[10] Coppo A, Bellani G, Winterton D, et al. Feasibility and physiological effects of prone positioning in Non-intubated patients with acute respiratory failure due to COVID-19 (PRON-COVID): A prospective cohort Study[J]. The Lancet Respiratory Medicine, 2020, 8(8): 765 ～ 774.

[11] Cinnella G, Rauseo M. Proning Responder or Not? This Is the Question*[J]. Critical Care Medicine, 2022, 50(4): 708 ～ 711.

[12] ARDS Definition Task Force, Ranieri V M, Rubenfeld G D, et al. Acute Respiratory Distress Syndrome[J]. JAMA, 2012, 307(23): 2526 ～ 2533.

[13] Yan Y, Geng B, Liang J, et al. A prediction model for nonresponsive outcomes in critically ill patients with acute respiratory distress syndrome undergoing prone position ventilation: A retrospective cohort Study[J]. Intensive and Critical Care Nursing, 2025, 86: 103804.

[14] Dong L, Yuan Y, Cai Y. Using Bagging classifier to predict protein domain structural Class[J]. Journal of Biomolecular Structure & Dynamics, 2006, 24(3): 239 ～ 242.

[15] Lai C, Monnet X, Teboul J-L. Hemodynamic Implications of Prone Positioning in Patients with ARDS[J]. Critical Care, 2023, 27(1): 98.

[16] Gattinoni L, Tognoni G, Pesenti A, et al. Effect of prone positioning on the survival of patients with acute respiratory Failure[J]. The New England Journal of Medicine, 2001, 345(8): 568 ～ 573.

[17] Abroug F, Ouanes-Besbes L, Elatrous S, et al. The effect of prone positioning in acute respiratory distress syndrome or acute lung injury: A meta-analysis. Areas of uncertainty and recommendations for research[J]. Intensive Care Medicine, 2008, 34(6):

1002 ～ 1011.

[18] Chiumello D, Carlesso E, Cadringher P, et al. Lung Stress and Strain during Mechanical Ventilation for Acute Respiratory Distress Syndrome[J]. American Journal of Respiratory and Critical Care Medicine, 2008, 178(4): 346 ～ 355.

[19] Albert R K, Keniston A, Baboi L, et al. Prone Position–induced Improvement in Gas Exchange Does Not Predict Improved Survival in the Acute Respiratory Distress Syndrome[J]. American Journal of Respiratory and Critical Care Medicine, 2014, 189(4): 494 ～ 496.

[20] Grasselli G, Calfee C S, Camporota L, et al. ESICM guidelines on acute respiratory distress syndrome: Definition, phenotyping and respiratory support Strategies[J]. Intensive Care Medicine, 2023, 49(7): 727 ～ 759.

[21] Fosset M, von Wedel D, Redaelli S, et al. Subphenotyping prone position responders with machine Learning[J]. Critical Care, 2025, 29(1): 116.

Table 1. Performance of machine learning models for predicting 28-day mortality

	AUC	PR-AUC	Accuracy	Sensitivity	Specificity	Precision	F1-score	Brier
LR	0.749	0.906	0.664	0.642	0.731	0.881	0.743	0.216
RF	0.753	0.913	0.720	0.815	0.423	0.815	0.815	0.170
SVM	0.751	0.866	0.589	0.506	0.846	0.911	0.651	0.165
XGBoost	0.790	0.927	0.692	0.679	0.731	0.887	0.769	0.181

LR, logistic regression; RF, random forest; SVM, support vector machine; AUC, area under the receiver operating characteristic curve; PR-AUC, area under the precision–recall curve.

Supplementary Table S1. Demographic and clinical characteristics of the study population

Variables	Total (n = 358)	Survivor (n = 110)	Non-survivor (n = 248)	P
Male, n (%)	275 (77)	86 (78)	189 (76)	*0.785*
Age, years	71 (64, 79)	68 (60, 76)	72.5 (65.75, 80)	***< 0.05***
BMI, kg/m²	23.26 (20.76, 25.4)	23.89 (21.48, 25.59)	22.86 (20.31, 25.39)	*0.106*
Covid-19, n (%)	81 (23)	21 (19)	60 (24)	*0.354*
ARDS severity, n (%)				*0.134*
1	35 (10)	12 (11)	23 (9)	
2	174 (49)	61 (55)	113 (46)	
3	148 (41)	37 (34)	111 (45)	
APACHE II	21 (14, 27)	20 (13.5, 23.5)	21 (14, 29)	***< 0.05***
ICU LOS	15.99 (9, 28.48)	22.86 (13.65, 37.78)	13.9 (8, 21.63)	***< 0.05***
Pneumonia, n (%)	240 (67)	67 (61)	173 (70)	*0.128*
Sepsis, n (%)	49 (14)	14 (13)	35 (14)	*0.853*
Aspiration, n (%)	50 (14)	21 (19)	29 (12)	*0.090*
Trauma, n (%)	13 (4)	4 (4)	9 (4)	*1.000*
Tumor, n (%)	116 (32)	32 (29)	84 (34)	*0.442*
HTN, n (%)	213 (59)	62 (56)	151 (61)	*0.492*
DM, n (%)	91 (25)	25 (23)	66 (27)	*0.517*
CAD, n (%)	59 (16)	13 (12)	46 (19)	*0.153*
Stroke, n (%)	52 (15)	22 (20)	30 (12)	*0.073*
COPD, n (%)	9 (3)	2 (2)	7 (3)	*0.727*
CLD, n (%)	73 (20)	21 (19)	52 (21)	*0.791*
Immunologic	48 (14)	10 (9)	38 (15)	*0.153*

disease, n (%)				
Viral infection, n (%)	112 (31)	26 (24)	86 (35)	*0.051*
Bacterial infection, n (%)	237 (66)	78 (71)	159 (64)	*0.257*
Fungal infection, n (%)	82 (23)	20 (18)	62 (25)	*0.106*
CT pattern, n (%)				***< 0.05***
1	152 (45)	60 (58)	92 (39)	
2	185 (55)	44 (42)	141 (61)	
CRRT, n (%)	109 (30)	21 (19)	88 (35)	***< 0.05***
ECMO, n (%)	29 (8)	5 (5)	24 (10)	*0.152*

Data are presented as median (interquartile range) for continuous variables and as counts (percentages) for categorical variables.

BMI, body mass index; ARDS, acute respiratory distress syndrome; APACHE II, Acute Physiology and Chronic Health Evaluation II; ICU, intensive care unit; LOS, length of stay; HTN, hypertension; DM, diabetes mellitus; CAD, coronary artery disease; COPD, chronic obstructive pulmonary disease; CLD, chronic lung disease; CT, computed tomography; CRRT, continuous renal replacement therapy; ECMO, extracorporeal membrane oxygenation.

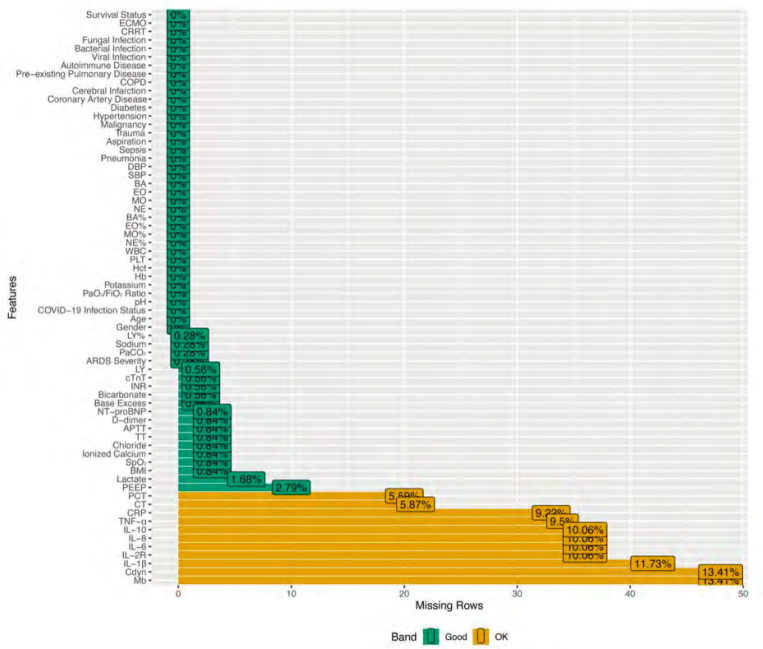
Supplementary Table S2. Laboratory findings at enrollment

Variables	Total (n = 358)	Survivor (n = 110)	Non-survivor (n = 248)	P
PH	7.37 (7.29, 7.42)	7.38 (7.32, 7.43)	7.36 (7.28, 7.42)	***<0.05***
$PaCO_2$, mmHg	43.04 (36.22, 52.07)	41.53 (36.7, 49.3)	43.78 (35.77, 52.74)	*0.299*
PaO_2/FiO_2	113.49 (82.5, 153.38)	119.5 (94, 154.62)	111.41 (80.61, 153)	*0.070*
SpO_2, %	96.8 (93, 98.5)	96.9 (93.6, 98.3)	96.8 (93, 98.6)	*0.729*
K^+, mmol/L	3.84 ± 0.62	3.68 ± 0.56	3.91 ± 0.64	***<0.05***
Na^+, mmol/L	139.4 (135.3, 144.5)	139.42 (136.07, 143.95)	139.4 (135.04, 145.04)	*0.655*
iCa^{2+}, mmol/L	1.01 (0.94, 1.07)	1.02 (0.96, 1.08)	1 (0.93, 1.06)	***<0.05***
Cl^-, mmol/L	110.03 (106.86, 115.66)	109.64 (106.75, 114.72)	110.64 (107, 116)	*0.317*
BE, mmol/L	-1.79 (-4.95, 1.61)	-1.61 (-3.87, 2)	-1.83 (-5.2, 1.02)	*0.129*
HCO_3^-, mmol/L	23.6 (20.9, 26.63)	23.6 (21.1, 27.2)	23.6 (20.8, 26.4)	*0.430*
Lac, mmol/L	1.74 (1.31, 2.38)	1.47 (1.17, 2.13)	1.83 (1.37, 2.56)	***<0.05***
AG, mmol/L	8.7 (6.2, 11.1)	8.6 (6.3, 10.97)	8.8 (6.1, 11.95)	*0.506*
CRP, mg/L	90 (66.1, 186.8)	112.45 (76.65, 225.45)	90 (61.15, 177.85)	***<0.05***
INR	1.24 (1.14, 1.38)	1.22 (1.12, 1.31)	1.26 (1.15, 1.42)	***<0.05***
TT, s	15.7 (14.6, 17)	15.35 (14.4, 16.4)	15.9 (14.7, 17.3)	***<0.05***
APTT, s	33.6 (29.3, 39.6)	32.2 (28.8, 37.2)	34.5 (29.75, 40.88)	***<0.05***
D-dimer, mg/L	5.52 (2.79, 10.02)	4.96 (2.88, 9.26)	5.6 (2.77, 10.56)	*0.636*
cTnT, ng/L	0.04 (0.02, 0.09)	0.02 (0.01, 0.05)	0.05 (0.03, 0.1)	***<0.05***
Mb, ng/mL	2 (1.15, 3.88)	1.85 (0.9, 3.15)	2.3 (1.3, 4)	***<0.05***
NT-proBNP, pg/mL	147.6 (66.25, 396.35)	91.1 (50.15, 194.5)	195 (75.2, 487.15)	***<0.05***
PCT, ng/mL	1859 (597.9, 4686.5)	1458.5 (532.02, 3287.75)	2076 (682.4, 5583)	***<0.05***
TNF-α, pg/mL	1.25 (0.33, 4.79)	1.42 (0.38, 6.71)	1.21 (0.33, 4.18)	*0.435*
IL-1β, pg/mL	6.65 (5, 13.98)	6.8 (5, 15.65)	6.6 (5, 13.4)	*0.700*
IL-2R, U/mL	1173.5 (816.75, 2135)	1123 (757.5, 1698.5)	1195 (861, 2164)	*0.214*

IL-6, pg/mL	107.5 (28.77, 448.5)	92.25 (38.2, 535.25)	120.55 (26.4, 419.25)	*0.886*
IL-8, pg/mL	78 (42, 163.5)	61 (33.5, 125)	87 (45, 184.5)	***<0.05***
IL-10, pg/mL	13.5 (6.5, 28.82)	10.8 (6, 21.1)	14.5 (7.2, 34.9)	***<0.05***
Hb, g/L	95 (74, 115)	100.5 (83, 115)	93 (71.75, 115)	***<0.05***
Hct, %	29.2 (23.1, 34.75)	30.7 (25.3, 35.27)	28.3 (22.6, 34.3)	***<0.05***
PLT, $\times10^9$/L	148 (84.5, 210.75)	176 (127, 240.75)	132 (72.5, 205.25)	***<0.05***
WBC, $\times10^9$/L	11.14 (7.35, 15.46)	10.78 (6.71, 14.16)	11.59 (7.78, 16.79)	*0.133*
NE%	91 (86.9, 94.1)	89.65 (85.35, 93.38)	91.6 (88.07, 94.35)	***<0.05***
LY%	4.6 (2.7, 7.2)	5.3 (3.52, 7.3)	4.1 (2.6, 7)	***<0.05***
MO%	3.4 (2, 5.3)	4 (2.32, 7.4)	3.3 (1.9, 4.93)	***<0.05***
EO%	0 (0, 0.38)	0 (0, 0.5)	0 (0, 0.3)	*0.245*
BA%	0.1 (0.1, 0.2)	0.1 (0.1, 0.3)	0.1 (0, 0.2)	***<0.05***
NE, $\times10^9$/L	10.05 (6.4, 13.88)	9.65 (5.85, 12.78)	10.4 (6.88, 15.55)	*0.105*
LY, $\times10^9$/L	0.5 (0.3, 0.8)	0.5 (0.3, 0.8)	0.4 (0.3, 0.8)	*0.273*
MO, $\times10^9$/L	0.36 (0.2, 0.63)	0.38 (0.22, 0.66)	0.35 (0.2, 0.62)	*0.239*
EO, $\times10^9$/L	0 (0, 0.04)	0 (0, 0.05)	0 (0, 0.03)	*0.255*
BA, $\times10^9$/L	0.01 (0.01, 0.03)	0.01 (0.01, 0.03)	0.01 (0, 0.03)	*0.415*
SBP, mmHg	123 (107, 138)	130 (116, 145.5)	118.5 (105, 135.25)	***<0.05***
DBP, mmHg	61 (54, 70)	64 (56, 74)	60 (52, 68)	***<0.05***
PEEP, cmH_2O	8 (6, 10)	8 (6, 10)	8 (6, 10)	*0.516*
Cdyn, mL/cmH_2O	30 (23, 40)	33 (26, 45.3)	29 (22, 38)	***<0.05***

Data are presented as median (interquartile range) for continuous variables and as counts (percentages) for categorical variables.

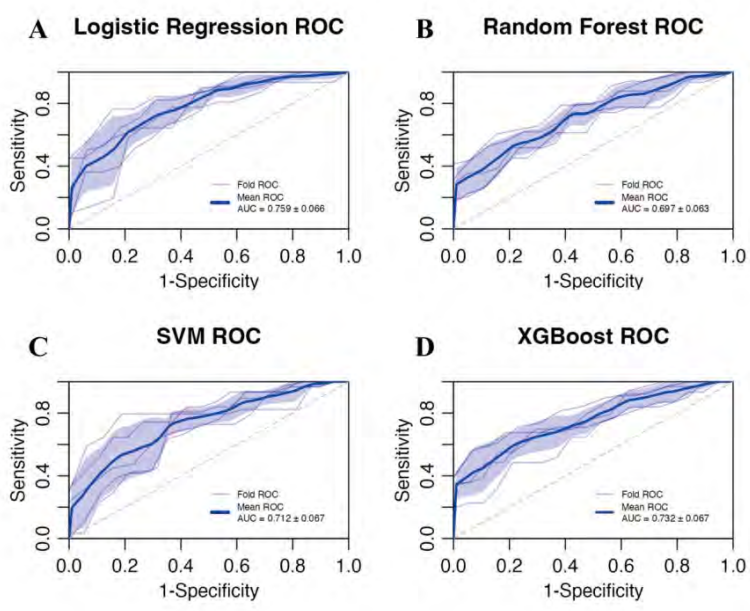
pH, potential of hydrogen; $PaCO_2$, partial pressure of arterial carbon dioxide; PaO_2/FiO_2, ratio of arterial oxygen partial pressure to fractional inspired oxygen; SpO_2, peripheral oxygen saturation; K^+, potassium; Na^+, sodium; iCa^{2+}, ionized calcium; Cl^-, chloride; BE, base excess; HCO_3^-, bicarbonate; Lac, lactate; AG, anion gap; CRP, C-reactive protein; INR, international normalized ratio; TT, thrombin time; APTT, activated partial thromboplastin time; cTnT, cardiac troponin T; Mb, myoglobin; NT-proBNP, N-terminal pro–brain natriuretic peptide; PCT, procalcitonin; TNF-α, tumor necrosis factor alpha; IL, interleukin; IL-2R, interleukin-2 receptor; Hb, hemoglobin; Hct, hematocrit; PLT, platelet count; WBC, white blood cell count; NE, neutrophil count; LY, lymphocyte count; MO, monocyte count; EO, eosinophil count; BA, basophil count; SBP, systolic blood pressure; DBP, diastolic blood pressure; PEEP, positive end-expiratory pressure; Cdyn, dynamic compliance.



Supplementary Figure S1. Missing data distribution across all variables

Bar plot showing the proportion of missing values for each variable after excluding features with >20% missingness. Each bar represents the percentage of missing observations per variable. Variables are color-coded by missingness level: green indicates low missingness (“Good”), and yellow indicates moderate missingness (“OK”).

Supplementary Figure S2. ROC curves of machine learning models in the training set based on 5-fold cross-validation



Receiver operating characteristic (ROC) curves of four models in the training set: (A) Logistic Regression, (B) Random Forest, (C) Support Vector Machine (SVM), and (D) Extreme Gradient Boosting (XGBoost). ROC curves were generated using 5-fold cross-validation. Thin lines represent ROC curves from individual folds, while the solid line indicates the mean ROC curve. The shaded area represents ±1 standard deviation. The diagonal dashed line indicates random classification. The area under the curve (AUC) is reported as mean ± standard deviation.

Development and validation of a glucose-to-calcium ratio clinical prediction model for progression to severe acute pancreatitis:A cohort study based on the MIMIC-IV and eICU databases

姓名：汤宏杰，张凤冉，李家琼，杜文婧
单位：徐州市中心医院

Abstract

Background. Most acute pancreatitis (AP) resolves without organ support, yet the minority progressing to severe acute pancreatitis (SAP) account for most deaths. Hypocalcaemia and stress hyperglycaemia both mark early metabolic derangement, so their ratio may flag progression earlier than either value alone. We tested this in two intensive care unit (ICU) databases.

Methods. We studied adults with AP and an ICU stay of at least 24 h in MIMIC-IV v3.1 (development, n=959) and the eICU Collaborative Research Database (external validation, n=1102). Time zero was ICU admission. Predictors were taken from the first 24 h and SAP was ascertained only afterwards, so that no predictor could be measured after the outcome it was used to predict. GCR was the first glucose divided by the first total calcium (both mg/dL) within that window. Adjusted odds ratios (ORs) came from logistic regression with prespecified covariates. For the model, arterial blood gas and coagulation assays were excluded from the candidate pool in advance because they are not measured routinely in every centre; remaining candidates were completed by multiple imputation by chained equations (five imputations), and LASSO and Boruta were run separately in each imputed dataset, features surviving in at least three of five by both methods being retained. Logistic regression was the primary model, with XGBoost, random forest and LightGBM as comparators, assessed by tenfold cross-validation and rendered as a nomogram. Coefficients were then applied to eICU unchanged, recalibrated, and refitted.

Results. SAP occurred in 268 of 959 patients (27.9%) in the development cohort, a higher proportion than in community AP because eligibility required ICU care. Each log-unit rise in GCR was associated with SAP after full adjustment (OR 1.99, 95% CI 1.44–2.74; P for trend <0.001), and the spline relationship rose monotonically. Seven predictors were retained: GCR, alkaline phosphatase, aspartate aminotransferase, urea, haematocrit, phosphate and white cell count. Cross-validated AUROC was 0.702 (0.666–0.739) with a calibration slope of 0.96; the nomogram C-index was 0.707 after bootstrap correction. None of the machine-learning comparators improved on this. Discrimination exceeded BISAP (0.639), Ranson (0.552) and SOFA (0.584) (DeLong P<0.05). Applied unchanged to eICU, the model gave an AUROC of 0.648 with a calibration slope of 0.595, indicating overconfident risk estimates; recalibration returned the slope to 1.00 and reduced the integrated calibration index from 0.069 to 0.037, and refitting locally gave an AUROC of 0.699. Aetiology modified the association: the GCR–SAP OR was 4.87 in biliary AP versus 1.44 in non-biliary AP (interaction P=0.003, and 0.0195 after both Bonferroni and false-discovery-rate correction). E-values were 2.49 for the point estimate and 1.88 for the confidence bound.

Conclusions. GCR measured in the first 24 ICU hours identifies patients with AP who go on to develop severe disease, most clearly in biliary AP. A seven-variable nomogram built around it discriminates moderately — better than BISAP, Ranson or SOFA, but not well enough to decide individual management alone — and transports to an independent cohort once recalibrated. Prospective evaluation is needed before clinical use.

1 Introduction

Acute pancreatitis (AP) is among the commonest gastrointestinal causes of hospital admission. Most episodes settle with supportive care, but those that progress to severe acute pancreatitis (SAP) — organ failure persisting beyond 48 h[1] — carry a far worse prognosis and account for the bulk of deaths from the disease. The difficulty is timing: by the point at which persistent organ failure declares itself, the window for pre-emptive escalation has largely closed. Bedside scores such as BISAP and Ranson were built for this purpose but discriminate only modestly, and the more accurate general severity scores incorporate organ failure itself, which limits their use as early warnings.

Two routine measurements carry early information in AP. Hypocalcaemia reflects fat saponification and inflammatory consumption of calcium and tracks with adverse outcomes[2]; stress hyperglycaemia reflects the intensity of the inflammatory

and counter-regulatory response. Because the two move in opposite directions as illness worsens, their ratio should separate progressing from resolving disease more sharply than either alone, while requiring nothing beyond a routine biochemistry panel. The glucose-to-calcium ratio (GCR) has not been evaluated for this purpose in a cohort with external validation[3].

2 Objective

We asked whether GCR in the first 24 ICU hours is associated with subsequent progression of AP to SAP, and whether a model built around it can predict that progression using only variables available in any hospital laboratory, using MIMIC-IV for development and eICU for external validation.

3 Study design

We analysed MIMIC-IV v3.1 as the development cohort[4] and the eICU Collaborative Research Database v2.0 as the external validation cohort[5], both obtained from PhysioNet under its data use agreements. Two analyses were prespecified: an association analysis of GCR and SAP, reported following STROBE[6], and a prediction model, reported following TRIPOD+AI[7]. Time zero was the first ICU admission. Predictors were drawn from [t0, t0+24 h) and SAP was ascertained only from t0+24 h to ICU discharge, so that predictors could never postdate the outcome — the design feature that makes the estimates prognostic rather than concurrent.

4 Methods

Participants, exposure and outcome. We included adults (⩾ 18 years) with diagnostic codes for AP (ICD-9 577.0; ICD-10 K85.x) whose first ICU stay lasted at least 24 h and in whom GCR could be calculated within the first 24 h, excluding repeat AP admissions for the same patient. GCR was the first in-window glucose divided by the first total calcium, both in mg/dL after unit harmonisation. Because insulin and intravenous calcium both move the ratio, we also prespecified a pre-treatment GCR using only values recorded before the first such dose. The outcome was SAP: persistent failure of the respiratory, renal or cardiovascular system for more than 48 h, adjudicated by modified Marshall/SOFA criteria[8].

Association analysis. We estimated the OR of SAP per log-unit of GCR by logistic regression, adding covariates in three prespecified steps; the fully adjusted model held age, sex, aetiology, the Charlson comorbidity index and chronic kidney disease. Dose–response was examined with restricted cubic splines. Covariates were chosen on clinical grounds before analysis rather than by stepwise selection, and variables lying on the causal path between GCR and SAP were left out to avoid over-adjustment.

Candidate predictors and feature selection. Candidates were routine measurements from the first 24 ICU hours. Three groups were removed before selection began. Components used to define organ failure were removed because they partly constitute the outcome. Arterial blood gas (pH, lactate, base excess) and coagulation assays (PT, aPTT, INR) were removed because they are not drawn routinely in every centre, and a model requiring them cannot be deployed where they are unavailable; their high missingness in eICU (pH 63%, aPTT 75%) bears this out. Candidates missing in more than 25% of patients were also dropped.

Neither LASSO nor Boruta tolerates missing data, so the remaining candidates were completed by multiple imputation by chained equations (five imputations, Bayesian ridge with posterior sampling). We used multiple imputation rather than median substitution deliberately: median filling stacks every missing value on a single point, and a tree-based selector can split on that artefact, inflating the apparent importance of incompletely measured variables. LASSO (1-SE rule) and Boruta (perc=100) were run separately in each imputed dataset. A variable counted as selected by a method if it survived in at least three of the five datasets, and the final set was the intersection of the two pooled selections. GCR was retained by protocol as the exposure under study.

Model development and validation. Logistic regression was the primary model, chosen so the result could be expressed as a nomogram and inspected coefficient by coefficient; XGBoost, random forest and LightGBM served as comparators to show what, if anything, flexible methods added. Tenfold cross-validation gave discrimination (AUROC with DeLong intervals), calibration (slope and integrated calibration index) and net benefit by decision-curve analysis. Imputation was refitted inside each training fold so that held-out data never informed it. Nomogram optimism was corrected over 1000 bootstrap replicates.

External validation, subgroups and sensitivity analyses. We applied the MIMIC coefficients to eICU three ways: unchanged, after logistic recalibration, and after refitting the model locally. This separates two questions that a single external AUROC conflates

— whether the predictor–outcome relationships hold in a new population, and whether the risk estimates themselves are numerically correct there. Effect modification was tested across six prespecified subgroups (age, sex, diabetes, aetiology, chronic kidney disease, hypertension). Six interaction tests invite false positives, so we treated them as one family and applied both Bonferroni and Benjamini–Hochberg correction, reporting corrected values throughout. Sensitivity to unmeasured confounding was quantified by E-values; as SAP was not rare, ORs were square-root-transformed to approximate risk ratios first[9].

5 Results

Of 959 patients in the development cohort, 268 (27.9%) developed SAP (Figure 1, left panel). This is higher than the roughly one in five quoted for AP overall, as expected where eligibility requires ICU care. Patients who progressed had a higher median GCR (3.0 vs 2.8), with lower total calcium, higher glucose and worse inflammatory and organ-function measurements at baseline. The association held across all three adjustment steps, reaching an OR of 1.99 per log-unit (95% CI 1.44–2.74, P<0.001) in the fully adjusted model. Risk rose across GCR quartiles (P for trend <0.001) and the spline was monotonic, with no threshold below which the relationship disappeared (Figure 2).

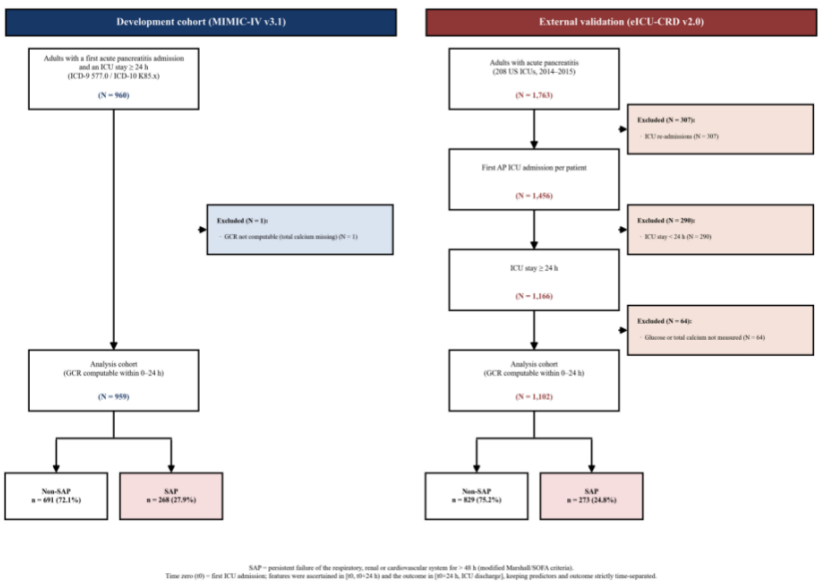


Figure 1 CONSORT participant flow diagrams. Left, development cohort (MIMIC-IV v3.1, 960 → 959); right, external validation cohort (eICU-CRD v2.0, 1763 → 1102).

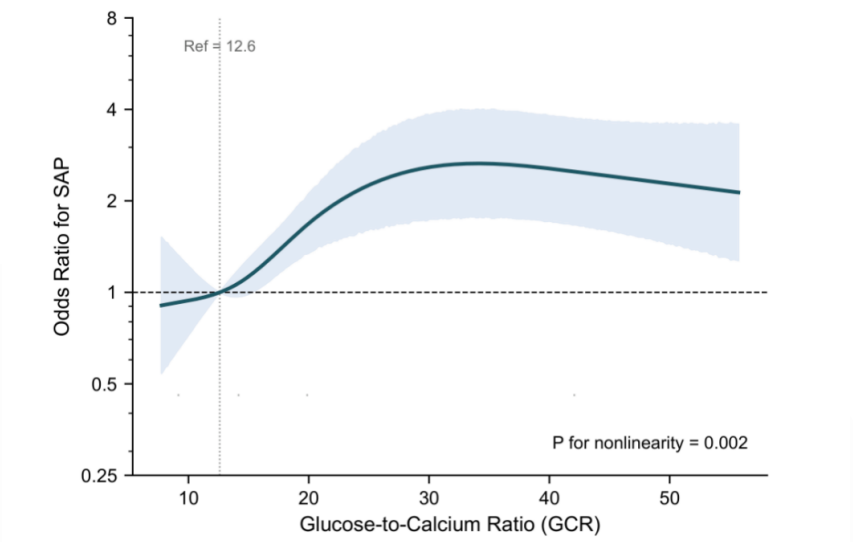


Figure 2 Restricted cubic spline for the association between GCR and SAP.

Seven predictors survived both selectors: GCR, alkaline phosphatase, aspartate aminotransferase, urea, haematocrit, phosphate and white cell count. Six were selected in all five imputed datasets by both methods and white cell count in four of five, so the set was not an artefact of any single imputation. Cross-validated AUROC was 0.702 (0.666–0.739) with a calibration slope of 0.96 and an integrated calibration index of 0.011. None of XGBoost, random forest or LightGBM differed from logistic regression on DeLong testing, so the simpler model was kept (Figure 3). As a nomogram it gave a C-index of 0.707 and a calibration slope of 0.941 after bootstrap correction (Figure 4). To check that the retained features behaved consistently under a flexible learner, we inspected SHAP values from the XGBoost comparator: phosphate and GCR ranked highest and each contributed in the same direction as its coefficient in the primary logistic model, supporting the logistic result rather than replacing it (Figure 5).

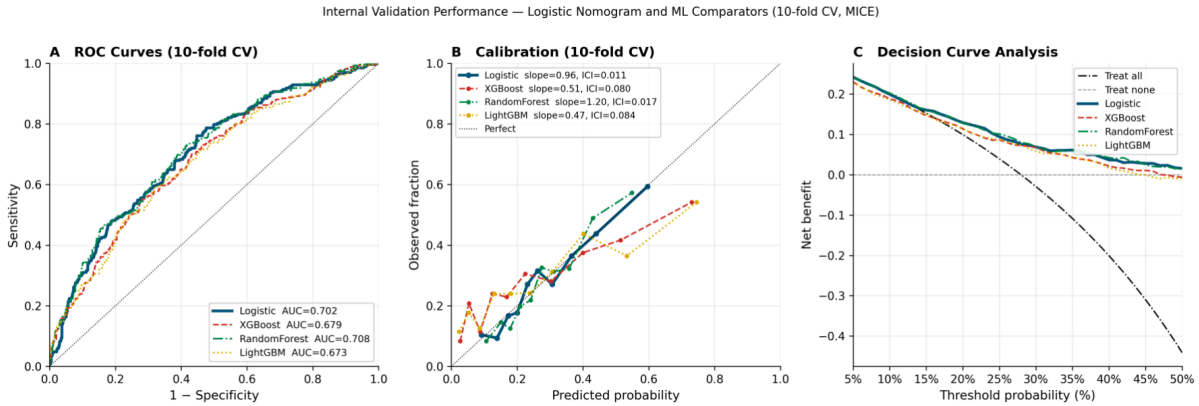


Figure 3 Composite predictive performance (ROC, calibration and decision curves; four models overlaid).

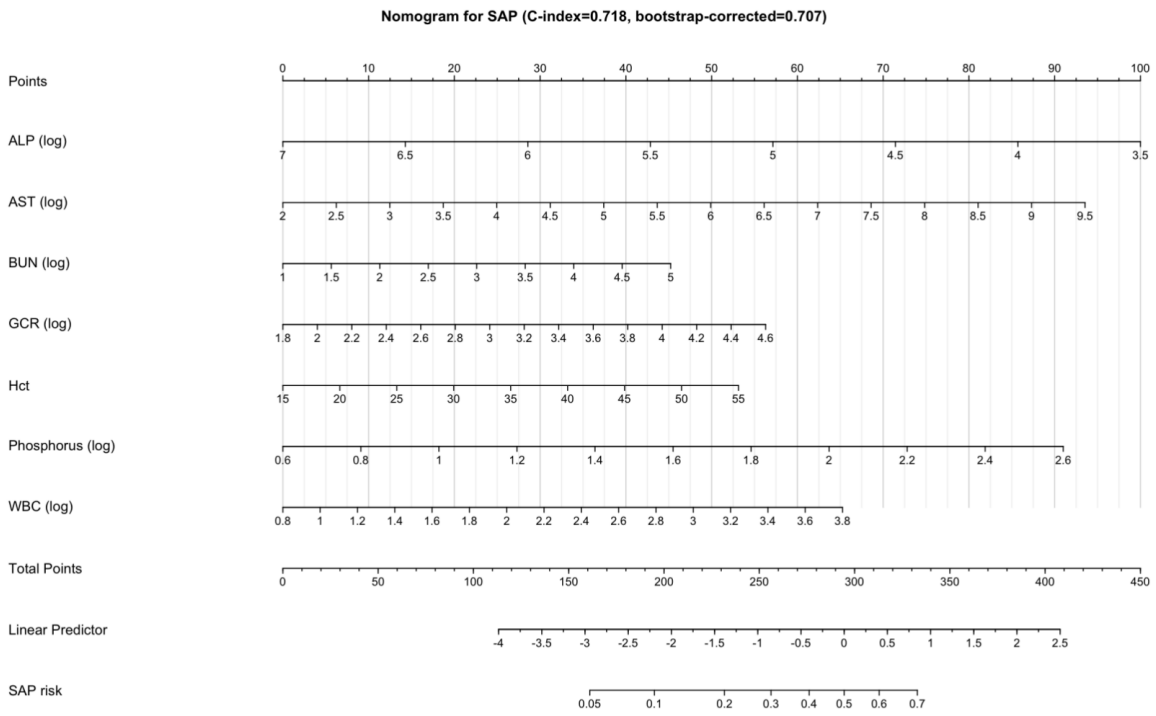


Figure 4 Nomogram for predicting SAP from the seven retained features.

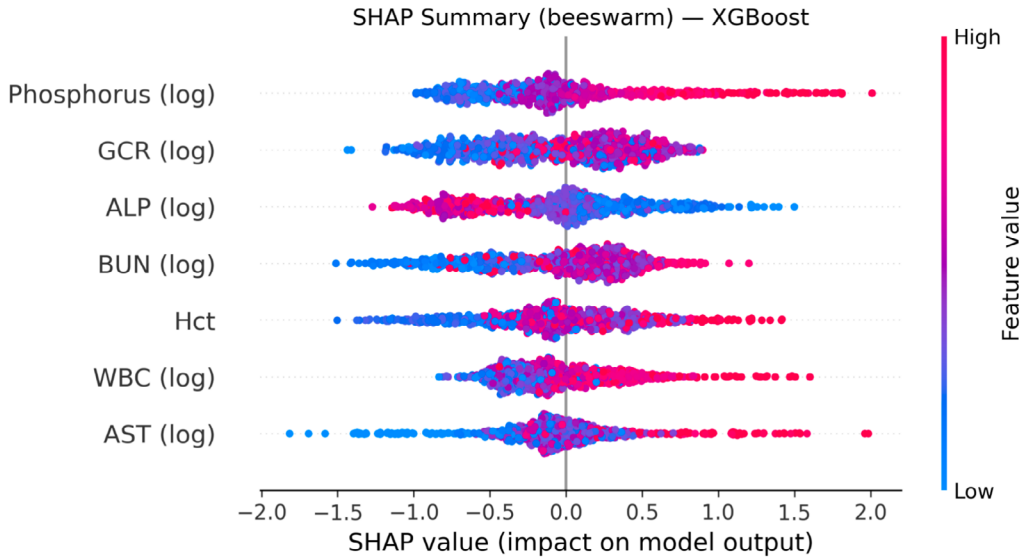


Figure 5 SHAP beeswarm plot for the XGBoost comparator model, used as a consistency check on the primary logistic regression. Feature ranking and the direction of each contribution agree with the logistic coefficients.

The nomogram discriminated better than BISAP (0.639), Ranson (0.552) and SOFA (0.584), with DeLong P<0.05 against each and positive IDI and NRI. It did not differ from APS III (0.777) or SAPS II (0.731). That comparison is not like for like: both scores contain organ-failure terms that overlap with the outcome being predicted, and both require variables collected over the whole ICU day rather than the first laboratory panel. Our model contains no organ-failure term.

Applied to eICU without modification (n=1102, SAP 24.8%; Figure 1, right panel), the model gave an AUROC of 0.648 and a calibration slope of 0.595 — it ranked patients acceptably but overstated their absolute risk. Logistic recalibration returned the slope to 1.00 and cut the integrated calibration index from 0.069 to 0.037; refitting in eICU gave an AUROC of 0.699, close to internal performance. What transports, then, is the shape of the predictor–outcome relationship; the intercept and slope do not, and would need local recalibration before the predicted probabilities could be trusted at a new site (Figure 6).

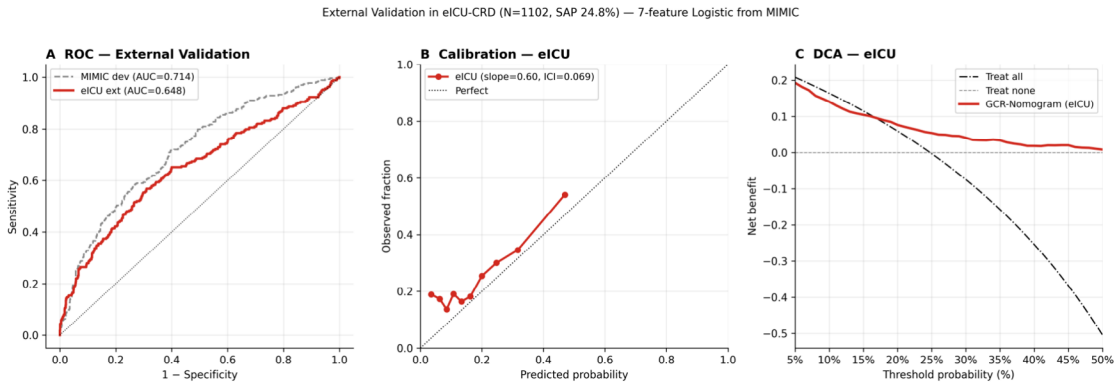


Figure 6 External validation in eICU (ROC, calibration and decision curves).

Adjusted ORs for GCR were directionally consistent across all six prespecified subgroups, and aetiology was the only significant effect modifier: the GCR–SAP association was considerably stronger in biliary than in non-biliary AP (OR 4.87 [2.40–9.86] vs 1.44 [1.00–2.08]). Treating the six interaction tests as a single family, the aetiology interaction survived correction (raw P=0.003; Bonferroni P=0.0195; BH-FDR q=0.0195). The other five interactions were null before and after correction (Figure 7).

Three sensitivity analyses bear on interpretation. Pre-treatment GCR was more strongly associated with SAP than the main exposure (OR 2.44 vs 1.99), which fits the expectation that insulin and calcium replacement pull the ratio back toward normal and thus dilute rather than create the signal. Removing phosphate lowered the AUROC from 0.702 to 0.681, so its contribution is real but not the whole model. Expanding from seven predictors to the 16-variable union changed AUROC by 0.015, which does not

justify the added measurement burden. E-values were 2.49 for the point estimate and 1.88 for the confidence bound, rising to 4.66 and 3.06 in biliary AP: an unmeasured confounder would need associations of that magnitude with both GCR and SAP to explain away what we observed.

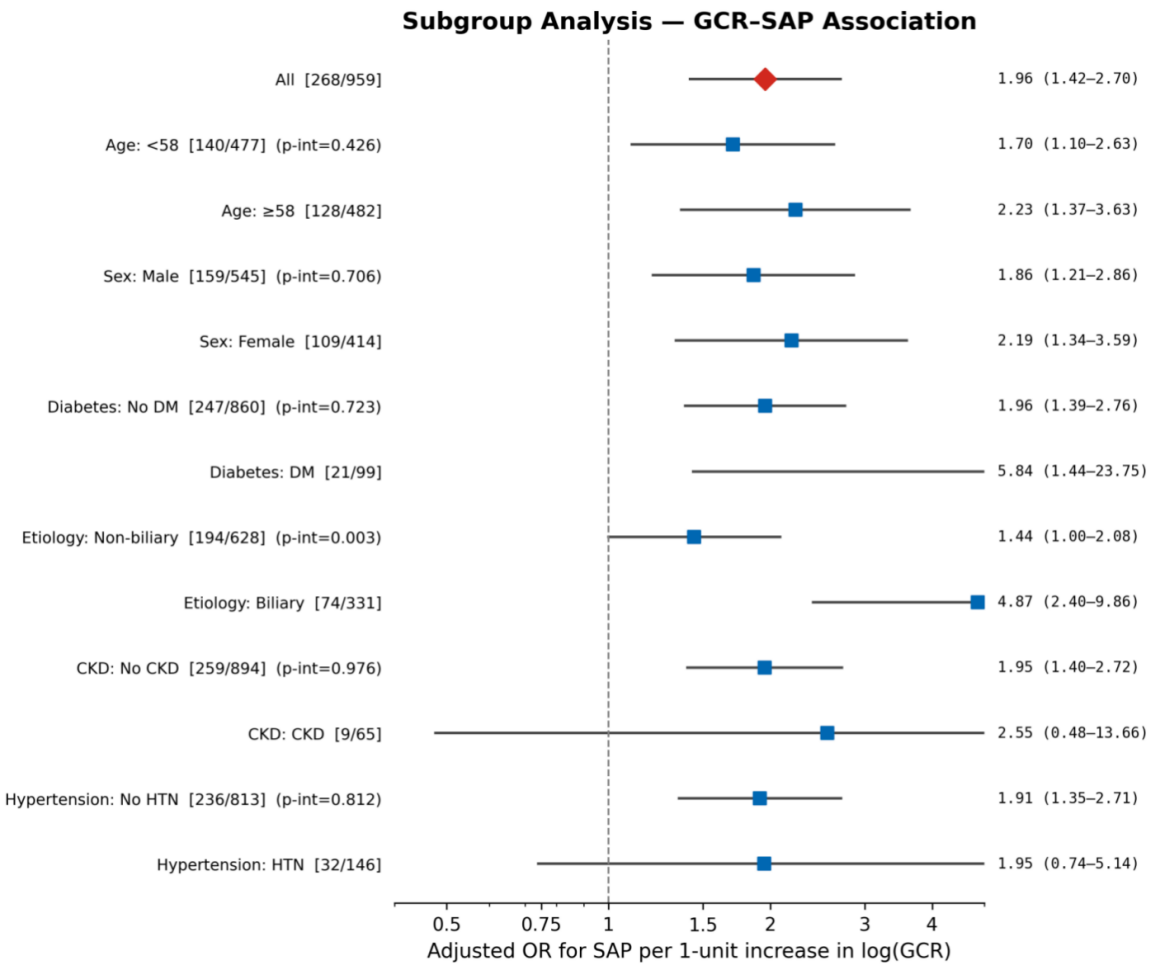


Figure 7 Forest plot of adjusted ORs for GCR across prespecified subgroups (aetiology interaction P=0.003).

6 Conclusions

Glucose-to-calcium ratio in the first 24 ICU hours is associated with subsequent progression of AP to severe disease, most strongly in biliary AP, and a seven-variable model built around it predicts progression with moderate discrimination that exceeds established bedside scores and holds up in an independent cohort after recalibration. Both inputs come from a routine biochemistry panel, which makes the ratio easy to adopt where it proves useful. Discrimination was moderate and both databases are from the United States, so the model should be recalibrated before use at other sites and prospective testing is needed to establish whether acting on the prediction changes outcome.

References

[1] Banks PA, Bollen TL, Dervenis C, et al. Classification of acute pancreatitis—2012: revision of the Atlanta classification and definitions by international consensus. Gut, 2013, 62(1): 102-111.

[2] Chen X, Huang Y, Xu Q, Zhang B, Wang Y, Huang M. C-reactive protein to serum calcium ratio as a novel biomarker for predicting severity in acute pancreatitis: a retrospective cross-sectional study. Front Med (Lausanne), 2025, 12: 1506543.

[3] Ustaalioğlu İ, Ak R. Integrating feature selection, machine learning, and SHAP explainability to predict severe acute pancreatitis. Diagnostics (Basel), 2025, 15(19): 2473.

[4] Johnson AEW, Bulgarelli L, Shen L, et al. MIMIC-IV, a freely accessible electronic health record dataset. Sci Data, 2023, 10(1): 1.

[5] Pollard TJ, Johnson AEW, Raffa JD, Celi LA, Mark RG, Badawi O. The eICU Collaborative Research Database, a freely available multi-center database for critical care research. Sci Data, 2018, 5: 180178.

[6] von Elm E, Altman DG, Egger M, Pocock SJ, Gøtzsche PC, Vandenbroucke JP; STROBE Initiative. The Strengthening the Reporting of Observational Studies in Epidemiology (STROBE) statement: guidelines for reporting observational studies. Lancet, 2007, 370(9596): 1453-1457.

[7] Collins GS, Moons KGM, Dhiman P, et al. TRIPOD+AI statement: updated guidance for reporting clinical prediction models that use regression or machine learning methods. BMJ, 2024, 385: e078378.

[8] Vincent JL, Moreno R, Takala J, et al. The SOFA (Sepsis-related Organ Failure Assessment) score to describe organ dysfunction/failure. Intensive Care Med, 1996, 22(7): 707-710.

[9] VanderWeele TJ, Ding P. Sensitivity analysis in observational research: introducing the E-value. Ann Intern Med, 2017, 167(4): 268-274.

Development of a Nomogram to Predict the Risk of Feeding Intolerance in Patients Undergoing Prone Position Ventilation

姓名：翟青晨

单位：东南大学附属中大医院

Abstract

Aim: To develop and validate a predictive nomogram for early identification of feeding intolerance (FI) in critically ill patients receiving prone position ventilation (PPV) combined with enteral nutrition (EN).

Methods: This retrospective cohort study included 644 patients who received concurrent PPV and EN support in the intensive care unit of a tertiary teaching hospital between January 2021 and December 2025. Patients were chronologically divided into a training cohort (n = 457) and a temporal external validation cohort (n = 187). Least Absolute Shrinkage and Selection Operator (LASSO) regression combined with multivariate logistic regression was used to identify independent risk factors and construct a nomogram. Model performance was evaluated by discrimination (area under the receiver operating characteristic curve, AUC), calibration (calibration plots, Brier score, and Spiegelhalter Z-test), and clinical utility (decision curve analysis and clinical impact curves).

Results: The overall incidence of FI was 39.82% in the training cohort and 41.18% in the validation cohort, with no significant difference between the two groups (P = 0.751). The daily FI rate peaked on day 2 (10.38%) and remained high through days 3–4 after EN initiation. Five independent predictors were identified: pre-existing diabetes mellitus (OR = 2.05, 95% CI: 1.23–3.42), ECMO support (OR = 2.30, 95% CI: 1.14–4.62), number of antibiotic categories (OR = 2.10, 95% CI: 1.56–2.82), cumulative prone ventilation duration (OR = 1.08, 95% CI: 1.02–1.15), and nasojejunal tube feeding (OR = 0.19, 95% CI: 0.12–0.32). The nomogram demonstrated good discriminative ability, with an AUC of 0.752 (95% CI: 0.704–0.801) in the training cohort and 0.729 (95% CI: 0.652–0.806) in the external validation cohort. Calibration curves showed satisfactory agreement between predicted and observed probabilities, and decision curve analysis confirmed superior net clinical benefit across a wide range of threshold probabilities.

Conclusion: We developed and temporally externally validated a novel nomogram for predicting FI in patients undergoing PPV. The model incorporates five routinely available clinical variables and exhibits robust predictive performance, offering clinicians a practical bedside tool for early risk stratification. This instrument may facilitate personalized EN strategies and timely preventive interventions, thereby potentially improving clinical outcomes in this high-risk population.

Keywords: prone position ventilation, feeding intolerance, predictive model, nomogram, critical care

1 Introduction

Prone position ventilation (PPV) has become a cornerstone strategy for improving oxygenation in patients with acute respiratory distress syndrome (ARDS) and severe pneumonia [1]. Concurrently, early enteral nutrition (EN) serves as a critical supportive intervention in critically ill populations, playing an essential role in preserving intestinal mucosal integrity, modulating immune responses, and reducing infectious complications [2,3]. However, the anatomical and physiological alterations induced by the prone position, compounded by the concomitant use of deep sedation and neuromuscular blocking agents, frequently impair gastrointestinal motility. Consequently, the risk of feeding intolerance (FI) increases markedly when EN is initiated in patients receiving PPV[4,5].Owing to substantial heterogeneity in FI diagnostic criteria, study populations, and regional practices, the reported incidence of FI among PPV patients varies widely, ranging from 36.09% to 82.00% across different reports[6-8]. FI not only compromises adequate caloric and protein delivery but also predisposes patients to gastric regurgitation and aspiration, ultimately exerting a detrimental effect on clinical outcomes[9,10]. Therefore, early identification of individuals at heightened risk for FI during PPV is of considerable clinical importance.

Although FI has attracted growing attention in intensive care medicine, and several risk prediction models have been developed for general critically ill populations, these existing models typically lack clinical variables specific to the prone position, such as cumulative PPV duration or the use of neuromuscular blockers[11-14]. As a result, their applicability and predictive performance in the PPV subgroup remain severely limited. To date, the literature concerning this specific population has largely concentrated

on epidemiological descriptions of FI incidence and cross-sectional analyses of isolated risk factors [5,15-23], with a notable scarcity of rigorously validated prognostic tools suitable for bedside translation. Recently, a few preliminary nomogram-based prediction models for FI in PPV patients have been proposed [6,24]; however, these efforts are substantially constrained by small sample sizes, absence of independent external validation, and omission of decision curve analysis (DCA), all of which undermine their generalizability and clinical reliability. Moreover, although some investigators have attempted to incorporate point-of-care ultrasound (POCUS) metrics of gastric motility (e.g., antral cross-sectional area) into predictive algorithms, the mechanical and spatial limitations imposed by the prone position frequently preclude adequate acoustic window acquisition, making standardized, routine bedside ultrasound monitoring impractical[25]. Thus, to our knowledge, no specific prediction model for PPV patients that simultaneously balances bedside feasibility with robust validity has been established in the international literature.

To address these knowledge gaps, we conducted a retrospective cohort study of critically ill patients receiving PPV. Using Least Absolute Shrinkage and Selection Operator (LASSO) regression combined with multivariate logistic regression, we systematically screened candidate predictors to develop and internally validate a novel nomogram for predicting FI risk in this population. Furthermore, we performed temporal external validation using an independent cohort. This study aims to provide clinicians with a visualized, individualized bedside risk-stratification tool. The implementation of this model is expected to facilitate early identification of high-risk patients during the initial phase of PPV, thereby offering an objective basis for tailoring EN regimens and implementing timely prophylactic interventions, ultimately contributing to improved clinical outcomes in critically ill patients.

2 Methods

2.1 Study Design

This retrospective cohort study was designed and conducted in accordance with the Transparent Reporting of a Multivariable Prediction Model for Individual Prognosis or Diagnosis + Artificial Intelligence (TRIPOD+AI) statement [26] (Supplementary File 1).

2.2 Participants

We retrospectively reviewed clinical data of consecutive patients admitted to the Intensive Care Unit (ICU) of a tertiary teaching hospital in Nanjing who received concurrent PPV and EN support between January 2021 and December 2025. Eligible patients were those aged 18 years or older who received mechanical ventilation in the prone position and enteral nutrition support for at least 48 hours. Exclusion criteria comprised transfer from another ICU after already initiating PPV or EN therapy, pregnancy or lactation, pre-existing chronic constipation or diarrhea prior to ICU admission, or incomplete essential clinical records.

2.3 Data Collection

2.3.1 Candidate Predictor Variables

Based on an extensive literature review and multidisciplinary expert consensus, we identified a comprehensive set of candidate predictors for FI in PPV patients, which were subsequently extracted from the electronic medical record system. All predictor variables were captured within two predefined temporal windows: at ICU admission for baseline characteristics and within the first 24 hours following initiation of concurrent PPV and EN. Demographic data included age, sex, and body mass index. Clinical severity at admission was assessed using comorbidities, the Acute Physiology and Chronic Health Evaluation (APACHE II) score, the Sequential Organ Failure Assessment (SOFA) score, and the modified Nutrition Risk in the Critically Ill (mNUTRIC) score. The worst laboratory values recorded within the first 24 hours of concurrent PPV and EN were collected, including the lowest values for oxygenation index (PaO2/FiO2), hemoglobin, and serum albumin, as well as the highest value for blood lactate. Therapeutic interventions within the same 24-hour window included continuous renal replacement therapy, extracorporeal membrane oxygenation, number of analgesic and sedative categories, use of neuromuscular blocking agents, vasopressor use, and number of antibiotic categories. Respiratory parameters included the maximum positive end-expiratory pressure. Prone position exposure was quantified as cumulative duration of actual prone positioning in hours. Enteral nutrition dynamics comprised time to EN initiation, enteral access route (nasogastric versus nasojejunal tube), maximum enteral infusion rate,and cumulative enteral feeding volume. For patients who developed FI within the first 24 hours, the latter two variables, as well as PEEP and prone duration, were calculated strictly up to the time immediately preceding FI diagnosis. Data extraction and entry were

independently performed and cross-checked by two investigators to ensure data integrity.

2.3.2 Assessment of FI

Currently, there is no universally accepted international consensus on the definition of FI. Therefore, this study adopted the clinical diagnostic criteria adapted from the Guidelines for Clinical Application of Parenteral and Enteral Nutrition for Adult Patients in China (2023 Edition) [3]. FI was diagnosed if a patient developed any of the following gastrointestinal symptoms during EN therapy that required reduction, interruption, or cessation of the infusion: (1) vomiting or regurgitation, defined as visible ejection of gastric contents from the oral cavity or retrograde backflow through the feeding tube; (2) abdominal distension, defined as patient-reported distressing bloating, physical examination showing a tympanitic and distended abdomen, or an objective increase in abdominal circumference compared with baseline measurements; (3) diarrhea, defined as liquid or unformed stools occurring at least three times within 24 hours; or (4) elevated gastric residual volume, defined as a single measurement of $\geqslant$ 250 mL within a 4-hour interval. Previous literature indicates that the incidence of FI typically peaks between days 3 and 5 after EN initiation [27]. To capture the full trajectory of FI in this high-risk population, all patients were continuously monitored using nursing charts and clinical records for the first 7 days after EN initiation. Based on these records, patients were subsequently categorized into the feeding tolerance or feeding intolerance group. For those who experienced multiple overlapping FI symptoms within this 7-day window, the time of the first documented symptom was defined as the onset of FI.

2.4 Data Processing

Variables with a missing data rate exceeding 50% were entirely excluded from the analysis to avoid bias [28]. For variables with a missing proportion below 50%, missing data were imputed using the non-parametric random forest algorithm as implemented in the missForest package in R. In our training cohort, the baseline missing rates for hemoglobin and serum albumin were 1.7% and 2.6%, respectively, and both were successfully imputed with this method. We compared the distributions and summary statistics before and after imputation. No statistically significant differences were observed, confirming that the imputation procedure preserved the original data structure (Supplementary Table S1).

2.5 Statistical Analysis

Data normality was assessed using the Shapiro-Wilk test. Normally distributed continuous variables were expressed as mean $\pm$ standard deviation and compared using the independent-samples t-test, while non-normally distributed continuous data were expressed as median with interquartile range and analyzed using the Mann–Whitney U test. Categorical variables were expressed as absolute frequencies and percentages and evaluated using the chi-square test, with Fisher’ s exact test or continuity-corrected chi-square tests applied when expected cell counts fell below standard thresholds.To prevent overfitting and address potential collinearity among the high-dimensional clinical dataset, the Least Absolute Shrinkage and Selection Operator (LASSO) regression model with 10-fold cross-validation was applied for variable screening, and those predictors with non-zero coefficients were subsequently entered into a multivariate logistic regression analysis to identify independent risk factors for FI. Based on the regression coefficients from the multivariate model, a visualized bedside nomogram was constructed. The performance of the nomogram was rigorously appraised in both the training cohort and the independent temporal external validation cohort across three core dimensions: discrimination, calibration, and clinical utility. Discriminative ability was quantified using the area under the receiver operating characteristic curve (AUC), with an AUC exceeding 0.70 signifying acceptable-to-good discriminative accuracy. Calibration was assessed via calibration curves plotting predicted probabilities against observed outcomes, supplemented by calculation of the Brier score, maximum error (Emax), average error (Eavg), and the Spiegelhalter Z-test (S:p) to verify goodness-of-fit. Clinical net benefit was evaluated using decision curve analysis across a spectrum of threshold probabilities, and further illustrated by clinical impact curves to visually depict the expected rate of true positives versus predicted high-risk classifications. All statistical analyses, modeling, and visualization were performed using R software version 4.5.2, with a two-sided $P < 0.05$ considered statistically significant.

2.6 Ethical Considerations

This study was approved by the Institutional Ethics Committee of Southeast University Zhongda Hospital (Approval Number: 2024ZDSYLL412-P01) and conducted in strict adherence to the ethical tenets of the Declaration of Helsinki. Owing to the retrospective nature of the study utilizing fully de-identified and anonymized clinical data, the requirement for written informed

consent was waived by the committee. Patient confidentiality was strictly protected throughout the investigation.

3 Results

3.1 Baseline Characteristics of Enrolled Patients

A total of 644 patients were enrolled and chronologically split into a training cohort of 457 patients and a temporal external validation cohort of 187 patients. The overall incidence of FI was 39.82% (182/457) in the training set and 41.18% (77/187) in the validation set, with no statistically significant difference between the two cohorts ($x2= 0.10$, $P = 0.751$). As shown in Supplementary Table S2, significant inter-cohort differences were observed in several clinical variables, including mNUTRIC score, maximum enteral feeding rate, 28d-ICU-free days, and in-ICU mortality (all $P < 0.05$), providing a rigorous test of the real-world generalizability of our predictive model. Table 1 summarizes the baseline characteristics stratified by FI status within the training cohort. Several indicators, including age, mean prone duration, continuous renal replacement therapy, extracorporeal membrane oxygenation, and neuromuscular blocking agents, differed significantly between the FI and non-FI subgroups (all $P < 0.05$).

3.2 Daily FI Trend Within the First 7 Days After EN Initiation

As illustrated in Figure 1, the daily percentage of FI demonstrated an initial rise followed by a gradual fall across the first 7 EN days. The baseline FI rate was 4.07% on day 1, reaching its maximum at 10.38% on day 2. High FI rates persisted on day 3 (9.85%) and day 4 (8.28%), before a continuous downward trend emerged starting on day 5, with FI proportions falling to 3.41%, 2.75%, and 1.09% on days 5, 6, and 7, respectively. Episodes of FI were predominantly concentrated within days 2 to 4 of EN, with subsequent steady declines in incidence thereafter.

3.3 Variable Selection and Nomogram Construction

To construct the risk prediction model in a rigorous manner, we first performed LASSO regression with 10-fold cross-validation on all potential characteristic parameters within the training cohort (Figure 2). Under the optimal λ value corresponding to minimum deviance, five predictors with non-zero coefficients were retained in the final model: pre-existing diabetes mellitus, ECMO support, number of antibiotic categories, cumulative prone ventilation duration, and enteral feeding route. Subsequent multivariate logistic regression analysis (Table 2) confirmed that all five variables were independent risk factors for FI (all $P < 0.05$). Among these, pre-existing diabetes mellitus (odds ratio [OR] = 2.05, 95% confidence interval [CI]: 1.23–3.42), ECMO support (OR = 2.30, 95% CI: 1.14–4.62), treatment with a greater number of antibiotic categories (OR = 2.10, 95% CI: 1.56–2.82), and prolonged cumulative prone ventilation duration (OR = 1.08, 95% CI: 1.02–1.15) were independently associated with increased FI risk. In contrast, post-pyloric nasojejunal tube feeding served as a strong protective factor against FI (OR = 0.19, 95% CI: 0.12–0.32). Based on the regression coefficients derived from the multivariate model, a visualized nomogram was established to enable bedside individualized quantitative estimation of FI risk probability (Figure 3).

3.4 Model Performance

The nomogram exhibited satisfactory discriminative performance, achieving an AUC of 0.752 (95% CI: 0.704–0.801) in the training cohort and 0.729 (95% CI: 0.652–0.806) in the temporal external validation cohort, both exceeding the conventional threshold of 0.7 (Figure 4). Notably, the AUC remained stable, showing only a slight decrease in the external cohort despite substantial baseline differences compared with the training set, demonstrating robust temporal generalizability. Calibration metrics, including the Brier score, Emax, Eavg, and the Spiegelhalter Z-test, all indicated good agreement between predicted and observed risks in both cohorts (Figure 5). A mild overestimation at lower predicted probabilities was observed in the training set but was largely mitigated in the external validation cohort, further confirming the reliability of the nomogram. Regarding clinical utility, decision curve analysis demonstrated that the net benefit of our model surpassed that of the "treat all" and "treat none" strategies across the commonly used threshold probability range of approximately 0.1 to 0.8 (Figure 6). Furthermore, clinical impact curves (CICs) visually demonstrated that as the risk threshold increased, the predicted number of high-risk patients closely matched the actual number of true positive events in both cohorts (Figure 7). This further confirmed reasonable risk stratification performance, collectively supporting the model’ s practical value for bedside clinical nutrition decision-making.

4. Discussion

In this retrospective cohort study of 644 patients receiving PPV with concurrent EN, we developed and temporally externally validated a novel clinical nomogram for predicting the risk of FI. The overall FI incidence in our cohort was 40.22%. The final model incorporated five independent predictors: a history of diabetes mellitus, ECMO support, the number of antibiotic categories, cumulative PPV duration, and the route of enteral feeding. Exhibiting robust predictive performance and satisfactory temporal generalizability, this model provides a reliable bedside tool for early risk stratification in this highly susceptible patient population.

Notably, our study revealed a high incidence of FI in PPV patients, with a temporal trajectory distinctly different from that of the general critically ill population. While existing literature indicates that the onset of FI in ICU patients typically peaks between days 3 and 5 after EN initiation[29-31], the peak incidence in our PPV cohort was markedly advanced to days 2 through 4, reaching a maximum of 10.38% on day 2. This earlier onset and accelerated progression are primarily attributable to the compounding effects of positional alterations. The prone position inherently induces significant anatomical and physiological changes; when coupled with the deep sedation[32,33] and neuromuscular blocking agents routinely required during PPV, it profoundly exacerbates the suppression of gastrointestinal motility, thereby precipitating an earlier onset of gastrointestinal dysfunction.

Our final model included five readily available clinical indicators. Cumulative prone positioning duration (OR = 1.08) was identified as a risk factor, likely reflecting sustained abdominal compression that elevates intra-abdominal pressure and chronically impairs gastrointestinal motility[4,34]. Diabetes mellitus (OR = 2.05) predisposes patients to gastric retention, as pre-existing autonomic neuropathy and delayed emptying are further exacerbated by the prone position[35,36]. In contrast, nasojejunal feeding (OR = 0.19) was protective by bypassing the stomach and directly mitigating reflux and intragastric pressure elevation[37]. ECMO support (OR = 2.30) denotes severe circulatory failure, which compromises intestinal mucosal perfusion and barrier integrity, synergistically worsening splanchnic ischemia already induced by prone-related abdominal compression[38,39]. The number of antibiotic categories (OR = 2.10) reflects gut microbiota disruption and direct mucosal irritation, potentially precipitating diarrhea and dysmotility, particularly when basal motility is reduced by positioning[40].

Regarding model performance and clinical utility, our constructed nomogram demonstrates substantial advantages. The model exhibited satisfactory discriminative ability, achieving AUC values of 0.752 and 0.729 in the training and validation cohorts, respectively, alongside excellent calibration. Furthermore, DCA and CIC confirmed its superior net clinical benefit across a broad range of threshold probabilities (0.1 to 0.8). A paramount strength of this model is its bedside feasibility: all five predictors are routinely acquired from daily ICU records without the need for additional invasive procedures or specialized assessments. In clinical practice, healthcare professionals can utilize this visualized tool to rapidly quantify the individualized probability of FI during the early phase of EN initiation. For those identified as high-risk, clinicians can proactively implement tailored interventions, such as early placement of a nasojejunal tube for post-pyloric feeding, adjustment of enteral infusion rates, or prompt administration of prokinetic agents, thereby mitigating risks and improving patient outcomes.

Limitations

Nevertheless, several limitations must be acknowledged to appropriately frame the interpretability and generalizability of our findings. First, given the retrospective and single-center nature of the design, the potential for selection bias and unmeasured confounding cannot be entirely excluded, despite the execution of temporal external validation. Multicenter prospective studies are imperatively required to confirm the model's generalizability across diverse geographic regions and healthcare systems. Second, the absence of a universally accepted gold standard for diagnosing FI remains a persistent challenge; the subjective assessment of certain symptoms, particularly abdominal distension, may introduce inter-observer variability. Third, because clinical practices and treatment protocols can vary considerably across different institutions, local recalibration of the model is strongly recommended prior to widespread external deployment. Ultimately, as with any prognostic tool, this nomogram is intended to serve as a valuable clinical adjunct rather than a substitute for professional medical decision-making. Its definitive clinical impact relies on its careful integration into standardized, multidisciplinary nutritional care pathways.

5. Conclusion

In conclusion, we successfully developed and temporally validated a novel nomogram to predict the risk of feeding intolerance in critically ill patients receiving prone position ventilation. By integrating five readily accessible clinical variables, including a history

of diabetes mellitus, ECMO support, the number of antibiotic categories, cumulative prone ventilation duration, and the route of enteral feeding, the model demonstrated robust discrimination, excellent calibration, and substantial clinical utility. This visual, individualized bedside instrument empowers clinicians to perform early risk stratification, facilitating the timely implementation of tailored enteral nutrition strategies and proactive preventative measures. Ultimately, this tool holds the potential to improve clinical outcomes in this highly vulnerable population, though future multicenter prospective studies are warranted to firmly establish its generalizability across diverse healthcare settings.

Table 1. Baseline characteristics of the training cohort stratified by feeding intolerance status.

Variables	Total (n = 457)	Non-FI group (n = 275)	FI group (n = 182)	P
Age(years), Mean ± SD	66.13 ± 15.55	67.35 ± 15.18	64.29 ± 15.95	0.040
Gender, n (%)				0.221
Male sex	327 (71.55)	191 (69.45)	136 (74.73)	
Female sex	130 (28.45)	84 (30.55)	46 (25.27)	
BMI(kg/m^2), Mean ± SD	23.87 ± 4.62	23.83 ± 4.93	23.93 ± 4.13	0.815
Prone duration(hour), Mean ± SD	13.00 ± 3.47	12.64 ± 3.33	13.56 ± 3.61	0.005
PaO_2/FiO_2(mmHg), M (Q_1, Q_3)	195.60 (124.20, 245.30)	203.50 (125.05, 250.10)	189.70 (123.90, 235.47)	0.453
PEEP(cmH_2O), M (Q_1, Q_3)	10 (8, 12)	10.00 (8, 12)	10(8, 12)	0.690
APACHE II score, M (Q_1, Q_3)	22 (17, 27)	22.00 (17, 28)	21 (16, 26)	0.209
SOFA score, M (Q_1, Q_3)	9 (6,12)	9(6,12)	9(6, 11)	0.834
mNUTRIC score, M (Q_1, Q_3)	5 (4, 6)	5(4, 6)	5 (4, 6)	0.916
Comorbid conditions, n(%)				
Hypertension	230 (50.33)	132 (48.00)	98 (53.85)	0.221
Cerebrovascular disease	154 (33.70)	98 (35.64)	56 (30.77)	0.281
Diabetes mellitus	149 (32.60)	89 (32.36)	60 (32.97)	0.893
Coronary artery disease	100 (21.88)	55 (20.00)	45 (24.73)	0.232
CRRT, n(%)	145 (31.73)	77 (28.00)	68 (37.36)	0.035
ECMO, n(%)	52 (11.38)	18 (6.55)	34 (18.68)	<0.001
Muscle relaxants,n(%)	76 (16.63)	38 (13.82)	38 (20.88)	0.047
Vasopressors,n(%)	371 (81.18)	223 (81.09)	148 (81.32)	0.951
Categories of Analgesics and/or Sedatives,n(%)				0.410
1	78 (17.07)	47 (17.09)	31 (17.03)	
2	192 (42.01)	123 (44.73)	69 (37.91)	
3	156 (34.14)	86 (31.27)	70 (38.46)	
4	31 (6.78)	19 (6.91)	12 (6.59)	
Categories of Antibiotics, n(%)				<0.001
0	35 (7.66)	28 (10.18)	7 (3.85)	
1	169 (36.98)	120 (43.64)	49 (26.92)	
2	207 (45.30)	115 (41.82)	92 (50.55)	
3	46 (10.07)	12 (4.36)	34 (18.68)	
Hb(g/L), Mean ± SD	97.04 ± 21.61	96.01 ± 21.76	98.60 ± 21.35	0.209
ALB(g/L), Mean ± SD	31.24 ± 5.06	31.35 ± 4.70	31.07 ± 5.57	0.570
Lac(mmol/L), Mean ± SD	1.90 (1.30, 2.50)	1.90 (1.40, 2.50)	1.80 (1.20, 2.40)	0.195
EN within 48h, n(%)	396 (86.65)	236 (85.82)	160 (87.91)	0.519
EN infusion rate(ml/h), M (Q_1, Q_3)	50(50, 75)	50 (50, 75)	50 (50, 75)	0.596

EN volume(ml/d), M (Q_1, Q_3)	666.65 (449.17, 848.33)	700.00 (475.00, 850.42)	633.75 (440.00, 820.83)	0.369
Types of enteral feeding tubes, n(%)				<0.001
Nasogastric tube	284 (62.14)	140 (50.91)	144 (79.12)	
Nasojejunal tube	173 (37.86)	135 (49.09)	38 (20.88)	
28-d ICU-free days, M (Q_1, Q_3)	0.00 (0.00, 7.14)	0.00 (0.00, 9.06)	0.00 (0.00, 4.04)	0.008

t: t-test, Z: Mann-Whitney test, χ^2: Chi-square test

SD: standard deviation, M: Median, Q_1: 1st Quartile, Q_3: 3rd Quartile

Abbreviations: FI,Feeding Intolerance; BMI, Body Mass Index; PEEP,Positive End-Expiratory Pressure; APACHE II, Acute Physiology and Chronic Health Evaluation II; SOFA, Sequential Organ Failure Assessment; mNutric, Modified Nutrition Risk in the Critically Ill ; Hb, hemoglobin; ALB, Albumin; Lac, Lactate; ECMO, Extracorporeal Membrane Oxygenation; CRRT, Continuous Renal Replacement Therapy; EN, Enteral nutrition; ICU, Intensive Care Unit.

Table 2. Multivariable logistic regression analysis of independent risk factors for feeding intolerance.

Variables	**β**	**S.E**	**Z**	**P**	**OR (95%CI)**
Diabetes mellitus	0.72	0.26	2.76	0.006	2.05 (1.23 ~ 3.42)
ECMO	0.83	0.36	2.33	0.020	2.30 (1.14 ~ 4.62)
Antibiotics	0.74	0.15	4.92	<0.001	2.10 (1.56 ~ 2.82)
Prone duration	0.08	0.03	2.45	0.014	1.08 (1.02 ~ 1.15)
Nasojejunal tube	-1.65	0.26	-6.31	<0.001	0.19 (0.12 ~ 0.32)

OR: Odds Ratio, CI: Confidence Interval

ECMO, Extracorporeal Membrane Oxygenation;

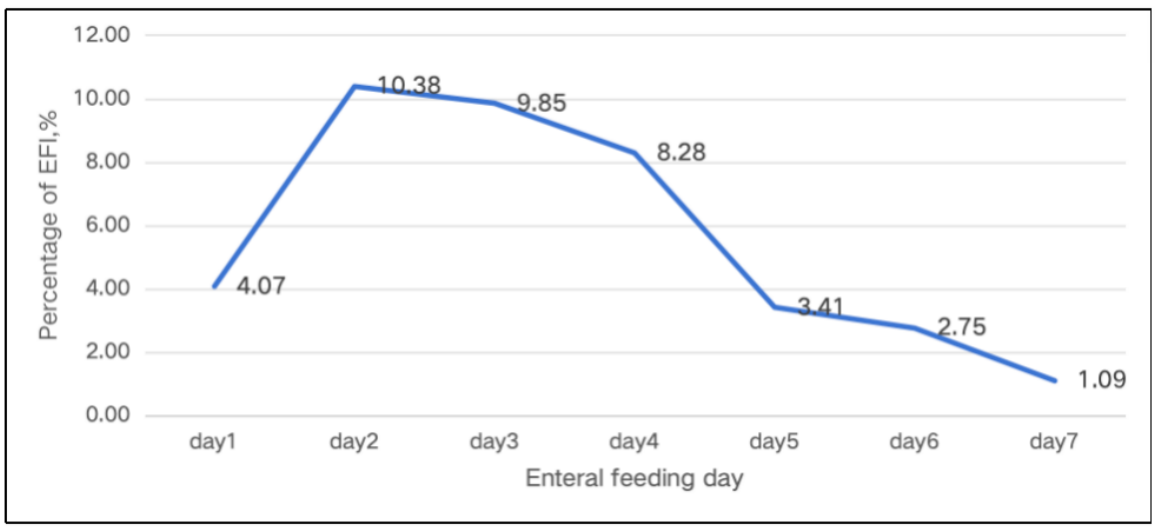


Figure 1 Daily incidence of feeding intolerance during the first 7 days after enteral nutrition initiation in the training cohort.

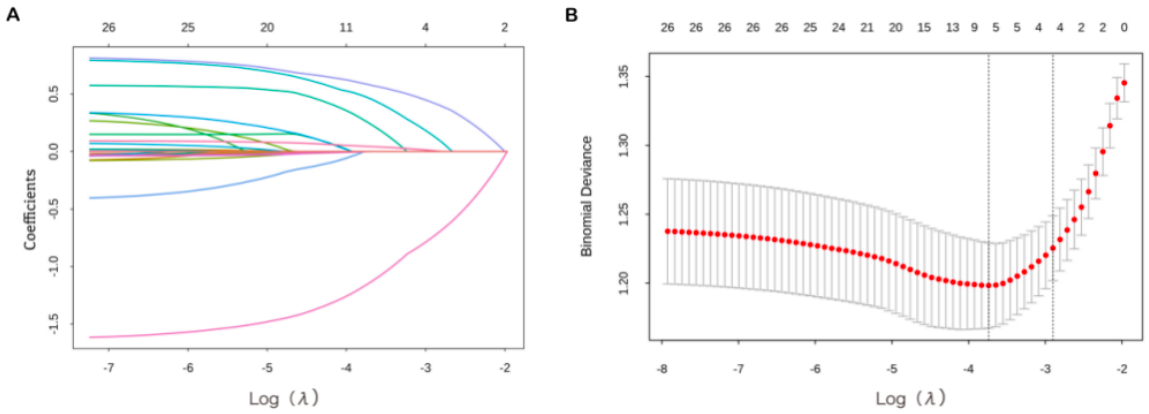


Figure 2 .LASSO regression analysis for variable selection in the FI risk prediction model. (A) Cross - validation deviance plot; (B) coefficient trajectory plot.

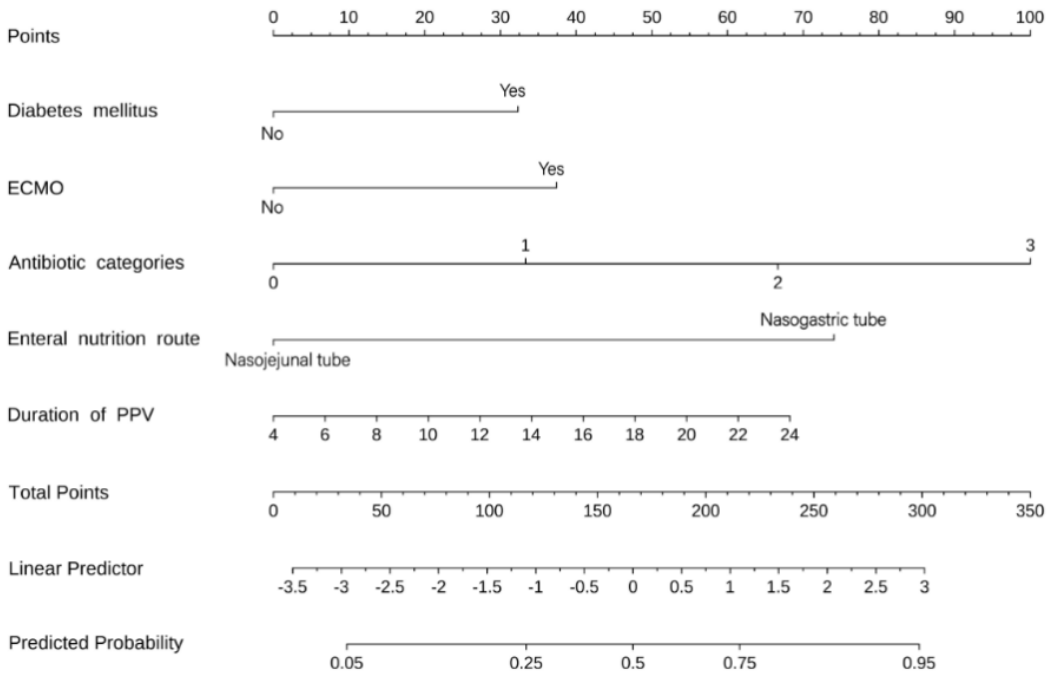


Figure 3. Nomogram for predicting the risk of feeding intolerance in patients undergoing prone position ventilation.

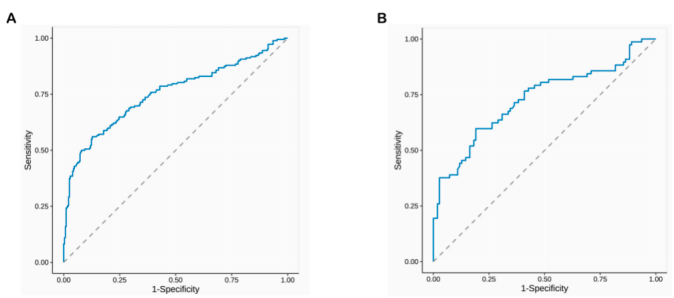


Figure 4. Receiver operating characteristic curves of the prediction model in the (A) training cohort and (B) temporal external validation cohort.

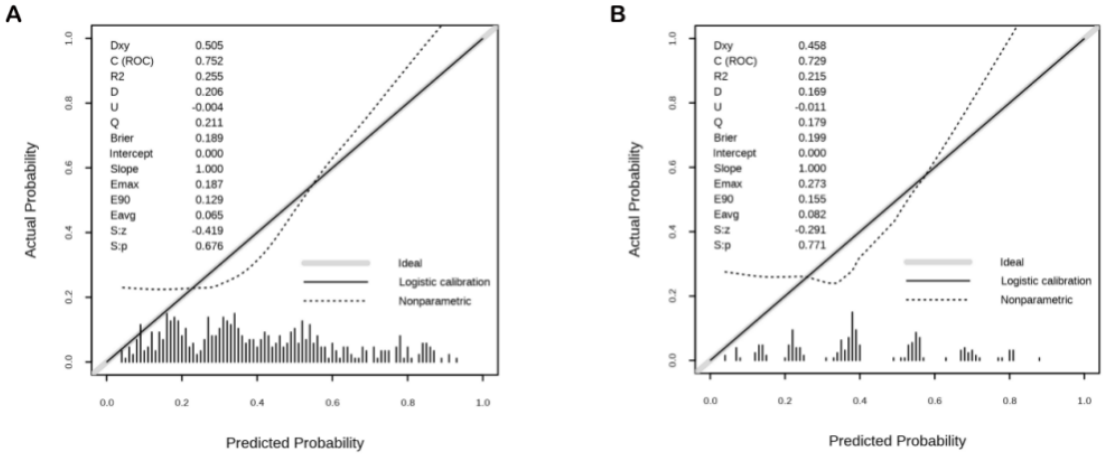


Figure 5. Calibration curves of the prediction model in the (A) training cohort and (B) temporal external validation cohort.

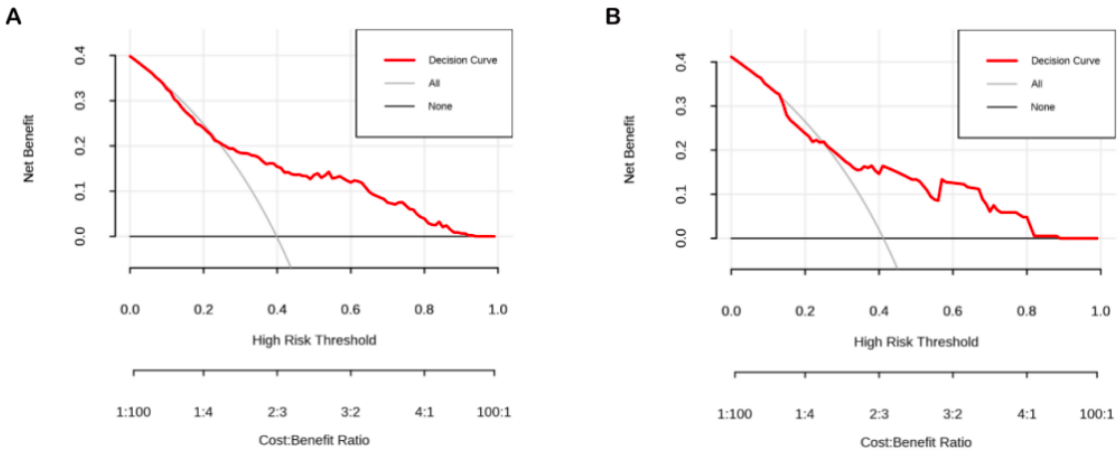


Figure 6. Decision curve analysis of the prediction model in the (A) training cohort and (B) temporal external validation cohort.

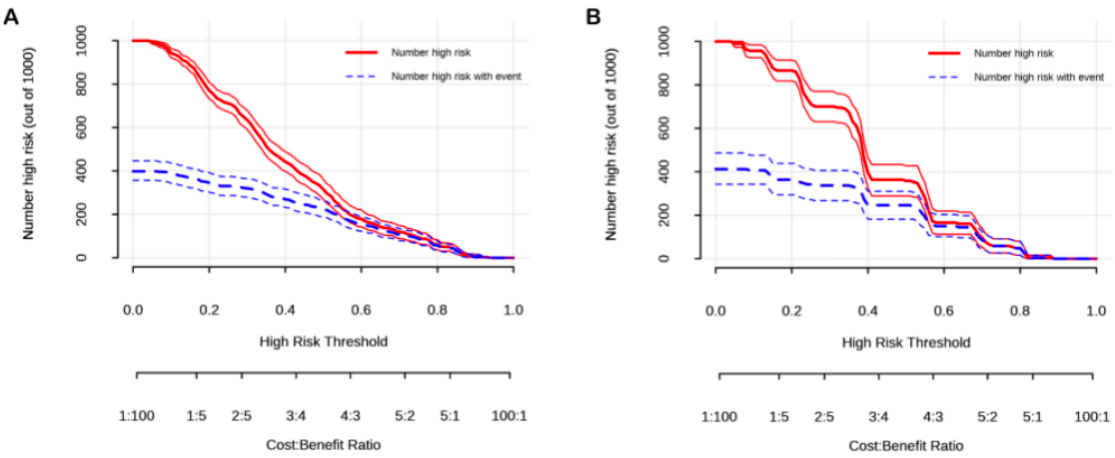


Figure 7. Clinical impact curves of the prediction model in the (A) training cohort and (B) temporal external validation cohort.

References

[1]Qadir N, Sahetya S, Munshi L, et al. An update on management of adult patients with acute respiratory distress syndrome: an official American thoracic society clinical practice guideline[J]. Am J Respir Crit Care Med, 2024, 209(1): 24-36.

[2]McClave S A, Taylor B E, Martindale R G, et al. Guidelines for the provision and assessment of nutrition support therapy in the adult critically ill patient: Society of Critical Care Medicine and American Society for Parenteral and Enteral Nutrition [J]. Critical Care Medicine, 2016, 44 (2): 390-438.

[3] 中华医学会肠外肠内营养学分会 . 中国成人患者肠外肠内营养临床应用指南 (2023 版)[J]. 中华医学杂志 , 2023, 103(13): 946-974.

[4]Hintersteininger M, Haselwanter P, Maleczek M, Laxar D, Hermann M, Hermann A, Buchtele N, Staudinger T, Zauner C, Schneeweiss-Gleixner M. The Influence of Prone Positioning on Energy and Protein Delivery in COVID-19 Patients Requiring ECMO Support. Nutrients. 2024 Oct 18;16(20):3534. doi: 10.3390/nu16203534. PMID: 39458527; PMCID: PMC11510455.

[5]Zhao ML, Hou YF, Zong LW, Yue YF, Ma S. Effects of prone versus supine position during enteral nutrition on clinical outcomes and complications in mechanically ventilated patients: a systematic review and meta-analysis. Front Nutr. 2026 Jan 8;12:1685664. doi: 10.3389/fnut.2025.1685664. PMID: 41586217; PMCID: PMC12823493.

[6] 刘超 , 袁海艳 , 季梦婷 , 等 . ICU 俯卧位通气患者肠内喂养不耐受风险预测模型的构建 [J]. 护理管理杂志 , 2024, 24(12): 1024-1029. DOI: 10.3969/j.issn.1671-315x.2024.12.003.

[7] 梁微波 , 何为群 , 桑岭 , 等 . 俯卧位通气患者肠内营养耐受性的影响因素分析 [J]. 中国呼吸与危重监护杂志 , 2020, 19(5): 478-482. DOI: 10.7507/1671-6205.201910082.

[8]Brown T，Touger-Decker R，Roberts S，et al.Challenges to provision of adequate medical nutrition therapy in a critically ill COVID-19 patient fed in the prone position[J].Top Clin Nutr，2022，37 (3)：218-226. DOI：10.1097/tin.0000000000000285.

[9]Li J，Wang L，Zhang H，et al.Different definitions of feeding intolerance and their associations with outcomes of critically ill adults receiving enteral nutrition：a systematic review and Meta-analysis[J]. J Intensi Care，2023，11 (1)：29-43.DOI：10.1186/s40560-023-00674-3.

[10]Salciute-Simene E，Stasiunaitis R，Ambrasas E，et al.Impact of enteral nutrition interruptions on underfeeding in intensive care unit[J].Clin Nutr，2021，40 (3)：1310-1317.DOI：10.1016/j.clnu.2020.08.01

[11]Cao X, Wang H, Song Y, Yan X, Wu W, Li W, Chen L. Development and evaluation of a risk prediction model for enteral nutrition feeding intolerance in intensive care units. Front Nutr. 2025 Sep 18;12:1667046. doi: 10.3389/fnut.2025.1667046. PMID: 41049372; PMCID: PMC12488460.

[12]Pan Y, Min C, Li J, Lin W, Li B, Wang Y, Zhang S, Jing W, Dang X. Development and validation of a dynamic nomogram for predicting enteral nutrition feeding intolerance in patients with severe traumatic brain injury: An external validation study. Medicine (Baltimore). 2025 Jun 27;104(26):e42993. doi: 10.1097/MD.0000000000042993. PMID: 40587708; PMCID: PMC12212860.

[13]Hu K, Xiang S, Pang J, Huang B, Xiong B. Metabolomic biomarkers enhance prediction of feeding intolerance in ICU septic patients. Clin Res Hepatol Gastroenterol. 2025 Dec;49(10):102731. doi: 10.1016/j.clinre.2025.102731. Epub 2025 Nov 7. PMID: 41207616.

[14]Luan X, Lin Y, Ke L, Xu J, Xi M, Xia Y, Wang D. Individualized Implementation of Enteral Nutrition Adjusted by Laboratory Indicators and Clinical Parameter Scoring. J Burn Care Res. 2026 Mar 4;47(2):558-565. doi: 10.1093/jbcr/iraf194. PMID: 41071105.

[15] 陈建勤 , 戴珍娟 , 王洁 , 等 . 持续腹内压监测预警系统在俯卧位机械通气患者肠内营养中的应用 [J]. 中华急危重症护理杂志 ,2025,6(7):798-804.

[16]Wang S, He Y, Yi J, et al. Risk factors for enteral feeding intolerance in critically ill patients: an updated systematic review and meta-analysis[J]. BMC Gastroenterol, 2025, 25: 233. DOI: 10.1186/s12876-025-03837-8.

[17] 袁丽 , 侯胜男 . 重症喂养流程下早期肠内营养干预对重症脑卒中病人营养吸收效率及胃肠道耐受性的影响 [J]. 循证护理 ,2025,11(24):5159-5164.

[18] 江文昊 , 卢祖谊 , 牟正贤 , 等 . 基于误吸风险评估的幽门后喂养策略对重症脑卒中患者肠内营养耐受性及临床预后的影响 [J]. 医学理论与实践 ,2025,38(17):3008-3010.DOI:10.19381/j.issn.1001-7585.2025.17.042.

[19] 艾晨阳 , 谭玉惠 , 李金亭 . 耳穴贴压对重症急性胰腺炎患者早期肠内营养喂养耐受性的临床研究 [J]. 中国中西医结合外科杂志 ,2024,30(3):401-404.

[20] 李冰 , 楚晓飞 , 马景丹 , 等 . 肠内营养不同递增输注速度对食管癌术后患者喂养耐受性的影响 [J]. 临床医学工程 ,2023,30(9):1251-1252.

[21] 未培轩 , 兰晓敬 , 吴亭亭 , 等 . 间断喂养与持续喂养对行机械通气患者耐受性、营养指标及预后的影响 [J]. 临床荟萃 ,2023,38(10):907-911.

[22]Dickerson RN, Farrar JE, Byerly S, Filiberto DM. Enteral feeding tolerance during pharmacologic neuromuscular blockade. Nutr Clin Pract. 2023 Dec;38(6):1236-1246. doi: 10.1002/ncp.11045. Epub 2023 Jul 20. PMID: 37475530.

[23]Xu Y, Hu Q, Pei D, Zhang Y, Zhu H, Hui Y, Guan W, Xu M, Chen L. Construction of a preoperative emotional state and postoperative intra-abdominal pressure based prediction model for early enteral feeding intolerance in postoperative patients with gastric cancer. Front Nutr. 2024 Nov 26;11:1480390. doi: 10.3389/fnut.2024.1480390. PMID: 39659911; PMCID: PMC11628306.

[24] 谢幼妮 , 刘媛航 , 黎艳 , 等 . 俯卧位通气患者肠内营养喂养不耐受风险预测模型的构建 [J]. 现代医药卫生 ,2025,41(5):1134-1139+1144.

[25]Neves RPS, Assis AP, Russo CMC. Monitoring enteral feeding tolerance in a critically ill patient using point-of-care ultrasound. Rev Bras Enferm. 2025 Dec 8;78(6):e20250033. doi: 10.1590/0034-7167-2025-0033. PMID: 41370602; PMCID: PMC12707605.

[26]Collins, G. S., K. G. M. Moons, P. Dhiman, et al. 2024. “TRIPOD+AI Statement: Updated Guidance for Reporting Clinical Prediction Models That Use Regression or Machine Learning Methods.” BMJ 385: e078378. https://doi.org/10.1136/bmj-2023-078378.

[27]Heyland DK, Ortiz A, Stoppe C, et al. Incidence, risk factors, and clinical consequence of enteral feeding intolerance in the mechanically ventilated critically ill: an analysis of a multicenter, multinational database[J]. Crit Care Med, 2021, 49(9): e835-e844. DOI: 10.1097/CCM.0000000000005058.

[28]Heymans MW, Twisk JWR. Handling missing data in clinical research[J]. J Clin Epidemiol, 2022, 151: 185-188. DOI: 10.1016/j.jclinepi.2022.08.016.

[29]ZHU Lihong, ZHUANG Yiyu. The predictive value of glycemic variability in early enteral feeding intolerance in critically ill patients[J]. Chinese Journal of Emergency and Critical Care Nursing, 2025, 6(6): 645-652.

[30]Xia Xu, Jiamin Hu, Liping Huang, Long Cheng, Shuliu Zhang, Weiwei Zhao, Panpan Gu, Cheng Cao. Current status of early enteral nutrition feeding intolerance in elderly critically ill patients and the construction and validation of a risk prediction nomogram[J/OL]. Chinese Journal of Critical Care Medicine(Electronic Edition), 2025, 18(01): 11-17. DOI: 10.3877/cma.j.issn.1674-6880.2025.01.003

[31]Jenkins B, Hossain MJ, Beja MM, Calder PC, Marino LV. Investigating the prevalence, predictors and outcomes associated with enteral feeding intolerance in critically ill adults: A retrospective cohort study. Clin Nutr ESPEN. 2026 Jun;73:103269. doi: 10.1016/j.clnesp.2026.103269. Epub 2026 Apr 1. PMID: 41932610.

[32]Mei M, Yao M, Li J, Qiu C, Wang Y, Li Y, Shi L, Wang L, uyang B. Influences of different sedatives on gastric antrum contraction in patients with acute brain injury. Front Neurol. 2024 Dec 20;15:1492604. doi: 10.3389/fneur.2024.1492604. PMID: 39758778; PMCID: PMC11695409.

[33]Herbert, M., Holzer, P., Roewer, N., & Roth-Goldbrunner, S. (2002). Clonidine and Dexmedetomidine Potently Inhibit Peristalsis in the Guinea Pig Ileum In Vitro . Anesthesiology, 97(6), 1491–1499. https://doi.org/10.1097/00000542-200212000-00022

[34]Dincer, E., Gundogan, S., Tomruk, S., & Ozgultekin, A. (2008). The effects of prone position on intraabdominal pressure, hemodynamics,and alveoler oxygenation in patients with ALI/ARDS: 12AP2-5. European Journal of Anaesthesiology, 25, 168.

[35]Kornum, D.S., Krogh, K., Keller, J. et al. Diabetic gastroenteropathy: a pan-alimentary complication. Diabetologia 68, 905–919 (2025). https://doi.org/10.1007/s00125-025-06365-y

[36]Galeano, F., Tumminia, A., Oteri, V. et al. Diabetic gastroparesis: pathophysiology and impact on insulin timing choices. Endocrine 91, 211 (2026). https://doi.org/10.1007/s12020-026-04693-6

[37] 国家急诊医学专业医疗质量控制中心 , 北京市急诊质量控制和改进中心 , 中华护理学会急诊护理专业委员会 . 急危重症患者鼻空肠营养管管理专家共识 . 中华急诊医学杂志 , 2024, 33(6): 761-766.

[38]Wang, Q., Liu, L., Ma, X., & Xiao, T. (2025). Gastric Mucosal Injury in Patients Undergoing Venoarterial Extracorporeal Membrane Oxygenation (VA-ECMO): A Pilot Endoscopic Study. ASAIO Journal, 71(Supplement 5), 6. https://doi.org/10.1097/01.mat.0001171200.06070.b6

[39]Omar, A. Heart–gut interaction in veno-arterial extracorporeal membrane oxygenation: a forgotten axis in critical care perfusion. J Artif Organs 29, 16 (2026). https://doi.org/10.1007/s10047-025-01543-6

[40]Wang, J.-H.; Han, S.-Y.; Lee, K.; Han, U.; Cho, S.-K.; Kim, H. Antibiotic Cocktail Exacerbates Esomeprazole-Induced Intestinal Dysmotility While Ameliorating Gastric Dyspepsia in Mice. Antibiotics 2025, 14, 442. https://doi.org/10.3390/antibiotics14050442

类别 :// 临床研究：设计规范的各类临床研究及研究方案报告

Dynamic Changes of Diaphragmatic Function and Its Association with Weaning Outcomes in Critically Ill: A Single-Center, Prospective, Longitudinal Study

姓名：罗佳忍，王陆豪，韦碧琳，郑慧芳，刘洋，常泽楠，刘紫锰

单位：中山大学附属第一医院

Diaphragmatic function is a key prognostic factor for critically ill patients, especially those receiving mechanical ventilation. However, systematic research on the longitudinal dynamic changes of global diaphragmatic function in ICU patients remains insufficient. We aim to explore the dynamic evolution of global diaphragmatic function in critically ill patients and it's association with weaning outcomes in mechanically ventilated patients.

This single-center, prospective observational study enrolled 80 mechanically ventilated and 24 non-mechanically ventilated critically ill patients. Daily bedside ultrasound assessments were performed to measure diaphragmatic motion (DM), end-inspiratory diaphragm thickness (Ti), end-expiratory diaphragm thickness (Te), and diaphragmatic thickening fraction (DTF).

Diaphragmatic parameters exhibited distinct dynamic trajectories depending on patient status. For mechanically ventilated patients, diaphragmatic function declined immediately after ICU admission; the impairment of diaphragmatic contractility progressively aggravated within the first 48 hours and then tended to recover gradually. In contrast, diaphragm thickness began to decline after 48 hours of ICU stay. None of these parameters returned to baseline levels by ICU discharge. Compared with mechanically ventilated patients, non-mechanically ventilated patients maintained relatively higher levels of DM and DTF throughout the ICU stay. Mechanically ventilated patients who failed extubation exhibited more prominent fluctuations in DM, DTF, Ti and Te than those with successful extubation. After extubation, patients receiving high-flow nasal cannula (HFNC) oxygen therapy showed more stable changes in all diaphragmatic parameters compared with those using conventional nasal cannula oxygen therapy (COT). Within the first 72 hours of MV, 33 patients (41.25%) developed diaphragmatic atrophy (thickness reduction >10%), and 16 patients (20%) had diaphragmatic thickening (thickness increase >10%). The incidence of early diaphragmatic dysfunction (DM < 1.4 cm combined with DTF < 20%) was 55%. Multivariate logistic regression analysis revealed that early diaphragmatic atrophy was an independent risk factor for short-term weaning failure (OR=3.12, 95%CI [1.07, 9.09], p=0.04). The area under the curve (AUC) of the prediction model for short-term weaning failure was 0.82, with a sensitivity of 83% and a specificity of 80% at the optimal cutoff value of 0.48.

Diaphragmatic function in ICU patients deteriorates rapidly within 24 to 48 hours and undergoes continuous dynamic changes, which requires close monitoring. Post-extubation HFNC is associated with more stable diaphragmatic function. Early diaphragmatic atrophy is an independent risk factor for short-term weaning failure.

类别 :// 临床研究：设计规范的各类临床研究及研究方案报告

Early energy delivery trajectories and prolonged organ failure in hypertriglyceridaemia-associated acute pancreatitis: a multicentre cohort study

姓名：周灵亮，柯路，李维勤

单位：中国人民解放军东部战区总医院

Background: Optimal early energy delivery in acute pancreatitis remains uncertain, and hypertriglyceridaemia-associated acute pancreatitis (HTG-AP) may pose distinct metabolic challenges. We aimed to identify early energy delivery trajectories in patients with HTG-AP and examine their association with organ failure.

Methods: The analyses were based on data extracted from a multicentre, prospective cohort study of patients with HTG-AP. Daily energy delivery from recorded enteral and parenteral nutrition during study days 1 to 7 was used to identify trajectories by latent class mixed modelling. The primary outcome was prolonged organ failure (PrOF), defined as the presence of an individual Sequential Organ Failure Assessment subscore ⩾ 2in the respiratory, renal, or cardiovascular system on study day 7. Associations were estimated using modified Poisson regression with robust standard errors, adjusted for age, sex, body mass index, the Acute Physiology and Chronic Health Evaluation II score, and baseline organ failure. Sensitivity analyses evaluated mean energy delivery during study days 1 to 3 and study days 1 to 4 as alternative early exposure windows.

Results:A total of 301 patients were included in the analysis.Three early energy delivery trajectories were identified: low energy delivery (n = 170), moderate energy delivery (n = 85), and high energy delivery (n = 46). Mean daily energy delivery was 1.0, 8.6, and 13.1 kcal/kg/day, respectively.Overall, PrOF occurred in 61 patients (20.3%). Compared with low energy delivery, both moderate energy delivery and high energy delivery were associated with a higher risk of PrOF, with adjusted RRs of 3.21 (95% CI, 1.90 to 5.43) and 2.84 (95% CI, 1.60 to 5.02), respectively. Early window sensitivity analyses showed directionally consistent associations.

Conclusions: In patients with HTG-AP, higher early energy delivery trajectories were associated with a higher risk of PrOF. These findings are hypothesis-generating.

类别 :// 临床研究：设计规范的各类临床研究及研究方案报告

Early fresh frozen plasma transfusion and clinical outcomes of patients with sepsis-induced coagulopathy: a retrospective cohort study

姓名：李玉婷，李洪祥，张兴达，张凤，包玲玲，王友泉，张东

单位：吉林大学第一医院

Background: The impact of early fresh frozen plasma (FFP)administration on clinical outcomes for patients with sepsis-induced coagulopathy (SIC) uponintensive care unit(ICU)admission has not been well elucidated due to limited existing research in this field. Accordingly, thisstudy sought to investigate its correlation with clinical prognosis within this patient cohort.

Methods: This study is a single-center retrospective cohort study, enrolling patients with SICadmitted to the ICU from March 2023 to June2025. Patients were divided into the early FFP transfusion group and the non-early FFP transfusion group according to whether FFP was transfused within the first 24 h of ICU admission. We compared clinical outcomes between the two groups, including in-hospital mortality, 28-day mortality, mechanical ventilation time, receipt of continuous renal replacement therapy (CRRT), vasoactive drug duration, ICU length of stay, hospital length of stay, as well as the incidence of bleeding events and deep vein thrombosis (DVT). Multivariable logistic regression was applied to evaluate the association between early FFP transfusion and clinical outcome. A restricted cubic spline (RCS) model was adopted to explore the linear relationship between the volume of transfused FFP and in-hospital mortality.

Results: This study included a total of 322patients with SIC, among whom67 (20.81%) were assigned to the early FFP transfusion group and 255 (79.19%) to the non-early FFP transfusion group.The in-hospital mortality of early FFP transfusion group was higher than that of non-early FFP transfusion group(14.93% vs 6.27%, P=0.021). In addition, The DVT incidence of early FFP transfusion group was higher than that of non-early FFP transfusion group (7.46% vs 2.75%, P=0.006). Both the mechanical ventilation time (P=0.005) and vasoactive drug duration (P=0.03) were significantly prolonged in early FFP transfusion group compared with non-early FFP transfusion group. The multivariate regression analysis indicated that early FFP transfusion was an independent risk factor for in-hospital mortality in patients with SIC (P=0.005, OR=3.546, 95% CI 1.457-8.631). The restricted cubic spline curve indicated the linear relationship between early FFP transfusion volume and in-hospital mortality in critically ill patients with SIC (P for nonlinearity >0.05). Higher volume of early FFP transfusion was associated with high in-hospital mortality.

Conclusions: Early FFP administration in patients with SIC may correlate with higher in-hospital mortality, with this relationship demonstrating a linear dose-dependent pattern. Early FFP transfusion is additionally linked to an increased risk of DVT, alongside longer mechanical ventilation time and extended vasopressor requirements in this patient population.

类别 :// 临床研究：设计规范的各类临床研究及研究方案报告

Early Mean Perfusion Pressure Trajectories and Clinical Outcomes in Patients Receiving VA-ECMO: A Retrospective Cohort Study

姓名：王妍，王粮山，王可心，符鸿福，于欣睿，鲁瑞轲，王奕文，李呈龙，张帅，郝星，王红，杜中涛，侯晓彤

单位：首都医科大学附属北京安贞医院

Adequate mean perfusion pressure (MPP = MAP - CVP) may be important during veno-arterial extracorporeal membrane oxygenation (VA-ECMO) for cardiogenic shock. However, management typically focuses on mean arterial pressure (MAP), and the prognostic relevance of early MPP trajectories remains unclear.

This retrospective study included 670 adults with cardiogenic shock who received VA-ECMO at Beijing Anzhen Hospital between February 1, 2018, and September 30, 2025. MPP was measured at 4, 12, and 24 h after ECMO initiation. Ensemble clustering was used to identify MPP trajectories. Inverse probability of treatment weighting was applied to adjust for baseline differences, and weighted regression examined associations with clinical outcomes. Multivariable logistic regression using unweighted data served as a sensitivity analysis.

Four distinct MPP trajectories were identified. In-hospital mortality ranged from 39.0% in Class 1 (persistent hyperperfusion) to 71.2% in Class 4 (persistent hypoperfusion). With Class 4 as the reference, Class 1 was associated with lower odds of in-hospital mortality (OR = 0.35, 95% CI 0.18-0.68; P = 0.002) and CRRT use (OR = 0.40, 95% CI 0.21-0.77; P = 0.006) in weighted analyses. Outcomes in Class 2 (resuscitation improvement) and Class 3 (decompensation) were intermediate. Findings from the unweighted multivariable analyses were broadly consistent with the weighted results.

Early MPP trajectories identified four hemodynamic phenotypes that were associated with in-hospital mortality and CRRT use. These trajectories may support early risk stratification and individualized hemodynamic management.

Early PaO2/FiO2 and PaCO2 Trajectories Across Prone Positioning Cycles and 28-Day Mortality in ARDS: A Retrospective Trajectory Analysis

姓名：Yuxian Wang[1#], Shimin Zhang[1#], Yongsheng Guo[2#], Xin Zheng[1*], Kai Liu[1*], MingZhong[1,3*]

单位：1 Zhongshan Hospital, Fudan University

2 Shanghai Geriatric Medical Center

3 Shanghai Institute of Infectious Disease and Biosecurity, School of Public Health, Fudan University

Abstract

Background: Early respiratory evolution during prone positioning may provide prognostic information beyond single cross-sectional measurements in patients with acute respiratory distress syndrome (ARDS). We aimed to identify distinct respiratory subphenotypes based on the trajectories of the PaO_2/FiO_2 (P/F) ratio and $PaCO_2$ across sequential prone positioning cycles and to evaluate their associations with 28- day mortality.

Methods: Latent class trajectory models were constructed for univariate P/F, univariate $PaCO_2$, and joint P/F-$PaCO_2$ trajectories across three prespecified observation windows, including Cycle 1 (T1–T5), Cycles 1–2 (T1–T10), and Cycles 1–3 (T1–T15). Within each cycle, T1 represented the pre-prone supine position, T2 the early prone phase, T3 the middle prone phase, T4 the end of the prone phase, and T5 the return to supine position; subsequent cycles were defined analogously. Model selection considered statistical fit, class size, and clinical interpretability. Kaplan – Meier analysis and Cox proportional hazards models were used to assess the associations between trajectory class membership and 28-day mortality.

Results: Among the candidate models, analyses based on the first two prone positioning cycles (T1 – T10) yielded the most clinically interpretable class distributions and were selected for the primary trajectory analyses. In the univariate P/F model, 350 patients were classified into Class 1 (n = 180) and Class 2 (n = 170). Class 2 showed consistently higher P/F values across the first two prone positioning cycles and had better 28-day survival than Class 1 (log-rank p = 0.00017). Correspondingly, 28-day mortality was significantly lower in Class 2 than in Class 1 (45.3% vs. 66.1%, p < 0.001). In multivariable analysis, Class 2 remained independently associated with a lower hazard of 28-day mortality than Class 1 (HR 0.63, 95% CI 0.45–0.90, p = 0.011). In the joint P/F-$PaCO_2$ model, 350 patients were classified into Class 1 (n = 186) and Class 2 (n = 164). Class 1 was characterized by lower $PaCO_2$ and higher P/F values, whereas Class 2 showed higher $PaCO_2$ and lower P/F values across the first two prone positioning cycles. Kaplan–Meier analysis demonstrated significantly better 28-day survival in Class 1 than in Class 2 (log-rank p = 0.039). In the adjusted Cox model, Class 2 was independently associated with a higher hazard of 28-day mortality relative to Class 1 (HR 1.55, 95% CI 1.11–2.15, p = 0.009). By contrast, $PaCO_2$ trajectory alone was not independently associated with 28-day mortality after adjustment (HR 1.46, 95% CI 0.81–2.64, p = 0.209).

Conclusions: Early PaO_2/FiO_2 and joint PaO_2/FiO_2 – $PaCO_2$ trajectories across the first two prone positioning cycles were associated with 28-day mortality in patients with ARDS. A persistently higher PaO_2/FiO_2 trajectory was associated with lower mortality, whereas the combination of higher $PaCO_2$ and lower PaO_2/FiO_2 identified a higher-risk trajectory pattern. These findings suggest that dynamic respiratory monitoring during prone positioning may provide additional prognostic information beyond single time-point measurements, although the exploratory nature of trajectory classification warrants further validation.

Keywords: acute respiratory distress syndrome; prone positioning; PaO_2/FiO_2 ratio; $PaCO_2$; latent class trajectory analysis; 28-day mortality

Introduction

Acute respiratory distress syndrome (ARDS) is a heterogeneous syndrome characterized by diffuse inflammatory lung injury, impaired gas exchange, and substantial short-term mortality despite advances in supportive care [1,2]. Among evidence-based supportive strategies, prone positioning has been shown to improve oxygenation and reduce mortality in patients with moderate-to-severe ARDS, and it is now widely recommended as a standard intervention in appropriately selected patients [3–5]. However, the physiological response to prone positioning is not uniform. Some patients show sustained improvement in oxygenation and ventilatory status, whereas others derive limited or transient benefit, underscoring the marked biological and clinical

heterogeneity of ARDS during treatment [6,7]. In routine clinical practice, the response to prone positioning is often evaluated using single time-point measurements, particularly the PaO_2 /FiO_2 (P/F) ratio. Although the P/F ratio remains a key indicator of oxygenation impairment, it reflects only one dimension of respiratory dysfunction and may not fully capture the dynamic evolution of pulmonary status during repeated prone positioning cycles [8,9]. $PaCO_2$ provides complementary information regarding ventilatory efficiency and dead-space-related physiological derangements, which may also be clinically relevant during prone positioning [10,11]. Nevertheless, most previous studies have focused on static measurements obtained before or after a prone cycle, rather than on longitudinal respiratory patterns across repeated prone positioning cycles. Trajectory-based approaches may offer a more informative framework for characterizing such dynamic changes. By modeling repeated measurements over time, latent class trajectory analysis can identify subgroups of patients with distinct temporal patterns that may not be apparent from conventional cross-sectional assessments [12,13]. In ARDS, this approach may be particularly useful for distinguishing respiratory subphenotypes with different responses to prone positioning and different clinical outcomes. Moreover, joint modeling of oxygenation and ventilation variables may better reflect the complexity of respiratory physiology than either variable alone. Therefore, in the present study, we used latent class mixed modeling to characterize early respiratory trajectories of the PaO_2 /FiO_2 ratio and $PaCO_2$ across sequential prone positioning cycles in patients with ARDS. We evaluated univariate PaO_2 /FiO_2 trajectories, univariate $PaCO_2$ trajectories, and joint PaO_2 /FiO_2 –$PaCO_2$ trajectories across predefined observation windows spanning the first one, two, and three prone positioning cycles. We then examined whether these trajectory-derived respiratory patterns were associated with 28-day mortality. We hypothesized that early dynamic respiratory trajectories during prone positioning would identify clinically interpretable risk strata with different prognostic profiles.

Methods

Study design and patient population

This was a single-center retrospective observational study conducted in the intensive care unit of ZhongShan Hospital of Fudan University between July 2019 and August 2025. Adult patients with acute respiratory distress syndrome (ARDS) who underwent prone positioning during invasive mechanical ventilation were screened for eligibility. Patients were included if they (1) were aged ⩾ 18 years, (2) met the diagnostic criteria for ARDS, (3) underwent prone positioning during mechanical ventilation, and (4) had available arterial blood gas measurements required for the predefined trajectory analyses. Patients were excluded if they had incomplete longitudinal respiratory data for the corresponding observation window, duplicate admissions, or missing 28-day mortality data. For patients with multiple ICU admissions, only the first eligible admission was included. A total of 350 patients were ultimately included in the analysis.

The study was approved by the ethics committee (approval No. [B2026-019]). The requirement for written informed consent was waived by the ethics committee due to the retrospective design and use of de-identified data.

2.2. Definition of prone positioning cycles and longitudinal respiratory measurements

Longitudinal respiratory measurements were organized according to sequential prone positioning cycles. Cycle 1 (T1–T5) represented the first prone positioning cycle and included pre-prone supine position (T1), early prone phase (T2), middle prone phase (T3), end of prone phase (T4), and return to supine position (T5). Cycle 2 (T6–T10) and Cycle 3 (T11 – T15) were defined analogously for the second and third prone positioning cycles, respectively. At each predefined time point, arterial blood gas variables were collected, including PaO_2 , FiO_2 , and $PaCO_2$. The PaO_2 /FiO_2 (P/F) ratio was calculated as PaO_2 divided by FiO_2 . Within each prone positioning cycle, T1 was defined as the pre- prone supine measurement, T2 as the early prone-phase measurement, T3 as the middle prone-phase measurement, T4 as the end-prone measurement, and T5 as the post-prone supine measurement. Cycle 2 and Cycle 3 were defined analogously. The timing of arterial blood gas sampling was determined according to the institutional prone positioning protocol and was synchronized with the corresponding ventilator settings, including FiO_2 and PEEP. Baseline clinical variables were extracted from the medical records, including age, sex, body mass index (BMI), systolic blood pressure (SBP), diastolic blood pressure (DBP), positive end-expiratory pressure (PEEP), dynamic compliance (Cdyn), Acute Physiology and Chronic Health Evaluation II (APACHE II) score, ARDS severity category, major etiologies/comorbidities, CT pattern, continuous renal replacement therapy (CRRT), and extracorporeal membrane oxygenation (ECMO).

2.3. Outcome

The primary endpoint was 28-day mortality, defined as death from any cause within 28 days after initiation of the first prone positioning cycle.

2.5. Survival analysis

Kaplan –Meier curves were generated to compare 28-day survival across trajectory classes, and differences between groups were assessed using the log-rank test. To further evaluate the association between trajectory class membership and 28-day mortality, Cox proportional hazards regression models were constructed and presented as hazard ratios (HRs) with 95% confidence intervals (CIs). Separate multivariable models were fitted for the selected P/F trajectory model, $PaCO_2$ trajectory model, and joint P/F+$PaCO_2$ trajectory model. In these analyses, Class 1 served as the reference category for trajectory membership. For categorical covariates, the reference groups were defined a priori, including male sex and mild ARDS, as applicable.

2.6. Statistical analysis 179

Data Processing and Latent Class Mixed Modeling 180

Latent class mixed models were fitted using the lcmm package in R. The PaO_2 /FiO_2 ratio and $PaCO_2$ were standardized using Z-scores before modeling to improve numerical stability and to allow joint modeling of variables measured on different scales. Time was modeled according to the predefined observation order, and natural cubic splines with 3–4 degrees of freedom were used to capture nonlinear trajectories. A random intercept was included to account for between-patient heterogeneity. For each observation window, one-, two-, and three-class models were fitted using multiple sets of initial values to reduce the risk of convergence to local maxima. Model selection was based on a combination of BIC, minimum class size, posterior classification quality, and clinical interpretability. Models generating very small or clinically implausible classes were not selected even when they showed lower BIC values. Patients were assigned to the trajectory class with the highest posterior probability. Classification quality was assessed using entropy, class-specific average posterior probability, and odds of correct classification. Because trajectory class assignment may be affected by classification uncertainty, all trajectory-based survival analyses were considered exploratory and were interpreted together with model diagnostics.

Survival Analysis and Covariate Selection 200

The primary outcome was 28-day all-cause mortality. Kaplan – Meier curves were constructed and compared using the log-rank test. Cox proportional hazards models were used to assess the association between trajectory classes and mortality risk. Potential confounders were selected based on clinical relevance and univariate Cox regression. Age, sex, and APACHE II score were included in all multivariable models regardless of statistical significance. Additional covariates with $P < 0.10$ in univariate Cox analysis were considered for inclusion, while avoiding overfitting and collinearity. The proportional hazards assumption was assessed using Schoenfeld residuals. Results are presented as hazard ratios with 95% confidence intervals. All analyses were performed using R version 4.5.2 (lcmm, survival, and ggplot2 packages), with two-sided $P < 0.05$ considered statistically significant.

Results

Study population

A total of 350 adult patients with ARDS who underwent prone positioning during invasive mechanical ventilation were included in the final analysis. All patients had available longitudinal arterial blood gas measurements for the prespecified trajectory analyses and complete 28-day mortality data. Baseline characteristics according to the selected PaO_2 /FiO_2 and joint PaO_2 /FiO_2 – $PaCO_2$ trajectory classes are summarized in Table 2.

Model Fitting and Selection

Using Z-score standardized longitudinal data, LCMMs with natural cubic splines were applied to identify trajectory patterns of P/F and PaCO2 across different time windows (5, 10, and 15 time points). Based on BIC, class size, and clinical interpretability, optimal trajectory models were selected for each time window. The use of maximum likelihood estimation allowed for robust handling of missing and irregular data. Although the one-class models yielded slightly lower BIC values in some T1 –T10 analyses, they did not allow clinically meaningful prognostic stratification. The two- class T1–T10 models were retained for the primary analyses because

they produced balanced class sizes, clinically interpretable trajectory patterns, and significant separation in subsequent time-to-event analyses. Therefore, the selected models were intended to support exploratory risk stratification rather than to establish definitive biological subphenotypes.

PaO2 /FiO2 trajectory model across the first two prone positioning cycles

In the selected T1–T10 PaO_2 /FiO_2 trajectory model, patients were classified into two groups: Class 1 (n = 180) and Class 2 (n = 170). Class 2 showed consistently higher predicted PaO_2 /FiO_2 values across the first two prone positioning cycles than Class 1. The 28-day mortality rate was significantly lower in Class 2 than in Class 1 (45.3% vs. 66.1%, P < 0.001). Kaplan – Meier analysis demonstrated significantly better survival in Class 2 than in Class 1 over 28 days. In the multivariable Cox model, Class 2 remained independently associated with a lower hazard of 28-day mortality compared with Class 1.

Joint PaO 2 /FiO 2 – PaCO 2 trajectory model across the first two prone positioning cycles

In the selected joint T1–T10 model, patients were classified into Class 1 (n = 186) and Class 2 (n = 164). Class 1 was characterized by lower $PaCO_2$ and higher PaO_2 /FiO_2 values, whereas Class 2 showed higher $PaCO_2$ and lower PaO_2 /FiO_2 values across the first two prone positioning cycles. Although the crude 28-day mortality difference did not reach statistical significance, mortality was numerically higher in Class 2 than in Class 1. Kaplan–Meier analysis showed significant separation between the two classes, and the adjusted Cox model demonstrated that Class 2 was independently associated with a higher hazard of 28-day mortality compared with Class 1.

PaCO2 -only trajectory model

The $PaCO_2$ -only trajectory model did not provide robust independent prognostic information after adjustment. Although $PaCO_2$ trajectories captured differences in ventilatory status, trajectory class membership was not independently associated with 28-day mortality in the multivariable Cox model. This finding suggests that $PaCO_2$ may be more informative when interpreted jointly with oxygenation rather than as an isolated trajectory marker.

Early Phase (5 Time Points): Limited Prognostic Discrimination

In the early monitoring window, univariate models did not identify subgroups with significant differences in 28-day mortality. Kaplan – Meier curves based on P/F or PaCO2 trajectories showed no significant separation. Similarly, the bivariate model identified two classes, but no significant survival difference was observed (log-rank P > 0.05). These findings suggest limited prognostic discrimination of early trajectory patterns.

Intermediate Phase (10 Time Points): Improved Prognostic Stratification

With extended monitoring to 10 time points, trajectory patterns showed improved discriminatory ability. The P/F model identified two subgroups with significantly different survival outcomes (log-rank P < 0.05). After adjustment for age and sex, trajectory class remained significantly associated with 28-day mortality (HR = 0.63, 95% CI: 0.45–0.90, P < 0.05). The bivariate model (P/F and PaCO2) demonstrated similar findings (HR = 1.55, 95% CI: 1.11–2.15, P < 0.05), whereas the PaCO2-only model did not yield clinically or statistically meaningful groupings.

Late Phase (15 Time Points): Reduced Stability of Prognostic Associations

At 15 time points, the prognostic performance of trajectory models became less stable. The P/F model did not distinguish survival outcomes, and although the PaCO2 model showed significant differences in Kaplan – Meier analysis (P < 0.05), this was not sustained in multivariable Cox models (P > 0.05). The bivariate model remained statistically significant; however, one subgroup approached the minimum size threshold, and Kaplan–Meier curves exhibited crossing, suggesting potential non-proportional hazards. Therefore, results from this time window should be interpreted with caution. Overall, the intermediate time window (10 time points) provided more stable and reliable prognostic information.

Trajectory-Based Classification and Exploratory Survival Analysis

Trajectory classification showed non-negligible uncertainty, as reflected by modest posterior classification indices. Therefore,

the selected trajectory classes were interpreted as exploratory trajectory-derived risk strata rather than definitive biological subphenotypes. Survival analyses based on trajectory class membership were consequently interpreted in conjunction with trajectory patterns, class size, and clinical plausibility.

Discussion 307

In this retrospective trajectory analysis of patients with ARDS undergoing prone positioning, early respiratory trajectories across the first two prone positioning cycles were associated with 28-day mortality. The main findings are threefold. First, a persistently higher PaO_2 /FiO_2 trajectory was associated with better 28-day survival and remained independently associated with lower mortality after adjustment. Second, joint modeling of PaO_2 /FiO_2 and $PaCO_2$ refined risk stratification by identifying a higher-risk trajectory pattern characterized by lower oxygenation and higher $PaCO_2$. Third, $PaCO_2$ trajectory alone did not retain an independent association with 28- day mortality after adjustment, suggesting that $PaCO_2$ may be more clinically informative when interpreted together with oxygenation rather than in isolation.The association between a more favorable P/F trajectory and lower 28-day mortality is biologically plausible. Compared with a single baseline oxygenation measurement, longitudinal P/F trajectories across repeated prone positioning cycles are more likely to capture the dynamic evolution of lung injury and the early response to supportive treatment. In our cohort, the less favorable P/F trajectory was also accompanied by a higher proportion of severe ARDS and a significantly different CT pattern distribution, supporting the interpretation that trajectory membership reflected clinically meaningful heterogeneity rather than statistical clustering alone. Taken together, these findings suggest that early temporal changes in oxygenation during prone positioning may provide prognostic information beyond a cross-sectional assessment at a single time point. The joint trajectory analysis extends this observation by showing that the combination of $PaCO_2$ and P/F captures prognostically relevant information that may not be fully represented by either variable alone. Patients in the less favorable joint class exhibited persistently higher $PaCO_2$ together with lower P/F, a pattern that may reflect simultaneous impairment in oxygenation and ventilatory efficiency during repeated prone positioning cycles. From a physiological perspective, such a pattern is consistent with more severe respiratory dysfunction and a higher-risk clinical course. Notably, although the crude between-group difference in 28-day mortality in Table 2 did not reach statistical significance, both the Kaplan–Meier analysis and the adjusted Cox model demonstrated significant prognostic separation. This discrepancy is not unexpected, as time-to-event analyses account for event timing and censoring and may therefore detect prognostic differences that are less apparent in unadjusted mortality proportions alone. Another noteworthy finding is that the $PaCO_2$ trajectory alone was not independently associated with 28-day mortality after multivariable adjustment. This result suggests that isolated $PaCO_2$ patterns may be influenced by multiple factors beyond the severity of pulmonary dysfunction, including ventilatory strategy, compensatory changes in minute ventilation, and systemic metabolic conditions. By contrast, when $PaCO_2$ was interpreted together with P/F, its prognostic relevance became more evident. This finding supports a more integrated view of respiratory monitoring during prone positioning, in which oxygenation and ventilation are considered complementary dimensions of disease evolution rather than separate competing markers. These findings may have practical clinical implications. Repeated assessment of routinely available respiratory variables across the early prone positioning cycles may provide more informative risk stratification than a single cross-sectional measurement. In particular, trajectory-based classification over the first two prone positioning cycles may help identify patients with persistently unfavorable respiratory evolution who may require closer surveillance and more individualized management. The observation that trajectory class remained informative after adjustment for established clinical factors further suggests that dynamic respiratory phenotyping during prone positioning may add prognostic value beyond conventional baseline severity assessment. In addition, model selection was not based solely on the lowest BIC. Some candidate models with favorable statistical fit generated very small or clinically implausible classes, limiting their usefulness for bedside interpretation. We therefore prioritized models that balanced statistical fit, adequate class size, clinical plausibility, and prognostic separation. This pragmatic approach is appropriate for exploratory risk stratification but requires prospective validation before clinical implementation. Several issues should be considered when interpreting the present findings. Class selection was guided not only by statistical fit, but also by class size and clinical interpretability, because some candidate models generated very small subgroups. In addition, trajectory membership was derived from observational longitudinal data and should not be interpreted causally. Residual confounding cannot be excluded, and external validation will be required before broader clinical application. Nevertheless, the consistency between trajectory patterns, survival curves, and adjusted risk estimates supports the robustness of the main findings. An important methodological limitation is the uncertainty inherent in latent class assignment. Posterior classification indices indicated that separation between classes was modest, and therefore trajectory classes should not be

interpreted as definitive biological subphenotypes. Instead, they should be viewed as exploratory, clinically interpretable trajectory-derived risk strata. Future studies should validate these trajectory patterns in external cohorts and assess whether posterior probability weighting or other methods accounting for classification uncertainty improve risk estimation.

Conclusion

In conclusion, early PaO_2 /FiO_2 and joint PaO_2 /FiO_2 –$PaCO_2$ trajectories across the first two prone positioning cycles were associated with 28-day mortality in patients with ARDS. A persistently higher PaO_2 /FiO_2 trajectory identified a lower- risk pattern, whereas the combination of higher $PaCO_2$ and lower PaO_2 /FiO_2 identified a higher-risk pattern. Dynamic respiratory trajectories during prone positioning may provide a pragmatic framework for prognostic enrichment and bedside risk stratification, but further validation is required before these trajectory classes can be considered definitive respiratory subphenotypes.

Abbreviations

ABG: arterial blood gas ARDS: acute respiratory distress syndrome APACHE II: Acute Physiology and Chronic Health Evaluation II AvePP: average posterior probability BIC: Bayesian information criterion BMI: body mass index CI: confidence interval CRRT: continuous renal replacement therapy CT: computed tomography Cdyn: dynamic lung compliance ECMO: extracorporeal membrane oxygenation FiO_2 : fraction of inspired oxygen HR: hazard ratio ICU: intensive care unit KM: Kaplan–Meier LCMM: latent class mixed model OCC: odds of correct classification $PaCO_2$: partial pressure of arterial carbon dioxide PaO_2 : partial pressure of arterial oxygen P/F: PaO_2 /FiO_2 ratio PEEP: positive end-expiratory pressure

Declarations

Ethics approval and consent to participate

This study was approved by the Medical Ethics Committee of Zhongshan Hospital, Fudan University (No. B2026-019). The requirement for informed consent was waived due to the retrospective nature of the study and use of de-identified data.

Consent for publication

Not applicable.

Availability of data and material

The datasets used and/or analyzed in the present study are available from the corresponding author on reasonable request.

Competing interests

The authors declare no competing interests.

Funding

This work was supported by the Shanghai Municipal Health Commission Fund(GWVI-11.1-14), the Open Project of State Key Laboratory of Respiratory Disease (SKLRD-OP-202321), the Shanghai Key Laboratory of Lung Inflammation and Injury, the Shanghai Health Commission Clinical Research Project (202240334), and the Youth Fund of Zhongshan Hospital, Fudan University (No.2024ZSQN48).

Authors' contributions

Yuxian Wang, Shimin Zhang, Yongsheng Guo, Xin Zheng, and Kai Liu conceived and designed the study. Yuxian Wang, Shimin Zhang, and Yongsheng Guo collected and curated the clinical data. Yuxian Wang, Shimin Zhang, Yongsheng Guo, and Xin Zheng performed the statistical analyses and interpreted the data. Yuxian Wang and Shimin Zhang drafted the manuscript. Xin Zheng, Kai Liu, and Ming Zhong critically revised the manuscript for important intellectual content. All authors reviewed and approved the final manuscript.

Acknowledgments

The authors thank the clinical staff of the Department of Critical Care Medicine, Zhongshan Hospital, Fudan University, for their

support in patient care and data collection.

References

Figure Legends

Figure 1. PaO_2 /FiO_2 trajectory groups across the first two prone positioning cycles and corresponding 28-day Kaplan–Meier survival curves.

(A) Estimated trajectories of the predicted PaO_2 /FiO_2 ratio across the first two prone positioning cycles (T1–T10). T1–T5 represent Cycle 1, and T6–T10 represent Cycle 2. (B) Kaplan–Meier survival curves according to PaO_2 /FiO_2 trajectory class. Shaded areas indicate 95% confidence intervals, tick marks indicate censored observations, and numbers at risk are shown below the plot. The P value was calculated using the log-rank test.

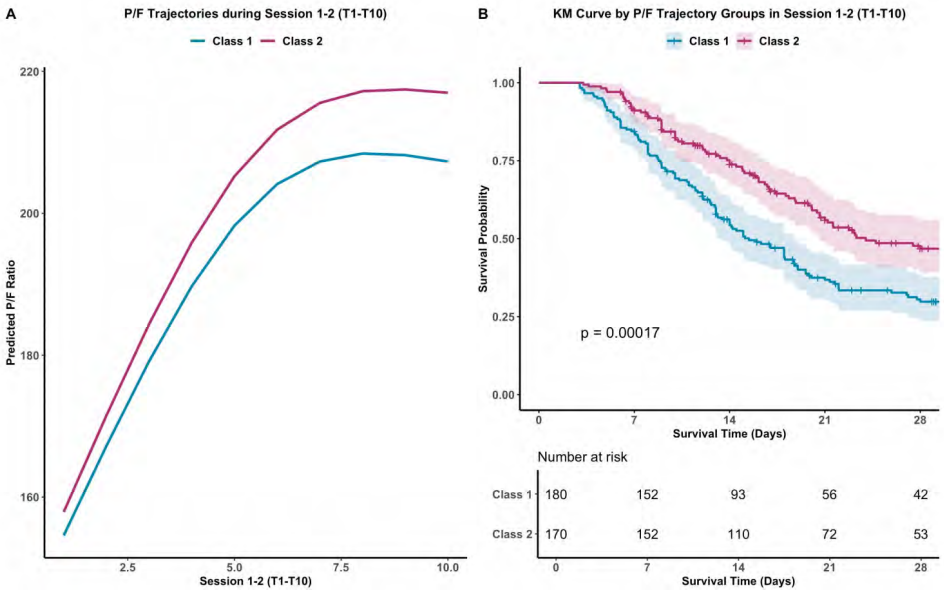


Figure 2. Joint $PaCO_2$ and PaO_2 /FiO_2 trajectory groups across the first twoprone positioning cycles and corresponding 28-day Kaplan–Meier survival curves.

(A) Estimated joint trajectories of $PaCO_2$ and PaO_2 /FiO_2 ratio across the first two prone positioning cycles (T1–T10). T1–T5 represent Cycle 1, and T6–T10 represent Cycle 2. The upper panel shows $PaCO_2$ trajectories, and the lower panel shows PaO_2 / FiO_2 trajectories. Solid lines represent class-specific mean trajectories, and shaded areas indicate 95% confidence intervals. (B) Kaplan–Meier survival curves according to joint trajectory class. Shaded areas indicate 95% confidence intervals, tick marks indicate censored observations, and numbers at risk are shown below the plot. The P value was calculated using the log-rank test.

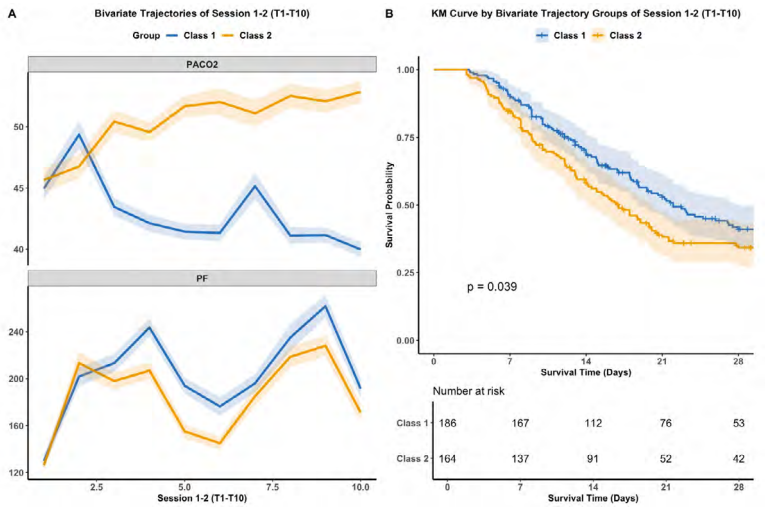


Figure 3. Multivariable Cox regression analyses for 28-day mortality.

Forest plots show adjusted hazard ratios and 95% confidence intervals for variables included in the $PaCO_2$ -only, PaO_2 /FiO_2 -only, and joint PaO_2 /FiO_2 –$PaCO_2$ trajectory models. The vertical reference line denotes a hazard ratio of 1.0. Class 1, male sex, and mild ARDS served as reference categories. Trajectory classes should be interpreted as exploratory trajectory-derived risk strata.

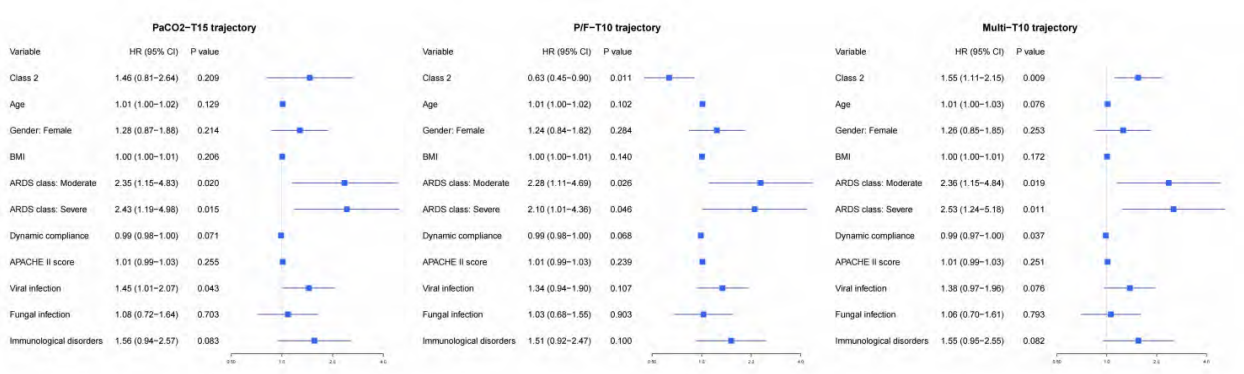


Table 1. Model fit, class distribution, and selection of latent class mixed models across predefined prone positioning windows

Analysis window	Model	Group	BIC	Class
cycle 1 (T1-T5)	Univariate (P/F)	1	16738.80	100%
	Univariate (P/F)	2	16724.82	97.7%/2.3%
	Univariate (P/F)	3	16749.93	0%/97.2%/2.8%
	Univariate (PACO2)	1	10745.12	100%
	Univariate (PACO2)	2	10718.37	96.3%/3.7%
	Univariate (PACO2)	3	10741.83	96.0%/0%/4.0%
	Joint model (P/F+PACO2)	1	7815.60	100%
	Joint model (P/F+PACO2)	2	7818.24	79.5%/20.5%
	Joint model (P/F+PACO2)	3	7841.45	0%/81.5%/18.5%
cycle 1-2 (T1-T10)	Univariate (P/F)	1	2914.61	100%
	Univariate (P/F)	2	2917.16	51.4%/48.6%
	Univariate (PACO2)	1	18153.72	100%
	Univariate (PACO2)	2	18135.89	95.5%/4.5%
	Joint model (P/F+PACO2)	1	13400.33	100%
	Joint model (P/F+PACO2)	2	13422.71	53.1%/46.9%
cycle 1-3 (T1-T15)	Univariate (P/F)	1	36837.50	100%
	Univariate (P/F)	2	36831.42	97.7%/2.3%
	Univariate (P/F)	3	36854.68	67.3%/30.7%/2.0%
	Univariate (PACO2)	1	22907.09	100%
	Univariate (PACO2)	2	22891.77	91.8%/8.2%
	Univariate (PACO2)	3	22921.09	0%/89.2%/10.8%
	Joint model (P/F+PACO2)	1	16925.50	100%
	Joint model (P/F+PACO2)	2	16949.12	5.1%/94.9%
	Joint model (P/F+PACO2)	3	16884.74	3.7%/95.7%/0.6%

BIC, Bayesian information criterion; P/F, PaO_2 /FiO_2 ratio. Models were selected based on a combination of BIC, class size, posterior classification quality, and clinical interpretability. Models with very small or clinically implausible classes were not selected for primary analyses.

Table 2.Baseline characteristics and outcomes according to PaO_2 /FiO_2 and joint PaO_2 /FiO_2 –$PaCO_2$ trajectory classes

	P/F Class 1(n=180)	P/F Class 2(n=170)	p	SMD	Joint Class 1(n=186)	Joint Class 2(n=164)	p	SMD
Age, mean (SD)	69.66(12.56)	70.96(13.73)	0.356	0.099	70.19(13.44)	70.40(12.83)	0.882	0.016
Gender (%),			0.330	0.118			0.380	0.108
Male	134(74.4)	135(79.4)			139(74.7)	130(79.3)		
BMI, mean (SD)	25.58(3.55)	22.81(4.32)	0.243	0.127	22.90(3.60)	25.75(3.08)	0.230	0.125
SBP, mean (SD)	121.96(21.32)	127.17(25.54)	0.038	0.222	124.89(23.12)	124.04(24.14)	0.737	0.036
DBP, mean (SD)	62.46(12.02)	63.70(14.81)	0.390	0.092	63.74(12.49)	62.29(14.45)	0.315	0.107
PEEP, mean (SD)	8.15(2.80)	8.07(2.38)	0.755	0.034	8.16(2.47)	8.06(2.74)	0.707	0.041
Cdyn, mean (SD)	34.68(4.99)	36.33(26.53)	0.696	0.045	33.04(14.58)	38.02(19.94)	0.236	0.135
APACHE II, mean (SD)	21.83(9.41)	20.30(9.08)	0.159	0.165	20.99(9.10)	21.14(9.48)	0.894	0.016
COVID-19 (%)	42(23.3)	39(22.9)	0.999	0.009	38(20.4)	43(20.7)	0.380	0.108
ARDS Class (%),			<0.001	0.693			0.723	0.087
1	9(5.0)	25(14.7)			20(10.8)	14(8.5)		
2	68(37.8)	101(59.4)			87(46.8)	82(50.0)		
3	103(57.2)	44(25.9)			79(42.5)	68(41.5)		
Pneumonia (%)	129(71.7)	107(62.9)	0.104	0.187	122(65.6)	114(69.5)	0.505	0.084
Sepsis (%)	24(13.3)	22(12.9)	0.999	0.012	30(16.1)	16(9.8)	0.109	0.191
Aspiration (%)	22(12.2)	27(15.9)	0.405	0.105	26(14.0)	23(14.0)	0.999	0.001
Trauma (%)	3(1.7)	10(5.9)	0.072	0.223	7(3.8)	6(3.7)	0.999	0.006
Cancer (%)	58(32.2)	56(32.9)	0.977	0.015	59(31.7)	55(33.5)	0.805	0.039
HBP (%)	108(60.0)	100(58.8)	0.908	0.024	110(59.1)	98(59.8)	0.994	0.013
Diabetes (%)	47(26.1)	43(25.3)	0.958	0.019	49(26.3)	41(25.0)	0.869	0.031
Coronary artery disease (CAD) (%)	32(17.8)	27(15.9)	0.741	0.051	33(17.7)	26(15.9)	0.743	0.051
Ischemic stroke (%)	22(12.2)	29(17.1)	0.258	0.137	35(18.8)	16(9.8)	0.025	0.261
Chronic lung disease (%)	37(20.6)	35(20.6)	0.999	0.001	29(15.6)	43(26.2)	0.02	0.264
COPD (%)	5(2.8)	4(2.4)	0.999	0.027	2(1.1)	7(4.3)	0.122	0.199
Immunological disorders (%)	27(15.0)	21(12.4)	0.573	0.077	26(14.0)	22(13.4)	0.999	0.016
Viral infection (%)	62(34.4)	50(29.4)	0.371	0.108	56(30.1)	56(34.1)	0.488	0.087
Bacterial infection (%)	115(63.9)	115(67.6)	0.530	0.079	125(67.2)	105(64.0)	0.608	0.067
Fungal infection (%)	50(27.8)	31(18.2)	0.049	0.265	45(24.2)	36(21.9)	0.472	0.128
CT (%)			<0.001	0.426			0.223	0.147
1	62(35.6)	88(56.4)			86(48.9)	64(41.6)		
2	112(64.4)	68(43.6)			90(51.1)	90(58.4)		
CRRT (%)	58(32.2)	49(28.8)	0.566	0.074	55(29.6)	52(31.7)	0.751	0.046
ECMO (%)	18(10.1)	11(6.5)	0.308	0.130	16(8.6)	13(7.9)	0.960	0.026
28-day mortality (%)	119(66.1)	77(45.3)	<0.001	0.429	95(51.1)	101(61.6)	0.062	0.213

Values are presented as mean (SD) or n (%), as appropriate. SMD, standardized mean difference; BMI, body mass index; PEEP, positive end-expiratory pressure; Cdyn, dynamic lung compliance; APACHE II, Acute Physiology and Chronic Health Evaluation II; CRRT, continuous renal replacement therapy; ECMO, extracorporeal membrane oxygenation.

Table S1.Univariate Cox Regression Analysis

Variable	HR	95% CI	P
Age	1.013	1.002-1.024	0.018
Gender	1.315	0.958-1.806	0.090
BMI	1.005	1.000-1.011	0.073
COVID-19	1.160	0.838-1.606	0.372
ARDS Class	1.233	0.988-1.538	0.064
PEEP	1.011	0.955-1.070	0.705
Cdyn	0.987	0.976-0.998	0.019
APACHE II	1.020	1.004-1.037	0.016
Pneumonia	1.185	0.875-1.605	0.273
Sepsis	1.118	0.754-1.659	0.579
Aspiration	0.801	0.522-1.227	0.307
Trauma	0.868	0.408-1.846	0.714
Cancer	0.893	0.660-1.207	0.461
HBP	0.919	0.690-1.223	0.561
Diabetes	0.990	0.720-1.362	0.953
Coronary artery disease (CAD)	0.968	0.669-1.401	0.862
Ischemic stroke	0.723	0.468-1.118	0.145
Chronic lung disease	1.079	0.767-1.518	0.661
COPD	1.434	0.589-3.488	0.427
Immunological disorders	1.432	0.985-2.082	0.060
Viral infection	1.381	1.031-1.850	0.030
Bacterial infection	0.816	0.609-1.092	0.171
Fungal infection	1.317	0.960-1.807	0.087

Early Warning Value of Electrical Impedance Tomography Combined with Lung Ultrasound for Pulmonary Infection in Neurocritical Care Patients

姓名：胡丽蓉

单位：西南医科大学附属医院

Abstract

Early Warning Value of Electrical Impedance Tomography Combined with Lung Ultrasound for Pulmonary Infection in Neurocritical Care Patients

Objective: To investigate the early warning value of electrical impedance tomography (EIT) combined with lung ultrasound (LUS) for pulmonary infection in neurocritical care patients.

Methods: A total of 330 neurocritical care patients admitted to the Department of Critical Care Medicine at the Affiliated Hospital of Southwest Medical University between January 2025 and January 2026 were retrospectively enrolled. All patients underwent dynamic EIT and LUS monitoring. According to whether pulmonary infection occurred during hospitalization, the patients were divided into an infection group (n = 108) and a non-infection group (n = 222). General clinical characteristics, oxygenation index, inflammatory markers, EIT parameters, and LUS scores were collected. The EIT parameters included the global inhomogeneity index (GI), dorsal ventilation proportion, regional ventilation delay (RVD), and changes in end-expiratory lung impedance. Differences in these indicators were compared between the two groups. Multivariable logistic regression analysis was performed to identify independent factors associated with pulmonary infection in neurocritical care patients. Receiver operating characteristic (ROC) curves were constructed to evaluate the early warning performance of EIT, LUS, and their combination. The DeLong test was used to compare the areas under the ROC curves among the different prediction models.

Results: The LUS score, GI, and RVD in the infection group were 16.82 ± 4.26 points, 0.49 ± 0.08, and 8.71 ± 2.15%, respectively, which were significantly higher than those in the non-infection group (8.36 ± 3.14 points, 0.41 ± 0.07, and 5.46 ± 1.83%, respectively). The dorsal ventilation proportion and oxygenation index in the infection group were 42.63 ± 7.85% and 214.36 ± 48.27 mmHg, respectively, which were significantly lower than those in the non-infection group (49.74 ± 8.16% and 286.52 ± 55.41 mmHg, respectively). All differences were statistically significant (all $P < 0.001$). Multivariable logistic regression analysis showed that an increased LUS score, an elevated GI, prolonged RVD, and a decreased dorsal ventilation proportion were independently associated with pulmonary infection in neurocritical care patients (all $P < 0.05$). ROC curve analysis showed that the area under the curve (AUC) of EIT alone was 0.781 (95% confidence interval [CI]: 0.731–0.831), with a sensitivity of 75.0% and a specificity of 72.1%. The AUC of LUS alone was 0.824 (95% CI: 0.780–0.869), with a sensitivity of 78.7% and a specificity of 76.6%. The AUC of EIT combined with LUS was 0.901 (95% CI: 0.868–0.934), with a sensitivity of 86.1% and a specificity of 83.8%. The DeLong test showed that the AUC of the combined model was significantly higher than those of EIT alone and LUS alone ($P < 0.001$ and $P = 0.006$, respectively).

Conclusion: Pulmonary infection in neurocritical care patients is characterized by increased pulmonary ventilation heterogeneity, prolonged regional ventilation delay, a decreased dorsal ventilation proportion, and an elevated LUS score. The combination of EIT and LUS enables bedside, non-invasive, and dynamic assessment of both regional pulmonary ventilation and lung morphological changes. Its early warning performance is superior to that of EIT or LUS alone and may provide a useful reference for the early identification and timely clinical management of pulmonary infection in neurocritical care patients.

Keywords: electrical impedance tomography; lung ultrasound; neurocritical care; pulmonary infection; early warning

类别 :// 临床研究：设计规范的各类临床研究及研究方案报告

Effect of age on comorbidities and occurrence and outcome of sepsis in ICU patients in China: a national cohort study

姓名：史楠，李文韬，陈辉，谢剑锋

单位：东南大学附属中大医院

Age and comorbidities are established risk factors for sepsis occurrence and poor clinical outcomes. However, national data on their age-specific joint associations with sepsis occurrence and outcome in China are limited.

We conducted this hospital-based observational study using data from intensive care units (ICUs) in the National Hospital Quality Monitoring System (HQMS) for 2023. Sepsis was identified using explicit ICD‐10 codes or implicit criteria defined as infection with organ dysfunction. Comorbidities were classified and scored by the Charlson Comorbidity Index (CCI). The primary outcome was defined as in-hospital death or discharge against medical advice (DAMA). Multivariable logistic regression was employed to assess associations of comorbidity number with sepsis occurrence and exacerbated outcome. Age-stratified analyses across eight age groups were performed to evaluate how age modified these associations.

In 2023, the HQMS database included 3,984,278 ICU patients from 4,113 hospitals, the mean age was 62 (standard deviation 17) years, and 2,226,586 (55.88%) were male. Of these, 1,442,113 (36.20%) patients were diagnosed with sepsis. Among sepsis patients, 171,802 (11.91%) died in hospital, and in-hospital death/DAMA rate was 40.18%. In terms of hospitalization costs, with increasing comorbidity burden and age, the out-of-pocket proportion of total expenses decreased. For sepsis occurrence, a higher number of comorbidities was independently associated with increased occurrence of sepsis. This association was strongest in younger patients and weakened progressively with age. In adultsyounger than 30 years, CCI was the dominant determinant of sepsis occurrence (aOR = 5.02, 95%CI 4.90-5.13, $p < 0.001$), whereas age showed a modest protective effect (aOR = 0.98, 95% CI 0.98-0.98, $p < 0.001$). In patients aged 50-89 years, the CCI effect declined steadily (aOR range: 2.12-1.66, $p < 0.001$), while the age effect was gradually enhanced (aOR range: 1.01-1.05, $p < 0.001$). Besides, the number of comorbidities wasidentified as a risk factor for exacerbated outcome, and similar age-dependent patterns were observed.

Sepsis remains a substantial burden in ICUs across China. For sepsis occurrence and exacerbated outcome, the dominant risk factor shifted from comorbidity in adults aged < 30 years to age in those aged 50-89 years. These findings may offer some insights into the formulation of health policies.

Effect of anisodamine hydrobromide on improving early microcirculation disturbance in septic shock patients

姓名：Xiaoxu Ding[a1]，Liwei Yan[b1]，Qi Yan[c2]，Xin Zhang[a3]，Hao LI[d*]，Zhanbiao Yu[a*]

单位：1 Department of Critical Care Medicine, Affiliated Hospital of Hebei University

2 Department of Gynecology, Affiliated Hospital of Hebei University

3 Department of Pharmacy, Affiliated Hospital of Hebei University

Summary:

BACKGROUND: Septic shock, prevalent in critical care medicine, poses significant treatment challenges and high mortality rates. Its pathogenesis involves an inflammatory cytokine storm and microcirculatory dysfunction, potentially leading to fatal multiple organ failure. Microcirculation alterations during septic shock critically impact patient outcomes. Anisodamine hydrobromide, a commonly used anticholinergic, mitigates oxidative stress and modulates cell apoptosis, notably enhancing microcirculation by targeting cholinergic receptors. This study investigates the efficacy of anisodamine hydrobromide in ameliorating microcirculatory disorders in septic shock patients.

Methods: This article collects 72 cases of patients with septic shock from the Department of Critical Care Medicine, Affiliated Hospital of Hebei University from 2024 to 2025. Participants were assigned to either a treatment group or a control group based on the administration of anisodamine hydrobromide. Data on heart rate, mean arterial pressure (MAP), blood lactate (LAC) levels, peripheral blood perfusion index (PI), and mottling scores were collected at 0, 6, 24, and 48 hours post-admission. Additionally, the 28-day mortality rate and progression from acral cyanosis to acral necrosis were assessed. Statistical analysis was conducted to compare differences in these indices between the groups.

Results: No statistically significant difference was observed in 28-day mortality between the treatment and control groups (14% vs. 16%; p =0.86). Norepinephrine dosage also showed no significant difference. Heart rates at 6 and 24 hours post-treatment were statistically similar; however, at 48 hours, the treatment group exhibited a significantly lower heart rate than the control group. ScvO2 and Pcv-aCO2 levels did not differ significantly between groups at any time point (all p >0.05). Comparison of microcirculatory oxygen metabolism indicators between the groups: The treatment group exhibited significant improvements in lactate and PI compared to the control group (P ＜ 0.05). At 6 and 24 hours post-treatment, the SMS scores were lower in the treatment group, though no significant difference was observed at 48 hours. CRT showed no difference at 6 hours, but the treatment group demonstrated significant improvement at 24 and 48 hours (P >0.05). No statistically significant difference was found in the progression from acral cyanosis to acral necrosis between the groups.

Conclusion: The standardized treatment of septic shock, when combined with anisodamine hydrobromide infusion, enhances early microcirculation indicators in septic shock patients.

Keywords: Anisodamine hydrobromide; Septic shock; Microcirculation disorder; Blood lactic acid (LAC); Peripheral perfusion index (PI); Mottling score; Acral cyanosis; Acral necrosis.

Septic shock is characterized by sepsis with severe circulatory and cellular metabolic dysfunctions. The infection initiates an innate immune response, activating immune cells like mononuclear macrophages to release inflammatory mediators such as tumor necrosis factor-α (TNF-α), interleukin (IL)-1, and IL-6. Normally, the body’s anti-inflammatory mechanisms maintain equilibrium, but in septic shock, the inflammatory response becomes excessive and persistent, disrupting this balance and causing tissue damage. Inflammatory mediators harm vascular endothelial cells, increase vascular permeability, and lead to plasma exudation into tissue spaces, reducing effective circulating blood volume. Concurrently, vasomotor dysfunction results in abnormal vasodilation and microthrombus formation, impairing blood perfusion and depriving tissues and organs of adequate oxygen and nutrients[1].

Microcirculatory dysfunction is pivotal in the development of tissue hypoxia and organ failure during sepsis [2]. Despite achieving macro-hemodynamic resuscitation targets, microvascular perfusion alterations often persist. These microcirculatory issues intensify tissue hypoxia, shifting energy metabolism from aerobic to anaerobic, resulting in lactic acid accumulation and acidosis. Septic shock frequently involves decreased effective volume, leading to peripheral circulatory failure. Numerous studies have

focused on evaluating peripheral circulation in shock treatment.[3]. In septic shock, peripheral vasoconstriction prioritizes blood flow to vital organs, reducing the perfusion index (PI). The extent of PI reduction correlates with shock severity. Research indicates that lower PI values are associated with severe microcirculatory disorders, such as poor skin perfusion, serving as an early indicator and severity assessment tool for shock.

The presence of mottled skin during an initial patient assessment is a strong indicator of critical illness, often signaling hypoxia and blood stasis in terminal vessels. The mottling score serves as a semi-quantitative index for evaluating the severity of sepsis [4]. Elucidating the pathophysiological basis of the mottling score enhances its utility in assessing microcirculation. Bourcier's vascular reactivity tests revealed that patients with mottled skin frequently exhibit endothelial dysfunction [5]. Additionally, some researchers suggest that coagulation cascade activation and vasoconstriction, triggered by heightened sympathetic stress, contribute to mottling [6].

The primary pathophysiological mechanism of septic shock is microcirculatory dysfunction, leading to tissue hypoxia, organ dysfunction, and potentially life-threatening conditions. This can be viewed as a severe endothelial dysfunction syndrome. Infection triggers reversible or irreversible microcirculatory damage, significantly contributing to multiple organ failure [7]. Thus, regulating the inflammatory response and repairing endothelial damage are crucial in treating septic shock. Anisodamine hydrobromide has demonstrated efficacy in enhancing microcirculation and mitigating reperfusion injury by reducing oxidative stress, inhibiting apoptosis, alleviating inflammation, and activating the cholinergic anti-inflammatory pathway [8][9]. The current research on anisodamine for treating septic shock remains inadequate. Studies have not demonstrated that anisodamine reduces in-hospital mortality among critically ill adults with septic shock in intensive care [10]. Consequently, we conducted a randomized controlled trial focusing on microcirculation indicators, including blood lactic acid levels, peripheral perfusion index, mottling score, and the progression of acral cyanosis to necrosis. This trial aims to assess whether anisodamine hydrobromide can enhance microcirculation.

1 Data and methods

1.1 General Data：Clinical data from 72 septic shock patients admitted to the Department of Critical Care Medicine at the Affiliated Hospital of Hebei University between January 2024 and June 2025 were analyzed. Of these, 41 patients treated with anisodamine hydrobromide constituted the experimental group, while 31 untreated patients formed the control group. The mean age was 64 ± 10 years. Predominant conditions included severe pneumonia, urinary tract infections, enterogenic infections, and postoperative intra-abdominal infections.

1.2 Inclusion Criteria: ① Confirmed infection site. ② Systolic blood pressure (SBP) below 90 mmHg, necessitating vasopressors for stabilization. ③ Blood lactate levels exceeding 2 mmol/L.

1.3 Exclusion criteria：Patients younger than 18 years of age, pregnant women and patients with known peripheral vascular disease (e.g. peripheral arterial occlusive disease, vasculitis) were excluded.

1.4 Grouping Methods: Patients with septic shock were divided into two groups based on the administration of anisodamine hydrobromide. Both groups received standard septic shock treatment, including fluid resuscitation, vasopressors, empirical antibiotics, and organ support. In the experimental group, anisodamine hydrobromide was delivered via pump. The initial intravenous bolus was 0.5 mg/kg, with a minimum of 20 mg and a maximum of 40 mg. The maintenance dose ranged from .02 to .1 mg/kg/h, adjusted by the treating physician according to vital signs, lactate levels, and adverse reactions, with a daily maximum of 200 mg. Drug withdrawal criteria included: 1) recovery from shock (normal serum lactate levels and cessation of vasopressors); 2) unresolved drug-related complications despite symptomatic treatment (e.g., arrhythmia, allergic reaction, intestinal obstruction); 3) patient death.

1.5 Methods: A central venous catheter was inserted via the internal jugular or subclavian vein to simultaneously collect central venous and peripheral arterial blood for gas analysis. Indicators measured at admission and 12, 24, and 48 hours post-treatment included central venous oxygen saturation ($ScvO_2$), central venous partial pressure of carbon dioxide ($PcvCO_2$), peripheral arterial blood lactate (Lac), arterial partial pressure of carbon dioxide, pulse perfusion index (PI), capillary refill time (CRT), and skin mottling score (SMS). Statistical differences in these indicators, 28-day mortality, and the number of patients with acral cyanosis or progressing to acral necrosis were compared between the two groups.

1.6 Microcirculation monitoring indicators: Skin mottling score (SMS) was assessed using the criteria by Ait-Oufella et al. to evaluate peripheral microcirculatory perfusion. Capillary refill time (CRT) involved raising the patient's right index finger to heart level and pressing the fingertip with a glass slide until blanching occurred. After 10 seconds, the slide was removed, and the time for color return was recorded with a stopwatch; this process was repeated twice for an average. A CRT of ⩾ 3 seconds indicated microcirculatory impairment. Pulse perfusion index (PI) was measured using a Mindray pulse oximetry monitor, with the middle finger as the consistent measurement site.

1.7 Statistical Methods: Statistical analyses were conducted using SPSS software. Non-normally distributed measurement data were reported as medians with interquartile ranges Q2 (Q1, Q3). Group comparisons employed the Mann-Whitney U test, while paired samples with non-normal distributions were analyzed using the Wilcoxon signed-rank test. Binary variable comparisons between two groups utilized the Pearson chi-square test. Statistical significance was set at $P < .05$. Survival curves for 28-day survival trends were generated using the Kaplan-Meier method, and the Fine-Gray test assessed differences in extremity necrosis risk between the groups.

2.Outcomes

2.1 Participants

Baseline characteristics of the patient groups: From the Department of Critical Care Medicine at the Affiliated Hospital of Hebei University, 85 patients were initially screened. Exclusions included 2 patients who died within 6 hours of admission, 2 with intestinal obstruction, 5 with an ICU stay exceeding 24 hours at enrollment, 1 with glaucoma, and 3 in the acute phase of cerebral hemorrhage. Ultimately, 72 patients were included: 41 in the treatment group and 31 in the control group. All patients were on mechanical ventilation; 46 underwent CRRT, and 2 received ECMO. In the treatment group, anisodamine hydrobromide was administered for an average of 3.1 days.

Table 1 Baseline characteristics of control and treatment groups

Variables	Total (n = 72)	Control (n = 31)	Treated (n = 41)
Age (years), Median (Q1, Q3)	67(56, 75)	67(54, 76)	68(60, 71)
Gender, male n (%)	39 (55%)	21(51%)	18 (58%)
Disease n(%)			
Craniocerebral injury	1(1.39%)	1(2.44%)	0(0.00%)
Intestinal perforation	3(4.17%)	3(7.32%)	0(0.00%)
Pneumonia	30(41.67%)	16(39.02%)	14(45.16%)
Cholangitis	5(6.94%)	3(7.32%)	2(6.45%)
Intestinal necrosis	1(1.39%)	1(2.44%)	0(0.00%)
Intestinal infection	2(2.78%)	1(2.44%)	1(3.23%)
Urinary tract infection	6(8.33%)	3(7.32%)	3(9.68%)
Gastric cancer	1(1.39%)	1(2.44%)	0(0.00%)
Abdominal infection	1(1.39%)	1(2.44%)	0(0.00%)
Gastric perforation	4(5.56%)	3(7.32%)	1(3.23%)
Uterine perforation	1(1.39%)	1(2.44%)	0(0.00%)
Skin and soft tissue infection	2(2.78%)	1(2.44%)	1(3.23%)
Appendicitis	1(1.39%)	1(2.44%)	0(0.00%)
Liver abscess	2(2.78%)	1(2.44%)	1(3.23%)
Infective endocarditis	1(1.39%)	1(2.44%)	0(0.00%)
Abdominal trauma	1(1.39%)	1(2.44%)	0(0.00%)
Intestinal tumor	1(1.39%)	0(0.00%)	1(3.23%)
Leukemia	1(1.39%)	0(0.00%)	1(3.23%)
COPD	3(4.17%)	1(2.44%)	2(6.45%)
Pancreatitis	3(4.17%)	1(2.44%)	2(6.45%)
Intracranial infection	1(1.39%)	0(0.00%)	1(3.23%)
Peritonsillar inflammation	1(1.39%)	0(0.00%)	1(3.23%)
Main infection site n(%)			
Lung n(%)	35(48.61%)	19(46.34%)	16(51.61%)
Biliary system n(%)	5(6.94%)	3(7.32%)	2(6.45%)
Abdominal cavity n(%)	16(22.22%)	12(29.27%)	4(12.90%)
Intracranial n(%)	1(1.39%)	0(0.00%)	1(3.23%)
Blood n(%)	3(4.17%)	1(2.44%)	2(6.45%)
Endocardium n(%)	1(1.39%)	1(2.44%)	0(0.00%)
Intestine n(%)	2(2.78%)	1(2.44%)	1(3.23%)
Skin and soft tissue n(%)	2(2.78%)	1(2.44%)	1(3.23%)

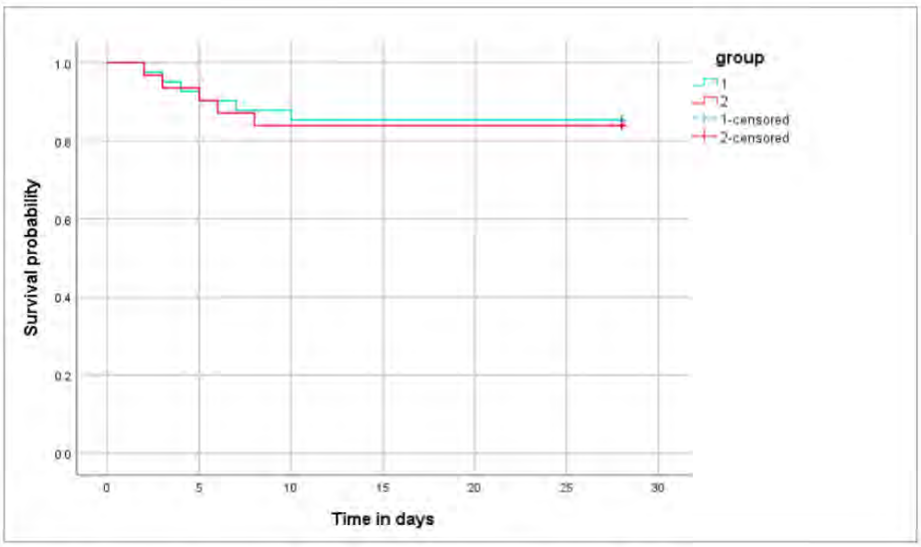
Urinary system n(%)	6(8.33%)	3(7.32%)	3(9.68%)
Other sites n(%)	1(1.39%)	0(0.00%)	1(3.23%)
Condition upon admission to the department			
SOFA (Q1、Q3)	12(12,14)	13(12,14)	12(12,15)
APEACHii score (Q1, Q3)	14(15,16)	13(15,16)	14(15,16)

Note:Both patient groups received septic shock treatment according to the Sepsis-3 Guidelines bundle. The control group additionally received an intravenous infusion of anisodamine hydrobromide alongside standard treatment. Lac denotes blood lactate, ScvO2 central venous oxygen saturation, PcCO2 (v-a) the central venous-arterial carbon dioxide partial pressure difference, PI the pulse perfusion index, SMS the skin mottling score, and CRT the capillary refill time.

2.2 Comparison of mortality between treatment and control groups

The in-hospital mortality rate for the treatment group was marginally lower than that of the control group, though the difference was not statistically significant (14% vs. 16%; p = .86). The log-rank test of the Kaplan-Meier survival curves indicated no significant survival difference between the groups (Figure 1).

Figure 1 Kaplan-Meier survival curve



Note：1 represents treatment group and 2 represents control group.

2.3 Comparison of clinical indicators between the treatment group and the control group

No significant difference in 28-day mortality was observed between the patient groups. Norepinephrine dosage within 48 hours post-treatment and heart rate at 6 and 4 hours post-treatment showed no significant differences between the groups. However, at 48 hours, the treatment group exhibited a statistically significant decrease in heart rate compared to the control group. $ScvO_2$ and $Pcv\text{-}aCO_2$ levels showed no significant differences across all time points (P >0.05). In terms of microcirculatory oxygen metabolism, lactic acid and PI levels significantly improved in the treatment group compared to the control group ($P < 0.05$). SMS scores were lower in the treatment group at 6 and 24 hours post-treatment, with no notable difference at 48 hours. Conversely, CRT scores showed no difference at 6 hours but significantly improved in the treatment group at 24 and 48 hours ($P < 0.05$) (Table 2)..

Regarding the comparison of oxygen metabolism indicators in the microcirculation between the two groups, levels of lactic acid and perfusion index (PI) were significantly improved in the treatment group compared to the control group (P>0.05). The Sequential Organ Failure Assessment (SOFA) scores in the treatment group were lower than those in the control group at 6 hours and 24 hours post-treatment, with no significant difference between the groups at 48 hours. Conversely, when comparing the groups using the Capillary Refill Time (CRT) parameter, there was no distinction at 6 hours, but significant improvement was

observed in the treatment group at 24 hours and 48 hours (P>0.05) (Table 2).

Table 2 Comparison of primary and secondary clinical outcomes between treatment and control groups

Variables	Total (n=72)	Control (n=31)	Treated (n=41)	p value
28-day mortality rate	11 (15%)	6 (14%)	5 (16%)	0.860
Median NE dosage Median(Q1、Q3)				
0h	0.5(0.4,0.65)	0.5 (0.4,0.6)	0.5 (0.4,0.675)	0.880
6h	0.4(0.4,0.5)	0.4(0.3,0.4)	0.5(0.4,0.6)	0.122
24h	0.3(0.3,0.4)	0.3(0.2,0.3)	0.4(0.3,0.4)	0.271
48h	0.1(0.1,0.2)	0.1(0.1,0.1)	0.2(0.2,0.2)	0.101
heart rate median(Q1、Q3)				
0h	98(84.5,109.5)	98(78,110)	99(88,109)	0.350
6h	86.5(75,98)	78(68,95)	87(78,98)	0.178
24h	78(67,86.5)	76(67,86)	78(68.5,87)	0.218
48h	69.5(65.75,78.5)	68(65,76)	78(67,89)	0.005
LAC median(Q1、Q3)				
0h	3.35(2.75,4.4)	3.2(2.8,4.7)	3.4(2.6,3.4)	0.945
6h	2.1(1.6,3.1)	1.4(1.3,1.6)	3.1(2.1,4.2)	0.000
24h	1.55(1.375,2.5)	1.4(1.3,1.6)	2.5(1.55,4.225)	0.000
48h	1.35(1.1,2.05)	1.1(1,1.3)	2.1(1.5,2.1)	0.000
ScVO2% median(Q1、Q3)				
0h	58(54,65)	58(54,65)	57(54,65)	0.750
6h	64(57.75,65)	64(62,65)	63(56,65)	0.102
24h	65(61.75,67)	5(63,67)	64(58,68.75)	0.141
48h	67(63.75,69)	67(65,69)	68(62,72.75)	0.454
P(v-a)CO2 median(Q1、Q3)				
0h	7(6,8)	7(6,8)	7(6,8.75)	0.754
6h	5(4,6)	5(5,6)	5(4,6)	0.053
24h	5(4,6)	5(4,5)	5(3.5,6)	0.500
48h	4(3,5)	4(4,5)	4(3,5)	0.326

Variables	Total (n=72)	Control (n=31)	Treated (n=41)	p value
PI median(Q1、Q3)				
0h	1.1(0.515,1.35)	1.1 (0.5,1.4)	1.1 (0.525,0.75)	0.954
6h	1.6(1.275,2.1)	1.7 (1.5,2.3)	1.28 (0.965,1.95)	0.020
24h	2.1(1.4,2.5)	2.4 (2.1,3.1)	1.45 (1.07,1.885)	0.000
48h	2.4(1.875,2.4)	2.7 (2.4,3.2)	1.9 (1.8,2.2)	0.000
SMS median(Q1、Q3)				
0h	3 (2,4)	3(3,4)	4(3,5)	0.199
6h	1.5 (1,2)	1(1,2)	2 (1.5,3)	0.001
24h	1 (1,2)	1(1,1)	2 (1,2)	0.014
48h	1(0,2)	0(0,1)	2 (0,2)	0.057
CRT median(Q1、Q3)				
0h	4 (3,5)	4 (3,5)	4 (3,5)	0.341
6h	4 (3,4.5)	4 (3,5)	3 (3,4)	0.708
24h	3 (2,4)	3 (2,4)	3 (3,4)	0.010
48h	3 (2,4)	2 (2,4)	3 (2.5,4)	0.021

2.4 Comparison of patients with acral cyanosis progressing to acral necrosis between the two groups.

Table 3 details the incidence of acral cyanosis in each group.

Group	Number of cases	Acrocyanosis	No acral cyanosis	Statistic	P value
Control	41	9 (21.95%)	32 (78.05)	χ^2=1.12	0.29
Treatment	31	10 (32.26)	21 (67.74)	df=1	—
Total	72	19 (26.39)	53 (73.61)	—	—

Table 4: Distribution of acral cyanosis eve[+]rogressing to necrosis and mortality across two patient groups.

Group	Total	Limb Necrosis	Death (Competing event)	Censored
Control	10	2 (20.0%)	4 (40.0%)	4 (40.0%)
Treatment	9	1 (11.1%)	4 (44.4%)	4 (44.4%)

Table 5: Fine—Gray competing risks analysis results.

Variable	sHR	95% CI	P value
Treatment vs Control	0.51	0.07 - 3.48	0.49

sHR: Subdistribution Hazard Ratio



Figure 1: Limb necrosis in patients with acral necrosis.



Panel A illustrates early-stage right thumb necrosis in the treatment group. Panel B depicts late-stage right thumb necrosis in the treatment group. Panel C shows early-stage necrosis of the right toes and sole in the control group. Panel D presents late-stage necrosis of the right toes and sole in the control group.

Symmetric peripheral gangrene (SPG) is characterized by cyanosis and ecchymosis of the extremities, typically starting at the fingers and progressing proximally, potentially leading to necrosis, ulcers, and ultimately gangrene. Table 3 compares acrocyanosis occurrence between two patient groups. In the experimental group, 9 out of 41 cases (21.95%) exhibited acrocyanosis, whereas in the control group, 10 out of 31 cases (32.26%) showed this symptom. A chi-square test yielded X2 = 1.12, df = 1, and P = .29, indicating no statistically significant difference in acrocyanosis incidence between the groups. Table 4 details patient outcomes with acral cyanosis. In the control group, 2 out of 10 patients (20%) progressed to acral necrosis, 4 (40.%) died before necrosis could be observed, and 4 (40.%) did not develop necrosis. In the experimental group, 1 out of 9 patients (11.1%) progressed to acral necrosis, 4 (44.4%) died before necrosis observation, and 4 (44.4%) did not develop necrosis. The Fine-Gray competing risk model (Table 5) yielded a sub-distribution hazard ratio (sHR) of .51 (95% CI: .07–3.48) for the experimental group compared to the control, with a P-value of 0.49, indicating no significant difference in acral necrosis risk between the groups.

3. discussion

Advancements in septic shock treatments reveal that achieving macro-hemodynamic stability is merely a component of sepsis management; the primary objective is optimizing microvascular blood flow. Septic shock often disrupts "hemodynamic coherence," indicating a disconnect between systemic and microcirculatory responses[11]. Clinically, using high-dose vasoactive drugs to maintain mean arterial pressure (MAP) above 65 mmHg frequently results in extremity necrosis[12]. Effective organ and tissue perfusion necessitates optimizing microcirculatory regulation—targeting arterioles, capillaries, and venules—rather than solely maintaining blood pressure, which can lead to peripheral vascular occlusion[13]. Thus, identifying methods and drugs to enhance microcirculation is imperative.

This study assessed anisodamine hydrobromide's impact on microcirculation and clinical outcomes. No significant difference in 28-day mortality was observed between the groups, likely due to the multifactorial nature of septic shock, which involves complex interactions such as multiple organ failure, gastrointestinal ischemia, and the adequacy of cardiopulmonary resuscitation [14]. While anisodamine hydrobromide enhances microcirculation, it may not mitigate other lethal risk factors like uncontrolled infection sources and organ failure. The "macrovasodilation and microvasoconstriction" seen in septic shock reflects pathological disparities in systemic inflammatory responses and vascular regulation across different vessel levels, influenced by vascular structure, regulatory mechanisms, and local microenvironment changes [15]. The tension in large blood vessels, such as the aorta, middle artery, and vein, is primarily influenced by neurohumoral regulation and systemic inflammatory mediators[16]. Infections activate immune cells to release inflammatory factors like TNF-α and IL-6, prompting cells in the liver, kidney, and intestine to produce substantial amounts of nitric oxide (NO)[17]. As a potent vasodilator, NO penetrates vascular smooth muscle cells, activating guanylate cyclase and increasing cGMP, which leads to smooth muscle relaxation. Research indicates that anisodamine hydrobromide's antishock effect is mediated by IL-10, and this effect is significantly reduced in IL-10-deficient mice[18]. However, not all septic shock patients exhibit elevated IL-10 levels; insufficient anti-inflammatory compensation can result in an excessive pro-inflammatory response, causing severe tissue damage. This impairs immune cell function, diminishes pathogen clearance, complicates infection control, and worsens prognosis. In such cases, the antishock efficacy of anisodamine hydrobromide is limited. The lack of statistical difference in norepinephrine (NE) dosage between the two groups within 48 hours post-treatment can be attributed to the regulation of large vessel tension primarily by sympathetic nerves (via α-adrenergic receptors), the renin-angiotensin system, and humoral factors like catecholamines and endothelin[19]. M-choline receptors are sparsely distributed on smooth muscle cells. Anisodamine hydrobromide, a selective M-choline receptor antagonist, primarily affects M-receptors on small vessel smooth muscle, alleviating spasms by counteracting acetylcholine and other vasoconstrictors. In contrast, its direct impact on large vessels such as the aorta, superior mesenteric artery, and renal artery is minimal due to the low density of M receptors, thus not significantly altering basal tension. Consequently, any improvement in blood pressure or reduction in blood pressure medication is negligible.

Macrocirculatory parameters, such as central venous oxygen saturation ($ScvO_2$) and the central veno-arterial carbon dioxide gradient (Pcv-aCO_2), are often used to evaluate systemic oxygen metabolism and tissue perfusion [20, 21]. In this study, no

significant differences in $ScvO_2$ and Pcv-aCO_2 were observed between the treatment and control groups at any time point. This suggests that anisodamine hydrobromide primarily enhances microcirculation perfusion with minimal impact on systemic oxygen metabolism. Whole-body oxygen metabolism is influenced by factors such as respiratory function and hemoglobin levels. Following microcirculation improvement by anisodamine hydrobromide, noticeable changes in systemic oxygen metabolism may require extended time or complex physiological adjustments.

In the microcirculation oxygen metabolism index, the lactic acid levels in the PI treatment group showed a significant improvement compared to the control group. Lactate is crucial for diagnosing and assessing septic shock [22] and serves as a vital marker of tissue hypoxia and anaerobic metabolism [23]. A reduction in lactate levels suggests that anisodamine hydrobromide effectively alleviates tissue hypoxia. This effect is attributed to anisodamine hydrobromide's ability to block M choline receptors on vascular smooth muscle, thereby alleviating microvasospasm (including arterioles, venules, and pre-capillary sphincters), stabilizing the endothelium, and inhibiting microthrombosis [24, 25]. Enhancing microcirculatory blood flow improves tissue and organ oxygenation. Correcting tissue hypoxia mitigates anaerobic metabolism, thereby lowering lactic acid production and blood lactate levels. The perfusion index (PI), indicating local tissue blood flow, is calculated as the ratio of the pulse wave in pulsating to non-pulsating regions. While research on macrocirculatory stability in septic shock patients is well-established, microcirculation has emerged as a focal point of study. It is recognized that microcirculatory failure is a fundamental pathological feature of septic shock, with clinical challenges often arising from the decoupling of macro- and microcirculation [26]. During septic shock, the release of inflammatory mediators like TNF-α and IL-6, along with sympathetic excitation and vasoactive substances such as catecholamines and angiotensin, induces persistent spasms and contractions in systemic microvessels, particularly arterioles and precapillary sphincters. This phenomenon effectively "blocks" the microcirculation pathway entrance, hindering blood flow into the capillary bed and leading to tissue ischemia and hypoxia[27]. The study's observed improvement in PI underscores the regulatory impact of anisodamine hydrobromide on microcirculation, enhancing microvascular perfusion and tissue oxygenation. These findings indicate that anisodamine hydrobromide significantly improves microcirculatory oxygen metabolism, playing a crucial role in alleviating tissue hypoxia in septic shock patients.

The speckle score (SMS) was employed as a specific index to assess peripheral microcirculation disorders in shock severity[28]. Scores for the treatment group were significantly lower than those of the control group at 6 and 24 hours post-treatment, with no significant difference observed at 48 hours. The speckle score quantifies the extent and duration of skin speckle, directly reflecting the perfusion state of skin microcirculation. The early-stage decrease in scores suggests that anisodamine hydrobromide rapidly restores microcirculation perfusion in peripheral tissues, such as skin, by alleviating arteriolar spasm and improving capillary blood flow. However, the score difference diminished at 48 hours, possibly due to improved microcirculation in the control group from overall treatment measures like fluid resuscitation and antibiotic intervention. Additionally, the speckle score's sensitivity may decline in the later shock stages, as vascular endothelial damage from prolonged hypoxia necessitates more complex repair mechanisms[29].

Distal gangrene in septic shock patients typically signals severe hypotension or elevated vasoconstrictor drug use, manifesting symmetrically or locally in fingers, toes, and potentially extending to feet or legs[30]. Unlike large artery occlusion, SPG arises from microvascular dysfunction and small vessel thrombosis[31]. This pathophysiology likely stems from a significant imbalance between procoagulant and anticoagulant factors within the tissue vascular bed, leading to microthrombosis[32、33]. Anisodamine hydrobromide theoretically inhibits microthrombosis, yet the study failed to confirm its efficacy in reversing acrocyanosis and necrosis. This may be due to acrocyanosis necrosis being the end-stage manifestation of microcirculation disorders, which involves not only microthrombosis but also factors like vascular endothelial injury, apoptosis, and metabolic failure from prolonged tissue ischemia. Anisodamine hydrobromide primarily acts by inhibiting thromboxane synthesis and improving early microcirculation blood flow. However, it is insufficient as a single intervention to halt necrosis driven by irreversible cellular damage and multifactorial tissue necrosis. Its impact on microcirculation is more apparent in hemodynamic measures, such as improved perfusion index (PI) and reduced lactate (LAC) levels. Nonetheless, acronecrosis results from long-term severe ischemia, and short-term hemodynamic improvements may not fully reverse ischemic tissue damage, thus inadequately reducing necrosis incidence. Additionally, the study's small sample size warrants consideration, suggesting the need for larger-scale research to delve deeper into this area.

Anisodamine hydrobromide effectively enhances early microcirculation oxygen metabolism, reduces heart rate, and improves

peripheral circulation in septic shock patients. While it did not significantly impact 28-day mortality, NE dosage, systemic oxygen metabolism, or limb necrosis improvement in this study, its efficacy in addressing microcirculation disorders remains notable. Future research should increase sample size, extend observation periods, and investigate the mechanisms and combined effects with other treatments to develop more effective strategies for septic shock management.

References

[1] De Backer D, Ricottilli F, Ospina-Tascón GA. Septic shock: a microcirculation disease. Curr Opin Anaesthesiol. 2021 Apr 1;34(2):85-91. doi: 10.1097/ACO.0000000000000957

[2] Damiani E, Carsetti A, Casarotta E, Domizi R, Scorcella C, Donati A, Adrario E. Microcirculation-guided resuscitation in sepsis: the next frontier? Front Med (Lausanne). 2023 Jul 5;10:1212321. doi: 10.3389/fmed.2023.1212321

[3] Hariri G, Joffre J, Leblanc G, Bonsey M, Lavillegrand JR, Urbina T, Guidet B, Maury E, Bakker J, Ait-Oufella H. Narrative review: clinical assessment of peripheral tissue perfusion in septic shock. Ann Intensive Care. 2019 Mar 13;9(1):37. doi: 10.1186/s13613-019-0511-1

[4] Ait-Oufella H, Lemoinne S, Boelle PY, Galbois A, Baudel JL, Lemant J, Joffre J, Margetis D, Guidet B, Maury E, Offenstadt G. Mottling score predicts survival in septic shock. Intensive Care Med. 2011 May;37(5):801-7. doi: 10.1007/s00134-011-2163-y.

[5] Bourcier S, Joffre J, Dubée V, Preda G, Baudel JL, Bigé N, Leblanc G, Levy BI, Guidet B, Maury E, Ait-Oufella H. Marked regional endothelial dysfunction in mottled skin area in patients with severe infections. Crit Care. 2017 Jun 23;21(1):155. doi: 10.1186/s13054-017-1742-x.

[6] Lima A, Bakker J. Clinical assessment of peripheral circulation. Curr Opin Crit Care. 2015 Jun;21(3):226-31. doi: 10.1097/MCC.0000000000000194.

[7] Yu Y, Zhu C, Hong Y, Chen L, Huang Z, Zhou J, Tian X, Liu D, Ren B, Zhang C, Hu C, Wang X, Yin R, Gao Y, Zhang Z. Effectiveness of anisodamine for the treatment of critically ill patients with septic shock: a multicentre randomized controlled trial. Crit Care. 2021 Sep 27;25(1):349. doi: 10.1186/s13054-021-03774-4.

[8] Liu Z, Wang W, Luo J, Zhang Y, Zhang Y, Gan Z, Shen X, Zhang Y, Meng X. Anti-Apoptotic Role of Sanhuang Xiexin Decoction and Anisodamine in Endotoxemia. Front Pharmacol. 2021 Apr 21;12:531325. doi: 10.3389/fphar.2021.531325

[9] Qin Z, Xiang K, Su DF, Sun Y, Liu X. Activation of the Cholinergic Anti-Inflammatory Pathway as a Novel Therapeutic Strategy for COVID-19. Front Immunol. 2021 Feb 8;11:595342. doi: 10.3389/fimmu.2020.595342

[10] Yu Y, Zhu C, Hong Y, Chen L, Huang Z, Zhou J, Tian X, Liu D, Ren B, Zhang C, Hu C, Wang X, Yin R, Gao Y, Zhang Z. Effectiveness of anisodamine for the treatment of critically ill patients with septic shock: a multicentre randomized controlled trial. Crit Care. 2021 Sep 27;25(1):349. doi: 10.1186/s13054-021-03774-4

[11] González R, Urbano J, López-Herce J. Resuscitating the macro- vs. microcirculation in septic shock. Curr Opin Pediatr. 2024 Jun 1;36(3):274-281. doi: 10.1097/MOP.0000000000001345

[12] Buijs EA, Reiss IK, Kraemer U, Andrinopoulou ER, Zwiers AJ, Ince C, Tibboel D. Increasing mean arterial blood pressure and heart rate with catecholaminergic drugs does not improve the microcirculation in children with congenital diaphragmatic hernia: a prospective cohort study. Pediatr Crit Care Med. 2014 May;15(4):343-54. doi: 10.1097/PCC.0000000000000105

[13] LeDoux D, Astiz ME, Carpati CM, Rackow EC. Effects of perfusion pressure on tissue perfusion in septic shock. Crit Care Med. 2000 Aug;28(8):2729-32. doi: 10.1097/00003246-200008000-00007

[14] Driessen RGH, Heijnen NFL, Hulsewe RPMG, Holtkamp JWM, Winkens B, van de Poll MCG, van der Horst ICC, Bergmans DCJJ, Schnabel RM. Early ICU-mortality in sepsis - causes, influencing factors and variability in clinical judgement: a retrospective cohort study. Infect Dis (Lond). 2021 Jan;53(1):61-68. doi: 10.1080/23744235.2020.1821912.

[15] De Backer D, Ricottilli F, Ospina-Tascón GA. Septic shock: a microcirculation disease. Curr Opin Anaesthesiol. 2021 Apr

1;34(2):85-91. doi: 10.1097/ACO.0000000000000957

[16] Annane D, Bellissant E, Cavaillon JM. Septic shock. Lancet. 2005 Jan 1-7;365(9453):63-78. doi: 10.1016/S0140-6736(04)17667-8

[17] Bultinck J, Sips P, Vakaet L, Brouckaert P, Cauwels A. Systemic NO production during (septic) shock depends on parenchymal and not on hematopoietic cells: in vivo iNOS expression pattern in (septic) shock. FASEB J. 2006 Nov;20(13):2363-5. doi: 10.1096/fj.06-5798fje

[18] Li Q, Lei H, Liu A, Yang Y, Su D, Liu X. The antishock effect of anisodamine requires the upregulation of α7 nicotine acetylcholine receptors by IL-10. Life Sci. 2011 Sep 12;89(11-12):395-401. doi: 10.1016/j.lfs.2011.07.008

[19] Wieruszewski PM, Khanna AK. Vasopressor Choice and Timing in Vasodilatory Shock. Crit Care. 2022 Mar 22;26(1):76. doi: 10.1186/s13054-022-03911-7

[20] Blasco V, Leone M, Textoris J, Visintini P, Albanèse J, Martin C. Oxymétrie veineuse : physiologie et implications thérapeutiques [Venous oximetry: physiology and therapeutic implications]. Ann Fr Anesth Reanim. 2008 Jan;27(1):74-82. French. doi: 10.1016/j.annfar.2007.10.031

[21] Dubin A, Pozo MO, Hurtado J. Central venous minus arterial carbon dioxide pressure to arterial minus central venous oxygen content ratio as an indicator of tissue oxygenation: a narrative review. Rev Bras Ter Intensiva. 2020 Mar;32(1):115-122. doi: 10.5935/0103-507x.20200017

[22] Singer M, Deutschman CS, Seymour CW, Shankar-Hari M, Annane D, Bauer M, Bellomo R, Bernard GR, Chiche JD, Coopersmith CM, Hotchkiss RS, Levy MM, Marshall JC, Martin GS, Opal SM, Rubenfeld GD, van der Poll T, Vincent JL, Angus DC. The Third International Consensus Definitions for Sepsis and Septic Shock (Sepsis-3). JAMA. 2016 Feb 23;315(8):801-10. doi: 10.1001/jama.2016.0287

[23] BRODER G, WEIL MH. EXCESS LACTATE: AN INDEX OF REVERSIBILITY OF SHOCK IN HUMAN PATIENTS. Science. 1964 Mar 27;143(3613):1457-9. doi: 10.1126/science.143.3613.1457

[24] Xiu RJ, Hammerschmidt DE, Coppo PA, Jacob HS. Anisodamine inhibits thromboxane synthesis, granulocyte aggregation, and platelet aggregation. A possible mechanism for its efficacy in bacteremic shock. JAMA. 1982 Mar 12;247(10):1458-60. doi: 10.1001/jama.247.10.1458

[25] Du X, Liu H, Yue Y, Wu Q, Jiang W, Qiu Y, Zeng Y. Anisodamine Hydrobromide Protects Glycocalyx and Against the Lipopolysaccharide-Induced Increases in Microvascular Endothelial Layer Permeability and Nitric Oxide Production. Cardiovasc Eng Technol. 2021 Feb;12(1):91-100. doi: 10.1007/s13239-020-00486-8

[26] Ince C, Mik EG. Microcirculatory and mitochondrial hypoxia in sepsis, shock, and resuscitation. J Appl Physiol (1985). 2016 Jan 15;120(2):226-35. doi: 10.1152/japplphysiol.00298.2015IF: 3.3 Q1 . Epub 2015 Jun 11. PMID: 26066826.

[27] Vallet B. Endothelial cell dysfunction and abnormal tissue perfusion. Crit Care Med. 2002 May;30(5 Suppl):S229-34. doi: 10.1097/00003246-200205001-00010. PMID: 12004241.

[28] Dumas G, Lavillegrand JR, Joffre J, Bigé N, de-Moura EB, Baudel JL, Chevret S, Guidet B, Maury E, Amorim F, Ait-Oufella H. Mottling score is a strong predictor of 14-day mortality in septic patients whatever vasopressor doses and other tissue perfusion parameters. Crit Care. 2019 Jun 10;23(1):211. doi: 10.1186/s13054-019-2496-4. PMID: 31182133; PMCID: PMC6558704.

[29] Bourcier S, Joffre J, Dubée V, Preda G, Baudel JL, Bigé N, Leblanc G, Levy BI, Guidet B, Maury E, Ait-Oufella H. Marked regional endothelial dysfunction in mottled skin area in patients with severe infections. Crit Care. 2017 Jun 23;21(1):155. doi: 10.1186/s13054-017-1742-x. PMID: 28641580; PMCID: PMC5481873.

[30] Alhumam T, Alhumam AA, Alhumaidi I, Al Rajeh I, Alduhailan Y. Relationship Between Symmetrical Peripheral Gangrene Patients and Using Vasopressors in the Intensive Care Unit. Cureus. 2024 Apr;16(4):e58117. DOI: 10.7759/cureus.58117. PMID: 38741803; PMCID: PMC11088959.

[31] Foead AI, Mathialagan A, Varadarajan R, Larvin M. Management of Symmetrical Peripheral Gangrene. Indian J Crit Care Med. 2018 Dec;22(12):870-874. doi: 10.4103/ijccm.IJCCM_379_18. PMID: 30662227; PMCID: PMC6311972.

[32] Ghosh SK, Bandyopadhyay D. Symmetrical peripheral gangrene. Indian J Dermatol Venereol Leprol. 2011 Mar-Apr;77(2):244-8. doi: 10.4103/0378-6323.77481. PMID: 21393969.

[33] Warkentin TE, Ning S. Symmetrical peripheral gangrene in critical illness. Transfus Apher Sci. 2021 Apr;60(2):103094. doi: 10.1016/j.transci.2021.103094. Epub 2021 Feb 13. PMID: 33627309.

Effect of one dose of ceftriaxone during endotracheal intubation on the incidence of aspiration pneumonia in cerebral hemorrhage patients: A randomized, controlled, double-blind clinical study protocol

姓名：刘新艳[1]，宋璇[2]

单位：1 聊城市心脏病医院，2 山东大学附属公共卫生临床中心 / 山东第一医科大学

ABSTRACT

Introduction

Due to the use of analgesic and sedative drugs during endotracheal intubation and the opening of the glottis may easily cause aspiration pneumonia. Ceftriaxone is a semi-synthetic third-generation cephalosporin with strong antimicrobial activity against most gram-positive and gram-negative bacteria. It can effectively prevent and treat aspiration pneumonia.

Methods and analysis

This is a prospective, randomized, controlled, double-blind clinical study. Patients with intracerebral hemorrhage (ICH) undergoing endotracheal intubation in Dong E Hospital of Shandong Province from April 2023 to April 2024 will be enrolled and randomly assigned to the intervention group or control group. The intervention group will be treated using 100mL 0.9% sodium chloride with 2g ceftriaxone intravenously over the course of one hour beginning within two hours after endotracheal intubation. The control group will be given 100mL 0.9% sodium chloride injection intravenously of the course of one hour beginning within two hours after endotracheal intubation. The primary outcome is the incidence of aspiration pneumonia within 48 hours after endotracheal intubation. Secondary outcomes include: intensity of antimicrobial use, length of hospital stay, duration without mechanical ventilation, and 28-day mortality.

Discussion

The primary objective of this study is to explore whether a single dose of ceftriaxone administered during endotracheal intubation in patients with ICH reduced the incidence of pneumonia within 48 hours and provide evidence for the prevention of aspiration pneumonia in patients with ICH with endotracheal intubation.

Trial registration: The trial is registered at the Chinese Clinical Trial Registry: ChiCTR2200066837. Registered on December 19, 2022.

Keywords: Aspiration pneumonia; Endotracheal intubation; Cerebral hemorrhage; Ceftriaxone; Antibiotic

INTRODUCTION

Patients with intracerebral hemorrhage (ICH) often experience such complications as consciousness disorders, respiratory center damage, airway obstruction, and swallowing dysfunction [1]. Endotracheal intubation is often required to protect the airway and maintain oxygenation [2]. However, during endotracheal intubation, the application of analgesic sedative drugs and glottis exposure may lead to aspiration [3]. Inhaled substances may include secretions from the nasal cavity and oropharynx, residual food in the mouth, contents of gastrointestinal vomiting, and digestive fluid reflux, which may cause aspiration pneumonia, including aspiration lung inflammation and aspiration lung infection caused by chemical damage [4].

A prospective observational study involving a total of 879 cases of emergency endotracheal intubation patients found that, after excluding patients who were not eligible for prognostic assessment (those who died within 48 hours without detection of pneumonia), 29% developed pneumonia and 8% (66/823) developed aspiration pneumonia that may have been associated with emergency intubation [5]. A large study from a single center in Japan showed that the incidence of aspiration pneumonia in elderly patients (aged >70) was 67.2 per 10,000 people from 2010 to 2015, and the mortality rate was 13.6% [6]. A retrospective study including patients with an average age of 78 in a single center in South Korea showed that the 1-year, 3-year and 5-year mortality rates of patients with aspiration pneumonia were 49.0%, 67.1% and 76.9%, respectively [7]. Even when the data are

corrected, the case fatality rate of aspiration pneumonia is still higher than that of other forms of pneumonia [7]. Therefore, the prevention of aspiration pneumonia is particularly important.

Conventional measures to prevent aspiration pneumonia include: elevation of the head of the bed, good oral care, swallowing function assessment and training, comprehensive rehabilitation, nasogastric feeding, improvement of gastric emptying function, and monitoring of gastric residual volume [8]. Given the pathophysiology of aspiration pneumonia and infection caused by aspiration, the application of antibiotics before endotracheal intubation can be regarded as a preventive strategy. In the Expert Advice on the Diagnosis and Treatment of Aspiration Pneumonia in Adults, the preventive measures for aspiration pneumonia are recommended as ‘antibiotic treatment for 24 hours after emergency intubation in coma patients’ [9].

Previous studies have shown that the incidence of anaerobic bacterial infection in aspiration pneumonia cases is not high [10]. Primarily enterobacteria, Haemophilus influenzae, Streptococcus pneumoniae, and Staphylococcus aureus were isolated from community-acquired cases, while gram-negative bacilli, such as Pseudomonas aeruginosa, were isolated from hospital-acquired cases. Only one case of ventilator associated pneumonia was anaerobe infection [11]. El Solh et al. found that the most common post-stroke pneumonia pathogens were gram-negative bacilli (49%), anaerobic bacteria (16%), and S. aureus (12%); the gram-negative bacilli found were predominantly Klebsiella pneumoniae and Escherichia coli [12]. Another study included the distribution characteristics of respiratory pathogenic bacteria introduced by endotracheal intubation in 588 patients with ICH. They found that 314 cases had nosocomial respiratory infections, and the infection rate was 53.40%. Over three years, a total of 2808 strains were cultured, including 422 gram-positive bacteria (15.03%). There were 1854 strains (66.03%) of gram-negative bacteria, 527 strains (18.95%) of Candida and five strains (0.18%) of others [13].

Ceftriaxone is a semi-synthetic third-generation cephalosporin which has strong antibacterial activity against most gram-positive and -negative bacteria, including P. aeruginosa, Escherichia coli, Bacillus pneumoniae, H. influenzae, aeroenteric bacteria, and Proteus [14]. Given the characteristics of pneumonia pathogens in patients with aspiration pneumonia and ICH, ceftriaxone can be used as an effective option to prevent and treat aspiration pneumonia [15].

The aim of this study is to investigate whether a single dose of ceftriaxone during endotracheal intubation can reduce the incidence of pneumonia within 48 hours in patients with cerebral hemorrhage, and to provide a basis for the prevention of aspiration pneumonia in patients with cerebral hemorrhage.

METHODS AND ANALYSIS

This is a prospective, randomized, controlled, double-blind clinical study, which was reviewed by the ethics committee of Dong E Hospital. All methods will be performed in accordance with the relevant guidelines and regulations. Written informed consent will be obtained from the guardians of all patients and registered in the Chinese Clinical Trial Registry (Registration number: ChiCTR2200066837). All methods were reported according to Consolidated Standards of Reporting Trials (CONSORT) [16].

Study design

Patients with ICH undergoing endotracheal intubation in Dong E Hospital of Shandong Province from April 2023 to April 2024 will be included. Inclusion criteria are: (1) age > 18 years; (2) ICH due to various causes; (3) endotracheal intubation; and (4) subjects understood and signed the informed consent. The following patients will be excluded from this study: (1) pneumonia occurred before endotracheal intubation; (2) aspiration occurred before endotracheal intubation (e.g., aspiration that is considered possible clinically, such as epilepsy; prehospital vomiting; vomit on the patient's clothing; or vomit visible in the oropharynx at the beginning of intubation attempts); (3) received antibiotics before endotracheal intubation; (4) received other antibiotics within 48 hours after enrollment (especially before diagnosis of aspiration pneumonia); (5) patients who died within 48 hours after endotracheal intubation without aspiration pneumonia; (6) allergic history to cephalosporin antibiotics; and (7) drinking history within one week before endotracheal intubation, as the use of cephalosporin after drinking alcohol can cause a disulfiram reaction. Of note, patients with COPD will not be excluded from the study. Schedule of enrolment, interventions, and assessments are shown in Figure 1.A simplified schematic of the trial design is shown in Figure 2.

Intervention

Subjects will be randomly assigned 1:1 to the ceftriaxone intervention group or the control group after signing informed consent on a computer-generated randomization table generated by an investigator not involved in the clinical trial. Patients who meet the inclusion criteria will undergo endotracheal intubation routinely according to the operating specifications of our unit. Patients in the intervention group will be given 100mL 0.9% sodium chloride with 2g ceftriaxone sodium intravenously over the course of one hour within two hours after endotracheal intubation. Patients in the control group will receive 100 mL 0.9% sodium chloride injection intravenously over the course of one hour within two hours after endotracheal intubation. Other treatment measures after endotracheal intubation (ie: prevention of aspiration, withdrawal of mechanical ventilation) are the same as conventional treatment. Neither the investigators nor the patients will be aware of the group assignments during the study. Open label is allowed in case of serious adverse effects such as allergic reaction.

Data collection

Patient Characteristics

The general data of the patients will be collected, including gender, age, height, weight, BMI, comorbidities, Acute Physiology and Chronic Health Evaluation II (APACHE Ⅱ) score, Sequential Organ Failure Assessment (SOFA) score, history of medication allergy, diagnosis, smoking history, drinking history, bed rest history, chest radiograph or chest CT manifestations before endotracheal intubation, laboratory test results (white blood cell count, neutrophil ratio, C-reactive protein and procalcitonin), body temperature, cause of ICH, time of onset of aspiration pneumonia after enrollment, duration of mechanical ventilation, length of ICU stay, length of hospital stay, and 28-day survival.

Intubation Characteristics

Intubation characteristics will be collected, including whether vomiting occurred before endotracheal intubation; whether obvious aspiration occurred before endotracheal intubation; whether aspiration occurred during endotracheal intubation; whether mechanically ventilated; endotracheal intubation time; endotracheal intubation type; whether analgesic and sedative drugs were used before intubation; whether intubation was difficult; whether repeated intubation attempts were necessary.

Antibiotic Characteristics

Antibiotic characteristics will be collected, including time of administration, antibiotic type, dose, frequency, and days of antibiotic use after enrollment; sputum or broncho alveolar lavage fluid (BALF) culture results during endotracheal intubation and sputum or BALF culture results during aspiration pneumonia.

Research outcomes

The primary outcome is the incidence of aspiration pneumonia within 48 hours after endotracheal intubation. Aspiration pneumonia is defined the presence of new or advanced infiltrating shadows, consolidation shadow, or ground glass shadow on chest X-ray or CT in patients without a diagnosis of community-acquired pneumonia, healthcare-associated pneumonia, or aspiration pneumonia, combined with two or more of the following clinical symptoms: (1) fever, body temperature >38 ° C; (2) purulent airway discharge; (3) white blood cell count >10 ×10 ^ 9 / L or<4×10^9/L.

The intensity of antimicrobial use is defined as:

$$\frac{\text{Antimicrobial consumption (cumulative DDD)}}{\text{Days of patients admitted in the same period}} \times 100$$

where DDD is the defined daily dose.

The intensity of antibiotic use in a particular patient is defined as:

$$\frac{\text{Antimicrobial consumption (cumulative DDD)}}{\text{Days of hospital stay}} \times 100$$

$$\frac{\text{Antimicrobial drug consumption / } DDD}{\text{Days of hospital stay}} \times 100$$

$$\frac{\text{Single dose of antibiotics} \times \text{frequency of use} \times \text{days of use /DDD}}{\text{Days of hospital stay}} \times 100$$

Adverse event monitoring

Patients with a history of allergy to cephalosporins will be excluded to avoid allergic reactions to the drugs. Allergic reactions include high fever, rash, pruritus, dyspnea, laryngeal edema, and anaphylactic shock. Once allergy occurs, the drug will be stopped immediately, and epinephrine or appropriate first aid measures (e.g., airway management, intravenous rehydration, antihistamines, corticosteroids, vasoactive drugs) will be given to patients with severe acute hypersensitivity reaction according to clinical indications. Serious adverse reactions will be reported to the Ethics Committee immediately.

Sample size calculation

A total of 50 patients will be included in the preliminary study. For the preliminary results, the incidence of pneumonia within 48 hours after endotracheal intubation will be obtained in the two groups. The sample size estimation formula for the comparison of two sample rates will be used to estimate the sample size; the test level α was set at 0.05, and the type II error probability β was set at 0.2. The patients will be distributed according to 1:1 randomization, and the two-sided test will be used to calculate the required sample size.

Statistical analysis

SPSS 20.0 will be used for statistical analysis. Statistical descriptions of general data included the frequency and percentage of count data such as gender and disease diagnosis, and chi-square test or Fisher's exact probability method will be used for statistical analysis. Furthermore, the data will be described statistically with mean and standard deviation or median and quartile depending on the distribution. Age, APACHE II score, SOFA score, BMI, length of stay in ICU, length of hospital stay, and duration of mechanical ventilation will be statistically described by mean ± standard deviation or quartile, and analyzed by independent sample t-test or Mann-Whitney U rank sum test. The incidence of pneumonia within 48 hours of tracheal intubation and 28-day mortality will be statistically described by frequency and percentage. The significance level of all the above statistical tests is $P \leqslant 0.05$.

DISCUSSION

This is a prospective, randomized, controlled, double-blind clinical study to compare the effect of a single dose of ceftriaxone during endotracheal intubation on the incidence of aspiration pneumonia within 48 hours after endotracheal intubation in patients with ICH. To the best of our knowledge, this is the first clinical study of ceftriaxone to prevent the development of aspiration pneumonia in patients with ICH hemorrhage undergoing endotracheal intubation.

Aspiration pneumonia is a pulmonary inflammation caused by the inhalation of oropharyngeal secretions, gastric contents, or other exogenous foreign bodies into the lower respiratory tract [4]. One type of aspiration pneumonia is chemical inflammation caused by direct damage to lung tissue caused by inhalation of gastric contents; another type is pulmonary atelectasis and inflammation caused by inhalation of obstructive substances; and the third type is bacterial pneumonia caused by inhalation of oral secretions containing colonized bacteria, which is the most common clinical type and can be fatal in severe cases [17]. Patients with ICH often experience disturbance of consciousness and require endotracheal intubation, and these patients are typically in a non-fasting state. During intubation, analgesic and sedative drugs are administered and the glottis is exposed, allowing oral secretions to easily to enter the lower respiratory tract and cause aspiration pneumonia [18, 19].

A prospective study of emergency endotracheal intubation in the emergency department by Drive et al. [5] showed that 8% of patients developed aspiration pneumonia that could be associated with emergency endotracheal intubation. The number of intubation attempts did affect the occurrence of aspiration pneumonia. Aspiration pneumonia is commonly acute, with symptoms occurring within hours to days. Pneumonia caused by inhalation of anaerobic bacteria may be subacute because of the low virulence of the bacteria, but its clinical features are difficult to distinguish from other bacterial pneumonitis [20]. Studies have shown that the expected mortality of patients with aspiration pneumonia is higher than that of patients with other forms of pneumonia [21].

A recent study on oral microecology found 103 species of bacteria in the mouth of patients with acute stroke; 29 of these were previously unreported bacteria of which the pathogenicity is still unknown [22]. Previous studies have shown that aspiration

pneumonia is often due to infection with gram-negative bacteria (e.g., E. coli, K. pneumoniae, P. aeruginosa) and S. aureus [9, 17], and antibiotics used prophylactically should target these pathogens. Ceftriaxone, which is effective against both gram-positive and gram-negative bacteria, was found to be an effective agent for the prevention of bacterial aspiration pneumonia in intubated ICH patients.

In a study evaluating the risk factors for pneumonia within 48 hours after intubation, Rello et al. [23] found that patients with respiratory/cardiac arrest and coma had the highest incidence of pneumonia in the first 48 hours. Antibiotic use during this period reduced the incidence of pneumonia, while other preventive measures such as subglottic suction were ineffective. Sirvent et al. [24] conducted a randomized trial to evaluate the effectiveness of two doses of cefuroxime administered within 24 hours after intubation in reducing the incidence of early-onset ventilator-associated pneumonia (VAP) in patients with closed head injury (Glasgow Coma Scale score < 12). A retrospective cohort study by Vlad Dragan et al. [25] reached a different conclusion, finding instead that prophylactic antimicrobial therapy in patients with acute aspiration pneumonia does not provide clinical benefit, has no effect on mortality improvement, and may generate antibiotic selection pressure and increase the number of days of subsequent antibiotic treatment. In these cases, however, antibiotic use may be more akin to short-term treatment than true prevention, and long-term antibiotic use may increase the risk of subsequent infection by resistant microorganisms. For this reason, we decided to use a single dose of an antibiotic which has a long half-life and is effective against the main pathogens responsible for most endotracheal intubation-induced aspiration pneumonia.

A previous similar study by Valles et al. [26] showed that a single dose of antibiotics significantly reduced the incidence of VAP in mechanically ventilated comatose patients. It also reduced mechanical ventilation and ICU length of stay, and had no effect on mortality or the incidence of multidrug-resistant microbial infections. However, this was a non-randomized study, and there was bias in the selection of patients in the control group. The incidence of chronic obstructive pulmonary disease in the control group was higher, which resulted in a greater degree of airway pathogen colonization before intubation, and more patients requiring neurosurgical intervention were included in the control group.

Further prospective randomized controlled studies are necessary to explore whether a dose of ceftriaxone before endotracheal intubation can reduce the incidence of aspiration pneumonia in patients with ICH, so as to provide an option for the prevention of pneumonia in these patients.

Our study has some limitations. First, this study will be conducted in a single center and will include a small sample size, which may limit the broader applicability of our findings. Second, the definition of aspiration pneumonia may inadvertently include aspiration pneumonia before endotracheal intubation because we will exclude these patients on the basis of clinical speculation. Finally, it is difficult to distinguish between aspiration pneumonia and another type of pneumonia that develops within 48 hours of endotracheal intubation.

Trial status

At the time of manuscript submission, the study is in the preparation phase for recruitment. This is the first version of the protocol completed on September 30, 2022. Recruitment is scheduled to begin in April 2023 and expected to be completed by April 2024.

Figure captions

Figure 1. Schedule of enrolment, interventions, and assessments

Figure 2. Simplified schematic of the trial design

Declarations

Ethics and dissemination

This study was approved by the hospital ethics committees of Dong E Hospital. Informed consent will be obtained from the participants. Servers associated with this study will be encrypted and password-protected. They will be accessible only to designated researchers. The results of this trial will be disseminated in peer-reviewed journals and at scientific conferences. Anonymized data will be available upon request from the principal investigator. We do not expect any major protocol

modifications.

Patient and public involvement

Patients and/or the public were not involved in the design, or conduct, or reporting, or dissemination plans of this research.

Consent for publication

Not applicable

Data availability

The data used for this research will be available from the corresponding author on reasonable request and subject to Institutional Review Board guidelines.

Conflicts of interest

The authors have declared that no competing interests exist.

Funding

This work was supported by Natural Science Foundation of Shandong Province, China (Grant ZR202102210272), Taishan Scholars Program of Shandong Province (Grant tsqn202211347) and Shandong Provincial Postdoctoral Science Foundation (Grant N/A) . The funders did not and will not have a role in study design, data collection and analysis, decision to publish, or preparation of the manuscript.

Author contributions

Conceptualization, X.S.; methodology, X.L.; software, Y.B.; validation, X.L. and Y.B.; formal analysis, Y.Y..; investigation, X.L. and Q.W.; resources, X.S.; data curation, Y.Y.; writing—original draft preparation, X.L. and Q.W.; writing—review and editing, X.S.; visualization, X.L. and Q.W.; supervision, X.S.; project administration, X.S.; funding acquisition, X.S. All authors have read and agreed to the published version of the manuscript.

Acknowledgments

None.

References

1. Balami, J.S. and A.M. Buchan, Complications of intracerebral haemorrhage. Lancet Neurol, 2012. 11(1): p. 101-18.

2. Alvarado, A.C. and P. Panakos, Endotracheal Tube Intubation Techniques, in StatPearls. 2023: Treasure Island (FL) ineligible companies. Disclosure: Patricia Panakos declares no relevant financial relationships with ineligible companies.

3. Roshan, R., et al., Aspiration during Rapid Sequence Induction: Prevalence and Risk Factors. Indian J Crit Care Med, 2021. 25(2): p. 140-145.

4. Mandell, L.A. and M.S. Niederman, Aspiration Pneumonia. N Engl J Med, 2019. 380(7): p. 651-663.

5. Driver, B.E., et al., The occurrence of aspiration pneumonia after emergency endotracheal intubation. Am J Emerg Med, 2018. 36(2): p. 193-196.

6. Nonaka, S., et al., Incidence of aspiration pneumonia during hospitalization in Japanese hospitalized cases did not increase whereas concern factors were exacerbated in a time-dependent manner: analysis of Diagnosis Procedure Combination (DPC) data. J Clin Biochem Nutr, 2018. 63(1): p. 66-69.

7. Yoon, H.Y., et al., Long-Term Mortality and Prognostic Factors in Aspiration Pneumonia. J Am Med Dir Assoc, 2019. 20(9): p. 1098-1104.e4.

8. Feng, M.C., et al., The Mortality and the Risk of Aspiration Pneumonia Related with Dysphagia in Stroke Patients. J Stroke Cerebrovasc Dis, 2019. 28(5): p. 1381-1387.

9. Adult, E.G.o.t.D.a.T.o., Expert task force on diagnosis and treatment of aspiration pneumonia in adults. International Respiratory Journal, 2022. 42(2): p. 86-96.

10. Bartlett, J.G., How important are anaerobic bacteria in aspiration pneumonia: when should they be treated and what is optimal therapy. Infect Dis Clin North Am, 2013. 27(1): p. 149-55.

11. Marik, P.E. and P. Careau, The role of anaerobes in patients with ventilator-associated pneumonia and aspiration pneumonia: a prospective study. Chest, 1999. 115(1): p. 178-83.

12. El-Solh, A.A., et al., Microbiology of severe aspiration pneumonia in institutionalized elderly. Am J Respir Crit Care Med, 2003. 167(12): p. 1650-4.

13. Yang, H., et al., A retrospective study on risk factors and disease burden for hospital-acquired pneumonia caused by multi-drug-resistant bacteria in patients with intracranial cerebral hemorrhage. Neurol Sci, 2022. 43(4): p. 2461-2467.

14. Richards, D.M., et al., Ceftriaxone. A review of its antibacterial activity, pharmacological properties and therapeutic use. Drugs, 1984. 27(6): p. 469-527.

15. Kato, H., et al., Retrospective Comparison of the Effectiveness and Safety of Ceftriaxone 1 g Twice Daily versus 2 g Once Daily for Treatment of Aspiration Pneumonia. Antibiotics (Basel), 2022. 11(8).

16. Moher, D., et al., CONSORT 2010 explanation and elaboration: updated guidelines for reporting parallel group randomised trials. Bmj, 2010. 340: p. c869.

17. DiBardino, D.M. and R.G. Wunderink, Aspiration pneumonia: a review of modern trends. J Crit Care, 2015. 30(1): p. 40-8.

18. Sousa, A.S., C. Ferrito, and J.A. Paiva, Intubation-associated pneumonia: An integrative review. Intensive Crit Care Nurs, 2018. 44: p. 45-52.

19. Sathishkumar, S. and J. Fassl, Endotracheal tube-associated pneumonia. Anesthesiology, 2009. 111(4): p. 922; author reply 922-3.

20. Son, Y.G., J. Shin, and H.G. Ryu, Pneumonitis and pneumonia after aspiration. J Dent Anesth Pain Med, 2017. 17(1): p. 1-12.

21. Neill, S. and N. Dean, Aspiration pneumonia and pneumonitis: a spectrum of infectious/noninfectious diseases affecting the lung. Curr Opin Infect Dis, 2019. 32(2): p. 152-157.

22. Boaden, E., et al., Oral flora in acute stroke patients: A prospective exploratory observational study. Gerodontology, 2017. 34(3): p. 343-356.

23. Rello, J., et al., Risk factors for developing pneumonia within 48 hours of intubation. Am J Respir Crit Care Med, 1999. 159(6): p. 1742-6.

24. Sirvent, J.M., et al., Protective effect of intravenously administered cefuroxime against nosocomial pneumonia in patients with structural coma. Am J Respir Crit Care Med, 1997. 155(5): p. 1729-34.

25. Dragan, V., et al., Prophylactic Antimicrobial Therapy for Acute Aspiration Pneumonitis. Clin Infect Dis, 2018. 67(4): p. 513-518.

26. Vallés, J., et al., Efficacy of single-dose antibiotic against early-onset pneumonia in comatose patients who are ventilated. Chest, 2013. 143(5): p. 1219-1225.

Effects of Early Pulmonary Rehabilitation Training on Ventilator-Induced Diaphragmatic Dysfunction in ICU Mechanically Ventilated Patients

姓名：Baoyi Yang，Rong Wang，Qi Tang
单位：Taihe Hospital, Hubei University of Medicine

Abstract

Objective: To investigate the preventive effects of early pulmonary rehabilitation training on ventilator-induced diaphragmatic dysfunction (VIDD) in ICU mechanically ventilated patients and its impact on clinical outcomes.

Methods: A prospective randomized controlled trial was conducted. A total of 82 mechanically ventilated patients admitted to the intensive care unit of a tertiary hospital from January 2025 to December 2025 were enrolled and randomly assigned to either the experimental group (n=41) or the control group (n=41) using a random number table. The control group received routine ICU care and an early mobilization protocol, while the experimental group received systematic early pulmonary rehabilitation training in addition to the control protocol. Ultimately, 75 patients completed the study. Diaphragm excursion (DE), diaphragmatic thickening fraction (DTF), maximum inspiratory pressure (MIP), duration of mechanical ventilation, ICU length of stay, incidence of VIDD, and adverse events were compared between the two groups.

Results: On day 5 and day 7 of the intervention, DE and DTF in the experimental group were significantly higher than those in the control group ($P<0.05$). MIP on day 7 was significantly higher in the experimental group than in the control group ($P<0.001$). The experimental group had significantly shorter durations of mechanical ventilation (6.2±2.1 days vs. 8.7±3.4 days) and ICU stays (9.5±3.2 days vs. 12.8±4.6 days) compared to the control group ($P<0.001$). The incidence of VIDD was significantly lower in the experimental group (15.8%, 6/38) than in the control group (40.5%, 15/37; $P=0.017$). No significant difference was found in the incidence of adverse events between the two groups ($P>0.05$).

Conclusion: Early pulmonary rehabilitation training effectively improves diaphragmatic function, reduces the incidence of VIDD, shortens the duration of mechanical ventilation and ICU length of stay in mechanically ventilated patients, and demonstrates good safety.

Keywords: Pulmonary rehabilitation; Mechanical ventilation; Ventilator-induced diaphragmatic dysfunction; Diaphragmatic ultrasound; Intensive care

1. Introduction

Mechanical ventilation (MV) is a core life-support technology in intensive care units (ICUs), with approximately 30%–88% of critically ill patients requiring MV. However, while MV saves lives, it places the diaphragm in a partial or complete unloading state, leading to decreased diaphragmatic tension, muscle fiber atrophy, and contractile dysfunction, known as ventilator-induced diaphragmatic dysfunction (VIDD) [1]. Studies indicate that the incidence of VIDD ranges from 60% to 80%, and 33% of patients with VIDD fail to fully recover diaphragmatic function after rehabilitation [2]. Evidence has confirmed that diaphragmatic atrophy and functional decline can occur within 24 hours after the initiation of MV, with atrophy progressing faster than in other skeletal muscles [3].

The pathophysiology of VIDD is complex, involving multiple molecular pathways such as mitochondrial oxidative stress, excessive activation of the ubiquitin-proteasome pathway, calpain and caspase-3-mediated proteolysis, and inhibition of protein synthesis [1,3]. VIDD not only severely affects the recovery of respiratory function but also leads to weaning difficulties, prolonged MV, extended ICU stays, increased medical costs, and even higher mortality [4]. Therefore, finding effective intervention strategies to prevent and improve VIDD has become a research hotspot in the field of critical care rehabilitation.

In recent years, pulmonary rehabilitation (PR), as a comprehensive non-pharmacological intervention, has received widespread attention for its application in ICU mechanically ventilated patients [5]. Studies have shown that early rehabilitation, including physical therapy, breathing training, and exercise training, can effectively prevent and improve respiratory muscle atrophy, enhance muscle strength, reduce in-hospital mortality, and improve overall prognosis [6-8]. However, high-quality randomized

controlled trials focusing on the preventive effects of early pulmonary rehabilitation centered on respiratory muscle training for VIDD remain limited, particularly in the ICU setting in China. Therefore, this prospective randomized controlled trial aims to investigate the protective effects of early pulmonary rehabilitation training on diaphragmatic function and its impact on clinical outcomes in ICU mechanically ventilated patients, providing evidence-based support for critical care nursing practice.

2. Methods

2.1 Participants

This prospective randomized controlled trial was conducted in the ICU of a tertiary hospital from January 2025 to December 2025. Inclusion criteria: (1) age ⩾ 18 years; (2) undergoing invasive MV via orotracheal intubation or tracheostomy; (3) expected duration of MV ⩾ 72 hours; (4) relatively stable hemodynamics upon ICU admission (mean arterial pressure ⩾ 65 mmHg); (5) informed consent provided by the patient or a family member. Exclusion criteria: (1) history of neuromuscular disease or diaphragmatic paralysis before ICU admission; (2) previous diaphragmatic surgery; (3) conditions unsuitable for respiratory rehabilitation (e.g., cervical spine fracture, intracranial hypertension); (4) severe hemodynamic instability requiring high-dose vasoactive agents; (5) pregnancy; (6) terminal illness with expected survival <6 months. Elimination criteria: (1) MV duration <72 hours due to extubation or death; (2) transfer out of the ICU during the study period; (3) withdrawal of informed consent.

Sample size calculation: Using PASS 15.0, based on pre-trial results (VIDD incidence of approximately 18% in the experimental group and 42% in the control group), with α=0.05 (two-tailed), power 1-β=0.80, a 1:1 allocation, and accounting for a 15% dropout rate, 82 patients were required. A random number table generated by SPSS 26.0 was used by a statistician not involved in the intervention to randomly assign 82 patients to the experimental group (n=41) and control group (n=41). Allocation concealment was achieved using sealed envelopes. The study was approved by the hospital ethics committee (approval number: XM2025115).

2.2 Interventions

2.2.1 Control group

The control group received routine ICU care and an early mobilization protocol, including: (1) basic care (vital sign monitoring, airway management, oral care); (2) passive/active range of motion exercises (twice daily, 15–20 min each) based on consciousness and muscle strength; (3) head-of-bed elevation to 30° –45° ; (4) suctioning as needed; (5) minimal sedation strategy.

2.2.2 Experimental group

In addition to the control protocol, the experimental group received a 7-day systematic early pulmonary rehabilitation training program delivered by a trained critical care rehabilitation team (including one ICU head nurse, two ICU specialist nurses, and one respiratory therapist). All team members completed a 2-week standardized training program and passed assessments covering bedside diaphragmatic ultrasound, respiratory muscle training techniques, airway clearance techniques, early mobilization protocols, and safety monitoring.

(1) Bedside diaphragmatic ultrasound and individualized plan

Within 24 hours of enrollment, a nurse trained in diaphragmatic ultrasound assessed baseline diaphragmatic function using a bedside ultrasound system (convex probe 2–5 MHz; linear probe 7–12 MHz), measuring DE and DTF. Based on the results, along with the patient’ s consciousness level (RASS score), Medical Research Council score (MRC-Score), and hemodynamic status, the rehabilitation team developed an individualized pulmonary rehabilitation plan specifying training methods, intensity, frequency, and progression criteria.

(2) Progressive respiratory muscle training

Passive stimulation phase (for RASS -3 to -1 or unable to cooperate): Patients in semi-recumbent position (head-of-bed 30° –45°) received passive respiratory muscle stimulation by adjusting ventilator trigger sensitivity (initial setting -3 cmH2O, decreased by 0.5–1 cmH2O every 24 hours to a target of -1 cmH2O, twice daily, 15 min each) [9-10].

Active training phase (for RASS -1 to +1 able to follow commands): Included diaphragmatic breathing [11], deep breathing

exercises [12], and threshold inspiratory muscle training (initial load at 30% of MIP, 10–15 breaths per session, twice daily, with load increased by 5%–10% weekly up to 50% of MIP, Borg dyspnea score ⩽ 5) [13]. Each session lasted 15–20 min with at least 4 hours between sessions.

(3) Effective coughing and airway clearance training

For conscious patients (RASS -1 to +1) able to follow commands: effective coughing training (deep inspiration – 2-second breath hold – forceful cough) and active cycle of breathing technique (ACBT) [14-15]. Manual chest compression was applied if needed.

(4) Early progressive positioning management

Daily positioning level determined by the ICU mobility scale (IMS): IMS 0–1: passive repositioning and range of motion; IMS 2–3: additional semi-recumbent active maintenance; IMS 4–5: transition to sitting at the bedside; IMS 6–7: standing or sitting in a chair [16].

(5) Dynamic diaphragmatic ultrasound monitoring and adjustment

DE and DTF were assessed at days 1, 3, 5, and 7 by the same trained nurse. Training intensity was adjusted based on diaphragmatic function trends (increase load if DTF improved by ⩾ 5%; maintain if DTF decreased by ⩾ 10% or no improvement; initiate enhanced stimulation if DTF <20% for >72 hours).

(6) Safety stopping criteria

Training was immediately stopped if any of the following occurred: heart rate >140/min or <40/min; new arrhythmias; systolic blood pressure >180 mmHg or <85 mmHg, or fluctuation >20% from baseline; SpO_2 <88% or >5% drop from baseline; respiratory rate >35/min; overt patient intolerance.

2.3 Outcome Measures

2.3.1 Primary outcome

VIDD incidence, defined as DTF <20% combined with DE <10 mm (during quiet breathing) [14], assessed on day 7.

2.3.2 Secondary outcomes

(1) Diaphragmatic ultrasound parameters (DE and DTF) measured on days 1, 3, 5, and 7 [9].

(2) Maximum inspiratory pressure (MIP) measured on days 1 and 7 [4].

(3) Clinical outcomes: duration of mechanical ventilation (from intubation to successful extubation with spontaneous breathing ⩾ 48 hours) and ICU length of stay.

(4) Adverse events: unplanned extubation, catheter displacement, falls, severe arrhythmias, and marked blood pressure fluctuations.

2.4 Statistical Analysis

SPSS 26.0 was used. The per-protocol (PP) set was used for primary efficacy analysis. Normally distributed continuous data were expressed as mean ± standard deviation ($\bar{x} \pm s$) and compared using independent samples t-test or repeated measures ANOVA. Non-normally distributed data were expressed as median (IQR) and compared using Mann-Whitney U test. Categorical data were expressed as frequencies and percentages and compared using χ^2 test or Fisher's exact test. $P<0.05$ was considered statistically significant.

3. Results

3.1 Baseline Characteristics

Of the 82 enrolled patients, 75 completed the study (38 in the experimental group, 37 in the control group). No significant

differences were found between the two groups in age, sex, BMI, APACHE II score, primary diagnosis, or PaO_2/FiO_2 ratio at ICU admission (P>0.05), indicating comparability

3.2 Diaphragmatic Ultrasound Indicators

On days 5 and 7, DE and DTF in the experimental group were significantly higher than those in the control group (P<0.05). Repeated measures ANOVA showed significant time, group, and interaction effects for both DE and DTF (P<0.001) (Table 1).

Table 1. Comparison of DE and DTF between the two groups ($\bar{x}\pm s$)

Parameter	Group	Day 1	Day 3	Day 5	Day 7	F-time	F-group	F-interaction
DE (mm)	Experimental	13.8±2.8	14.2±3.1	15.9±3.4	17.1±3.2	42.158	8.952	12.346
	Control	14.1±3.0	13.5±3.2	13.2±3.5	13.4±3.6			
DTF (%)	Experimental	28.5±6.2	27.8±5.9	31.2±7.1	34.6±7.8	36.724	10.158	15.637
	Control	29.1±6.5	26.4±6.3	24.8±6.8	23.5±7.2			

3.3 Maximum Inspiratory Pressure (MIP)

On day 7, MIP in the experimental group was significantly higher than that in the control group and significantly improved from day 1 (P<0.001), while no significant change was observed in the control group (P>0.05) (Table 2).

Table 2. Comparison of MIP between the two groups (cmH_2O, $\bar{x}\pm s$)

Group	Day 1	Day 7	t	P
Experimental	38.6±8.4	52.4±9.7	-8.432	＜0.001
Control	39.2±9.1	36.5±8.8	1.856	0.068
t	-0.298	7.456		
P	0.766	＜0.001		

3.4 Clinical Outcomes and VIDD Incidence

The experimental group had significantly shorter duration of MV (6.2±2.1 vs. 8.7±3.4 days, P<0.001) and ICU length of stay (9.5±3.2 vs. 12.8±4.6 days, P<0.001). VIDD incidence was significantly lower in the experimental group (15.8% vs. 40.5%, P=0.017) (Table 3).

Table 3. Comparison of clinical outcomes between the two groups

Outcome	Experimental (n=38)	Control (n=37)	t/χ^2	P
MV duration (days, $\bar{x}\pm s$)	6.2±2.1	8.7±3.4	-3.978*	＜0.001
ICU LOS (days, $\bar{x}\pm s$)	9.5±3.2	12.8±4.6	-3.756*	＜0.001
VIDD [n (%)]	6（15.8）	15（40.5）	5.70△	0.017

3.5 Adverse Events

In the experimental group, transient blood pressure fluctuations (3 cases, 7.9%) and tachycardia (2 cases, 5.3%) occurred, all resolving after pausing or reducing training intensity. No severe adverse events (unplanned extubation, catheter displacement, falls) occurred. No significant difference in total adverse events was found between the two groups (P=0.673).

4. Discussion

This study demonstrates that early pulmonary rehabilitation training effectively protects diaphragmatic function in ICU

mechanically ventilated patients, as evidenced by significantly higher DE and DTF in the experimental group compared to the control group ($P<0.05$). These findings are consistent with previous studies showing that early pulmonary rehabilitation combined with bundled nursing care improves diaphragmatic excursion [6], and that inspiratory muscle training significantly enhances diaphragmatic excursion in mechanically ventilated patients [2,4]. Notably, diaphragmatic function in the control group progressively declined on days 5 and 7, confirming the pathophysiological effect of MV-induced diaphragmatic unloading and atrophy [1,3]. In contrast, the experimental group showed no decline but rather an improvement in diaphragmatic function, suggesting that early pulmonary rehabilitation effectively counteracts the adverse effects of MV on the diaphragm [17].

The VIDD incidence in the experimental group (15.8%) was significantly lower than that in the control group (40.5%), and both MV duration and ICU length of stay were significantly shortened. Given that reported VIDD incidence can reach 60%–80% [2], and VIDD-related weaning difficulties increase complications, costs, and mortality[1,4], the comprehensive and phased nature of our intervention—integrating respiratory muscle training, airway clearance techniques, and early progressive positioning with ultrasound-based dynamic adjustment—likely contributed to its success. This reflects a closed-loop management concept of "assessment–intervention–reassessment" [18].

Safety is a primary concern when implementing early rehabilitation in ICU patients with critical illness, multiple catheters, and hemodynamic instability [19-20]. Consistent with prior studies [4-5], the experimental group in our study experienced only minor, transient adverse events (blood pressure fluctuations, tachycardia) that resolved quickly, with no increase in serious adverse events compared to the control group. These results confirm that early pulmonary rehabilitation training can be safely implemented in ICU mechanically ventilated patients under close monitoring and standardized management.

5. Conclusion

Early pulmonary rehabilitation training effectively improves diaphragmatic function, reduces the incidence of VIDD, shortens the duration of mechanical ventilation and ICU length of stay in ICU mechanically ventilated patients, and demonstrates good safety. We recommend that individualized early pulmonary rehabilitation training based on bedside ultrasound assessment be routinely implemented for mechanically ventilated patients in ICU clinical nursing practice to protect diaphragmatic function and improve patient outcomes.

References

[1] Fu W, Guan LL, Liu Q, et al. Ventilator-induced diaphragmatic dysfunction: pathophysiology, monitoring and advances in potential treatment and prevention. European Respiratory Review. 2025;34(178):250069.

[2] Benli RK, Yurdalan U, Yılmaz B, et al. Effect of post-extubation inspiratory muscle training on diaphragmatic function in mechanically ventilated patients: a randomized controlled trial. Advances in Clinical and Experimental Medicine. 2024;33(10):1077-1085.

[3] Khwaja SA, Habib MA, Gupta R, et al. Unraveling ventilator-induced diaphragmatic dysfunction: a comprehensive narrative review on pathogenesis, diagnosis and management. Current Respiratory Medicine Reviews. 2025;21(1):1-15.

[4] Wang SJ, Chen YJ, Lin SY, et al. Inspiratory muscle training facilitates liberation from mechanical ventilation in subacute critically ill patients: a randomized controlled trial. Frontiers in Medicine. 2025;11:1503678.

[5] Farley C, Newman A, Ho J, et al. The effects of inspiratory muscle training in critically ill adults: a systematic review and meta-analysis. Journal of Intensive Care Medicine. 2025;40(3):238-252.

[6] Liu HW, Ni PJ, Li L, et al. Effect of early pulmonary rehabilitation combined with ESCAPE bundled nursing on ventilator-induced diaphragmatic dysfunction in ICU patients undergoing invasive mechanical ventilation. Qilu Journal of Nursing. 2024;30(10):23-27. (in Chinese)

[7] Wang JG, Li SM, Zhang Y, et al. Relationship between mechanical ventilation duration and diaphragmatic function recovery under integrated rehabilitation intervention. Chinese Journal of Integrated Traditional and Western Medicine Surgery. 2025;31(1):50-55. (in Chinese)

[8] Hao T, Cheng J, Li Q, et al. Effect of phrenic nerve electrical stimulation on extubation outcomes in ICU mechanically ventilated patients: a meta-analysis. Chinese Journal of Respiratory and Critical Care Medicine. 2025;24(1):9-17. (in Chinese)

[9] Chen LH, Zhao M, Sun T, et al. Effect of early out-of-bed activity on diaphragmatic function in ICU mechanically ventilated patients. Chinese Journal of Nursing. 2025;60(4):456-462. (in Chinese)

[10] Lin XF, Zhang M, Huang L, et al. Effect of respiratory muscle training combined with lung ultrasound monitoring on diaphragmatic function and weaning in mechanically ventilated patients. Contemporary Nurse (First Issue). 2024;31(3):42-46. (in Chinese)

[11] Critical Care Rehabilitation Committee of Chinese Rehabilitation Medical Association. Chinese expert consensus on severe-subacute organ rehabilitation – pulmonary rehabilitation section. Chinese Journal of Rehabilitation Medicine. 2025;40(7):1-15. (in Chinese)

[12] Zhou WJ, Li S, He P, et al. Summary of best evidence for diaphragmatic rehabilitation in ICU mechanically ventilated patients. Chongqing Medicine. 2025;54(6):1-6. (inChinese)

[13] Tong SQ, Yang Y, Li Y, et al. Consequences in critically ill patients with prolonged mechanical ventilation after diaphragmatic stimulation techniques: a systematic review and meta-analysis. Intensive and Critical Care Nursing. 2025;86:103789.

[14] Dres M, Goligher EC, Heunks LMA, et al. Monitoring and preserving diaphragmatic function in critically ill patients. Current Opinion in Critical Care. 2025;31(2):132-141.

[15] He L, Zhou P, Zheng HY, et al. Research progress on diaphragmatic rehabilitation in critically ill mechanically ventilated patients. Chinese Journal of Nursing. 2025;60(14):1785-1791. (in Chinese)

[16] Ma J, Yang L, Han B. Monitoring and rehabilitation of diaphragmatic dysfunction in mechanically ventilated patients. In: Proceedings of the First Symposium on Clinical Medicine Application Development and Integrated Medical and Nursing Care. 2025:15-20. (in Chinese)

[17] Li T, Zhang W, Xu J, et al. Effect of MDT-assisted early graded respiratory rehabilitation training on respiration, oxygenation, DE and DTF in mechanically ventilated patients. Nursing Research. 2025;39(3):510-515. (in Chinese)

[18] Rochester CL, Singh SJ, Spruit MA, et al. Respiratory muscle dysfunction in older critically ill patients: implications for rehabilitation. Critical Care Clinics. 2025;41(4):671-686.

[19] Mitchell R, Davies A, Chen L. Rehabilitating the diaphragm: an integrated approach to intensive care unit-acquired dysfunction in critical illness: a narrative review. Annals of Clinical Care and Critical Care. 2026;5(1):25-36.

[20] Zhang L, Wang F, Liu C, et al. Summary of best evidence for diaphragmatic function training in mechanically ventilated patients. Chinese Nursing Management. 2025;25(8):1275-1282. (in Chinese)

类别 :// 临床研究：设计规范的各类临床研究及研究方案报告

Effects of positive end expiratory pressure on brain lung interaction in severe acute brain injury patients with moderate to severe acute respiratory distress syndrome: the role of lung recruitability

姓名：汤睿，汪影，杜敏，周敏

单位：中国科学技术大学附属第一医院（安徽省立医院）

The effect of positive end expiratory pressure (PEEP) on brain lung interaction in severe acute brain injury (ABI) patients with acute respiratory distress syndrome (ARDS) is not fully elucidated. To investigate the relationship between lung recruitability and the effect of PEEP on brain lung interaction in patients with severe ABI and ARDS.

A prospective study investigated 9 severe ABI patients with moderate to severe ARDS. PEEP was respectively set according to ARDSnet protocol (low PEEP level) and Express study protocol (high PEEP level). Respiratory mechanics, hemodynamics, arterial blood gases values, lung recruitment (lung ultrasound, LUS, 12 region LUS scores), transcranial doppler (TCD, measuring the bilateral middle cerebral artery (MCA) flow velocity), estimated intracranial pressure (eICP) using TCD data, non-invasive cerebral perfusion pressure (nCPP), and brain regional saturation in oxygen (rSO2 measured by Near-infrared spectroscopy) were recorded at two PEEP levels. Patients were divided into high or low recruiter depending on whether recruitment-to-inflation ratio (R/I ratio) was higher/lower than 0.5. The study was registered at chictr.org.cn (ChiCTR2000037804).

9 patients were high recruiter (R/I ratio, 0.71±0.14) and 8 patients were low recruiter (R/I ratio, 0.39±0.05). In low recruiters, compared with low PEEP (10±0cmH2O), PaO2/FiO2, dead space, LUS score, rSO2 did not improve, eICP, nCPP and MCA flow velocity worsened at high PEEP (16±1cmH2O). In high recruiters, compared with low PEEP (11±1cmH2O), PaO2/FiO2, dead space, LUS score improved, rSO2, eICP, nCPP and MCA flow velocity did not deteriorate at high PEEP (17±1cmH2O). However, the relationships were not found between R/I ratio and changes in eICP and nCPP.

Lung recruitability may take part in the effect of PEEP on brain lung interaction in severe ABI with moderate to severe ARDS. In high recruiters, high PEEP may have both lung and brain protection. In severe ABI patients with moderate-to-severe ARDS, lung recruitability had significant effects of PEEP on brain lung interaction. In high recruiter, high PEEP exerted both lung and brain protection which were not shown in low recruiter.

类别 :// 临床研究：设计规范的各类临床研究及研究方案报告

Empiric Extended Anaerobic Coverage Is Associated with Ecological Infectious Harm but No Survival Benefit in Sepsis Patients at Low Risk for Anaerobic Infection: A Retrospective Cohort Study

姓名：林婉婷，于伟杰，徐静媛

单位：东南大学附属中大医院，江苏省重症医学重点实验室

Early broad-spectrum antibiotic therapy is essential in sepsis, but empiric regimens frequently include anaerobic activity even when the clinical phenotype suggests low anaerobic infection risk. Whether this practice improves survival or mainly causes downstream ecological harm remains uncertain. We examined the clinical and ecological consequences of empiric extended anaerobic coverage in critically ill adults with sepsis and low apparent risk for anaerobic infection, with particular attention to the impact of 72-hour reassessment and de-escalation.

This is a retrospective cohort study using the Medical Information Mart for Intensive Care IV 3.1 database. Adult intensive care unit patients meeting Sepsis-3 criteria and receiving intravenous antibiotics within 24 hours of suspected infection were included. Patients with high-risk anaerobic infection syndromes, baseline Clostridioides difficile infection, or predefined strict anaerobic organisms at baseline were excluded. Empiric extended anaerobic coverage was defined as receipt of anaerobic-active antibiotics within 24 hours. The primary outcome was 28-day all-cause mortality. Secondary outcomes included Clostridioides difficile infection, fungal culture positivity, new secondary positive cultures, multidrug-resistant organism culture positivity, and a composite new infectious outcome. Propensity-score overlap weighting was used to balance baseline characteristics. A 72-hour landmark analysis compared limited or no anaerobic coverage, early de-escalation, and continuation beyond 72 hours.

Among 18,568 patients, 5,868 (31.6%) received empiric extended anaerobic coverage. After overlap weighting, extended anaerobic coverage was not associated with lower 28-day mortality (hazard ratio [HR], 1.00; 95% CI, 0.93–1.08, P=0.994). Extended coverage was associated with higher risks of Clostridioides difficile infection (risk ratio [RR], 1.51; 95% CI, 1.39-1.63, P<0.001), fungal culture positivity (RR, 1.14; 95% CI, 1.04-1.26, P=0.007), and the composite new infectious complication (RR, 1.22; 95% CI, 1.16-1.29, P<0.001). In the landmark analysis, de-escalation within 72 hours was not associated with excess mortality or infectious risk, whereas continuation beyond 72 hours was associated with greater ecological infectious burden without mortality benefit.

In critically ill adults with sepsis but low apparent anaerobic infection risk, empiric extended anaerobic coverage did not improve survival and was associated with increased ecological infectious complications. These findings support a phenotype-guided, 72-hour reassessment strategy to limit unnecessary anaerobic coverage and advance more precise antimicrobial stewardship in sepsis care.

Empiric Extended Anaerobic Coverage Is Associated with Ecological Infectious Harm but No Survival Benefit in Sepsis Patients at Low Risk for Anaerobic Infection: A Retrospective Cohort Study

姓名：Yihuan Lai[1,2]，Feifei Guo[1]，Kun Zhou[1]，Yichun Wang[1*]

单位：1 The Third Affiliated Hospital of Guangzhou Medical University

Abstract

Background: Maternal sepsis is a leading cause of obstetric morbidity and mortality worldwide. Acute respiratory distress syndrome (ARDS) is a frequent and lethal complication of sepsis in pregnancy, yet epidemiological data, pathogen profiles, and validated prediction tools specific to obstetric populations in low- and middle-income countries remain scarce. We aimed to characterise the epidemiology and pathogen distribution of maternal sepsis in the intensive care unit (ICU) and to develop a bedside clinical prediction model for ARDS among septic pregnant and postpartum women.

Methods: We conducted a retrospective cohort study of pregnant and postpartum women admitted to the ICU of a tertiary obstetric referral centre in southern China (Guangzhou Medical University Third Affiliated Hospital) between January 2013 and April 2019. Sepsis was defined according to the Sepsis-3.0 criteria (infection + Sequential Organ Failure Assessment [SOFA] score ⩾ 2). ARDS was diagnosed using the Berlin Definition (2012). Clinical characteristics, laboratory parameters, pathogen culture results, antimicrobial susceptibility profiles, and maternal–fetal outcomes were compared between groups. A multivariable logistic regression model was constructed to identify independent predictors of ARDS in septic patients, presented as a nomogram, and internally validated using receiver operating characteristic (ROC) curve analysis, calibration plots, and comparison with SOFA and APACHE II scores.

Results: Among 780 ICU admissions, 309 (39.6%) met sepsis criteria, of whom 138 (44.7%) developed ARDS. The in-hospital mortality was 6.1% for sepsis overall and 10.9% for sepsis-associated ARDS. Septic patients exhibited significantly higher illness severity, longer ICU stays, and greater healthcare costs than non-septic patients. Pathogen analysis in a contemporaneous cohort of 744 patients revealed that Acinetobacter baumannii (9.2%), Escherichia coli (7.1%), and Candida albicans (4.6%) were the most frequently isolated organisms among septic patients, with high rates of multidrug resistance (carbapenem-resistant A. baumannii and methicillin-resistant Staphylococcus aureus). Independent predictors of ARDS in septic patients included lower systolic blood pressure, higher heart rate, higher respiratory rate, lower partial pressure of oxygen, multiple organ dysfunction syndrome (MODS), invasive mechanical ventilation, continuous renal replacement therapy (CRRT), and vasoactive drug use. The resulting nomogram demonstrated excellent discrimination (area under the curve [AUC] 0.986, 95% confidence interval [CI] 0.978–0.996; sensitivity 0.949, specificity 0.947), significantly outperforming SOFA (AUC 0.669) and APACHE II (AUC 0.597) (both $P < 0.001$). The calibration curve indicated good agreement between predicted and observed probabilities.

Conclusions: Maternal sepsis in this Chinese ICU was characterised by a high burden of ARDS, prolonged hospitalisation, and a distinct pathogen profile dominated by multidrug-resistant A. baumannii. The developed nomogram accurately predicted ARDS risk in septic obstetric patients and may serve as a simple bedside tool to facilitate early recognition and resource allocation. External validation in diverse obstetric ICUs is warranted before widespread clinical adoption.

Keywords: Maternal sepsis, ARDS, pregnancy, intensive care unit, prediction model, nomogram, antimicrobial resistance, obstetric critical care

1. Introduction

Sepsis during pregnancy and the puerperium remains a leading cause of maternal mortality and morbidity globally. The World Health Organization (WHO) estimates that infection accounts for approximately 10.7% of maternal deaths worldwide, with sepsis contributing substantially to this burden [1]. In China, sepsis is the primary indication for obstetric ICU admission, complicating up to 25% of critical maternal transfers [2]. Despite advances in critical care, maternal sepsis continues to carry significant mortality, particularly in low- and middle-income countries (LMICs) where diagnostic delays and antimicrobial resistance are prevalent [3].

Acute respiratory distress syndrome (ARDS) is a devastating pulmonary complication of sepsis, occurring in up to 40% of septic patients in the general population and associated with substantially worse outcomes [4]. Pregnant and postpartum women are particularly vulnerable due to physiological adaptations including increased oxygen consumption, decreased functional residual capacity, and relative immunomodulation [5]. These changes not only increase the risk of respiratory failure but also mask early clinical deterioration, delaying diagnosis and intervention [6]. Current international guidelines, including the Surviving Sepsis Campaign (SSC) 2021 and the Society for Maternal-Fetal Medicine (SMFM) 2019 recommendations, emphasise early recognition and the "1-hour bundle"; however, they lack obstetric-specific tools for predicting ARDS progression [7, 8].

Epidemiological and pathogen data from obstetric ICUs in China remain limited. Existing studies from high-income countries report group B streptococcus and Escherichia coli as predominant pathogens [9], yet ICU-acquired infections in Chinese centres frequently involve multidrug-resistant organisms such as Acinetobacter baumannii and carbapenem-resistant Enterobacterales (CRE), reflecting differences in hospital-acquired infection ecology and antibiotic stewardship practices [10]. Understanding local pathogen distribution and resistance patterns is essential for guiding empirical antimicrobial therapy and infection prevention strategies.

Furthermore, while general severity scores such as SOFA and APACHE II are widely used in ICU prognostication, their predictive performance in pregnant populations is suboptimal due to physiological alterations in haemodynamic and respiratory parameters during gestation [11]. To date, no validated bedside tool specifically predicts ARDS risk among septic obstetric patients. Such a tool could enable risk stratification at the time of ICU admission, inform decisions regarding mechanical ventilation preparedness, and facilitate timely multidisciplinary management involving obstetrics, anaesthesia, and neonatology.

Therefore, this study had three primary objectives: (1) to describe the epidemiology and clinical characteristics of maternal sepsis in a Chinese tertiary obstetric ICU; (2) to characterise the pathogen profile and antimicrobial resistance patterns of septic obstetric patients; and (3) to develop and internally validate a clinical prediction model for ARDS specifically among pregnant and postpartum women with sepsis.

2. Methods

2.1 Study design and setting

This was a retrospective cohort study conducted at the Intensive Care Unit of the Third Affiliated Hospital of Guangzhou Medical University, a provincial and municipal tertiary referral centre for critically ill pregnant women in southern China. The ICU admits approximately 100–150 obstetric patients annually from Guangdong Province and neighbouring regions. The study comprised two overlapping patient cohorts extracted from the same electronic medical record database: a primary cohort of 780 pregnant and postpartum women admitted between January 2013 and April 2019 (used for ARDS prediction model development and clinical characterisation), and a contemporaneous cohort of 744 patients (used for detailed pathogen and antimicrobial susceptibility analysis).

2.2 Participants

Inclusion criteria: (1) pregnant or postpartum women (within 42 days of delivery or pregnancy termination) admitted to the ICU; (2) age $\geqslant$ 18 years; and (3) availability of complete electronic medical records.

Exclusion criteria: (1) non-pregnant/non-postpartum status; (2) ICU length of stay $\leqslant$ 24 hours; (3) incomplete clinical data; and (4) transfer from another ICU without primary data availability.

2.3 Definitions and diagnostic criteria

Sepsis and septic shock were defined according to the Third International Consensus Definitions for Sepsis and Septic Shock (Sepsis-3.0): sepsis was identified as infection with a SOFA score $\geqslant$ 2; septic shock was defined as sepsis with persisting hypotension requiring vasopressors to maintain mean arterial pressure (MAP) $\geqslant$ 65 mmHg and serum lactate >2 mmol/L despite adequate fluid resuscitation [12].

ARDS was diagnosed using the Berlin Definition (2012): acute onset within 7 days of a known clinical insult; bilateral opacities on

chest imaging not fully explained by effusions, lobar/lung collapse, or nodules; respiratory failure not fully explained by cardiac failure or fluid overload; and impaired oxygenation categorised as mild (200 mmHg < PaO_2/FiO_2 ⩽ 300 mmHg), moderate (100 mmHg < PaO_2/FiO_2 ⩽ 200 mmHg), or severe (PaO_2/FiO_2 ⩽ 100 mmHg) with positive end-expiratory pressure (PEEP) ⩾ 5 cmH_2O [13].

Multiple organ dysfunction syndrome (MODS) was defined as the simultaneous or sequential dysfunction of two or more organ systems in response to an acute insult [14].

Pathogen identification was performed using standard microbiological cultures from blood, sputum, urine, vaginal secretions, and other clinically relevant sites. Antimicrobial susceptibility testing followed Clinical and Laboratory Standards Institute (CLSI) guidelines.

2.4 Data collection

Clinical data were extracted from the hospital electronic medical record system, laboratory information system, and microbiology database by trained researchers using a standardised case report form. Variables included:

(1)General characteristics: age, gestational age, gravidity, parity, body mass index (BMI), mode of ICU admission (emergency, intra-hospital, inter-hospital transfer), and underlying comorbidities.

(2)Clinical parameters: vital signs (temperature, heart rate, respiratory rate, blood pressure, MAP), Glasgow Coma Scale (GCS), and illness severity scores (SOFA, APACHE II) within 24 hours of ICU admission.

(3)Laboratory investigations: complete blood count, procalcitonin (PCT), C-reactive protein (CRP), serum lactate, creatinine, blood urea nitrogen (BUN), total bilirubin, alanine aminotransferase, albumin, coagulation profile (prothrombin time [PT], activated partial thromboplastin time [APTT], international normalised ratio [INR]), and arterial blood gas analysis.

(5)Microbiological data: culture sites, isolated organisms, and antimicrobial susceptibility profiles.

(6)Treatment modalities: mechanical ventilation (invasive/non-invasive), vasoactive agents, blood transfusion, anticoagulation, continuous renal replacement therapy (CRRT), and empirical antibiotic regimens.

(7)Outcomes: ICU length of stay, total hospital length of stay, total hospitalisation costs, maternal in-hospital mortality, and pregnancy outcomes (abortion, preterm delivery, term delivery, stillbirth).

2.5 Statistical analysis

Data were analysed using SPSS version 26.0 (IBM Corp., Armonk, NY, USA) and R software version 4.3.1 (R Foundation for Statistical Computing, Vienna, Austria). Continuous variables were tested for normality using the Shapiro-Wilk test. Normally distributed data were expressed as mean ± standard deviation (SD) and compared using independent samples t-tests. Non-normally distributed data were presented as median (interquartile range [IQR]) and compared using the Mann-Whitney U test. Categorical variables were expressed as frequencies (percentages) and compared using the chi-squared test or Fisher's exact test, as appropriate.

To identify independent predictors of ARDS among septic patients, variables with $P < 0.05$ in univariate analysis were entered into a multivariable logistic regression model using backward stepwise selection (likelihood ratio). Collinearity was assessed using the variance inflation factor (VIF), with VIF > 10 indicating significant multicollinearity. A nomogram was constructed based on the final regression coefficients to provide a visual bedside prediction tool.

Model discrimination was evaluated using the area under the receiver operating characteristic curve (AUC-ROC) with 95% confidence intervals (CI). Model calibration was assessed using the Hosmer-Lemeshow goodness-of-fit test and calibration plots. The net reclassification improvement (NRI) and integrated discrimination improvement (IDI) were calculated to quantify the incremental predictive value of the new model compared with SOFA and APACHE II. Internal validation was performed using 1000 bootstrap resamples to estimate optimism-corrected performance.

A two-sided P value < 0.05 was considered statistically significant.

3. Results

3.1 Epidemiology and baseline characteristics

Between January 2013 and April 2019, 780 pregnant and postpartum women were admitted to the ICU. Of these, 309 (39.6%) met Sepsis-3.0 criteria. Among septic patients, 126 (40.8%) progressed to septic shock, and 19 (6.1%) died during hospitalisation. The overall ARDS rate was 32.9% (257/780); among septic patients, 138 (44.7%) developed ARDS, while 119 (15.3%) of the 471 non-septic patients met ARDS criteria (primarily due to obstetric haemorrhage, amniotic fluid embolism, or preeclampsia).

Septic patients were significantly younger (median age 29.5 vs. 30.0 years, P = 0.483), presented with higher illness severity (SOFA score 8.2 vs. 5.0, P < 0.001), and required more intensive organ support than non-septic patients. Septic patients had higher rates of invasive mechanical ventilation (65.1% vs. 35.5%), blood transfusion (61.6% vs. 28.2%), vasopressor use (43.4% vs. 16.3%), and CRRT (40.9% vs. 9.7%) (all P < 0.001). Hospitalisation costs and lengths of stay were also significantly greater in the sepsis group (Table 1).

3.2 Pathogen distribution and antimicrobial resistance

In the contemporaneous cohort of 744 patients, 648 (87.1%) had microbiological specimens collected. Among 279 septic patients, 273 (97.8%) were sampled, yielding 204 positive cultures (74.7%). A total of 435 pathogen isolates were identified from septic patients. The six most common organisms were Acinetobacter baumannii (40 isolates, 9.2%), Escherichia coli (31 isolates, 7.1%), Candida albicans (20 isolates, 4.6%), Staphylococcus aureus (19 isolates, 4.4%), Enterococcus faecium (15 isolates, 3.4%), and Klebsiella pneumoniae (13 isolates, 3.0%). Notably, 31 methicillin-resistant S. aureus (MRSA) strains (7.1%), 28 ceftriaxone-resistant gram-negative organisms (CTX-RO) (6.4%), and 4 carbapenem-resistant Enterobacterales (CRE) (0.9%) were identified.

The predominant infection sites were the respiratory system (83/279, 29.8%) and genital/reproductive tract (79/279, 28.3%). A. baumannii was most frequently isolated from sputum (60.0%), whereas E. coli was predominantly recovered from blood (47.0%) and C. albicans from vaginal secretions (50.0%).

Antimicrobial susceptibility testing revealed that A. baumannii was extensively drug-resistant, with high resistance rates to carbapenems, aminoglycosides, fluoroquinolones, and most cephalosporins; only polymyxins, cefoperazone-sulbactam, and tigecycline retained high sensitivity. E. coli remained highly susceptible to carbapenems and amikacin but exhibited 75.0% resistance to ceftriaxone. Coagulase-negative staphylococci and E. faecium demonstrated variable resistance patterns, with preserved sensitivity to linezolid, tigecycline, and glycopeptides (Table 2).

Empirical antibiotic therapy in septic patients most commonly involved carbapenems (37.2%), followed by ceftriaxone (15.2%), latamoxef (15.0%), and first-/second-generation cephalosporins (9.5%).

3.3 Clinical characteristics of sepsis-associated ARDS

Among the 257 ARDS patients, those with sepsis-associated ARDS (n = 138) were more severely ill than non-septic ARDS patients (n = 119). Septic ARDS patients had higher rates of moderate-to-severe ARDS (76.8% vs. 61.3%, P < 0.001), greater requirement for invasive mechanical ventilation (72.5% vs. 49.6%, P < 0.001), longer ICU stays (median 7 vs. 4 days, P < 0.001), and higher in-hospital mortality (10.9% vs. 3.4%, P = 0.022). However, pregnancy outcomes (abortion, preterm delivery, live birth, stillbirth) did not differ significantly between the two ARDS groups.

Within the septic cohort, ARDS patients (n = 138) exhibited more pronounced physiological derangement than non-ARDS septic patients (n = 171), including lower systolic blood pressure (102.2 ± 23.3 vs. 141.0 ± 23.4 mmHg), higher heart rate (126.2 ± 26.1 vs. 85.3 ± 19.2 beats/min), faster respiratory rate (22.1 ± 7.3 vs. 16.7 ± 4.8 breaths/min), and lower PaO_2 (94.0 vs. 122.0 mmHg) (all P < 0.001). They also had higher rates of MODS (79.7% vs. 22.8%), septic shock (52.2% vs. 31.6%), DIC (15.2% vs. 7.6%), and CRRT requirement (52.2% vs. 20.9%) (all P < 0.05) (Table 3).

3.4 Risk factors and prediction model for ARDS in septic patients

Univariate logistic regression identified 14 variables significantly associated with ARDS in septic patients. After multivariable adjustment, eight independent predictors remained: systolic blood pressure (OR 0.926, 95% CI 0.884–0.961, P < 0.001), heart rate (OR 1.069, 95% CI 1.041–1.013, P < 0.001), respiratory rate (OR 1.136, 95% CI 0.996–1.296, P = 0.048), PaO_2 (OR 0.989, 95% CI 0.978–

0.999, P = 0.031), MODS (OR 9.731, 95% CI 3.113–35.390, P < 0.001), invasive mechanical ventilation (OR 4.287, 95% CI 1.070–19.330, P = 0.046), CRRT (OR 4.744, 95% CI 1.204–21.380, P = 0.031), and vasoactive drug use (OR 0.059, 95% CI 0.004–0.613, P = 0.027).

A nomogram was constructed incorporating these eight variables (Figure 1). The model demonstrated excellent discrimination with an AUC of 0.986 (95% CI 0.978–0.996), sensitivity of 0.949, and specificity of 0.947. This significantly outperformed SOFA (AUC 0.669, 95% CI 0.609–0.729) and APACHE II (AUC 0.597, 95% CI 0.533–0.660) (DeLong test, both P < 0.001). The calibration curve indicated good agreement between predicted and observed ARDS probabilities (Hosmer-Lemeshow test P = 0.834), and bootstrap validation confirmed robustness (optimism-corrected AUC 0.982). Decision curve analysis demonstrated positive net benefit across clinically relevant threshold probabilities (Figure 2).

4. Discussion

4.1 Principal findings

This study provides a comprehensive characterisation of maternal sepsis in a Chinese tertiary obstetric ICU, integrating epidemiological, pathogen, and predictive modelling data. Three principal findings emerge. First, maternal sepsis affected nearly 40% of obstetric ICU admissions and was associated with substantial organ dysfunction, prolonged hospitalisation, and considerable healthcare costs. Second, the pathogen profile was dominated by ICU-acquired multidrug-resistant organisms, particularly A. baumannii, contrasting with community-acquired profiles reported in Western obstetric populations. Third, we developed and internally validated a simple eight-variable nomogram that accurately predicted ARDS risk among septic obstetric patients, substantially outperforming generic severity scores.

4.2 Epidemiology in context

The observed sepsis incidence (39.6%) and mortality (6.1%) in this cohort are higher than those reported in many high-income countries but comparable to other Chinese and Indian ICU series [15, 16]. This likely reflects the referral pattern of our centre, which receives the most complex cases from across southern China, and the application of stringent Sepsis-3.0 criteria in a population with high baseline physiological reserve. The 44.7% ARDS rate among septic patients underscores the pulmonary vulnerability of pregnant women, likely mediated by the physiological reduction in functional residual capacity, increased oxygen consumption, and the pro-inflammatory milieu of sepsis [17].

Notably, pregnancy outcomes (preterm delivery, stillbirth) did not differ significantly between septic ARDS and non-ARDS patients, suggesting that timely obstetric intervention—particularly emergency caesarean section for fetal salvage—may mitigate some adverse fetal effects of maternal respiratory failure. However, this observation should be interpreted cautiously given the absence of long-term neonatal follow-up data.

4.3 Pathogen profile and antimicrobial implications

The predominance of A. baumannii and other ICU-acquired pathogens differs markedly from Western reports where group B streptococcus and community-acquired E. coli predominate [9]. This discrepancy highlights the importance of local epidemiology in guiding empirical therapy. The high rate of carbapenem resistance in A. baumannii and the frequent use of carbapenems as first-line empirical therapy (37.2%) raise significant antimicrobial stewardship concerns. While carbapenems remain appropriate for critically ill septic patients given their broad spectrum, the low CRE rate (0.9%) suggests that de-escalation to narrower agents (e.g., piperacillin-tazobactam or cefoperazone-sulbactam) should be pursued once susceptibilities return, in line with SSC 2021 recommendations [7]. The high proportion of respiratory and genital tract infections also emphasises the need for rigorous infection prevention bundles, including ventilator-associated pneumonia prevention and peripartum antibiotic prophylaxis.

4.4 The prediction model: clinical utility and innovation

To our knowledge, this is the first nomogram specifically developed to predict ARDS risk among septic pregnant and postpartum women. Existing general ICU scores (SOFA, APACHE II) performed poorly in this population (AUC < 0.70), likely because they fail to account for pregnancy-specific physiological adaptations. For example, the relative "protective" effect of vasoactive drug use in our model (OR 0.059) may reflect earlier haemodynamic resuscitation in patients presenting with septic shock, preventing progression to ARDS—an effect obscured by generic scores.

The eight variables included in the nomogram are readily available at the bedside within the first hours of ICU admission, requiring only vital signs, arterial blood gas, and awareness of organ support requirements. This facilitates real-time risk stratification without specialised biomarkers. In clinical practice, a septic obstetric patient with low blood pressure, tachycardia, tachypnoea, hypoxaemia, and evolving MODS could be identified within the first hour as having >80% predicted ARDS risk, prompting immediate preparation for invasive mechanical ventilation, lung-protective strategies, and multidisciplinary obstetric planning.

4.5 Strengths and limitations

Strengths include the relatively large obstetric ICU cohort, the application of contemporary Sepsis-3.0 and Berlin definitions, and the direct comparison with established severity scores. However, several limitations must be acknowledged. First, the retrospective design and single-centre setting introduce selection bias and limit generalisability. Second, the pathogen analysis was derived from a slightly smaller contemporaneous cohort (744 vs. 780 patients) due to database extraction timing; while both cohorts share the same centre and time period, unified data extraction would strengthen consistency. Third, the prediction model requires external validation in independent obstetric ICUs before clinical implementation. Fourth, we lacked long-term maternal and neonatal follow-up data beyond hospital discharge. Finally, the absence of viral and molecular diagnostics (e.g., metagenomic next-generation sequencing) may have underestimated viral or rare pathogen contributions.

4.6 Future directions

Future research should prioritise external validation of this nomogram in multi-centre prospective studies across diverse healthcare settings, particularly in LMICs with similar pathogen profiles. Integration of the model into electronic health record systems as a clinical decision support tool would facilitate bedside adoption. Additionally, studies examining the impact of model-guided early intervention on ARDS incidence and maternal mortality are warranted. The inclusion of novel biomarkers (e.g., presepsin, sTREM-1) or machine learning approaches may further refine predictive accuracy.

5. Conclusions

Maternal sepsis in this Chinese ICU cohort was associated with a high incidence of ARDS, significant mortality, and a pathogen profile dominated by multidrug-resistant ICU-acquired organisms. The developed eight-variable nomogram accurately predicted ARDS among septic obstetric patients and outperformed generic severity scores. If externally validated, this tool could support early recognition, resource allocation, and improved maternal outcomes in obstetric critical care.

Abbreviations

ARDS: Acute respiratory distress syndrome

APACHE II: Acute Physiology and Chronic Health Evaluation II

AUC: Area under the curve

BMI: Body mass index

CI: Confidence interval

CRRT: Continuous renal replacement therapy

DIC: Disseminated intravascular coagulation

GCS: Glasgow Coma Scale

ICU: Intensive care unit

IQR: Interquartile range

MAP: Mean arterial pressure

MODS: Multiple organ dysfunction syndrome

OR: Odds ratio

PaO_2: Partial pressure of arterial oxygen

PEEP: Positive end-expiratory pressure

ROC: Receiver operating characteristic

SD: Standard deviation

SOFA: Sequential Organ Failure Assessment

SSC: Surviving Sepsis Campaign

References

[1] Say L, Chou D, Gemmill A, et al. Global causes of maternal death: a WHO systematic analysis. Lancet Glob Health. 2014;2(6):e323-e333.

[2] Zhao Z, Han S, Yao G, et al. Pregnancy-Related ICU Admissions From 2008 to 2016 in China: A First Multicenter Report. Crit Care Med. 2018;46(10):e1002-e1009.

[3] Acosta C, Knight M. Sepsis and maternal mortality. Curr Opin Obstet Gynecol. 2013;25(2):109-116.

[4] Englert JA, Bobba C, Baron RM. Integrating molecular pathogenesis and clinical translation in sepsis-induced acute respiratory distress syndrome. JCI Insight. 2019;4(2).

[5] Lapinsky SE. Management of Acute Respiratory Failure in Pregnancy. Semin Respir Crit Care Med. 2017;38(2):201-207.

[6] Parfitt SE, Hering SL. Recognition and Management of Sepsis in the Obstetric Patient. AACN Adv Crit Care. 2018;29(3):278-288.

[7] Evans L, Rhodes A, Alhazzani W, et al. Surviving sepsis campaign: international guidelines for management of sepsis and septic shock 2021. Intensive Care Med. 2021;47(11):1181-1247.

[8] Plante LA, Pacheco LD, Louis JM. SMFM Consult Series #47: Sepsis during pregnancy and the puerperium. Am J Obstet Gynecol. 2019;220(4):B2-B10.

[9] Knowles SJ, O'sullivan NP, Meenan AM, et al. Maternal sepsis incidence, aetiology and outcome for mother and fetus: a prospective study. BJOG. 2015;122(5):663-671.

[10] Qin Yuanyi, Chen Xuemei, Huang Dongjian, et al. [Pathogen distribution and drug resistance analysis of nosocomial infection in ICU]. Nan Fang Yi Ke Da Xue Xue Bao. 2012;32(10):1473-1476. (In Chinese)

[11] Albright CM, Has P, Rouse DJ, et al. Internal Validation of the Sepsis in Obstetrics Score to Identify Risk of Morbidity From Sepsis in Pregnancy. Obstet Gynecol. 2017;130(4):747-755.

[12] Singer M, Deutschman CS, Seymour CW, et al. The Third International Consensus Definitions for Sepsis and Septic Shock (Sepsis-3). JAMA. 2016;315(8):801-810.

[13] Force ADT, Ranieri VM, Rubenfeld GD, et al. Acute respiratory distress syndrome: the Berlin Definition. JAMA. 2012;307(23):2526-2533.

[14] Bone RC, Balk RA, Cerra FB, et al. Definitions for sepsis and organ failure and guidelines for the use of innovative therapies in sepsis. Chest. 1992;101(6):1644-1655.

[15] Balki I, Baghirzada L, Walker A, et al. Incidence, morbidity, and associated factors for sepsis in women hospitalized for delivery: a nationwide retrospective observational population-based study in Canada. Can J Anaesth. 2022;69(3):298-310.

[16] Muthu V, Agarwal R, Dhooria S, et al. Epidemiology, lung mechanics and outcomes of ARDS: A comparison between pregnant

and non-pregnant subjects. J Crit Care. 2019;50:207-212.

[17] Lim MJ, Lakshminrusimha S, Hedriana H, et al. Pregnancy and Severe ARDS with COVID-19: Epidemiology, Diagnosis, Outcomes and Treatment. Semin Fetal Neonatal Med. 2023;28(1):101426.

类别 :// 临床研究：设计规范的各类临床研究及研究方案报告

Etiology-Specific Clinical Phenotypes and Outcomes in Patients Receiving Venoarterial Extracorporeal Membrane Oxygenation: A Nationwide Multicenter Cohort Study in China

姓名：Wang YIwen，Li Chenglong，Hou Xiaotong

单位：首都医科大学附属北京安贞医院

为了描述中国国家登记册中成人 VA ECMO 患者的病因分布、基线特征、支持特征、并发症和住院结果，并按年龄和性别进行分层。

我们利用中国体外生命支持学会（CSECLS）注册库开展了一项全国多中心回顾性队列研究。自 2015 年以来，该学会共记录了 18,043 例体外膜肺氧合（ECMO）病例。纳入标准为：年龄≥ 18 岁，接受静脉 - 动脉（VA）ECMO 治疗，且关键基线和临床变量的完整性超过 70%。最终分析队列包含 12,043 例患者。纳入的变量包括人口统计学特征、病因分类、血流动力学和实验室指标、ECMO 支持持续时间、机械通气时间、重症监护室（ICU）住院时间、并发症以及出院生存情况。对不同病因组的患者进行比较，并进一步按年龄（≤ 45 岁、45-65 岁和 >65 岁）和性别进行分层。连续变量以中位数（四分位间距）表示，分类变量以例数（百分比）表示。组间比较采用 Kruskal-Wallis 检验或卡方检验（视情况而定）。

患者的中位年龄为 54 岁（44-65 岁）；8748 例患者（73%）为男性，3295 例（27%）为女性。体外膜肺氧合（ECMO）的中位持续时间为 96 小时（48-168 小时），9431 例患者（78%）接受了机械通气，ICU 的中位住院时间为 10 天（5-17 天）。观察到明显的病因特异性异质性。暴发性心肌炎约占该队列的 8%，患者年龄最小（中位年龄 38 岁），女性患者占多数（男性比例为 49%），需要相对较长的支持治疗，且出院生存率最高（约 74%）。急性心肌梗死约占病例的 21%；这些患者年龄较大（中位年龄 61 岁），以男性为主（64%），合并症负担较重，生存率约为 59%。心脏手术后患者的年龄分布介于两者之间（中位年龄 56 岁），男性比例最高（70%），生存率约为 47%，出血并发症发生率较高，ICU 住院时间较长。脓毒症相关的体外膜肺氧合（VA ECMO）患者的生存率最低，约为 41%。按年龄分层分析显示病因逐渐发生变化：≤ 45 岁患者中以心肌炎为主（54%），45-65 岁患者中急性心肌梗死增多（42%），>65 岁患者中急性心肌梗死最为常见（61%）。女性仅占总队列的 27%，但在心肌炎病例中却占一半以上。在急性心肌梗死患者中，女性比男性年龄大（中位数为 67 岁，男性为 59 岁），且 ECMO 治疗时间较短。

迄今为止，这项规模最大的全国性中国 VA ECMO 队列研究表明，病因对患者的表型、并发症情况和预后有显著影响。心肌炎、急性心肌梗死和心脏手术后休克不应被视为 VA ECMO 的可互换适应症。年龄和性别不仅是混杂因素，更是病因分布和预后的重要临床相关调节因素。针对特定病因的风险模型以及基于年龄和性别的个体化管理方案可能有助于改善患者选择、并发症监测、撤机策略和预后判断。

类别 :// 基础研究：涉及重症相关问题的基础研究

Exendin-4 Attenuates mPFC–Hippocampal Circuit Dysfunction after Severe Traumatic Brain Injury via Glp1r Activation

姓名：徐璠，周敏

单位：中国科学技术大学附属第一医院（安徽省立医院）

Severe traumatic brain injury (sTBI) causes high disability and mortality.[1]. The mPFC–hippocampal circuit is vulnerable to sTBI, but its molecular mechanisms are unclear[1]. Exendin 4 has been reported to exert potential neuroprotective effects[2]; however, its role and underlying mechanisms in sTBI remain unclear[3]. This study aimed to investigatewhether Exendin-4 ameliorates sTBI-induced circuit dysfunction via Glp1r and potential Potential downstream pathways.

Single-cell sequencing data of the mPFC tissue from severe TBI patients and normal donors were analyzed to explore the mechanisms of severe TBI-induced cortical injury. Severe TBI models were established using mechanically scratched HT22 and SH-SY5Y neuronal cell lines[4] and severe CCI-induced C57 mice (groups: sham, TBI, TBI+Exendin 4, n=6)[5]. MTT assay was used to assess neuronal viability, combined with quantitative real-time PCR (qPCR) to evaluate cellular injury. And MitoTracker Red CMXRos was used to detect Mitochondrial damage. Neurological and cognitive impairments were assessed by mNSS score[6] and immunofluorescence (IF). Blood-brain barrier integrity was assessed by Evans blue extravasation. Furthermore, Glp1r flox/flox Camk2a Cre+ conditional knockout mice were used in behavioral experiments (Open field, New object recognition and Morris water maze test) to verify the impact of Glp1r deletion on severe TBI-induced neurological damage.

ingle cell sequencing showed that 103 genes in GLP1R positive cortical neurons of severe TBI patients (n=3) were significantly upregulated compared to normal donors (n=3), among which the top ten genes were HSP90AA1, PTPRZ1, MTRNR2L8, LHFPL3, VCAN, CTTNBP2, NOVA1, DSCAM, PID1 and SFPQ (Figure 1A). The enrichment analysis of differentially expressed genes in Glp1r positive neurons between severe TBI patients and normal control group showed that the main functional changes were in inflammation, metabolism, and cell connectivity, including Focal adhesion, Adherens junction, Lysosome, Cell adhesion molecules (CAMs), Noteh signaling pathway, P3K-Akt signaling pathway and ErbB signaling pathway (Figure 1B). qPCR, MTT tests and IF results demonstrated that Exendin 4 alleviated severe TBI-induced oxidative damage and apoptosis in HT22 and SH-SY5Y neurons (Figure 2A-C). mNSS scores, Evans blue staining, and IF results showed that Exendin 4 ameliorated severe TBI-induced mPFC and hippocampal neurological dysfunction in mice (Figure 2D-F). Behavioral experiments further revealed that Glp1r conditionl knockout significantly exacerbated hippocampal neurological deficits and cognitive impairment in severe TBI mice (Figure 3A-C).

Single-cell sequencing of mPFC tissue, together with in vitro and in vivo experiments, confirms that Exendin 4 alleviates severe TBI-induced mPFC and hippocampal neurological damage and cognitive dysfunction by activating Glp1r and reducing inflammation and oxidative damage, highlighting its therapeutic potential. Studies are warranted to elucidate the further mechanisms of severe TBI injury and the therapeutic action of Exendin 4.

FTO-mediated m6A Demethylation of PRKCB mRNA Activates NF-κB to Trigger Alveolar Fibrin Deposition in ARDS

姓名：Xianjun Chen [1,#]，Ying Liu [1,2,#]，Jia Yuan [1]，Chuan Xiao [1]，Qi Dong[1]，Qing Li [1]，Ying Wang [1]
Qimin Chen[1]，Shuwen Li [1]，Wei Li [1]，Feng Shen [1,*]
单位：1 The Affiliated Hospital of Guizhou Medical University，2 Wuhan No. 1 Hospital

Abstract

Background: Acute Respiratory Distress Syndrome (ARDS) is characterized by alveolar fibrin deposition, driven by dysregulated hypercoagulation and impaired fibrinolysis. Although alveolar epithelial type II (AEC II) cells contribute to this imbalance by overexpressing Tissue Factor (TF) and Plasminogen Activator Inhibitor-1 (PAI-1), the upstream regulatory mechanisms, particularly at the epitranscriptomic level, remain unclear. The potential role of the N6-methyladenosine (m6A) RNA demethylase FTO in ARDS pathogenesis is unexplored.

Methods: In this study, we employed lipopolysaccharide (LPS)-induced rat ARDS models and LPS-stimulated AEC II cells as primary experimental systems to investigate the underlying mechanisms. Multi-omics profiling, combining methylated RNA immunoprecipitation sequencing (MeRIP-seq) and RNA sequencing (RNA-seq), was performed. Gain and loss-of-function studies were conducted using lentiviral vectors both in vitro and in vivo. Mechanistic investigations involved MeRIP-qPCR, mRNA stability assays, co-immunoprecipitation (Co-IP), Western blot, immunofluorescence, and pharmacological modulation of the NF-κB pathway.

Results: Lungs from ARDS rats showed decreased global m6A levels and increased FTO expression. Knockdown of FTO alleviated lung injury, reduced pulmonary edema, and suppressed the expression of TF and PAI-1, concomitant with inhibition of NF-κB signaling. Integrated multi-omics analysis identified PRKCB as a key target of FTO. Mechanistically, FTO demethylated PRKCB mRNA, thereby enhancing its stability and translation. Elevated PRKCB promoted IKKβ phosphorylation and subsequent NF-κB activation. Rescue experiments confirmed that FTO regulates alveolar hypercoagulation and fibrinolytic inhibition in ARDS via PRKCB-dependent activation of the NF-κB pathway.

Conclusion:

Our study identifies the FTO-PRKCB-NF-κB axis as a novel epitranscriptomic pathway driving alveolar fibrin deposition in ARDS. These findings reveal FTO as a potential therapeutic target for mitigating alveolar hypercoagulation and fibrinolysis inhibition in ARDS.

Keywords: Acute Respiratory Distress Syndrome, N6-methyladenosine, FTO, PRKCB, NF-κB signaling, alveolar fibrin deposition.

Gastric Antral Motility Rhythm Phenotypes Derived From Bedside Ultrasound Are Associated With Gastrointestinal Dysfunction and Enteral Nutrition Delivery in Patients With Acute Brain Injury: A Single-Center Retrospective Cohort Study

姓名：Tongjuan Zou，Wanhong Yin
单位：四川大学华西医院

Abstract

Objective To investigate the associations of gastric antral motility rhythm phenotypes, defined from continuous cross-sectional area (CSA) traces acquired by bedside ultrasound, with gastrointestinal dysfunction (GID) and enteral nutrition delivery in patients with acute brain injury (ABI).

Methods This single-center retrospective cohort study included adult patients with ABI from the 2023–2024 gastric ultrasound video database of the Department of Critical Care Medicine, West China Hospital, Sichuan University. Eligible patients had a quality-controlled 6-min short-axis antral ultrasound video acquired within 24 h of ICU admission and complete core clinical data. An artificial intelligence system performed frame-wise gastric antral segmentation and generated continuous CSA traces. The study team manually reviewed the traces according to prespecified phenotypic criteria and classified them as regular, irregular, or gastroparesis-like; regular and irregular phenotypes were also combined as the non-gastroparesis-like group. The primary outcome was GID, defined as a Gastrointestinal Dysfunction Score (GIDS) ⩾ 1 on the day of ultrasound acquisition. Nutritional outcomes included enteral nutrition status on the day of ultrasound acquisition, initiation of enteral nutrition within 48 h of ICU admission, and achievement of 80% of target feeding volume within 3 d of ICU admission. Dynamic ultrasound measures included the motility index (MI), antral contraction frequency (ACF), antral contraction amplitude (ACA), and the number of antral contractions within 6 min.

Results A total of 267 patients with ABI were included: 82 (30.71%) had a regular phenotype, 71 (26.59%) an irregular phenotype, and 114 (42.70%) a gastroparesis-like phenotype. Age, sex, Glasgow Coma Scale category, Sequential Organ Failure Assessment score, targeted temperature management, arrhythmia, ICU length of stay, hospital length of stay, and in-hospital mortality did not differ significantly across the three phenotypes. Median MI values were 0.97 (0.70–1.42), 0.72 (0.58–1.02), and 0.41 (0.29–0.57), respectively (P<0.001); median numbers of antral contractions within 6 min were 8.00 (2.50–12.00), 6.00 (2.00–10.00), and 2.00 (0.00–6.00), respectively (P<0.001). Overall, 163 patients (61.05%) had GIDS ⩾ 1; proportions differed across phenotypes (47.56%, 64.79%, and 68.42%; P=0.010). Compared with the gastroparesis-like phenotype, the regular phenotype was associated with lower odds of GID (OR 0.42, 95% CI 0.23–0.75; P=0.005). Initiation of enteral nutrition within 48 h also differed across phenotypes (85.36%, 73.24%, and 68.42%; P=0.024). In the two-group analysis, the non-gastroparesis-like group had lower odds of GID than the gastroparesis-like group (55.56% vs 68.42%; OR 0.58, 95% CI 0.35–0.96; P=0.042) and higher rates of enteral nutrition in place on the day of ultrasound acquisition and of enteral nutrition initiated within 48 h.

Conclusion Gastric antral motility rhythm phenotypes derived from continuous bedside ultrasound CSA traces were supported by dynamic motility measures and were associated with GID burden and early enteral nutrition delivery in patients with ABI. A gastroparesis-like phenotype may identify patients with a higher GID burden and more limited early enteral nutrition delivery. This dynamic phenotype may support bedside, visual risk stratification of GID in neurocritical care.

Keywords: Acute brain injury; Gastrointestinal dysfunction; Gastric antral ultrasound; Gastric antral motility rhythm; Enteral nutrition; Artificial intelligence

类别 :// 基础研究：涉及重症相关问题的基础研究

GRN-Sort1 轴介导小胶质细胞 - 神经元交互调控脓毒症脑病损伤的机制研究

姓名：张译之

单位：湖南医药学院总医院

脓毒症脑病是重症脓毒症患者常见的严重神经系统并发症，以认知功能障碍、神经炎症损伤、神经元凋亡为核心病理特征，是重症患者预后不良、远期认知残留损伤的重要独立危险因素。目前临床缺乏针对性的靶向干预靶点，其核心分子调控机制尚未完全阐明，尤其脑组织内免疫细胞与神经细胞的交互调控机制亟待深入探究。本研究以盲肠结扎穿刺（CLP）诱导的脓毒症小鼠模型为研究载体，动态观察脓毒症小鼠行为学及脑组织病理损伤特征，通过单细胞 RNA 测序解析海马组织细胞异质性及细胞间通讯网络，筛选核心调控信号轴，并结合体外细胞实验验证 GRN-Sort1 信号轴对脓毒症神经炎症及神经元损伤的调控作用，旨在阐明脓毒症脑病的潜在发病机制，为临床重症脓毒症脑病的靶向治疗提供全新的实验依据与分子靶点。

本研究分为动物模型体内实验、组织测序分析及体外细胞验证实验三部分。第一部分，采用中度盲肠结扎穿刺（CLP）法构建小鼠脓毒症模型，设置假手术（Sham）对照组，分别在造模后 24h、48h 对小鼠背部外观、眼部状态、呼吸功能、自主活动、肌肉张力、翻正反射、消化功能及体表温度进行多维度行为学评分；造模 2 周后通过 Morris 水迷宫实验检测小鼠学习记忆认知功能。实验结束后取小鼠海马脑组织，采用免疫荧光染色检测小胶质细胞激活标志物 Iba1、星形胶质细胞活化标志物 GFAP 表达水平，通过尼氏染色观察海马 CA1 区神经元损伤情况。第二部分，选取行为学及病理证实存在脓毒症脑病损伤的 CLP 组与 Sham 组小鼠海马组织，制备单细胞悬液进行单细胞 RNA 测序（scRNA-seq），利用 fastMNN 算法完成批次校正，通过 tSNE 聚类分析划分细胞亚簇，结合标志基因及 SingleR 注释完成细胞类型鉴定，构建细胞间单向通讯网络，筛选小胶质细胞与神经元之间的核心受配体信号对。第三部分，通过 qPCR 筛选 BV2 小胶质细胞中 Sort1 有效干扰 siRNA，以 LPS 诱导炎症细胞模型，采用 CCK8 实验检测 HT22 神经元细胞增殖活性，Western Blot 检测细胞凋亡标志物 Cleaved-Caspase3 表达，流式细胞术检测细胞凋亡率，qPCR 检测炎症因子 IL-6、TNF-α、IL-10 mRNA 表达水平，ELISA 检测 GRN 蛋白分泌水平，验证 Sort1 敲降对脓毒症神经炎症及神经元损伤的调控作用。

动物行为学评分结果显示，

CLP 造模后小鼠出现明显脓毒症全身症状及神经功能异常，48h 各维度行为学评分显著高于 24h，且同期评分显著高于 Sham 组，提示脓毒症小鼠随病程进展出现进行性加重的脓毒症相关脑损伤行为学改变。

造模 2 周水迷宫结果表明，CLP 组小鼠穿越原平台位置次数显著减少，逃避潜伏期明显延长，证实脓毒症小鼠存在持续性学习、记忆认知功能损伤。

脑组织病理检测显示，CLP 组小鼠海马组织 Iba1、GFAP 荧光表达强度显著升高，提示小胶质细胞、星形胶质细胞大量活化；海马 CA1 区尼氏小体数量显著减少，神经元损伤、凋亡数量明显增加。

单细胞测序结果将小鼠海马组织细胞划分为 25 个亚簇，成功注释小胶质细胞、神经元、星形胶质细胞等 10 余种细胞类型；细胞通讯分析证实小胶质细胞向神经元的信号传递为海马组织核心信号流，显著强于神经元对小胶质细胞的反向通讯，其中 Grn-Sort1 为二者间最关键的受配体对，通讯活性最强。

组织验证实验证实脓毒症脑病小鼠海马组织中 GRN、Sort1 蛋白表达水平均显著上调，且 GRN 主要表达于小胶质细胞，Sort1 特异性富集于神经元。体外细胞实验显示，LPS 炎症刺激可显著抑制 HT22 细胞增殖、促进细胞凋亡，上调炎症因子及 Cleaved-Caspase3 表达，提升 GRN 分泌水平；敲降 Sort1 后可显著逆转上述损伤，促进 HT22 细胞增殖、降低凋亡率，抑制炎症因子表达，同时进一步上调 GRN 蛋白水平，有效缓解炎症介导的神经元损伤。

CLP 诱导的脓毒症可诱发小鼠持续性神经炎症、神经元损伤及认知功能障碍，成功构建稳定的脓毒症脑病动物模型。脓毒症状态下海马组织小胶质细胞异常活化，通过 Grn-Sort1 信号轴与神经元产生强效异常通讯，介导神经炎症级联反应及神经元凋亡损伤。靶向敲降 Sort1 可通过调控 GRN 表达，抑制小胶质细胞过度活化、减轻神经炎症反应、缓解神经元凋亡损伤。GRN-Sort1 轴是调控脓毒症脑病小胶质细胞 - 神经元交互损伤的核心信号通路，可作为临床重症脓毒症脑病精准干预的潜在新型靶点。

类别 :// 临床研究：设计规范的各类临床研究及研究方案报告

Haemodynamic Stability of Cipepofol versus Propofol in Critically Ill Adults Undergoing Emergency Rapid-Sequence Intubation: An Exploratory Randomised Controlled Pilot Trial

姓名：韩霏

单位：复旦大学附属中山医院

Propofol is the most widely used induction agent for rapid-sequence intubation (RSI) in critically ill patients, yet its vasodilatory and negative inotropic effects frequently provoke peri-intubation hypotension. Cipepofol, a structurally optimised alkylphenol, suppresses vascular smooth-muscle tone less than propofol at equi-sedative doses in preclinical and early-phase studies. Randomised data in critically ill adults undergoing emergency RSI are lacking.

We conducted an investigator-initiated, parallel-group, centrally randomised, open-label pilot trial in three tertiary ICUs in Shanghai (November 2024 to November 2025). Adults requiring emergency tracheal intubation were assigned 1:1 to cipepofol (0.1–0.2 mg/kg) or propofol (0.5–1.0 mg/kg), each given over 30 ± 5 s after standardised remifentanil and rocuronium. The pre-specified primary composite outcome was cardiovascular collapse within 30 min of intubation (any of SBP < 65 mmHg, initiation of a new vasoactive agent, sustained SBP fall ⩾ 20% from baseline, or SBP < 90 mmHg for ⩾ 30 min). The intention-to-treat analysis used the χ^2 test, with a pre-specified logistic model adjusting for baseline shock, GCS, and MAP. Identical-appearance masking was not feasible, so treating clinicians were unblinded while outcome adjudicators and the analyst were blinded. As a pilot, the trial was not powered for confirmatory inference and all analyses are exploratory.

All 100 randomised patients (49 cipepofol, 51 propofol) were analysed with no loss to follow-up. Cardiovascular collapse occurred in 18 of 49 cipepofol recipients (36.7%) and 29 of 51 propofol recipients (56.9%): risk difference (RD) − 20.2% (95% CI, − 39.1 to − 1.3; P = 0.044). The association persisted after adjustment (adjusted OR 0.42; 95% CI, 0.18–0.98; P = 0.048). It was carried mainly by the new-vasopressor component, which is open to performance bias under an unblinded design (43.1% vs 22.4%; P = 0.029). Sedation success (89.8% vs 90.2%) and first-attempt intubation (100% in both) were equivalent. Bradycardia occurred only with propofol (11.8% vs 0%; P = 0.027). Twenty-eight-day mortality was 22.4% versus 25.5% (P = 0.72).

In this underpowered, open-label pilot trial, cipepofol was associated with less peri-intubation cardiovascular collapse and bradycardia than propofol, with equivalent sedation. Borderline significance, the susceptibility of the leading endpoint component to performance bias, and baseline imbalance confine these findings to the hypothesis-generating level. They justify, but do not pre-empt, an adequately powered, double-dummy, multicentre trial with 28-day mortality as a co-primary outcome.

HDAC11 敲低改善 LPS 诱导 H9C2 心肌细胞脂肪酸氧化障碍

姓名：陈伟[1]，赵泽泽[1]，耿争光[1]，郑晓茜[1]，付豹[1]，傅小云[1]*

单位：遵义医科大学附属医院

摘要

背景：脓毒症相关心肌功能障碍与线粒体能量代谢紊乱密切相关。脂肪酸氧化受抑可造成 ATP 生成不足和脂质蓄积，但组蛋白去乙酰化酶 11（HDAC11）在该过程中的作用尚不明确。目的：观察 HDAC11 敲低对脂多糖（LPS）诱导 H9C2 心肌细胞脂肪酸氧化障碍的影响，并初步评价肉碱棕榈酰转移酶 1B（CPT1B）的作用。方法：采用 10 μg/mL LPS 刺激 H9C2 细胞。通过腺病毒敲低 HDAC11，检测 PGC-1α、ACADVL、CPT1B、CD36 及 PLIN5 的 mRNA 和蛋白表达；采用 BODIPY 493/503 染色、FAO-Glo 法和 ATP 检测试剂盒分别评价脂质蓄积、相对脂肪酸氧化活性及 ATP 水平。进一步采用 CPT1B shRNA 慢病毒感染细胞 48 h（MOI=300），观察 CPT1B 敲低对 HDAC11 敲低效应的影响。结果：LPS 刺激后 HDAC11 表达升高，CPT1B 及其他脂肪酸氧化相关分子表达下降，并伴随脂肪酸氧化活性降低和脂质蓄积增加。HDAC11 敲低可部分恢复相关分子表达，提高脂肪酸氧化活性并减少脂质蓄积。进一步敲低 CPT1B 后，脂肪酸氧化活性和 ATP 水平再次下降，脂质蓄积增加，HDAC11 敲低的代谢改善效应受到削弱。结论：HDAC11 敲低可改善 LPS 诱导的 H9C2 细胞脂肪酸氧化障碍，其作用可能部分依赖 CPT1B 介导的脂肪酸氧化恢复。

关键词：HDAC11；CPT1B；脂肪酸氧化；脂多糖；H9C2 细胞

1 研究背景与现状

脓毒症相关心肌功能障碍是脓毒症重要的器官并发症，其发生涉及炎症反应、氧化应激和线粒体能量代谢异常等多重机制 [1-2]。正常心肌具有较高的能量需求，脂肪酸氧化是其重要供能途径。脓毒症状态下，脂肪酸向线粒体转运及 β- 氧化受阻，可导致 ATP 生成不足、脂质中间产物蓄积并进一步加重细胞损伤 [2]。HDAC11 是唯一的Ⅳ类组蛋白去乙酰化酶，除参与表观遗传调控外，还具有脂酰化修饰调节功能，并与炎症和能量代谢密切相关 [3-4]。已有研究提示 HDAC11 可限制骨骼肌脂肪酸氧化 [5]，但其是否参与 LPS 诱导的心肌细胞脂肪酸氧化障碍仍缺乏直接证据。

2 研究目的

观察 LPS 刺激后 H9C2 细胞 HDAC11 和脂肪酸氧化相关分子的变化，评价 HDAC11 敲低对脂肪酸氧化功能及脂质蓄积的影响，并通过 CPT1B 敲低实验初步判断其作用是否依赖 CPT1B。

3 研究设计与方法

本研究为体外对照实验。首先以 10 μg/mL LPS 刺激 H9C2 细胞 0、3、6、12、24 和 48 h，采用 Western blot 检测 HDAC11 及 CPT1B 蛋白表达，确定后续干预时间。随后采用腺病毒介导 HDAC11 敲低，设置 shNC 组、LPS+shNC 组、shHDAC11 组及 LPS+shHDAC11 组。采用 RT-qPCR 和 Western blot 检测 HDAC11、PGC-1α、ACADVL、CPT1B、CD36 及 PLIN5 表达；BODIPY 493/503 联合 MitoTracker、Hoechst 染色观察脂滴及线粒体分布；FAO-Glo 法检测相对脂肪酸氧化活性。机制验证阶段，在 HDAC11 敲低基础上采用 CPT1B shRNA 慢病毒感染 H9C2 细胞 48 h（MOI=300），设置 shNC 组、LPS+shNC 组、LPS+shHDAC11 组、LPS+shCPT1B 组及 LPS+shHDAC11+shCPT1B 组，并检测脂质蓄积、脂肪酸氧化活性及 ATP 水平。采用 GraphPad Prism 软件进行统计分析。各实验独立重复 3 次，数据以均数 ± 标准差表示，多组间比较采用单因素方差分析，以 $P<0.05$ 为差异有统计学意义。

4 结果

4.1 LPS 诱导 HDAC11 升高并抑制 CPT1B 表达

随 LPS 刺激时间延长，H9C2 细胞 HDAC11 蛋白总体呈升高趋势，CPT1B 蛋白总体呈下降趋势，24 h 时变化明确，故后续实验采用 LPS 10 μg/mL 刺激 24 h（图 1）。

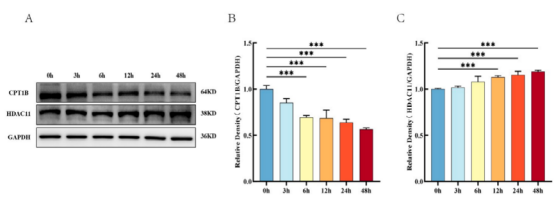


图 1　LPS 时间梯度刺激对 H9C2 细胞 HDAC11 和 CPT1B 蛋白表达的影响。A：代表性 Western blot 条带；B、C：CPT1B 和 HDAC11 灰度定量。n=3，*P<0.05，**P<0.01，***P<0.001。

4.2 HDAC11 敲低恢复脂肪酸氧化相关分子表达

与 shNC 组相比，LPS+shNC 组 HDAC11 mRNA 和蛋白表达升高，PGC-1α、ACADVL、CPT1B、CD36 及 PLIN5 表达下降。HDAC11 敲低后，上述脂肪酸氧化及脂质代谢相关分子的表达得到不同程度恢复（图 2、图 3），提示 HDAC11 可能参与 LPS 诱导的脂肪酸氧化转录及蛋白表达异常。

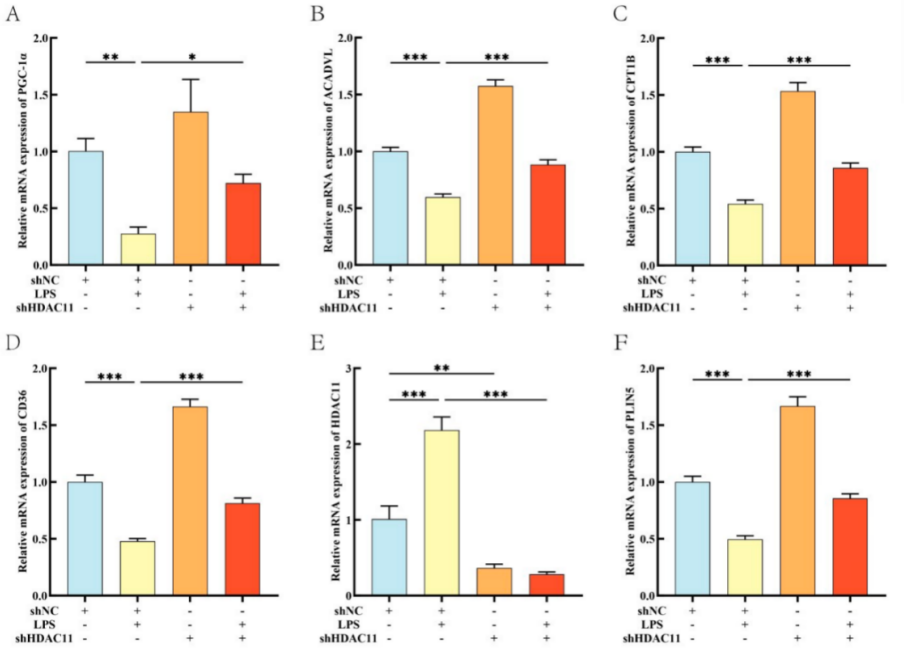


图 2　HDAC11 敲低对 LPS 诱导 H9C2 细胞脂肪酸氧化相关基因 mRNA 表达的影响。A-F 依次为 PGC-1α、ACADVL、CPT1B、CD36、HDAC11 及 PLIN5。n=3

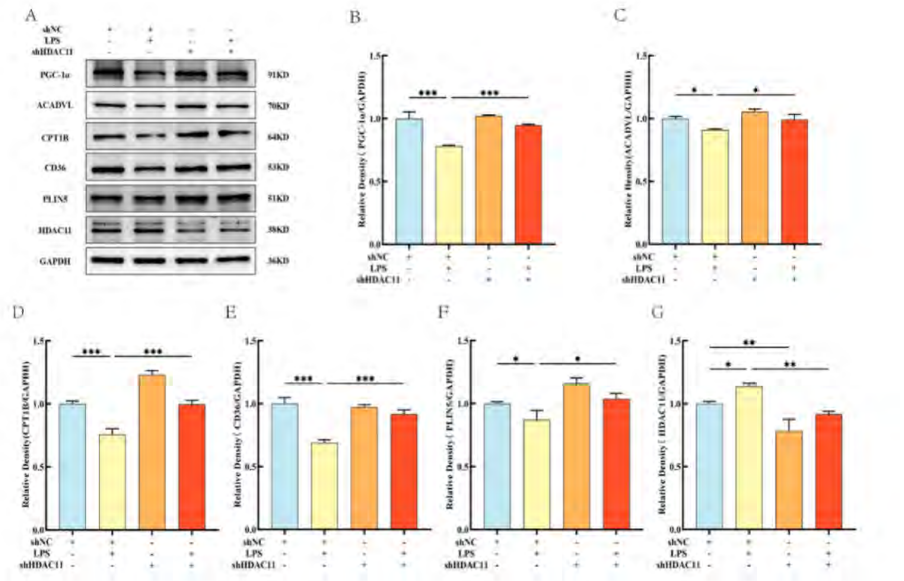


图 3　HDAC11 敲低对 LPS 诱导 H9C2 细胞脂肪酸氧化相关蛋白表达的影响。A：代表性 Western blot 条带；B-G：相应蛋白灰度定量。n=3。

4.3 HDAC11 敲低改善脂肪酸氧化功能，CPT1B 敲低削弱其作用

LPS 刺激后，H9C2 细胞内脂滴相对荧光强度明显升高，相对脂肪酸氧化活性下降；HDAC11 敲低可减少脂质蓄积并部分恢复脂肪酸氧化活性。进一步敲低 CPT1B 后，脂滴相对荧光强度再次升高，脂肪酸氧化活性明显下降，表明 CPT1B 敲低削弱了 HDAC11 敲低对 LPS 诱导脂肪酸氧化障碍的改善作用（图 4）。

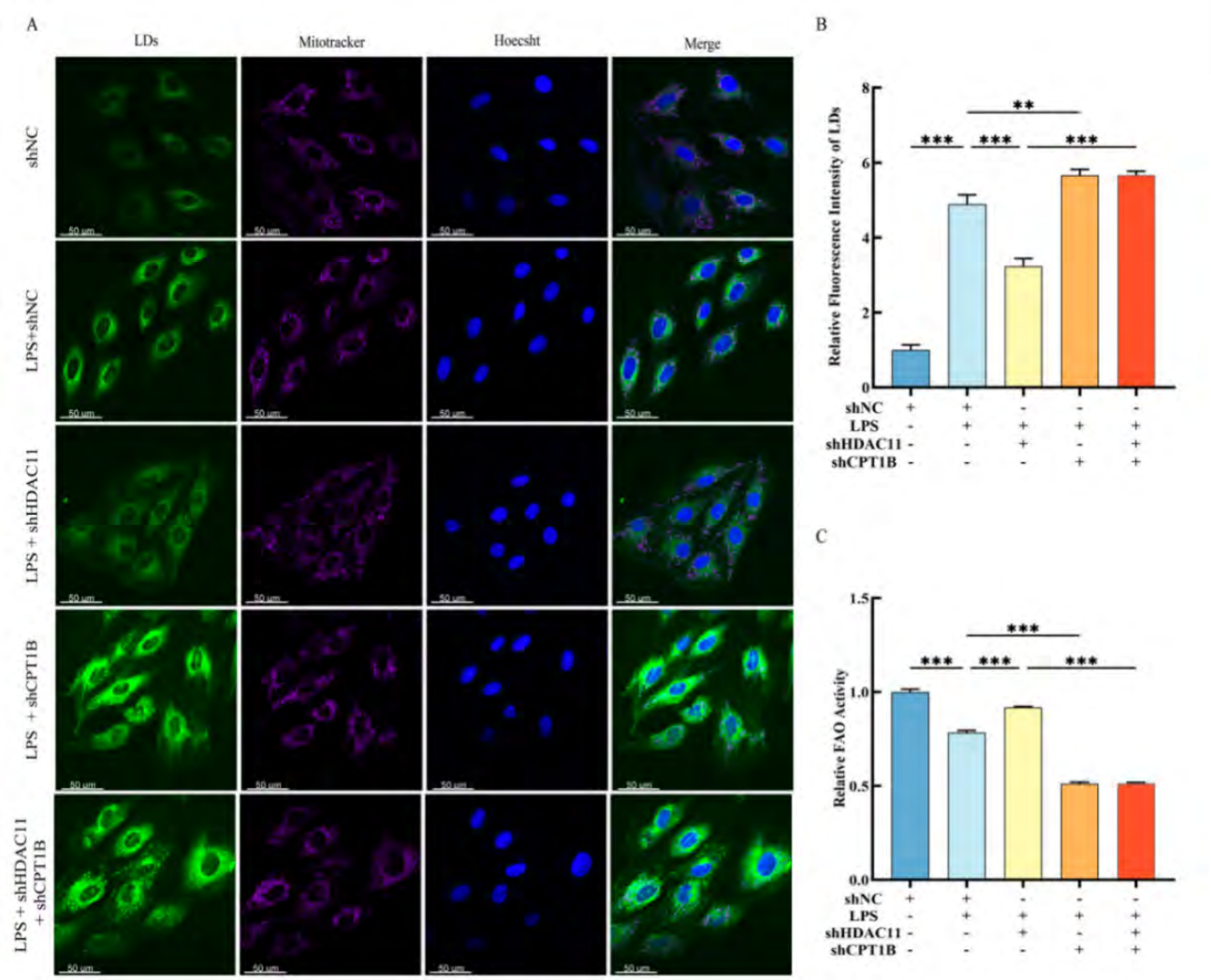


图 4　CPT1B 敲低削弱 HDAC11 敲低对 LPS 诱导 H9C2 细胞脂质蓄积和脂肪酸氧化障碍的改善作用。A：BODIPY 493/503、MitoTracker 及 Hoechst 染色代表性图像；B：脂滴相对荧光强度；C：相对脂肪酸氧化活性。标尺=50 μm，n=3，P<0.01，***P<0.001。**

4.4 CPT1B 敲低削弱 HDAC11 敲低对 ATP 水平的改善作用

LPS 刺激后，H9C2 细胞 ATP 水平明显下降；HDAC11 敲低可使 ATP 水平部分恢复。在 HDAC11 敲低基础上进一步敲低 CPT1B 后，ATP 水平再次下降，提示 CPT1B 介导的脂肪酸氧化恢复可能参与 HDAC11 敲低对细胞能量稳态的改善（图 5）。

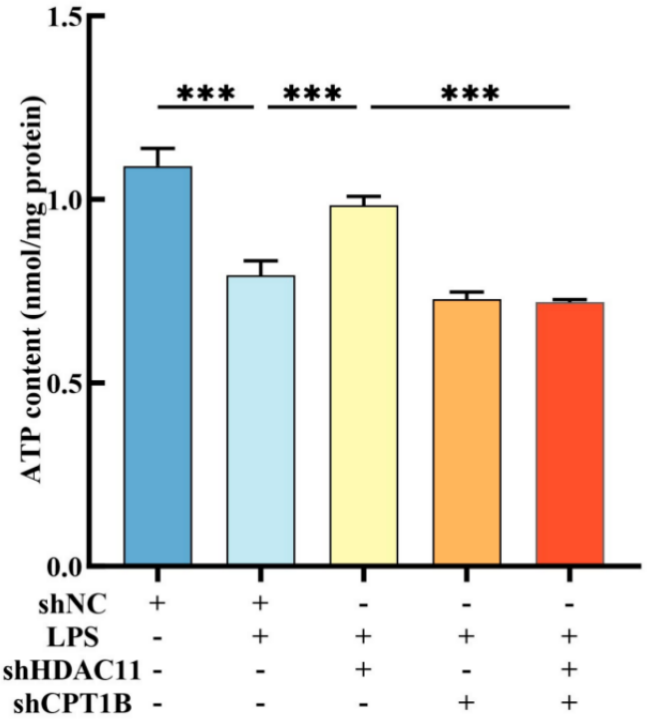


图 5　CPT1B 敲低削弱 HDAC11 敲低对 LPS 诱导 H9C2 细胞 ATP 水平下降的改善作用。ATP 含量按蛋白量归一化，n=3，*P<0.001。**

5 讨论与结论

本研究从分子表达和功能表型两个层面显示，LPS 可诱导 H9C2 细胞 HDAC11 升高及脂肪酸氧化受抑，而 HDAC11 敲低能够恢复 CPT1B 等相关分子表达、提高脂肪酸氧化活性、减少脂质蓄积并改善 ATP 水平。进一步敲低 CPT1B 后，上述脂肪酸氧化及能量代谢改善作用受到明显削弱，支持 HDAC11 敲低的代谢效应至少部分依赖 CPT1B 介导的脂肪酸氧化恢复。现有结果尚不能证明 HDAC11 直接调控 CPT1B，且研究限于 H9C2 细胞和较小重复数，后续仍需结合直接调控实验及体内模型验证。综上，HDAC11 可能是 LPS 诱导心肌细胞脂肪酸氧化障碍的潜在干预靶点。

参考文献

[1] Poveda-Jaramillo R. Heart dysfunction in sepsis[J]. Journal of Cardiothoracic and Vascular Anesthesia, 2021, 35(1): 298-309.

[2] Yu X, Gao J, Zhang C. Sepsis-induced cardiac dysfunction: mitochondria and energy metabolism[J]. Intensive Care Medicine Experimental, 2025, 13(1): 20.

[3] Jia G, Liu J, Hou X, et al. Biological function and small molecule inhibitors of histone deacetylase 11[J]. European Journal of Medicinal Chemistry, 2024, 276: 116634.

[4] Nunez-Alvarez Y, Suelves M. HDAC11: a multifaceted histone deacetylase with proficient fatty deacylase activity and its roles in physiological processes[J]. FEBS Journal, 2022, 289(10): 2771-2792.

[5] Hurtado E, Nunez-Alvarez Y, Munoz M, et al. HDAC11 is a novel regulator of fatty acid oxidative metabolism in skeletal muscle[J]. FEBS Journal, 2021, 288(3): 902-919.

Hemodynamic Response Phenotypes in Patients Receiving Intra-Aortic Balloon Pump Support: A Hierarchical Clustering Study

姓名：江春景
单位：北京安贞医院

[Abstract] Objective: To identify baseline hemodynamic phenotypes in patients receiving intra-aortic balloon pump (IABP) support, compare dynamic responses to IABP among phenotypes, and explore the potential value of phenotype-based stratification for individualized IABP management. Methods: Ninety-one consecutive patients who received IABP support after cardiac surgery were included. Within 2 h after IABP implantation, baseline hemodynamic variables were obtained with bioimpedance spectroscopy cardiography (BSC) while IABP support was temporarily discontinued. Unsupervised hierarchical clustering was used to identify baseline phenotypes. Paired measurements obtained daily with IABP off and on were compared among phenotypes. Results Three baseline phenotypes were identified: a low-output/high-resistance phenotype (type 1, n=28), an intermediate-output/intermediate-resistance phenotype (type 2, n=34), and a high-output/low-resistance phenotype (type 3, n=29). On Day 1, stroke volume (SV) increased in Type 1 patients (10.25% +/- 15.0%, P=0.003) but did not change significantly in Type 2 patients (-0.08% +/- 10.3%, P=0.74). In type 3 patients, SV increased on Day 2 (7.37% +/- 11.9%, P=0.03). On Day 3, changes in SV, cardiac output, and velocity index remained significantly different among the three groups (P=0.028, 0.048, and 0.016, respectively). Conclusion Patients receiving IABP support exhibit distinct baseline hemodynamic phenotypes and early response patterns. Combining baseline phenotyping with serial hemodynamic monitoring may help distinguish immediate, delayed, and limited responses, thereby informing dynamic assessment and individualized IABP management.

[Keywords] intra-aortic balloon pump; hemodynamic phenotype; hierarchical clustering; treatment response; bioimpedance spectroscopy cardiography

Intra-aortic balloon pump (IABP) counterpulsation is a commonly used form of mechanical circulatory support. By synchronizing balloon inflation and deflation with the cardiac cycle, IABP augments diastolic coronary perfusion and reduces left ventricular afterload immediately before systole, thereby improving myocardial oxygen supply-demand balance and cardiac output [1-3].

Despite its sound pathophysiological rationale, whether IABP improves clinical outcomes remains controversial. Several large randomized controlled trials failed to demonstrate reductions in short- or long-term mortality among patients with cardiogenic shock [4-6], leading to downgrading of IABP recommendations in national and international guidelines. However, population-level results may obscure clinically important differences in response among patients with different baseline circulatory states.

Previous studies have demonstrated substantial heterogeneity in hemodynamic response to IABP [7-11]. Some patients show increased cardiac output and reduced left ventricular workload, whereas others exhibit only modest improvement or changes in the opposite direction. More recently, unsupervised clustering has identified reproducible cardiogenic shock phenotypes with distinct clinical characteristics and outcomes [12-13]. Average treatment effects may obscure clinically important differences in individual hemodynamic responses. Identifying baseline circulatory phenotypes and monitoring their dynamic responses may provide a new basis for patient selection, treatment evaluation, and adjustment of support strategies.

In this study, multiple hemodynamic variables were continuously acquired using bioimpedance spectroscopy cardiography (BSC). Unsupervised hierarchical clustering was applied to identify baseline circulatory phenotypes in patients receiving IABP support, and dynamic changes between IABP-off and IABP-on states were compared across phenotypes. The study aimed to characterize heterogeneity in IABP response and evaluate the potential clinical value of phenotype-based stratification.

1 Materials and Methods

1.1 Study Population

Patients who underwent cardiac surgery and received IABP support at Beijing Anzhen Hospital, Capital Medical University, between December 2025 and July 2026 were consecutively included. Indications for IABP at our center included mean arterial pressure (MAP) <60 mmHg; left atrial pressure or pulmonary capillary wedge pressure >20 mmHg; central venous pressure >15 cmH2O; urine output <20 mL/h; or evidence of impaired peripheral perfusion, such as cold and clammy extremities.

1.2 Study Protocol

Hemodynamic monitoring with BSC (YECO Hemodynamic and Cardiac Function Monitoring System) was initiated within 2 h after IABP implantation. IABP support was temporarily discontinued only when all of the following conditions were met: (1) heart rate (HR) <120 beats/min or an increase of <10 beats/min from the pre-interruption value; (2) a vasoactive-inotropic score (VIS) below the protocol-defined threshold of 20-30; and (3) MAP >=60-65 mmHg. After the hemodynamic curves stabilized, baseline data were recorded with IABP off. IABP was then restarted, and data were recorded again after stabilization. Stabilization required approximately 10-15 min after each adjustment. If a patient failed to meet all criteria after IABP interruption, support was resumed immediately and that observation was excluded from paired analysis. Paired measurements were obtained daily until IABP removal using the sequence 'IABP off - stabilization - data acquisition - IABP on - stabilization - data acquisition.'

The relative change between IABP-on and IABP-off states was calculated as follows:

$$\Delta X = \frac{X_{on} - X_{off}}{X_{off}} \times 100\% \qquad (1)$$

1.3 Hemodynamic Monitoring

This study used BSC, a patented monitoring technology independently developed by YECO. BSC analyzes thoracic bioimpedance spectral characteristics and their dynamic changes during the cardiac cycle to obtain multiple hemodynamic variables continuously and noninvasively. Its continuous monitoring capability enabled paired acquisition of IABP-off and IABP-on measurements within a short time window to assess the immediate hemodynamic effects of IABP support.

The principal variables included cardiac output (CO), stroke volume (SV), HR, systemic vascular resistance (SSVR), acceleration index (ACI), thoracic fluid content (TFC), pre-ejection period (PEP), left ventricular ejection time (LVET), velocity index (VI), and stroke volume variation (SVV). CO and SV reflect cardiac pump performance; SSVR reflects peripheral vascular resistance; ACI, PEP, LVET, and VI characterize left ventricular systolic function; TFC reflects thoracic fluid status; and SVV reflects volume responsiveness.

1.4 Hierarchical Clustering Analysis

Baseline hemodynamic variables obtained on day 1 with IABP off were selected as clustering features, including CO, SV, HR, SSVR, ACI, TFC, PEP, LVET, VI, and SVV. Unsupervised hierarchical clustering was performed to identify latent phenotypes based on the overall hemodynamic profile. Response variables obtained after IABP activation and clinical outcomes were not included in clustering, thereby reducing outcome-driven classification bias.

1.5 Statistical Analysis

Continuous variables are presented as mean +/- standard deviation or median (Q1, Q3), as appropriate, and categorical variables as number (percentage). Continuous variables were compared among the three groups using one-way analysis of variance; when the overall difference was significant, Tukey's honestly significant difference test was used for post hoc pairwise comparisons. Relative changes in SV, CO, SSVR, HR, TFC, and other variables between IABP-on and IABP-off states were analyzed to characterize early response patterns. All tests were two-sided, and $P<0.05$ was considered statistically significant. Data management and statistical analyses were conducted using Python version 3.12. Hierarchical clustering was implemented with the SciPy package (scipy.cluster.hierarchy), using Euclidean distance and Ward's minimum variance linkage.

2 Results

2.1 Patient and Operative Characteristics

The mean preoperative left ventricular ejection fraction was 48.1% +/- 12.7%. New York Heart Association (NYHA) class III or IV heart failure was present in 47.3% of the study population, whereas preoperative cardiogenic shock was uncommon (1.8%) (Table 1).

Operative characteristics are presented in Table 2. Nearly 60% of patients underwent coronary artery bypass grafting (CABG) alone or CABG combined with valve surgery. Urgent surgery or surgery during the same hospitalization was performed in 51 patients (55.5%), primarily because patients with newly diagnosed triple-vessel coronary artery disease were referred directly from the cardiac catheterization laboratory for surgery after preoperative optimization. Reoperative cardiac surgery was performed in 18.1% of patients. The median cardiopulmonary bypass (CPB) time was 180.0 min, and the median aortic cross-clamp time was 119.5 min. Cold blood cardioplegia was used in 68 patients (74.7%). During CPB, 74 patients (81.3%) underwent mild hypothermia and 5 (6.0%) underwent deep hypothermic circulatory arrest.

Table 1. Patient Demographics and Baseline Characteristics

Variable	Overall (N=91)
Age (years)	63.8 ± 11.4
Female	26 (28.7%)
BMI (kg/m²)	24.4 ± 6.8
Obesity (BMI ≥30 kg/m²)	20 (21.9%)
Diabetes	36 (39.1%)
End-stage renal disease	8 (8.7%)
Chronic lung disease	10 (11.4%)
Peripheral artery disease	9 (10.1%)
Cerebrovascular disease	12 (12.7%)
NYHA heart class	
No heart failure	34 (36.9%)
Class I	4 (4.8%)
Class II	9 (10.0%)
Class III	31 (34.0%)
Class IV	12 (13.3%)
History of MI	35 (38.6%)
Pre-operative CS	2 (1.8%)
LVEF (%)	48.1 ± 12.7

Values are presented as mean ± SD or n (%). BMI = body mass index; NYHA = New York Heart Association; CS = cardiogenic shock; LVEF = left ventricular ejection fraction.

Table 2. Operative Characteristics

Variable	Overall (N=91)
Index surgery	
CABG	25 (27.0%)
CABG + Valve	27 (29.6%)
Mitral valve ± Tricuspid valve	17 (18.2%)
AVR	3 (3.7%)
Multi-valve	7 (7.6%)
Aorta ± AVR	4 (3.9%)
Other	9 (9.9%)
Re-operative cardiac surgery	16 (18.1%)
Surgical status	
Elective	34 (37.4%)
Urgent	51 (55.5%)
Emergent	6 (7.1%)
CPB time (min)	180.0 (134.0–225.0)
Cross-clamp time (min)	119.5 (89.3–156.8)
Type of cardioplegia	
Cold blood	68 (74.7%)
Del Nido	8 (8.8%)
Warm blood	1 (0.5%)
No cardioplegia / Not applicable	14 (15.9%)
Cardioplegia delivery (n=74)	
Antegrade	77 (85.0%)
Retrograde	11 (11.8%)
Antegrade & Retrograde	3 (3.3%)
Systemic temperature	
Normothermia	9 (10.4%)
Mild hypothermia	74 (81.3%)
Moderate hypothermia	2 (2.2%)
Deep hypothermia	5 (6.0%)
Circulatory arrest	5 (6.0%)

Values are presented as n (%) or median (IQR). CABG = coronary artery bypass grafting; AVR = aortic valve replacement; CPB = cardiopulmonary bypass.

2.2 Characteristics and Outcomes of IABP Support

Postcardiotomy shock and failure to wean from CPB were the two most common indications for rescue IABP support (35.3% and 32.9%, respectively), followed by myocardial ischemia (15.5%), cardiac arrest (14.7%), and ventricular arrhythmia (1.6%). The median duration of IABP support was 3.0 days (interquartile range, 3.0-4.0 days). In-hospital mortality was 14.6%, with 13 deaths during the index hospitalization. Cardiogenic shock was the most common cause of death, and most affected patients also had multiorgan failure.

Table 3. **IABP Support Characteristics and Clinical Outcomes**

Variable	Overall (N=91)
IABP indication	
Post-cardiotomy shock	32 (35.3%)
Failure to wean from CPB	30 (32.9%)
Myocardial ischemia	14 (15.5%)
Cardiac arrest	13 (14.7%)
Ventricular arrhythmia	1 (1.6%)
IABP duration (days)	3.0 (3.0–4.0)
In-hospital mortality	13 (14.6%)
Etiologies of mortality	
Cardiogenic shock	8 (62.9%)
Cardiogenic shock with MOF	7 (93.3%)
Cardiac arrest in the setting of CS	1 (6.7%)
Respiratory failure	2 (15.7%)
Septic shock	2 (13.3%)
Unknown	1 (8.1%)
ICU length of stay (days)	6.0 (4.0–10.0)
In-hospital length of stay (days)	12.0 (8.0–17.8)

Values are presented as n (%) or median (IQR). IABP = intra-aortic balloon pump; CPB = cardiopulmonary bypass; CS = cardiogenic shock; MOF = multi-organ failure; ICU = intensive care unit.

2.3 Hierarchical Clustering Identified Three Baseline Hemodynamic Phenotypes

A total of 91 patients receiving IABP support completed hemodynamic monitoring. Hierarchical clustering of baseline variables obtained on day 1 with IABP off identified three phenotypes with distinct circulatory profiles (types 1-3).

Type 1 was characterized by low cardiac output, high vascular resistance, and a faster heart rate. Type 2 showed intermediate cardiac output and vascular resistance; its PEP was longer than that of types 1 and 3 (both pairwise Tukey comparisons, $P<0.001$). Type 3 was characterized by high cardiac output and low vascular resistance; its ACI and LVET were higher than those of types 1 and 2 (all pairwise Tukey comparisons, $P<0.05$). Type 3 also had the highest VI, with significant pairwise differences among all three groups (all $P<0.02$).

Table 4. Baseline Hemodynamic Parameters of the Three Clusters

Variables	Cluster 1 (n=28)	Cluster 2 (n=34)	Cluster 3 (n=29)	P value
Cardiac performance				
CO (L/min)	3.18 ± 0.82	3.96 ± 0.87	4.57 ± 0.85	<0.001
SV (mL)	31.07 ± 6.70	44.35 ± 7.61	54.64 ± 12.43	<0.001
HR (bpm)	101.89 ± 12.47	89.62 ± 14.49	85.55 ± 13.56	<0.001
Afterload				
SSVR	203.54 ± 54.77	134.77 ± 32.28	111.16 ± 29.20	<0.001
Left ventricular systolic function				
ACI	39.86 ± 11.42	52.15 ± 19.52	70.93 ± 35.82	<0.001
PEP (ms)	72.50 ± 17.62	104.26 ± 15.68	78.28 ± 15.23	<0.001
LVET (ms)	220.86 ± 22.92	239.18 ± 33.69	259.41 ± 33.38	<0.001
Flow				
VI	13.74 ± 4.59	21.01 ± 6.71	27.04 ± 11.26	<0.001

Data are presented as mean ± SD. P values were calculated using one-way ANOVA.
CO, cardiac output; SV, stroke volume; HR, heart rate; SSVR, stroke systemic vascular resistance; ACI, acceleration index; PEP, pre-ejection period; LVET, left ventricular ejection time; VI, velocity index.

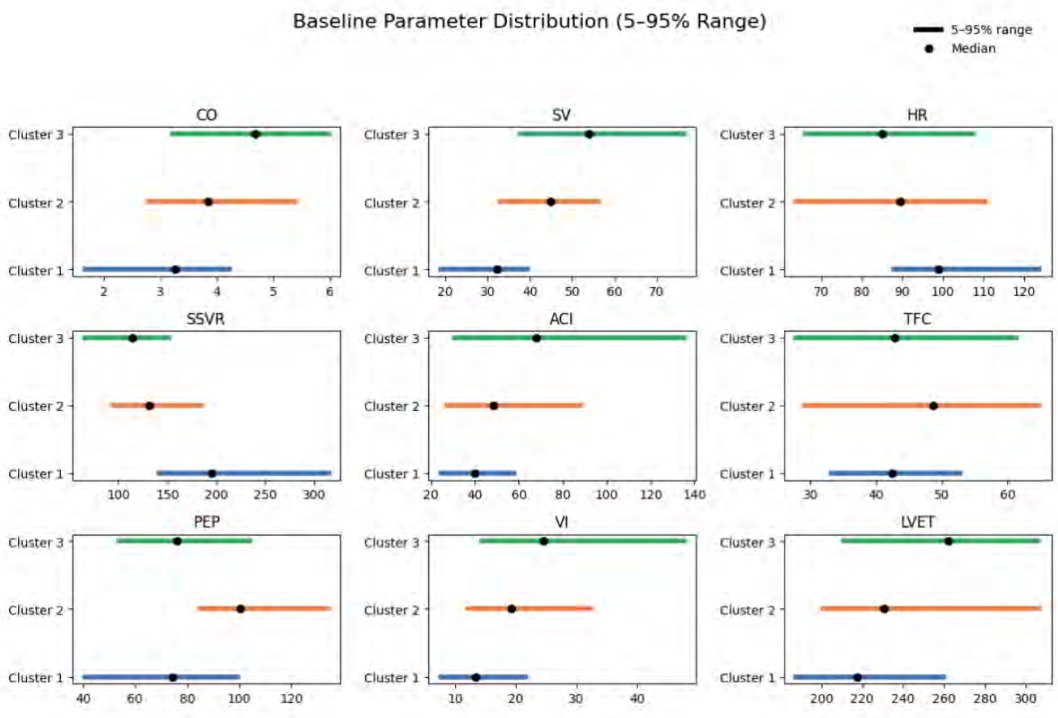


Figure 1. Distribution of Major Hemodynamic Variables Across the Three Baseline Phenotypes

Note: Black dots indicate medians, and horizontal lines indicate the 5th-95th percentile range. All variables were baseline measurements obtained on day 1 after IABP implantation with IABP off. CO, cardiac output; SV, stroke volume; HR, heart rate; SSVR, systemic vascular resistance; ACI, acceleration index; TFC, thoracic fluid content; PEP, pre-ejection period; VI, velocity index; LVET, left ventricular ejection time.

2.4 Early Hemodynamic Responses to IABP Differed Among Baseline Phenotypes

On day 1, SV increased after IABP activation in type 1 patients (10.25% +/- 15.0%, P=0.003) but did not change significantly in type 2 patients (-0.08% +/- 10.3%, P=0.74). In type 3 patients, SV increased on day 2 (7.37% +/- 11.9%, P=0.03). CO, SSVR, and other hemodynamic variables also differed in direction and magnitude of change across phenotypes (Figure 2 and Table 5).

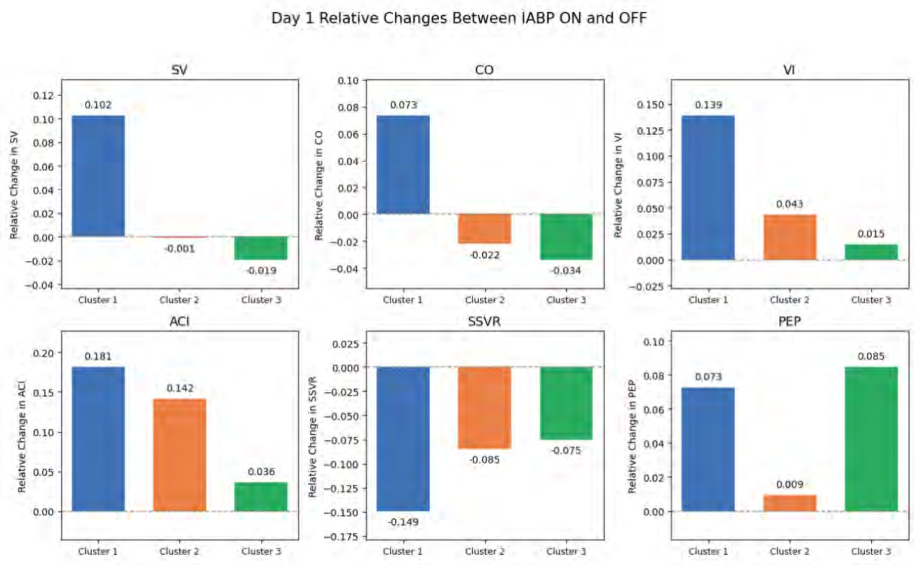


Figure 2. Relative Changes in Major Hemodynamic Variables Between IABP-On and IABP-Off States on Day 1

Note: Bars indicate mean relative changes within each phenotype. Day 1 denotes the first day after IABP implantation. Relative change was calculated from paired IABP-on and IABP-off measurements in the same patient using equation (1). SV, stroke volume; CO, cardiac output; VI, velocity index; ACI, acceleration index; SSVR, systemic vascular resistance; PEP, pre-ejection period.

Table 5. Relative Hemodynamic Changes Between IABP ON and OFF

Parameter	IABP day	Cluster 1 (n=28)	Cluster 2 (n=34)	Cluster 3 (n=29)	P value
SV	Day 1	0.102 ± 0.150 (n=28)	−0.001 ± 0.103 (n=34)	−0.019 ± 0.103 (n=29)	<0.001
	Day 2	0.097 ± 0.173 (n=18)	0.032 ± 0.152 (n=26)	0.074 ± 0.119 (n=20)	0.345
	Day 3	0.154 ± 0.176 (n=11)	0.036 ± 0.156 (n=16)	−0.025 ± 0.140 (n=13)	0.028
CO	Day 1	0.073 ± 0.155 (n=28)	−0.022 ± 0.089 (n=34)	−0.034 ± 0.090 (n=29)	<0.001
	Day 2	0.078 ± 0.179 (n=18)	0.024 ± 0.130 (n=26)	0.026 ± 0.123 (n=20)	0.417
	Day 3	0.116 ± 0.137 (n=11)	0.062 ± 0.173 (n=16)	−0.038 ± 0.129 (n=13)	0.048
VI	Day 1	0.139 ± 0.277 (n=28)	0.043 ± 0.216 (n=34)	0.015 ± 0.167 (n=29)	0.095
	Day 2	0.188 ± 0.401 (n=18)	0.057 ± 0.175 (n=26)	0.070 ± 0.166 (n=20)	0.220
	Day 3	0.305 ± 0.406 (n=11)	0.081 ± 0.238 (n=16)	−0.050 ± 0.212 (n=13)	0.016
HR	Day 1	−0.029 ± 0.044 (n=28)	−0.017 ± 0.041 (n=34)	−0.014 ± 0.060 (n=29)	0.498
	Day 2	−0.007 ± 0.042 (n=18)	−0.011 ± 0.039 (n=26)	−0.047 ± 0.072 (n=20)	0.033
	Day 3	−0.014 ± 0.064 (n=11)	0.026 ± 0.089 (n=16)	−0.011 ± 0.039 (n=13)	0.252
SSVR	Day 1	−0.149 ± 0.173 (n=28)	−0.085 ± 0.151 (n=34)	−0.075 ± 0.155 (n=29)	0.168
	Day 2	−0.137 ± 0.195 (n=18)	−0.101 ± 0.214 (n=26)	−0.138 ± 0.192 (n=20)	0.785
	Day 3	−0.201 ± 0.171 (n=11)	−0.104 ± 0.184 (n=16)	−0.046 ± 0.210 (n=13)	0.149
PEP	Day 1	0.073 ± 0.193 (n=28)	0.009 ± 0.146 (n=34)	0.085 ± 0.182 (n=29)	0.182
	Day 2	0.021 ± 0.154 (n=18)	0.035 ± 0.101 (n=26)	0.115 ± 0.311 (n=20)	0.290
	Day 3	−0.040 ± 0.186 (n=11)	0.017 ± 0.090 (n=16)	−0.007 ± 0.141 (n=13)	0.581

Day 1 Day 2 Day 3

Data are presented as mean ± SD; the number of patients contributing to each time point is shown in parentheses.
Relative change refers to the within–patient change between IABP ON and OFF.
P values were calculated using one–way ANOVA at each time point.
SV, stroke volume; CO, cardiac output; VI, velocity index; HR, heart rate; SSVR, stroke systemic vascular resistance; PEP, pre–ejection period.

Note: Values in parentheses indicate the number of patients included at each time point. Days 1, 2, and 3 denote the first, second, and third days after IABP implantation, respectively. Relative change was calculated from paired IABP-on and IABP-off measurements in the same patient. Comparisons among the three groups at each time point were performed using one-way analysis of variance.

2.5 Three Early Response Patterns Across Baseline Phenotypes

On day 1, SV and CO increased by 10.2% +/- 15.0% and 7.3% +/- 15.5%, respectively, in type 1 patients, whereas no clear increases were observed in types 2 and 3. Type 1 also showed the largest increase in ACI (18.1% +/- 29.4%) and the greatest decrease in SSVR (-14.9% +/- 17.3%), indicating early improvement in pump performance and reduction in afterload.

On day 2, type 1 maintained relatively large changes in SV, CO, and VI. Type 3 showed further increases in SV, CO, and VI compared with day 1, consistent with delayed improvement, whereas changes in type 2 remained small, indicating a limited early hemodynamic response.

On day 3, relative changes in SV, CO, and VI remained significantly different among the three groups (P=0.028, 0.048, and 0.016, respectively), with type 3 showing the greatest increase in VI. Across time points, types 1, 2, and 3 exhibited immediate, limited, and delayed response patterns, respectively.

The distribution of relative SV changes in type 3 patients on days 1 and 2 further supported a delayed response (Figure 3): the distribution shifted upward on day 2, and the median changed from approximately zero to a positive value.

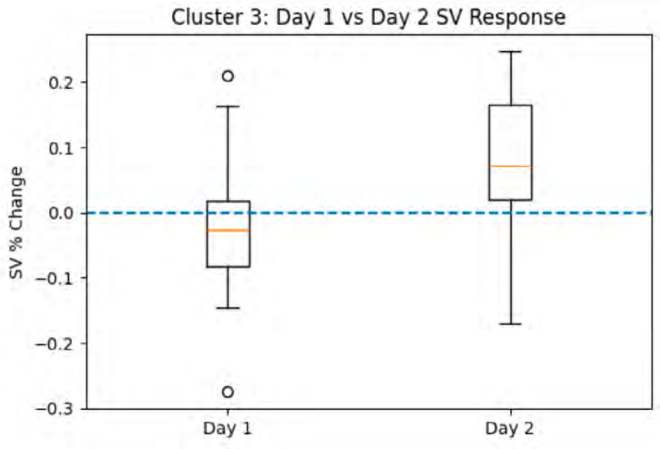


Figure 3. Distribution of Relative SV Changes in Type 3 Patients on Days 1 and 2

Note: On day 1, relative SV changes were concentrated around or below zero. On day 2, the distribution shifted upward and the median became positive, suggesting progressive hemodynamic improvement during continued IABP support.

3 Discussion

Hierarchical clustering of baseline hemodynamic variables obtained with IABP off identified three circulatory phenotypes with distinct magnitudes and temporal patterns of response after IABP activation. Patients with the low-output/high-resistance phenotype showed early increases in SV and CO and a decrease in SSVR. Patients with the intermediate-output/intermediate-resistance phenotype showed limited early changes, whereas those with the high-output/low-resistance phenotype showed progressive improvement on day 2. These findings are consistent with previous observations that IABP response is heterogeneous and influenced by baseline hemodynamics [7-11].

IABP augments diastolic coronary perfusion and reduces left ventricular afterload before systole, thereby decreasing myocardial oxygen demand and improving cardiac output [1-3]. Type 1 patients had low cardiac output and high vascular resistance at baseline; after IABP activation, SV and CO increased and SSVR decreased, which is consistent with the classic afterload-reducing mechanism of IABP. Early hemodynamic improvement in this phenotype may indicate greater sensitivity to the mechanical effects of IABP. Whether this phenotype predicts clinical benefit, however, requires validation against organ perfusion, vasoactive drug requirements, and clinical outcomes.

Type 2 patients had intermediate cardiac output and vascular resistance but a markedly prolonged PEP, potentially indicating abnormal left ventricular systolic timing. Their overall changes in SV and CO after IABP activation were small, suggesting that afterload reduction may not translate into short-term improvement in pump performance. In patients with a limited early response, volume status, myocardial function, cardiac rhythm, pharmacological therapy, and organ perfusion should be reassessed rather than declaring IABP ineffective on the basis of a single hemodynamic variable.

Type 3 patients had relatively high cardiac output and low vascular resistance at baseline. Their hemodynamic changes were minimal on day 1, whereas SV, CO, and VI increased further on day 2, suggesting a time-dependent response in some patients. A single or very early assessment may therefore underestimate the effect of IABP in this phenotype, and serial monitoring may help define the direction and time course of response. Nevertheless, delayed improvement may also reflect postoperative recovery, volume management, or adjustment of vasoactive therapy and cannot be attributed entirely to IABP.

Previous IABP studies have mainly used predefined thresholds to classify responders and nonresponders or regression models to examine associations between baseline factors and longitudinal changes [7-11]. Direct clinical evidence using unsupervised hierarchical clustering to identify IABP hemodynamic response phenotypes remains limited. In parallel, clustering studies in cardiogenic shock have shown that data-driven methods can identify subgroups with distinct pathophysiological features and outcomes [12-13]. The present findings suggest that the same support strategy may generate different response patterns depending on baseline circulatory status. Combining baseline phenotype classification with serial monitoring may help distinguish

immediate, delayed, and limited responses and may inform the timing of assessment and treatment adjustment. This study has several limitations. It was a single-center observational study with a limited sample size; the number of patients available for paired analysis decreased over time; the clusters have not been externally validated; and we did not analyze successful IABP weaning, organ function, short-term mortality, or long-term outcomes. The findings should therefore be regarded as hypothesis-generating and should not be used directly to define thresholds for initiating, discontinuing, or escalating mechanical circulatory support.

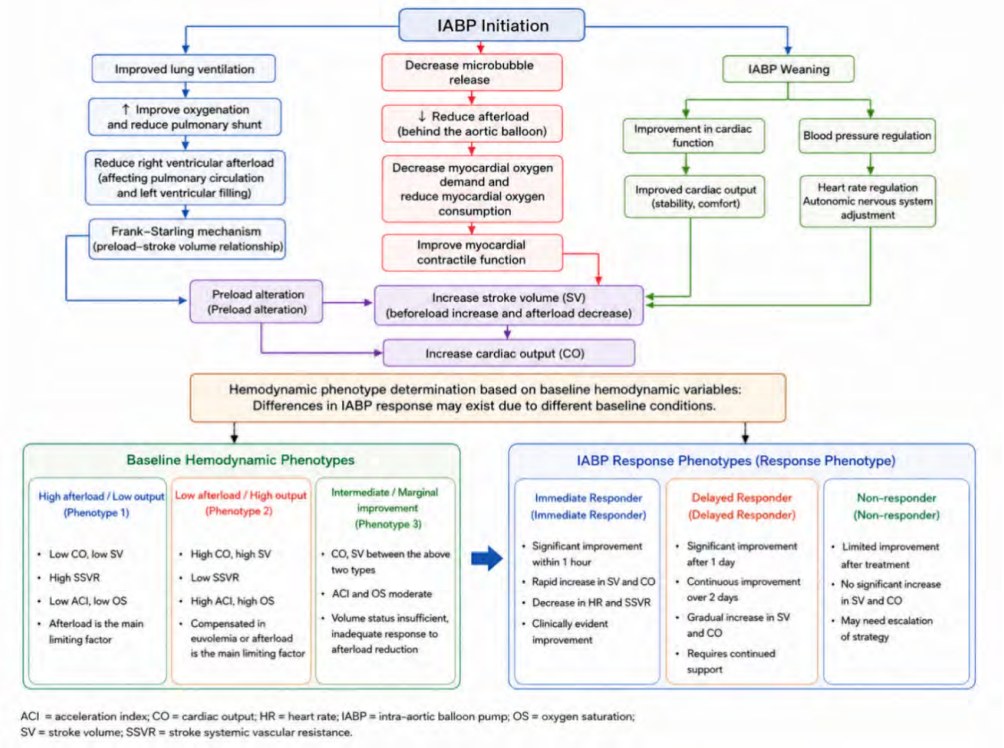


Figure 4. Principal Hemodynamic Mechanisms of IABP and the Response Patterns Proposed in This Study

Note: IABP may influence SV and CO by modifying preload, reducing afterload, and improving myocardial perfusion. Depending on baseline hemodynamic status, patients may exhibit an immediate, delayed, or limited response. SV, stroke volume; CO, cardiac output.

4 Conclusion

Patients receiving IABP support exhibit distinct baseline hemodynamic phenotypes and early response patterns. The low-output/high-resistance phenotype showed earlier improvement; the high-output/low-resistance phenotype showed possible delayed improvement; and the intermediate-output/intermediate-resistance phenotype showed a relatively limited early response. Baseline circulatory phenotyping combined with serial hemodynamic monitoring may support dynamic assessment and individualized IABP management. Its predictive value requires confirmation in multicenter prospective studies incorporating clinical outcomes.

5 References

[1] Parissis H, Graham V, Lampridis S, et al. IABP: history-evolution-pathophysiology-indications: what we need to know[J]. J Cardiothorac Surg, 2016, 11: 122. DOI: 10.1186/s13019-016-0513-0.

[2] Buckley MJ, Leinbach RC, Kastor JA, et al. Hemodynamic evaluation of intra-aortic balloon pumping in man[J]. Circulation, 1970, 41(5 Suppl): II130-II136. DOI: 10.1161/01.CIR.41.5S2.II-130.

[3] Stefanadis C, Dernellis J, Tsiamis E, et al. Aortic function in patients during intra-aortic balloon pumping determined by the pressure-diameter relation[J]. J Thorac Cardiovasc Surg, 1998, 116(6): 1052-1059. DOI: 10.1016/S0022-5223(98)70058-3.

[4] Thiele H, Zeymer U, Neumann FJ, et al. Intraaortic balloon support for myocardial infarction with cardiogenic shock[J]. N Engl J Med, 2012, 367(14): 1287-1296. DOI: 10.1056/NEJMoa1208410.

[5] Thiele H, Zeymer U, Neumann FJ, et al. Intra-aortic balloon counterpulsation in acute myocardial infarction complicated by cardiogenic shock (IABP-SHOCK II): final 12 month results of a randomised, open-label trial[J]. Lancet, 2013, 382(9905): 1638-1645. DOI: 10.1016/S0140-6736(13)61783-3.

[6] Thiele H, Zeymer U, Thelemann N, et al. Intraaortic balloon pump in cardiogenic shock complicating acute myocardial infarction: long-term 6-year outcome of the randomized IABP-SHOCK II trial[J]. Circulation, 2019, 139(3): 395-403. DOI: 10.1161/CIRCULATIONAHA.118.038201.

[7] Annamalai SK, Buiten L, Esposito ML, et al. Acute hemodynamic effects of intra-aortic balloon counterpulsation pumps in advanced heart failure[J]. J Card Fail, 2017, 23(8): 606-614. DOI: 10.1016/j.cardfail.2017.05.015.

[8] Huang AL, Fried JA, Malick W, et al. Predictors of hemodynamic response to intra-aortic balloon pump therapy in patients with acute decompensated heart failure and cardiogenic shock[J]. J Invasive Cardiol, 2021, 33(4): E275-E280. DOI: 10.25270/jic/20.00473.

[9] Baran DA, Visveswaran GK, Seliem A, et al. Differential responses to larger volume intra-aortic balloon counterpulsation: hemodynamic and clinical outcomes[J]. Catheter Cardiovasc Interv, 2018, 92(4): 703-710. DOI: 10.1002/ccd.27387.

[10] Imamura T, Juricek C, Nguyen A, et al. Predictors of hemodynamic improvement and stabilization following intraaortic balloon pump implantation in patients with advanced heart failure[J]. J Invasive Cardiol, 2018, 30(2): 56-61.

[11] Castagna F, Viswanathan S, Chalhoub G, et al. Predicting hemodynamic changes during intra-aortic balloon pump support with a longitudinal evaluation[J]. ASAIO J, 2023, 69(11): 977-983. DOI: 10.1097/MAT.0000000000002014.

[12] Zweck E, Thayer KL, Helgestad OKL, et al. Phenotyping cardiogenic shock[J]. J Am Heart Assoc, 2021, 10(14): e020085. DOI: 10.1161/JAHA.120.020085.

[13] Jentzer JC, Soussi S, Lawler PR, et al. Validation of cardiogenic shock phenotypes in a mixed cardiac intensive care unit population[J]. Catheter Cardiovasc Interv, 2022, 99(4): 1006-1014. DOI: 10.1002/ccd.30103.

Hemodynamic-Metabolic Discordance During Early Sepsis Resuscitation and In-Hospital Mortality: A Sequential Three-Cohort Observational Study

姓名：Yuxue Feng[1]，Na Yu[1*]

单位：1 The Fifth People’ s Hospital of Chongqing

Abstract

Background

Early sepsis resuscitation aims to restore tissue perfusion. However, mean arterial pressure (MAP) and lactate levels often fail to align. Some patients reach blood pressure targets but still have elevated lactate. We refer to this gap as hemodynamic-metabolic discordance (HMD). It remains unclear if HMD acts as an independent predictor of patient outcomes and whether regional tissue oxygenation drives this prognostic signal..

Objective

We aimed to develop and externally validate HMD as a mortality predictor during early sepsis care. We also explored how HMD relates to regional tissue oxygen saturation (StO_2) in a prospective clinical cohort.

Methods

We conducted a prespecified sequential observational study. We used the MIMIC-IV database to develop the HMD phenotype and the eICU-CRD database for external validation. We then analyzed a local patient cohort using near-infrared spectroscopy and transpulmonary thermodilution to understand the underlying mechanisms. We evaluated patient status at 6 hours after starting resuscitation. Patients were grouped into four states. State A achieved both blood pressure and metabolic recovery. State B achieved blood pressure recovery but lacked metabolic recovery (HMD). State C achieved metabolic recovery only. State D achieved neither target. We defined blood pressure recovery as a MAP of at least 65 mm Hg. Metabolic recovery was defined as lactate levels of 2 mmol/L or lower, or a lactate decrease of at least 20%. Our primary outcome was all-cause hospital mortality.

Results

The MIMIC-IV cohort included 4,409 evaluable patients. Hospital mortality was 21.3% for State A and 38.5% for State B. State B independently predicted higher hospital mortality, with an adjusted odds ratio (OR) of 1.93 (95% CI 1.59–2.34; $P < 0.001$). This represented a 13.1% absolute increase in mortality risk. The eICU-CRD validation cohort included 648 patients across 78 hospitals. Mortality was 23.6% in State A compared to 50.3% in State B (adjusted OR 3.23; 95% CI 1.79–5.83; $P < 0.001$). The transferred prediction model achieved an area under the curve (AUC) of 0.757. The local mechanistic cohort included 55 patients. The adjusted difference in 24-hour composite StO_2 between State B and State A was − 1.33 percentage points, which was not statistically significant. All regional StO_2 and thermodilution variables showed no significant differences after correcting for multiple comparisons.

Conclusion

Discordance between blood pressure and metabolic recovery during early sepsis resuscitation independently predicts hospital mortality. This finding remained consistent across two large databases. The underlying mechanisms do not appear to involve macroscopic regional tissue oxygenation. Clinicians can easily use this simple phenotype at the bedside to stratify patient risk early in the treatment process.

Keywords

Sepsis, early resuscitation, Hemodynamic-metabolic discordance, tissue oxygen saturation, near-infrared spectroscopy

1. Background

Sepsis causes a high number of deaths in intensive care units (ICU) worldwide. Early and effective resuscitation serves as the

cornerstone for improving patient survival [1]. Current clinical guidelines recommend restoring tissue perfusion, typically monitored through blood pressure targets and lactate clearance [2]. However, these two measures often fail to align in clinical practice. Many patients reach the recommended MAP threshold but maintain elevated lactate levels [3]. We operationally refine this into a 6-hour landmark phenotype, which we term hemodynamic-metabolic discordance (HMD), to emphasize the discordance between achieved hemodynamic targets and persistent metabolic derangement.

Most previous studies examined blood pressure and lactate as separate predictors of outcome [4]. Standard care bundles also treat them as parallel goals rather than a combined clinical state. Very few researchers have merged these parameters into a specific phenotype to test its predictive value across different hospital databases. Furthermore, the biological mechanisms behind HMD remain debated. Persistent high lactate despite normal blood pressure might indicate poor microcirculatory flow, mitochondrial damage, accelerated aerobic glycolysis, or an impaired ability to clear lactate.

Near-infrared spectroscopy (NIRS) offers a noninvasive way to measure regional tissue oxygen saturation (StO_2). When combined with transpulmonary thermodilution (Pulse Indicator Continuous Cardiac Output, PiCCO) , doctors can access detailed volumetric measurements. These tools help reveal if HMD actually masks hidden tissue hypoxia. Therefore, we designed a sequential three-cohort study. First, we developed and validated the HMD phenotype using the MIMIC-IV database [5]. Second, we externally validated our prediction model using the eICU-CRD database [6]. Third, we explored the biological basis of HMD using local clinical data collected from NIRS and PiCCO.

2. Objective

We aimed to determine if HMD independently predicts hospital mortality. We defined HMD as achieving blood pressure goals without metabolic recovery 6 hours into sepsis resuscitation. We also sought to externally validate this prediction model in a separate multicenter database. Finally, we wanted to evaluate if HMD correlates with regional tissue oxygen deficits in a specific mechanistic cohort.

3. Study Design

We conducted a prespecified sequential observational study using three distinct cohorts. First, we developed the phenotype and analyzed its association with outcomes using MIMIC-IV (version 3.1). Second, we validated the model and tested its transportability using eICU-CRD (version 2.0). Third, we explored underlying mechanisms using local clinical data. We froze all definitions, analysis timeframes, covariates, and statistical plans before starting the outcome modeling. We also locked the MIMIC-IV model coefficients before applying them to the eICU-CRD data. We kept the three cohorts separate and did not calculate a pooled P value. We followed STROBE and RECORD guidelines for reporting our findings [7].

4. Methods

4.1 Data Sources and Populations

MIMIC-IV is a de-identified database from a single critical care center. We included adult patients aged 18 or older during their first ICU admission. These patients met the Sepsis-3 criteria, defined as a suspected infection combined with a SOFA score increase of 2 or more points. We set the index time as the first moment a patient received vasopressors while having a lactate level above 2 mmol/L within a prespecified 6-hour window. We excluded patients who died before the 6-hour mark to prevent immortal time bias.

The eICU-CRD is a deidentified multicenter database. We applied the MIMIC-IV eligibility rules to this cohort as closely as possible, harmonizing the SOFA scores and Charlson Comorbidity Index definitions between datasets. Our local cohort enrolled consecutive adult Sepsis-3 patients. We required these patients to have complete records of blood pressure, lactate, and StO_2. We restricted the primary mechanistic analysis to patients with documented septic shock. The Research Ethics Committee of The Fifth People’ s Hospital of Chongqing approved this study (Approval No: 2026CQSDWRMYYEC-Iw001, February 14, 2026).

4.2 HMD Classification

We used T0 to denote the start of resuscitation. The T0 lactate was the value recorded closest to the index time, allowing a margin

of 2 hours. The T0 MAP was the median value recorded within 1 hour of the index time. We assessed follow-up values at 6 hours (T6). The T6 lactate was the value closest to the 6-hour mark. The T6 MAP was the median value between hours 5 and 7.

We defined blood pressure recovery as a MAP of at least 65 mm Hg at T6. We defined metabolic recovery as a T6 lactate of 2 mmol/L or lower, or a relative lactate decrease of at least 20% from T0. Based on these targets, we assigned patients to four mutually exclusive states. State A represented full recovery of both blood hemodynamic and metabolism. State B represented blood hemodynamic recovery without metabolic recovery (HMD). State C represented metabolic recovery without blood hemodynamic recovery. State D meant the patient achieved neither target. Our primary analysis compared State B to State A.

4.3 Variables and Outcomes

We adjusted for several covariates, including age, sex, T0 SOFA score, Charlson Comorbidity Index, T0 lactate, and baseline creatinine. We also accounted for invasive mechanical ventilation, liver disease, and vasopressor doses converted to norepinephrine equivalents. The main outcome for the database cohorts was all-cause hospital mortality after the 6-hour landmark. We evaluated 28-day mortality as a secondary outcome. For the local cohort, the primary mechanistic outcome was the composite StO_2 at 24 hours. We calculated this as the equally weighted mean of cerebral, periumbilical, and peripheral readings.

4.4 Statistical Analysis

In the MIMIC-IV dataset, we estimated the association between HMD and mortality using binomial generalized linear models with a logit link. Our prespecified adjustment variables included HMD State B, age, sex, T0 SOFA score, Charlson Comorbidity Index, T0 lactate, invasive ventilation, creatinine levels, liver disease status, norepinephrine equivalent dose, and the number of active vasopressors. We reported the adjusted odds ratio for State B compared to State A. We evaluated model discrimination using the area under the curve (AUC) and the Brier score. Internal validation involved 500 bootstrap resamples.

We applied the exact same model structure to the eICU-CRD dataset. We used hospital cluster-robust standard errors to account for the multicenter design. To test transport validation, we applied the fixed MIMIC-IV linear predictor to the eICU-CRD data without recalculating any coefficients. In the local cohort, we evaluated the 24-hour composite StO_2 using analysis of covariance. We adjusted this model for baseline tissue oxygenation, age, baseline SOFA score, and T0 lactate. We controlled the false discovery rate (FDR) for multiple comparisons using the Benjamini-Hochberg method. We performed all statistical analyses in Python 3.12 and created figures using R 4.6.1. All statistical tests were two-sided with an alpha level of 0.05.

5. Results

5.1 Study Populations

We initially identified 8,092 patients in MIMIC-IV who met our feasibility criteria. Out of these, 4,409 patients were evaluable for the outcome analysis. This group included 1,873 patients in State A, 1,732 in State B, 328 in State C, and 476 in State D. Our primary complete case model included 2,169 patients and 785 deaths. In the eICU-CRD database, the external validation analysis included 648 evaluable patients from 78 different hospitals (280 in State A; 368 in State B). Our local cohort ultimately analyzed 55 patients who met the strict criteria for septic shock (23 in State A; 32 in State B) (Figure 1 Table 1).

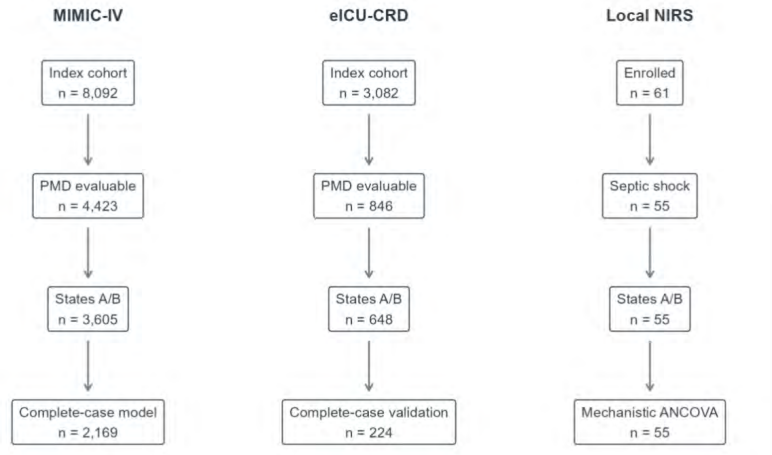


Figure 1. Study architecture and analysis populations. Flow of participants through the MIMIC-IV development cohort, eICU-CRD external-validation cohort, and local NIRS mechanistic cohort. HMD, Hemodynamic-metabolic discordance; NIRS, near-infrared spectroscopy; ANCOVA, analysis of covariance.

Table 1. Baseline Characteristics at T0 of Patients in HMD States A and B Across Cohorts

Panel A. MIMIC-IV development cohort

Characteristic	State A (n=1,873)	State B (n=1,732)	Absolute SMD
Age, y	64.4 (15.6)	64.2 (15.4)	0.02
Female sex	723/1,873 (38.6)	676/1,732 (39.0)	0.01
SOFA score at T0	4.0 [3.0–7.0]; n=1,280	5.0 [3.0–8.0]; n=1,250	0.23
Charlson Comorbidity Index	5.0 [3.0–7.0]	5.0 [3.0–7.0]	0.05
Lactate at T0, mmol/L	3.2 [2.4–4.9]	3.3 [2.5–4.9]	0.09
MAP at T0, mm Hg	75.3 (11.8); n=1,854	73.4 (11.9); n=1,710	0.16
Creatinine at T0, mg/dL	1.2 [0.9–1.9]; n=1,496	1.4 [1.0–2.2]; n=1,441	0.13
Invasive mechanical ventilation at T0	1,292/1,873 (69.0)	1,211/1,732 (69.9)	0.02
Renal disease	419/1,873 (22.4)	363/1,732 (21.0)	0.03
Mild or severe liver disease	316/1,873 (16.9)	428/1,732 (24.7)	0.19
Norepinephrine-equivalent dose at T0, μg/kg/min	0.100 [0.050–0.200]; n=1,776	0.140 [0.060–0.301]; n=1,668	0.22
Active vasopressor agents at T0, n	1.0 [1.0–1.0]; n=1,838	1.0 [1.0–2.0]; n=1,716	0.22

Panel B. eICU-CRD external-validation cohort

Characteristic	State A (n=280)	State B (n=368)	Absolute SMD
Age, y	64.6 (14.6)	64.8 (16.0)	0.01
Female sex	126/280 (45.0)	174/368 (47.3)	0.05
Met strict septic shock definition	153/280 (54.6)	203/368 (55.2)	0.01
SOFA score at T0	9.0 [6.0–12.0]	10.0 [8.0–13.0]	0.34
Charlson Comorbidity Index	1.0 [0.0–2.0]	2.0 [0.0–3.0]	0.17
Lactate at T0, mmol/L	3.5 [2.3–5.9]	3.7 [2.5–6.0]	0.07
MAP at T0, mm Hg	69.2 (13.0); n=277	68.4 (12.2); n=364	0.06
Creatinine at T0, mg/dL	1.6 [1.0–2.8]	1.9 [1.2–2.8]	0.08
Invasive mechanical ventilation at T0	152/280 (54.3)	240/368 (65.2)	0.22
Mild or severe liver disease	14/280 (5.0)	33/368 (9.0)	0.16
Norepinephrine-equivalent dose at T0, μg/kg/min	0.145 [0.079–0.315]; n=95	0.220 [0.100–0.393]; n=129	0.11
Active vasopressor agents at T0, n	1.0 [1.0–1.0]	1.0 [1.0–2.0]	0.30

Panel C. Local NIRS mechanistic cohort

Characteristic	State A (n=23)	State B (n=32)	Absolute SMD
Age, y	69.1 (14.1)	66.2 (15.5)	0.20
Female sex	6/23 (26.1)	13/32 (40.6)	0.31
Baseline SOFA score	11.0 [9.0–12.0]	10.0 [9.0–13.0]	0.13
Baseline Glasgow Coma Scale score	12.0 [11.0–13.0]	12.5 [10.5–13.0]	0.07
Lactate at T0, mmol/L	4.5 [3.8–6.7]	4.3 [3.8–5.0]	0.24
MAP at T0, mm Hg	80.4 (17.2)	80.4 (13.4)	0.00
Composite StO_2 at T0, %	60.1 (3.0)	61.2 (3.3)	0.34
Cerebral StO_2 at T0, %	57.1 (4.2)	58.6 (4.5)	0.33
Periumbilical StO_2 at T0, %	67.8 (2.8)	68.7 (3.3)	0.27
Peripheral StO_2 at T0, %	55.5 (3.0)	56.5 (3.6)	0.30
Cardiac index at T0, L/min/m²	3.06 (0.56)	3.04 (0.69); n=31	0.04
SVRI at T0, dyn·s·cm⁻⁵ ·m²	1,677 [1,467–1,768]	1,877 [1,733–2,738]; n=31	0.71
EVLWI at T0, mL/kg	9.5 [8.2–11.6]	8.9 [7.8–12.6]; n=31	0.11
GEDVI at T0, mL/m²	724 (114)	760 (93); n=31	0.35
Cardiac function index at T0, min⁻¹	4.37 (1.34)	4.05 (1.10); n=31	0.26
Norepinephrine dose at T0, µg/kg/min	0.45 [0.30–0.80]; n=22	0.50 [0.30–0.80]; n=29	0.04

Data are mean (SD), median [interquartile range], or n/N (%). Values after semicolons indicate the nonmissing sample size when a continuous variable was incomplete. Absolute standardized mean differences (SMDs) are reported; no baseline hypothesis tests were performed. MAP, mean arterial pressure; SOFA, Sequential Organ Failure Assessment; StO_2, tissue oxygen saturation; SVRI, systemic vascular resistance index; EVLWI, extravascular lung water index; GEDVI, global end-diastolic volume index; NIRS, near-infrared spectroscopy.

5.2 Association Between HMD and Mortality in MIMIC-IV

In the MIMIC-IV cohort, hospital mortality reached 21.3% for State A and 38.5% for State B. State B strongly predicted higher hospital mortality. The adjusted OR was 1.93 (95% CI 1.59–2.34; P < 0.001). This resulted in an absolute risk difference of 13.1 percentage points. We found consistent results when using multiple imputation methods and inverse probability weighting. Incorporating the HMD state into our baseline clinical model improved the AUC from 0.717 to 0.732. After correcting for optimism through bootstrapping, the final model AUC stood at 0.724 (Table 2 Figure 2).

Table 2. MIMIC-IV Association and Sensitivity Analyses

Analysis	N	Events	Effect estimate (95% CI)	*P* value
Primary complete-case adjusted OR	2,169	785	1.93 (1.59–2.34)	<0.001
Multiple-imputation adjusted OR	3,605	1,065	2.02 (1.71–2.37)	—
IPOW adjusted OR	2,169	785	1.88 (1.52–2.32)	—
Adjusted standardized risk difference	2,169	785	13.1 pp (9.4–16.9)	—

OR, odds ratio; CI, confidence interval; IPOW, inverse probability of observation weighting; pp, percentage points.

5.3 External Validation in eICU-CRD

In the eICU-CRD dataset, hospital mortality was 23.6% for State A and 50.3% for State B. Our complete case model showed that State B correlated with significantly higher odds of death (adjusted OR 3.23; 95% CI 1.79–5.83; P < 0.001). When we applied the locked MIMIC-IV prediction model to the eICU-CRD data without altering the coefficients, the AUC reached 0.757. A simple intercept recalibration improved the Brier score to 0.197 (Table 3 Figure 2).

Table 3. eICU-CRD External-Validation Results

Analysis	N	Events	Estimate (95% CI)	*P* value
Complete-case cluster-robust adjusted OR	224	93	3.23 (1.79–5.83)	<0.001
Multiple-imputation adjusted OR	648	251	3.16 (2.26–4.41)	—
IPOW adjusted OR	224	—	3.66 (2.04–6.58)	—
Frozen-model AUC	224	93	0.757 (0.696–0.804)	—

OR, odds ratio; CI, confidence interval; IPOW, inverse probability of observation weighting; AUC, area under the receiver operating characteristic curve. The AUC confidence interval used hospital-cluster bootstrap resampling.

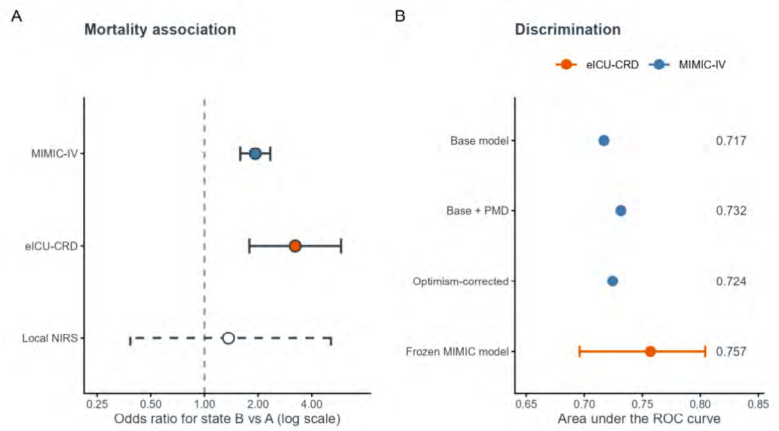


Figure 2. Cross-cohort mortality associations and model discrimination. (A) Odds ratios for mortality comparing HMD state B with state A. Estimates were 1.93 (95% CI 1.59–2.34) in MIMIC-IV, 3.23 (95% CI 1.79–5.83) in eICU-CRD, and 1.36 (95% CI 0.38–5.12) in the local cohort. The local estimate was exploratory and is displayed with an open symbol and dashed interval. The vertical line denotes an odds ratio of 1. (B) Model discrimination in MIMIC-IV and transport performance in eICU-CRD. The frozen MIMIC-IV model achieved an AUC of 0.757 (hospital-cluster bootstrap 95% CI 0.696–0.804) in eICU-CRD. CI, confidence interval; AUC, area under the receiver operating characteristic curve.

5.4 Local NIRS-PiCCO Mechanistic Cohort

At the 24-hour mark, the adjusted estimated mean composite StO_2 was 62.1% for State A and 60.8% for State B. The adjusted difference between the two states was − 1.33 percentage points, which was not statistically significant (95% CI − 4.52 to 1.87; P = 0.408). We also found no significant differences in regional measurements across the cerebral, periumbilical, and peripheral sites after FDR correction. Among our exploratory thermodilution metrics, no parameter met the prespecified significance threshold after multiple comparison adjustments (Table 4 Figure 3).

Table 4. Local NIRS Mechanistic Results

Analysis	N	Adjusted difference (95% CI)	*P* value	Multiplicity
Primary 24-h composite StO_2	55	−1.33 (−4.52 to 1.87)	0.408	Primary
Cerebral StO_2	55	−1.41 (−4.27 to 1.45)	0.327	FDR *P*=0.533
Periumbilical StO_2	55	−1.23 (−4.04 to 1.58)	0.382	FDR *P*=0.533
Peripheral StO_2	55	−1.16 (−4.88 to 2.56)	0.533	FDR *P*=0.533
Exploratory 28-d mortality OR	55	1.36 (0.38–5.12)	0.775	Exploratory

Differences in StO_2 are expressed in percentage points for state B minus state A. CI, confidence interval; FDR, false discovery rate; NIRS, near-infrared spectroscopy; OR, odds ratio; StO_2, tissue oxygen saturation.

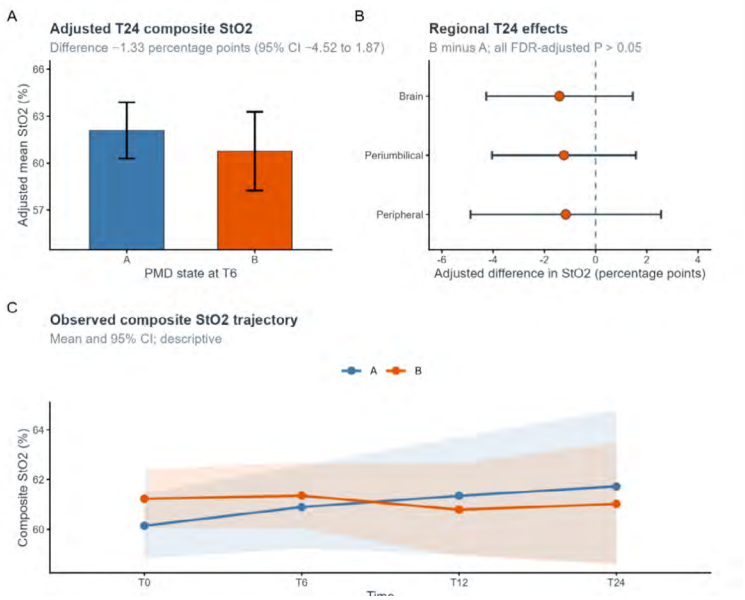


Figure 3. Local mechanistic results. (A) Covariate-adjusted mean 24-hour composite tissue oxygen saturation (StO_2) according to HMD state at 6 hours. The adjusted state B minus state A difference was − 1.33 percentage points (95% CI − 4.52 to 1.87; P = 0.408). Error bars indicate 95% CIs. (B) Adjusted regional 24-hour differences for cerebral, periumbilical, and peripheral StO_2. All Benjamini–Hochberg false-discovery-rate-adjusted P values exceeded 0.05. (C) Observed composite StO_2 trajectories from baseline to 24 hours; points represent means and shaded bands represent 95% CIs. Panel C is descriptive and is not a repeated-measures causal estimate.

5.5 Sensitivity Analyses

We verified the robustness of our findings in both large databases. The association between HMD and mortality remained stable even when we changed the lactate clearance thresholds to 10% or 30%. Altering the MAP targets to 60 or 70 mm Hg did not change the overall trend. The adjusted odds ratios ranged from 1.81 to 2.08 in MIMIC-IV and from 2.97 to 3.24 in eICU-CRD (Figure 4).

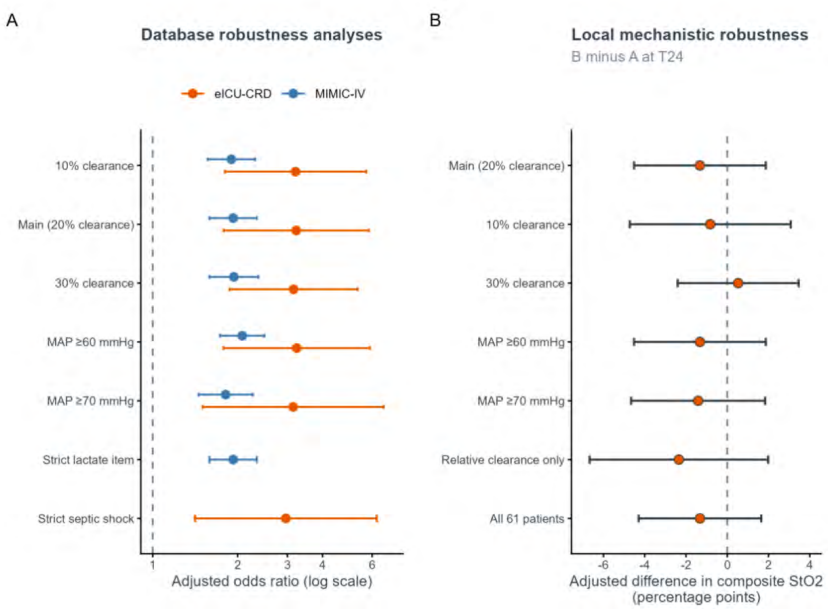


Figure 4. Sensitivity analyses. (A) Adjusted mortality odds ratios in MIMIC-IV and eICU-CRD under alternative lactate-clearance, mean arterial pressure, and cohort definitions. The direction of association was consistent across database analyses. (B) Local adjusted 24-hour composite StO_2 differences under prespecified alternative operational definitions. Confidence intervals crossed zero in all local analyses. Vertical reference lines denote an odds ratio of 1 in panel A and a mean difference of 0 in panel B.

6. Conclusion

Experiencing a disconnect between blood Hemodynamic recovery and metabolic improvement during early sepsis care independently predicts higher hospital mortality. We consistently observed this association across two large, independent patient databases. Furthermore, the prediction model transferred well to an external multicenter cohort, showing strong discrimination and calibration.

However, our local cohort analysis revealed that macroscopic tissue oxygen saturation does not significantly differ between these patient states. This suggests that the high mortality risk associated with HMD likely stems from other factors, such as microcirculatory failure, mitochondrial damage, or abnormal lactate processing. Identifying patients with HMD offers a straightforward way to assess risk at the bedside. It helps clinicians spot patients who seem stable based on blood pressure but still face a high risk of death. Future studies should investigate targeted interventions—such as microcirculatory optimization or metabolic modulation—for patients trapped in this discordant state.

7.References

[1] Singer M, Deutschman CS, Seymour CW, et al. The Third International Consensus Definitions for Sepsis and Septic Shock (Sepsis-3). JAMA. 2016;315(8):801-810.

[2] Evans L, Rhodes A, Alhazzani W, et al. Surviving Sepsis Campaign: International Guidelines for Management of Sepsis and Septic Shock 2021. Intensive Care Med. 2021;47(11):1181-1247.

[3] Howell MD, Donnino M, Clardy P, Talmor D, Shapiro NI. Occult hypoperfusion and mortality in patients with suspected infection. Intensive Care Med. 2007;33(11):1892-1899.

[4] Jones AE, Shapiro NI, Trzeciak S, et al. Lactate clearance vs central venous oxygen saturation as goals of early sepsis therapy: a randomized clinical trial. JAMA. 2010;303(8):739-746.

[5] Johnson AEW, Bulgarelli L, Shen L, et al. MIMIC-IV, a freely accessible electronic health record dataset. Sci Data. 2023;10(1):1.

[6] Pollard TJ, Johnson AEW, Raffa JD, Celi LA, Mark RG, Badawi O. The eICU Collaborative Research Database, a freely available multi-center database for critical care research. Sci Data. 2018;5:180178.

[7] von Elm E, Altman DG, Egger M, et al. The Strengthening the Reporting of Observational Studies in Epidemiology (STROBE) statement: guidelines for reporting observational studies. Lancet. 2007;370(9596):1453-1457.

HMOX1 Ameliorates Sepsis-Induced Acute Lung Injury by Suppressing a Single-Cell-Defined Pathogenic Slc11a1-High Macrophage Subpopulation

姓名：杨艺博
单位：天津市中西医结合医院（天津市南开医院）

Abstract

Background

Sepsis-induced acute lung injury (ALI) is characterized by severe alveolar damage, immune dysfunction, and high mortality. Although alveolar macrophages are central to pulmonary inflammation, the specific macrophage subsets responsible for driving excessive inflammation in the septic microenvironment are not fully understood. Here, we investigate how the cytoprotective enzyme heme oxygenase-1 (HMOX1) regulates macrophage heterogeneity to alleviate septic ALI.

Methods: We mapped the pulmonary immune landscape of septic ALI mice (cecal ligation and puncture model) using single-cell RNA sequencing (scRNA-seq) and pseudotime trajectory analysis. Molecular docking and dynamics simulations were used to evaluate HMOX1-target interactions, with cross-validation in human clinical transcriptomic datasets. In vivo mechanisms were validated using the HMOX1 agonist hemin and HO-1 knockout mice, supported by histopathology, immunofluorescence, and Western blotting.

Results: ScRNA-seq revealed a distinct, early-responding pathogenic macrophage subpopulation characterized by high Slc11a1 expression, which is closely linked to early pro-inflammatory cascades. Molecular dynamics simulations demonstrated a stable, direct binding interaction between HMOX1 and SLC11A1. This interaction aligns with their concurrent dysregulation observed in clinical sepsis samples. In vivo, hemin-mediated HMOX1 activation suppressed the expansion of these Slc11a1-high macrophages, reducing pulmonary edema, reactive oxygen species (ROS) accumulation, and cellular apoptosis. Conversely, HO-1 knockout mice exhibited massive infiltration of this pathogenic subset, leading to more severe lung lesions and poorer survival.

Conclusions: HMOX1 interacts directly with SLC11A1 to block differentiation and proliferation of harmful Slc11a1-high macrophages, exerting potent protective effects against sepsis-triggered ALI.

Introduction

Sepsis is defined as a life-threatening organ dysfunction triggered by a dysregulated host response to infection (1). Due to its extensive capillary network and direct environmental exposure, the lung is exceptionally vulnerable during sepsis, making acute lung injury (ALI) and acute respiratory distress syndrome (ARDS) leading causes of mortality in intensive care units worldwide (2, 3). The pathophysiology of sepsis-induced ALI involves a complex cascade of increased alveolar-capillary permeability, protein-rich pulmonary edema, and widespread apoptosis of pulmonary cells (4, 5). Notably, this severe tissue destruction is predominantly driven by a "cytokine storm" resulting from hyperactive innate immune cells(6).

Within the pulmonary immune system, macrophages play a paradoxical role: they initiate the inflammatory response but are equally critical for coordinating tissue repair(7). Traditionally, macrophage activation has been categorized using a simplified binary model—the pro-inflammatory M1 and anti-inflammatory M2 phenotypes(8, 9). However, this in vitro-derived classification fails to accurately capture the high phenotypic plasticity and continuous transcriptomic states of macrophages within the dynamic in vivo septic microenvironment(10, 11). Although single-cell RNA sequencing (scRNA-seq) now allows for high-resolution mapping of cellular heterogeneity(12), the specific macrophage subpopulations driving irreversible tissue injury in septic ALI, and their dynamic polarization trajectories, remain poorly defined(13, 14).

At the molecular level, Solute Carrier Family 11 Member 1 (Slc11a1), a divalent metal ion transporter localized on the macrophage lysosomal membrane, is crucial for innate antimicrobial immunity(15, 16). However, its persistent overexpression disrupts intracellular iron homeostasis, fueling the Fenton reaction and excessive reactive oxygen species (ROS) production, which subsequently hyperactivates pro-inflammatory pathways such as NF-κB(17, 18). Conversely, Heme Oxygenase-1 (HMOX1/HO-1), an endogenous stress-inducible enzyme, confers potent cytoprotection (19). By degrading free heme, HMOX1 mitigates pulmonary

edema and improves survival in septic mice (20). Indeed, our previous laboratory work has established the multifaceted protective roles of HMOX1 in sepsis-induced ALI, demonstrating that it mitigates Golgi stress in macrophages(21) and suppresses MAPK-driven inflammation(22).

Building on this foundation, we hypothesized that HMOX1 mitigates septic ALI by actively targeting and regulating specific, highly pathogenic macrophage subpopulations. To address this, the present study utilizes scRNA-seq to construct a high-resolution immune map of sepsis-induced ALI to identify the core macrophage subset driving excessive inflammation. Furthermore, we systematically investigate the previously unexplored molecular interplay between HMOX1 and SLC11A1, elucidating the mechanisms underlying HMOX1-mediated immunometabolic regulation.

Materials and Methods

Animal Models and Ethical Approval

Wild-type (WT) male C57BL/6J mice (6–8 weeks old) and HMOX1 whole-gene knockout (HO-1-/-) mice sharing the same genetic background were obtained from Speford (Beijing) Biotechnology Co., Ltd. Mouse genotypes were confirmed via PCR prior to experimentation. All animal procedures strictly adhered to the guidelines established by the Tianjin Medical Experimental Animal Care Center and received approval from the Animal Ethical and Welfare Committee of Tianjin Nankai Hospital (Approval No: NKYY-DWLL-2024-045). All procedures were performed in compliance with the ARRIVE 2.0 guidelines. Mice were housed under standard specific pathogen-free (SPF) laboratory conditions (12-h light/dark cycle, 22 ± 2° C, 50–60% humidity) with ad libitum access to food and water.

Sepsis-induced ALI was induced via the standard Cecal Ligation and Puncture (CLP) model. Briefly, under continuous anesthesia (2% isoflurane inhalation), the cecum was exteriorized, ligated at the midpoint between the distal pole and the base with a 3-0 silk suture, and subjected to a single through-and-through puncture with a 20G sterile needle. A small droplet of feces was extruded to ensure a consistent, polymicrobial infection. Sham-operated control mice underwent laparotomy and bowel exteriorization without ligation or puncture. Post-surgery, all mice received immediate fluid resuscitation via subcutaneous injection of pre-warmed physiological saline (5 mL/100 g body weight). Post-operative analgesics were withheld to avoid confounding effects on the immunological and inflammatory responses under investigation.

Where indicated, mice were intraperitoneally administered the HMOX1 agonist Hemin (50 mg/kg, dissolved in 0.1 M NaOH and neutralized to pH 7.4 with HCl) 1 h prior to CLP surgery. Lung tissues were harvested 24 h post-surgery for downstream analyses. At the experimental endpoint, mice were euthanized by cervical dislocation under deep anesthesia (5% isoflurane).

Single-Cell RNA Sequencing (scRNA-seq) and Bioinformatics

Freshly harvested lung tissues were mechanically minced into approximately 1 mm^3 pieces and subjected to enzymatic digestion using the automated Singleron PythoT® system (37° C, 15 min). Following erythrocyte depletion with GEXSCOPE® RBC lysis buffer, the resulting single-cell suspensions were adjusted to a concentration of 2×10^5 cells/mL. To ensure high-quality sequencing inputs, only cell suspensions exceeding 90% viability (assessed via trypan blue exclusion) proceeded to library construction. Sequencing libraries were prepared utilizing the GEXSCOPE® Single-Cell RNA Library Kit and sequenced on the Illumina NovaSeq 6000 platform (PE150 strategy).

Downstream transcriptomic analyses were performed in R (v4.4.1) utilizing the Seurat package (v4.4.3). To guarantee a robust dataset, rigorous quality control filters were applied: cells were excluded if they presented <200 or >98th percentile total detected genes, displayed abnormally high Unique Molecular Identifier (UMI) counts, or exhibited >25% mitochondrial transcript ratios. To construct a high-fidelity integrated single-cell atlas, we combined Canonical Correlation Analysis (CCA) and Mutual Nearest Neighbors (MNN) algorithms, which efficiently regress out batch effects across biological replicates.

Dimensionality reduction was performed using Uniform Manifold Approximation and Projection (UMAP), and cellular identities were established through a consensus approach combining the SingleR pipeline (v1.4.0) with expert-curated canonical markers. Differentially expressed genes (DEGs) were rigorously identified using the Wilcoxon rank-sum test (adjusted $P < 0.05$, $|\log_2 FC| > 0.25$). Finally, to reconstruct the in vivo developmental and activation pathways of pathogenic macrophages within the septic

microenvironment, pseudotime trajectory mapping was strategically executed using both Monocle2 and Monocle3.

Molecular Docking and Molecular Dynamics (MD) Simulations

To investigate the structural basis of the novel HMOX1-SLC11A1 interaction, three-dimensional structures of human HMOX1 (PDB ID: 6EHA) and SLC11A1 (PDB ID: 9F6P) were retrieved from the Protein Data Bank. Global rigid-body protein-protein docking was executed locally using HDOCKlite (v1.1). The optimal binding conformation, selected based on a high confidence score (> 0.7), was further analyzed to map interfacial non-covalent interactions via the PLIP platform and visualized in PyMOL (v2.5.4).

To validate the dynamic stability of this protein-protein complex under physiological conditions, we performed 100-ns MD simulations utilizing the GROMACS 2022 suite, parameterized with the AMBER14SB force field and the TIP3P water model. The simulation box was neutralized and adjusted to a physiological ionic strength of 0.15 M NaCl. After thorough energy minimization (steepest descent algorithm, 50,000 steps) and standard equilibration phases, the production run was conducted in an NPT ensemble (310 K, 1 bar) with a 2 fs integration step. We monitored the structural integrity and interaction dynamics of the complex by extracting trajectories for Root Mean Square Deviation (RMSD), Root Mean Square Fluctuation (RMSF), Radius of Gyration (Rg), Solvent Accessible Surface Area (SASA), and dynamic hydrogen bond populations. Finally, the thermodynamic binding affinity was quantified by calculating the binding free energy using the MM-PBSA method.

Histopathology and Immunofluorescence

To assess severe architectural damage, harvested lung tissues were fixed in 4% paraformaldehyde (24 h, 4 ° C), paraffin-embedded, and sectioned at 4 μm. Hematoxylin and Eosin (H&E) staining was performed, and tissue injury was quantified using a standardized Lung Injury Score (LIS; scale 0–4) based on the severity of alveolar hemorrhage, interstitial edema, neutrophil infiltration, and fibrin exudation. To eliminate observation bias, scoring was performed independently by two blinded pathologists.

To visualize the in situ spatial relationship between HO-1 and SLC11A1, sections were subjected to double immunofluorescence (dIF). Following standard heat-induced antigen retrieval (citrate buffer, pH 6.0, 95 ° C, 20 min) and permeabilization (0.3% Triton X-100, 10 min), sections were blocked with 5% bovine serum albumin (BSA) supplemented with a Mouse-on-Mouse (M.O.M.) blocking reagent for 1 h to eliminate non-specific binding of endogenous mouse IgG. Sections were then co-incubated overnight at 4 ° C with primary antibodies against HO-1 (Rabbit, 1:200; Abcam, ab13243) and SLC11A1 (Mouse, 1:100; Thermo Fisher, PA5-21346). Corresponding fluorophore-conjugated secondary antibodies (FITC-conjugated goat anti-rabbit IgG and Cy3-conjugated goat anti-mouse IgG; both 1:500) were subsequently applied for 1 h at room temperature. Nuclei were counterstained with DAPI (1 μg/mL), and representative images were captured via a Leica TCS SP8 confocal laser scanning microscope.

Furthermore, to monitor pulmonary oxidative stress, Reactive Oxygen Species (ROS) accumulation was detected on 8 μm frozen sections employing a Dihydroethidium (DHE) fluorescent probe (10 μmol/L, 30 min, 37 ° C, protected from light). Finally, in situ cellular apoptosis was mapped utilizing a robust TUNEL assay kit (Roche, 11684817910) subsequent to proteinase K permeabilization (20 μg/mL, 15 min, 37° C).

Western Blot Analysis

To evaluate the protein expression profiles of the HMOX1/SLC11A1 axis, total protein was extracted from lung tissues utilizing RIPA lysis buffer (Beyotime, P0013B) supplemented with both protease (Roche, 04693132001) and phosphatase inhibitors (Roche, 04906845001). After quantifying protein concentrations via the BCA assay (Thermo Fisher, 23225), equal amounts of denatured protein (30 μg per lane) were resolved on 12% SDS-PAGE gels and electrotransferred onto 0.45 μm PVDF membranes (Millipore, IPVH00010). To minimize non-specific background signals, membranes were blocked with 5% non-fat milk in TBST for 1 h at room temperature.

The membranes were then probed overnight at 4 ° C with specific primary antibodies against HO-1 (Rabbit, 1:1000; Abcam, ab13243), SLC11A1 (Mouse, 1:500; Thermo Fisher, PA5-21346), and β-actin (Rabbit, 1:5000; Abcam, ab8227) as the internal loading control. Following a 1-h incubation with the corresponding HRP-conjugated secondary antibodies (1:5000, room temperature), immunoreactive signals were developed utilizing an ECL substrate (Thermo Fisher, 32106) and quantified densitometrically via

ImageJ software (v1.53k).

Validation in Human Clinical Cohorts

To determine whether the HMOX1/SLC11A1 regulatory axis observed in our murine model accurately reflects human pathology, we analyzed transcriptomic data from human peripheral blood mononuclear cells (PBMCs). Clinical datasets comprising critically ill sepsis patients and healthy donors were retrieved from the Gene Expression Omnibus (GEO) database (Accession: GSE279452). Standardized expression matrices were downloaded and processed utilizing the GEOquery R package (v2.66.0). This approach enabled the precise extraction and comparative analysis of HMOX1 and SLC11A1 mRNA expression levels across the distinct clinical cohorts.

Statistical Analysis

Data for continuous variables are expressed as the mean ± standard deviation (SD). Prior to analytical testing, data distribution normality and variance homogeneity were confirmed employing the Shapiro-Wilk and Levene's tests, respectively. Comparisons between two independent groups were evaluated using an unpaired Student's t-test, whereas multi-group comparisons were analyzed utilizing a one-way analysis of variance (ANOVA) followed by Tukey's post-hoc test. For non-normally distributed data, non-parametric equivalents such as the Mann-Whitney U or Kruskal-Wallis tests were applied.Survival curves were plotted using the Kaplan-Meier method and statistically compared via the log-rank (Mantel-Cox) test. All statistical analyses and graphical visualizations were performed using GraphPad Prism 8.0 (GraphPad Software, San Diego, CA, USA). Statistical significance was defined as $P < 0.05$. To ensure reproducibility, all in vitro and in vivo experiments were independently replicated a minimum of three times.

Results

Result 1 Mapping the Single-Cell Landscape of the Septic Lung Microenvironment

To characterize the dynamic cellular alterations during sepsis-induced ALI, we performed scRNA-seq on lung tissues harvested from Sham and CLP-treated mice (Fig. 1A). Unsupervised UMAP clustering defined 10 major cell lineages (Fig. 1B). The accuracy of these cellular annotations was confirmed by the distinct transcriptomic signatures and top differentially expressed marker genes unique to each lineage (Supplementary Figure S1). Overall cellular proportions highlighted neutrophils and mononuclear phagocytes as the predominant immune infiltrates (Fig. 1D). The induction of sepsis triggered a profound restructuring of the pulmonary immune niche. Notably, we observed a massive expansion of neutrophils concomitant with a marked depletion of B cells (Fig. 1C).

Interestingly, while other immune populations fluctuated drastically, the mononuclear phagocyte system (MPS) maintained a highly consistent proportional representation across both control and CLP samples (Fig. 1E). This stable presence amidst severe inflammation prompted us to further investigate the internal heterogeneity of this lineage. Subsequent high-resolution sub-clustering of the MPS compartment delineated classical and non-classical monocytes, macrophages, and specific dendritic cell subsets (Fig. 1F), culminating in a refined 14-cluster immune atlas of the septic lung (Fig. 1G).

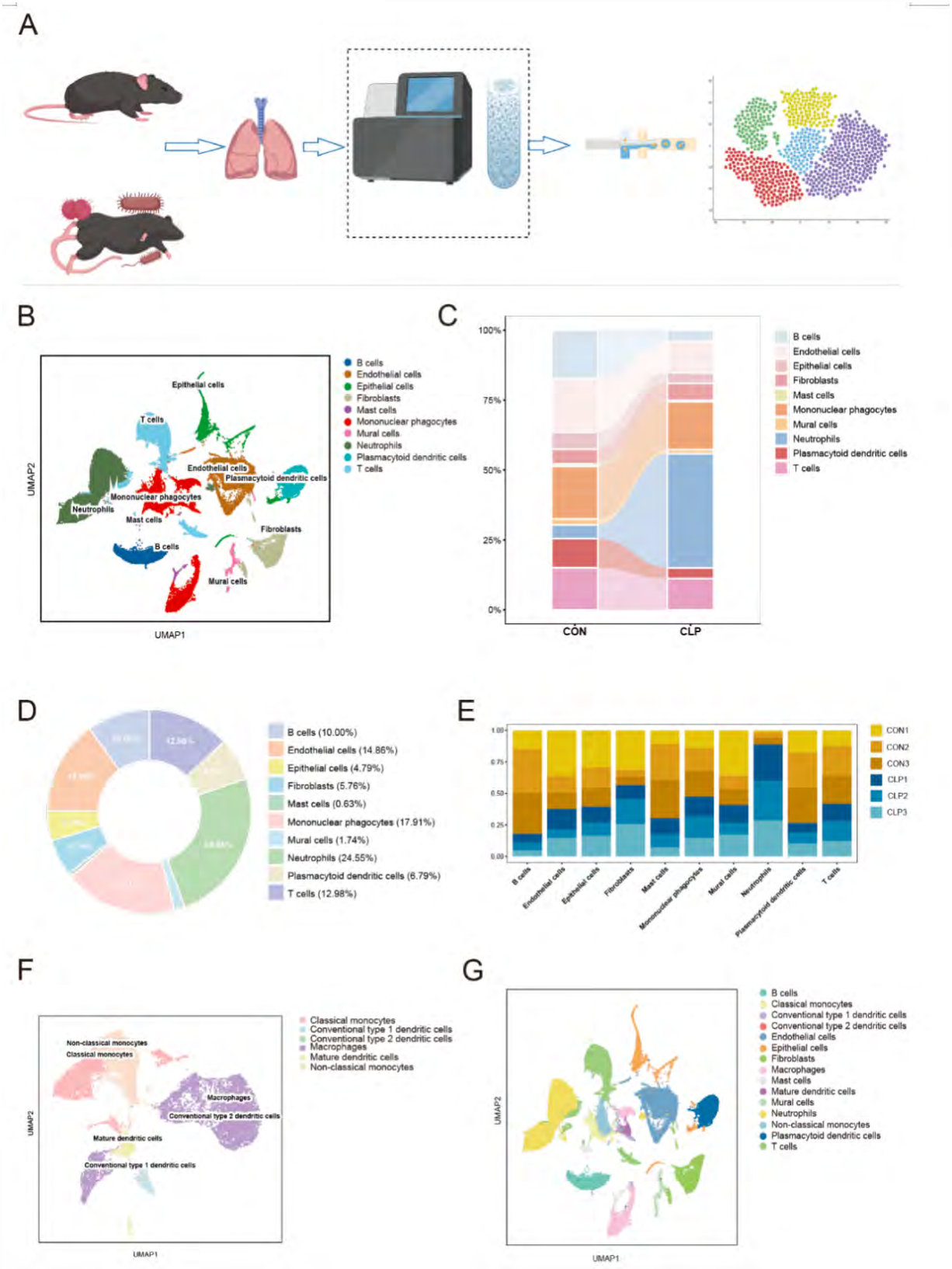


Figure 1. Single-cell transcriptomic landscape of the murine lung during sepsis-induced acute lung injury. (A) Schematic illustration of the experimental design. Lung tissues from Sham (CON) and CLP-treated mice were harvested 24 h post-surgery for single-cell RNA sequencing (scRNA-seq). **(B)** Uniform Manifold Approximation and Projection (UMAP) plot visualizing the 10 major cell lineages identified in the integrated pulmonary dataset. **(C)** Stacked bar chart showing the dynamic proportional changes of the 10 major cell lineages between the CON and CLP groups. **(D)** Pie chart detailing the overall percentage distribution

of the major cell populations across all samples. **(E)** Relative abundance of the major cell lineages across individual biological replicates (CON1-3 and CLP1-3), highlighting the proportional stability of the mononuclear phagocyte system (MPS). **(F)** High-resolution UMAP plot of the sub-clustered MPS compartment, delineating seven distinct immune subsets including classical/non-classical monocytes, macrophages, and specific dendritic cell (DC) populations. **(G)** Comprehensive UMAP plot presenting the final 14-cluster pulmonary single-cell atlas, stratified by treatment condition (CON vs. CLP). Abbreviations: CLP, cecal ligation and puncture; CON, control (Sham); UMAP, uniform manifold approximation and projection.

Result 2 Identification of a Pathogenic, Slc11a1-High Macrophage Subpopulation

To dissect macrophage heterogeneity during sepsis, we computationally subsetted the macrophage population. The high purity of this isolated compartment was confirmed by the widespread expression of the canonical macrophage marker Cd68 (Supplementary Figure S2A). Secondary unsupervised clustering delineated 8 transcriptionally distinct subclusters (Fig. 2A). The biological validity of this sub-clustering was robustly supported by transcriptomic profiling, which demonstrated distinct, non-overlapping gene expression signatures for each of the 8 subsets (Supplementary Figure S2B). Compositional analysis revealed a marked shift in the macrophage compartment following CLP. Specifically, Subclusters 2 (Mac2) and 3 (Mac3) exhibited significant disease-associated expansion, supported by both relative proportional increases and an observed-to-expected (Ro/e) ratio > 1 (Fig. 2B, C).

To understand the functional specialization of these expanded subsets, we performed Gene Ontology (GO) functional enrichment. Strikingly, Mac3 was highly enriched for hyper-inflammatory pathways, including the positive regulation of cytokine production and leukocyte chemotaxis (Fig. 2F). This specialized transcriptomic signature strongly implicates Mac3 as a core initiator of the septic inflammatory cascade. Furthermore, unbiased differential gene expression analysis identified the divalent metal transporter Slc11a1 as the defining marker for Mac3, with its expression spatially restricted almost exclusively to this specific pathogenic subpopulation (Fig. 3A). Quantitative distribution analysis further confirmed that Slc11a1 expression was overwhelmingly enriched in Mac3 compared to all other macrophage subclusters (Supplementary Figure S2C).

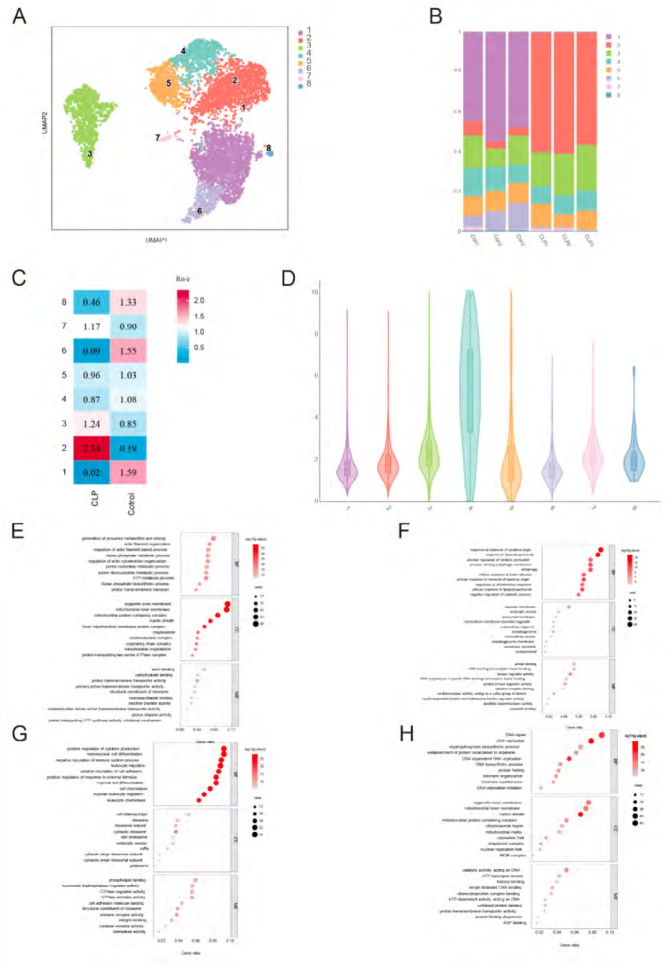


Figure 2. Identification and functional characterization of macrophage heterogeneity in the septic lung.

(A) UMAP visualization of the computationally isolated macrophage compartment, delineating 8 transcriptionally distinct subclusters (Mac1-8). (B) Stacked bar plot illustrating the relative proportional distribution of the 8 macrophage subclusters across individual Control (Sham) and CLP biological replicates. (C, D) Quantitative analysis of compositional shifts, including the observed-to-expected (Ro/e) ratios (C) and cellular abundance variations (D), highlighting the profound disease-associated expansion of specific subsets (e.g., Mac2 and Mac3) following CLP induction.

(E-H) Gene Ontology (GO) functional enrichment analysis of differentially expressed genes defining key macrophage subclusters. Notably, panel (F) demonstrates the profound enrichment of hyper-inflammatory and chemotactic pathways (e.g., positive regulation of cytokine production, leukocyte chemotaxis) specifically within the pathogenic Mac3 subpopulation.

Result 3 Pseudotime Trajectory Positions the Slc11a1-High Subpopulation as an Early Initiator

To delineate the developmental dynamics of these macrophages during sepsis, we performed pseudotime trajectory inference. Trajectory analysis revealed that the highly pro-inflammatory Mac3 subpopulation localized predominantly at the root of the differentiation trajectory (Pseudotime ≈ 0) (Fig. 3B-D). This unique spatial positioning aligned perfectly with the algorithm-defined initial cellular state (Supplementary Figure S3A). Furthermore, faceted trajectory and density analyses confirmed that cells clustering at this early developmental root were heavily enriched in the CLP group, underscoring their rapid, disease-specific emergence (Supplementary Figure S3B, C).

This positioning suggests that Mac3 represents an acute, early-responder state rather than a terminally differentiated or exhausted phenotype. Consistently, the expression signal of Slc11a1 aligned closely with this trajectory origin (Fig. 3E). Dynamic gene expression modeling along the pseudotime axis further revealed a distinct cluster of critical pro-inflammatory chemokines (including Ccl3 and Ccl4). These genes exhibited an early burst of high expression at the onset of pseudotime—concurrent with the emergence of the Mac3 population—before being subsequently downregulated as differentiation progressed (Supplementary Figure S3D). Together, these trajectory dynamics support the hypothesis that the Slc11a1-high subpopulation serves as an early cellular initiator of the septic inflammatory cascade.

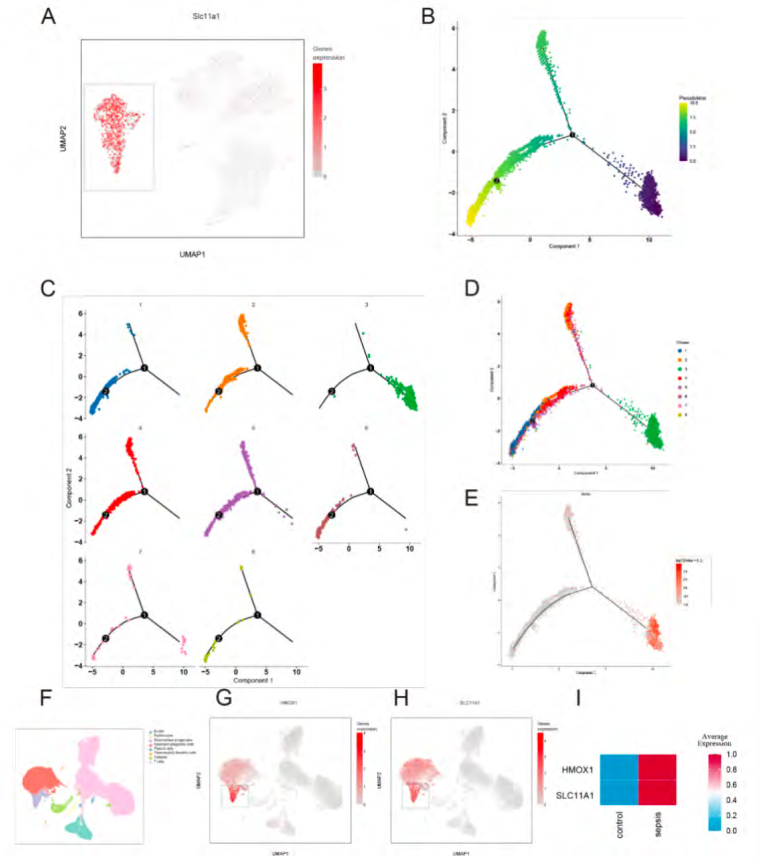


Figure 3. Pseudotime trajectory inference of pulmonary macrophages and clinical validation of the HMOX1/SLC11A1 axis.

(A) UMAP feature plot visualizing the highly specific and spatially restricted expression of the divalent metal transporter Slc11a1 within the pathogenic macrophage subpopulation. (B-D) Pseudotime trajectory analysis mapping the developmental dynamics of the macrophage compartment. The cellular differentiation trajectory is visualized by pseudotime progression (B), faceted by individual macrophage subclusters (C), and colored by distinct cluster identities (D), demonstrating the predominant localization of the pathogenic subset at the developmental root (Pseudotime $\approx$ 0). (E) Trajectory plot illustrating the dynamic expression of Slc11a1 along the pseudotime axis, confirming its acute, early-onset upregulation at the trajectory origin. (F-H) Cross-species clinical validation utilizing human peripheral blood mononuclear cell (PBMC) transcriptomics. UMAP projection annotating major human immune cell lineages (F), alongside corresponding feature plots revealing the spatially coupled enrichment of HMOX1 (G) and SLC11A1 (H) specifically within the human monocyte/macrophage lineage. (I) Heatmap comparing the average expression levels of HMOX1 and SLC11A1 between healthy controls and clinical sepsis patients, validating their synchronized dysregulation in human sepsis.

Result 4 HMOX1 and SLC11A1 Exhibit Direct Molecular Interaction and Coupled Clinical Dysregulation

Protein-protein interaction (PPI) network analysis initially suggested a functional relationship between HMOX1 and SLC11A1. This was supported by their spatially coupled upregulation within the pathogenic Mac3 macrophage subpopulation (Fig. 4A, B). To structurally characterize this interaction, we performed molecular docking. The predicted complex revealed a stable three-dimensional interface driven by critical non-covalent interactions, including specific hydrogen bonds (e.g., HMOX1 ARG-113 to SLC11A1 TRP-59) and salt bridges (e.g., SLC11A1 ARG-226 to HMOX1 ASP-156) (Fig. 4C).

To evaluate the dynamic conformational stability of the HMOX1-SLC11A1 complex in an aqueous environment, we conducted a 100-ns molecular dynamics (MD) simulation. The complex demonstrated robust structural stability, as evidenced by the Root Mean Square Deviation (RMSD) converging and stabilizing at approximately 3.8 Å (Fig. 4D). Complementary geometric metrics, including the Radius of Gyration (Rg) and Solvent Accessible Surface Area (SASA), alongside sustained hydrogen bond networks and low Root Mean Square Fluctuation (RMSF) profiles, collectively verified the structural compactness and interaction consistency over the simulation trajectory (Fig. 4E-I).

Finally, comprehensive thermodynamic MM-PBSA calculations yielded a highly favorable total binding free energy () of − 47.6 kcal/mol, confirming a potent binding affinity (Supplementary Table S1; Fig. 4J). Per-residue free energy decomposition further revealed that this robust stability is predominantly driven by strong electrostatic contributions from key anchor residues, notably ARG-108, ARG-226, and GLU-215 (Supplementary Table S2; Fig. 4K).

Crucially, analysis of human PBMC transcriptomics (GSE279452) validated the clinical relevance of this axis: both SLC11A1 and HMOX1 mRNAs were significantly upregulated in clinical sepsis patients compared to healthy donors, exhibiting synchronized dysregulation specifically within the monocyte/macrophage lineages (Fig. 3F-I).

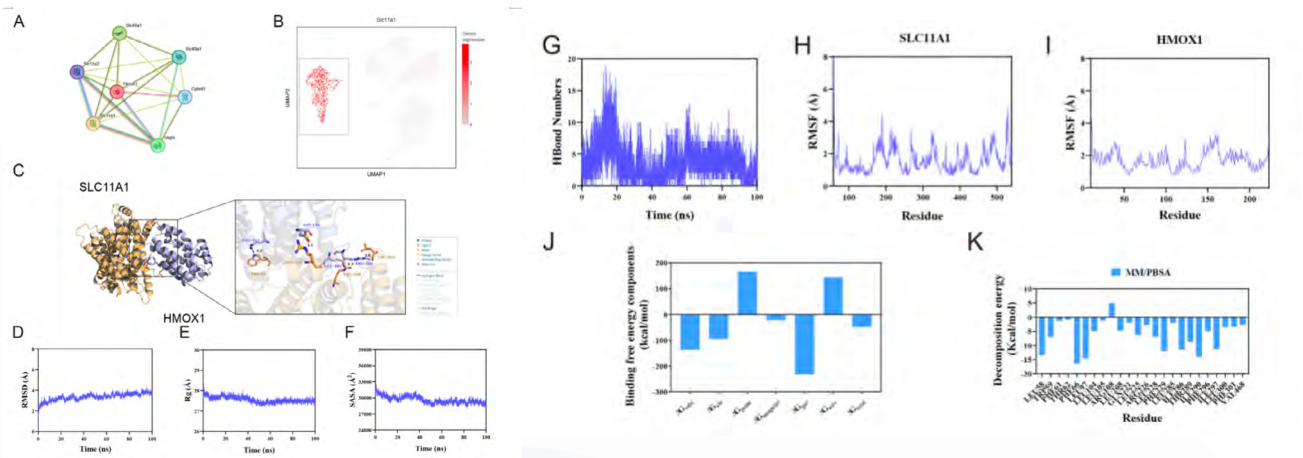


Figure 4. Structural basis and molecular dynamics of the HMOX1-SLC11A1 interaction.

(A) Protein-protein interaction (PPI) network analysis predicting a direct functional relationship between HMOX1, SLC11A1, and other iron metabolism-associated proteins. **(B)** UMAP feature plot visualizing the expression pattern of Slc11a1 across the macrophage subclusters. **(C)** 3D structural model of the HMOX1-SLC11A1 complex generated via molecular docking. The magnified inset details the critical non-covalent interactions at the binding interface, highlighting specific anchoring hydrogen bonds and salt bridges between key amino acid residues. **(D–I)** A 100-ns molecular dynamics (MD) simulation assessing the dynamic conformational stability of the docked complex in an aqueous environment. Structural integrity is validated by **(D)** Root Mean Square Deviation (RMSD), **(E)** Radius of Gyration (Rg), **(F)** Solvent Accessible Surface Area (SASA), **(G)** the fluctuation of intermolecular hydrogen bond numbers, and the Root Mean Square Fluctuation (RMSF) profiles for **(H)** SLC11A1 and **(I)** HMOX1. **(J)** Thermodynamic analysis detailing the individual energy components and the highly favorable total binding free energy calculated using the MM-PBSA method. **(K)** Per-residue free energy decomposition profile identifying the specific amino acids that contribute most significantly to the interaction affinity between HMOX1 and SLC11A1.

Result 5 Pharmacological Activation of HMOX1 Abrogates Slc11a1-Mediated ALI

To validate the regulatory impact of HMOX1 in vivo, we administered Hemin, a potent HMOX1 agonist, to CLP-treated mice. Western blot and qPCR analyses confirmed that Hemin treatment markedly upregulated HO-1 expression while simultaneously suppressing the CLP-induced surge in Slc11a1 protein and mRNA levels (Fig. 5A-C).

Histopathologically, Hemin administration significantly mitigated lung damage, as evidenced by reduced alveolar architectural collapse, decreased septal thickening, and lower overall Lung Injury Scores (LIS) compared to the CLP group (Fig. 5D, E). Consistently, Kaplan-Meier survival analysis showed that the activation of the HMOX1/SLC11A1 axis significantly improved the survival rate of septic mice (Fig. 5F).

Given that Slc11a1 overexpression potentially drives iron-mediated oxidative stress, we further evaluated pulmonary redox status and cell death. DHE staining revealed that Hemin treatment effectively reduced the massive ROS accumulation characteristic of septic lungs (Fig. 5G). Concomitantly, TUNEL staining demonstrated that this reduction in oxidative damage was associated with a substantial decrease in parenchymal cell apoptosis in the CLP+Hemin group (Fig. 5H). These findings suggest that HMOX1 activation alleviates sepsis-induced ALI by counteracting Slc11a1-driven oxidative injury and subsequent cell death.

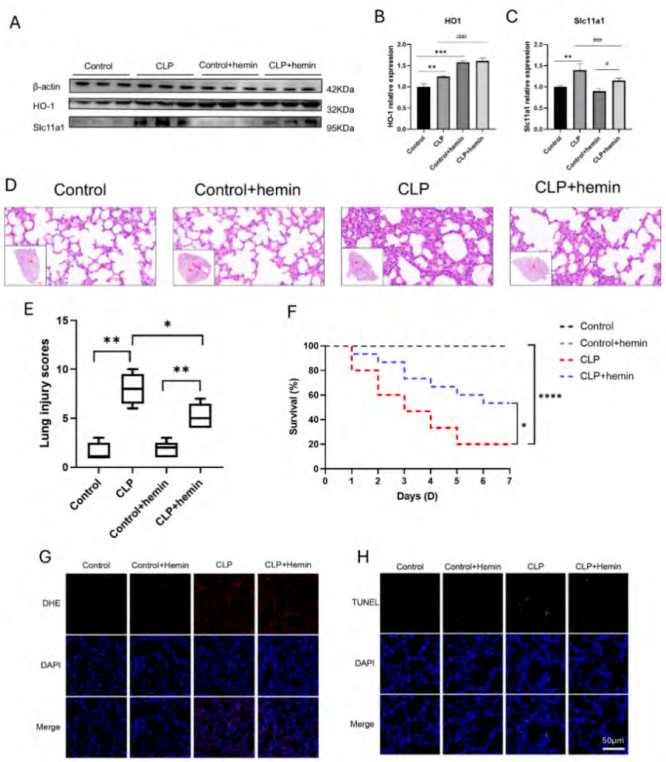


Figure 5. Pharmacological activation of HMOX1 mitigates Slc11a1-mediated acute lung injury.

(A) Western blot analysis of HO-1 and its downstream target Slc11a1 protein expression levels in lung tissues across the experimental groups (Control, Control+Hemin, CLP, and CLP+Hemin).(B, C) Relative densitometric quantification of HO-1 (B) and Slc11a1 (C) protein levels (n = 3 per group).

(D) Representative hematoxylin and eosin (H&E) staining images of lung tissues from each group. The bottom-left insets display whole-lung scans, indicating the corresponding magnified regions.(E) Semi-quantitative Lung Injury Score (LIS) based on the H&E-stained sections. Statistical differences were assessed using the Mann-Whitney U test ($P < 0.05$, $^{*}P < 0.01$, $P < 0.001$).(F) Kaplan-Meier survival curves of the mice in the indicated groups (n = 15 per group).(G) In situ evaluation of reactive oxygen species (ROS) levels in lung tissues via DHE fluorescence staining. Red fluorescence indicates ROS accumulation, and blue DAPI staining indicates the nuclei.(H) TUNEL multiplex fluorescence assay evaluating parenchymal cell apoptosis in lung tissues. Green fluorescence indicates apoptotic cells with DNA fragmentation, and blue DAPI staining indicates the nuclei.

Result 6 HMOX1 Deletion Exacerbates Slc11a1 Overload and Pathogenesis

To further investigate the role of HMOX1, we subjected Hmox1 global knockout (Hmox1 $^{-/-}$) mice to the CLP model (Fig. 6A). In the absence of this endogenous regulatory checkpoint, Hmox1 $^{-/-}$ mice displayed a significantly enhanced, compensatory upregulation of Slc11a1 expression compared to wild-type (WT) CLP-treated mice (Fig. 6B, C).

Consistent with this molecular phenotype, Hmox1 $^{-/-}$ mice exhibited significantly more severe lung injury, manifested as extensive alveolar consolidation and elevated Lung Injury Scores (LIS) (Fig. 6D, E). Furthermore, the lack of HMOX1-mediated protection led to markedly reduced survival rates in septic Hmox1 $^{-/-}$ mice compared to their WT counterparts (Fig. 6F). Mechanistically, the unrestricted Slc11a1 activity in Hmox1 $^{-/-}$ mice was associated with a more pronounced oxidative stress burden, as evidenced by intensified DHE staining (Fig. 6G), which preceded a dramatic increase in diffuse parenchymal cell apoptosis observed via TUNEL staining (Fig. 6H). These findings identify HMOX1 as a critical negative regulator of the Slc11a1-high pathogenic macrophage subpopulation, essential for maintaining pulmonary homeostasis during septic stress.

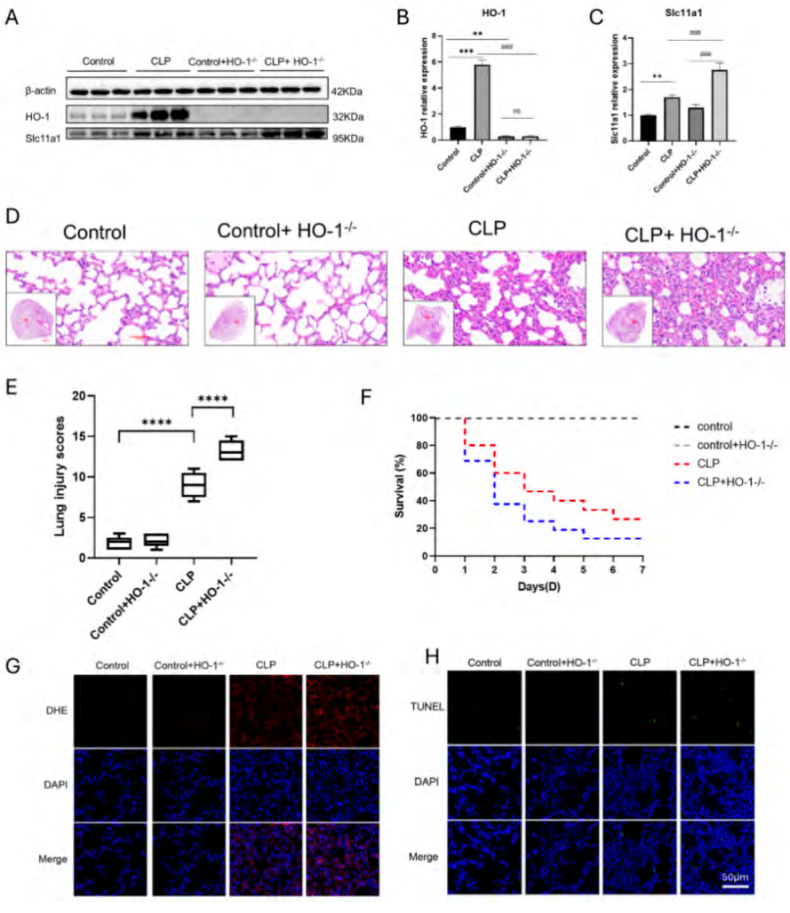


Figure 6. Genetic ablation of Hmox1 releases the inhibition on Slc11a1 and exacerbates sepsis-induced oxidative stress, apoptosis, and acute lung injury.

(A–C) Representative Western blot images (A) and relative densitometric quantification of HO-1 (B) and Slc11a1 (C) protein levels in the lung tissues of wild-type (WT) and Hmox1 knockout (HO-1) mice subjected to sham or CLP surgery. -actin was used as the loading control. (D, E) Representative hematoxylin and eosin (H&E) staining of lung tissue sections (D) and the corresponding semi-quantitative Lung Injury Score (LIS) evaluation (E). The bottom-left insets in panel D display whole-lung lobe scans indicating the regions of magnification. Statistical differences for LIS were determined using the Mann-Whitney U test. (F) Kaplan-Meier overall survival curves of the mice over a 7-day observation period post-CLP (n = 15 per group). (G, H) Representative fluorescence images assessing the pulmonary microenvironment. Panel (G) shows dihydroethidium (DHE) staining evaluating in situ reactive oxygen species (ROS) accumulation (red fluorescence). Panel (H) displays multiplex TUNEL staining evaluating parenchymal cell apoptosis (green fluorescence indicating DNA fragmentation). Nuclei were counterstained with DAPI (blue) in both assays. Scale bar = 50 μm. *(Data in bar graphs are presented as mean ± SD, n = 3. *P < 0.05, P < 0.01, P < 0.001 vs. respective control groups).

Discussion

The pathophysiology of sepsis-induced acute lung injury (ALI) is closely linked to innate immune dysregulation. While broad-spectrum immunosuppression has shown limited clinical efficacy, targeting specific hyper-inflammatory cellular subsets offers a more precise therapeutic strategy(23-25). In this study, we utilized single-cell transcriptomics to map the immune landscape of the septic lung, identifying a pathogenic macrophage subpopulation characterized by high Slc11a1 expression. Integrating computational modeling with in vivo functional assays, we demonstrated that the cytoprotective enzyme HMOX1 directly interacts with and inhibits SLC11A1, mitigating the iron-mediated oxidative stress that drives ALI progression.

Traditional in vitro binary M1/M2 macrophage polarization models often fail to capture the phenotypic plasticity present in vivo(10, 26). Our pseudotime trajectory analysis indicates that the Slc11a1-high (Mac3) subpopulation is not a terminal or exhausted state, but rather an early-responder phenotype located at the developmental root. This transcriptomic profile aligns with the acute clinical onset of Systemic Inflammatory Response Syndrome (SIRS) in sepsis, positioning Slc11a1 as a key initiator gene(27, 28).

Physiologically, Slc11a1 functions as a divalent metal transporter to restrict nutrient access for intracellular pathogens(29). During sepsis, however, its sustained upregulation contributes to metabolic dysfunction. Excessive cytosolic iron transport expands the labile iron pool, driving the Fenton reaction and promoting reactive oxygen species (ROS) accumulation(30-32). Our in vivo data position HMOX1 as a critical negative regulator of this cascade. Pharmacological HMOX1 activation attenuated Slc11a1 expression, reduced oxidative lung injury, and improved survival. Conversely, Hmox1 ablation removed this checkpoint, leading to unchecked Slc11a1 expression, exacerbated apoptosis, and increased mortality(33-35).

Molecular dynamics simulations provided a structural basis for this targeted inhibition, identifying a stable binding interface (− 47.6 kcal/mol) between HMOX1 and SLC11A1(36, 37). This direct physical interaction offers a mechanistic explanation for how HO-1 constrains Slc11a1 activity. Cross-validation with human clinical transcriptomics (GEO: GSE279452) suggests that this HMOX1/SLC11A1 regulatory axis is conserved and clinically relevant in human sepsis (38). Furthermore, HMOX1 has been reported to modulate macrophage polarization via endothelial exosomal miR-184-3p(39), adding another layer to its protective role against ALI. Collectively, these findings reinforce HMOX1 as a central node in sepsis-induced innate immune regulation.

Targeting specific macrophage subsets aligns with our ongoing research into precision immunometabolism in critical illness. We previously found that nicotinamide mononucleotide and alveolar epithelial-derived interleukin-17D alleviate endotoxin-induced ALI by modulating macrophage polarization and the Nrf2 pathway, respectively(40). Additionally, our work demonstrating that dexmedetomidine preserves mitochondrial dynamics via HIF-1α/HO-1 signaling highlights the interplay between HMOX1 and mitochondrial quality control (41). (Fig. 7)

In the broader context of anesthesiology and perioperative medicine, precision immunomodulation is gaining significant clinical traction. The identification of specific immune targets, such as plasmacytoid dendritic cells (pDCs)(42), alongside the immunomodulatory effects of perioperative interventions—including anesthetics—on inflammatory cell death(43, 44) and systemic neuroinflammation(45), emphasize the necessity for targeted, cell-specific therapies to improve critical care outcomes.

Finally, several limitations should be noted. Although our computational and in vivo data support the HMOX1-mediated inhibition of SLC11A1, the exact molecular mechanism remains to be fully elucidated. It is unclear whether HMOX1 promotes SLC11A1 degradation via direct protein-protein interactionor if its metabolic byproducts，such as carbon monoxide or biliverdin，exert transcriptional repression on the Slc11a1 promoter. Future studies utilizing Co-IP or ChIP-seq are required to resolve this. Additionally, in vivo lineage tracing is needed to determine whether the Slc11a1-high subpopulation originates from resident alveolar macrophages or recruited monocyte-derived macrophages.

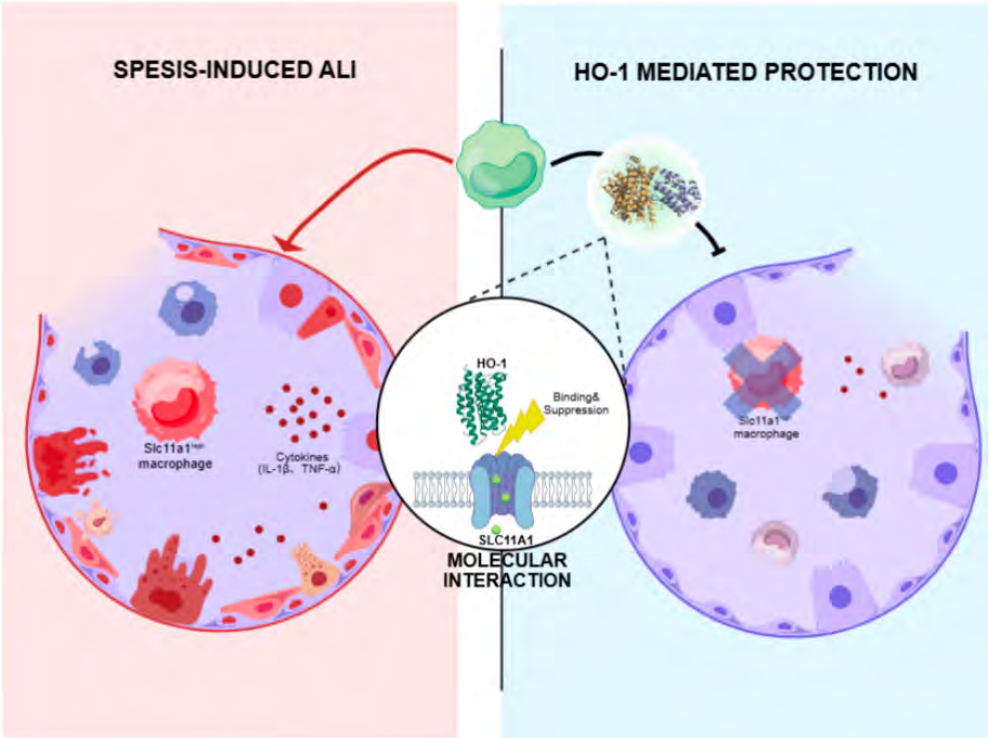


Figure 7. Proposed mechanistic model of HMOX1-mediated regulation of Slc11a1-high macrophage-driven acute lung injury.

HMOX1 confers pulmonary protection by specifically targeting and inhibiting the differentiation and expansion of the pathogenic macrophage subpopulation. This suppression effectively neutralizes downstream ROS accumulation and mitigates cellular apoptosis, thereby preserving lung tissue integrity. Consequently, the HMOX1/SLC11A1 axis represents a promising, precision-targeted therapeutic strategy for mitigating severe lung injury in critically ill patients.

Conclusions

This study challenges classical macrophage polarization paradigms by identifying a specific, early-acting Slc11a1-high pathogenic subpopulation that is a primary driver of sepsis-induced ALI. We establish that HMOX1 affords vital pulmonary protection by specifically targeting and inhibiting the differentiation and expansion of this subpopulation, effectively neutralizing downstream ROS accumulation and apoptosis. Modulating the HMOX1/SLC11A1 axis offers a highly promising, precision-targeted therapeutic intervention for severe lung injury in the critically ill.

References

1. Singer, M., Deutschman, C.S., Seymour, C.W., Shankar-Hari, M., Annane, D., Bauer, M. et al. (2016) The Third International Consensus Definitions for Sepsis and Septic Shock (Sepsis-3). Jama. 315, 801-810. 10.1001/jama.2016.0287

2. Matthay, M.A., Zemans, R.L., Zimmerman, G.A., Arabi, Y.M., Beitler, J.R., Mercat, A. et al. (2019) Acute respiratory distress syndrome. Nat Rev Dis Primers. 5, 18. 10.1038/s41572-019-0069-0

3. Rudd, K.E., Johnson, S.C., Agesa, K.M., Shackelford, K.A., Tsoi, D., Kievlan, D.R. et al. (2020) Global, regional, and national sepsis incidence and mortality, 1990-2017: analysis for the Global Burden of Disease Study. Lancet. 395, 200-211. 10.1016/s0140-

6736(19)32989-7

4. Meyer, N.J., Gattinoni, L.and Calfee, C.S. (2021) Acute respiratory distress syndrome. Lancet. 398, 622-637. 10.1016/s0140-6736(21)00439-6

5. van der Poll, T., van de Veerdonk, F.L., Scicluna, B.P.and Netea, M.G. (2017) The immunopathology of sepsis and potential therapeutic targets. Nat Rev Immunol. 17, 407-420. 10.1038/nri.2017.36

6. Hotchkiss, R.S., Monneret, G.and Payen, D. (2013) Sepsis-induced immunosuppression: from cellular dysfunctions to immunotherapy. Nat Rev Immunol. 13, 862-874. 10.1038/nri3552

7. Malainou, C., Abdin, S.M., Lachmann, N., Matt, U.and Herold, S. (2023) Alveolar macrophages in tissue homeostasis, inflammation, and infection: evolving concepts of therapeutic targeting. J Clin Invest. 133. 10.1172/jci170501

8. Sica, A.and Mantovani, A. (2012) Macrophage plasticity and polarization: in vivo veritas. J Clin Invest. 122, 787-795. 10.1172/jci59643

9. Murray, P.J., Allen, J.E., Biswas, S.K., Fisher, E.A., Gilroy, D.W., Goerdt, S. et al. (2014) Macrophage activation and polarization: nomenclature and experimental guidelines. Immunity. 41, 14-20. 10.1016/j.immuni.2014.06.008

10. Strizova, Z., Benesova, I., Bartolini, R., Novysedlak, R., Cecrdlova, E., Foley, L.K. et al. (2023) M1/M2 macrophages and their overlaps - myth or reality? Clin Sci (Lond). 137, 1067-1093. 10.1042/cs20220531

11. Guilliams, M., Ginhoux, F., Jakubzick, C., Naik, S.H., Onai, N., Schraml, B.U. et al. (2014) Dendritic cells, monocytes and macrophages: a unified nomenclature based on ontogeny. Nat Rev Immunol. 14, 571-578. 10.1038/nri3712

12. Jovic, D., Liang, X., Zeng, H., Lin, L., Xu, F.and Luo, Y. (2022) Single-cell RNA sequencing technologies and applications: A brief overview. Clin Transl Med. 12, e694. 10.1002/ctm2.694

13. Reyfman, P.A., Walter, J.M., Joshi, N., Anekalla, K.R., McQuattie-Pimentel, A.C., Chiu, S. et al. (2019) Single-Cell Transcriptomic Analysis of Human Lung Provides Insights into the Pathobiology of Pulmonary Fibrosis. Am J Respir Crit Care Med. 199, 1517-1536. 10.1164/rccm.201712-2410OC

14. Liao, M., Liu, Y., Yuan, J., Wen, Y., Xu, G., Zhao, J. et al. (2020) Single-cell landscape of bronchoalveolar immune cells in patients with COVID-19. Nat Med. 26, 842-844. 10.1038/s41591-020-0901-9

15. Wessling-Resnick, M. (2015) Nramp1 and Other Transporters Involved in Metal Withholding during Infection. J Biol Chem. 290, 18984-18990. 10.1074/jbc.R115.643973

16. Peracino, B., Wagner, C., Balest, A., Balbo, A., Pergolizzi, B., Noegel, A.A. et al. (2006) Function and mechanism of action of Dictyostelium Nramp1 (Slc11a1) in bacterial infection. Traffic. 7, 22-38. 10.1111/j.1600-0854.2005.00356.x

17. Lafuse, W.P., Alvarez, G.R.and Zwilling, B.S. (2000) Regulation of Nramp1 mRNA stability by oxidants and protein kinase C in RAW264.7 macrophages expressing Nramp1(Gly169). Biochem J. 351 Pt 3, 687-696.

18. Gozzelino, R., Jeney, V.and Soares, M.P. (2010) Mechanisms of cell protection by heme oxygenase-1. Annu Rev Pharmacol Toxicol. 50, 323-354. 10.1146/annurev.pharmtox.010909.105600

19. Wu, X., Wu, L., Wu, Y., Chen, W., Chen, J., Gong, L. et al. (2023) Heme oxygenase-1 ameliorates endotoxin-induced acute lung injury by modulating macrophage polarization via inhibiting TXNIP/NLRP3 inflammasome activation. Free Radic Biol Med. 194, 12-22. 10.1016/j.freeradbiomed.2022.11.032

20. Chen, W., Zhang, Y., Chen, J., Dong, S., Wu, X., Wu, Y. et al. (2025) Heme Oxygenase-1 Modulates Macrophage Polarization Through Endothelial Exosomal miR-184-3p and Reduces Sepsis-Induce Lung Injury. Int J Nanomedicine. 20, 5039-5057. 10.2147/ijn.S506830

21. Kong, C., Zhang, Y., Li, X., Ren, G., Guo, C., Li, M. et al. (2026) Heme oxygenase-1 attenuates sepsis-associated acute lung injury

by suppressing the CREB3/ARF4 signaling pathway to mitigate Golgi stress in macrophages. Free Radic Biol Med. 251, 91-107. 10.1016/j.freeradbiomed.2026.04.007

22. Yang, J., Zhang, L., An, H., Guan, X., Zhang, Y., Zhang, J. et al. (2026) HO-1/Nrf2 activation orchestrates protection in sepsis-induced lung injury by suppressing CCR2(hi) monocyte recruitment and MAPK-driven inflammation. Free Radic Biol Med. 247, 122-138. 10.1016/j.freeradbiomed.2026.02.004

23. Li, W., Li, D., Chen, Y., Abudou, H., Wang, H., Cai, J. et al. (2022) Classic Signaling Pathways in Alveolar Injury and Repair Involved in Sepsis-Induced ALI/ARDS: New Research Progress and Prospect. Dis Markers. 2022, 6362344. 10.1155/2022/6362344

24. Luo, F., Jiang, W., Xu, Y., Liu, X.M., Wang, W., Zhang, W. et al. (2020) The Mechanisms Involved in Mesenchymal Stem Cell Alleviation of Sepsis-Induced Acute Lung Injury in Mice: A Pilot Study. Curr Ther Res Clin Exp. 93, 100593. 10.1016/j.curtheres.2020.100593

25. Zou, S., Bai, J., Liang, C., Yang, J.and Xiao, J. (2025) Plasmacytoid dendritic cells in sepsis-associated acute lung injury: a potential therapeutic target. Anesthesiology and Perioperative Science. 3. 10.1007/s44254-025-00121-6

26. Rasmussen, K.H.and Hawkins, C.L. (2022) Role of macrophage extracellular traps in innate immunity and inflammatory disease. Biochem Soc Trans. 50, 21-32. 10.1042/bst20210962

27. Shi, Y., Wan, J., Zhang, X., Liang, T.and Yin, Y. (2024) scCRT: a contrastive-based dimensionality reduction model for scRNA-seq trajectory inference. Brief Bioinform. 25. 10.1093/bib/bbae204

28. van der Poll, T.and Meijers, J.C. (2010) Systemic inflammatory response syndrome and compensatory anti-inflammatory response syndrome in sepsis. J Innate Immun. 2, 379-380. 10.1159/000318190

29. Mulero, V., Searle, S., Blackwell, J.M.and Brock, J.H. (2002) Solute carrier 11a1 (Slc11a1; formerly Nramp1) regulates metabolism and release of iron acquired by phagocytic, but not transferrin-receptor-mediated, iron uptake. Biochem J. 363, 89-94. 10.1042/0264-6021:3630089

30. Nairz, M., Fritsche, G., Crouch, M.L., Barton, H.C., Fang, F.C.and Weiss, G. (2009) Slc11a1 limits intracellular growth of Salmonella enterica sv. Typhimurium by promoting macrophage immune effector functions and impairing bacterial iron acquisition. Cell Microbiol. 11, 1365-1381. 10.1111/j.1462-5822.2009.01337.x

31. Awomoyi, A.A. (2007) The human solute carrier family 11 member 1 protein (SLC11A1): linking infections, autoimmunity and cancer? FEMS Immunol Med Microbiol. 49, 324-329. 10.1111/j.1574-695X.2007.00231.x

32. Blackwell, J.M., Goswami, T., Evans, C.A., Sibthorpe, D., Papo, N., White, J.K. et al. (2001) SLC11A1 (formerly NRAMP1) and disease resistance. Cell Microbiol. 3, 773-784. 10.1046/j.1462-5822.2001.00150.x

33. Nakajima, M., Matsuyama, M., Kawaguchi, M., Kiwamoto, T., Matsuno, Y., Morishima, Y. et al. (2021) Nrf2 Regulates Granuloma Formation and Macrophage Activation during Mycobacterium avium Infection via Mediating Nramp1 and HO-1 Expressions. mBio. 12. 10.1128/mBio.01947-20

34. Poss, K.D.and Tonegawa, S. (1997) Heme oxygenase 1 is required for mammalian iron reutilization. Proc Natl Acad Sci U S A. 94, 10919-10924. 10.1073/pnas.94.20.10919

35. Poss, K.D.and Tonegawa, S. (1997) Reduced stress defense in heme oxygenase 1-deficient cells. Proc Natl Acad Sci U S A. 94, 10925-10930. 10.1073/pnas.94.20.10925

36. Liu, Z., Sun, Y., Zhen, H.and Nie, C. (2022) Network Pharmacology Integrated with Transcriptomics Deciphered the Potential Mechanism of Codonopsis pilosula against Hepatocellular Carcinoma. Evid Based Complement Alternat Med. 2022, 1340194. 10.1155/2022/1340194

37. Zhao, J., Tian, S., Lu, D., Yang, J., Zeng, H., Zhang, F. et al. (2021) Systems pharmacological study illustrates the immune regulation, anti-infection, anti-inflammation, and multi-organ protection mechanism of Qing-Fei-Pai-Du decoction in the

treatment of COVID-19. Phytomedicine. 85, 153315. 10.1016/j.phymed.2020.153315

38. Tang, X., Liu, J., Yao, S., Zheng, J., Gong, X.and Xiao, B. (2022) Ferulic acid alleviates alveolar epithelial barrier dysfunction in sepsis-induced acute lung injury by activating the Nrf2/HO-1 pathway and inhibiting ferroptosis. Pharm Biol. 60, 2286-2294. 10.1080/13880209.2022.2147549

39. Li, Y., Shi, J., Yu, T., Piao, M., Tan, J., Miao, Y. et al. (2025) FPR1-dependent Pro-inflammatory Ccl4(high) monocytes/macrophages drive and predict sepsis-induced acute lung injury. Respir Res. 26, 308. 10.1186/s12931-025-03385-5

40. He, S., Jiang, X., Yang, J., Wu, Y., Shi, J., Wu, X. et al. (2024) Nicotinamide mononucleotide alleviates endotoxin-induced acute lung injury by modulating macrophage polarization via the SIRT1/NF-κB pathway. Pharm Biol. 62, 22-32. 10.1080/13880209.2023.2292256

41. Dong, S., Liu, S., Gao, Q., Shi, J., Song, K., Wu, Y. et al. (2023) Interleukin-17D produced by alveolar epithelial type II cells alleviates LPS-induced acute lung injury via the Nrf2 pathway. Clin Sci (Lond). 137, 1499-1512. 10.1042/cs20230354

42. Shi, J., Yu, T., Song, K., Du, S., He, S., Hu, X. et al. (2021) Dexmedetomidine ameliorates endotoxin-induced acute lung injury in vivo and in vitro by preserving mitochondrial dynamic equilibrium through the HIF-1a/HO-1 signaling pathway. Redox Biol. 41, 101954. 10.1016/j.redox.2021.101954

43. Fagundes, T.R., Coradi, C., Sotomayor, M.R., Campos, A.G.H., da Silva, L.C.F., Ferneda, H.A. et al. (2025) Mechanisms of anesthetic-induced immune dysregulation. Anesthesiology and Perioperative Science. 3. 10.1007/s44254-025-00117-2

44. Long, M., Hu, Z., Long, F., Chen, Y., Liu, L.and Wang, M. (2025) The capsaicin receptor TRPV1 reduces sepsis-associated brain injury in mice by inhibiting pyroptosis. Anesthesiology and Perioperative Science. 3. 10.1007/s44254-025-00115-4

45. Thedim, M.and Vacas, S. (2025) Anesthetic sensitivity and resilience in the aging brain: implications for perioperative neurocognitive disorders. Anesthesiology and Perioperative Science. 3. 10.1007/s44254-025-00094-6

hucMSCs alleviate LPS-induced endothelial glycocalyx damage by secreting Cxcl12 to activate CXCR4

姓名：崔金锋，王涛，王晓芝
单位：山东医药大学附属医院

Abstract

Acute respiratory distress syndrome (ARDS) has a high clinical mortality rate and continues to draw research attention regarding its mechanisms and potential treatments. Disruption of the endothelial barrier is a primary pathological feature, and glycocalyx degradation is a key factor contributing to this disruption. hucMSCs exhibit strong anti-inflammatory and immunomodulatory effects, making their application in ARDS treatment an area of increasing interest. Proteomic screening identified Cxcl12 as a protein secreted by hucMSCs. In male C57 mice and cell models, LPS was used to induce injury, followed by interventions with hucMSCs or hucMSCs with silenced Cxcl12 to assess glycocalyx-related proteins SDC-1, HS, and the repair marker EXT-1. To evaluate downstream signaling, the CXCR4 receptor was inhibited and related indicators were examined. Silencing Cxcl12 reduced the therapeutic effect of hucMSCs on LPS-induced glycocalyx damage. Inhibition of CXCR4 also weakened the effect of Cxcl12. These findings indicate that hucMSCs alleviate LPS-induced glycocalyx damage in pulmonary vascular endothelial cells by secreting Cxcl12, which activates the downstream receptor CXCR4, providing a therapeutic effect for ARDS.

Introduction

Sepsis is an inflammatory disease triggered by acute infection and can lead to multiple organ dysfunction and life-threatening conditions. It is a common cause of acute respiratory distress syndrome (ARDS). The primary pathological mechanism of ARDS is the disruption of the vascular endothelial barrier, which increases lung tissue permeability and leads to pulmonary edema. Clinical treatment relies mainly on mechanical ventilation support; however, this approach requires advanced medical resources and is associated with complications, such as respiratory tract infections. Consequently, investigating the pathogenesis of sepsis-induced ARDS and identifying appropriate treatment strategies have emerged as critical issues in contemporary clinical and basic research. Establishing an animal model of acute lung injury (ALI) is a commonly utilized approach to study this condition.

The glycocalyx is essential for maintaining the endothelial barrier and enables material exchange at the endothelial surface. Damage to the structure and function of the endothelial glycocalyx is a key factor contributing to the heightened permeability of pulmonary capillary endothelium. The glycocalyx consists mainly of negatively charged proteins and polysaccharide complexes; its key components include the core protein syndecan-1 (SDC-1) and its heparan sulfate (HS) side chain. Because endothelial cells experience continuous shear stress, enzymes such as heparinase (HPA) and hyaluronidase (HAase) maintain the glycocalyx in a dynamic balance between degradation and repair. Exostosin-1 (EXT-1), a key enzyme in the synthesis of HS, plays an essential role in the glycocalyx repair process.

hucMSCs, a type of pluripotent stem cell, have attracted considerable interest for their therapeutic potential. Their wide availability, ease of expansion, low immunogenicity, and strong tissue repair capacity contribute to their suitability for translational research. hucMSCs demonstrate self-renewal and multidirectional differentiation, and they release cytokines, growth factors, and exosomes through paracrine activity. These factors play a crucial role in tissue repair, immune regulation, and anti-inflammatory responses[1, 2]. Studies have demonstrated that hucMSCs and their derived exosomes (hucMSC-Exos) exhibit remarkable therapeutic effects in various disease models, including pulmonary fibrosis, acute kidney injury, myocardial infarction, and skin injury. Furthermore, hucMSCs can migrate to the site of injury, positioning them as an ideal vehicle for precision therapy.

Interest in the CXC chemokine family in ARDS has increased, particularly regarding the dual roles of Cxcl12 (also known as stromal cell-derived factor-1, SDF-1) in inflammation and repair. Cxcl12 binds to CXCR4 to mediate inflammatory cell chemotaxis and plays a key role in tissue repair and regeneration. Its effects on endothelial cells and the activation of downstream signaling pathways support endothelial cell survival and function, contributing to restoration of the endothelial barrier.

To investigate the molecular mechanisms underlying the therapeutic effects of hucMSCs in ARDS, we established an ALI mouse model by intraperitoneal injection of lipopolysaccharide (LPS) followed by tail vein administration of hucMSCs. Proteomic analysis

of lung tissue after hucMSC intervention identified Cxcl12 as a differentially expressed protein, consistent with previous findings. By generating hucMSCs with silenced Cxcl12 through lentiviral transfection, we evalted the role of Cxcl12 in the treatment of ARDS with hucMSCs in both in vivo and in vitro experiments. Furthermore, we investigated whether Cxcl12 ameliorates LPS-induced endothelial glycocalyx damage and promotes glycocalyx repair through its downstream receptor CXCR4.

Materials and Methods

In vivo construction of a mouse model of ALI

Mice were randomly assigned to six groups (n = 6 per group): Control, LPS, LPS+hucMSCs, LPS+shCxcl12 hucMSCs, LPS+NC hucMSCs, hucMSCs. Each mouse received 100 μL of LPS solution intraperitoneally at 20 mg/kg. Two hours later, 100 μL of hucMSCs (2×10^5 cells/mouse) was administered via tail vein injection, with random selection of animals during handling to reduce bias. At 8 hours after LPS injection, the mice were anesthetized with tribromoethanol, and lung tissue and serum were collected and stored at − 80° C.

Histopathology

After anesthesia, pulmonary circulation was perfused, and lung tissues were removed and fixed in 4% paraformaldehyde for at least 48 hours. Samples were dehydrated, embedded in paraffin, and cut into 5-μm sections (Novland, Shanghai, China). Hematoxylin and eosin (HE) staining was performed, and lung injury was scored under an optical microscope (Olympus Optics, Tokyo, Japan). Six random high-power fields were evaluated, and the mean score represented each sample.

In vivo fluorescence imaging of hucMSCs

hucMSCs were transfected with Luc-tagged lentivirus and selected using puromycin. Mice were assigned to three groups (n = 3 per group): Control, LPS+hucMSCs, and hucMSCs. Two hours after LPS injection, Luc-labeled hucMSCs were administered via tail vein. At 6, 12, and 24 hours after injection, potassium luciferin was administered intraperitoneally, and hucMSC distribution was visualized using the AniView100 Pro multimodal in vivo imaging system.

The pulmonary vascular permeability was evaluated by injecting FITC- albumin

For fluorescence imaging, mice were randomly assigned to six groups (n = 6 per group): Control, LPS, LPS+hucMSCs, LPS+shCxcl12 hucMSCs, LPS+NC hucMSCs, hucMSCs. The AniView100 Pro system was pre-cooled. Animals were anesthetized, and the thoracic cavity was exposed. After complete perfusion and lung extraction, lung tissues were rinsed, dried, placed on black background paper, and imaged using the FITC probe.

Cell culture

hucMSCs were sourced from Shandong Qilu Stem Cell Engineering Co., Ltd, and human microvascular endothelial cells (HULEC-5a) were purchased from the American Type Culture Collection (ATCC) . The cells were seeded in a 25 cm^2 cell culture flask and cultured in a sterile incubator at 37 ° C with 5% CO_2. All hucMSCs utilized in the animal experiments were maintained within three passages. Based on cell culture observations, hucMSCs exhibit slower division and growth after the third passage.The hucMSCs counted using a cell counter (Halo counter).

In vitro construction of ALI cell model

Transwell co-cultured endothelial cells (lower wells) with hucMSCs/shCxcl12-hucMSCs (upper inserts). After LPS stimulation for 6 h, endothelial proteins were harvested. For supplementary assays, recombinant Cxcl12 or AMD3100 was added alongside LPS before protein collection at 6 h.

Western blot verification

Total proteins were extracted from lung tissues and cells using RIPA buffer. Protein concentrations were determined using the Enhanced BCA Assay Kit. Initially, 20 μg of the sample was added to the respective wells. The samples were subsequently separated by 10% SDS-PAGE gel electrophoresis. Following this, the separated proteins were transferred to a PVDF membrane,

blocked with TBST containing 5% skim milk, and incubated at room temperature for 2 hours. The membrane was then incubated with primary antibodies, including anti-SDC-1, HS, EXT-1, Cxcl12, CXCR4, and GAPDH, overnight at 4 ° C. Finally, the membrane was treated with a horseradish peroxidase-conjugated secondary antibody at room temperature for 1 hour, and the protein bands were visualized using a chemiluminescence kit. Density analysis was conducted using ImageJ software.

Immunofluorescence staining

Endothelial cells (1×10^5/well) were seeded into 24-well plates with pre-placed slides. After washing with PBS, cells were fixed in 4% paraformaldehyde for 30 minutes, blocked with goat serum for 30 minutes, and incubated with primary antibodies overnight at 4° C. After washing, cells were incubated with fluorescent secondary antibodies for 1 hour at room temperature. DAPI staining solution (200 µL) was added for 5 minutes. Slides were mounted with anti-fade medium and imaged using a fluorescence microscope.

FITC-albumin permeability detection

HULEC-5a cells (15,000 cells/well) were seeded into the upper chambers of a 24-well Transwell plate. hucMSCs or shCxcl12 hucMSCs (20,000 cells/well) were seeded into the lower wells for co-culture. After 6 hours of LPS treatment, medium in the Transwell chamber was replaced. FITC-albumin (1 mg/mL) was added under light-protected conditions to the upper chamber and incubated for 30 minutes. Then, 100 µL of medium from the upper and lower chambers was transferred to a 96-well plate. Absorbance at 490 nm and 525 nm was measured, and permeability was assessed by the lower-to-upper chamber absorbance ratio.

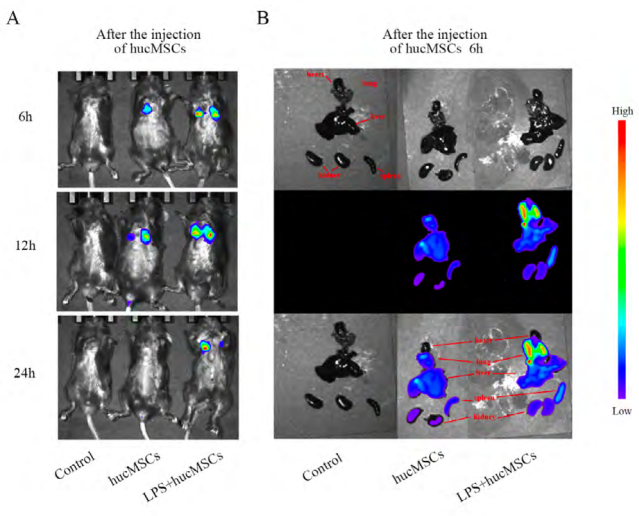
Transendothelial electrical resistance (TEER)

Co-culture was conducted as previously described. LPS was added for 6 hours. The two electrodes of the Michel® ERS-2 resistance meter were placed above and below the filter membrane. Baseline (blank) resistance was measured, and TEER was calculated as: (Ω/cm^2) = (measured resistance − blank resistance) × effective membrane area.

Results

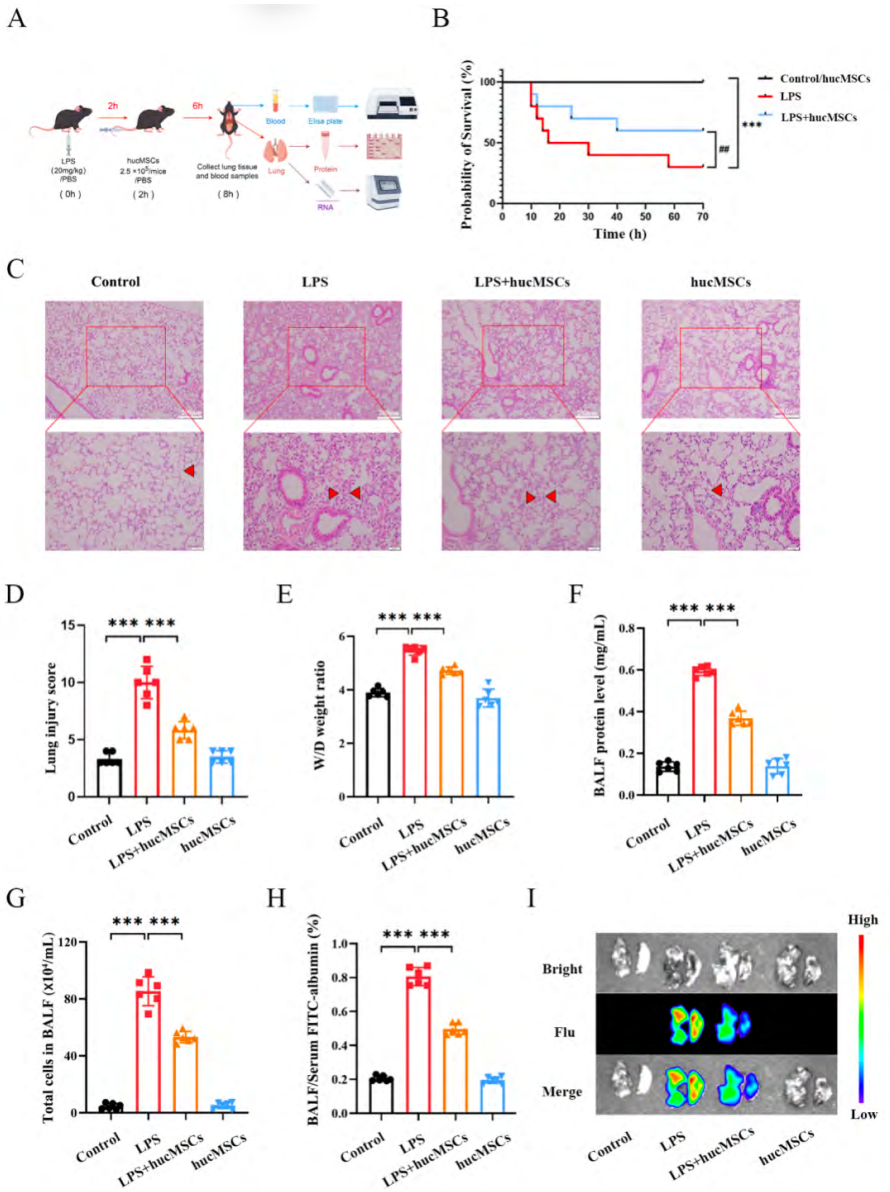
1. Localization of hucMSCs in normal mice and septic mice

To examine the distribution of hucMSCs after tail vein injection and to assess their homing to the lungs following injury, an LPS-ALI model was established through intraperitoneal LPS administration. hucMSCs were labeled with a Luc-tagged lentiviral vector and then injected into normal mice and LPS-ALI mice, while control mice received saline. Fluorescence imaging of whole-body distribution was performed at 6, 12, and 24 hours after injection (Figure 1A). Organs were also collected for imaging at the 6-hour time point (Figure 1B). The results showed that intravenously administered hucMSCs localized to the lung tissue in normal mice. The fluorescence intensity in the lungs of LPS-ALI mice was notably higher than in normal mice, indicating that hucMSCs migrate to and accumulate in injured lung tissue.



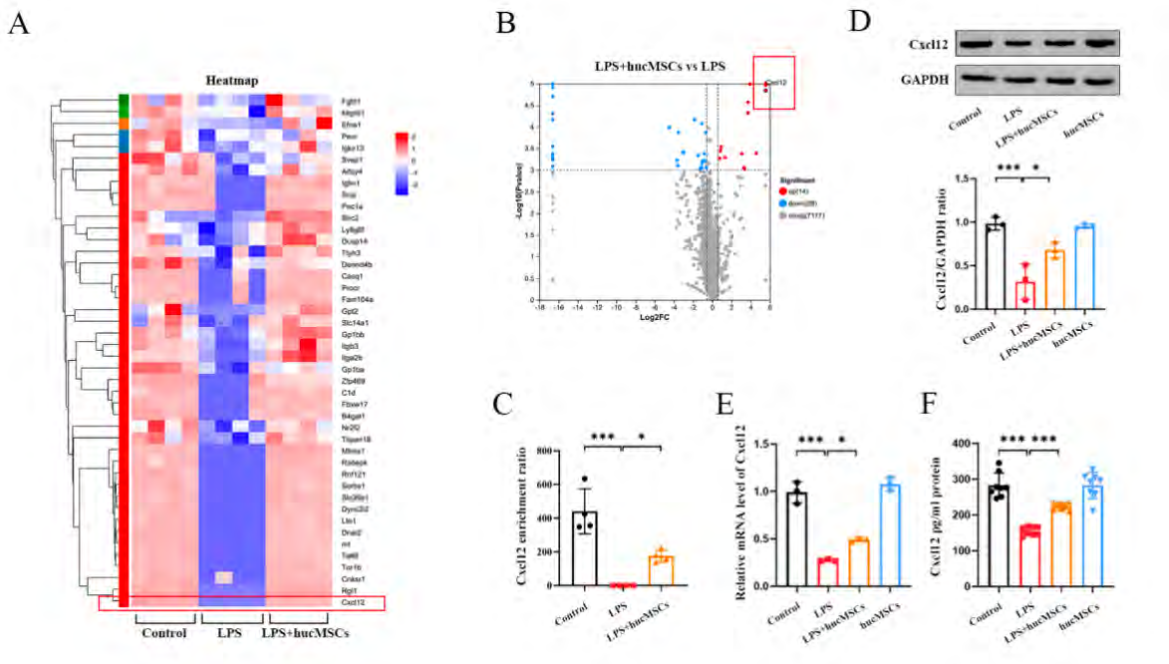
2.Injection of hucMSCs improves ALI

A mouse model of acute lung injury was established to investigate the mechanisms underlying ARDS and explore potential therapeutic approaches. The ALI model was induced by intraperitoneal LPS injection, followed by tail vein delivery of hucMSCs two hours later. After six additional hours, blood and lung tissue were collected for analysis (Figure 2A). The survival rate improved in LPS-ALI mice that received hucMSCs (Figure 2B). Histopathology showed that LPS caused marked structural disruption, including blurred alveolar architecture, interstitial edema, congestion, and increased tissue debris. These abnormalities were reduced after hucMSC treatment (Figure 2C-D). The lung wet/dry ratio, total cell count, and protein content in BALF were also decreased (Figure 2E-G). FITC-albumin permeability analysis further confirmed that hucMSCs lowered LPS-induced pulmonary vascular permeability (Figure 2H-I).



3.Proteomic analysis suggests Cxcl12 as a key protein

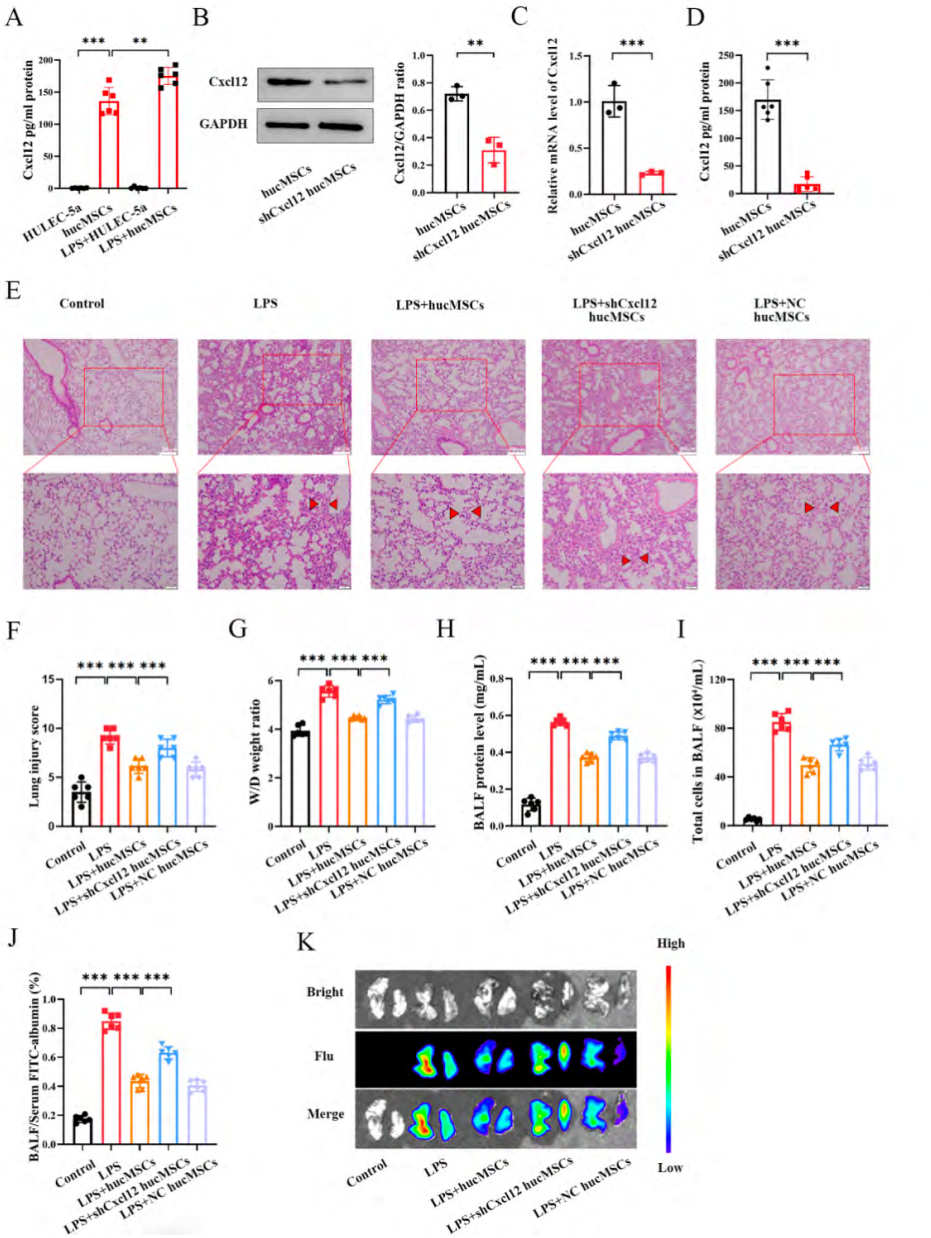
Proteomic analysis revealed a decrease in the expression of Cxcl12 in lung tissues following LPS injection, with an increase in expression observed after hucMSCs treatment (Figure 3A-C). To validate the accuracy of the proteomic findings, this study employed Western blot and qRT-PCR to assess Cxcl12 expression in lung tissues, and the results were consistent with those obtained from the proteomic analysis (Figure 3D-E). Additionally, changes in Cxcl12 levels in mouse serum were detected using an ELISA kit, demonstrating a trend that aligns with the findings in lung tissues (Figure 3F).



4.Cxcl12 plays a crucial role in the hucMSCs-mediated amelioration of LPS-ALI

Cxcl12 is known to be one of the secreted proteins of hucMSCs. ELISA analysis showed that hucMSCs secreted higher amounts of Cxcl12 than HULEC-5a cells, and secretion increased after LPS stimulation (Figure 4A). Lentiviral transfection was used to silence Cxcl12 in hucMSCs, and silencing efficiency was verified by Western blot, qRT-PCR, and ELISA (Figure 4B-D).

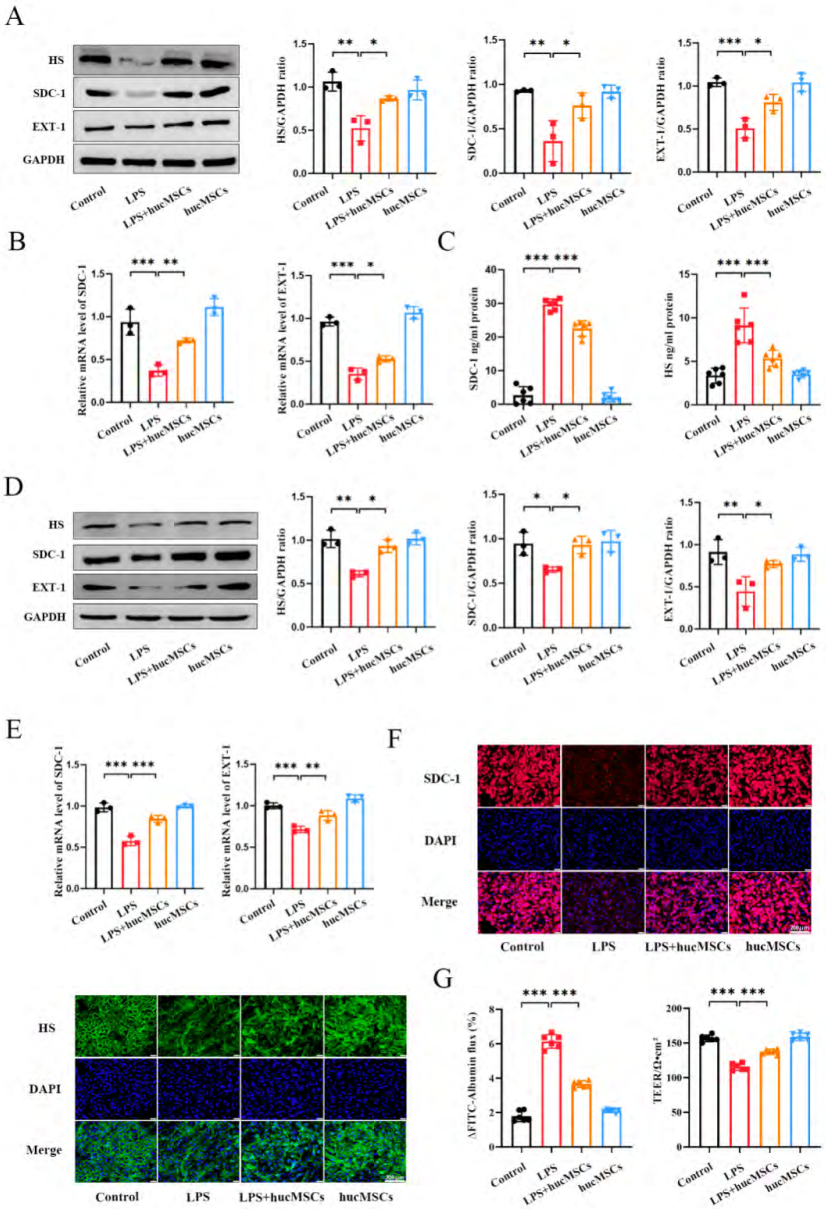
To determine the role of Cxcl12 in vivo, shCxcl12 hucMSCs were injected into LPS-ALI mice. Compared with mice receiving normal hucMSCs, the Cxcl12-silenced group showed more severe pulmonary edema and septal damage, a higher wet/dry ratio, and increased cell and protein levels in BALF (Figure 4E-I). FITC-albumin permeability also increased (Figure 4J-K). These findings indicate that Cxcl12 contributes to the ability of hucMSCs to reduce lung tissue permeability and alleviate lung injury.



5.hucMSCs ameliorate LPS-induced endothelial glycocalyx damage

This study examined the effect of hucMSCs delivered via tail vein injection on the endothelial glycocalyx in mouse lung tissue. Western blot and qRT-PCR analyses were used to measure glycocalyx-related proteins, including HS, SDC-1, and EXT-1, the key enzyme responsible for HS synthesis. LPS-ALI mice showed reduced expression of HS, SDC-1, and EXT-1, whereas hucMSC treatment increased their expression (Figure 5A-B). ELISA results further demonstrated that hucMSCs decreased levels of free SDC-1 and HS in serum (Figure 5C).

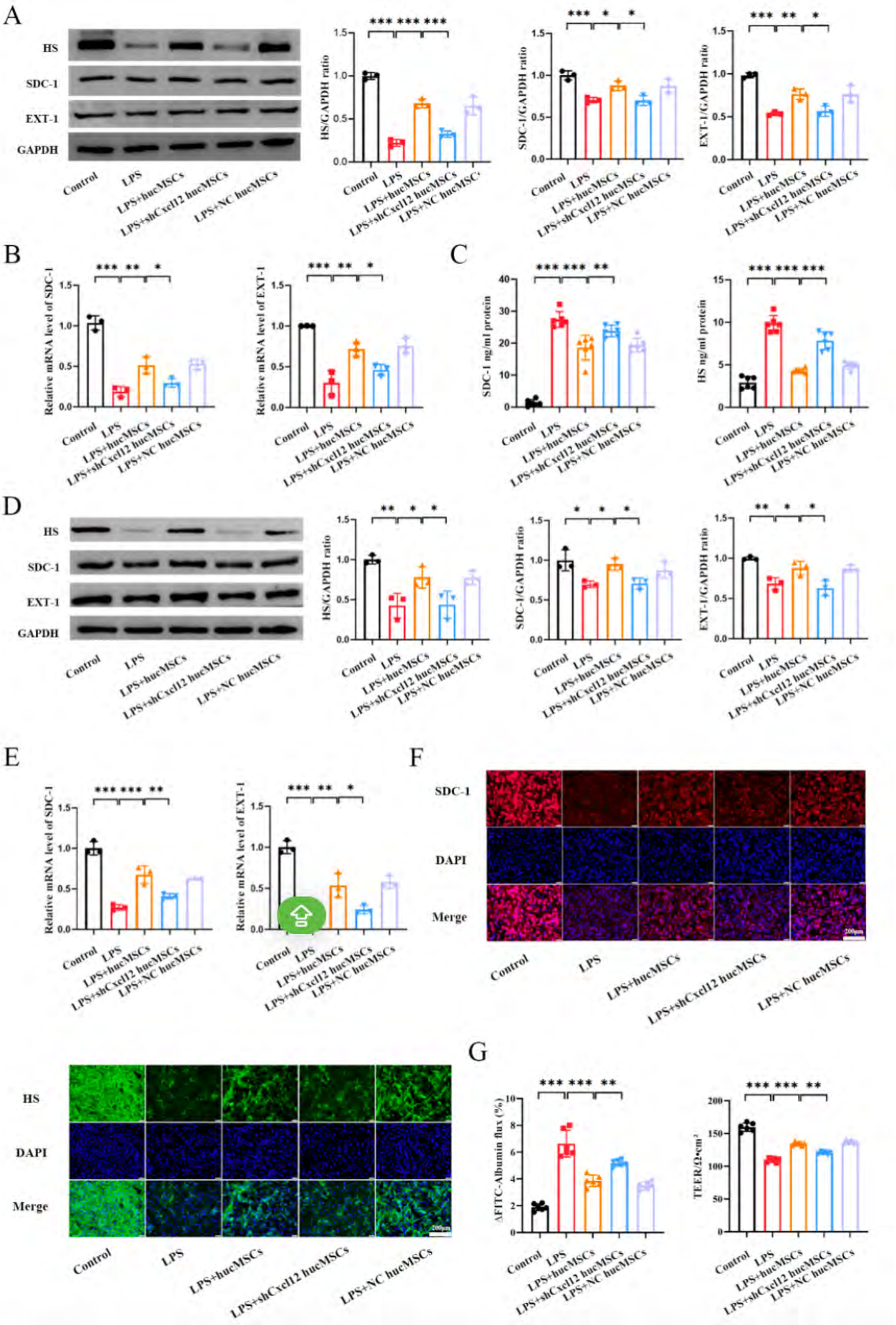
To determine whether hucMSCs exert similar effects in vitro, a co-culture model of endothelial cells and hucMSCs was established, with LPS added to induce inflammatory injury (Supplementary Figure 2). Western blot and qRT-PCR analyses showed that LPS reduced HS, SDC-1, and EXT-1 expression in endothelial cells, while co-culture with hucMSCs restored their expression (Figure 5D-E). Immunofluorescence staining demonstrated that LPS caused shedding of SDC-1 and HS from the endothelial surface; this effect was reduced after co-culture with hucMSCs (Figure 5F). FITC–albumin permeability and TEER assays confirmed that hucMSC co-culture reduced the LPS-induced increase in endothelial permeability (Figure 5G). These findings indicate that hucMSCs ameliorate LPS-induced endothelial glycocalyx damage, enhance EXT-1 expression, promote glycocalyx repair, and reduce endothelial permeability.



6.Cxcl12 is a crucial protein for hucMSCs in ameliorating LPS-induced endothelial glycocalyx damage

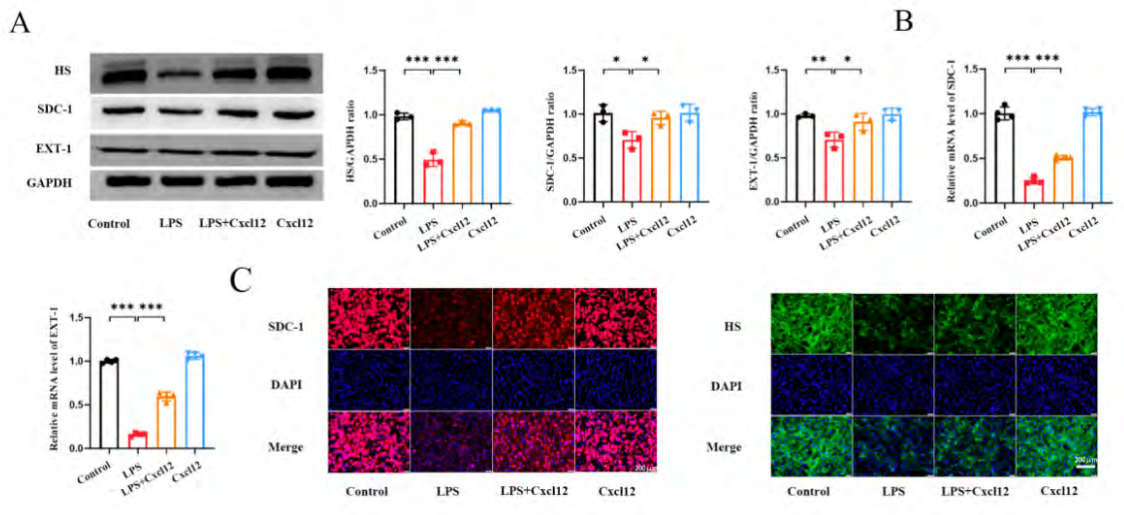
The contribution of Cxcl12 to the effect of hucMSCs on the endothelial glycocalyx in LPS-ALI mice was assessed by injecting shCxcl12 hucMSCs via the tail vein. Western blot and qRT-PCR showed that HS, SDC-1, and EXT-1 were decreased in LPS-ALI lung tissue, increased after hucMSC injection, and then reduced again when Cxcl12-silenced hucMSCs were administered (Figure 6A-B). ELISA showed increased serum levels of free SDC-1 and HS in mice treated with shCxcl12 hucMSCs compared with mice receiving hucMSCs (Figure 6C).

To confirm these findings in a cellular model, endothelial cells were co-cultured with shCxcl12-hucMSCs and then exposed to LPS. Western blot and qRT-PCR showed that HS, SDC-1, and EXT-1 decreased after LPS stimulation, increased after co-culture with hucMSCs, and decreased again when co-cultured with shCxcl12-hucMSCs (Figure 6D-E). Immunofluorescence analysis showed that LPS increased the shedding of SDC-1 and HS from the endothelial surface, whereas hucMSC co-culture reduced this effect. Co-culture with shCxcl12 hucMSCs reduced SDC-1 and HS retention to a lesser extent than co-culture with normal hucMSCs (Figure 6F). FITC-albumin permeability and TEER measurements showed that endothelial permeability increased after co-culture with shCxcl12-hucMSCs (Figure 6G). These results demonstrate that hucMSCs reduce LPS-induced glycocalyx injury and promote glycocalyx repair through secretion of Cxcl12.


A
HS
SDC-1
EXT-1
GAPDH
HS/GAPDH ratio
SDC-1/GAPDH ratio
EXT-1/GAPDH ratio
B
Relative mRNA level of SDC-1
Relative mRNA level of EXT-1
C
SDC-1 ng/ml protein
HS ng/ml protein
D
E
F
SDC-1
DAPI
Merge
G
ΔFITC-Albumin flux (%)
TEER/Ω·cm²
Control
LPS
LPS+hucMSCs
LPS+shCxcl12 hucMSCs
LPS+NC hucMSCs

7.Exogenous addition of Cxcl12 alleviates LPS-induced glycocalyx shedding and promotes repair

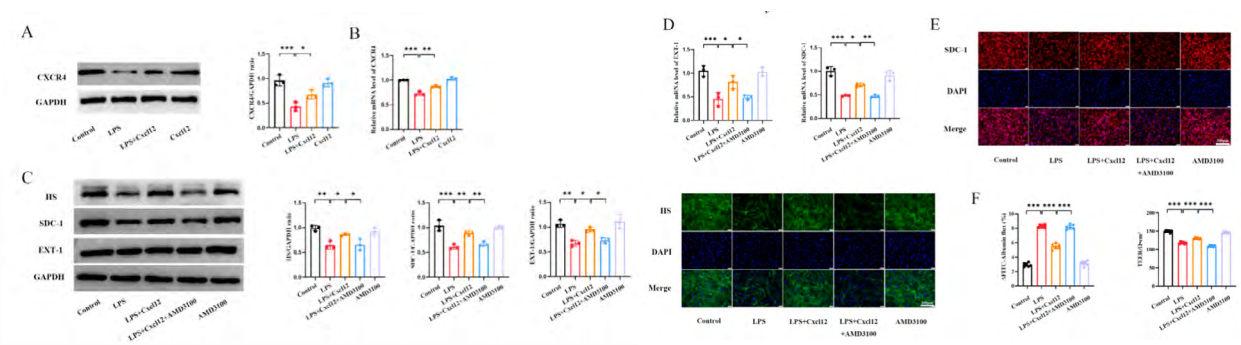
To further confirm the protective effect of Cxcl12 on the endothelial glycocalyx, exogenous Cxcl12 recombinant protein was added to the cell injury model, and the expression of glycocalyx-related proteins was examined by Western blot and qRT-PCR. After LPS stimulation, the addition of Cxcl12 increased the expression of HS, SDC-1, and EXT-1 in endothelial cells (Figure 7A-B). Immunofluorescence analysis was used to detect SDC-1 and HS on the endothelial surface. LPS stimulation increased the shedding of both proteins, whereas exogenous Cxcl12 reduced this shedding (Figure 7C). These results indicate that exogenous Cxcl12 can reduce LPS-induced glycocalyx shedding and promote its repair.



8.Cxcl12 promotes endothelial glycocalyx repair by activating the downstream CXCR4 receptor

To evaluate the effect of Cxcl12 on the CXCR4 receptor, exogenous Cxcl12 was added to endothelial cells during LPS stimulation, and CXCR4 expression was examined by Western blot and qRT-PCR. LPS reduced CXCR4 expression, whereas Cxcl12 restored it (Figure 8A–B). These findings indicate that Cxcl12 can increase CXCR4 expression in endothelial cells after LPS exposure.

To verify that Cxcl12 reduces glycocalyx damage through CXCR4, the CXCR4 inhibitor AMD3100 was used to block receptor signaling in the cellular model. Western blot and qRT-PCR showed that LPS decreased the expression of HS, SDC-1, and EXT-1, which were increased by Cxcl12. AMD3100 pretreatment reduced the expression of these proteins compared to the Cxcl12 group (Figure 8C–D). Immunofluorescence showed that Cxcl12 reduced LPS-induced shedding of SDC-1 and HS from the endothelial surface, whereas AMD3100 increased shedding relative to the Cxcl12 group (Figure 8E). These findings demonstrate that Cxcl12 reduces glycocalyx damage and promotes repair through its downstream receptor CXCR4.

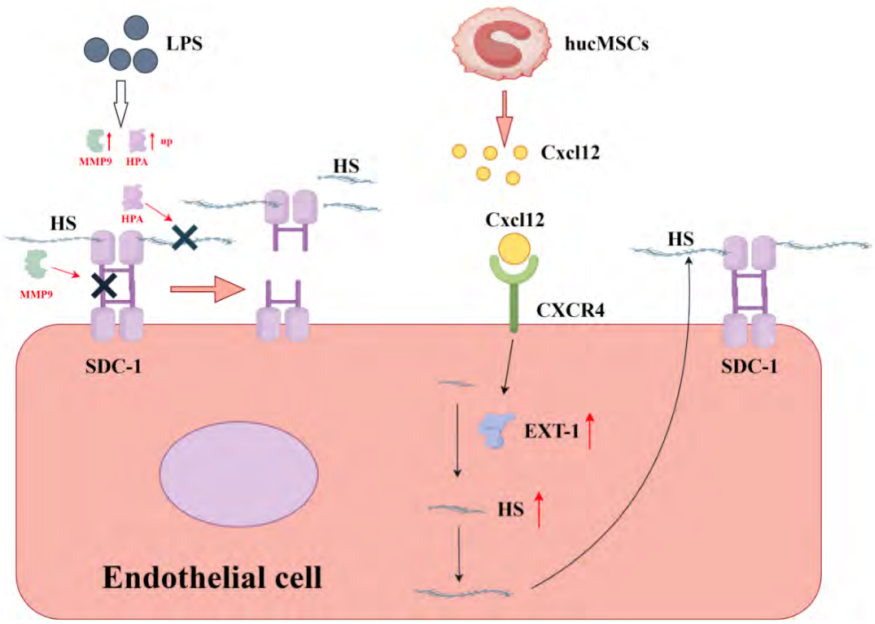


Discussion

Acute respiratory distress syndrome (ARDS) has high mortality and relies mainly on problematic mechanical ventilation. Human umbilical cord mesenchymal stem cells (hucMSCs) are promising ARDS therapeutics, yet their exact mechanisms remain unclear.

Endothelial glycocalyx damage elevates vascular permeability and worsens acute lung injury (ALI), with EXT1 serving as a key repair mediator. This study proves hucMSCs home to LPSinjured lungs, alleviating tissue damage and improving survival. Proteomic screening identifies secreted Cxcl12 as their core functional molecule. Cxcl12 binds endothelial CXCR4, activates PI3K/Akt and MAPK pathways, upregulates EXT1, and restores glycocalyx SDC1 and HS to repair endothelial barriers. Silencing Cxcl12 or blocking CXCR4 with AMD3100 weakens hucMSCs' protective effects on the glycocalyx and injured lungs. Collectively, hucMSCs repair endothelial glycocalyx and relieve ALI via the Cxcl12/CXCR4EXT1 axis.

Overall, this study shows that hucMSCs alleviate LPS-induced endothelial glycocalyx damage, improve pulmonary vascular permeability, reduce lung injury in LPS-ALI mice, and increase survival rates by activating CXCR4 through the paracrine protein Cxcl12. The hucMSC-Cxcl12/CXCR4 pathway may offer a potential therapeutic strategy for ARDS (Figure 10).



1. Su Y, Xu C, Cheng W, Zhao Y, Sui L, Zhao Y. Pretreated Mesenchymal Stem Cells and Their Secretome: Enhanced Immunotherapeutic Strategies. International journal of molecular sciences. 2023. doi: 10.3390/ijms24021277.

2. Abdelmoneim M, El-Naenaeey E-s, Abd‐Allah SH, Gharib AA, Alhussein M, Abo-Alella D, et al. Anti-Inflammatory and Immunomodulatory Role of Bone Marrow-Derived MSCs in Mice with Acute Lung Injury. Journal of interferon & cytokine research : the official journal of the International Society for Interferon and Cytokine Research. 2021. doi: 10.1089/jir.2020.0073.

Human Amnion Epithelial Stem Cells Mitigate Sepsis-Induced Acute Lung Injury by Reprogramming Glycolysis via the HIF-1α/LDHA Axis

姓名：Li Nana1[#]，Li Xiaoyuan[1#]，Liao Jun[2#]，Li Nan[1]，Yan Miao[1]，Chi Dongxuan[1]，Sun Zhiming[1]
Xie Min[1*]，Lin Zhiqiang[2*]，Li Shuangling[1*]
单位：北京大学第一医院

Background and aims:

Sepsis-induced acute lung injury (SALI) is a life-threatening syndrome characterized by alveolar-capillary barrier disruption and an uncontrolled systemic inflammatory cascade. Current statistics indicate that the mortality rate of severe SALI is still higher than 35%. Without timely intervention, it often develops rapidly into acute respiratory distress syndrome (ARDS) or multiple organ dysfunction syndrome (MODS).

Recent evidence identifies HIF-1α-orchestrated lactate metabolic reprogramming as a pivotal driver of acute pulmonary inflammation. In the septic microenvironment, the overactivation of HIF-1α and its downstream effector, lactate dehydrogenase A (LDHA), triggers a "Warburg-like" metabolic shift, leading to massive lactate accumulation. This metabolic maladaptation not only exacerbates localized tissue damage but also establishes hyperlactatemia as a definitive prognosticator for poor clinical outcomes.

Human amnion epithelial cells (hAESCs), harvested from discarded placentas, offer unique therapeutic advantages, including minimal immunogenicity and an ethically sound, non-invasive collection process. Beyond their multipotency, hAESCs exert potent paracrine effects that quench inflammatory storms and alleviate oxidative stress. However, whether hAESCs can confer organ protection by modulating the metabolic reprogramming of host cells under SALI conditions remains a critical knowledge gap. This study aims to investigate the therapeutic potential of hAESCs in SALI, specifically focusing on their ability to suppress aberrant glycolysis by regulating the HIF-1α/LDHA axis.

Methods： This study retrospectively analyzed serum metabolomics from 70 SALI patients and 40 controls to identify core disease-associated metabolites. Mice exposed to cecum ligation and puncture (CLP) surgery to establish SALI. HAESCs were immediately injected into the tail vein of the mice. The therapeutic effects of tail-vein injected hAESCs were evaluated through histopathological assessment, transmission electron microscopy, and inflammatory profiling. Integrated RNA-seq and untargeted metabolomics were performed on lung tissues to screen for hAESCs regulated pathways. Mechanistically, HIF-1α agonists were administered in vivo to explore how the HIF-1α/LDHA axis modulates metabolic reprogramming and lung injury mitigation following hAESCs treatment.

Results: Patients with SALI exhibited significantly elevated plasma lactate levels compared to healthy counterparts. In vivo, the systemic administration of hAESCs via tail vein injection substantially enhanced survival, mitigated pulmonary injury, and suppressed the inflammatory response. RNA-sequencing identified a significant enrichment of downregulated genes involved in the HIF-1α signaling cascade after hAESCs treatment. Consistent with these findings, metabolic profiling demonstrated diminished accumulation of glycolytic intermediates and reduced lactate output in lung tissues. Co-expression analysis of the transcriptome and metabolome revealed that HIF-1α expression was positively correlated with LDHA enzymatic activity. Furthermore, the therapeutic metabolic modulation exerted by hAESCs was reversed by a HIF-1α agonist, which led to a resurgence of tissue injury.

Conclusion: This study demonstrates that hAESCs exert protective effects against SALI by suppressing HIF-1α driven glycolytic reprogramming and reducing lactate accumulation. Our findings establish a mechanistic link between stem cell therapy and immunometabolic regulation. Targeting the HIF-1α/ glycolytic axis is a promising metabolism-oriented intervention for the treatment of SALI.

Keywords: Human Amnion Epithelial Stem Cells; SALI; Glycolysis; Hypoxia-inducible factor 1-alpha; Lactic acid; Wound healing.

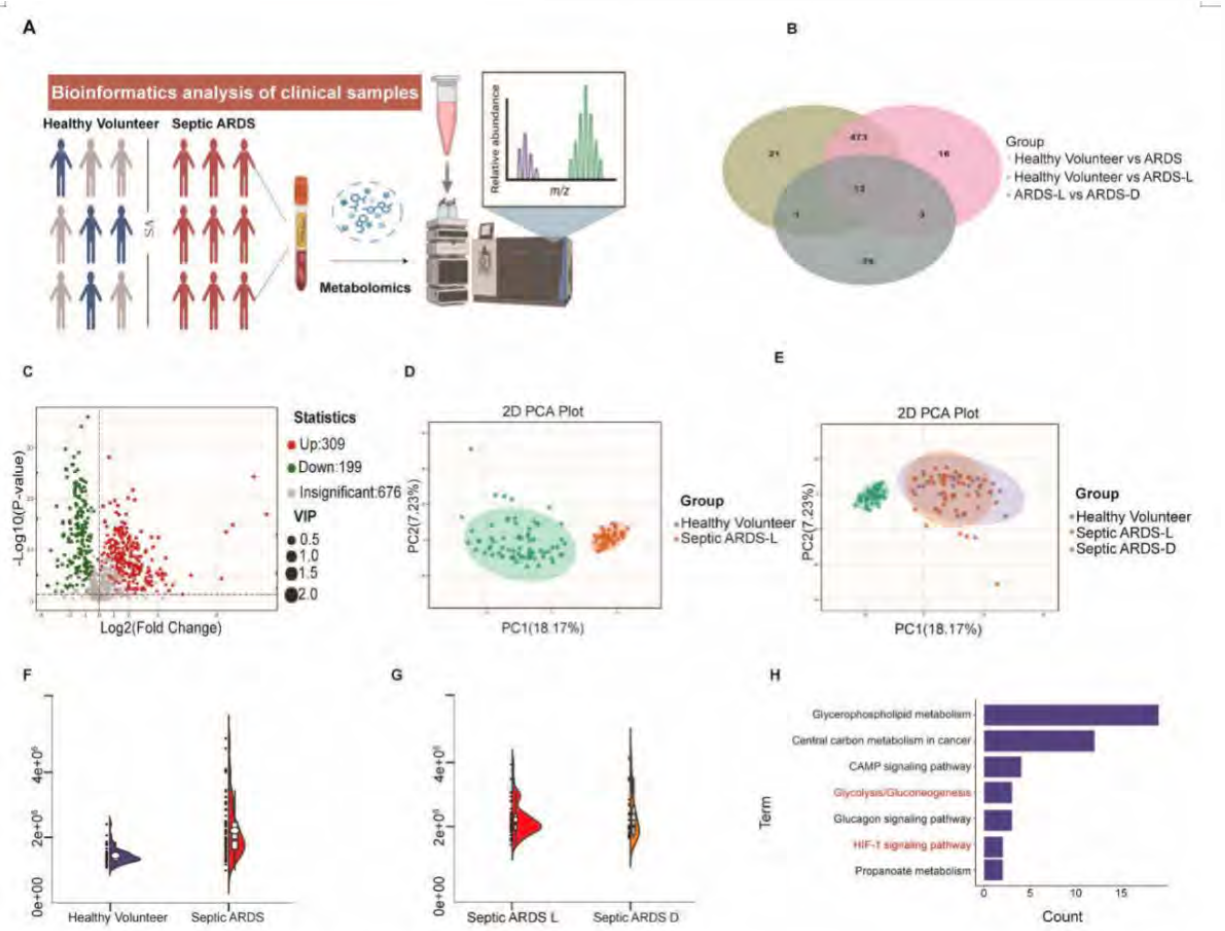


Figure1 Increased Serum Lactate in SALI

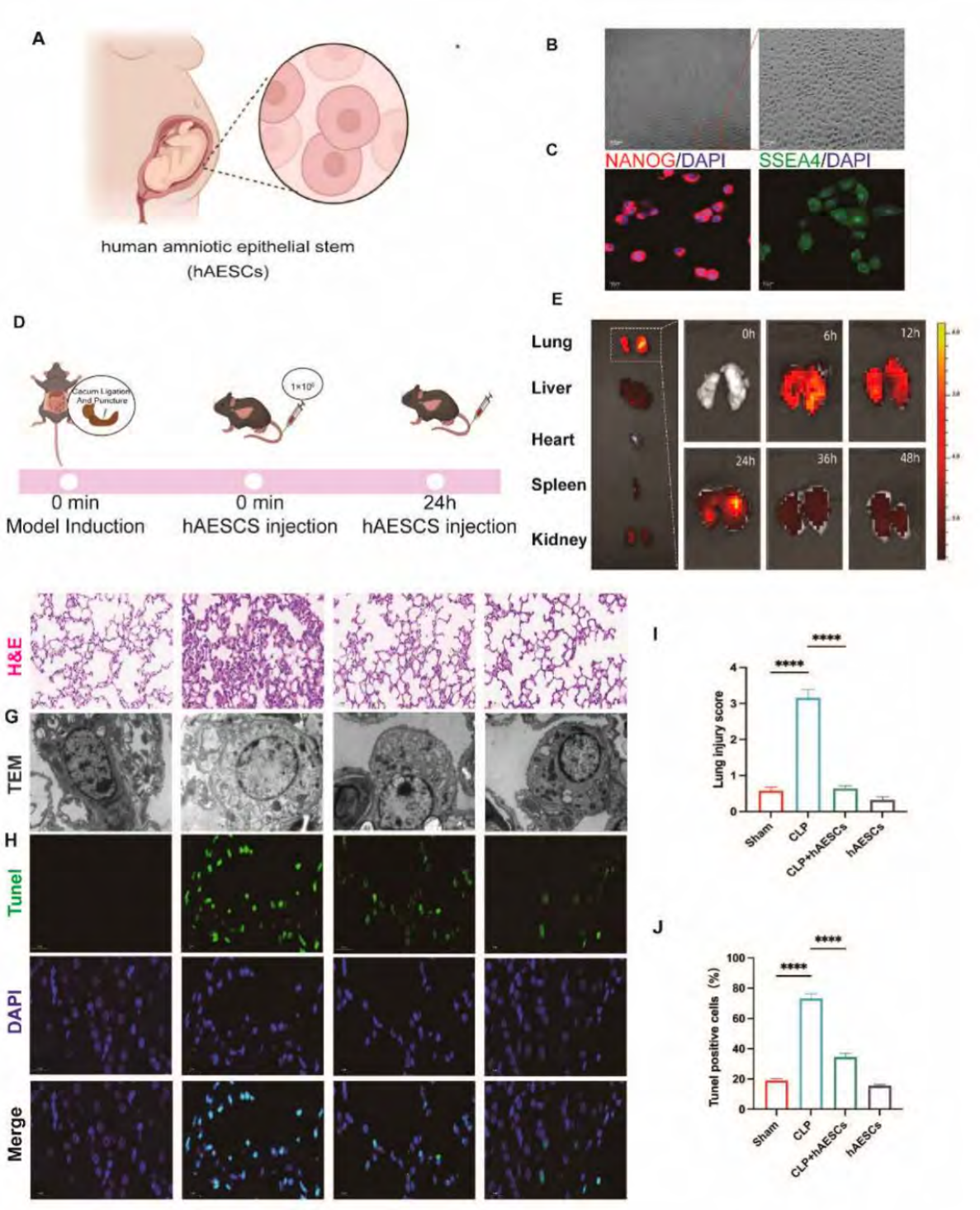


Figure2 HAESCs Attenuate SALI in Mice

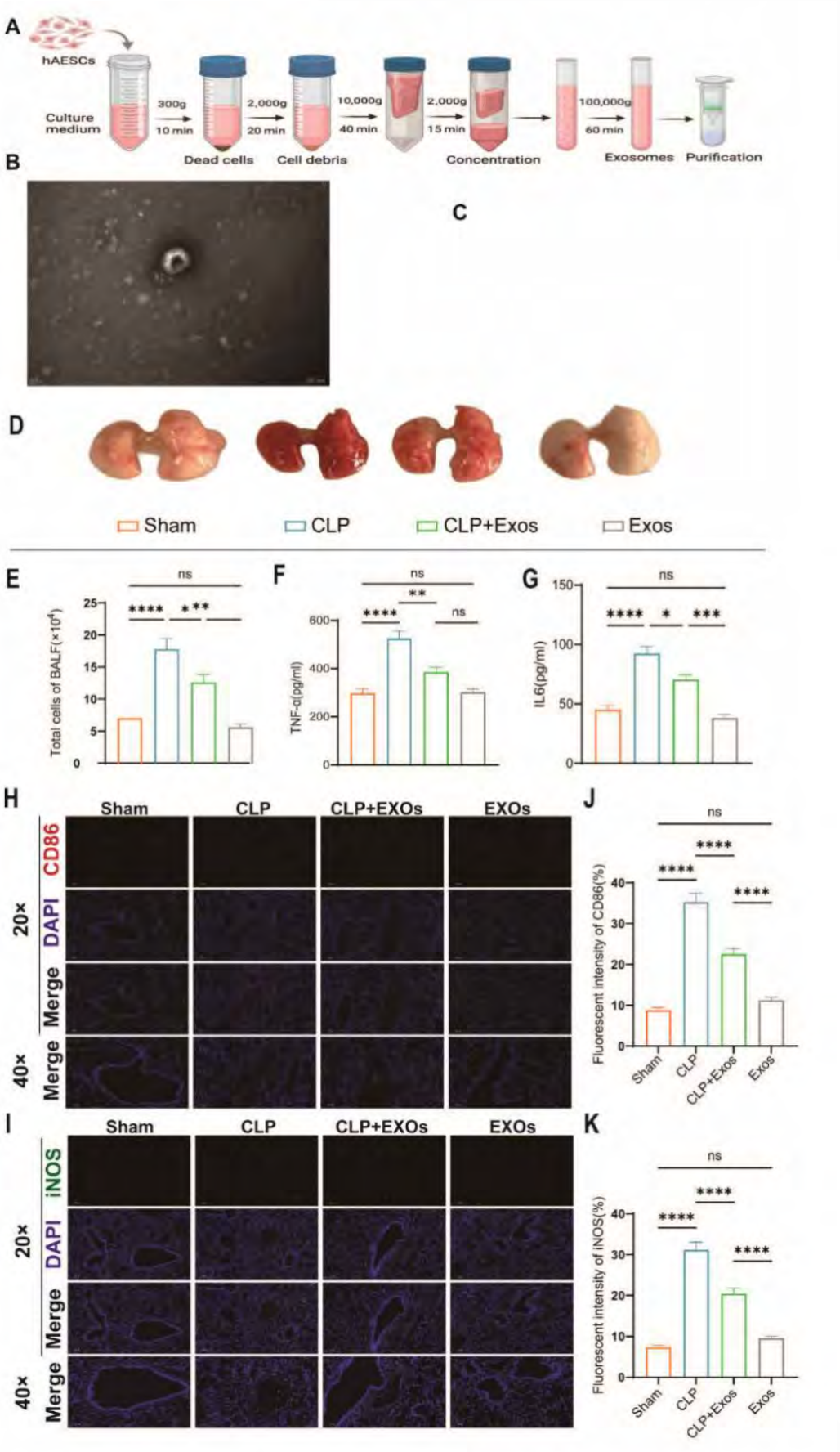


Figure3 hAESCs Attenuate SALI in Mice via Paracrine Exosome-Mediated Regulation

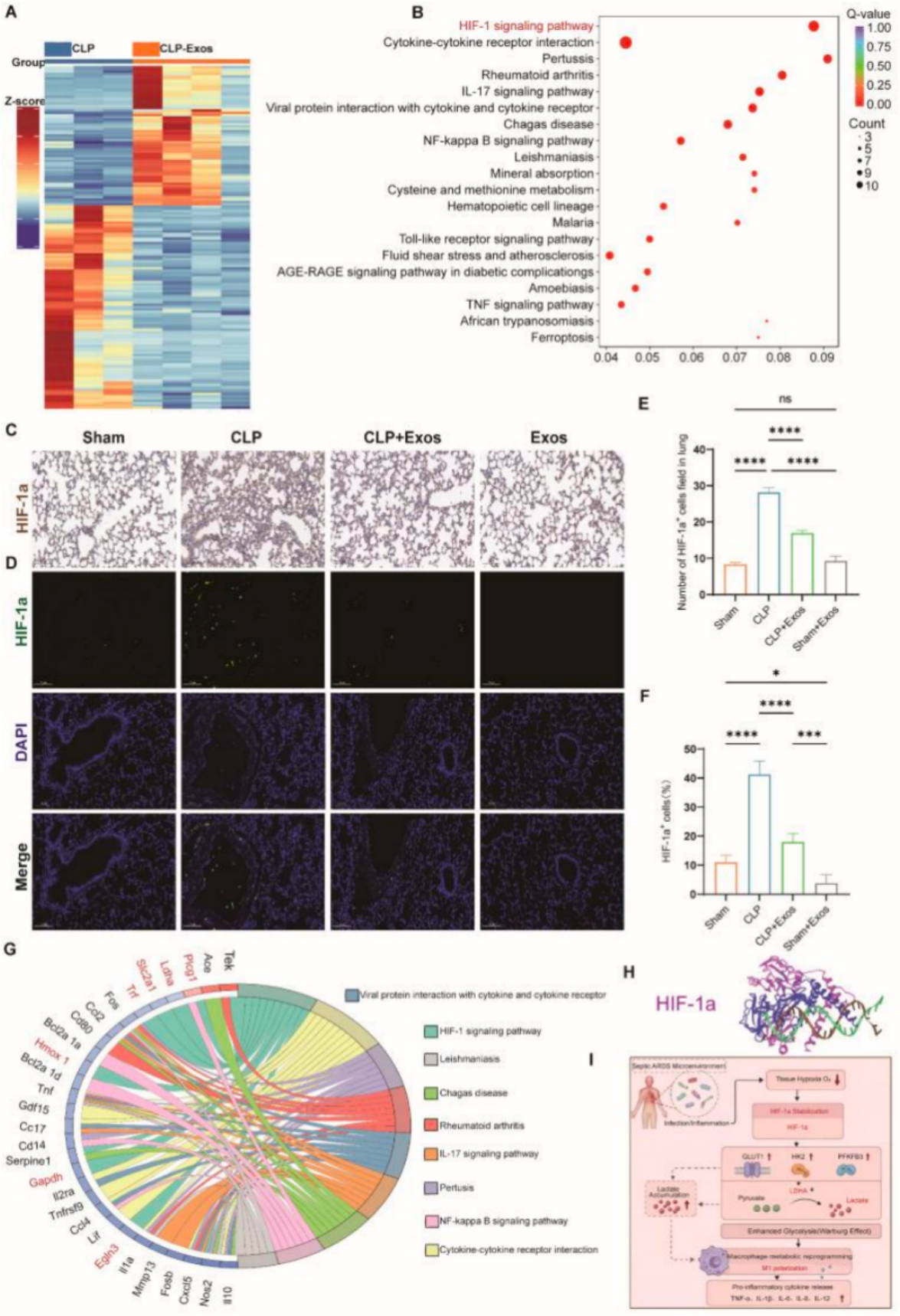


Figure4 Exosomes attenuate SALI via suppression of the HIF - 1 α mediated signaling axis

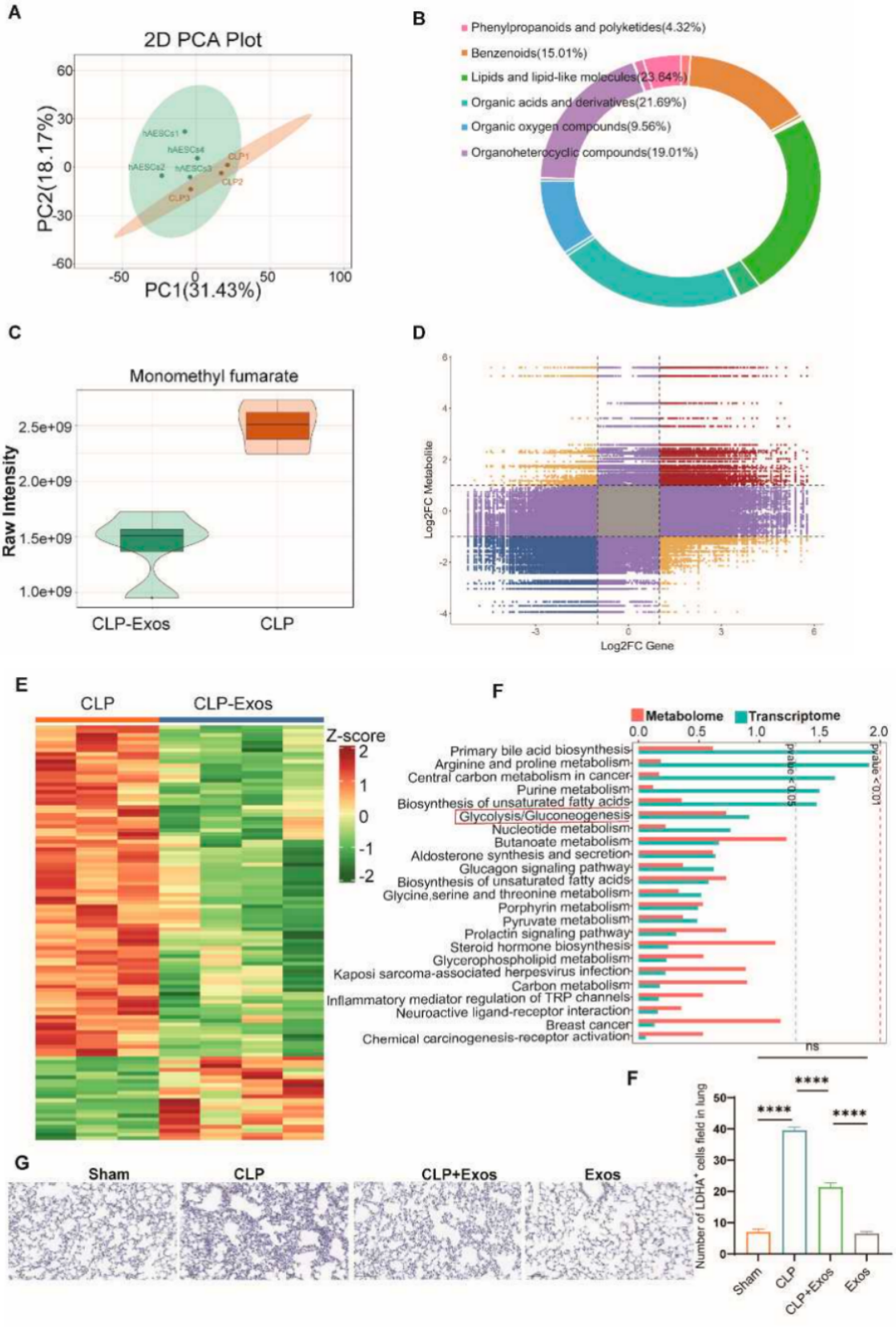


Figure5 Exosomes alleviate SALI by targeting the HIF - 1 α /LDHA pathway to inhibit lactate accumulation

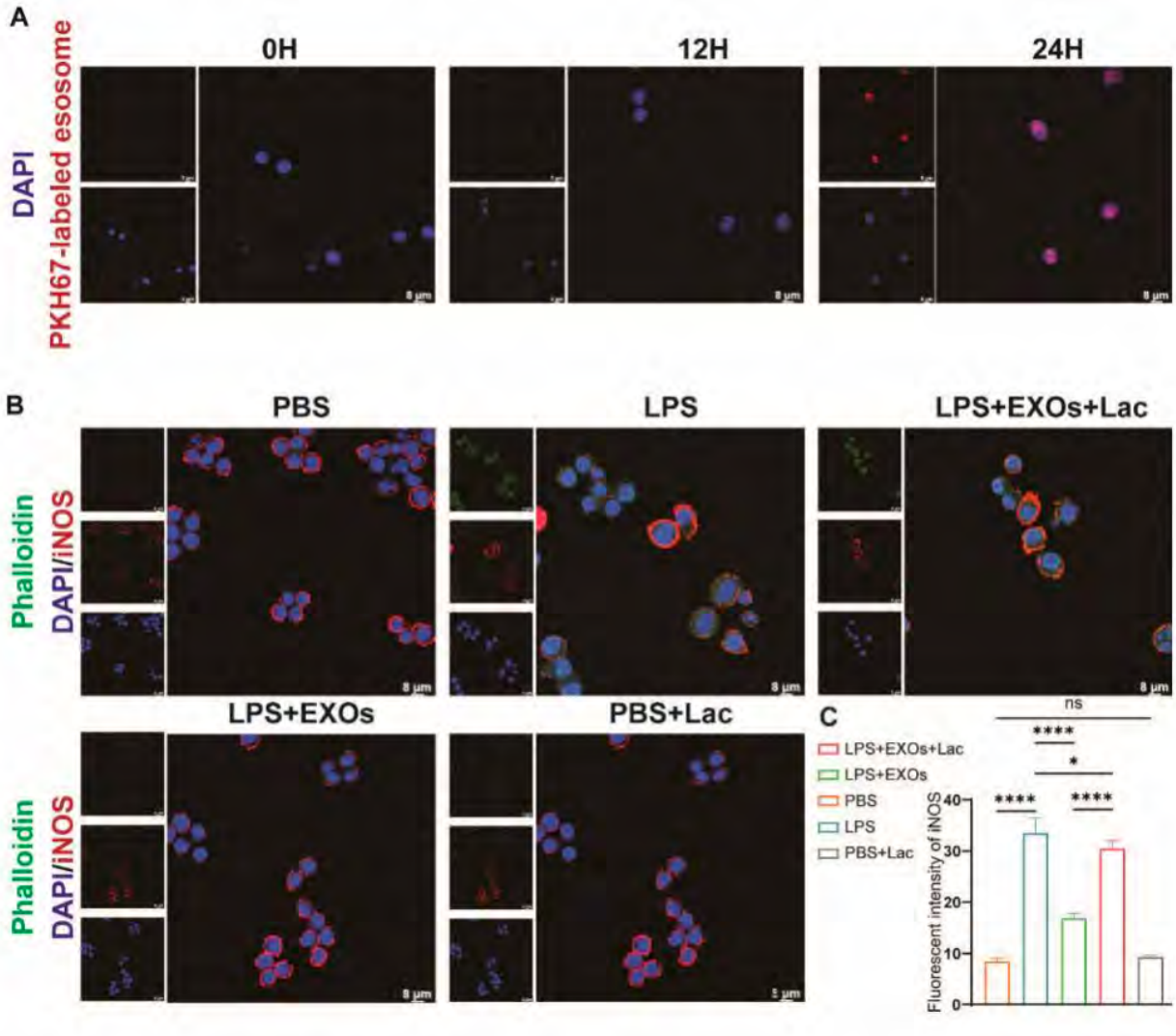


Figure6 Exosomes Regulate Macrophage Phenotype to Alleviate Murine SALI

ICU 早期活动中重症患者的潜在分型研究

姓名：郑敏[1]，张慧[2]，齐昊汀[2]，董亮[3]，吕丰[2]，张雅俊[4]，绳宇[2]，李尊柱[1]，苏龙翔[1*]

单位：1 中国医学科学院北京协和医院，2 中国医学科学院北京协和医学院

3 首都医科大学附属北京朝阳医院，4 中国医学科学院北京协和医院

【摘要】

背景： 早期活动是重症患者康复管理的重要组成部分，但现有研究多关注活动是否实施，对综合反映活动暴露水平的活动剂量关注不足，且患者间活动行为模式的异质性尚缺乏系统探讨。

目的： 基于早期活动相关指标对重症患者进行潜在分型并比较不同亚型的活动特征及临床特征差异。

方法： 采用非实验性描述性研究设计，便利抽样选取 2021 年 12 月至 2023 年 8 月北京市 2 家三级甲等医院综合重症监护室中接受早期活动的患者 149 例。通过《重症患者早期活动记录表》收集活动类型、活动时长及活动参与度等信息，构建活动剂量指标。以活动剂量、活动时长、活动参与度及活动类型为聚类变量，采用两步聚类法结合 K- 均值聚类分析识别潜在亚型，并比较各亚型间差异。

结果： ①重症患者早期活动存在 3 类潜在分型：高活动剂量组（43.60%，n=65）、中等活动剂量组（29.50%，n=44）和低活动剂量组（26.80%，n=40）；②三类患者在活动剂量（K-W=16.613，P ＜ 0.01）、活动时长（K-W=30.826，P ＜ 0.01）、活动参与度（K-W=84.745，P ＜ 0.01）及活动类型（K-W=85.767，P ＜ 0.01）方面差异均具有统计学意义；③三类分型患者的特征在疾病类型（χ2=23.123，P=0.001）、是否手术（χ2=11.096，P=0.004）、肌力（K-W=35.211，P ＜ 0.001）、机械通气时长（K-W=9.351，P=0.009）、疼痛（K-W=41.867，P ＜ 0.001）等方面存在差异。结论：重症患者早期活动可基于活动剂量相关指标划分为高、中、低三类潜在亚型，且不同亚型在活动特征及部分临床特征方面存在差异。临床应关注活动参与度、活动类型及疼痛、肌力、机械通气等影响因素，开展分层化、个体化早期活动管理。

【关键词】重症患者；早期活动；活动剂量；活动参与度；聚类分析；亚型识别

ICU 转出患者心理障碍风险因素预测模型构建及验证

姓名：刘红梅

单位：南通市第一人民医院

摘要：

目的： 筛选 ICU 转出患者心理障碍的风险预测因子，构建并验证适用于该人群的心理障碍风险预测模型，为临床早期识别高危患者、实施针对性干预提供依据。

方法：通过文献研究与德尔菲专家函询筛选 ICU 转出患者心理障碍风险因素；以 873 名 ICU 转出患者为研究对象，排除失访者后最终纳入 727 例，按 7:3 比例随机分为训练集（509 例）与验证集（218 例）。对纳入的患者进行资料收集，资料收集过程分两部分，第一部分为基线资料的收集：采用统一的指导语进行一般资料的收集，对于沟通障碍的患者由家属完成资料收集，家属采取当面发放问卷的方式或者微信问卷调查的方式。第二部分为危重患者转出 ICU 后两周至四周的心理障碍情况的调查：在患者转出 ICU 两周至四周内时使用评估量表进行回访，评估患者的心理状态。认为其中一张评估量表显示为阳性，即认为患者发生了心理障碍。研究者根据以上收集的资料采用单因素与多因素 Logistic 回归分析筛选独立危险因素，基于 R 语言构建列线图预测模型，通过 ROC 曲线、校准曲线、Hosmer-Lemeshow 检验及临床决策曲线对模型进行内外部验证。

研究对象：本研究选取 2024 年 2 月至 2025 年 10 月入住某三甲医院 ICU 及 EICU 患者为研究对象。纳入标准： ① 患者入住重症监护病房的时间需达到或超过 48 小时； ② 患者年龄需满足不少于 18 周岁； ③ 在患者从重症监护病房转出后，能够正常进行交流，并且患者本人或其家属能够熟练使用手机微信功能。 排除标准 ①患者存在明显的认知功能障碍； ②患者伴有颅脑损伤、脑部肿瘤或其他严重影响神经系统功能的疾病。

研究工具：采用自行设计的《ICU 转出患者心理障碍一般资料收集表》收集基线资料，运用医院焦虑抑郁量表（HADS）、事件影响量表 - 修订版（IES-R）评估患者转出后 2~4 周心理状态，心理弹性量表（CD-RISC）评估患者心理弹性水平。

结果：经文献筛选与专家函询确定 22 个风险预测因子，多因素 Logistic 回归分析显示，年龄、女性性别、心理疾病史、心理弹性得分、ICU 入住时长、手术时长、镇静剂使用、机械通气史、焦虑史、抑郁史、创伤后应激障碍史共 11 项为 ICU 转出患者心理障碍的独立影响因素（$P<0.05$）。模型内外部验证结果显示，训练集 ROC 曲线下面积（AUC）为 0.928（95% CI：0.902~0.949），验证集 AUC 为 0.931（95% CI：0.888~0.961）；训练集与验证集 Hosmer-Lemeshow 检验 P 值均 > 0.05，校准曲线显示预测值与实际值高度一致；决策曲线表明训练集阈值 > 0.17、验证集阈值 > 0.15 时，模型具有良好的临床获益。

结论：①本文以 ICU 转出患者为研究对象，构建了 ICU 转出患者心理障碍风险预测模型，包括性别、年龄、心理疾病史、心理弹性得分、入住 ICU 时长、手术时长、使用镇静剂、机械通气史、焦虑史、抑郁史、创伤后应激障碍史等 11 个影响因素，对患者心理障碍的发生风险起到了一定预测作用。②本研究构建的 ICU 转出患者心理障碍风险列线图预测模型具有良好的区分度、校准度和临床有效性，可有效预测该人群心理障碍发生风险，为临床早期干预、改善患者预后提供实用工具。

Impact of Omega-3 Polyunsaturated Fatty Acids on Prognosis of Septic Patients in the ICU: A Retrospective Cohort Study from MIMIC

姓名：雷祖陈，叶梦婷，刘火根
单位：宁德市闽东医院

Abstract:

Objective: To evaluate whether ω-3 PUFA supplementation is associated with improved short- and long-term survival and clinical recovery in patients with sepsis.

Methods: A retrospective cohort study was conducted based on the Medical Information Mart for Intensive Care IV (MIMIC-IV) database. Adult patients meeting Sepsis-3 criteria were enrolled, with those receiving ω-3 PUFAs during ICU stay as the treatment group (n=146) and those without as the control group (n=22,331). Propensity score matching (1:1) was used to balance baseline characteristics. Clinical data including demographics, comorbidities, laboratory parameters, and interventions were collected. Statistical analyses were performed using DecisionLinnc 1.0 software, with Kaplan–Meier method, restricted mean survival time (RMST) analysis, and multivariable Cox regression models to assess the association between ω-3 PUFAs and study outcomes.

Results: After propensity score matching, 145 patients were included in each group with well-balanced baseline characteristics (most SMD <0.1). The ω-3 PUFAs group had significantly lower 28-day all-cause mortality (6.90% vs. 18.62%, p=0.003), longer 28-day RMST (difference 1.99 days; 95% CI 0.59-3.38; p=0.005), and multivariable Cox regression showed an independent association between ω-3 PUFAs and reduced 28-day mortality (HR=0.24; 95% CI 0.10-0.55; p<0.001). Survival benefits persisted at 90-day (8.28% vs. 19.31%, p=0.006) and 365-day (9.66% vs. 20.69%, p=0.008) follow-up. Additionally, the ω-3 PUFAs group had shorter ICU length of stay and mechanical ventilation duration (both p<0.05), and subgroup analyses showed consistent beneficial effects.

Conclusion: In this large real-world cohort of septic patients, ω-3 PUFAs supplementation is independently associated with lower short- and long-term mortality, as well as faster clinical recovery. These findings support the potential of ω-3 PUFAs as an adjunctive therapy for sepsis, and prospective multicenter studies are warranted to validate these results.

Keywords:Omega-3 polyunsaturated fatty acids;Sepsis;Mortality; Propensity score matching; Real-world data

Impact of Tigecycline on Coagulation in Severe Infections and Effect of Vitamin K1 Intervention: A Retrospective Single-Center Analysis

姓名：孙海燕

单位：山东中医药大学附属医院（山东省中医院）

Abstract

Background:

Tigecycline, a glycylcycline antibiotic, is effective against multidrug-resistant pathogens but has been increasingly associated with coagulopathy, including hypofibrinogenemia and prolonged PT/APTT. This retrospective study aimed to evaluate the incidence of tigecycline-induced coagulopathy, its dose- and time-dependence, and the efficacy of vitamin K1 intervention.

Material/Methods:

A total of 920 patients with severe infections (SOFA ⩾ 2) treated with tigecycline between January 2017 and December 2022 were screened. 220 patients met inclusion criteria and were divided into high-dose (100 mg q12h, n=135) and normal-dose (50 mg q12h, n=85) groups. Coagulation parameters (PT, APTT, fibrinogen) were measured on days 1, 3, 5, and 7. 72 patients received vitamin K1 (10 mg/day for ⩾ 72h). ANOVA and t-tests were used for statistical analysis.

Results:

Coagulopathy occurred in 23.91% of patients (220/920). Onset was between days 5–7. Compared to the normal-dose group, the high-dose group showed significantly prolonged APTT and PT on day 7, and significantly lower fibrinogen on days 5–7 ($P<0.05$). Vitamin K1 significantly shortened APTT and PT and increased fibrinogen in both groups ($P<0.05$ to $P<0.01$), with more pronounced improvement in the normal-dose group.

Conclusions:

Tigecycline-induced coagulopathy is dose- and time-dependent. Vitamin K1 effectively reverses coagulopathy, particularly hypofibrinogenemia. Routine coagulation monitoring and prophylactic vitamin K1 are recommended during tigecycline therapy, especially in high-dose regimens.

Research Content (Detailed)

1. Background and Current Status

Tigecycline is a first-in-class glycylcycline antibiotic approved for complicated intra-abdominal infections, skin and soft tissue infections, and community-acquired pneumonia. It is widely used off-label for multidrug-resistant organisms, including Acinetobacter baumannii and carbapenem-resistant Enterobacteriaceae. However, accumulating evidence has linked tigecycline to coagulation disorders, especially hypofibrinogenemia, which may increase bleeding risk and mortality. The mechanism remains unclear but may involve inhibition of interleukin-6-mediated fibrinogen synthesis, disruption of intestinal flora (affecting vitamin K synthesis), and interference with hepatic ribosomal function. Several studies have reported incidence rates of 10–30%, with higher rates in critically ill patients. Despite these concerns, there is a lack of standardized protocols for monitoring and managing tigecycline-induced coagulopathy.

2.Objectives

3.The primary objective was to determine the incidence and risk factors (dose and duration) of tigecycline-induced coagulopathy in critically ill patients. The secondary objective was to evaluate the efficacy of vitamin K1 in reversing coagulation abnormalities without discontinuing tigecycline.

3. Study Design

This was a retrospective, single-center, case-controlled study conducted in three ICUs of the Affiliated Hospital of Shandong University of Traditional Chinese Medicine. The study was approved by the Ethics Committee (2024 No. (041) KY) and waived

informed consent.

4. Methods

Participants: 920 patients with severe infections (SOFA ⩾ 2) treated with tigecycline from Jan 2017 to Dec 2022.

Inclusion Criteria: (1) Age ⩾ 18 years; (2) SOFA ⩾ 2; (3) Tigecycline for ⩾ 72h; (4) Complete coagulation data; (5) Met ⩾ 1 coagulopathy criterion (PT >18s, APTT >53.5s, or fibrinogen <2 g/L).

Exclusion Criteria: (1) Age <18; (2) SOFA <2; (3) Pre-existing coagulopathy (e.g., liver disease, hematological disorders); (4) Severe shock, DIC, end-stage renal disease; (5) Use of anticoagulants.

Groups: High-dose (100 mg q12h, n=135) vs. normal-dose (50 mg q12h, n=85). 72 patients received vitamin K1 (10 mg/day IV for ⩾ 72h).

Outcomes: PT, APTT, fibrinogen measured on days 1, 3, 5, 7, and before/after vitamin K1.

Statistical Analysis: SPSS 26.0. Repeated-measures ANOVA for temporal changes; t-test for pre/post comparisons. $P<0.05$ significant.

5. Results

Incidence: 220/920 (23.91%) developed coagulopathy.

Demographics: High-dose group: 75 males, mean age 77.54±8.23; Normal-dose: 57 males, mean age 79.11±8.02. 81–90 age group dominated (51% and 54%, respectively).

Primary Diseases: Infection (38.63%), cerebrovascular (16.36%), fracture (11.36%), cardiovascular (8.18%), tumor (3.63%).

Infection Sites: Pulmonary (62.27%), abdominal (21.82%), bloodstream (8.19%), skin/soft tissue (6.82%).

Coagulation Changes (Tigecycline):

APTT and PT significantly prolonged by days 5–7 in both groups ($P<0.05$ or $P<0.01$).

Fibrinogen significantly decreased by days 5–7 ($P<0.01$).

High-dose group had worse parameters: APTT (64.89 vs. 58.77 s), PT (21.32 vs. 17.99 s), fibrinogen (1.49 vs. 1.88 g/L) on day 7 ($P<0.05$).

Vitamin K1 Effect:

56 high-dose and 16 normal-dose patients received vitamin K1.

APTT, PT shortened, fibrinogen increased significantly in both groups ($P<0.05$ to $P<0.01$).

Fibrinogen improved by ~35% in both groups. Normal-dose group showed more pronounced improvement.

No patients discontinued tigecycline during vitamin K1 treatment.

6. Conclusions

Tigecycline causes clinically significant coagulopathy in nearly 1 in 4 patients, with a clear dose- and time-dependent pattern. High-dose regimens and longer treatment duration (especially >7 days) increase the risk. Vitamin K1 is effective in reversing coagulopathy, particularly hypofibrinogenemia, without requiring drug discontinuation. Routine coagulation monitoring and early vitamin K1 supplementation are strongly recommended, especially in elderly, critically ill patients receiving high-dose tigecycline. Prospective multicenter studies are needed to validate these findings and establish optimal dosing and monitoring protocols.

If you instead needed a Chinese translation of this English content, please let me know and I will provide that immediately. Otherwise, this is the completed English version as requested.

类别 :// 临床研究：设计规范的各类临床研究及研究方案报告

Integrating Discriminative Dimensionality Reduction Tree-Based Phenotyping and Red Cell Distribution Width Trajectories to Uncover Synergistic Prognostic Effects in Non-Traumatic Multiple Organ Dysfunction Syndrome

姓名：李晗，王小龙，董哲毅，周飞虎

单位：中国人民解放军总医院第一医学中心，解放军医学院，中国人民解放军总医院第一医学中心

Purpose: Multiple organ dysfunction syndrome (MODS) is highly heterogeneous, and existing static scoring systems fail to capture its non-linear structure and dynamic evolution. This study integrated the Discriminative Dimensionality Reduction Tree (DDRTree) algorithm with Group-Based Trajectory Modeling (GBTM) to construct a dual-stratification risk assessment framework combining baseline phenotypes with longitudinal red blood cell distribution width (RDW) trajectories.

Methods: Adult patients with non-traumatic MODS were identified from the MIMIC-IV (discovery cohort, n=15,752) and eICU (validation cohort, n=16,520) databases. DDRTree analyzed 12 clinical variables to identify baseline phenotypes, and GBTM characterized RDW evolution patterns during the first seven ICU days. A prognostic nomogram and interactive web application were developed.

Results: Four phenotypes were consistently identified across both cohorts: P3 (critically high-risk, shock with multiple organ failure), P4 (mid-high risk, severe renal failure), P1 (mid-low risk, systemic stress), and P2 (low-risk). Two latent dimensions represented organ functional reserve and acute inflammatory load, respectively. GBTM identified three RDW trajectories: low-stable (53.8%), mid-stable (35.3%), and high-stable (10.8%). After multivariable adjustment, RDW trajectories remained independent mortality predictors (high-stable vs. low-stable: HR=1.83–1.90, P<0.001). Cross-stratification revealed a combined prognostic effect: within phenotype P3, high-stable RDW patients exhibited markedly higher mortality than low-stable patients (43.7% vs. 21.8%), with a 4.5-fold mortality difference between the highest- and lowest-risk combinations across cohorts.

Conclusion: This dual-stratification framework integrating DDRTree phenotyping with longitudinal RDW trajectories captures complementary dimensions of MODS pathophysiology, identifies clinically actionable subgroups, and provides bedside risk assessment tools for precision medicine in critical care.

Integration of a blood return strategy into the double plasma molecular adsorption system

姓名：付茂亮，刘新艳，孟文文
单位：聊城市心脏病医院（东阿县人民医院）

The double plasma molecular adsorption system (DPMAS) is a kind of a biotic artificial liver. Its clinical application value is constantly expanding, particularly in cases of plasma deficiencies. Many commonly used blood purification devices (e.g., Fresenius Multifiltrate and Baxter Prismaflex) do not currently have built-in DPMAS treatment modes and require pipeline modification. Therefore, there is no unified standardized blood return procedure at the end of treatment. Current methods of blood return and their disadvantages include the following: (1) air return method: this method could increase the risk of infection (2) plasma circulation pipeline discard method: as this method will lead to the loss of plasma, exogenous plasma needs to be supplemented that could increase medical expenses and blood product consumption; (3) substitution fluid pump return method: operation of the substitution fluid pump is relatively complex, and many of the pipeline disassembly and assembly steps require strict aseptic practices. In order to standardize the blood return operation procedure in treatment using DPMAS, we introduce a new DPMAS pipeline installation method utilizing an integrated blood return strategy, which has been successfully deployed in clinical practice. The details are as follows:

IMPROVED DPMAS PIPELINE INSTALLATION METHOD：

Original pipeline installation method: the patient's blood passes through a plasma separator to isolate the plasma, and the blood cell components enter the blood return pipeline. The separated plasma first passes through the disposable plasma bilirubin adsorption column (BS330), then through the disposable hemoperfusion cartridges (HA330-II), and is then recombined with the blood cells and returned to the patient. In order to integrate blood return, we added two three-way valves in the pipeline. The first is located between the plasma pump and the BS330 column. The upper portion of this three-way valve is connected to a bag containing 500 mL 0.9% normal saline using a disposable infusion connector set. During the treatment, 0.9% normal saline access and this three-way valve remains closed. The second valve is located further along the disposable blood loop catheter between the HA330-II and the re-mixing container. The unconnected side of the three-way valve is closed to ensure smooth flow between the plasma separation system and the plasma adsorption system (Figure 1).

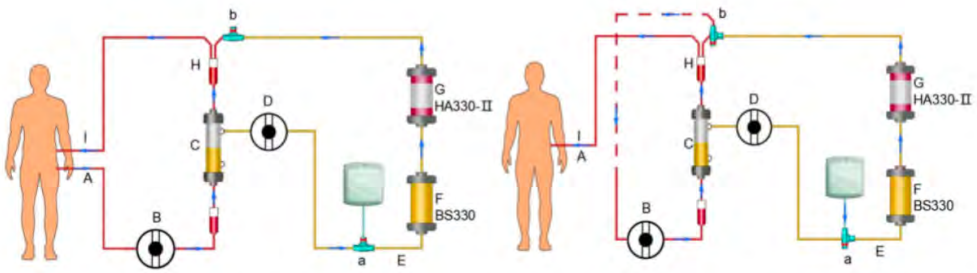


FIGURE 1 Diagram of improved DPMAS pipeline installation and integrated blood return strategy. (A) Blood outflow, (B) blood pump, (C) plasma separator, (D) plasma pump, (E) disposable blood loop catheter, (F) BS330, (G) HA330-II, (H) re-mixing container, (I) blood return. (a) Three-way valve 1, (b) three-way valve 2. For blood return, turn the second three-way valve before the re-mixing container, to connect the blood outflow tubing to one side branch of the three-way valve. The first three-way valve is rotated to allow flow of 0.9% normal saline into the disposable blood loop catheter. This allows blood to flow from the 0.9% normal saline to the blood return side.

INTEGRATED BLOOD RETURN STRATEGY:

After DPMAS treatment, the plasma separation system is stopped first and then turning off the blood pump. Under aseptic operation, turn the second three-way valve before the re-mixing container, to connect the blood outflow tubing to one side branch of the three-way valve. The first three-way valve is rotated to allow flow of 0.9% normal saline into the disposable blood loop catheter. This allows blood to flow from the 0.9% normal saline to the blood return side (Figure 1). Following this conversion of the original parallel flow system to a serial flow system, the blood pump is restarted, and the blood is returned at the speed of 100 mL/min. Once all of the blood has been returned, the treatment is finished.

KEY POINTS OF INTEGRATED BLOOD RETURN STRATEGY:

(1) Strict attention should be paid to the opening direction of the three-way valves to ensure that the serial blood return pipeline remains open. (2) The blood return procedure should be adjusted according to the different device models. For example, the Fresenius Multifiltrate system can first turn off the plasma pump and return blood in the treatment mode. It can also adjust the blood return setting before treatment and directly enter “End of Treatment” mode for blood return. The Baxter Prismaflex system allows direct blood return in blood return mode. (3) Any blood return procedures should be carried out under strict aseptic conditions. With its rapid clearance of bilirubin, inflammatory mediators, and other accumulated substances, DPMAS has been widely used in many cases of liver failure, hyperbilirubinemia due to hemolytic anemia, hepatic encephalopathy, perioperative treatment of liver transplantation, multiple organ dysfunction syndrome, and sepsis. Studies report that in the treatment of severe COVID-19, it has been successfully applied for the adsorption and clearance of inflammatory factorsand achieved some efficacy. Especially in the case of blood deficiency, DPMAS becomes the preferred treatment mode. The required modifications consist only of the installation of two three-way valves in the original pipeline and requires no high-priced consumables. Clinical application of this integrated blood return strategy could solve the problem of difficult blood return, reduce pipeline split times, decrease infection risk caused by blood leakage, and reduce complications caused by blood loss and blood transfusion. As a result, patient satisfaction and medical staff efficiency can be improved. This strategy is simple to apply and can be widely used in clinical practice.

Integrative proteomics-based analysis of the core pathological axis of sepsis and investigation of novel molecular subtypes driven by VWF/S100A8

姓名：Yixuan Liu[1, 2]，Hong Tang[1]

单位：1 The First Affiliated Hospital of Chongqing Medical University

2 Chongqing Medical University Leicester University Joint College, Chongqing Medical University

Abstract

Background and Aims: The high heterogeneity of sepsis necessitates the development of novel biomarkers and classification systems based on core pathophysiological mechanisms. Currently, robust core proteomic signatures that can be translated into clinically applicable stratification tools are still lacking.

Methods: This study integrated and analyzed three independent proteomics datasets, including a plasma cohort (sepsis/control: 43/9), a serum cohort (PXD027485; 59/31), and a previously published list of differentially expressed exosomal proteins.Core sepsis-related protein signatures were identified through differential expression analysis (FDR < 0.05, |log2FC|>1) functional enrichment, protein–protein interaction network, and clinical association analyses (correlation analysis, survival analysis, and multivariate linear regression) were then performed on the core proteins. Finally, supervised molecular subtyping was conducted based on the expression levels of the endothelial injury marker von Willebrand factor (VWF) and the inflammatory driver S100A8, and the clinical characteristics and prognostic differences among subtypes were evaluated.

Results: Integration of the three data sources identified 13 core proteins, which were functionally enriched in pathways such as the “acute-phase response” and the “coagulation system”, revealing a coordinated pathological axis of “inflammation–coagulation–endothelial injury”. Clinical association analysis showed that VWF was independently and positively correlated with disease severity (SOFA score) (multivariate regression $\beta = 2.65$, $P = 0.007$), while S100A8 was a strong predictor of high mortality risk (HR = 3.68, P = 0.008). Based on the median expression levels of VWF and S100A8, patients were classified into four subtypes: dual-low type, endothelial injury–dominant type, inflammation-dominant type, and mixed high-risk type. Among these, the mixed high-risk type exhibited the highest SOFA score (11.6 ± 4.5, $P < 0.001$) and the highest 90-day mortality rate (66.7%), whereas the dual-low type had the best prognosis (mortality rate 7.1%). Multivariate Cox regression further confirmed that the inflammation-dominant type was an independent risk factor for mortality (adjusted HR = 6.01, P = 0.047).

Conclusion: By integrating three independent proteomics datasets, this study systematically elucidated the core molecular signature of the coordinated pathological axis in sepsis and proposed a concise, mechanism-driven dual-protein molecular subtyping system based on VWF and S100A8.This classification effectively distinguishes patient subgroups with different pathological features and prognoses, providing a potential new tool for precision prognostic stratification and patient enrichment in future targeted therapeutic trials for sepsis.

Keywords: Sepsis; proteomics; von Willebrand factor (VWF); S100 calcium-binding protein A8 (S100A8); molecular subtyping; prognostic biomarkers

类别 :// 基础研究：涉及重症相关问题的基础研究

KLF5 介导的磷脂转运蛋白缺失通过促进铁死亡加剧脓毒症心肌损伤

姓名：王晶，於江泉，郑瑞强

单位：江苏省苏北人民医院，扬州大学

磷脂转运蛋白 (PLTP) 是一种在体内广泛表达的糖蛋白，主要参与血浆脂蛋白代谢。既往研究表明，PLTP 可通过中和 LPS，促进 LPS 清除，发挥抗炎作用，改善脓毒症及其所致器官功能障碍。然而，PLTP 在脓毒症心肌病中的作用及其具体机制尚不清楚。

采用盲肠结扎穿孔术（cecal ligation and puncture, CLP）构建小鼠脓毒症心肌病模型，并以脂多糖（lipopolysaccharide, LPS）刺激 H9C2 心肌细胞建立体外模型。通过 qPCR、Western blot、免疫组化或免疫荧光检测 PLTP 及铁死亡相关蛋白 ACSL4、GPX4、4-HNE 等的表达变化。采用 PLTP 敲除小鼠或重组 PLTP 干预模型观察 PLTP 下调对脓毒症心肌损伤的影响，并通过血浆 LDH 水平、心脏超声、HE 染色及生存分析评估心肌损伤程度。利用 JASPAR 数据库预测 PLTP 启动子区域潜在转录因子结合位点，并检测 KLF5 在脓毒症心肌组织中的表达变化。进一步采用 KLF5 抑制剂 ML264 干预 LPS 刺激的 H9C2 细胞，观察抑制 KLF5 后 PLTP 表达及铁死亡相关指标的变化。

CLP 后小鼠心脏组织及 LPS 刺激的 H9C2 细胞中 PLTP 表达明显下调，同时伴随心肌损伤加重和铁死亡相关改变，表现为 ACSL4、4-HNE 表达升高，GPX4 表达下降。与 WT+CLP 组相比，PLTP 缺失进一步加重脓毒症小鼠心肌损伤，表现为血浆 LDH 水平升高、心功能下降、心肌组织病理损伤加重及生存率降低，并进一步增强心肌组织铁死亡相关改变。生物信息学预测显示，PLTP 启动子区域存在潜在 KLF5 结合位点；同时，CLP 后小鼠心脏组织中 KLF5 表达显著升高。体外实验中，KLF5 抑制剂 ML264 干预后可部分恢复 LPS 诱导的 PLTP 下调，并减轻 ACSL4、4-HNE 升高及 GPX4 下降等铁死亡相关改变。

脓毒症时，KLF5 异常升高可能参与 PLTP 表达下调，导致心肌细胞磷脂转运稳态受损，并促进脂质过氧化和铁死亡发生，从而加剧脓毒症心肌损伤。KLF5/PLTP 轴可能是干预脓毒症心肌铁死亡和改善脓毒症相关心功能障碍的潜在治疗靶点。

Lymphocyte–C-reactive Protein Ratio upon Admission Predicts Resistance to Initial Intravenous Immunoglobulin in Pediatric Patients with Kawasaki Disease: A Two-center Retrospective Cohort Study

姓名：Ya-Jun Wang1*, Lei Zhang2*, Jin-Xia Lan1*, Yan Zhang3*, Yu-Jia Tang3, Hui-Ying Liu3, Yi-Lu Lin3, Yao Li3, Jia-Le Deng3, Kai Kang4, Zhi-Hui Wang5, Yang Gao3

单位：1 Department of Pediatrics, The Sixth Affiliated Hospital of Harbin Medical University

2 Department of Emergency, The First Affiliated Hospital of Harbin Medical University

3 Department of Critical Care Medicine, The Sixth Affiliated Hospital of Harbin Medical University

4 Department of Critical Care Medicine, The First Affiliated Hospital of Harbin Medical University

5 Department of Emergency, The Sixth Affiliated Hospital of Harbin Medical University

Abstract

Objective: To evaluate whether the lymphocyte–C-reactive protein ratio (LCR) at admission predicts resistance to initial intravenous immunoglobulin (IVIG) in children with Kawasaki disease (KD).

Methods: We retrospectively analyzed children with KD treated at two centers between January 1, 2014, and December 31, 2024. Admission LCR was natural-log transformed (lnLCR). Patients were classified as initial IVIG responsive or resistant, and clinical variables were compared using multivariable logistic regression and receiver operating characteristic (ROC) analysis.

Results: Among 317 children, 18 (5.68%) were resistant to initial IVIG. Each one-unit increase in admission lnLCR was associated with lower odds of resistance (odds ratio, 0.509; 95% confidence interval, 0.319–0.813). The area under the ROC curve was 0.760. At a cutoff of 6.170, sensitivity was 88.90%, specificity 65.20%, positive predictive value 13.33%, and negative predictive value 98.98%.

Conclusion: Admission LCR is an inexpensive, readily available immunoinflammatory marker that may support early risk stratification for initial IVIG resistance in pediatric KD. Its modest specificity and the small number of resistant cases require external validation before clinical implementation.

Keywords: lymphocyte–C-reactive protein ratio; Kawasaki disease; resistance to initial intravenous immunoglobulin; risk stratification; personalized medicine

Introduction

Kawasaki disease (KD) is an acute systemic vasculitis that predominantly affects children younger than 5 years and is a leading cause of acquired pediatric heart disease and coronary artery lesions (CAL) [1–7]. Its pathogenesis is thought to involve an immune-mediated inflammatory response to environmental triggers in genetically susceptible children [8–10]. Although intravenous immunoglobulin (IVIG) plus aspirin is first-line therapy, IVIG resistance increases the risk of CAL and long-term cardiovascular complications [11,12]. Early identification of high-risk patients could enable closer monitoring and individualized treatment, yet simple, inexpensive admission markers remain limited [13,14].

The lymphocyte–C-reactive protein ratio (LCR) integrates adaptive immune status and systemic inflammation. It has shown prognostic value in malignancy and acute inflammatory illnesses when measured at admission, perioperatively, or serially [15–22]. Our previous study found that admission LCR combined with albumin predicted coronary artery dilation and aneurysm formation in children with KD [16]. However, its association with initial IVIG resistance has not been established.

We therefore investigated whether admission LCR could serve as an early warning marker for initial IVIG resistance in pediatric KD and provide a basis for future risk-stratified treatment strategies.

Methods

Study design

This two-center retrospective cohort study included children with KD admitted to the First Affiliated Hospital of Harbin Medical University from January 1, 2014, to August 7, 2022, or to the Sixth Affiliated Hospital from August 8, 2022, to December 31, 2024. Initial therapy consisted of IVIG (400 mg/kg daily for 5 days or 1 g/kg daily for 2 days) and oral aspirin. Aspirin was given at 30–50 mg/kg/day in 2–3 divided doses, then reduced to 3–5 mg/kg once daily for 6–8 weeks beginning 3 days after defervescence. Demographic data, admission laboratory findings, fever duration before IVIG, and length of stay were extracted from medical records. Patients were classified as initial IVIG responsive or resistant. The ethics committees of both hospitals approved the study (IRB Nos. 2025117 and LC2025-004).

Study population

Eligible participants were 28 days to 16 years of age, had a definitive diagnosis of KD, and received standard-dose IVIG and aspirin as initial treatment. Exclusion criteria were concurrent infection or another autoimmune disease, primary or acquired immunodeficiency, chronic organ failure, malignancy, severe malnutrition, immunotherapy or organ transplantation within the previous 6 months, or incomplete records (Figure 1).

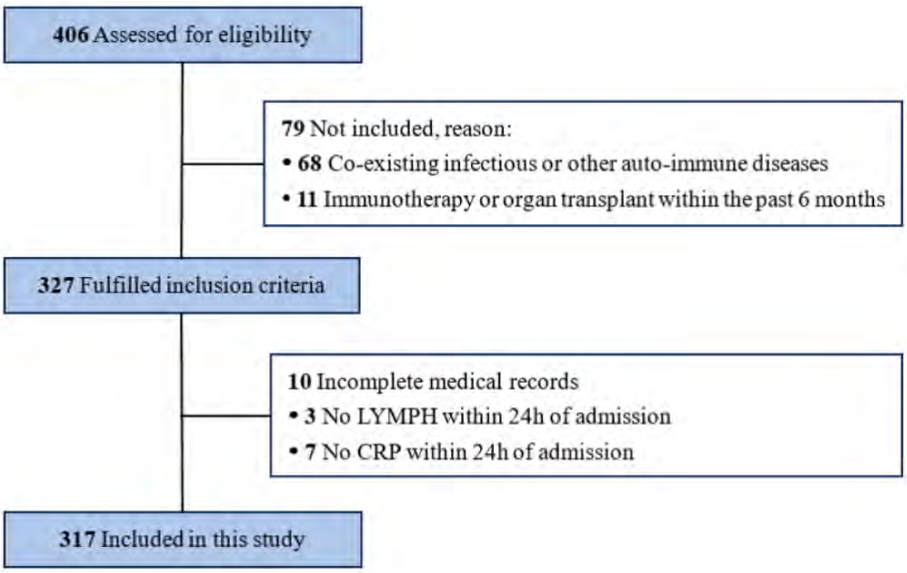


Figure 1 Flowchart of the study participants. Abbreviations: LYMPH: Lymphocyte, CRP: C-reactive Protein.

Diagnosis and treatment of KD

KD, including classic and incomplete presentations, was diagnosed using clinical findings, laboratory results, and echocardiography in accordance with relevant guidelines [23–25]. Standard initial treatment was IVIG plus aspirin; repeat IVIG or IVIG combined with corticosteroids could be considered for resistant cases [23–26].

Determination of resistance to initial IVIG

After exclusion of other causes, initial IVIG resistance was defined as persistent fever above 38 ° C within 36 hours after IVIG and aspirin, or recurrent fever with at least one principal KD feature within 2 weeks, most commonly 2–7 days, after treatment [27].

Calculation of LCR upon admission

Admission LCR was calculated from lymphocyte count (LYMPH) and C-reactive protein (CRP) measured within 24 hours: LCR = LYMPH ($\times 10^9$/L) $\times$ 10,000 / CRP (mg/L) [16–19].

Data collection

De-identified data were obtained from the medical record departments by trained study personnel. The requirement for written informed consent was waived under institutional policy.

Statistical analyses

Analyses were performed with SPSS version 22.0. Admission LCR was natural-log transformed and reported as lnLCR. Normally distributed continuous variables are presented as mean ± standard deviation and were compared with independent-samples t tests; non-normally distributed variables are presented as median (P25, P75) and were compared with Mann–Whitney U tests. Categorical variables were compared with chi-square tests. Because the study was exploratory, no adjustment was made for multiple comparisons. Variables with $P < 0.05$ in between-group analyses entered a multivariable logistic regression model using backward Wald selection. ROC analysis provided the area under the curve (AUC), optimal cutoff, sensitivity, specificity, positive predictive value (PPV), and negative predictive value (NPV). Given the small resistant group, significant predictors underwent post hoc power analysis in G*Power and 1,000-sample bootstrap validation in STATA 15.0. Two-sided $P < 0.05$ indicated statistical significance.

Results

Comparison of demographic characteristics and clinical parameters upon admission and during hospitalization between the initial IVIG-responsive group and the initial IVIG-resistant group

The cohort included 317 children (male-to-female ratio, 1.66:1): 299 were responsive and 18 were resistant to initial IVIG, yielding a resistance rate of 5.68%. Compared with responsive patients, resistant patients had higher neutrophil percentage, CRP, alanine aminotransferase, aspartate aminotransferase, and direct bilirubin; lower lymphocyte percentage, lymphocyte count, and lnLCR; and longer hospital stays (Table 1).

Table 1 Comparison of demographic characteristics and clinical parameters upon admission and during hospitalization between the initial IVIG-responsive group and the initial IVIG-resistant group

Variable(s)	The initial IVIG–responsive group (n = 299)	The initial IVIG–resistant group (n = 18)	$t/Z/X^2$	*P*
Gender (male/female)	184/115	14/4	1.910	0.167
Age (year)	2.67 (1.25, 4.25)	2.04 (1.48, 5.04)	−0.122	0.903
Weight (kilogram)	14.00 (11.00, 17.10)	13.00 (10.88, 16.25)	−1.039	0.299
WBC (× 10^9/L)	13.18 (10.25, 16.80)	12.32 (8.71, 17.16)	−0.602	0.547
NEUT% (%)	63.85 ± 16.07	72.68 ± 13.51	2.281	0.023
NEUT (× 10^9/L)	8.70 (5.56, 11.45)	8.77 (5.23, 12.48)	−0.281	0.779
LYMPH% (%)	24.20 (15.64, 34.94)	17.00 (11.15, 25.59)	−2.251	0.024
LYMPH (× 10^9/L)	3.10 (2.00, 4.51)	1.86 (0.98, 3.42)	−2.588	0.010
PLT (× 10^9/L)	336.04 ± 122.54	340.12 ± 170.12	−0.850	0.396
CRP (mg/L)	46.27 (18.44, 81.26)	79.44 (48.82, 109.25)	−2.419	0.016
ESR (mm/h)	47.12 ± 23.29	55.22 ± 23.74	−1.431	0.153
D–Dimer (μg/L)	1.07 (0.73, 1.56)	1.60 (0.83, 2.34)	−1.613	0.107
ALT (U/L)	24.70 (15.50, 53.77)	53.92 (22.80,126.70)	−2.174	0.030
AST (U/L)	29.00 (23.00, 41.00)	47.50 (26.95, 98.40)	−2.673	0.008
ALB (g/L)	36.87 (33.82, 39.46)	35.96 (30.10, 38.46)	−1.111	0.26

				7
TBIL (umol/L)	8.20 (6.05, 11.76)	9.85 (4.97, 24.65)	−0.857	0.392
DBIL (umol/L)	1.21 (0.00, 2.34)	2.04 (1.04, 5.28)	−2.367	0.018
IBIL (umol/L)	6.73 (4.95, 9.54)	7.20 (3.29, 19.37)	−0.075	0.940
CK–MB (ng/ml)	14.00 (9.00, 20.00)	14.25 (6.08, 16.25)	−0.842	0.400
lnLCR	6.70 ± 1.35	5.61 ± 0.82	−3.367	0.001
Fever duration prior to initial IVIG (day)	7.00 (5.00, 8.00)	6.00 (4.00, 8.00)	−1.027	0.305
Hospital stay (day)	7.00 (5.00, 8.00)	10.00 (7.75, 14.00)	−4.704	0.000

Abbreviations: IVIG: Intravenous Immunoglobulin, WBC: White Blood Cell, NEUT%: Neutrophil Percentage, NEUT: Neutrophil, LYMPH%: Lymphocyte Percentage, LYMPH: Lymphocyte, PLT: Platelet, CRP: C-reactive Protein, ESR: Erythrocyte Sedimentation Rate, ALT: Alanine Aminotransferase, AST: Aspartate Aminotransferase, ALB: Albumin, TBIL: Total Bilirubin, DBIL: Direct Bilirubin, IBIL: Indirect Bilirubin, CK-MB: Creatine Kinase-MB, LCR: Lymphocyte-C-reactive Protein Ratio.

Analysis of the factors related to resistance to initial IVIG

Admission lnLCR was independently associated with lower odds of initial IVIG resistance. Each one-unit increase reduced the odds to 0.509 of the previous value (95% confidence interval, 0.319–0.813; P = 0.005) (Table 2). Although length of stay was significant, it was considered a consequence rather than an early predictor of resistance.

Table 2 Analysis of the factors related to resistance to initial IVIG

Variable(s)	B	SE	Wald	df	Sig	Exp(B)	95% CI for Exp(B)	
							Lower	Upper
lnLCR upon admission	−0.675	0.239	7.981	1.000	0.005	0.509	0.319	0.813
Hospital stay	0.350	0.080	18.907	1.000	0.000	1.419	1.212	1.661
Constant	−1.634	1.532	1.137	1.000	0.286	0.195		

Abbreviations: IVIG: Intravenous Immunoglobulin, SE: Standard Error, df: Degrees of Freedom, CI: Confidence Interval, LCR: Lymphocyte-C-reactive Protein Ratio.

The ROC curve of lnLCR upon admission to classify pediatric patients with KD into the initial IVIG-resistant group

Admission lnLCR yielded an AUC of 0.760 (95% confidence interval, 0.668–0.852) (Table 3; Figure 2). At the 6.170 cutoff, sensitivity

was 88.90%, specificity 65.20%, PPV 13.33%, NPV 98.98%, and the maximum Youden index 0.541.

Table 3 The AUC of lnLCR upon admission

Variable(s)	Area	SE	Asymptotic Sig	Asymptotic 95% CI	
				Lower Bound	Upper Bound
lnLCR upon admission	0.760	0.047	0.000	0.668	0.852

Abbreviations: AUC: Area Under the ROC Curve, ROC: Receiver Operating Characteristic, LCR: Lymphocyte-C-reactive Protein Ratio, SE: Standard Error, CI: Confidence Interval.

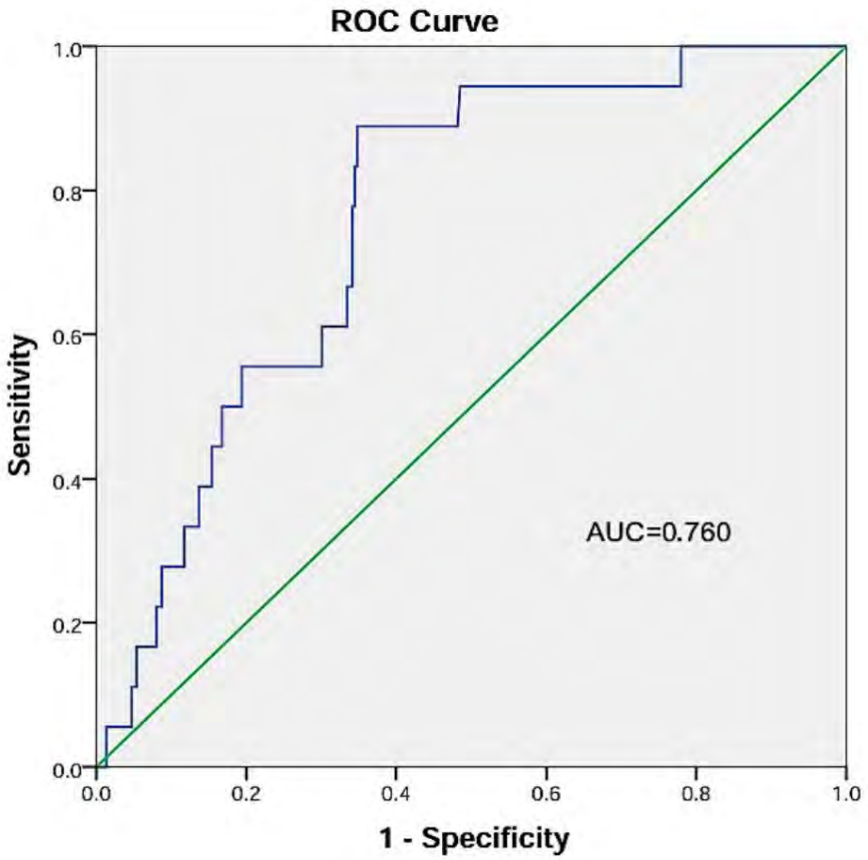


Figure 2 The ROC curve of lnLCR upon admission to classify pediatric patients with KD into the initial IVIG-resistant group. Abbreviations: AUC: Area Under the ROC Curve, ROC: Receiver Operating Characteristic, LCR: Lymphocyte-C-reactive Protein Ratio, KD: Kawasaki Disease, IVIG: Intravenous Immunoglobulin.

Post hoc power analysis

Post hoc power for the observed effect was 100%; however, this does not overcome the limitation imposed by only 18 resistant cases.

Bootstrap resampling analysis

In 1,000 bootstrap samples, admission lnLCR remained the only variable retained in the multivariable model.

Discussion

In this two-center cohort, 5.68% of children with KD were resistant to initial IVIG, a rate lower than that reported in several domestic and international series but similar to another study from eastern China [28–32]. Regional, ethnic, treatment, or case-mix differences may contribute. Although several admission variables differed between groups, only lnLCR remained an independent early factor after multivariable analysis and bootstrap validation. The association was clinically plausible: a lower lymphocyte count combined with a higher CRP concentration reflects a stronger systemic inflammatory response and weaker adaptive immune balance. Hospital stay was also associated with resistance but is unsuitable for prediction because it occurs after the treatment response is known.

Current KD management generally uses the same initial IVIG–aspirin regimen for most patients, whereas a reliable early risk marker could support more individualized care. Additional immunomodulators, including infliximab, cyclosporine, and corticosteroids, have been studied in resistant or high-risk KD [33–35]. Existing scores such as the Kobayashi, Formosa, Egami, Sano, and Harada models have limited transportability across Japanese and non-Japanese populations [36–39]. In our study, the probability of resistance increased as admission lnLCR decreased. A value below 6.170 identified a higher-risk group, whereas a value above this threshold had a high NPV and effectively excluded resistance in this cohort (Figure 3). The low PPV, however, means that lnLCR should not be used alone to justify intensified therapy. Rather, it may complement clinical assessment, echocardiography, and other laboratory markers, identify children who warrant closer surveillance, and inform the development of multivariable prediction tools. Prospective studies should determine whether LCR-guided strategies improve coronary outcomes or reduce unnecessary treatment.

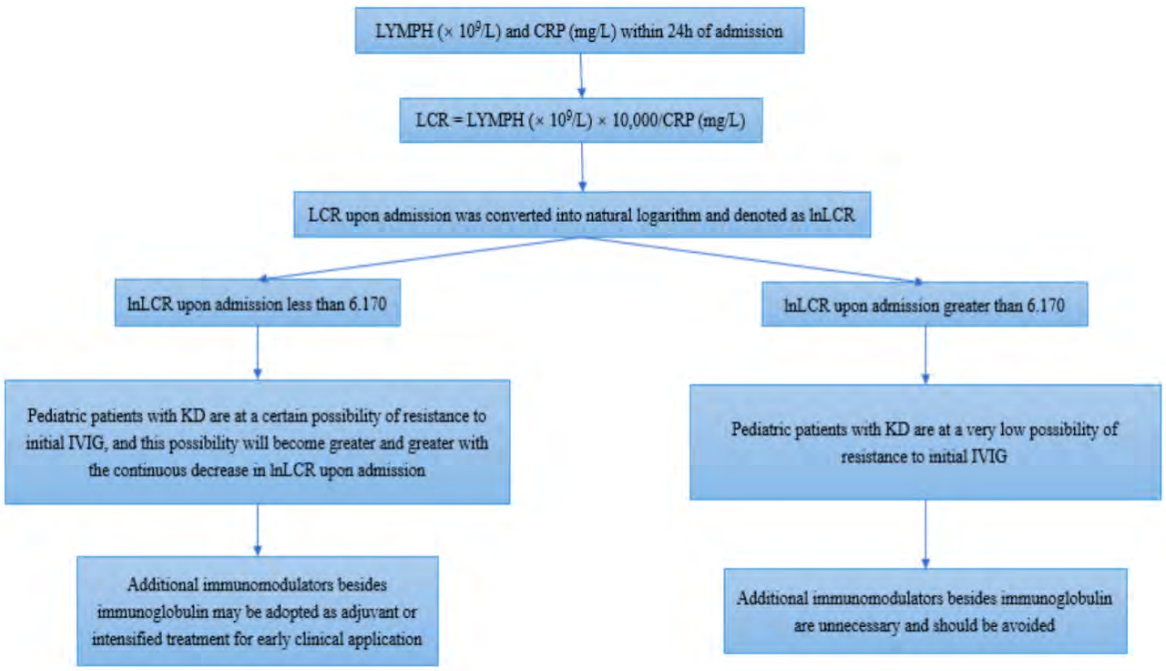


Figure 3 Schematic diagram of clinical application of lnLCR upon admission.

Abbreviations: LYMPH: Lymphocyte, CRP: C-reactive Protein, LCR: Lymphocyte-C-reactive Protein Ratio, KD: Kawasaki Disease, IVIG: Intravenous Immunoglobulin.

This study has several limitations. Its retrospective design and modest sample size limit causal inference and generalizability. Only 18 children were IVIG resistant, reducing model stability despite bootstrap validation. The high NPV partly reflects the low prevalence of resistance and may not apply to populations with higher event rates. Specificity was modest, and the single-marker model requires improvement. Finally, the findings were not externally validated. Large, prospective, multicenter studies should validate the cutoff and evaluate a multivariable model incorporating LCR before routine clinical use.

Conclusion

Admission LCR is a readily available, low-cost biomarker with potential value for predicting initial IVIG resistance and supporting risk stratification in pediatric KD. Because this exploratory study included few resistant cases and showed modest specificity, external prospective validation is required before LCR is used to guide treatment.

References

1.Day-Lewis M, Son MBF, Lo MS. Kawasaki disease: contemporary perspectives. Lancet Child Adolesc Health. 2024;8(10):781-792. doi: 10.1016/S2352-4642(24)00169-X

2.Jiao F, Pan Y, Du Z, et al. Guideline for the diagnosis and treatment of incomplete Kawasaki disease in children in China. BMC Pediatr. 2024;24(1):477. doi: 10.1186/s12887-024-04961-2

3.Aggarwal R, Pilania RK, Sharma S, et al. Kawasaki disease and the environment: an enigmatic interplay. Front Immunol. 2023;14:1259094. doi: 10.3389/fimmu.2023.1259094

4.Wen H, Hun M, Zhao M, et al. Serum ferritin as a crucial biomarker in the diagnosis and prognosis of intravenous immunoglobulin resistance and coronary artery lesions in Kawasaki disease: A systematic review and meta-analysis. Front Med (Lausanne). 2022;9:941739. doi: 10.3389/fmed.2022.941739

5.Robinson C, Chanchlani R, Gayowsky A, et al. Incidence and short-term outcomes of Kawasaki disease. Pediatr Res. 2021;90(3):670-677. doi: 10.1038/s41390-021-01496-5

6.Nielsen TM, Andersen NH, Torp-Pedersen C, et al. Kawasaki disease, autoimmune disorders, and cancer: a register-based study. Eur J Pediatr. 2021;180(3):717-723. doi: 10.1007/s00431-020-03768-4

7.Lin CH, Lai JN, Lee IC, et al. Kawasaki Disease May Increase the Risk of Subsequent Cerebrovascular Disease. Stroke. 2022;53(4):1256-1262. doi: 10.1161/STROKEAHA.120.032953

8.Rife E, Gedalia A. Kawasaki Disease: an Update. Curr Rheumatol Rep. 2020;22(10):75. doi: 10.1007/s11926-020-00941-4

9.Xiong Y, Xu J, Zhang D, et al. MicroRNAs in Kawasaki disease: An update on diagnosis, therapy and monitoring. Front Immunol. 2022;13:1016575. doi: 10.3389/fimmu.2022.1016575

10.Kang JM, Jung J, Kim YE, et al. Temporal Correlation Between Kawasaki Disease and Infectious Diseases in South Korea. JAMA Netw Open. 2022;5(2):e2147363. doi: 10.1001/jamanetworkopen.2021.47363

11.Wang Y, Huang S, Wang P, et al. Novel Predictive Scoring System for Intravenous Immunoglobulin Resistance Helps Timely Intervention in Kawasaki Disease: The Chinese Experience. J Immunol Res. 2023;2023:6808323. doi: 10.1155/2023/6808323

12.Iio K, Morikawa Y, Miyata K, et al. Risk Factors of Coronary Artery Aneurysms in Kawasaki Disease with a Low Risk of Intravenous Immunoglobulin Resistance: An Analysis of Post RAISE. J Pediatr. 2022;240:158-163.e4. doi: 10.1016/j.jpeds.2021.08.065

13.Li C, Wu S, Shi Y, et al. Establishment and Validation of a Multivariate Predictive Scoring Model for Intravenous Immunoglobulin-Resistant Kawasaki Disease: A Study of Children From Two Centers in China. Front Cardiovasc Med. 2022;9:883067. doi: 10.3389/fcvm.2022.883067

14.Wang J, Huang X, Guo D. Predictors and a novel predictive model for intravascular immunoglobulin resistance in Kawasaki disease. Ital J Pediatr. 2023;49(1):126. doi: 10.1186/s13052-023-01531-7

15.Zhang JN, Gao Y, Wang XT, et al. Lymphocyte-C-reactive protein ratio can differentiate disease severity of COVID-19 patients and serve as an assistant screening tool for hospital and ICU admission. Front Immunol. 2022;13:957407. doi: 10.3389/fimmu.2022.957407

16.Wang Y, Lin Y, Zhang L, et al. Lymphocyte-C-reactive protein ratio combined with albumin upon admission predicts coronary artery dilation and aneurysm formation in pediatric patients with Kawasaki disease: a retrospective cohort study. Expert Rev Clin Immunol. 2024;20(9):1127-1133. doi: 10.1080/1744666X.2024.2385765

17.Hu YJ, Qiu SX, Zhang JN, et al. Lymphocyte-C-reactive protein ratio upon admission to predict disease progression and ICU admission in adult patients with diabetic ketoacidosis. Sci Rep. 2025;15(1):3012. doi: 10.1038/s41598-024-84054-3

18.Xu XY, Gao Y, Yue CS, et al. Predictive and Prognostic Potentials of Lymphocyte-C-Reactive Protein Ratio Upon Hospitalization in Adult Patients with Acute Pancreatitis. J Inflamm Res. 2024;17:1659-1669. doi: 10.2147/JIR.S450587

19.Wang D, Gao Y, Lai QQ, et al. Dynamic lymphocyte-CRP ratio as a predictor: a single-centre retrospective study on disease severity and progression in adult COVID-19 patients. J Int Med Res. 2024;52(3):3000605241236278. doi: 10.1177/03000605241236278

20.Okugawa Y, Toiyama Y, Fujikawa H, et al. Cumulative perioperative lymphocyte/C-reactive protein ratio as a predictor of the long-term outcomes of patients with colorectal cancer. Surg Today. 2021;51(12):1906-1917. doi: 10.1007/s00595-021-02291-9

21.Zhang YF, Lu LH, Zhong C, et al. Prognostic Value of the Preoperative Lymphocyte-C-Reactive Protein Ratio in Hepatocellular Carcinoma Patients Treated with Curative Intent: A Large-Scale Multicentre Study. J Inflamm Res. 2021;14:2483-2495. doi: 10.2147/JIR.S311994

22.Miyatani K, Sawata S, Makinoya M, et al. Combined analysis of preoperative and postoperative lymphocyte-C-reactive protein ratio precisely predicts outcomes of patients with gastric cancer. BMC Cancer. 2022;22(1):641. doi: 10.1186/s12885-022-09716-9

23.Marchesi A, Tarissi de Jacobis I, Rigante D, et al. Kawasaki disease: guidelines of the Italian Society of Pediatrics, part I - definition, epidemiology, etiopathogenesis, clinical expression and management of the acute phase. Ital J Pediatr. 2018;44(1):102. doi: 10.1186/s13052-018-0536-3

24.McCrindle BW, Rowley AH, Newburger JW, et al. Diagnosis, Treatment, and Long-Term Management of Kawasaki Disease: A Scientific Statement for Health Professionals From the American Heart Association. Circulation. 2017;135(17):e927-e999. doi: 10.1161/CIR.0000000000000484

25.Shaanxi Provincial Kawasaki Disease Diagnosis and Treatment Center/Children’s Hospital of Shaanxi Provincial People’s Hospital, National Center for Children’s Health/Beijing Children’s Hospital Affiliated to Capital Medical University, Children’s Hospital of Shanghai Jiao Tong University School of Medicine, et al. Evidence-based Guidelines for the Diagnosis and Treatment of Kawasaki Disease in Chinese Children. Chinese Journal of Contemporary Pediatrics. 2023;25(12):1198–1210. doi: 10.7499/j.issn.1008-8830.2309038

26.Chang LS, Kuo HC. The role of corticosteroids in the treatment of Kawasaki disease. Expert Rev Anti Infect Ther. 2020;18(2):155-164. doi: 10.1080/14787210.2020.1713752

27.Subspecialty Group of Cardiology, the Society of Pediatrics, Chinese Medical Association; Subspecialty Group of Rheumatology, the Society of Pediatrics, Chinese Medical Association; Subspecialty Group of Immunology, the Society of Pediatrics, Chinese Medical Association, et al. The expert consensus on diagnosis and acute-phase treatment of Kawasaki disease. Zhonghua Er Ke Za Zhi. 2022;60(1):6-13. Chinese. doi: 10.3760/cma.j.cn112140-20211018-00879

28.Cheon EJ, Kim GB, Park S. Predictive modeling of consecutive intravenous immunoglobulin treatment resistance in Kawasaki disease: A nationwide study. Sci Rep. 2025;15(1):903. doi: 10.1038/s41598-025-85394-4

29.Huang H, Jiang J, Shi X, et al. Nomogram to predict risk of resistance to intravenous immunoglobulin in children hospitalized with Kawasaki disease in Eastern China. Ann Med. 2022;54(1):442-453. doi: 10.1080/07853890.2022.2031273

30.Yi C, Zhou YN, Guo J, et al. Novel predictors of intravenous immunoglobulin resistance in patients with Kawasaki disease: a retrospective study. Front Immunol. 2024;15:1399150. doi: 10.3389/fimmu.2024.1399150

31.Sunaga Y, Watanabe A, Katsumata N, et al. A simple scoring model based on machine learning predicts intravenous immunoglobulin resistance in Kawasaki disease. Clin Rheumatol. 2023;42(5):1351-1361. doi: 10.1007/s10067-023-06502-1

32.Kaya Akca U, Arslanoglu Aydin E, Aykan HH, et al. Comparison of IVIG resistance predictive models in Kawasaki disease. Pediatr

Res. 2022;91(3):621-626. doi: 10.1038/s41390-021-01459-w

33.Burns JC, Roberts SC, Tremoulet AH, et al. Infliximab versus second intravenous immunoglobulin for treatment of resistant Kawasaki disease in the USA (KIDCARE): a randomised, multicentre comparative effectiveness trial. Lancet Child Adolesc Health. 2021;5(12):852-861. doi: 10.1016/S2352-4642(21)00270-4

34.Wang L, He M, Wang W, et al. Efficacy and safety of infliximab in the treatment of Kawasaki disease: A systematic review and meta-analysis. Eur J Pediatr. 2024;183(4):1765-1776. doi: 10.1007/s00431-024-05437-2

35.Li X, Tang Y, Ding Y, et al. Higher efficacy of infliximab than immunoglobulin on Kawasaki disease, a meta-analysis. Eur J Pharmacol. 2021;899:173985. doi: 10.1016/j.ejphar.2021.173985

36.Faim D, Henriques C, Brett A, et al. Kawasaki Disease: Predictors of Resistance to Intravenous Immunoglobulin and Cardiac Complications. Arq Bras Cardiol. 2021;116(3):485-491. English, Portuguese. doi: 10.36660/abc.20190758

37.Kuniyoshi Y, Tsujimoto Y, Banno M, et al. Prediction Models for Intravenous Immunoglobulin Resistance in Kawasaki Disease: A Meta-analysis. Pediatrics. 2023;151(5):e2022059175. doi: 10.1542/peds.2022-059175

38.Guo MM, Kuo HC. The state of play in tools for predicting immunoglobulin resistance in Kawasaki disease. Expert Rev Clin Immunol. 2023;19(10):1273-1279. doi: 10.1080/1744666X.2023.2238122

39.Chiang WN, Huang PY, Kuo HC, et al. Evaluation of Formosa score and diagnostic sensitivity and specificity of four Asian risk scores for predicting intravenous immunoglobulin resistance in Kawasaki disease: a bivariate meta-analysis. Front Cardiovasc Med. 2023;10:1164530. doi: 10.3389/fcvm.2023.1164530

Mechanism-Guided Mobile Decision Support and Early Functional Outcomes After Severe Acute Brain Injury: A Two-Center Propensity Score-Matched Cohort Study

姓名：邱俊

单位：四川省宜宾市第二人民医院

Abstract

Background: Severe acute brain injury (SABI) produces interacting disturbances in systemic host responses, cerebral oxygen metabolism, intracranial compliance, cerebral perfusion/autoregulation, and cerebrospinal-fluid dynamics. Although contemporary guidelines address individual domains, bedside integration remains difficult when physiological priorities compete and reassessment is delayed. SMOOTH is a standardized, non-prescriptive mobile workflow comprising sedation and analgesia; targeted temperature management and multidisciplinary coordination; intracranial pressure/compliance management using optic nerve sheath diameter and invasive intracranial pressure when available; integrated cardiopulmonary-hemodynamic optimization; and time-sensitive TCD/TCCD cerebral blood-flow assessment. The “1+3+1” thinking chain provides the mechanism-guided sequence for clinical prioritization.

Objective: To evaluate whether documented SMOOTH-assisted management was associated with early functional outcomes in adults with SABI.

Methods: We conducted an exposure-defined, two-center, propensity score-matched retrospective cohort study. Adults with intracerebral hemorrhage, subarachnoid hemorrhage, or traumatic brain injury and admission Glasgow Coma Scale score ⩾ 4 were eligible. SMOOTH exposure required patient-level documentation of platform-supported physiological reassessment, structured SMOOTH assessment aligned with the “1+3+1” chain, TCD/TCCD-guided review, or severity-adaptive reassessment prompting. Controls had no documented SMOOTH workflow and were matched within center at a 1:1.5 ratio. The primary outcome was functional independence at discharge, defined as modified Rankin Scale (mRS) score ⩽ 2.

Results: The matched cohort included 40 SMOOTH-exposed patients and 60 standard-care controls. All postmatch absolute standardized mean differences were <0.10. Discharge functional independence occurred in 70.0% versus 41.7%, respectively. SMOOTH exposure was independently associated with the primary outcome (adjusted odds ratio 4.81, 95% CI 1.75–13.18; P=0.002), with an absolute between-group difference of 28.3 percentage points. The discharge mRS distribution shifted favorably (Mann–Whitney P=0.005; rank-biserial r=0.325). Favorable GOS-E and fewer intracranial pressure crises were consistent secondary signals; Firth and ridge-penalized models yielded concordant estimates.

Conclusion: Documented SMOOTH-assisted management was associated with better early functional outcomes and fewer intracranial pressure crises. These observational findings are hypothesis-generating and require prospective multicenter validation with standardized monitoring and blinded long-term outcome assessment.

Keywords: severe acute brain injury; clinical decision support; SMOOTH; “1+3+1” thinking chain; neurocritical care; propensity score matching; functional outcome

1. Research Background and Current Status

Severe acute brain injury includes clinically diverse disorders such as intracerebral hemorrhage, aneurysmal subarachnoid hemorrhage, and traumatic brain injury, but these conditions share a convergent secondary-injury physiology. After the primary insult, systemic stress responses, cerebral metabolic demand, intracranial compliance, autoregulation, perfusion, and cerebrospinal-fluid dynamics may deteriorate simultaneously and amplify one another. Sympathetic activation and extracerebral organ dysfunction can destabilize oxygen delivery; impaired compliance can promote intracranial pressure escalation; and disturbed perfusion or autoregulation can deepen ischemia–hypoxia. Timely coordination of these processes is central to preserving the neurovascular unit and preventing potentially reversible physiological abnormalities from becoming irreversible neuronal injury [1–4].

Guidelines for intracerebral hemorrhage, subarachnoid hemorrhage, traumatic brain injury, intracranial pressure management, multimodality monitoring, mechanical ventilation, and neurocritical ultrasound provide evidence-based recommendations for

individual domains [2–7]. However, real-world care requires clinicians to reconcile competing goals under time pressure. Osmotic therapy may lower intracranial pressure while complicating preload or perfusion targets; induced hypertension may be limited by cardiac reserve; and deeper sedation may reduce cerebral metabolic demand while delaying neurologic assessment. This gap is primarily one of decision architecture and implementation rather than absence of evidence [8,9].

SMOOTH was developed as a standardized bedside workflow for goal-oriented, multimodal SABI management [10]. It includes sedation and analgesia (S); targeted temperature management and multidisciplinary coordination (M); intracranial pressure and compliance management (O1), incorporating optic nerve sheath diameter and invasive intracranial pressure when available; cardiopulmonary-hemodynamic optimization (O2), integrating cardiac output/blood pressure, respiratory rate/drive, oxygenation, and carbon dioxide targets; and TCD/TCCD-based cerebral blood-flow assessment within 1 hour (T/H). The "1+3+1" thinking chain sequences these elements by prioritizing systemic host-response control, three cerebral microenvironment priorities—oxygen-metabolic balance, intracranial pressure/compliance, and cerebral perfusion/autoregulation—and cerebrospinal-fluid circulation and drainage. The mobile platform supports structured assessment, visualization, time-sensitive reassessment, and rule-based identification of cross-domain conflicts without prescribing treatment or replacing clinician judgment.

2. Objective

To determine whether documented SMOOTH-assisted management was associated with improved early functional outcomes in adults with SABI compared with propensity score-matched standard care.

3. Study Design and Methods

Design and setting: This was an exposure-defined, two-center, propensity score-matched retrospective cohort study conducted at West China Hospital, Sichuan University (Center A), and the Second People's Hospital of Yibin (Center B). Institutional ethics approval was obtained at both centers, and de-identified data were analyzed in accordance with institutional requirements.

Participants: Adults aged ⩾ 18 years admitted to the ICU with intracerebral hemorrhage, subarachnoid hemorrhage, or traumatic brain injury and admission GCS score ⩾ 4 were eligible. Exclusion criteria were age <18 years, GCS <4, withdrawal of life-sustaining treatment within 24 hours, ICU stay <48 hours, or incomplete primary outcome data.

Exposure and comparator: Because SMOOTH was introduced through phased bedside adoption, exposure was defined by patient-level documentation rather than calendar period alone. Exposure required a patient-specific record of structured physiological reassessment, structured SMOOTH assessment aligned with the "1+3+1" chain, TCD/TCCD-guided review, or severity-adaptive reassessment prompting before discharge outcome ascertainment. Standard-care patients had no documented SMOOTH-assisted workflow, structured prompts, or platform conflict alerts.

Matching: The complete screening files contained 527 records: 40 documented SMOOTH-exposed patients and 487 potential controls. After exclusion of 59 controls with admission GCS <4 and four with missing diagnosis or baseline matching variables, 424 controls entered the matching pool. Propensity scores were estimated using age, sex, admission GCS, diagnosis, pupillary reactivity, CT midline shift, and emergency surgery. Nearest-neighbor matching was performed independently within each center at a 1:1.5 ratio using a caliper of 0.2 standard deviations of the logit propensity score. The final cohort contained 40 exposed patients and 60 controls.

Outcomes and analysis: The primary outcome was discharge functional independence (mRS 0–2). Secondary outcomes included favorable GOS-E (⩾ 6), 28-day functional outcomes and survival, discharge GCS, intracranial pressure crisis, cerebral herniation, and systemic complications. The primary model used multivariable logistic regression adjusted for age, admission GCS, pupillary reactivity, CT midline shift, emergency surgery, diagnosis, and center. Firth and ridge-penalized logistic regression addressed sparse-data bias. Prespecified subgroup analyses evaluated center, diagnosis, age, GCS severity, and emergency surgery. Secondary binary outcomes were interpreted with false-discovery-rate control.

Table 1. Selected baseline characteristics of the matched cohort.

Characteristic	SMOOTH (n=40)	Standard care (n=60)	Abs SMD
Age, years, median (IQR)	59 (52–67)	58 (51–68)	0.017
Male sex, n (%)	25 (62.5)	37 (61.7)	0.017
Admission GCS, median (IQR)	9 (7–13)	9 (8–12)	0.037
Intracerebral hemorrhage, n (%)	22 (55.0)	31 (51.7)	0.067
Subarachnoid hemorrhage, n (%)	15 (37.5)	24 (40.0)	0.051
Traumatic brain injury, n (%)	3 (7.5)	5 (8.3)	0.031
Abnormal pupils, n (%)	9 (22.5)	13 (21.7)	0.020
CT midline shift, n (%)	8 (20.0)	12 (20.0)	0.000
Emergency surgery, n (%)	15 (37.5)	22 (36.7)	0.017

Note: SMD, standardized mean difference; GCS, Glasgow Coma Scale; IQR, interquartile range. Absolute SMD <0.10 was considered acceptable balance.

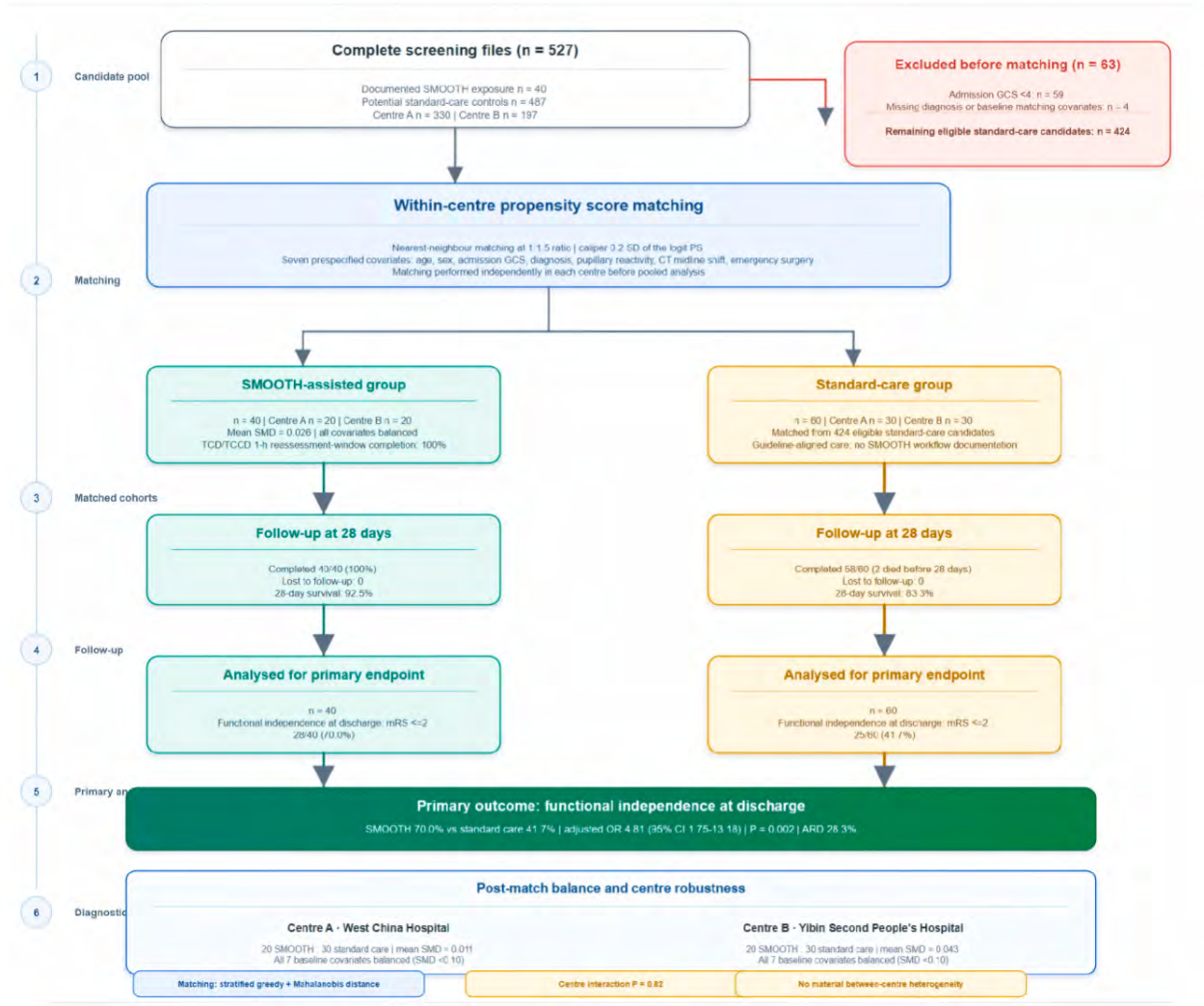


Figure 1. Study flow, patient-level SMOOTH exposure classification, within-center propensity score matching, and construction of the 100-patient matched analytic cohort.

4. Results

Cohort balance: Within-center matching selected 20 SMOOTH-exposed patients and 30 controls from each center. The matched groups were similar in age, sex, admission GCS, diagnosis, pupillary abnormalities, CT midline shift, and emergency surgery. All postmatch absolute standardized mean differences were <0.10, indicating acceptable measured covariate balance (Table 1).

Primary outcome: Discharge functional independence occurred in 28/40 SMOOTH-exposed patients (70.0%) and 25/60 controls (41.7%). The crude odds ratio was 3.27 (95% CI 1.40–7.64; P=0.008). In the prespecified adjusted model, SMOOTH exposure remained associated with functional independence (aOR 4.81, 95% CI 1.75–13.18; P=0.002). The absolute between-group difference was 28.3 percentage points. Because exposure was not randomized, this difference represents an observational association rather than a causal treatment effect.

Ordinal and secondary outcomes: The full discharge mRS distribution shifted toward lower disability in the SMOOTH group (P=0.005; rank-biserial r=0.325). Favorable GOS-E occurred more frequently at discharge and 28 days, and intracranial pressure crisis occurred less frequently. After false-discovery-rate assessment, discharge GOS-E, 28-day GOS-E, and intracranial pressure crisis remained the most robust secondary signals (Table 2; Figure 2).

Robustness: Firth penalized regression (aOR 4.03, 95% CI 1.53–10.59) and ridge regression (aOR 3.99, 95% CI 1.58–10.04) were consistent with the primary estimate. The association remained directionally concordant after excluding the small traumatic brain injury subgroup and across prespecified clinical strata; no interaction test identified statistically significant heterogeneity (Figure 3).

Table 2. Primary and key secondary outcomes.

Outcome	SMOOTH	Standard care	Adjusted OR (95% CI); P	FDR/role
mRS ≤2 at discharge	28/40 (70.0%)	25/60 (41.7%)	4.81 (1.75–13.18); 0.002	Primary
mRS ≤2 at 28 days	30/40 (75.0%)	30/58 (51.7%)	4.23 (1.47–12.16); 0.007	q=0.067
GOS-E ≥6 at discharge	32/40 (80.0%)	29/60 (48.3%)	6.71 (2.23–20.19); <0.001	q=0.020
GOS-E ≥6 at 28 days	32/40 (80.0%)	31/58 (53.4%)	5.92 (1.88–18.69); 0.002	q=0.045
GCS ≥13 at discharge	29/40 (72.5%)	31/60 (51.7%)	3.25 (1.21–8.71); 0.019	q=0.097
ICP crisis	8/40 (20.0%)	27/60 (45.0%)	0.20 (0.06–0.60); 0.004	q=0.045

Note: Adjusted models included age, admission GCS, pupillary reactivity, CT midline shift, emergency surgery, diagnosis, and center. FDR q values use the Benjamini–Hochberg method for secondary binary outcomes.

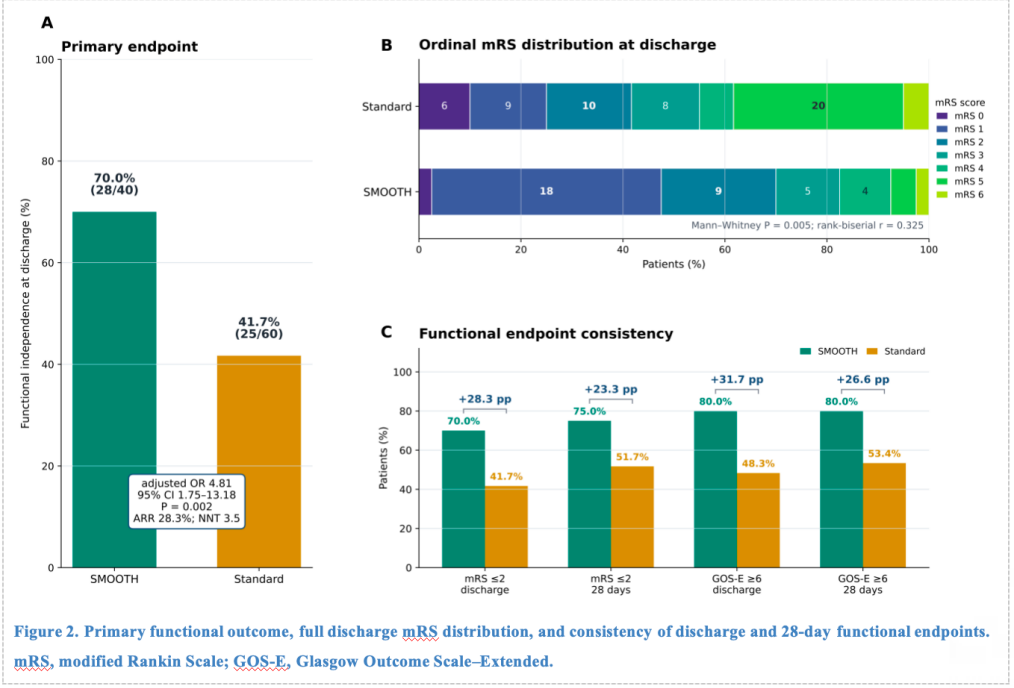


Figure 2. Primary functional outcome, full discharge mRS distribution, and consistency of discharge and 28-day functional endpoints. mRS, modified Rankin Scale; GOS-E, Glasgow Outcome Scale–Extended.

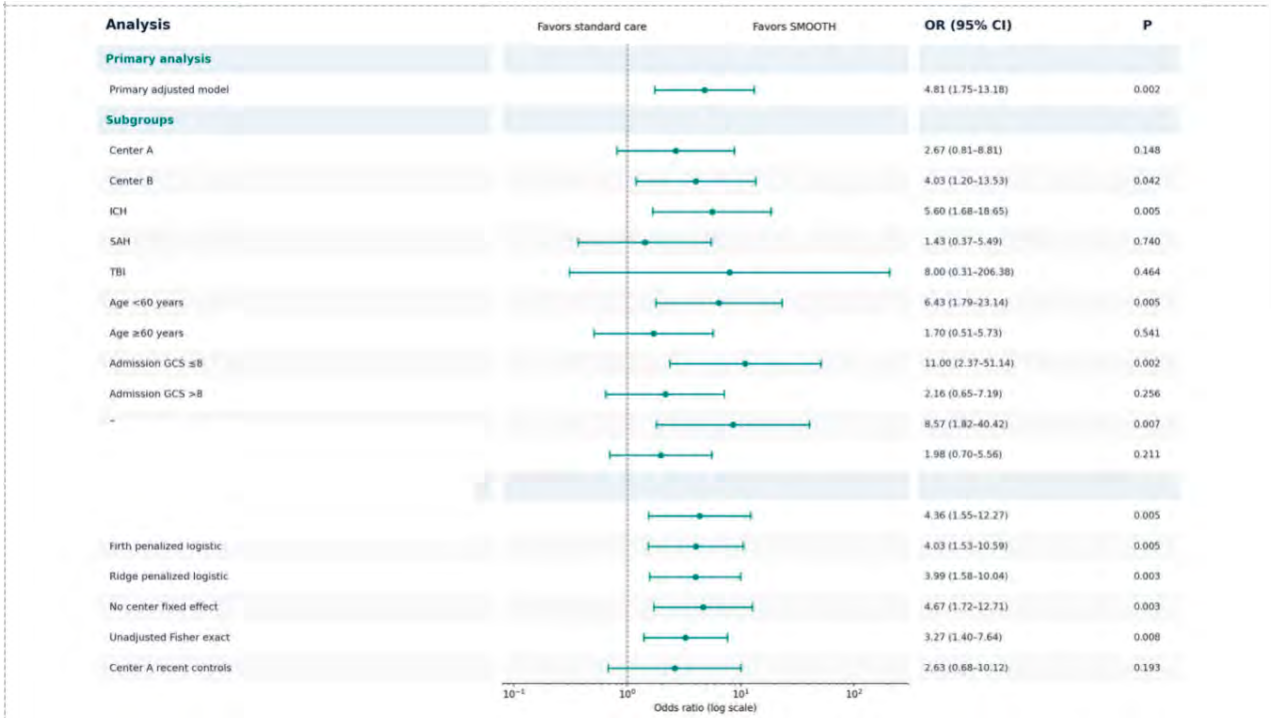


Figure 3. Prespecified subgroup analyses and robustness checks for discharge functional independence. Subgroup estimates are exploratory; interpretation is based on direction and interaction testing rather than within-subgroup significance.

5. Discussion

In this matched two-center cohort, documented SMOOTH-assisted management was associated with a clinically large early functional signal. The association was supported by an ordinal shift across the full mRS distribution, not only by a single dichotomization threshold, and by concordant secondary outcomes involving GOS-E, neurologic recovery, and intracranial pressure crisis. Penalized models and subgroup analyses reduced concerns regarding sparse-data instability but cannot establish causality.

SMOOTH should be interpreted as an implementation and decision-support intervention rather than a new treatment bundle. It does not mandate drugs, procedures, or fixed physiological targets. Its purpose is to organize existing evidence-supported actions, make physiological trade-offs explicit, prompt timely reassessment, and preserve a consistent reasoning sequence when systemic and cerebral priorities compete. This role is particularly relevant to neurocritical care, in which clinical quality depends on continuous coordination of multiple targets rather than one isolated intervention [8,9].

The lower frequency of intracranial pressure crisis is mechanistically coherent with earlier recognition of impaired compliance, more consistent TCD/TCCD reassessment, and structured prioritization of ICP–perfusion conflicts. Nevertheless, monitoring intensity may have differed between groups and could influence event detection. The study also has important limitations: nonrandom exposure, residual confounding, phased implementation, incomplete disease-specific severity variables, a small matched sample, exploratory subgroup analyses, and use of discharge rather than blinded 90-day outcomes. The contribution of individual workflow components cannot be separated.

Prospective multicenter evaluation should use standardized disease-specific severity measures, predefined adherence and process metrics, uniform neuromonitoring definitions, independent long-term outcome adjudication, and explicit control of center and calendar-time effects. Such studies should determine whether benefit is mediated mainly by structured reassessment, earlier recognition of intracranial vulnerability, TCD/TCCD integration, conflict recognition, or more reliable execution of evidence-based care.

6. Conclusion

Documented SMOOTH-assisted management was associated with higher early functional independence, a favorable discharge mRS shift, and fewer intracranial pressure crises in adults with SABI. These findings support prospective multicenter validation but should not be interpreted as causal evidence or a basis for immediate practice change.

Ethics, Funding, and Declarations

The study was approved by the Biomedical Ethics Review Committee of West China Hospital, Sichuan University (2025 Review No. 665; April 27, 2025) and the Medical Ethics Committee of the Second People's Hospital of Yibin (No. 2025-056-01; April 8, 2025). The study was funded by the Sichuan International Medical Exchange and Promotion Association (Grant No. 202500101-2). The authors declare no competing interests. As of July 31, 2026, this work has not been publicly published in a journal and has not received an award from another organization.

References

1. Maas AIR, Menon DK, Manley GT, et al. Traumatic brain injury: progress and challenges in prevention, clinical care, and research. Lancet Neurol. 2022;21:1004–1060.

2. Greenberg SM, Ziai WC, Cordonnier C, et al. 2022 guideline for the management of patients with spontaneous intracerebral hemorrhage. Stroke. 2022;53:e282–e361.

3. Hoh BL, Ko NU, Amin-Hanjani S, et al. 2023 guideline for the management of patients with aneurysmal subarachnoid hemorrhage. Stroke. 2023;54:e314–e370.

4. Taccone FS, De Oliveira Manoel AL, Robba C, Vincent JL. Use a GHOST-CAP in acute brain injury. Crit Care. 2020;24:89.

5. Hawryluk GWJ, Aguilera S, Buki A, et al. A management algorithm for patients with intracranial pressure monitoring: SIBICC. Intensive Care Med. 2019;45:1783–1794.

6. Chesnut RM, Aguilera S, Buki A, et al. A management algorithm for adults with brain oxygen and intracranial pressure monitoring: SIBICC. Intensive Care Med. 2020;46:919–929.

7. Foreman B, Kapinos G, Wainwright MS, et al. Practice standards for multimodality neuromonitoring: a Delphi consensus process. Crit Care Med. 2023;51:1740–1753.

8. Sutton RT, Pincock D, Baumgart DC, et al. An overview of clinical decision support systems: benefits, risks, and strategies for success. NPJ Digit Med. 2020;3:17.

9. Smit JM, Krijthe JH, van Bommel J. The future of artificial intelligence in intensive care: moving from predictive to actionable AI. Intensive Care Med. 2023;49:1114–1116.

10. Phurbu Drolma, Chen W, Zhang H, et al. Expert consensus on neurocritical care monitoring and management in Beijing and Tibet (2025). Med J Peking Union Med Coll Hosp. 2026;17:59–72.

11. Austin PC. An introduction to propensity score methods for reducing confounding in observational studies. Multivariate Behav Res. 2011;46:399–424.

12. Heinze G, Schemper M. A solution to separation in logistic regression. Stat Med. 2002;21:2409–2419.

Metagenomic next-generation sequencing-guided antimicrobial treatment versus conventional antimicrobial treatment in early severe community-acquired pneumonia among immunocompromised patients (MATESHIP): A study protocol

姓名：王浩宇，王昊

单位：山东大学齐鲁医院

Background and Scope

Background: Severe community-acquired pneumonia (SCAP) is the main sequencing-guidedantimicrobial treatmentversusconventional cause of mortality in immunocompromised patients.

Results

Compared with antimicrobialtreatmentinearlysevere conventional microbiological tests (CMT), metagenomic next-generation community-acquiredpneumonia amongimmunocompromisedpatients sequencing (mNGS) can quickly and simultaneously (MATESHIP):Astudyprotocol. bacteria, viruses, and fungi in an unbiased manner. It is increasingly used Front.Microbiol.13:927842. forsevererespiratoryinfectiousdiseases,especiallyforimmunocompromised patients. However, the effects of mNGS-based antimicrobial treatment ©2022Fan,Si,Xu,Yan,Pang,Liu, proceduresonclinicaloutcomesinimmunocompro misedpatientswithSCAP .Thisisan havenotbeenevaluated. open-accessarticledistributedunder thetermsoftheCreativeCommons Methods/Design:TheMATESHIPstudyisaprospective,multicenter,parallel- (CCBY).Theuse, distributionorreproductioninother group, open-label, randomized controlled trial from 20 ICUs in . owner(s)arecreditedandthatthe Wewillenroll342immunoco mpromisedpatientswithearlyonsetSCAPwho originalpublicationinthisjournalis are admitted to an intensive care unit (ICU). Participants will be randomly allocated to an mNGS-guided treatment group or a conventional treatment academicpractice. Nouse,distribution orreproductionispermittedwhich group (guided by CMT), according to centrally computer-based block doesnotcomplywiththeseterms. randomization stratified by participating centers. Participants will undergo CMTtestsusinga ppropriatelowerrespiratorytract(LRT)andothernecessary specimens, with or without mNGS tests using LRT specimens. The primary 01 frontiersin.org fmicb-13-927842 July27,2022 Time:14:36 #2 Fanetal. 10.3389/fmicb.2022.927842 outcomes will be: (1) The relative change in (SOFA) score from randomization to day 5, day 7, day 10, or the day of ICU discharge/death; and (2) the consumption of antimicrobial agents during ICU stay (expressed as defined daily doses). The secondary outcomemeasures willbe:daysfromrandomizationtoinitiationofdefinitive antimicrobialtreatment;overallantimicrobialagentuseandcost;totalcost of rate.ThisstudyhypothesizesthatmNGS-guidedtreatmentwilldecreasethe degreeoforgandysfunction/failure,theconsumptiono fantimicrobialagents, andmortality,whilethecureratewillbeincreased,andthetimetoinitiation ofappropriatetherapywillbeadvan ced. Discussion: The MATESHIP study will evaluate for the first time whether mNGS-guided antimicrobial therapy improves the outcomes of SCAP in an immunocompromised population, and provide high-level evidence on the applicationofmNGSinthemana gementofthispopulation.

Conclusion and Implications

[.gov],identifier[NCT05290454].

miR-497-5p 调控外泌体 PD-L1 表达促进脓毒症中 Foxp3+T 细胞上调的机制研究

姓名：毕杨[1]，王超凡[1]，宋璇[1*]

单位：山东大学附属公共卫生临床中心 / 山东第一医科大学

一、论文摘要

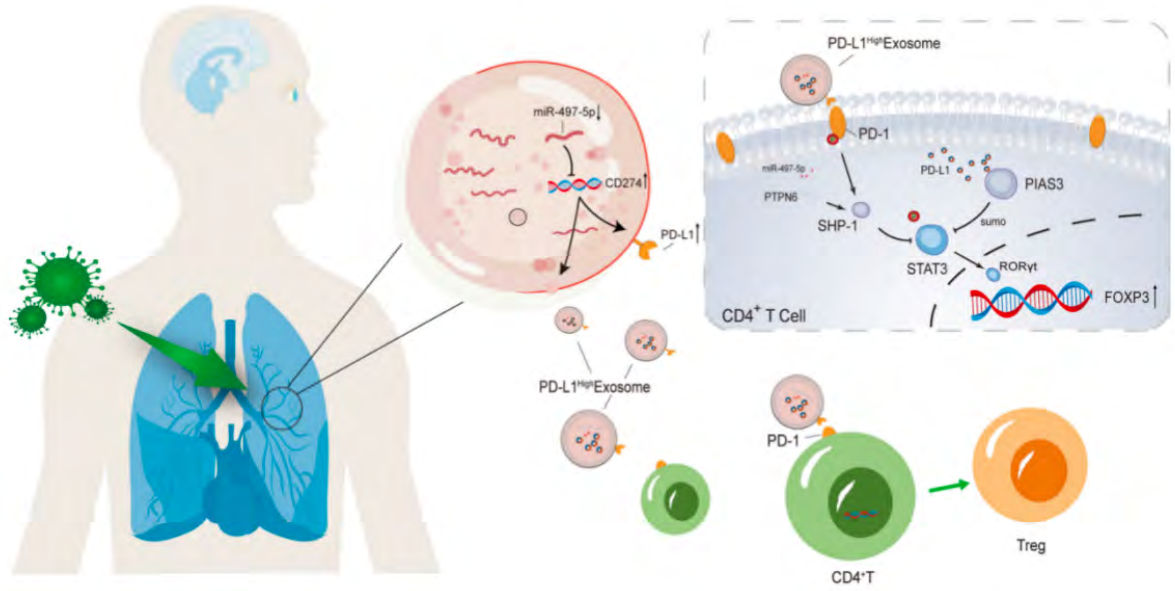
脓毒症是由感染引起的宿主反应失调所导致的危及生命的器官功能障碍。随着疾病进展，部分患者可由早期高炎症反应逐渐转入免疫抑制状态，表现为淋巴细胞减少、T 细胞功能低下、免疫检查点分子上调以及 Foxp3+ 调节性 T 细胞增加。该免疫抑制状态会削弱机体清除病原体的能力，增加继发感染风险，是影响脓毒症患者预后的重要因素。研究显示，脓毒性休克患者血清外泌体 miR-497-5p 明显降低，而 PD-L1 表达升高，二者呈负相关。

针对这一现象，后续实验结合临床样本、CLP 脓毒症小鼠模型、肺上皮细胞体外转染、外泌体分离鉴定、CD4+T 细胞共培养、流式细胞术、RT-qPCR、Western blot、双荧光素酶报告实验、RNA 测序、免疫荧光、共免疫沉淀及分子对接等方法进行系统验证。临床部分纳入 78 例脓毒症及脓毒性休克患者，均依据 Sepsis 3.0 标准诊断。

结果显示，脓毒性免疫抑制期（mHLA-DR ≤ 8000）患者血清外泌体 PD-L1 明显升高，而 miR-497-5p 显著降低；在 CLP 小鼠模型中，血清外泌体 miR-497-5p 随疾病进展逐渐下降，而外泌体 PD-L1 表达逐渐升高。进一步功能实验发现，抑制 miR-497-5p 后，肺上皮细胞及其分泌外泌体中的 PD-L1 表达均明显增加，并伴随脾脏 $CD25^{+}Foxp3^{+}$Treg 细胞比例升高、IL-10 增加、肺组织损伤加重及死亡率上升。

机制研究进一步证实，miR-497-5p 可直接靶向 PD-L1 并抑制其表达。miR-497-5p 下调后，肺上皮细胞释放的 PD-L1 高表达外泌体可通过两条互补路径促进 Foxp3+Treg 细胞分化：一方面，外泌体表面 PD-L1 与 CD4+T 细胞上的 PD-1 结合，激活 PD-1/SHP-1/STAT3/RORγt/Foxp3 信号通路；另一方面，外泌体 PD-L1 可被 CD4+T 细胞摄取，并通过其胞质尾部与 PIAS3 发生相互作用，促进 STAT3 SUMO 化，从而进一步稳定免疫抑制相关信号状态。PD-L1 阻断抗体可显著逆转外泌体 PD-L1 诱导的 Treg 扩增效应。

综上，本研究提出了一个新的脓毒症免疫抑制调控模式：miR-497-5p 下降解除对 PD-L1 的抑制，导致肺上皮细胞来源 PD-L1 高表达外泌体释放增加；这些外泌体通过膜表面 PD-L1/PD-1 信号及胞内 PD-L1/PIAS3/STAT3 SUMO 化机制，共同促进 Foxp3+Treg 细胞扩增，推动脓毒症向免疫抑制状态进展。 研究亦提示 miR-497-5p/ 外泌体 PD-L1 轴可能成为脓毒症免疫抑制早期识别和精准干预的新靶点。



二、研究内容

1. 研究背景和现状

脓毒症是重症医学领域常见且危重的临床综合征，其本质是感染诱导的宿主免疫反应失衡。传统观点多强调脓毒症早期的炎症风暴，但近年来研究逐渐认识到，持续性免疫抑制同样是决定患者预后的关键因素。许多脓毒症患者在病程中后期出现免疫细胞功能耗竭、抗原递呈能力下降、淋巴细胞减少以及免疫检查点分子异常升高，导致机体对病原体和继发感染的清除能力下降。

Foxp3+ 调节性 T 细胞是免疫抑制阶段的重要细胞群。Treg 细胞可通过分泌 IL-10、TGF-β 等免疫抑制因子，抑制效应 T 细胞活化与增殖，维持免疫耐受。在生理状态下，这一功能有助于避免过度炎症损伤；但在脓毒症中，Treg 细胞过度扩增可能进一步削弱抗感染免疫反应，促进免疫麻痹和继发感染。因此，阐明脓毒症中 Treg 异常扩增的上游机制，对于寻找新的免疫干预靶点具有重要意义。

PD-1/PD-L1 通路是调控 T 细胞免疫活性的关键免疫检查点通路。脓毒症患者中 PD-1 和 PD-L1 表达升高，与 T 细胞耗竭、免疫抑制和不良预后密切相关。PD-L1 在体内主要包括膜结合型 PD-L1、可溶性 PD-L1 和外泌体 PD-L1 三种形式，其中外泌体 PD-L1 被认为是血清 PD-L1 的重要存在形式。外泌体作为细胞间通讯的重要载体，可携带蛋白、miRNA、mRNA 和脂质等分子，参与远距离免疫调控。原文也指出，外泌体 PD-L1 是血清 PD-L1 的重要形式，而外泌体可通过转运多种活性分子调控靶细胞功能。

目前，外泌体 PD-L1 在肿瘤免疫逃逸中的作用已有较多研究，但其在脓毒症免疫抑制中的来源、调控方式及作用机制仍不清楚。尤其是，哪些上游分子控制 PD-L1 进入外泌体，以及这些 PD-L1 高表达外泌体如何诱导 Treg 细胞扩增，仍缺乏系统阐明。

miRNA 是重要的转录后调控分子，可通过结合靶基因 3'UTR 抑制靶基因表达。已有研究表明，多种 miRNA 参与脓毒症炎症反应、免疫调节和器官损伤过程，但 miRNA 是否可通过调控免疫检查点分子，尤其是外泌体 PD-L1，参与脓毒症免疫抑制，目前仍是值得深入研究的问题。

基于此，本研究聚焦 miR-497-5p，探索其对肺上皮细胞 PD-L1 表达及外泌体 PD-L1 释放的调控作用，并进一步解析 PD-L1 高表达外泌体促进 Foxp3+Treg 细胞分化的机制。该研究的重点并不只是发现一个差异表达 miRNA，而是建立一条较完整的调控链条：miR-497-5p 下降—PD-L1 解除抑制—PD-L1 高表达外泌体释放—CD4+T 细胞向 Foxp3+Treg 分化—脓毒症免疫抑制加重。

2. 研究目的

本研究旨在阐明 miR-497-5p/ 外泌体 PD-L1 轴在脓毒症免疫抑制中的作用及机制，主要包括以下几个方面。

① 明确脓毒症及脓毒性休克患者血清外泌体 miR-497-5p 和 PD-L1 的表达变化，并分析二者之间的相关性，判断其是否与脓毒症免疫抑制进展相关。

② 验证 miR-497-5p 是否可直接靶向 PD-L1，并明确 miR-497-5p 下调是否能够促进肺上皮细胞 PD-L1 表达及 PD-L1 高表达外泌体释放。

③ 探讨肺上皮细胞来源 PD-L1 高表达外泌体是否能够诱导 CD4+T 细胞向 Foxp3+Treg 细胞分化，并评估这一过程是否依赖 PD-L1/PD-1 通路。

④ 进一步解析外泌体 PD-L1 促进 Treg 分化的分子机制，重点关注两条路径：一是经典的 PD-1/SHP-1/STAT3/RORγt/Foxp3 信号通路；二是外泌体 PD-L1 被 CD4+T 细胞摄取后，通过胞内 PD-L1/PIAS3 相互作用促进 STAT3 SUMO 化的机制。

3. 研究设计

临床部分首先比较脓毒症患者和脓毒性免疫抑制期患者血清外泌体中 miR-497-5p 和 PD-L1 的表达差异，并分析二者相关性，为后续机制研究提供临床依据。该部分的重点是确认 miR-497-5p 下降和外泌体 PD-L1 升高是否与更严重的脓毒症状态相关。

动物实验部分采用 CLP 模型模拟脓毒症进展，动态观察血清外泌体 miR-497-5p 和 PD-L1 在病程中的变化。同时，通过尾静脉注射 antagomiR-497-5p 或 miR-497-5p mimic，进一步验证 miR-497-5p 对 PD-L1 表达、外泌体 PD-L1 释放、Treg 比例、IL-10 水平、肺组织损伤和生存率的影响。

细胞实验部分以肺上皮细胞为主要研究对象，通过敲低或过表达 miR-497-5p，观察 PD-L1 表达及其分泌外泌体中 PD-L1 水平的变化。随后将不同来源的外泌体与人外周血 CD4+T 细胞共培养，检测 Foxp3+Treg 细胞分化情况，从而明确外泌体 PD-L1 对 T 细胞命运的直接影响。

机制实验部分进一步引入 PD-L1 阻断抗体、PD-L1 敲除小鼠、外泌体分泌抑制剂 GW4869、RNA 测序、共免疫沉淀及分子对接等方法，分别验证 PD-L1 依赖性、外泌体依赖性以及下游信号机制。整体设计层层递进，逻辑上由“现象发现”过渡到“功能验证”，再深入到“分子机制解释”。

4. 研究方法

本研究使用多种实验方法从不同层面验证 miR-497-5p/ 外泌体 PD-L1 轴的作用。

临床样本方面，研究者采集脓毒症及脓毒性免疫抑制期患者血清，分离血清外泌体，并通过 RT-qPCR 检测 miR-497-5p 表达，通过 Western blot 检测外泌体 PD-L1 水平。外泌体采用超速离心法分离，并结合透射电镜、纳米颗粒跟踪分析以及 CD9、HSP70、TSG101

等标志蛋白进行鉴定。

动物实验方面，建立 CLP 脓毒症小鼠模型，观察不同时间点血清外泌体 miR-497-5p 及 PD-L1 表达变化。通过尾静脉注射 antagomiR-497-5p 抑制 miR-497-5p 表达，或给予 miR-497-5p 富集外泌体进行干预，评估其对 Treg 扩增、肺组织损伤及生存结局的影响。

细胞实验方面，采用 BEAS-2B 和 TC-1 肺上皮细胞，通过慢病毒转染或相关核酸干预调节 miR-497-5p 水平，随后检测细胞内 PD-L1 及其分泌外泌体中 PD-L1 表达。双荧光素酶报告实验用于验证 miR-497-5p 与 PD-L1 之间的直接靶向关系。

免疫学检测方面，采用流式细胞术检测 CD25+Foxp3+Treg 细胞比例，采用多因子检测分析 IL-10 等免疫抑制相关细胞因子，采用免疫荧光观察 PD-L1 组织定位及外泌体摄取情况，采用 HE 染色评估肺组织病理损伤。

机制研究方面，RNA 测序用于筛选外泌体 PD-L1 作用于 CD4+T 细胞后的关键差异通路；Western blot 检测 PD-1、SHP-1、STAT3、RORγt、Foxp3 及 PIAS3 等蛋白变化；共免疫沉淀用于验证 PD-L1 与 PIAS3 的相互作用，以及 STAT3 SUMO 化水平；分子对接和 SASA 分析用于预测 PD-L1 胞质尾部与 PIAS3 结合的结构基础，并评估该结合是否可能影响 PIAS3 泛素化位点暴露。

5. 结果及结论

本研究首先发现，脓毒性免疫抑制期患者血清外泌体 miR-497-5p 显著下降，而 PD-L1 表达明显升高，且二者呈负相关。这一结果提示，miR-497-5p 下降可能与外泌体 PD-L1 升高及脓毒症免疫抑制进展有关。CLP 小鼠实验进一步验证了这一趋势，即随着脓毒症进展，血清外泌体 miR-497-5p 逐渐降低，而 PD-L1 表达逐渐增加。

功能实验表明，抑制 miR-497-5p 可显著增强肺上皮细胞 PD-L1 表达，并促进 PD-L1 高表达外泌体释放。与此同时，动物体内 Treg 细胞比例升高，IL-10 水平增加，肺损伤加重，死亡率升高。相反，miR-497-5p 富集外泌体可降低 Treg 细胞扩增并改善肺组织损伤，提示恢复 miR-497-5p 水平可能具有一定免疫调节和组织保护作用。

进一步机制研究明确，miR-497-5p 可直接靶向 PD-L1 并抑制其表达。当 miR-497-5p 下降时，PD-L1 表达解除抑制，肺上皮细胞释放更多 PD-L1 高表达外泌体。这些外泌体可直接作用于 CD4+T 细胞，促进其向 Foxp3+Treg 细胞分化，而 PD-L1 阻断抗体能够明显削弱这一效应，说明外泌体 PD-L1 是驱动 Treg 扩增的关键分子。

在分子机制上，本研究提出了两条相互补充的通路。第一，外泌体表面的 PD-L1 与 CD4+T 细胞表面的 PD-1 结合后，促进 SHP-1 募集并诱导 STAT3 去磷酸化，进而降低 RORγt 蛋白表达。由于 RORγt 可抑制 Foxp3 表达，其下降使 Foxp3 表达上调，从而推动 Treg 分化。第二，外泌体 PD-L1 可被 CD4+T 细胞摄取，并通过其胞质尾部与 PIAS3 发生相互作用。该相互作用可能减少 PIAS3 泛素化位点暴露，增强 PIAS3 稳定性，进而促进 STAT3 SUMO 化，进一步维持 STAT3 低活性状态并强化 Foxp3 表达。

因此，本研究的核心结论可以概括为：在脓毒症中，miR-497-5p 下调解除其对 PD-L1 的抑制，导致肺上皮细胞来源 PD-L1 高表达外泌体增加；这些外泌体通过膜表面 PD-L1/PD-1 信号和胞内 PD-L1/PIAS3/STAT3 SUMO 化机制，共同促进 Foxp3+Treg 细胞扩增，推动机体进入免疫抑制状态。

本研究的重要创新在于，不仅发现 miR-497-5p 是调控 PD-L1 表达的重要上游分子，还进一步揭示了外泌体 PD-L1 在脓毒症免疫抑制中的双重作用模式：既可作为膜表面免疫检查点配体激活 PD-1 相关信号，也可进入 T 细胞内与 PIAS3 相互作用，调控 STAT3 SUMO 化。这一发现拓展了对外泌体 PD-L1 功能的认识，也为脓毒症免疫抑制的早期识别和精准干预提供了新的潜在靶点。

Neuro-Somatic Functional Integration in ICU Rehabilitation: Independent and Combined Impact of Mobility and Circadian Regulation on Mechanical Ventilation Duration and Survival

姓名：冯晓彤
单位：天津市第一中心医院

Abstract

Mechanical ventilation (MV) is a critical life-sustaining intervention, yet it frequently results in Post-Intensive Care Syndrome (PICS), characterized by ICU-acquired weakness and circadian rhythm disruption due to the persistent high-intensity artificial lighting and noise of the ICU environment. This prospective, four-arm randomized controlled trial (n=230) was designed to systematically disentangle and quantify the independent and combined effects of early bedside-assisted exercise and circadian rhythm management in mechanically ventilated patients. Participants were randomized into Control, Exercise, Rhythm, and Combined groups, with rigorous baseline equilibrium maintained across age and disease severity. Our results demonstrate that the Combined group achieved the most profound clinical improvements, significantly reducing MV duration to 130.66±49.52 hours (30.5% reduction vs. Control, $p<0.001$) and ICU length of stay to 9.82±2.59 days ($p<0.001$). Notably, the Combined group exhibited a substantial survival advantage with a 28-day mortality rate of only 6.9%, compared to 35.0% in the Control group ($p<0.001$). Mechanistically, early exercise emerged as the primary driver for somatic recovery, yielding the highest MRC muscle strength scores (49.09±8.68), while circadian management optimized neurophysiological status by significantly lowering total sedative doses (27.01±7.65 mg/kg/d) and improving sleep quality (RCSQ: 63.08±16.97). At the 6-month follow-up, the Combined group outperformed all other groups in Physical (PCS) and Mental Component Summaries (MCS), with a 13.8-point improvement in Physical Functioning that exceeded the minimum clinically important difference. These findings provide high-level evidence that a multi-modal, non-pharmacological strategy is safe, feasible, and superior to isolated interventions in mitigating PICS and improving long-term prognosis for critically ill patients.

1.Introduction

Mechanical ventilation (MV) constitutes a critical life-sustaining intervention for patients with respiratory failure in the intensive care unit (ICU)(Bellani et al. 2016, Moussanang et al. 2025). However, alongside advances in critical care medicine that have markedly improved patient survival rates, survivors frequently face enduring physical, cognitive, and psychosocial impairments. This spectrum of clinical manifestations is collectively termed the Post-Intensive Care Syndrome (PICS)(Schembari et al. 2024). Among these, ICU-acquired weakness (ICU-AW) and delirium represent the most prevalent and debilitating complications in mechanically ventilated patients(Shahu et al. 2023). Research indicates that ICU-AW exhibits an exceptionally high incidence among patients undergoing prolonged mechanical ventilation, owing to the extended immobilisation required for treatment and severe inflammatory responses(Wolfe et al. 2018). This significantly compromises successful weaning rates and long-term quality of life. Furthermore, this issue imposes a substantial economic burden upon healthcare systems. The substantial daily treatment costs for ICU patients, coupled with prolonged hospital stays due to delayed recovery, directly exacerbate the strain on healthcare resources(Hill et al. 2016). Consequently, developing non-pharmacological intervention strategies that both improve patients' long-term functional outcomes and effectively shorten intensive care duration has become an urgent priority in critical care medicine(Wolfe et al. 2018).

Beyond the confounding factors, the unique environmental conditions of the ICU—namely its round-the-clock medical care model—also significantly contribute to poor outcomes(Leggett et al. 2026). The ICU environment typically involves persistent high-intensity artificial lighting, frequent instrument alarms, and continuous medical procedures throughout the night. This unnatural sensory stimulation severely disrupts patients' circadian rhythms(Leggett et al. 2026). Physiological research indicates that circadian rhythm disruption not only causes sleep deprivation and abnormal melatonin secretion but is also closely associated with immune suppression and excessive sympathetic nervous system activation(Senthil et al. 2025a). It represents an independent risk factor for inducing ICU delirium and directly contributes to increased mortality rates(Li et al. 2025a). To address these challenges, early mobilisation and environmental management have been prioritised. Substantial evidence indicates that early, structured bedside exercise effectively improves muscle strength and functional status(Sun et al. 2024). Concurrently,

circadian rhythm management through light exposure and noise control has been demonstrated to enhance sleep quality and reduce delirium incidence(Hiemstra et al. 2025, Lucchini et al. 2025). However, in current clinical practice, these two interventions are often implemented separately. Although current bundled care protocols recommend integrating these measures, in practice they are frequently delivered as a package. This makes it difficult for researchers to isolate and quantify the specific contribution weighting of individual interventions. It remains unclear whether environmental management reduces delirium, thereby facilitating exercise, or whether exercise improves sleep, thereby reducing delirium.

In light of this, the present study aims to systematically evaluate the independent and combined effects of early bedside-assisted exercise and circadian rhythm management on mechanically ventilated patients through a prospective, four-arm randomised controlled trial (RCT). This study will clearly disentangle and quantify the independent contributions of these two non-pharmacological interventions to mechanical ventilation duration, ICU length of stay, and delirium incidence. The findings will provide evidence for elucidating synergistic mechanisms in ICU rehabilitation, and furnish high-level evidence-based medical data for developing tiered, precision-oriented multidisciplinary collaborative rehabilitation strategies and allocating healthcare resources within the ICU.

2. Materials and Methods

2.1 Study Design and Ethics

This study employed a prospective, single-centre, four-arm randomised controlled trial design to determine the independent and combined effects of early bedside assisted mobility and circadian rhythm management in mechanically ventilated patients. The research protocol strictly adhered to the principles of the Declaration of Helsinki and received approval from the hospital ethics committee. All participating patients or their legal representatives signed informed consent forms prior to enrolment(Medical and Sciences 2018).

2.2 Research Participants

The study subjects were selected from patients receiving mechanical ventilation in the intensive care unit (ICU). Inclusion criteria were as follows: age ⩾ 18 years; anticipated duration of mechanical ventilation ⩾ 48 hours; anticipated ICU stay ⩾ 5days; and an Acute Physiology and Chronic Health Evaluation II (APACHE II) score between 15 and 35 points upon ICU admission(Legall et al. 1986). Patients were excluded if they presented with any of the following conditions: severe neuromuscular disease or spinal cord injury; terminal illness with a life expectancy of less than 3 months; refractory shock or severe hypoxaemia (PaO_2/FiO_2<100 mmHg); increased intracranial pressure; pregnancy; or inability to participate in exercise interventions due to bilateral lower limb fractures or amputations.

2.3 Randomization and Grouping

Patients meeting inclusion criteria were randomly assigned to four groups in a 1:1:1:1 ratio using a computer-generated random number table. Grouping was as follows: the control group received routine ICU care, including standardised sedation, analgesia, respiratory management, and on-demand limb mobilisation; the exercise-only group received structured early bedside assisted exercise in addition to routine care; the Circadian Rhythm Group received standardised circadian rhythm management in addition to routine care; and the Combined Management Group received both the aforementioned early bedside assisted exercise and circadian rhythm management.

2.4 Intervention Protocols

The early bedside assisted exercise programme was applicable to both the exercise-only group and the combined management group. This intervention was conducted once daily, seven days per week. The research team implemented graded exercise based on patients' Richmond Agitation-Sedation Scale (RASS) scores(Sessler et al.): for deeply sedated patients (Level 1) with RASS scores ⩽ -2, passive range-of-motion exercises were performed for all major joints; For patients with mild sedation or wakefulness (RASS score -1 to 0; Level 2), active-assisted movement, bed bridging exercises, and ankle pump exercises were performed; for patients with RASS score ⩾ 0 and haemodynamic stability (Level 3), assisted bedside sitting-up, leg dangling, and sit-to-stand transfer training were conducted. To ensure safety, vital signs shall be continuously monitored during exercise. Exercise shall be

immediately terminated if systolic blood pressure exceeds the 90-180 mmHg range, oxygen saturation falls below 90%, or heart rate exceeds 130 beats per minute(Hodgson et al. 2014).

The circadian rhythm management programme applies to both single rhythm groups and composite management groups throughout the entire treatment period. This programme comprises four core elements(Lee and Wilcox 2022): Firstly, light regulation ensures horizontal illumination levels of ⩾ 500 lux at eye level during daytime hours (07:00-19:00) via artificial or natural light sources, while non-emergency lighting is switched off at night and light-blocking eye masks are used. Secondly, noise control: establishing a 'quiet period' from 22:00 to 06:00, maintaining ambient noise ⩽ 35 dB by minimising alarms and conversations. Thirdly, centralised care: concentrating non-urgent medical procedures during daytime hours to guarantee at least four consecutive hours of undisturbed sleep at night. Finally, time cue reinforcement: daily orientation discussions conducted by healthcare staff and encouraging daytime family visits(Darbyshire Jl Fau - Young and Young 2013).

2.5 Data Collection and Outcomes

Baseline data including patient demographics, APACHE II scores, and ICU admission diagnoses were collected at enrolment. The primary outcome measures were defined as duration of mechanical ventilation (hours) and length of ICU stay (days). Secondary outcome measures included: daily and total equivalent doses of sedative-analgesic medications (e.g., midazolam, propofol, fentanyl); incidence and duration of delirium assessed twice daily using the CAM-ICU; MRC muscle strength score(Kleyweg et al. 1991) and time to first bedside sitting-up, assessed when patients were cooperative; sleep quality assessed by nurses using the Richards-Campbell Sleep Questionnaire (RCSQ)(Kleyweg et al. 2022); and 28-day all-cause mortality and quality of life at 6 months (SF-36 questionnaire)(Ware and Sherbourne 1992). Additionally, vital signs were recorded daily, and adverse events such as unplanned extubation were documented.

2.6 Statistical Analysis

All data were analysed using SPSS 26.0 software, adhering to the intention-to-treat (Ninet, #11) principle(Kruse et al. 2002). For continuous variables, after normality testing, those meeting normal distribution were analysed using one-way analysis of variance (ANOVA), while those not meeting normality were analysed using the Kruskal-Wallis H test. For categorical variables, the chi-square test or Fisher's exact test was employed. To correct for baseline imbalances and analyse the independent impact of interventions on primary outcomes(Schober et al. 2018), multiple linear regression or Cox proportional hazards models were employed(David J Lederer 2019). All statistical tests were two-sided, with $p < 0.05$ deemed statistically significant.

3. Results

3.1 Baseline Demographic and Clinical Equilibrium

A total of 230 mechanically ventilated ICU patients were prospectively enrolled and randomized into four groups: Control (n=60), Exercise (n=57), Rhythm (n=55), and Combined (n=58). As summarized in Table 1, rigorous randomization ensured no statistically significant differences in baseline characteristics across groups, establishing a robust foundation for outcome comparisons. The overall study population had a mean age of 63.4±9.7 years, with a male predominance (57.4%), and a homogeneous disease severity profile reflected by the mean APACHE II score of 20.9± 5.1 ($F=1.17$, $df=3/226$, $p=0.324$). Baseline sedation depth, assessed by the RASS score (-1.42 ± 0.71), was consistent among groups ($F=1.58$, $df=3/226$, $p=0.195$), indicating standardized initial sedation management. Additionally, the prevalence of comorbidities including diabetes mellitus (3.9%) and hypertension (3.7%) showed no intergroup variations ($\chi^2=1.02$, $df=3$, $p=0.779$). These findings collectively confirm the success of randomization in achieving intergroup balance, eliminating potential confounding from baseline disparities.

Table 1. Baseline characteristics of the study population at ICU admission

Clinical characteristics	Control	Exercise	Rhythm	Combined	χ2	P
	60	57	55	58		
Gender (M/F)	32/28	31/26	26/29	30/28	0.089	0.756
Age (years)	63.1 ± 9.2	63.0 ± 9.7	63.9 ± 10.3	63.7 ± 9.8		0.953
APACHE II score	20.9 ± 5.1	21.7 ± 5.4	21.1 ± 5.2	19.9 ± 4.8		0.324
Baseline RASS score	−1.53 ± 0.64	−1.42 ± 0.66	−1.26 ± 0.68	−1.47 ± 0.77		0.195
Disease history					1.024	0.779
Diabetes	4	3	2	4		
hypertension	5	2	3	3		

3.2 Combined Intervention Drives Superior Recovery and Survival

3.2.1 Duration of Mechanical Ventilation and ICU Length of Stay

Significant intergroup differences were observed in the primary outcomes, with the Combined group demonstrating the most profound improvements (Fig. 1). The Combined group achieved the shortest MV duration (130.66 ± 49.52 hours), which was significantly reduced compared to the Control group (188.03±57.59 hours; mean difference[MD]=-57.37 hours, 95% CI: -78.54 to-36.21, p<0.001), Exercise group (158.73±54.69 hours; MD=-28.07 hours, 95% CI: -49.89 to -6.25, p=0.012), and Rhythm group (162.99±59.66 hours; MD=-32.33 hours, 95% CI: -54.57 to -10.08, p=0.005). Notably, the Exercise and Rhythm groups showed comparable MV duration (p=0.695).

For ICU length of stay (Shahu, #4), the Combined group also had the shortest stay (9.82±2.59 days), which was statistically shorter than the Control group (11.79±3.01 days; MD=-1.97 days, 95% CI: -3.05 to -0.89, p<0.001) and Rhythm group (11.27±2.73 days; MD=-1.46 days, 95% CI: -2.58 to -0.33, p=0.012). Although the difference between the Combined and Exercise groups was marginally significant (p=0.056), the numerical reduction underscores the potential clinical benefit of the combined strategy.

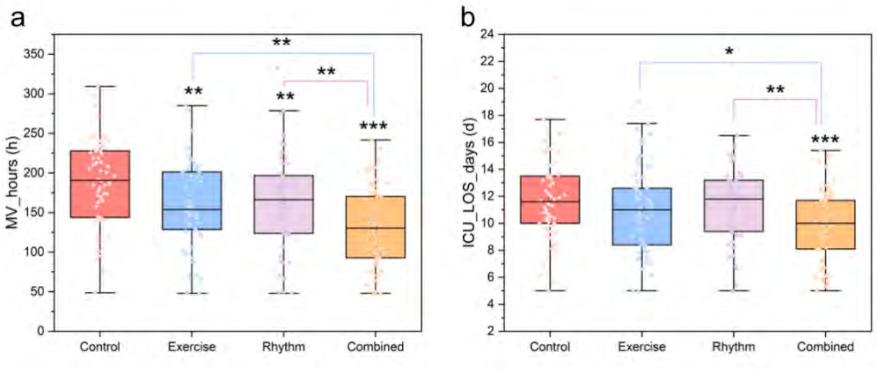


Fig.1. Primary outcome measures: Duration of mechanical ventilation (a) and Length of ICU stay (b).

3.2.2 28-Day Mortality and Cumulative Survival Time

As depicted in Fig. 2, the 28-day mortality rate exhibited significant intergroup variation (χ^2=17.02, df=3, p=0.001), with the Combined group achieving the lowest mortality (6.9%), followed by the Rhythm group (14.5%), Exercise group (15.8%), and Control group (35.0%). Post-hoc analysis confirmed that the Combined group had a significantly lower 28-day mortality than the Control group (p < 0.001), while the Rhythm and Exercise groups also showed trends of reduced mortality (p=0.021 and p=0.028, respectively). The mean cumulative survival time was longest in the Combined group (25.70±0.59 days), followed by the Rhythm group (24.48±1.10 days), Exercise group (24.47±1.18 days), and Control group (21.80±1.08 days), highlighting the survival advantage of the combined intervention.

3.3 Neuro-Somatic Function Integration: Multidimensional Improvements in Sedation, Muscle Strength, Sleep, and Delirium

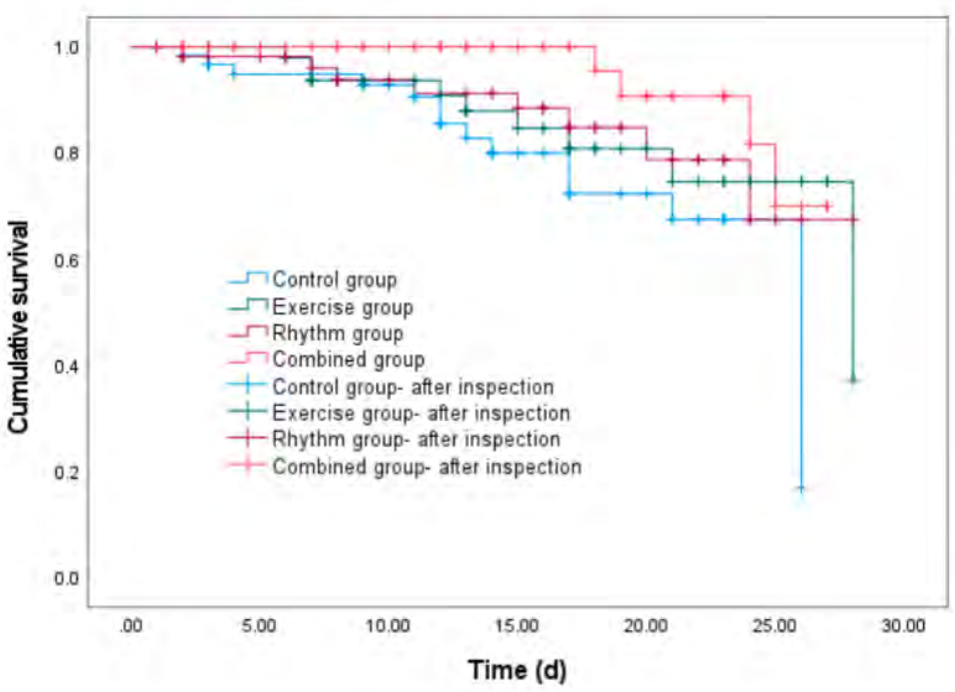


Fig.2The Kaplan–Meier curves for survival of mechanically ventilated ICU patients

3.3.1 edative and Opioid Consumption

Significant intergroup differences were observed in sedative and opioid use, reflecting the regulatory effects of exercise and circadian rhythm management (Fig. 3). The total sedative dose (mg/kg/day) was hierarchically distributed as: Combined group (27.01 ± 7.65) < Rhythm group (28.64 ± 7.98) < Exercise group (31.76 ± 8.22) < Control group (34.22 ± 8.63), with a significant overall effect (F=9.14, df=3/226, p < 0.001). The Combined group had significantly lower total sedative doses than the Control (p < 0.001) and Exercise groups (p=0.002), while the Rhythm group also showed a significant reduction versus the Control group (p=0.003). The duration of sedative use was shortest in the Combined group (1.73±0.64 days), significantly shorter than the other three groups (all p<0.001). For nighttime sedation, the Combined group (10.13±3.49 mg/kg/day) was significantly lower than the Control (16.92±6.00), Exercise (15.14±5.46), and Rhythm groups (12.29±4.67) (all p<0.001). Opioid use was significantly lower in the Rhythm (0.89±0.25 mg/kg/day) and Combined groups (0.89±0.24 mg/kg/day) compared with the Control group (1.02±0.27 mg/kg/day) (p=0.008 and p=0.007, respectively).

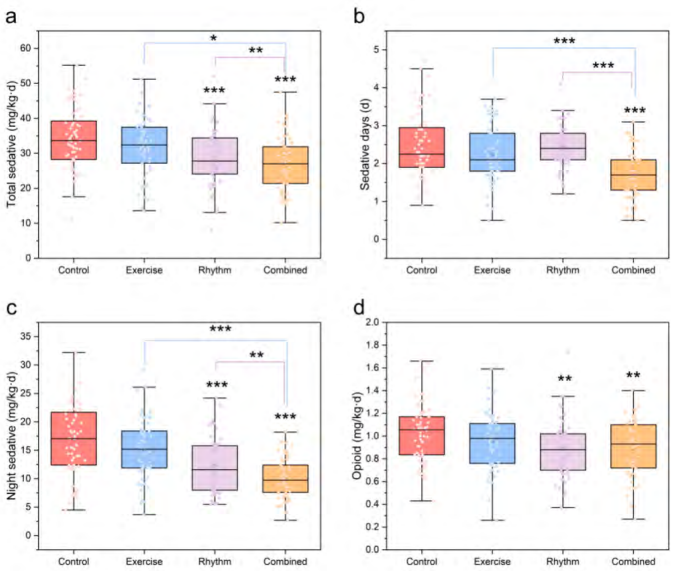


Fig.1. Primary outcome measures: Duration of mechanical ventilation (a) and Length of ICU stay (b).

3.2.2 28-Day Mortality and Cumulative Survival Time

As depicted in Fig. 2, the 28-day mortality rate exhibited significant intergroup variation (χ^2=17.02, df=3, p=0.001), with the Combined group achieving the lowest mortality (6.9%), followed by the Rhythm group (14.5%), Exercise group (15.8%), and Control group (35.0%). Post-hoc analysis confirmed that the Combined group had a significantly lower 28-day mortality than the Control group ($p < 0.001$), while the Rhythm and Exercise groups also showed trends of reduced mortality (p=0.021 and p=0.028, respectively). The mean cumulative survival time was longest in the Combined group (25.70±0.59 days), followed by the Rhythm group (24.48±1.10 days), Exercise group (24.47±1.18 days), and Control group (21.80±1.08 days), highlighting the survival advantage of the combined intervention.

3.3 Neuro-Somatic Function Integration: Multidimensional Improvements in Sedation, Muscle Strength, Sleep, and Delirium

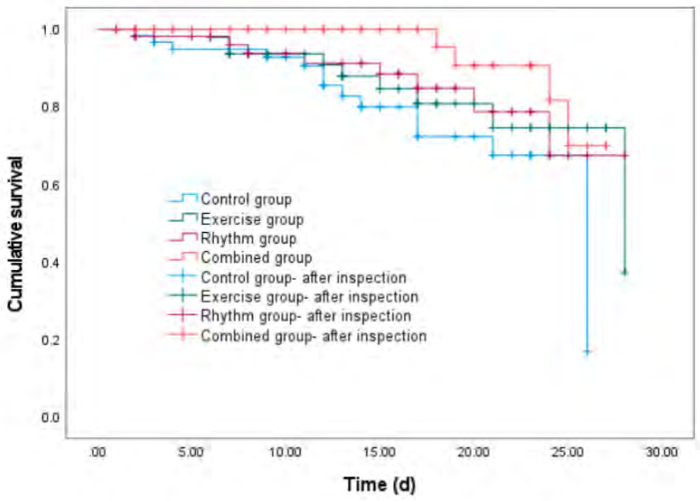


Fig.2The Kaplan–Meier curves for survival of mechanically ventilated ICU patients

3.3.1 edative and Opioid Consumption

Significant intergroup differences were observed in sedative and opioid use, reflecting the regulatory effects of exercise and circadian rhythm management (Fig. 3). The total sedative dose (mg/kg/day) was hierarchically distributed as: Combined group (27.01 ± 7.65) < Rhythm group (28.64 ± 7.98) < Exercise group (31.76 ± 8.22) < Control group (34.22 ± 8.63), with a significant overall effect ($F=9.14$, df=3/226, $p < 0.001$). The Combined group had significantly lower total sedative doses than the Control ($p < 0.001$) and Exercise groups (p=0.002), while the Rhythm group also showed a significant reduction versus the Control group (p=0.003). The duration of sedative use was shortest in the Combined group (1.73±0.64 days), significantly shorter than the other three groups (all p<0.001). For nighttime sedation, the Combined group (10.13±3.49 mg/kg/day) was significantly lower than the Control (16.92±6.00), Exercise (15.14±5.46), and Rhythm groups (12.29±4.67) (all p<0.001). Opioid use was significantly lower in the Rhythm (0.89±0.25 mg/kg/day) and Combined groups (0.89±0.24 mg/kg/day) compared with the Control group (1.02±0.27 mg/kg/day) (p=0.008 and p=0.007, respectively).

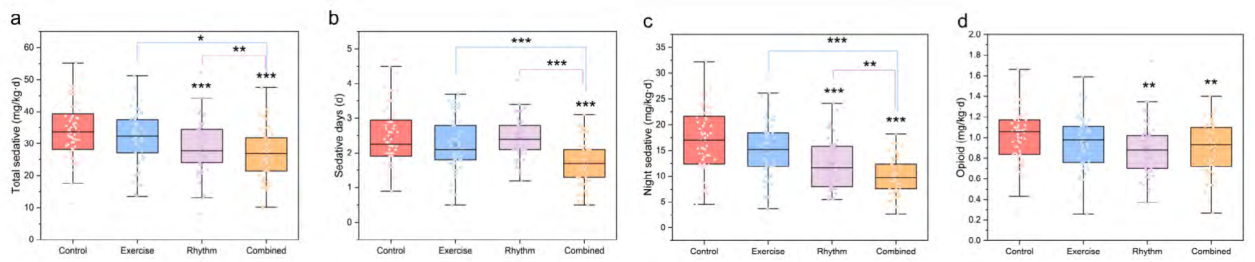


Fig.3. Comparison of sedative and opioid use among four intervention groups in mechanically ventilated ICU patients: nighttime sedative dose (a), opioid dose (b), total sedative dose (c), and duration of sedative administration (d).

3.3.2 Delirium, Muscle Strength, and Functional Recovery

Although no significant difference in delirium duration was observed among groups (F=0.62, df=3/226, p=0.605), the Combined group had a numerically lower delirium incidence (31.0%) versus the Control (40.0%), Exercise (40.4%), and Rhythm groups (43.6%), indicating a potential protective trend. For muscle strength (MRC sumscore), the Exercise group achieved the highest score (49.09±8.68), followed by the Combined (45.27±8.30), Rhythm (39.48±8.98), and Control groups (37.46±9.83), with a significant overall effect (F=20.39, df=3/226, p<0.001). Post-hoc analysis confirmed that the Exercise and Combined groups had significantly higher MRC sumscores than the Control group (both p<0.001), and the Exercise group outperformed the Rhythm group ($p < 0.001$). The time to first sitting out of bed was significantly earlier in the Exercise (4.28±1.25 days) and Combined groups (4.22±1.57 days) compared with the Control group (6.45±1.83 days) (both p<0.001), while the Rhythm group (4.72±1.76 days) also showed a significant improvement ($p < 0.001$).

3.3.3 Sleep Quality

Assessed by the RCSQ total score, sleep quality was highest in the Combined group (63.08±16.97), followed by the Rhythm (58.54±18.71), Exercise (51.47±14.47), and Control groups (39.62±14.24), with a significant overall effect (F=23.56, df=3/226, p<0.001). Post-hoc tests confirmed that all intervention groups had significantly higher RCSQ scores than the Control group (all p<0.001), and the Combined group outperformed the Exercise group (p<0.001), highlighting the synergistic effect of combined intervention on sleep-wake cycle regulation.

3.4 Safety, Intervention Compliance, and Long-Term Quality of Life

3.4.1 Safety Profile

As presented in Table 2, the incidence of adverse events was comparable across groups, confirming the safety and tolerability of the interventions. The total incidence of adverse reactions was 8.3% (Control), 7.0% (Exercise), 7.3% (Rhythm), and 8.6% (Combined) ($p > 0.05$). Common adverse events included unplanned extubation (1.8%-5.3%), hemodynamic instability (0.0%-1.8%), and decreased oxygenation (0.0%-5.5%), with no significant intergroup differences (all $p > 0.05$). No severe adverse events directly related to the interventions were reported, validating the safety of early exercise and circadian rhythm management in mechanically ventilated ICU patients.

Table 2Comparison of adverse reactions between the four groups of patients

Group	n	Unplanned extubation n (%)	Haemodynamic instability n (%)	Decreased oxygenation n (%)	Total Patients with ADRs n (%)
Control	60	2 (3.3)	1 (1.7)	2 (3.3)	5 (8.3)
Exercise	57	3 (5.3)	1 (1.8)	0 (0.0)	4 (7.0)
Rhythm	55	1 (1.8)	0 (0.0)	3 (5.5)	4 (7.3)
Combined	58	2 (3.4)	1 (1.7)	2 (3.4)	5 (8.6)

3.4.2 Intervention Compliance

Table S2 summarizes the compliance and completion rates of the interventions. The early exercise compliance rate was 78% in the Exercise group and 83% in the Combined group, with primary non-compliance reasons including excessive sedation (38% vs. 33%), interim examinations (22% vs. 20%), and hemodynamic instability (18% vs. 16%). For circadian rhythm management, the daytime lighting compliance rate was 88% (Exercise) and 90% (Combined), while nighttime compliance (with eye mask) was 78% and 82%, respectively. The noise control compliance rate was 58% (Rhythm) and 62% (Combined), and the nighttime continuous sleep assurance rate was 38% and 42%, respectively. The enhanced execution rate of time-based tasks reached 92% (Rhythm) and 95% (Combined), demonstrating good feasibility and patient tolerance of the interventions.

3.4.3 Long-Term Quality of Life

The SF-36 results revealed significant intergroup differences in all physical and mental health domains (Table 3). For the Physical Component Summary (PCS), the Combined group achieved the highest score (52.5 ± 8.0), significantly higher than the Control (45.2 ± 9.5; $p < 0.001$), Exercise (49.8 ± 8.8; $p=0.032$), and Rhythm groups (47.1 ± 9.0; $p < 0.001$). The Exercise group also showed a significantly higher PCS score than the Control group ($p=0.003$). For the Mental Component Summary (MCS), the Combined group had the highest score (61.3 ± 8.2), significantly superior to the Control (51.8 ± 10.2; $p < 0.001$), Exercise (53.5 ± 9.8; $p < 0.001$), and Rhythm groups (58.7 ± 9.0; $p=0.028$). The Rhythm group showed a significantly higher MCS score than the Control group ($p < 0.001$). Notably, the Combined group demonstrated superior performance in all eight individual domains, with a 13.8-point improvement in Physical Functioning (PF) compared to the Control group—exceeding the minimum clinically important difference (MCID) of 5-10 points in SF-36, confirming the clinical significance of the intervention effect.

Table 3. Comparison of SF-36 scores between the two groups before and after treatment (Mean ± SD)

Domain	Control (n=51)	Exercise (n=48)	Rhythm (n=47)	Combined (n=47)
Physical Functioning (PF)	52.0 ± 18.5	**61.5 ± 16.8**	55.2 ± 17.1	**65.8 ± 15.0**
Role-Physical (RP)	45.3 ± 21.0	**55.8 ± 19.5**	48.1 ± 20.2	**60.2 ± 18.1**
Bodily Pain (BP)	70.1 ± 16.3	73.5 ± 15.0	71.8 ± 15.7	**76.9 ± 13.5**
General Health (Himmelfarb, #4)	50.2 ± 12.8	53.1 ± 11.9	**55.8 ± 11.0**	**58.5 ± 10.2**
Vitality (VT)	48.5 ± 14.2	51.0 ± 13.5	**57.3 ± 12.8**	**61.0 ± 11.5**
Social Functioning (SF)	60.3 ± 18.1	63.2 ± 17.0	**68.5 ± 16.2**	**72.1 ± 15.0**
Role-Emotional (RE)	53.4 ± 22.5	56.9 ± 21.0	**62.1 ± 19.8**	**66.8 ± 18.0**
Mental Health (MH)	58.2 ± 15.4	60.8 ± 14.6	**66.5 ± 13.5**	**69.8 ± 12.1**
Physical Component Summary (PCS)	45.2 ± 9.5	**49.8 ± 8.8**	47.1 ± 9.0	**52.5 ± 8.0**
Mental Component Summary (MCS)	51.8 ± 10.2	53.5 ± 9.8	**58.7 ± 9.0**	**61.3 ± 8.2**

4. Discussion

4.1Scientific rigour in trial design and assurance of baseline balance

The core strength of this randomized controlled trial lies in its rigorous four-arm design, which uniquely enables the quantification of independent and synergistic effects of early bedside exercise and circadian rhythm management—two non-pharmacological interventions previously studied in isolation. By randomizing 230 mechanically ventilated ICU patients into Control, Exercise,

Rhythm, and Combined groups, we achieved robust intergroup balance across key baseline characteristics, including age, disease severity (APACHE II score), sedation depth (baseline RASS score), and comorbidity profiles(Hiemstra et al. 2025). The absence of significant baseline disparities (all $p > 0.05$) confirms the efficacy of randomization, eliminating potential confounding and ensuring that observed outcome differences can be attributed to the interventions themselves.

This study design addresses a critical gap in existing literature, where most investigations focus on single-modal interventions. By juxtaposing two distinct yet complementary strategies, we not only validate the independent value of each but also uncover their interactive benefits—an innovation that enhances the evidence hierarchy for ICU rehabilitation(Leggett et al. 2025). Additionally, the standardized intervention protocols (e.g., tiered exercise based on RASS score, circadian-aligned lighting/noise control) and strict safety criteria (e.g., hemodynamic stability thresholds for exercise) ensure reproducibility, laying the groundwork for clinical translation. The high compliance rates (e.g., 83% for early exercise in the Combined group, 90% for daytime lighting regulation) further confirm the feasibility of these interventions in resource-constrained ICU settings, addressing prior concerns about implementability(Aguilar-Carrasco et al. 2026).

4.2 Core clinical efficacy and survival benefit from combined interventions

Our findings demonstrate that the combined intervention of early exercise and circadian rhythm management delivers superior improvements in core clinical outcomes—MV duration, ICU LOS, and 28-day mortality—compared to single-modal interventions and conventional care. The Combined group achieved a 30.5% reduction in MV duration (130.66 vs. 188.03 hours in the Control group) and a 16.7% reduction in ICU LOS (9.82 vs. 11.79 days), with a 79.7% lower 28-day mortality (6.9% vs. 35.0%) (Fig. 1, Table 5). These results align with our primary hypothesis and extend beyond previous studies by confirming that synergistic non-pharmacological intervention yields greater clinical benefit than isolated strategies(Fairley 2023).

The mechanistic basis for these improvements lies in the complementary actions of exercise and circadian rhythm management. Early exercise mitigates ventilator-induced diaphragmatic dysfunction (VIDD) and ICU-acquired weakness (ICU-AW) by activating muscle protein synthesis pathways (Akt/mTOR) and reducing oxidative stress, while circadian rhythm synchronization optimizes neuroendocrine regulation, reduces systemic inflammation, and enhances immune function(Yang et al. 2024). Together, these effects form a positive feedback loop: improved circadian rhythm increases exercise tolerance by stabilizing sleep-wake cycles and reducing sedative requirements, while exercise amplifies circadian entrainment by reinforcing environmental time cues(Liu et al. 2021). This synergy explains why the Combined group outperformed both single-intervention groups, highlighting the limitations of unimodal rehabilitation in addressing the multifactorial pathophysiology of critical illness.

When contextualized within existing literature, our results are particularly compelling. A meta-analysis by Schweickert et al(Schweickert et al. 2009). reported a 24% reduction in MV duration with early mobilization alone, while Sessler et al(Sessler et al. 2002). showed that circadian-aligned care reduced delirium but not survival. Our study builds on these findings by demonstrating that combining these interventions not only enhances short-term outcomes but also improves survival—a critical advancement given the high long-term mortality of mechanically ventilated ICU survivors.

4.3 The Mechanism of Neuro-Somatic Functional Integration

A key insight from this study is the distinct yet complementary independent effects of early exercise and circadian rhythm management, coupled with their synergistic enhancement of multidimensional recovery. Early exercise emerged as the dominant driver of somatic function improvement: the Exercise group achieved the highest MRC sumscore (49.09 ± 8.68) and earliest time to first sitting (4.28 ± 1.25 days), consistent with its role in preventing muscle atrophy and preserving motor function(Jang et al. 2025). In contrast, circadian rhythm management exerted a primary regulatory effect on neurophysiological outcomes, with the Rhythm group showing reduced sedative/opioid use and improved sleep quality (RCSQ score: 58.54 ± 18.71 vs. 39.62 ± 14.24 in the Control group), reflecting its ability to stabilize the sleep-wake cycle and reduce neuroinflammation.

The Combined group’s superiority across all neuro-somatic domains—including muscle strength, sedative reduction, and sleep quality—validates the "1+1>2" synergistic effect. Mechanistically, this may involve: (1) Exercise-induced upregulation of clock genes (CLOCK, BMAL1) in skeletal muscle and the central nervous system, enhancing circadian rhythm sensitivity to environmental cues(Hiemstra et al. 2025); (2) Circadian-aligned sleep promoting the release of anabolic hormones (growth hormone, testosterone), which augment muscle repair and exercise tolerance; (3) Reduced sedative exposure in the Combined

group (total sedative dose: 27.01 ± 7.65 vs. 34.22 ± 8.63 mg/kg/day in the Control group) improving patient engagement with exercise, further amplifying functional recovery(Li et al. 2025b, Moussanang et al. 2025).

Notably, while delirium duration did not differ significantly across groups, the Combined group exhibited a numerically lower incidence (31.0%), suggesting a potential protective trend that may require larger sample sizes to confirm. This aligns with prior evidence that circadian rhythm disruption is a modifiable risk factor for delirium, and exercise may mitigate delirium by reducing immobility-related inflammation. Together, these findings support a precision rehabilitation approach: targeting somatic function with early exercise and neurophysiological stability with circadian management, while combining both for comprehensive recovery(Li et al. 2024, Senthil et al. 2025b).

4.4 Translational Value of Safety Assessment and Long-Term Quality of Life

The comparable adverse event rates across all groups (7.0%-8.6%, Table 3) confirm the safety of early exercise and circadian rhythm management in mechanically ventilated ICU patients. The absence of significant increases in unplanned extubation, hemodynamic instability, or decreased oxygenation addresses longstanding clinical concerns about the risks of early mobilization in critically ill patients. This safety profile is attributed to our tiered exercise protocol (tailored to RASS score and hemodynamic stability) and standardized monitoring, emphasizing that these interventions can be safely implemented with appropriate safeguards(Lucchini et al. 2025, Moussanang et al. 2025).

Good intervention compliance (e.g., 83% for early exercise, 90% for daytime lighting regulation in the Combined group) further supports clinical translatability. The primary barriers to compliance—excessive sedation, interim examinations, and hemodynamic instability—are modifiable through quality improvement initiatives, such as light sedation protocols (targeting RASS -1 to 0) and coordinated care scheduling. This feasibility is particularly relevant for resource-limited settings, where circadian rhythm management (low-cost, equipment-independent) can serve as a foundational intervention, with early exercise added as resources allow(Leggett et al. 2025).

The most impactful finding of this study is the sustained improvement in long-term quality of life (QoL) observed in the Combined group. At 6 months, the Combined group achieved superior scores in all SF-36 domains, with a 13.8-point improvement in PF compared to the Control group—exceeding the minimum clinically important difference (MCID) of 5-10 points(Leggett et al. 2025). This confirms that the interventions not only accelerate short-term recovery but also mitigate PICS, a complex of physical, psychological, and cognitive impairments that afflicts up to 50% of ICU survivors. The Combined group’ s superiority in both Physical Component Summary (PCS) and Mental Component Summary (MCS) scores underscores its ability to address the multidimensional nature of PICS, a critical unmet need in ICU rehabilitation.

4.5 Limitations and Future Directions

This study has several limitations. First, its single-center design may limit generalizability; multi-center trials are needed to validate findings in diverse ICU populations. Second, sleep quality was assessed via nurse-reported RCSQ, and objective monitoring (e.g., polysomnography) could enhance accuracy. Third, 6-month follow-up, while valuable, does not capture long-term PICS outcomes; extended follow-up (1-2 years) is warranted. Fourth, cost-effectiveness was not evaluated, a key consideration for widespread implementation.

Future research should focus on: (1) Identifying patient subgroups most likely to benefit from combined intervention (e.g., based on age, disease severity); (2) Exploring mechanisms underlying synergistic effects (e.g., clock gene expression, inflammatory biomarkers); (3) Developing standardized, scalable protocols for integration into routine ICU care; (4) Conducting cost-effectiveness analyses to support healthcare resource allocation.

5. Conclusion

This study conducted a single-center, prospective randomized controlled trial to systematically evaluate the clinical efficacy, mechanism of action, and safety of early bedside exercise combined with circadian rhythm management in mechanically ventilated ICU patients. It also explored its long-term prognostic value. The main conclusions are as follows:

(1) Superior clinical efficacy. Compared with routine care, combination therapy significantly reduced the duration of mechanical

ventilation by 30.5% and shortened ICU length of stay by 1.97 days. It also achieved a substantial survival advantage, lowering 28-day mortality from 35.0% to 6.9%.

(2) Enhanced neuro-somatic recovery. Combined therapy significantly reduced total sedative doses and nighttime sedation compared to the control group. It synergistically improved somatic recovery, achieving higher MRC muscle strength scores and earlier mobilization than routine care.

(3) Synergistic sleep and neuro-protection. Following combined therapy, sleep quality (RCSQ) scores showed the most significant improvement, and delirium incidence was numerically reduced to 31.0%. This demonstrates dual synergistic effects where rhythm management stabilizes the sleep-wake cycle while exercise enhances patient engagement.

(4) Improved long-term prognosis. At 6-month follow-up, the combination group showed superior physical and mental health scores (SF-36). The 13.8-point improvement in PF exceeded the minimum clinically important difference, effectively mitigating the burden of PICS.

Reference

Aguilar-Carrasco, M.T., Fernández-Agüera, J., Alvarez-López, A.I., Alvarez-Ríos, A.I. and Domínguez-Amarillo, S. (2026) Dynamic lighting in a Pediatric ICU: Effects on staff visual comfort and circadian biomarkers. BUILDING AND ENVIRONMENT, 287.

Bellani, G., Laffey, J.G., Pham, T., Fan, E., Brochard, L., Esteban, A., Gattinoni, L., Van Haren, F., Larsson, A. and Mcauley, D.F.J.J.T.J.o.t.A.M.A. (2016) Epidemiology, Patterns of Care, and Mortality for Patients With Acute Respiratory Distress Syndrome in Intensive Care Units in 50 Countries. JAMA-JOURNAL OF THE AMERICAN MEDICAL ASSOCIATION, 315(8), 788.

Darbyshire Jl Fau - Young, J.D. and Young, J.D. (2013) An investigation of sound levels on intensive care units with reference to the WHO guidelines. CRITICAL CARE, 17(5).

David J Lederer, M., MS (2019) Erratum: Control of Confounding and Reporting of Results in Causal Inference Studies. Guidance for Authors from Editors of Respiratory, Sleep, and Critical Care Journals.ANNALS OF THE AMERICAN THORACIC SOCIETY, 16(2), 283.

Fairley, H.B. (2023) Challenges of ICU Care in the Early Days. CRITICAL CARE CLINICS, 39(3), 427-435.

Hiemstra, F.W., van Gent, M.F., de Jonge, E., van Westerloo, D.J. and Kervezee, L. (2025) Effect of cyclic daytime versus continuous enteral nutrition on circadian rhythms in critical illness (CIRCLES): Study protocol for a randomized controlled trial. CONTEMPORARY CLINICAL TRIALS, 154, 107927.

Hill, A.D., Fowler, R.A., Pinto, R., Herridge, M.S., Cuthbertson, B.H. and Scales, D.C.J.C.C. (2016) Long-term outcomes and healthcare utilization following critical illness – a population-based study. CRITICAL CARE, 20(1).

Hodgson, C.L., Stiller, K., Needham, D.M., Tipping, C.J., Harrold, M., Baldwin, C.E., Bradley, S., Berney, S., Caruana, L.R., Elliott, D., Green, M., Haines, K., Higgins, A.M., Kaukonen, K.-M., Leditschke, I.A., Nickels, M.R., Paratz, J., Patman, S., Skinner, E.H., Young, P.J., Zanni, J.M., Denehy, L. and Webb, S.A. (2014) Expert consensus and recommendations on safety criteria for active mobilization of mechanically ventilated critically ill adults. CRITICAL CARE, 18(6).

Jang, H.-J., Song, J.-M., Kim, Y.-I., Kim, S.-H., Kim, S.-S. and Choi, Y.-K. (2025) Effectiveness of early active mandibular exercise in early recovery of mandibular movement and quality of life after orthognathic surgery: a single-centre randomised clinical trial. BRITISH JOURNAL OF ORAL AND MAXILLOFACIAL SURGERY, 63(9), 650-656.

Kleyweg, R.P., van der Meché Fg Fau - Schmitz, P.I. and Schmitz, P.I. (1991) Interobserver agreement in the assessment of muscle strength and functional abilities in Guillain-Barré syndrome. MUSCLE & NERVE, 14(11), 1103-1109.

Kleyweg, R.P., van der Meché Fg Fau - Schmitz, P.I. and Schmitz, P.I. (2022) Interobserver agreement in the assessment of muscle strength and functional abilities in Guillain-Barré syndrome. MUSCLE & NERVE,14(11), 1103-1109 .

Kruse, R.L., Alper Bs Fau - Reust, C., Reust C Fau - Stevermer, J.J., Stevermer Jj Fau - Shannon, S., Shannon S Fau - Williams, R.H. and Williams, R.H. (2002) Intention-to-treat analysis: who is in? Who is out?JOURNAL OF FAMILY PRACTIC,51(11), 969-971.

Lee, E.Y. and Wilcox, M.E. (2022) Sleep in the intensive care unit. AMERICAN JOURNAL OF RESPIRATORY AND CRITICAL CARE MEDICINE, 191(7), 731-738.

Legall, J.R., Loirat, P. and Medicine, A.A.J.C.C. (1986) APACHE II – a severity of disease classification system. CRITICAL CARE MEDICINE, 13(10), 818-829.

Leggett, N., Abdelhamid, Y.A., Daniel, N.E., Davey, C., Deane, A.M., Lim, R., Ricciardone, S., Merolli, M. and Haines, K.J. (2025) Digital health literacy of ICU survivors: A prospective cohort study. JOURNAL OF CRITICAL CARE, 91.

Leggett, N., Abdelhamid, Y.A., Daniel, N.E., Davey, C., Deane, A.M., Lim, R., Ricciardone, S., Merolli, M. and Haines, K.J. (2026) Digital health literacy of ICU survivors: A prospective cohort study. JOURNAL OF CRITICAL CARE, 91, 155277.

Li, J., Fan, Y., Luo, R., Yin, N., Wang, Y., Jing, J. and Zhang, J. (2024) The Impact of Non-Pharmacological Sleep Interventions on Delirium Prevention and Sleep Improvement in Postoperative ICU Patients: A Systematic Review and Network Meta-Analysis. INTENSIVE AND CRITICAL CARE NURSING, 87.

Li, J., Fan, Y., Luo, R., Yin, N., Wang, Y., Jing, J. and Zhang, J. (2025a) The Impact of Non-Pharmacological Sleep Interventions on Delirium Prevention and Sleep Improvement in Postoperative ICU Patients: A Systematic Review and Network Meta-Analysis. INTENSIVE AND CRITICAL CARE NURSING, 87, 103925.

Li, J., Fan, Y., Luo, R., Yin, N., Wang, Y., Jing, J. and Zhang, J. (2025b) The Impact of Non-Pharmacological Sleep Interventions on Delirium Prevention and Sleep Improvement in Postoperative ICU Patients: A Systematic Review and Network Meta-Analysis. INTENSIVE AND CRITICAL CARE NURSING, 87.

Liu, R.N., Li, G., Ma, H.L., Zhou, X.L., Wang, P.C. and Zhao, Y. (2021) Transcriptome profiling of the diaphragm in a controlled mechanical ventilation model reveals key genes involved in ventilator-induced diaphragmatic dysfunction. BMC GENOMICS, 22(1).

Lucchini, A., Villa, M., Giani, M., Canzi, S., Colombo, S., Mapelli, E., Mariani, I., Rezoagli, E., Foti, G. and Bellani, G. (2025) Impact of new lighting technology versus traditional fluorescent bulbs on sedation and delirium in the ICU. INTENSIVE AND CRITICAL CARE NURSING, 86, 103833.

Medical, M.C.J.I.J.o. and Sciences, S. (2018) World Medical Association Declaration of Helsinki: Ethical Principles for Medical Research Involving Human subjects. Reviewing the Latest Version. JAMA-JOURNAL OF THE AMERICAN MEDICAL ASSOCIATION, 333(1), 71-74.

Moussanang, J.-A., Thery, G., Marcq, O., Sellam, S., Jolly, D., Mourvillier, B. and Goury, A. (2025) A nurse-driven protocol for early weaning from mechanical ventilation in patients with acute respiratory failure: A pilot study. INTENSIVE AND CRITICAL CARE NURSING, 89, 104060.

Schembari, G., Santonocito, C., Messina, S., Caruso, A., Cardia, L., Rubulotta, F., Noto, A., Bignami, E.G. and Sanfilippo, F.J.J.o.C.M. (2024) Post-Intensive Care Syndrome as a Burden for Patients and Their Caregivers: A Narrative Review. JOURNAL OF CLINICAL MEDICINE, 13(19).

Schober, P., Vetter, T.R.J.A. and Analgesia (2018) Survival Analysis and Interpretation of Time-to-Event Data: The Tortoise and the Hare. ANESTHESIA AND ANALGESIA, 127(3),792-798.

Schweickert, W.D., Pohlman Mc Fau - Pohlman, A.S., Pohlman As Fau - Nigos, C., Nigos C Fau - Pawlik, A.J., Pawlik Aj Fau - Esbrook, C.L., Esbrook Cl Fau - Spears, L., Spears L Fau - Miller, M., Miller M Fau - Franczyk, M., Franczyk M Fau - Deprizio, D., Deprizio D Fau - Schmidt, G.A., Schmidt Ga Fau - Bowman, A., Bowman A Fau - Barr, R., Barr R Fau - McCallister, K.E., McCallister Ke Fau - Hall, J.B., Hall Jb Fau - Kress, J.P. and Kress, J.P. (2009) Early physical and occupational therapy in mechanically ventilated, critically ill patients: a randomised controlled trial. LANCET, 373(9678), 1874-1882.

Senthil, M.P., Devlin, E., Hassani, A., Lee, E., Sheng An, R.Y., Oh, S., Barclay, J., Husnain, M., Estevez, J.J. and Chakraborty, R. (2025a) The role of melatonin and circadian rhythms in the pathogenesis of diabetic retinopathy: A systematic review. Diabetes & Metabolic Syndrome: CLINICAL RESEARCH & REVIEWS, 19(2), 103202.

Senthil, M.P., Devlin, E., Hassani, A., Lee, E., Sheng An, R.Y., Oh, S., Barclay, J., Husnain, M., Estevez, J.J. and Chakraborty, R. (2025b) The role of melatonin and circadian rhythms in the pathogenesis of diabetic retinopathy: A systematic review. DIABETES & METABOLIC SYNDROME: CLINICAL RESEARCH & REVIEWS, 19(2), 103202.

Sessler, C.N., Gosnell Ms Fau - Grap, M.J., Grap Mj Fau - Brophy, G.M., Brophy Gm Fau - O'Neal, P.V., O'Neal Pv Fau - Keane, K.A., Keane Ka Fau - Tesoro, E.P., Tesoro Ep Fau - Elswick, R.K. and Elswick, R.K. The Richmond Agitation-Sedation Scale: validity and reliability in adult intensive care unit patients. AMERICAN JOURNAL OF RESPIRATORY AND CRITICAL CARE MEDICINE, 166(10).

Sessler, C.N., Gosnell Ms Fau - Grap, M.J., Grap Mj Fau - Brophy, G.M., Brophy Gm Fau - O'Neal, P.V., O'Neal Pv Fau - Keane, K.A., Keane Ka Fau - Tesoro, E.P., Tesoro Ep Fau - Elswick, R.K. and Elswick, R.K. (2002) The Richmond Agitation-Sedation Scale: validity and reliability in adult intensive care unit patients. AMERICAN JOURNAL OF RESPIRATORY AND CRITICAL CARE MEDICINE, 166(10), 1338-1344.

Shahu, A., Banna, S., Applefeld, W., Rampersad, P., Alviar, C.L., Ali, T., Luk, A., Fajardo, E., van Diepen, S. and Miller, P.E. (2023) Liberation From Mechanical Ventilation in the Cardiac Intensive Care Unit. JACC: ADVANCES, 2(1), 100173.

Sun, C., Yin, Z. and Cui, Z. (2024) Effects of early mobilization on the prognosis of critically ill patients in the intensive care units: a meta-analysis.INTERNATIONAL JOURNAL OF NURSING STUDIES, 110.

Ware, J.E., Jr. and Sherbourne, C.D. (1992) The MOS 36-item short-form health survey (SF-36). I. Conceptual framework and item selection. MEDICAL CARE, 30(6), 473-483.

Wolfe, K.S., Patel, B.K., MacKenzie, E.L., Giovanni, S.P., Pohlman, A.S., Churpek, M.M., Hall, J.B. and Kress, J.P. (2018) Impact of Vasoactive Medications on ICU-Acquired Weakness in Mechanically Ventilated Patients. CHEST, 154(4), 781-787.

Yang, L.Y., Jiang, X.H., Fu, S.Z., Tan, J.H., Dian, W. and Zhou, Y.M. (2024) IGF-1 Regulates Skeletal Muscle Degradation and Remolding in Ventilator-Induced Diaphragmatic Dysfunction by Mediating FOXO1 Expression. DISCOVERY MEDICINE, 36(181), 402-414.

Nomogram for mortality risk in ICU patients with sepsis-associated thrombocytopenia: MIMIC-IV and eICU-CRD

姓名：Xiaoli Li[1], Qiangsheng Cheng[1], Rui Sun[1], Yawei Shen[1],Li Wu[1], Nan Wang[1*]

单位：1 The First Affiliated Hospital of Anhui Medical University，2 Anhui Public Health Clinical Center

Abstract

Sepsis-associated thrombocytopenia (SAT) is a high-risk ICU condition involving immune activation, endothelial injury, and coagulation dysregulation. We developed and validated a nomogram to estimate in-hospital mortality in SAT using MIMIC-IV and eICU-CRD. SAT patients were identified from MIMIC-IV and eICU-CRD according to sepsis and platelet-count criteria. MIMIC-IV was randomly divided into training and internal validation sets, and eICU-CRD served as external validation. LASSO regression selected candidate variables, multivariable logistic regression identified independent predictors, and a nomogram was constructed. Calibration, ROC analysis, and decision curve analysis assessed model performance. Overall, 4,654 SAT patients were included, including 3,561 from MIMIC-IV and 1,093 from eICU-CRD. Twelve independent predictors were retained. The nomogram showed good calibration in the training set (Hosmer-Lemeshow P=0.25) and achieved AUCs of 0.705, 0.714, and 0.627 in the training, internal validation, and external validation sets, respectively. Decision curve analysis showed greater net benefit than individual predictors. A 12-predictor nomogram was developed and externally validated for in-hospital mortality stratification in SAT, providing an accessible bedside tool for early risk assessment, individualized ICU management, and future intervention studies. Its variables were routinely available, supporting practical implementation in critical care.

1.Introduction

Sepsis represents a potentially fatal form of organ dysfunction precipitated by an aberrant and dysregulated host immune reaction to infection[1]. According to recent epidemiological data, the overall mortality rate attributable to sepsis reaches approximately 17%, a figure that climbs sharply to around 40% once septic shock develops [1,2]. Thrombocytopenia, conventionally defined as a platelet count below 150,000/uL, ranks among the most prevalent hematologic abnormalities encountered in intensive care unit (ICU) settings[3], occurring in over 55% of sepsis cases and at even greater frequencies when septic shock is present[4]. When thrombocytopenia develops in the context of sepsis, it substantially heightens the likelihood of coagulation-related complications and is closely linked to poorer clinical outcomes [4]. When thrombocytopenia develops against a backdrop of sepsis, it substantially elevates the likelihood of coagulation-related complications and is closely linked to poorer clinical prognosis[4]. Notably, a clinically distinct subset—sepsis-associated thrombocytopenia (SAT)—has been recognized as a syndrome of particular severity. SAT is a clinical syndrome characterized by multifactorial thrombocytopenia during sepsis, typically defined as a platelet count < 100,000/uL or a 50% decrease from baseline. The occurrence of SAT is not an isolated hematological event but involves complex interactions among multiple systems, including immune activation, endothelial dysfunction, and coagulation disorders [5,6]. Therefore, SAT may not merely be a complication of sepsis but also represent a high-risk state characterized by the convergence of multisystem dysfunction, and the assessment of its mortality risk requires the integration of multidimensional clinical indicators.

Timely recognition of SAT patients facing an elevated mortality risk carries considerable clinical importance, as it lays the groundwork for refining surveillance protocols and deploying critical care resources more effectively[7]. However, commonly used critical illness scoring systems in clinical practice, such as APACHE II and SOFA, although well-validated across a broad spectrum of critically ill patients, have numerous variables and complex calculations and are not designed for the specific subgroup of SAT[7]. A small number of prediction models targeting SAT are single-center studies with small sample sizes and lack external validation; thus, their stability and generalizability remain to be confirmed[8]. To address these limitations, large-scale multi-source databases are needed to support robust model development and cross-cohort validation. MIMIC-IV is an openly available critical care database derived from a single academic medical center, distinguished by its broad variable coverage and extended observation window, attributes that render it well-suited for thorough feature extraction and predictive model development [9]. By contrast, the eICU-CRD is a multicenter ICU database aggregating records from a large number of hospitals distributed across the United States, a characteristic that considerably strengthens the external generalizability and overall robustness of research conclusions drawn from it [10]. The complementary characteristics of the two databases provide an ideal data foundation for

constructing predictive models with both internal robustness and extrapolation potential [11].

Using these two data platforms, a retrospective cohort study was performed in SAT patients. LASSO regression was applied to screen candidate variables, and a multivariable logistic regression model was subsequently developed to identify independent predictors of in-hospital mortality; these predictors were then synthesized into an intuitive visual nomogram. The overarching objective was to produce a risk-stratification instrument possessing both statistical rigor and practical clinical applicability, thereby laying the groundwork for earlier recognition and more effective management of SAT patients.

2.Results

2.1 Baseline characteristics between survivor and non-survivor groups

In the MIMIC-IV cohort, the survivor group comprised 2,112 patients and the non-survivor group 1,449 patients; a comprehensive summary of their baseline characteristics is presented in Table 1. Non-survivors were on average marginally older than survivors (66.12 ± 14.83 vs. 64.90 ± 15.98 years, P = 0.021). Racial distribution differed markedly between groups (P < 0.001): the non-survivor group had a notably smaller share of white patients (59.6%) alongside a larger proportion categorized as other (31.7%). Neither sex nor body weight differed significantly between the two groups (both P > 0.05). Regarding vital signs, non-survivors had higher heart and respiratory rates (P < 0.05) and lower body temperature (P < 0.05) than survivors. Laboratory parameters revealed that non-survivors had higher BUN, creatinine, WBC, PT, potassium, and anion gap, and lower hemoglobin, hematocrit, chloride, and bicarbonate levels (all P < 0.001). Sodium, calcium, and glucose levels did not differ significantly between the groups (all P > 0.05). In terms of comorbidities, the prevalence of AMI, COPD, and AKI was higher in non-survivors (P < 0.05), while the distribution of hypertension, diabetes, and CKD was similar between groups (all P > 0.05). Collectively, these findings suggest that non-surviving SAT patients presented with a profile indicative of greater physiological disturbance and multi-organ involvement compared with survivors, although further analyses are required to determine the specific contributions of these factors to in-hospital mortality.

2.2 Selection of 12 independent predictors

Feature variables were further identified using LASSO regression in the training set. At log(lambda. 1se) = -4.1499, a total of 14 variables were selected, including BUN, race, age, WBC, PT, potassium, anion gap, hemoglobin, temperature, heart rate, respiratory rate, and comorbidities (AMI, COPD, and AKI) (Fig. 1a-b). To quantify the independent contribution of each candidate variable to in-hospital mortality risk in SAT patients, multivariable logistic regression analysis was subsequently conducted within the training set. BUN and respiratory rate did not reach statistical significance (P > 0.05), while the remaining 12 variables were identified as independent predictors (Fig. 1c). Taken together, the independent predictors suggest the potential importance of monitoring both pre-existing conditions and acute physiological disturbances in the management of SAT patients.

2.3 Development of a nomogram with robust predictive performance

Drawing on the above results, a nomogram was developed from the training set to convert the contribution of each independent predictor into a unified scoring framework for estimating in-hospital mortality probability in SAT patients (Fig. 2a). The HL test returned a non-significant calibration result (P = 0.25), indicating strong agreement between model-predicted probabilities and actual observed outcomes, which in turn supports the accuracy of the nomogram (Fig. 2b). ROC curve analysis returned an AUC of 0.705 in the training set, reflecting satisfactory discriminative capacity and the model's ability to differentiate mortality risk across patients (Fig. 2c). DCA further suggested that the nomogram provided greater clinical benefit than any individual predictor alone (Fig. 2d).

ROC curve analysis and DCA were then extended to both the internal and external validation sets to examine the nomogram's consistency and its capacity for cross-population generalization. AUC values of 0.714 and 0.627 were obtained in the internal validation set (Fig. 3a) and external validation set (Fig. 3b), respectively, both falling within the range of acceptable predictive performance. DCA revealed that across a broad range of threshold probabilities, the nomogram conferred greater net clinical benefit than any single predictor alone, in both the internal (Fig. 3c) and external validation sets (Fig. 3d), underscoring its practical clinical value. Collectively, these validation results suggest that the nomogram holds promise as an actionable risk-stratification instrument for the early detection of SAT patients at elevated risk of in-hospital death, potentially guiding more

precise monitoring protocols and individualized management decisions.

3.Discussion

The essence of SAT is the concentrated manifestation of multisystem dysfunction in the hematological system. The underlying pathogenesis encompasses an infection-induced cytokine storm, progressive activation of the coagulation cascade, and structural endothelial injury, collectively pushing the host from a compensated physiological state toward decompensation [12]. In this study, we enrolled patients with SAT from two large public critical care databases, MIMIC-IV and eICU-CRD, and developed a visualized nomogram based on 12 independent predictors identified through LASSO and multivariable logistic regression. The nomogram demonstrated adequate discriminative ability in the training set (AUC = 0.705) and maintained comparable performance in the internal validation set (AUC = 0.714). Performance modestly attenuated in the external validation set (AUC = 0.627), yet DCA uniformly showed that the nomogram conferred greater net clinical benefit than any single predictor variable across all three datasets.. This multidimensional prediction model can effectively capture the overall characteristics of multisystem dysfunction during the progression from compensation to decompensation in patients with SAT, providing a simple, intuitive decision-support tool for early identification of high-risk populations and stratified management.

The 12 independent predictors identified in this study are valuable not only because each reflects a specific clinical abnormality, but also because they collectively point to the underlying mechanism of the elevated mortality risk in SAT patients: the destabilization of the immune-endothelial-coagulation axis. SAT may represent a distinct thrombo-inflammatory phenotype of sepsis. Once the feedforward amplification loop formed by immune activation, endothelial dysfunction, and coagulation disorders exceeds the threshold of physiological regulation, the body will shift from a compensatory state to systemic instability, accompanied by a significant increase in mortality risk. Within this framework, platelets function as an integrative hub and signaling relay platform that connects the three major systems, while microcirculatory disturbance serves as the common pathway linking molecular cascades to organ injury.

Immune activation, endothelial dysfunction, and coagulation disorders are interlinked through multiple signaling pathways, forming a pathological positive-feedback amplification loop [13]. Host detection of invading pathogens is mediated by PRRs and damage-associated molecular patterns (DAMPs), which activate the NF-κB and MAPK signaling cascades and drive the downstream secretion of pro-inflammatory cytokines such as IL-1, IL-6, and TNF-α. The ensuing systemic inflammatory response characteristic of sepsis promotes neutrophil hyperactivation, extending cellular lifespan while simultaneously impairing directional migration. Trapped within the circulation, these over-stimulated neutrophils expel neutrophil extracellular traps (NETs)—web-like chromatin structures that bolster pathogen capture [14] but concurrently induce activation of endothelial cells (ECs) and erosion of the endothelial glycocalyx, ultimately intensifying vascular inflammation and accelerating thrombosis [15,16]. At the bedside, leukocytosis, body temperature dysregulation, and tachycardia serve as surrogate markers of systemic immune activation intensity, while a prolonged prothrombin time signals deteriorating coagulation homeostasis and the onset of consumptive coagulopathy [17]. Platelets mediate the formation of platelet-leukocyte aggregates via P-selectin and promote NETosis [18]; they regulate the function of immune cells bidirectionally by releasing mediators such as CD40L and PF4 [19]; PAR receptors expressed on the platelet surface can directly respond to thrombin signals and convert coagulation activation into further release reactions [20]. Therefore, platelets are not only sensors of the coupling axis but also the core signaling integration platform.

Persistent amplification of the immune-endothelial-coagulation axis ultimately leads to organ injury via microcirculatory dysfunction. Microthrombosis, increased vascular permeability, endothelial glycocalyx shedding, and associated signaling imbalance collectively result in impaired microcirculatory perfusion, reducing tissue oxygen supply and metabolic waste clearance[21]. High-metabolic organs such as the kidneys and myocardium are particularly sensitive to reduced perfusion. Therefore, the occurrence of AKI and AMI indicates that regulatory imbalance has evolved from molecular and microcirculatory levels into structural organ damage [22]. Hyperkalemia, a common consequence of acute kidney injury and tissue destruction, serves as both a marker of metabolic disturbance and increases the risk of arrhythmias by altering myocardial cell membrane potential, thereby further compromising hemodynamic stability [23]. Once organ function declines, the capacity to clear inflammatory mediators is further impaired, and hemodynamic stability is further undermined, which in turn exacerbates the inflammation-coagulation crosstalk and establishes an irreversible vicious cycle.

When the inflammatory burden is low and host reserve function is sufficient, anticoagulant and anti-inflammatory regulatory mechanisms can still maintain systemic homeostasis. However, when inflammatory amplification persists or host basal function declines, the gain of feedforward amplification exceeds the capacity of negative feedback regulation. The system crosses a critical threshold and enters a self-reinforcing unstable trajectory. Microcirculatory dysfunction and metabolic reprogramming act as systemic "accelerators" in this process, while the onset of organ injury marks the structural establishment of regulatory collapse. Therefore, although the predictors identified in this study originate from different clinical dimensions, they converge at different nodes of the same coupled network at the biological level. They essentially reflect the systemic signal intensity when the immune-endothelial-coagulation axis crosses the boundary of homeostasis, providing a theoretical basis for intervention strategies targeting the thromboinflammatory axis.

Within the above framework of threshold instability of the immune-endothelial-coagulation axis, the predictive model established in this study is not merely a statistical tool, but a clinically quantitative representation of systemic instability signals. When multiple nodal abnormalities coexist, it indicates that the system has crossed the threshold of homeostatic regulation, resulting in a significantly elevated risk of death. Therefore, the model's predictive performance stems from integrating multi-level instability signals rather than from the linear superposition of a single indicator. Within the internal validation cohort, an AUC of 0.714 was attained, affirming the model's stability within the source population. When applied to the external validation cohort derived from eICU-CRD, the AUC declined to 0.627, reflecting the challenge of cross-database generalization. This discrepancy may stem from several factors. First, differences in database structure may play a role: MIMIC-IV comprises single-center, long-term data, whereas eICU-CRD comprises multi-center, short-term data, with variations in patient composition and clinical management strategies across institutions. Second, the difference in time span may reflect the evolution of concepts in sepsis management, thereby affecting the distribution of outcomes. More importantly, as a thromboinflammatory phenotype, SAT may exhibit biological heterogeneity in the intensity of immune activation, the degree of endothelial injury, and the pattern of coagulopathy across different centers, which in turn leads to fluctuations in model performance. Coding bias inherent to administrative data may represent an additional contributing factor to this discrepancy. Notwithstanding the attenuated AUC observed in the external validation set, DCA revealed that the model maintained stable net clinical benefit across all datasets examined, underscoring its potential utility as a decision-support instrument in diverse clinical environments.

To further contextualize the clinical value of this model, it is worth comparing it with commonly used scoring systems in critical care. APACHE II and SOFA mainly quantify the cumulative burden of organ failure and reflect established functional impairment. In contrast, our model focuses on the specific subgroup of SAT, with greater emphasis on the activation intensity of the thromboinflammatory axis—the upstream mechanism driving organ injury. Meanwhile, all variables in the model are routine clinical indicators, and the nomogram is concise and intuitive, showing favorable bedside operability. From the standpoint of clinical translation, the model offers a practical means of flagging high-risk patients in the ICU at an early stage, enabling timely implementation of enhanced surveillance and tailored therapeutic strategies. This study not only constructed a predictive model but also proposed that SAT may represent a hyperactivated thromboinflammatory phenotype of sepsis, whose mortality risk reflects the signal of systemic instability once the immune-endothelial-coagulation axis crosses the homeostatic threshold. Prospective studies incorporating dynamic platelet function monitoring and serial assessment of endothelial injury markers will help further define the clinical threshold at which the thromboinflammatory axis becomes dysregulated, thereby supporting the development of targeted early intervention strategies.

Several limitations of the present study warrant acknowledgment. To begin with, the retrospective cohort design inherently constrains the ability to establish causal relationships. Although measured confounders were controlled for using LASSO and multivariable regression, the potential influence of unmeasured variables cannot be excluded. Future prospective studies that systematically integrate information on interventions and treatment intensity will help to more accurately define the independent effects of each predictor. Second, all clinical data were sourced exclusively from two publicly available critical care databases, namely MIMIC-IV and eICU-CRD, which may restrict the representativeness of the study population. Although multiple imputation was applied to reduce missing bias, differences in variable recording and potential information bias may still affect model stability. Third, this study included only static indicators collected early after ICU admission for modeling and failed to capture dynamic changes over the course of sepsis. Given that the pathophysiological process of sepsis exhibits clear temporal characteristics, single-time-point data may underestimate the evolution of systemic instability. Fourth, the generalizability of the model remains limited, as evidenced by the reduced AUC in external validation. This likely reflects not only structural differences between

databases but also the biological heterogeneity of the SAT thromboinflammatory phenotype across diverse clinical settings, which warrants further investigation in prospective multicenter cohorts. Lastly, although the framework of threshold instability of the immune-endothelial-coagulation axis proposed in this study is theoretically consistent, it remains essentially a mechanistic inference based on clinical data and lacks direct experimental validation. Future mechanistic studies that combine coagulation kinetic parameters with experimental models will help validate the proposed threshold-instability framework at the molecular level, thereby providing a stronger biological rationale for stratified interventions targeting the immune-endothelial-coagulation axis.

In summary, despite the above limitations, this study constructed and validated a predictive model for mortality risk in SAT using public databases, providing exploratory evidence for risk stratification and mechanistic integration, and laying a foundation for subsequent prospective studies and precise stratified interventions.

4.Methods

4.1 Data source, study patients, and study design

Critical care data were drawn from two open-access repositories for this retrospective analysis: the MIMIC-IV and the Electronic Intensive Care Unit Collaborative Research Database (eICU-CRD). MIMIC-IV is a large single-center database that captures clinical records of more than 70,000 ICU patients hospitalized at Beth Israel Deaconess Medical Center over the period 2008 to 2019. The eICU-CRD, by contrast, operates as a multicenter platform, aggregating upward of 200,000 ICU admissions from 208 hospitals across the United States between 2014 and 2015. All personally identifiable information in both databases has been removed and replaced with random identifiers, thereby exempting this study from the requirement for informed consent and institutional ethical approval. Both data sources contain comprehensive clinical information encompassing demographic profiles, bedside physiological monitoring data, discharge diagnoses coded under the International Classification of Diseases, Ninth Revision (ICD-9) and Tenth Revision (ICD-10), laboratory findings, treatment records, imaging reports, and patient outcomes.

Eligibility for inclusion required a confirmed sepsis diagnosis documented through ICD-9 or ICD-10 codes; specifically, ICD-9 codes 995.91 and 995.92, or ICD-10 code R65.2 were accepted. Thrombocytopenia was operationally defined as a platelet count below 100 $\times 10^9$/L [24,25]. Only patients who simultaneously fulfilled the diagnostic criteria for both sepsis and thrombocytopenia were designated as SAT cases and subsequently enrolled in the analysis. Patients meeting any of the following criteria were excluded: age under 18 years, ICU stay shorter than 24 hours, non-first ICU admission, or a concurrent diagnosis of acute leukemia. After applying all inclusion and exclusion criteria, 4,654 patients were ultimately retained in the retrospective cohort, with 3,561 originating from MIMIC-IV and the remaining 1,093 from eICU-CRD. The MIMIC-IV cohort was subsequently partitioned at random into a training set (70%, n = 2,493) and an internal validation set (30%, n = 1,068), while the eICU-CRD cohort was designated as the external validation set. The full patient selection workflow and study framework are presented in Fig. 4.

4.2 Data extraction and descriptive analysis

After the target cohort was defined, pertinent clinical variables were systematically retrieved from the MIMIC-IV and eICU-CRD databases, with data accessibility and clinical relevance serving as the primary selection criteria to guarantee both practical applicability and analytical robustness. The entire data retrieval process was executed via structured query language (SQL). All extracted variables were organized into five categories: demographic characteristics (gender, age, race, and weight), vital signs (heart rate, respiratory rate, and temperature), laboratory parameters (blood urea nitrogen [BUN], hemoglobin, white blood cell [WBC] count, creatinine, potassium, sodium, calcium, chloride, anion gap, hematocrit, prothrombin time [PT], bicarbonate, and glucose), comorbid conditions (hypertension, diabetes, acute myocardial infarction [AMI], chronic kidney disease [CKD], acute kidney injury [AKI], and chronic obstructive pulmonary disease [COPD]), and the primary outcome defined as in-hospital survival status.

Incomplete data were handled through multiple imputation via the mice (v 3.18) package [26]. A missing rate threshold of 20% was applied: variables falling below this threshold underwent imputation, while those meeting or exceeding it were removed from subsequent analyses. The imputation strategy differed by variable type: binary variables were handled with the logistic regression (logreg) method, ordered categorical variables with the proportional odds logistic regression (polr) method, and continuous variables with predictive mean matching (pmm).

SAT patients were then divided into two groups—survivors and non-survivors—based on whether in-hospital death occurred during the index hospitalization. To explore the relationship between the extracted clinical variables and in-hospital mortality in SAT patients, between-group comparisons of baseline characteristics were carried out within the MIMIC-IV cohort. Categorical variables are reported as n (%) and tested with the chi-square test; continuous variables are summarized as mean ± standard deviation (SD) and examined by the Student's t-test or Wilcoxon rank-sum test depending on the distributional properties of the data. Statistical significance was set at a two-sided P-value below 0.05, and all comparative results are compiled in the baseline characteristics table.

4.3 Identification of independent predictors

Variables demonstrating statistically significant between-group differences in the baseline analysis were subsequently entered into a least absolute shrinkage and selection operator (LASSO) regression model for further screening. The procedure was implemented in the training set via 10-fold cross-validation with the glmnet (v 4.1.8) package[27]. Optimal penalty parameter (λ) selection followed the one-standard-error criterion (lambda.1se), retaining only those variables whose regression coefficients remained non-zero at the designated λ as candidate feature variables.

To examine the relationship between the retained feature variables and in-hospital mortality risk in SAT patients, multivariable logistic regression was then performed in the training set using the glm function within the stats (v 4.3.3) package [28]. Among the candidate variables, those that retained statistical significance ($P < 0.05$) after multivariable logistic regression adjustment were classified as independent predictors and carried forward into the subsequent analytical stages.

4.4 Construction and evaluation of the nomogram

Using the confirmed independent predictors, a nomogram was built in the training set through the rms (v 6.8.1) package[29]. Point values proportional to each predictor's regression coefficient were assigned, and the aggregate score was subsequently mapped to an individualized probability estimate of in-hospital death for each SAT patient. Calibration performance was examined through calibration analysis using the same rms (v 6.8.1) package, with consistency between model-predicted probabilities and actual observed outcomes serving as the primary evaluation criterion. The HL test was additionally applied to evaluate goodness-of-fit, whereby a non-significant P-value ($P > 0.05$) was taken as evidence of adequate fit. Discriminative capacity was quantified through ROC curve analysis implemented with the pROC (v 1.18.5) package [30], and the area under the curve (AUC) was computed as the primary performance metric; an AUC exceeding 0.60 was deemed indicative of acceptable discrimination. Clinical utility was further appraised through decision curve analysis (DCA) carried out with the rmda (v 1.6) package [31]. Validation of robustness and cross-setting generalizability relied on ROC and DCA analyses applied to both the internal validation set and the external validation set derived from eICU-CRD.

4.5 Statistical analysis

All statistical procedures were completed within the R (v 4.3.3) software environment. Unless stated otherwise, a two-sided P value of less than 0.05 served as the uniform criterion for declaring statistical significance. Detailed descriptions of each statistical test and analytical method are provided within their respective sections above.

List of abbreviations

Abbreviation	Full term
SAT	Sepsis-associated thrombocytopenia
ICU	Intensive care unit

MIMIC-IV	Medical Information Mart for Intensive Care IV
eICU-CRD	Electronic Intensive Care Unit Collaborative Research Database
ICD-9	International Classification of Diseases, Ninth Revision
ICD-10	International Classification of Diseases, Tenth Revision
BUN	Blood urea nitrogen
WBC	White blood cell
PT	Prothrombin time
AMI	Acute myocardial infarction
CKD	Chronic kidney disease
AKI	Acute kidney injury
COPD	Chronic obstructive pulmonary disease
LASSO	Least absolute shrinkage and selection operator
ROC	Receiver operating characteristic
AUC	Area under the curve
DCA	Decision curve analysis
HL	Hosmer-Lemeshow
SQL	Structured query language

SD	Standard deviation

References

1 Pisano, A., Venditto, M., Palmieri, C. & Landoni, G. Novel therapies and interventions in sepsis and septic shock. BJA Educ 25, 206-217, doi:10.1016/j.bjae.2025.01.003 (2025).

2 Evans, L. et al. Surviving sepsis campaign: international guidelines for management of sepsis and septic shock 2021. Intensive Care Med 47, 1181-1247, doi:10.1007/s00134-021-06506-y (2021).

3 Jonsson, A. B. et al. Thrombocytopenia in intensive care unit patients: A scoping review. Acta Anaesthesiol Scand 65, 2-14, doi:10.1111/aas.13699 (2021).

4 Anthon, C. T. et al. Thrombocytopenia and platelet transfusions in ICU patients: an international inception cohort study (PLOT-ICU). Intensive Care Med 49, 1327-1338, doi:10.1007/s00134-023-07225-2 (2023).

5 Maugeri, N. & Manfredi, A. A. Platelets as drivers of immunothrombosis in rheumatic diseases. Nat Rev Rheumatol 21, 478-493, doi:10.1038/s41584-025-01276-z (2025).

6 Setarehaseman, A., Mohammadi, A. & Maitta, R. W. Thrombocytopenia in Sepsis. Life (Basel) 15, doi:10.3390/life15020274 (2025).

7 Wang, L., Chen, J. & Zhou, X. Factors influencing sepsis associated thrombocytopenia (SAT): A multicenter retrospective cohort study. PLoS One 20, e0318887, doi:10.1371/journal.pone.0318887 (2025).

8 Ye, W. et al. Developing and validating a prognostic model to predict ICU mortality in patients with sepsis-associated thrombocytopenia: a retrospective cohort study based on MIMIC-IV. BMJ Open 15, e099691, doi:10.1136/bmjopen-2025-099691 (2025).

9 Johnson, A. E. W. et al. MIMIC-IV, a freely accessible electronic health record dataset. Sci Data 10, 1, doi:10.1038/s41597-022-01899-x (2023).

10 Pollard, T. J. et al. The eICU Collaborative Research Database, a freely available multi-center database for critical care research. Sci Data 5, 180178, doi:10.1038/sdata.2018.178 (2018).

11 Shen, J. et al. Multivitamin supplementation as a potential adjunctive therapy in post-cardiac arrest: insights from a multicenter retrospective analysis of MIMIC-IV and eICU-CRD. Front Nutr 12, 1602372, doi:10.3389/fnut.2025.1602372 (2025).

12 Satoh, K. et al. Practical approach to thrombocytopenia in patients with sepsis: a narrative review. Thromb J 22, 67, doi:10.1186/s12959-024-00637-0 (2024).

13 Girardis, M. et al. Understanding, assessing and treating immune, endothelial and haemostasis dysfunctions in bacterial sepsis. Intensive Care Med 50, 1580-1592, doi:10.1007/s00134-024-07586-2 (2024).

14 Liew, P. X. & Kubes, P. The Neutrophil's Role During Health and Disease. Physiol Rev 99, 1223-1248, doi:10.1152/physrev.00012.2018 (2019).

15 Vago, J. P. et al. Plasmin and plasminogen prevent sepsis severity by reducing neutrophil extracellular traps and systemic inflammation. JCI Insight 8, doi:10.1172/jci.insight.166044 (2023).

16 Chen, Z. et al. Review: The Emerging Role of Neutrophil Extracellular Traps in Sepsis and Sepsis-Associated Thrombosis. Front Cell Infect Microbiol 11, 653228, doi:10.3389/fcimb.2021.653228 (2021).

17 Zhu, L., Dong, H., Li, L. & Liu, X. The Mechanisms of Sepsis Induced Coagulation Dysfunction and Its Treatment. J Inflamm Res 18, 1479-1495, doi:10.2147/jir.S504184 (2025).

18 Liu, X., Li, T., Chen, H., Yuan, L. & Ao, H. Role and intervention of PAD4 in NETs in acute respiratory distress syndrome. Respir Res 25, 63, doi:10.1186/s12931-024-02676-7 (2024).

19 Bendas, G., Gobec, M. & Schlesinger, M. Modulating Immune Responses: The Double-Edged Sword of Platelet CD40L. Semin Thromb Hemost 51, 855-869, doi:10.1055/s-0044-1791512 (2025).

20 Iba, T. et al. Damage-associated Molecular Patterns, Immunothrombosis, and Intravascular Inflammation in Sepsis: A Narrative Integrative Review. Semin Thromb Hemost, doi:10.1055/a-2776-5999 (2025).

21 Lin, L. et al. HYDROGEN-RICH SALINE UPREGULATES THE SIRT1/NF-KB SIGNALING PATHWAY AND REDUCES VASCULAR ENDOTHELIAL GLYCOCALYX SHEDDING IN SEPSIS-INDUCED ACUTE KIDNEY INJURY. Shock 62, 416-425, doi:10.1097/shk.0000000000002404 (2024).

22 Atreya, M. R. et al. SERUM HUMANIN IN PEDIATRIC SEPTIC SHOCK-ASSOCIATED MULTIPLE-ORGAN DYSFUNCTION SYNDROME. Shock 61, 83-88, doi:10.1097/shk.0000000000002266 (2024).

23 Dépret, F. et al. Management of hyperkalemia in the acutely ill patient. Ann Intensive Care 9, 32, doi:10.1186/s13613-019-0509-8 (2019).

24 Menard, C. E. et al. Evolution and Impact of Thrombocytopenia in Septic Shock: A Retrospective Cohort Study. Crit Care Med 47, 558-565, doi:10.1097/ccm.0000000000003644 (2019).

25 Zhou, H., Li, Z., Liang, H. & Yan, Z. Thrombocytopenia and platelet count recovery in patients with sepsis-3: a retrospective observational study. Platelets 33, 612-620, doi:10.1080/09537104.2021.1970124 (2022).

26 Azur, M. J., Stuart, E. A., Frangakis, C. & Leaf, P. J. Multiple imputation by chained equations: what is it and how does it work? Int J Methods Psychiatr Res 20, 40-49, doi:10.1002/mpr.329 (2011).

27 Li, Y., Lu, F. & Yin, Y. Applying logistic LASSO regression for the diagnosis of atypical Crohn's disease. Sci Rep 12, 11340, doi:10.1038/s41598-022-15609-5 (2022).

28 Goncharova, I. A. et al. [Genetic Predisposition to Early Myocardial Infarction]. Mol Biol (Mosk) 54, 224-232, doi:10.31857/s0026898420020044 (2020).

29 Sachs, M. C. plotROC: A Tool for Plotting ROC Curves. J Stat Softw 79, doi:10.18637/jss.v079.c02 (2017).

30 Robin, X. et al. pROC: an open-source package for R and S+ to analyze and compare ROC curves. BMC Bioinformatics 12, 77, doi:10.1186/1471-2105-12-77 (2011).

31 Liu, C., He, Y. & Luo, J. Application of Chest CT Imaging Feature Model in Distinguishing Squamous Cell Carcinoma and Adenocarcinoma of the Lung. Cancer Manag Res 16, 547-557, doi:10.2147/cmar.S462951 (2024).

Declarations

Ethics approval and consent to participate

Not adapted.

Consent for publication

Not adapted.

Availability of data and materials

The dataset supporting the conclusions of this article is available in the [eICU- CRD] repository, [https://eicu-crd.mit.edu/]. The dataset supporting the conclusions of this article is available in the [mimic-IV] repository, [https://mimic.mit.edu/].

Competing interests

The authors declare that they have no competing interests.

Funding

The research reported in this project was generously supported by the 2023 Discipline Construction Project of Anhui Medical University, and the Anhui Provincial University Natural Science Research Project under grant agreement number [2023AH050518]. The funders had no role in study design, data collection and analysis, decision to publish, or preparation of the manuscript.

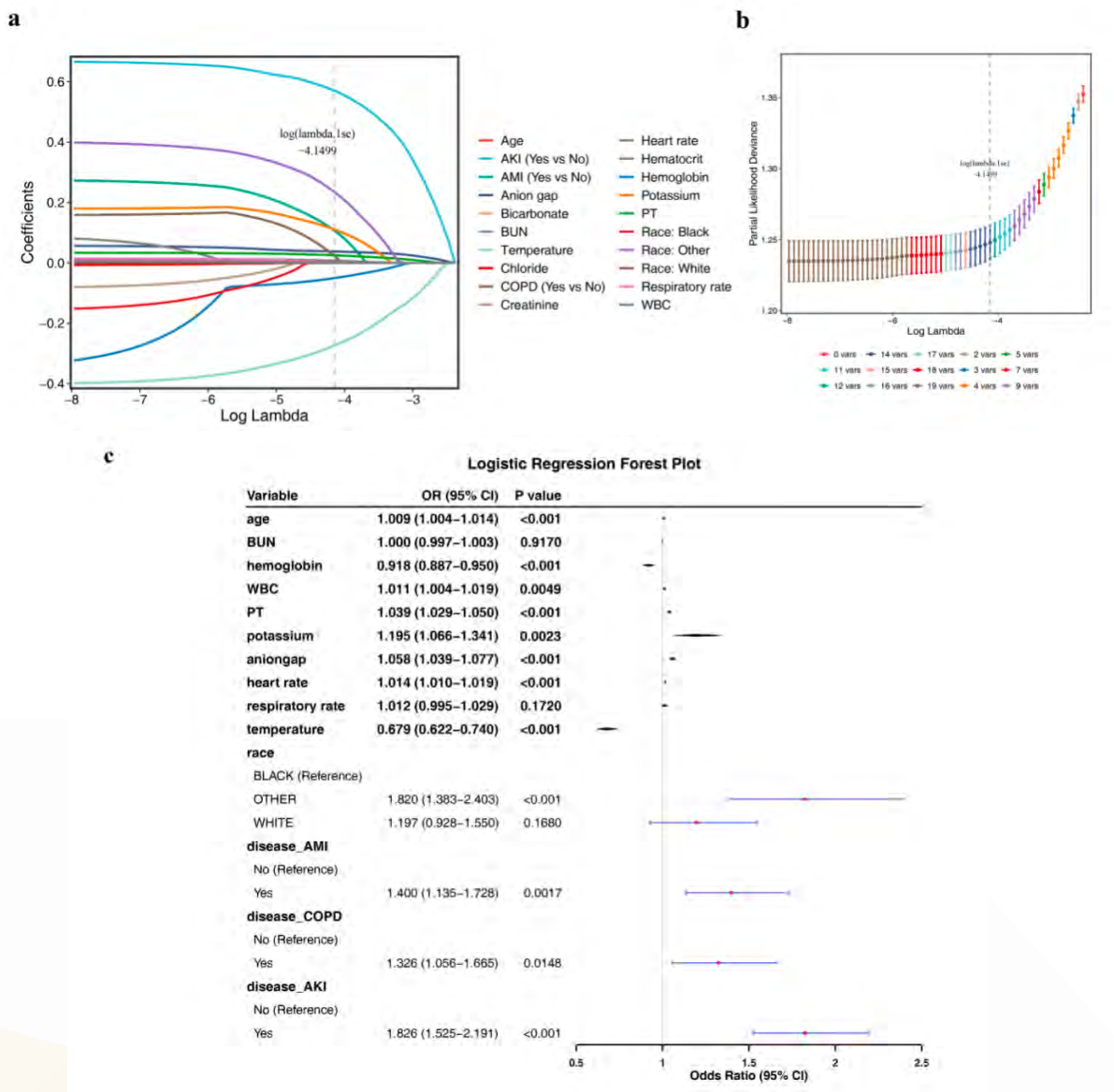
Authors' contributions

XL and NW conceived and designed the study. XL extracted data from the MIMIC-IV and eICU-CRD databases. XL, QC, and RS performed data curation and checked the integrity of the data. XL conducted the statistical analysis and developed the analytical workflow. YS drafted the manuscript with input from all authors. QC and RS contributed to data interpretation and manuscript revision. LW and NW supervised the study and critically revised the manuscript. All authors read and approved the final version of the manuscript.

Acknowledgements

The author would like to thank everyone on the research team for their contribution to this study.

Figure legends



Variable	OR (95% CI)	P value
age	**1.009 (1.004–1.014)**	**<0.001**
BUN	**1.000 (0.997–1.003)**	**0.9170**
hemoglobin	**0.918 (0.887–0.950)**	**<0.001**
WBC	**1.011 (1.004–1.019)**	**0.0049**
PT	**1.039 (1.029–1.050)**	**<0.001**
potassium	**1.195 (1.066–1.341)**	**0.0023**
aniongap	**1.058 (1.039–1.077)**	**<0.001**
heart rate	**1.014 (1.010–1.019)**	**<0.001**
respiratory rate	**1.012 (0.995–1.029)**	**0.1720**
temperature	**0.679 (0.622–0.740)**	**<0.001**
race		
BLACK (Reference)		
OTHER	1.820 (1.383–2.403)	<0.001
WHITE	1.197 (0.928–1.550)	0.1680
disease_AMI		
No (Reference)		
Yes	1.400 (1.135–1.728)	0.0017
disease_COPD		
No (Reference)		
Yes	1.326 (1.056–1.665)	0.0148
disease_AKI		
No (Reference)		
Yes	1.826 (1.525–2.191)	<0.001

Fig. 1. Selection of independent predictors. (a) Least absolute shrinkage and selection operator (LASSO) coefficient trajectory in the training set. (b) LASSO cross-validation plot showing optimal lambda in the training set. (c) Forest plot of multivariable logistic regression identifying independent predictors of in-hospital death.

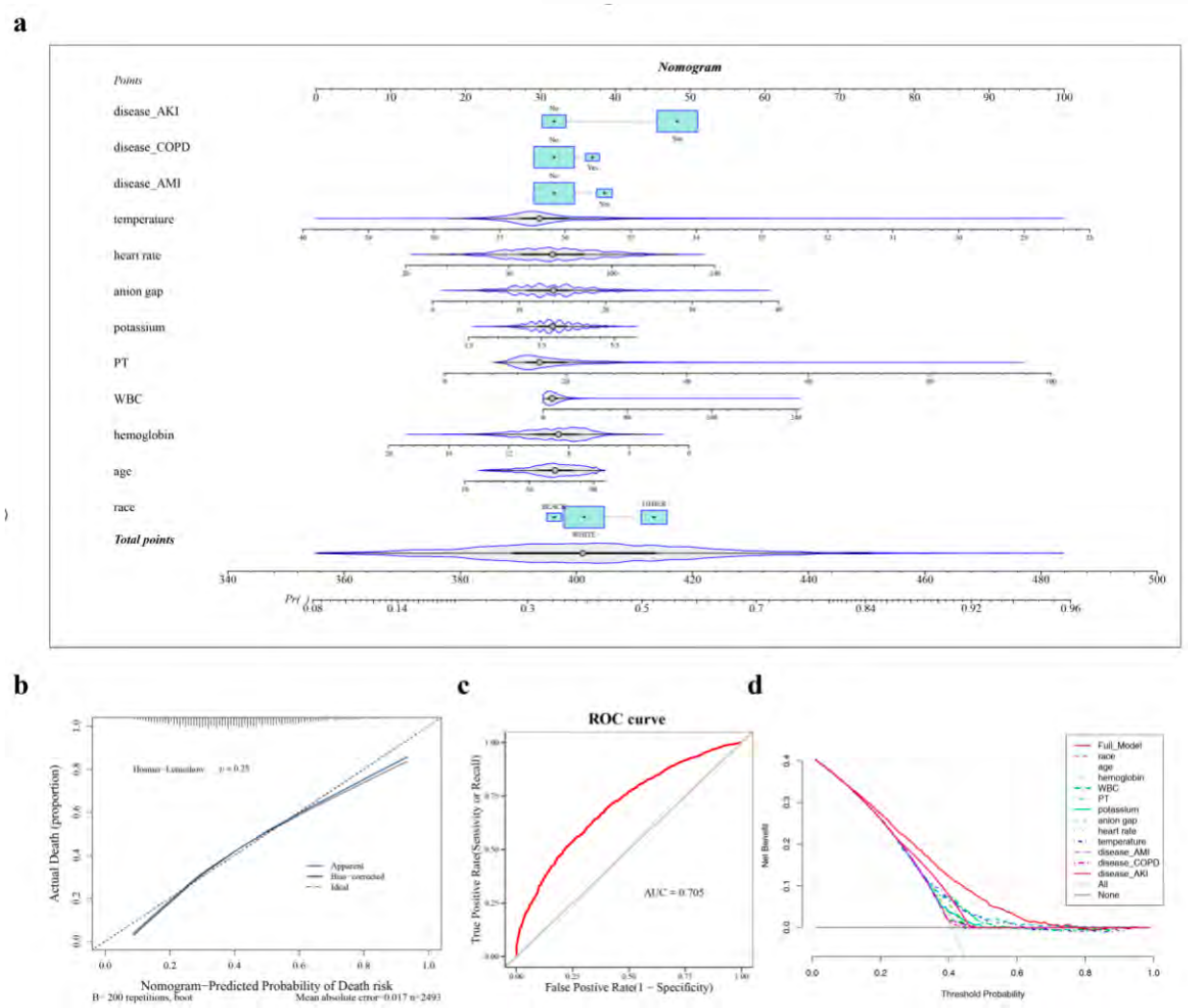


Fig. 2. Development and evaluation of the nomogram in the training set. (a) Nomogram integrating independent predictors for estimating in-hospital mortality risk. (b) Calibration curve showing agreement between predicted and observed outcomes. (c) ROC curve demonstrating discriminative performance of the nomogram. (d) Decision curve analysis (DCA) evaluates the clinical net benefit of the nomogram.

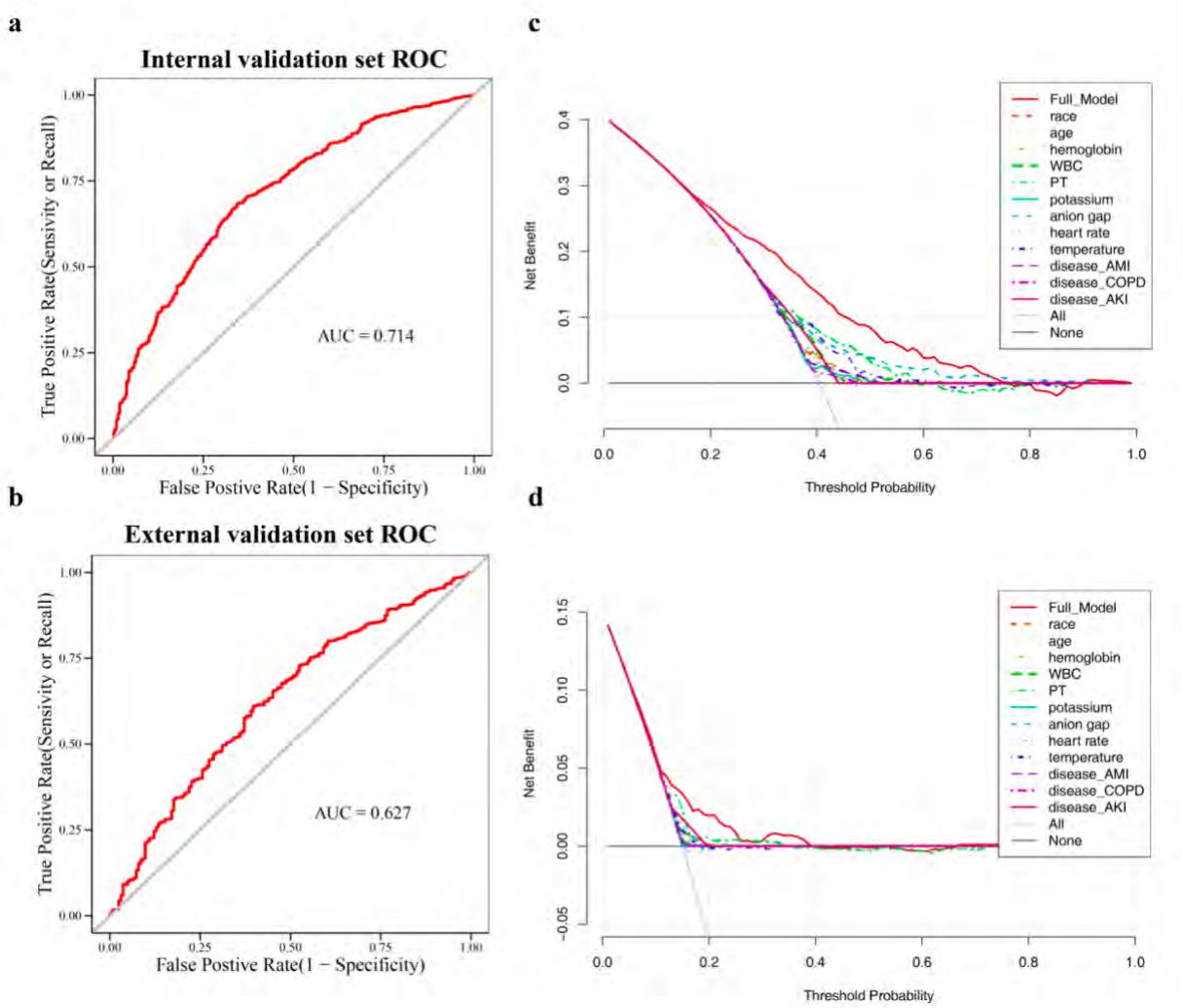


Fig. 3. Validation of the nomogram in internal and external cohorts. (a-b) ROC curves in the internal (a) and external (b) validation sets. (c-d) DCA in the internal (c) and external (d) validation sets assessing clinical utility.

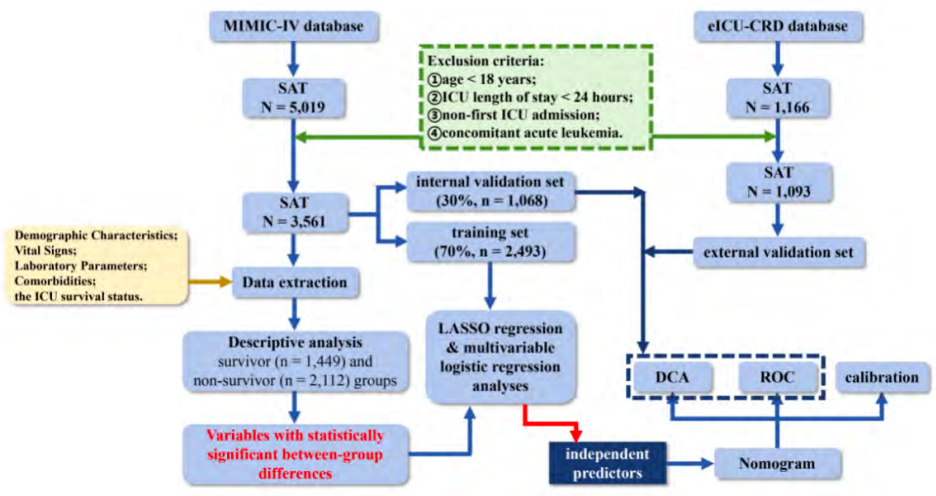


Fig. 4. Flowchart depicting sample inclusion and overall study workflow.

Tables

Table 1. Baseline characteristics of survivor and non-survivor groups in the MIMIC-IV cohort.

	Survivor (n = 2,112)	**non-survivor (n=1,449)**	**p**
Demographic Characteristics			
Gender, No. (%)			0.618
Female	876(41.5%)	614(42.4%)	
Male	1236(58.5%)	835(57.6%)	
Age (year)	64.90±15.98	66.12±14.83	0.021
Race, No. (%)			<0.001
Black	209(9.9%)	125(8.6%)	
Other	490(23.2%)	460(31.7%)	
White	1413(66.9%)	864(59.6%)	
Weight (kg)	82.46±23.72	83.06±24.33	0.465
Vital Signs			
heart rate (beats per minute, BPM)	76.43±16.88	78.87±17.24	<0.001
respiratory rate (breaths per minute, BPM)	13.13±4.17	13.43±4.53	0.042
temperature (℃)	36.31±0.82	36.00±1.02	<0.001
Laboratory Parameters			
BUN (blood urea nitrogen; mg/dL)	33.77±25.10	40.85±29.94	<0.001
hematocrit (%)	27.95±6.64	26.81±6.44	<0.001

	Survivor (n = 2,112)	**non-survivor (n=1,449)**	**p**
hemoglobin (g/dL)	9.17±2.18	8.71±2.12	<0.001
WBC (white blood cell; 10^9/L)	10.09±8.25	11.66±12.30	<0.001
PT (prothrombin time; s)	16.94±6.58	19.54±8.67	<0.001
creatinine (mg/L)	1.74±1.60	1.97±1.53	<0.001
potassium (mEq/L)	3.80±0.63	3.93±0.68	<0.001
sodium (mEq/L)	135.58±6.27	135.38±6.80	0.376
calcium (mg/dL)	7.65±0.90	7.71±1.04	0.096
chloride (mEq/L)	101.19±7.62	99.81±8.06	<0.001
anion gap (mEq/L)	13.38±3.95	15.19±5.13	<0.001
bicarbonate (mEq/L)	18.83±5.17	17.49±5.76	<0.001
glucose (mg/dL)	114.55±41.69	113.09±50.12	0.346
Comorbidities			
hypertension, No. (%)			0.952
No	877(41.5%)	604(41.7%)	
Yes	1235(58.5%)	845(58.3%)	
diabetes, No. (%)			0.843
No	1461(69.2%)	997(68.8%)	
Yes	651(30.8%)	452(31.2%)	
AMI (acute myocardial infarction), No. (%)			<0.001
No	1873(88.7%)	1217(84.0%)	
Yes	239(11.3%)	232(16.0%)	

	Survivor (n = 2,112)	**non-survivor (n=1,449)**	**p**
COPD (chronic obstructive pulmonary disease), No. (%)			0.014
No	1902(90.1%)	1266(87.4%)	
Yes	210(9.9%)	183(12.6%)	
CKD (chronic kidney disease), No. (%)			0.371
No	1553(73.5%)	1045(72.1%)	
Yes	559(26.5%)	404(27.9%)	
AKI (acute kidney injury), No. (%)			<0.001
No	671(31.8%)	241(16.6%)	
Yes	1441(68.2%)	1208(83.4%)	